The University of Adelaide
Department of Geology and Geophysics

A Geophysical Study of the Structure and Crustal Environment of the Polda Rift, South Australia

Irena Kivior
M. Sc., Eng. Geol. [A.G.H., Kraków]

January 1996

A thesis submitted to the University of Adelaide
in fulfilment of the requirements for the degree of
Doctor of Philosophy

Contents

List of Figures

List of Tables

Abstract

The Polda Trough, a major geological feature on the southern Gawler Craton in South Australia, has such meagre surface expression that its full extent was not recognised until the late sixties. Aeromagnetic surveys showed that the Polda Trough is a narrow graben, which extends for more than 400 km westward from the centre of Eyre Peninsula towards the edge of the continental margin in the Great Australian Bight and that its widest and deepest part lay offshore. The onshore part of the Polda Trough which is the eastern end of the larger structure and a small section offshore is the subject of this research.

The SADME/AGSO high quality aeromagnetic survey flown in 1987 when integrated with the available geological, drilling, gravity and seismic data, shows that the Polda Trough east of $134^{\circ}30' E$ has the following character:

- it narrows from 35 km to 5 km in width about the position of the coast line;
- the eastern part is an extension of the southern section of the wider rift;
- the sediments in the rift are 5 km thick in the west and about 1.2 km thick in the narrower part of the rift;
- onshore the Permian sediments revealed in drill holes are restricted to the area of the 5 km wide rift;
- where the angle of the dip can be determined from the modelling of the magnetic anomalies, the faults are normal and dip at a relatively high angle (about $75^{\circ} - 80^{\circ}$);
- at the eastern end of the Polda Trough, east of longitude 136°, the sediments occur in a northerly dipping wedge bounded in the north by step faults with a throw of about 2.5 km;
- the correlation of magnetic anomalies on the northern and southern margins of the Polda Trough suggests that there is a 30 km strike-slip dextral movement along this structure. The age of this movement is not known.

Gravity lows with an amplitude of about 40 *mgals* are the combined effect of both the low-density Precambrian basement and the younger sedimentary cover. Consequently the gravity lows in places give a misleading impression of the thickness of the sediments in the Polda Trough. In the past these negative gravity anomalies were considered to be due to only low-density sediments.

A number of major NE and NW faults, which are shown on regional tectonic maps, could not be identified in the new high resolution magnetic survey data apart from one large NW trending fault

which is located near the eastern end of the trough. It is suggested that the en echelon pattern of the rift segments previously attributed to cross faults may be the effect of relay ramps.

It has been suggested by several authors that the Polda Trough developed first as a graben in Late Proterozoic time. Although it seems probable that the Polda Trough developed along the line of a much older structure, there is no evidence onshore that the graben structure developed before the Mesozoic period.

There is a major change in the composition and thickness of the upper crust across an east-west striking boundary which coincides with the position of the Uno fault on the surface. This rather than the Polda Trough faults may mark the northern limit of a major unit in the Southern Australian Rift System in South Australia.

Spectral analysis applied to regional aeromagnetic data which covers an area between $26-35^{\circ}S$ and $129-141^{\circ}E$, indicates major magnetic inhomogeneities in the crust in South Australia.

Interpretation of the logarithmic radial energy spectrum of the study area and the surrounding Gawler Craton shows a more magnetic section of the crust lying at depth of between 10 and 20 km below the surface. In areas where seismic data is available this more magnetic section of the crust corresponds to a change in seismic velocity from about 4.9 km/sec to 5.6 km/sec.

The logarithmic radial energy spectrum also provides filter parameters to separate the regional and residual magnetic fields and allows the construction of depth slice maps at depths of 4 km, 16 km and 30 km.

The analysis of the upward continued regional field suggests that the magnetic crust beneath the Polda Trough is probably thinner than that beneath the crystalline Gawler Craton. However, it was not possible to show more distinctive features which would indicate a difference between rifted and normal crust.

Statement

To the best of the author's knowledge and belief, and except where reference is made herein, this thesis contains no material previously published or written by another person, nor any material that has been accepted for the award of any other degree or diploma in any University.

If this thesis is accepted for the award of the degree, the author consents to the thesis being made available for photocopying and loan.

Irena Kivior

January 1996

Acknowledgements

I am deeply grateful for the help and advice of the following people who gave me their encouragement and made it possible for me to carry on this research.

My very special thanks and gratitude to Professor David Boyd, my scientific mentor and thesis supervisor, for his untiring assistance, inspiring support and patient guidance. The wealth of his knowledge, wisdom and experience was invaluable and made it possible for me to continue my work. It was a real privilege to be his student and I deeply appreciate all the help and encouragement I have received from him.

Many thanks to my internal supervisors, Dr. Peter Brooker for helpful advice, reading and correcting my manuscript, and Dr. Pat James for partial review of my thesis.

My special thanks to Professor Ken McClay for his interest, advice and comments on my work.

I am very indebted to Dr. Zhiqun Shi for her friendly involvement and participation in my research. She opened to me the domain of potential field, assisting me with her knowledge and experience in that area, always encouraging and stimulating me to a further effort. I am very grateful for having such a true friend.

I would like to acknowledge Dr. John Parker help in critical review of my work and his many constructive suggestions, and also thank Dr. David Tucker, who first suggested to me the Polda Trough as my research project. I am very grateful for his support and faith in me.

I wish to thank Dr. Atchuta Rao for his interest in my research, stimulating discussion and very kind comments concerning my work.

My thanks and gratitude to Dr. Shanti Rajagopalan for her counsel and interest in my progress and for use of her 'colour image' software.

I wish to acknowledge Dr. John Cooper, Dr. David Johnson, Dr. Duncan Cowan, Professor Richard Jarrett, Dr. Tony White, Dr. Robin Oliver and Dr. Mike Sandiford for their helpful information and useful discussions concerning my research, also I would like to express my thanks to Andy Mitchell for his always willing help and for providing printing facilities.

I would like to convey my great appreciation to Ursula McGowan of the ACUE, at the University of Adelaide, who gave me guidance on the required structuring of the thesis and helped me with the English language.

I thank the University of Adelaide for granting me a Postgraduate Research Award and the Department of Geology and Geophysics for access to their facilities. I wish to thank Dr. Pat James, Dr. Vic Gostin and Dr. John Foden, who during their respective tenures as Chairmans of this Department extended all possible support. I specially thank Dr. Vic Gostin for his continuous help and understanding.

I am grateful to the Department of Geology and Geophysics, the Computing Centre of the University of Adelaide and the National Centre for Petroleum and Geophysics for providing computing facilities.

My research was greatly facilitated by the interest, and cooperation of the Officers of the University of Adelaide, John Willoughby, Chris Farmer, Don Creighton and Sherry Proferes, Richard Barrett, Sophie Craddock, Mary Odlum and Gerard Buttfield. I am particularly indebted to Murray Rogers for his friendly assistance and constant help. Also I would like to extend my appreciation to fellow postgraduate students during the past few years: Charles Sevcik, Stephen Markham and Mohammad Haidarian.

My grateful acknowledgements to Mines and Energy of South Australia for the provision of the 1987 Eyre Peninsula Survey aeromagnetic data sets, the grid of the State Aeromagnetic Map and the State gravity data base. I especially thank Mr. Rick Horn and Mr. Terry Crabb for their support.

It is my pleasant duty to thank Grazyna Smolucha and Gosia Panek for the diagrams they skilfully drew for me. Also my grateful thanks go to Enid Templeton-Tait and Basia Rajkowska for the proof-reading of my manuscript, Dr. Tom Flöttmann and Annette Bingemer for careful and critical review of part of my thesis, Dr. Sylvia Barber and Elizabeth Tasker for their friendly advice, and my special friend Yolanta Raggambi for proof-reading of my thesis, propping me up in difficult moments and always standing by ready for any emergency.

I wish to thank my parents, Lucy and Frank Burtan, and my family for always encouraging me in my studies and for their faith in me. Their support and generosity is deeply appreciated.

Finally my heartfelt thank you to my son Tomasz for his patient endurance during the years of my preoccupation with this thesis and his loving, never-failing cheer and encouragement. This thesis is dedicated to Him.

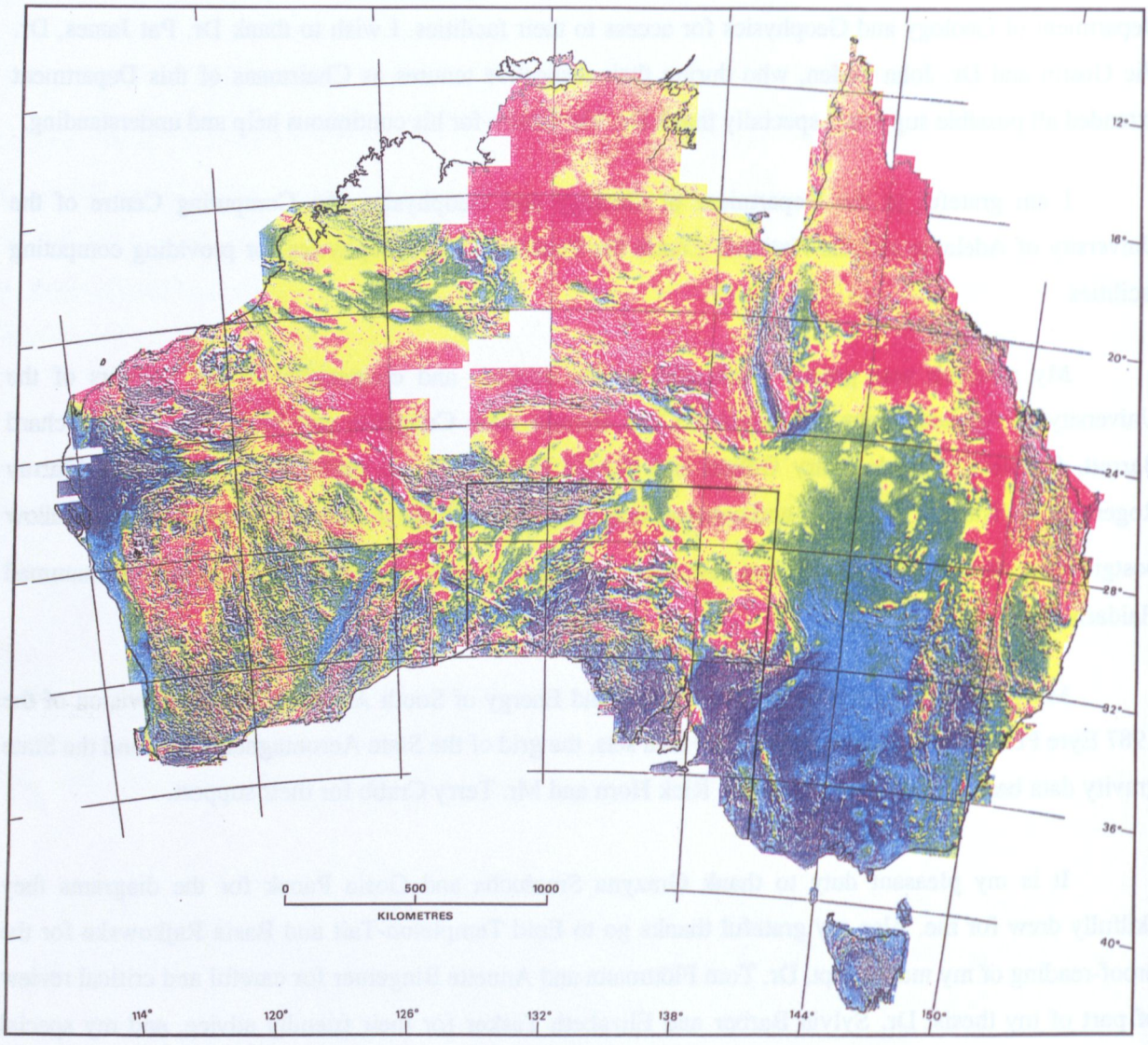

PLATE I Total magnetic intensity map of Australia. After Tarlowski (1991).

Motto

Prospecting for new deposits to meet future needs is increasingly active in those countries with long histories of political stability. While a good deal of favorable land surface remains to be prospected by conventional means in favored areas, it is already apparent that prospecting for deposits buried beneath thick blankets of surface rocks will become feasible. The search for buried mineral deposits will become intense over the next 50 years, and the places where searching is likely to be most rewarding will be in those countries that have made the long-term investments needed to measure and map the earth's crust in the third dimension to depths of 15 or 20 km. Such mapping is an expensive and exacting undertaking. The countries where the expertise exists, and where the investment is being made, are the present-day industrial countries. It is perceived, therefore, that the mining of metallic minerals may well start to return to shores of the industrial countries over the next 50 years.

McLaren and Skinner (1987)

Chapter 1

Introduction

Rifts are unique features of global geology. The formation and development of rifts were important events in the evolution of the earth's crust. During the evolution of the crust, rifting, leading to the break-up of continents and the opening of new oceanic basins, played an equally important role as orogenic processes, accompanied by the closure of oceans and the suturing of continents. The economic potential of many known world rifts is considerable. These features are sites of hydrocarbons, coals, and minerals including phosphates, Cu-Pb-Zn sulphides, diamonds, barite and uranium accumulations.

Rift valley basins are extensional features on a regional scale. In the evolution of the extensional rift valleys magmatic activity may reflect underlying heat sources such as a convection plume in the mantle or a hot spot, the rifting then being the consequence of expansion and thermal uplift. Alternatively the magmatic activity may be a result of regional or local extensional stresses. Studies of rifts and geodynamics of rifting may bring more light to understanding the earth's geological history. The processes which formed the passive continental margins are closely related to the mechanism of rifting and sea floor spreading.

Geodynamic processes controlling the development of continental margins are closely related to the rifting on the edges of the continents. Continental margin rift basins developed in association with the break-up of super-continents, sea floor spreading and the evolution of new oceans.

Global geological history based on plate tectonic evolution, lists records of important events in the break-up of Gondwanaland. The Mesozoic opening of the western Indian Ocean, separating East Gondwana (Madagascar, India, Antarctica, and Australia) from West Gondwana (Africa and South America), followed by the separation of India from Australia and Antarctica, are examples of major geological events, preceded by an appreciable amount of rifting over a long period of time. The lithospheric extension and related rifting between Australian and Antarctic plates began in Jurassic time. The break-up and separation of these two continents evolved into the opening of the Southern Ocean, and the development of the southern Australian and Antarctic continental margins. The opening of the Southern Ocean was initiated in the mid-Cretaceous and continues to the present day. The southern margin of the Australian continent, which is a divergent, passive, continental margin, extends for four thousand kilometres from the Perth Basin in Western Australia to the Tasman Plateau in the south-east. Extensive Mesozoic/Tertiary rifting on the edge of the southern margin of

the Australian continent resulted in a complex tectonic system referred to as the Southern Australian Rift System. The Polda Trough is a rift structure about 50 km wide and 400 km long, which is a small part of this extensive tectonic system.

The Polda rift is located on the south-eastern Gawler Craton and extends from the middle of Eyre Peninsula to the edge of the continental shelf in the Great Australian Bight. An integration of geological studies with an interpretation of the available geophysical survey data of the Polda rift and surrounding craton can be expected to increase our knowledge and understanding of the development of the Southern Australian Rift System and geological history of the southern margin of the Australian Continent. A principal aim of the research presented in this thesis is a detailed analysis of the major structural elements i.e. boundary faults and the interior structure of the Polda rift as well as the character of the deeper crust underlying rifted and stable cratonic regions. This analysis is based on aeromagnetic data.

The part of the Polda Trough designated and discussed in this thesis is a minor appendage at the eastern end of the much larger rift structure. There are hardly any outcrops of the Pre-Quaternary stratigraphic units in the study area; the whole region is covered by Tertiary and Quaternary sediments. Intensive drilling, being a part of the geological exploration carried out by various companies over the years, provides some information about litho-stratigraphy of the rock formations within the rift and the surrounding craton. As there is not much information about geology in the study area, geophysics was used to infer the structure of this rift basin, and to interpret and correlate some geological information and thereby reconstruct its tectonic history.

The attention in this study was mainly directed to that part of the trough which was covered by the new, good quality, aeromagnetic survey which was conducted over the Eyre Peninsula by SADME and BMR in 1987/88. As this survey extended about 40 km westwards offshore, the research presented in this thesis has focused mainly on the onshore portion of the Polda Trough. Therefore, only the eastern end (160 km long) of the much larger rift structure (over 400 km) has been the subject of this research. The offshore part of the rift was only briefly reviewed, based on the literature, as there was no access to any original geophysical data surveyed over the Polda Trough extension into the Great Australian Bight.

The literature review presented in Chapter 2, Chapter 3 and Chapter 6, raises several questions not considered by others in the past and also indicates a need for an extension of the undertaken study.

- While some studies have been done on the geological interpretation of the geophysical aspect of the Polda Trough, little information is available on detailed geology and particularly its relation to the structure of the Polda Trough.

- The question which has been addressed here is the position of the Polda Trough in the regional geological pattern, and how this structure fits into the Southern Australian Rift System. Although in the past much research has been devoted to the reconstruction of the break-up history of the Gondwana super-continent in relation to the development of the southern margin of the Australian continent, very little is known about the evolution of the Polda rift from the rift-genesis point of view. Many of the southern basins are very well known because of extensive oil exploration and this is in contrast to this particular part of the Polda Trough.

- No work has been done on understanding the nature of the crust in the rifted regions in South Australia and its variation from the normal non-rifted crust. There is little information available on the study of the deeper parts of the Earth's crust. Several authors report on such investigations (see Chapters 2 and 4) but only limited information is available on the crustal studies in South Australia (BUMP-Upper Mantle Project; few refraction seismic lines, analysis of minor earthquake epicentres, teleseismic stations in the Musgrave Block and recently deep seismic sounding in the Officer Basin). The study of the middle and the lower crust is a new unexplored field of knowledge, and understanding its nature and its magnetic character becomes an important question in the research reported here.

This research project is concerned with two major scientific problems which are addressed in two stages, and thus the thesis has been structured to emphasise these two separate aspects of research:

- Analysis and the interpretation of the high resolution aeromagnetic survey data as a main tool and compilation of all other available geophysical and geological data to understand the structure of the sediments within the Polda rift, which as has been said represents only the eastern portion of a much more extensive tectonic system;

- Establishment of the magnetic signature of the deeper crust within the Polda rift zone and its character within the non-rifted cratonic region using energy spectral analysis of the total magnetic intensity field in order to do this.

The first purpose of this research was, using the new aeromagnetic data, and available seismic and gravity data, to define the shape of the individual parts of the Polda Trough, most of which cannot be seen because the area is covered by a blanket of sand.

The major structural elements of the Polda rift, i.e. the position and geometry of the marginal faults, as well as its interior structure, were located and analysed. The structural pattern of the Polda rift segments was inferred, by a comparison with reported results obtained from analog sand-box modelling, simulating a real geological rift-setting, and the observed interior structure of other rift systems.

The thickness of the sediments in the western, central and eastern parts of the rift, which have different geological character, were established, either from the spectral analysis of the gridded magnetic data, or forward modelling of the magnetic data along the east-west flight lines or north-south tie lines. The depth to the basement and some of the interpreted structures were confirmed by reinterpretation of the existing gravity data.

The integration of all results concerning detailed geophysical and geological studies of the Polda Trough shows that this rift is of post-Permian age, that it follows an older structure and is not a purely extensional rift..

The second major aim of the presented research was to determine any differences in the character of the magnetic crust in the rift zone and non-rifted areas. The studies of the magnetic crust in rifted and non-rifted regions of South Australia were carried out on the gridded magnetic data which covers more than one million square kilometres (an area between 26°S-35°S and 129°E-141°E). A geological interpretation on the regional scale was integrated with an interpretation of the quantitative studies of complex and large aeromagnetic data sets.

The energy spectral analysis method was applied to regional aeromagnetic data to compute the approximate average depth to the top of the deepest magnetic interfaces within the crust. Results obtained show significant variation in thickness of the weakly magnetic upper crustal layer underlying different tectonic provinces across the South Australian State. The verification and confirmation of the results has been facilitated by comparison with deep seismic sounding studies of the deep crust underlying the Canadian, Ukrainian, Baltic Shields and an analogy drawn with crustal studies of the Indian subplate.

The crustal studies reported in this thesis were directed towards rifted regions: the Polda rift and the Adelaide Geosyncline which is rift-type structure, and stable cratonic regions: the Musgrave Block and the Gawler Craton.

The major magnetic patterns of the deep magnetic sources (DMS) map of South Australia show deep crustal features interpreted from seismic profiles and regional gravity data. In the region of the Polda rift a thickness of the upper crustal layer and character of the magnetic crust within the zone affected by rifting was established from the analysis of the magnetic field using the energy spectra method, separation filters of the low and high frequency components, and vertical and horizontal gradients of the 'depth slice maps'.

The results of the research presented in this thesis are of importance to other researchers exploring the character and nature of the deeper crust, especially the thickness of crustal layers and variation of the Curie point isotherm. This research is a pioneer guide to the study of the middle and the lower crust of the Australian continent. As conventional crustal studies using deep seismic

sounding are slow and expensive, the application of spectral analysis to the magnetic and the gravity data of the whole of Australia should serve as the basis for a better understanding of the structure and major processes controlling the Earth's crust and even possibly the upper mantle. The results of this study may suggest the position where further deep seismic sounding lines should be shot to obtain maximum benefit. This in itself would be useful as a seismic survey is very costly.

By showing where the boundary of the Polda Trough is, and describing its internal structure, i.e. the position of the internal faults, this research will assist in planning and conducting any further exploration for hydrocarbons, coal, diamonds and other mineral in the Polda Trough.

Plate II Earth picture taken from Apollo 17 at a distance of 90,000 miles. Reprint from 'Africa's Rift Valley' by Colin Willock.

Chapter 2

Review of the world's major rift systems

2.1 Introduction

Rifting is one of the most fundamental geological process. To understand the origin and development of the Polda Trough is essential to review and summarise the latest facts and hypotheses concerning the origin and classification of the world's major rift systems. This chapter provides the background, within which the context of the Polda rift is analysed by way of comparisons it will be referred to in other sections of this thesis.

The geophysical signature of a rift zone is often the only tool available to establish the structure and evolution of any particular rift systems. In the following sections an account of geophysical studies of several of the world's rift systems will be briefly presented. The experience of geophysicists and geologists interpreting geophysical surveys over other rifts, may add to the understanding of the crustal changes which occurred in the Polda Trough and adjacent Gawler Craton.

The first part of this chapter summarises general account of the rift valley; the second part provides specific examples of the rifts from the different part of the world; the final sections focus on the South Australian Rift System which is a tectonic setting of the Polda Trough.

2.2 Origin and classification of rifts

Pioneering work in the study of the origin of rifts commenced at the end of the last century, when J. W. Gregory (1894), based on his work in East Africa, introduced the notion of rifting into the geological literature. The term 'graben' had been applied much earlier to structures such as the Red Sea and the Upper Rhine Valley by Eduard Suess (1885). For almost three quarters of the century the full significance of the concept of rifting and its role in Earth's geological history was not recognised.

The recognition of the geological processes responsible for the formation and development of rifts and grabens, was not till the late sixties, when oil exploration brought about major progress in the development of this field of a geological knowledge.

In 1955 the Russian scientist N. S. Shatsky, for the first time, described the rift structure of the Pachelma area on the Russian Platform and named it an 'aulacogen' (Shatsky, 1964). The term

'aulacogen' was introduced to describe linear graben-like structures, which had subsided during the early stages of development of this ancient craton in the Late Proterozoic.

Rifts are one of the most spectacular features of global morphology. Within oceans they separate plates as new oceanic crust is created, whereas within continents they may form deep valleys. The processes which form passive continental margins are closely related to mechanism of rifting and sea floor spreading. All of these continental margins are underlain by rifted sedimentary basins, and failed rifts whether they formed within continents or at the junction of continents and oceans (Reading, 1986). Some rifts penetrating continents are clearly failed rifts or aulacogens, which began as one arm of a triple junction, as ocean floor spreading developed along the two remaining arms. The Benue Trough in western Africa and the northern Viking graben of the North Sea are claimed to be such failed rifts (Whiteman et al., 1975), and so is that part of the East African Rift System known as the Afar triangle where the Red Sea and Gulf of Aden Rifts successfully opened, whilst the Afar triangle 'failed'. Some rifts originated as a result of a continental collision; the impact of India with Asia is considered to have caused an east-west extension which formed the Baikal graben (Molnar and Tapponnier, 1975). The origin of the Rhine graben is also interpreted as a result of a stress regime generated in the Alps.

In the last few decades the events related to rifting and the evolution of passive continental margins have been discussed and described by numerous authors (e.g. Burke and Dewey, 1973; Burke and Whiteman, 1973; Burk and Drake, 1974; Falvey, 1974; Girod, 1978; Ramberg and Neumann, 1978; Keen, 1979; Watkins et al., 1979; Freund and Garfunkel, 1981; Morgan and Baker, 1983, Ramberg et al. (Eds), 1984; Frostick et al. (Eds), 1986; Neumann (Ed), 1990; Makris et al. (Eds), 1991a, 1991b; Watkins et al. (Eds), 1979, 1992; Ziegler (Ed), 1992a, 1992b; McKenzie, 1978b; White and McKenzie, 1987, 1988 1989, Etheridge et al., 1983, 1988, 1990).

2.2.1 Geotectonic setting of rifts

Throughout the Earth's history several discrete episodes of rifting have been identified (Khain, 1992; Milanovsky, 1992), during which the break-up of Pangea or Gondwana super-continents was accompanied by the development of major rift systems. Some intra-continental rift basins evolved through time under collisional settings.

Based on Ziegler's (1992b) description, the geotectonic setting of the major rifts systems, will be briefly summarised as follows:

(I) Atlantic-type rift systems

Atlantic-type rift systems originated and developed during the break-up of major continental plates presumably as a result of convection cell reorganisation (Ziegler, 1992a). Early stages of rifting are associated with regional tensional stresses predominantly in areas of potential crustal separation and also in the initiation of complex graben systems. With time, rifting activity concentrates on the zone of crustal separation and, as a consequence, tectonic activity in lateral graben systems decreases and become tectonically inactive. Together with crustal doming processes and progressive lithospheric

attenuation, the deviatoric tensional stress regime strongly influences the evolution of this rift system. Thereafter, the separation of the continental crust, the diverging continental margins and the failed arms (paleorifts, aulacogens) of the original system become tectonically inactive. Among the Atlantic-type intra-cratonic rifts there exist many variations, in terms of stages of development or the level of volcanic activities (McKenzie and Bickle, 1988; White and McKenzie, 1987; White et al., 1987; Ziegler, 1988, 1990).

(II) Back-arc rifts

Back-arc rifts originate in response to decreasing convergence rates and/or to the divergence of the colliding plates (Uyeda and Miyashiro, 1974; Uyeda and Kanamori, 1979; Uyeda, 1981, 1982). This type of rifting may cause splitting of the continental crust and opening of the limited oceanic basins (e.g. Sea of Japan, South China Sea; Ziegler, 1992b).

(III) Syn-orogenic rift deformations

Syn-orogenic rift/wrench deformations can be initiated by the following events:

- forland indenter effects and escape tectonics, often with the rotation of intramontain blocks; examples are the Pannonian Basin (Royden and Horvath, 1988) or the Late Carboniferous Variscan fold belt (Ziegler, 1990),

- lithospheric over-thickening in fold belts and consequent uplift and extension of the axial parts of the orogen; e.g. the Altiplano in the Andes (Dalmayrac and Molnar, 1981),

- compressional splitting of the foreland; such as in the Baikal rift zone (Molnar and Tapponnier, 1975) or the Late Carboniferous development of the Norwegian-Greenland Sea rift (Ziegler, 1989).

(V) Post-orogenic rifting

Post-orogenic rifting may result in the decay of regional compressional stress field, steepening of the subducted lithospheric slab and ultimately the detachment of the latter. As Dewey (1988) implies such a scenario gives rise to rapid post-orogenic uplift, and to deviatoric tensional stresses caused by orogenic over-thickening of the lithosphere (e.g. West Siberian Basin; Rudkewich, 1976; Aplanov, 1987). Modifications in the convergence direction of colliding continents is associated with stress reorientation which may result in the development of wrench fault systems and related pull-apart basins (Old Red Sandstone Basin of Arctic-North Atlantic area, Stephanian-Autunian evolution of Western Europe; Ziegler, 1990).

(IV) Basin-and-Range type rifting

Basin-and-Range type rifting, evolved in response to the North America craton having overridden the Yellowstone and Socorro hot spots, and later, at about 28 Ma, the East Pacific Rise, in conjunction with the rapid opening of the Atlantic Ocean (Verall, 1989).

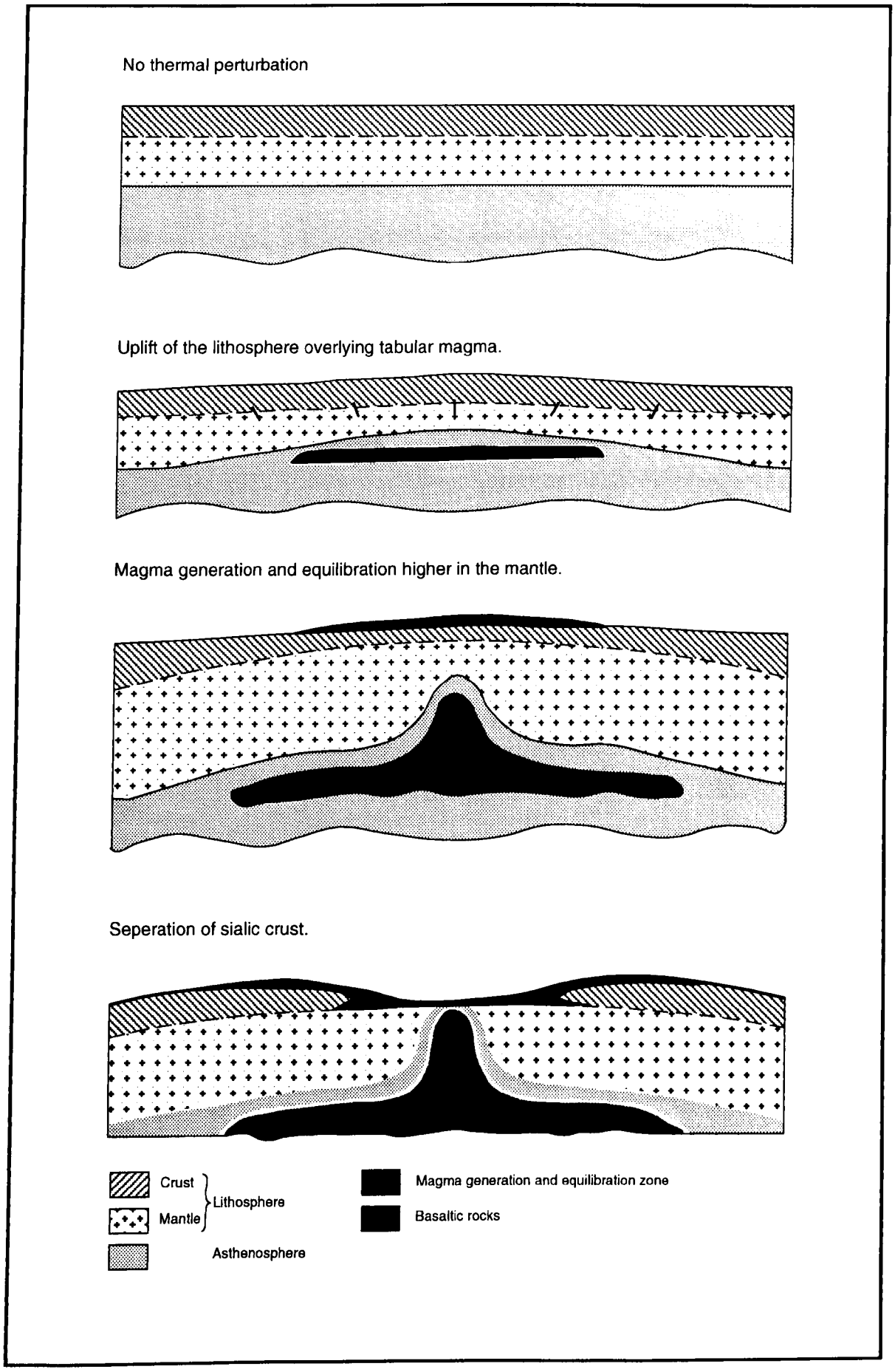

Figure 2.1 Diagrammatic representation of magmatic and structural processes related to a thermal perturbation in the lithosphere/asthenosphere boundary. After White and McKenzie (1989).

2.2.2 Thermal and mechanical state of the lithosphere

Continental rifts are generally considered to be essentially a surface manifestation of convective processes involving the upper mantle and perturbations in underlying zones of low viscosity. During geological history, large lithospheric plates with low thermal conductivity had insulating effect above the sub-lithospheric mantle. The accumulated heat caused development of new upwelling convective systems under the continental masses. This resulted in the exertion of drag forces on the base of the lithosphere and an increase in the melt content of the asthenosphere. During rifting, stress-induced lithospheric thinning causes decompression of the lower lithosphere and the upper asthenosphere, their partial melting and diapiric rise of melts into a zone of thinned lithosphere. Volume and composition of the melts generated by partial melting of the lower lithosphere and upper asthenosphere are related to the amount of extension, the thermal state of the lithosphere and asthenosphere at the initial stage and also strain rates (Spohn and Schubert, 1983; Neugebauer, 1983; McKenzie and Bickle, 1988; White and McKenzie, 1989b, Wilson, 1989; Latin et al., 1990, Ziegler, 1992b). Diapiric rise of melts causes large scale thermal doming of rift zones (Figure 2.1) observed for example in Early Jurassic Central Atlantic border lands (Favre and Stampfli, 1992) or the Red Sea Rift (e.g. Reading, 1986).

(I) Doming of the rift zone

Diapirically rising melts 'ponding' at the crust-mantle boundary, provide an additional mechanism for thermal doming of rift zones. Thermal response of the lithosphere to crustal extension is a slow process, which may take place 20-60 Ma after the initial extension (McKenzie, 1978a; McKenzie and Bickle, 1988; White and McKenzie, 1989). The doming of the rift zone causes uplift of the rift's flanks, sometimes even up to 2 km as for example the Red Sea or Lake Baikal - 450 m, Lake Tanganyika - 773 m, Lake Khubsugul - 1650m (Logatchev and Zorin, 1992). The West Antarctic rift system has a spectacular rift shoulder scarp which extends from northern Victoria Land-Queen Maud Mountains to the Ellsworth-Whitmore-Horlick Mountains and shows present physiographic relief of 5 km in the Ross Embayment and 7 km in the Ellsworth Mountains-Byrd Subglacial Basin area (Behrendt et al., 1991). However, there are also examples of rifts, such as the Mesozoic Polish Trough, where no regional doming or flank uplift is evident during the rift history (Ziegler, 1990).

The uplift of the rift basin can exceed the base level of the regional erosion and consequently may cause erosion of the sedimentary fill. This situation is exemplified in the Mid-Jurassic Central North Sea Rift dome (Hillis, 1991, 1992); the Miocene uplift of the Sayan-Baikal dome (Logatchev and Zorin, 1992); subsidence/uplift around the extensional rift basins in Greece (Collier (1988, 1990); Roberts and Jackson (1991)).

(II) Subsidence of the rift zone

McKenzie (1978b) and White (1989b) suggest that after rifting begins in some continental regions the lithosphere has been stretched by small amount only and the limited upwelling produces small amount of melt. Lithospheric stretching courses thinning of the continental crust which floats on the denser underying mantle causing it to subside below sea level. Sometimes the initial subsidence is offset by the thinning of the underlying lithospheric mantle, which is replaced by hotter and therefore less dense asthenospheric mantle. Cooling of added asthenospheric material to the normal lithospheric

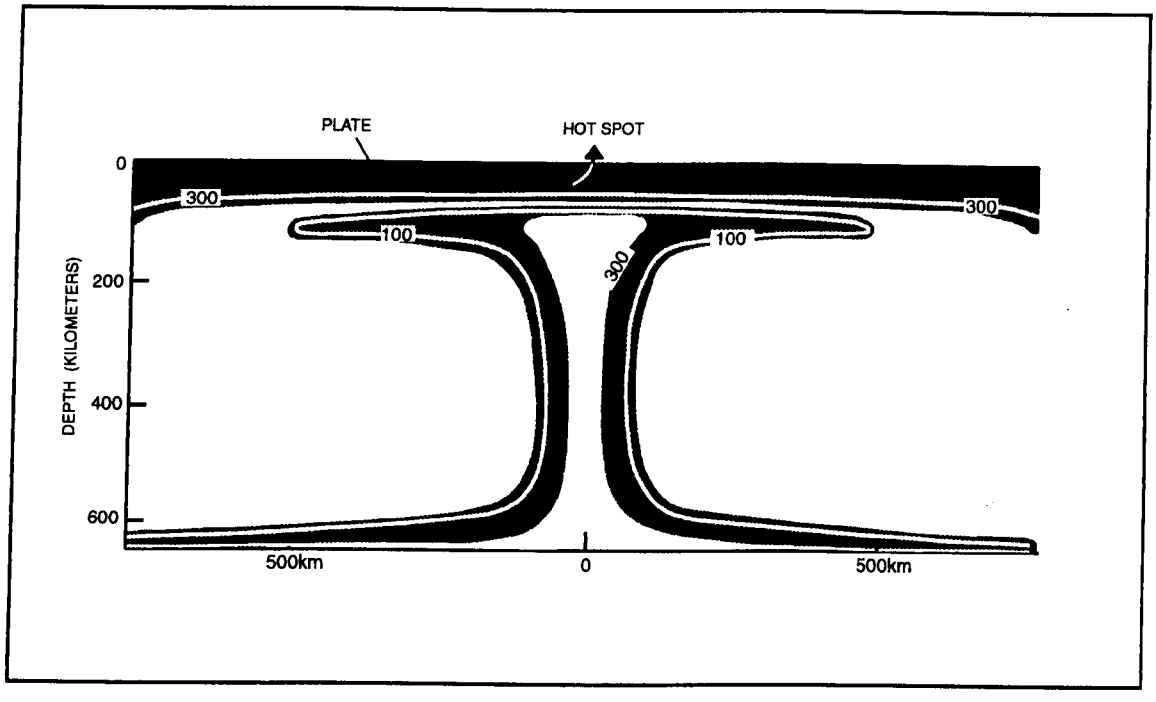

Figure 2.2 Hot spot and mantle plume. After White and Mc Kenzie (1989).

temperature causing futher subsidence. This process is called thermal subsidence. As a result basin sunks far below sea level enables deposition of the sediments (e.g. the North Sea). If the stretching of the continental lithosphere continues, causing eventually continental break-up and opening of new ocean.

(III) Volcanism at rifts

According to White and McKenzie (1989b) volcanic activity of the pre-separation stage is probably related to the thermal state of the asthenosphere and location of deep mantle plumes beneath the continental plate. The melt rising into the lithosphere causes decompression of the underlying asthenosphere and partial melting, and melt segregation at progressively deeper asthenospheric levels. The evolving mantle plume grows both upwards and downwards.

Melts may rise up to the lower crust causing intrusion, melting and secondary differentiation. The intrusion of the mantle derived melts into the lower crust may be associated with the development of lower crust laminations present within the actual rift zone. This process is known as 'magmatic underplating' (Keen and De Voogd, 1988) with reference to the addition of mantle derived material to the lower crust, causing its thickening, that apparently displaces geophysically defined Moho discontinuity upwards. White and McKenzie (1989b) suggest that, the vast amounts of lava flooded under the continental crust during the early stages of many rifts causing accumulation of volcanic deposits directly under the continental margin, between the thinned crust and the lithospheric mantle as defined by reflection seismic data (e.g. the North Atlantic, White and McKenzie, 1989b; the Oslo Rift or the Rhine Graben; Ziegler, 1992b). As Ziegler (1992b) suggests, if the lower crust lamination is indeed due to mantle injection, this process may ultimately lead to a basification of the lower crust, to such degree that the geophysically defined Moho is displaced upwards and crustal material is incorporated into the mantle lithosphere. The occurence of the crust-mantle transition zone was detected by seismic refraction for instance under the Mid-Norway continental shelf (Ziegler, 1988; Planke et al., 1991).

Based on the laboratory modelling and field observations (mapping a large scale thermal anomaly, mapping of the seafloor, study of the earth's gravity field) White and McKenzie (1989b) interpreted the data as the effects of a plume of unusually hot rock rising from deep in the mantle in relation to the hot spot that marks the plume axis. As shown in Figure 2.2 region of anomalous hot mantle surround the hot spot. If rift opens over mushroom head of hot mantle much more melt is generated by decompression of the upwelling material than from rifting over normal temperature mantle. Rifting over high-temperature mantle explains extrusion of voluminous plateau basalts onto the continental margins (e.g. Atlantic coast of South America and Africa; volcanic margin of the North Atlantic; west coast of India and the west coast of Australia; 10 km thick volcanic sequences on the margin of Antarctica). The melt also poured inland forming a basaltic plateau as for example the Deccan Traps.

White and McKenzie (1989b) also indicate that, as the hot spots are thought to be largely fixed in the mantle, but plates themselves wander, a rift can migrate away from a hot spot. The relative

motion of the hot spot could be traced because the plume leaves a trail of volcanic ridges, islands and sea mounts on the overlying plate. The North Atlantic, for example, has a plume under Iceland.

However, hot spots are not crucial for rifting, as a normal, nonvolcanic margins were formed well away from the mantle plume (White and McKenzie (1989)). Example of such a normal margin is the European margin at the Bay of Biscay, where little volcanism appears offshore at the edge of the streatched and thinned continental crust.

A dispute exists as to whether hot spot activity is a consequence of a pre-existing thermal perturbation of the asthenosphere, or, related to stress-induced lithospheric extension, triggering an upwelling of anomalous asthenosphere (Wilson, 1989; White and McKenzie, 1989a, 1989b; White, 1992).

(IV) Geochemical signature of the magmatic activity associated with continental rifts

A wide spectrum of magmatic activity may be associated with rifting of the continental lithosphere. The geochemical characteristics of the primary, mantle derived, mafic magmas, ranging from silica undersaturated alkaline magmas (nephelinites, basanites and alkali basalts;), through transitional-tholeiitic basalts to subalkaline continental tholeiites, reflect degree of partial melting of both lithospheric and asthenospheric mantle sources (Wilson, 1989; Wilson and Guiraud, 1992). These parental magma types may undergo crystal fractionation, combined with crustal contamination, in high-level magma chamber systems and evolved to more complex magma types.

Trace element and Sr-Nd-Pb-O isotopic data may constrain both the depth and degree of partial melting and the nature of the mantle source. The transitional-tholeiitic basalts are indicative of high degree of partial melting (20-30%) of sub-lithospheric mantle source. The geochemical characteristic of rift-related alkali basalts indicates a low degree of partial melting of incompatible element enriched mantle sources which may reside within mantle plumes or within the continental lithosphere.

An upwelling asthenospheric mantle diapir which intrudes the overlying lithosphere may be composed of normal depleted asthenospheric mantle or it may be a chemically distinct mantle plume (hotspot) derived from a boundary within the mantle at a depth of 670 km seismic discontinuity or the core/mantle boundary (Wilson and Guiraud, 1992).

According to Wilson and Guiraud (1992) the onset of magmatic activity for passive type of rifting (the upwelling asthenosphere is filling the gap produced by lithospheric extension; e.g. Buck, 1986) should occur after the initiation of rifting and that the magmas should show decrease in alkalinity with time. In contrary in the case of active rifting (a dynamically upwelling asthenosphere forcibly intrudes and deforms the overlying lithosphere) domal uplift and magmatism should precede the onset of rifting and the erupted magmas may have geochemical signature indicating partial melting of geochemically distinct plume components. However, in general the recognition of timing of rifting and associated magmatic activity can be complicated by development of individual sub-basins within

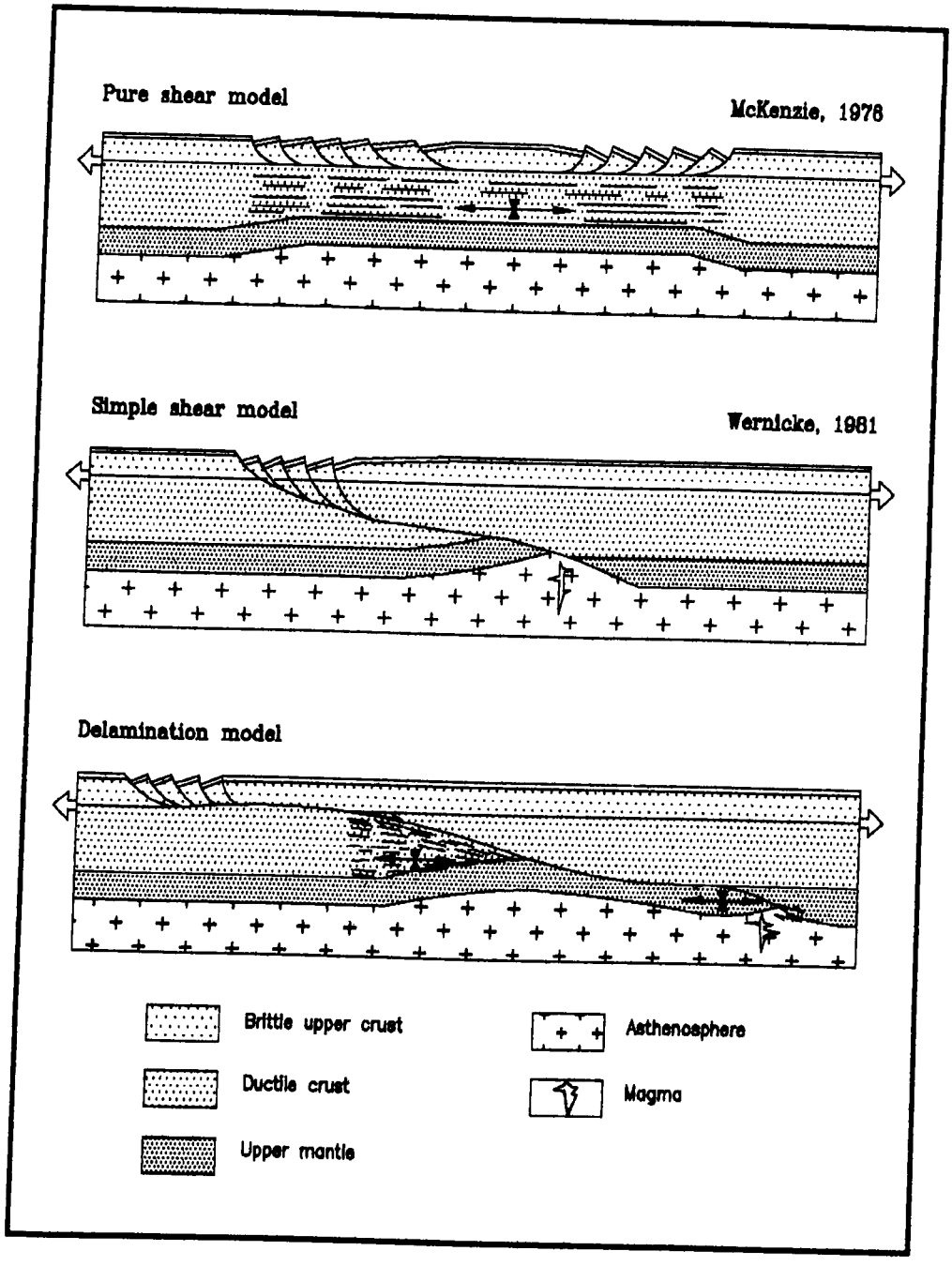

Figure 2.3 Lithospheric stretching models.

a particular rift and by younger volcanic activities and cover of sedimentary rocks that tend to obscure the early rift sequences.

(V) Stretching models

The extension of the upper crust corresponding to the subsiding rift is explained with purely mechanical stretching models (Figure 2.3).

(a) Pure-shear model

McKenzie (1978b) proposed lithospheric stretching model to explain the crustal thinning, rifting, and subsidence histories. This symmetrical, pure-shear extension model has many sophisticated variations (Sclater and Christie, 1980; Schuepbach and Vail, 1980; Le Pichot and Sibuet, 1981; Keen et al., 1982; Vierbuchen et al., 1982; White and McKenzie, 1988), however, does not predict the wide variations observed in continental margins architecture.

(b) Simple-shear model

Wernicke (1981) proposed simple-shear model which is based on the structural asymetryof the continental extension (shallow-dipping crustal shear zones). Wernicke (1981, 1985) suggest that detachment faults represent low-angle normal faults that cut through the entire lithosphere.

(c) Combination models (delamination)

As major detachment faults play a key role in the lithospheric extension processes several detachment models have been applied to the formation of passive continental margins. Lister et al. (1986, 1991) suggest that detachment faulting is an integral part of the continental extension process, therefore, detachment faults are to be expected beneath passive continental margins. They developed asymmetric detachement model which predicts the existence of upper-plate (above the detachment fault) and lower-plate passive margins after continental break-up.

Several other variations of the crustal deformations models have been developed, e.g. Barbier et al. (1986), Kusznir et al. (1987, 1991), Kusznir and Egan (1989). These models do not take into account the thermally induced upward displacement of asthenosphere-lithosphere boundary.

(VI) Deformation mechanisms

'Simple-shear' is the dominant deformation mechanism in the early stages of rifting, which transects the entire crust and may extend into the subcrustal lithosphere. During the advance rifting stages 'simple-shear' still controls the deformation, but at a lower crustal level and within the mantle lithosphere mechanism of a 'pure-shear' deformations becoming dominant.

The pre-existing structural discontinuity in the crust plays an important role in the localisation of rift systems and they influence the geometry of the rift's faults, as in the East Africa rift system (McConnell, 1980; Rosendahl, 1987; Rosendahl et al., 1992); South Atlantic rifts (Chang et al., 1992) and the Cainozoic rift system of Europe (Ziegler, 1990; Ziegler, 1992b). Crustal discontinuity may be reactivated during rifting if their orientation coincides with the direction of the faults of the respective tensional stress field. Under favourable conditions, ancient rift systems can be reactivated,

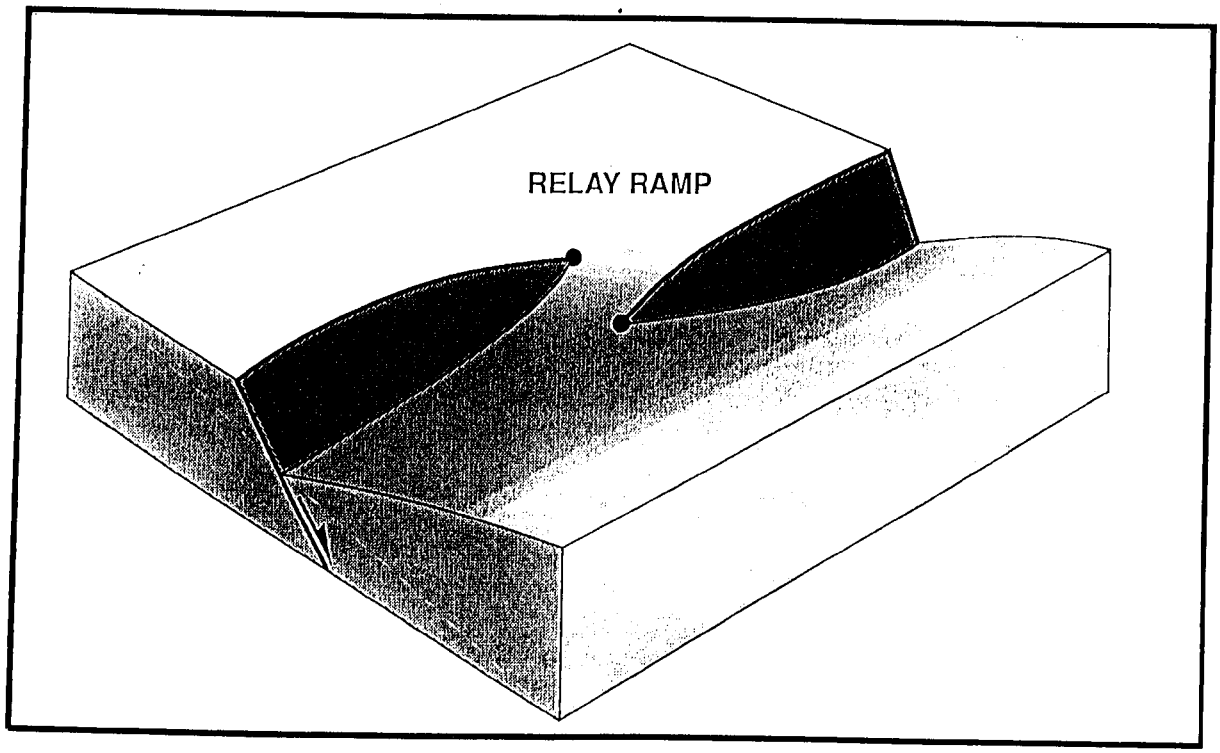

Figure 2.5 Relay ramp. After McClay (1993)

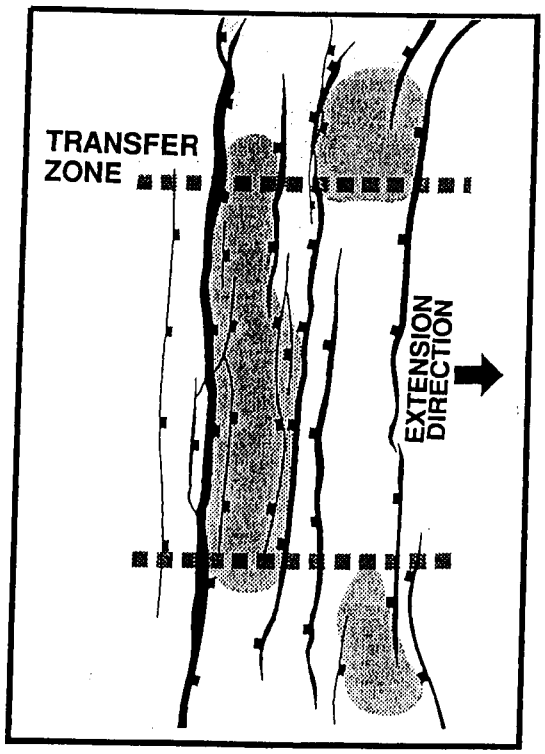

Figure 2.6 Sand-box analog model. Oblique direction of rift extension. After McClay (1993)

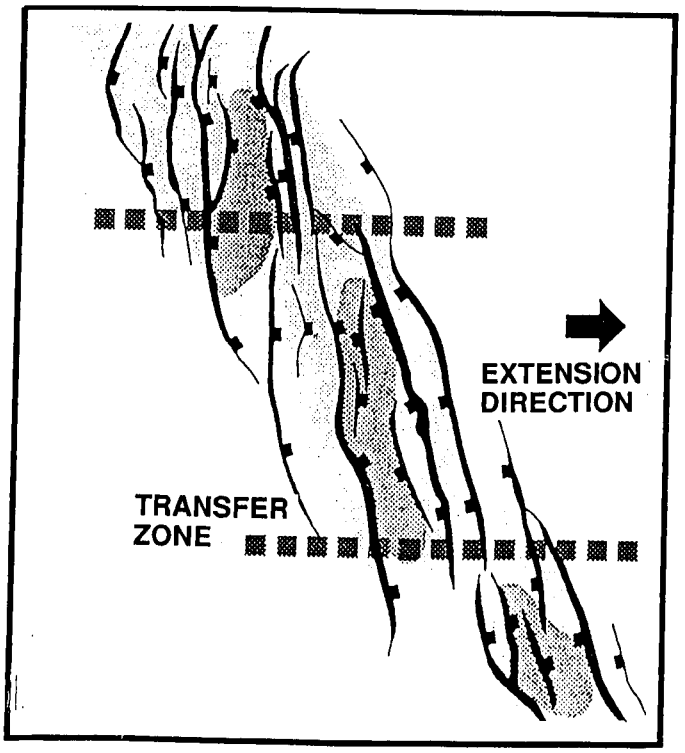

Figure 2.7 Sand-box analog model - rift structure. Orthogonal direction of rift extension. After McClay (1993)

Planar faults which extend through the middle crust reaching the brittle-ductile boundary in the rifts zones are described by Jackson and McKenzie (1983), Jackson and White (1989), Kusznir et al. (1991). The evidence of existence of planar faults has been proved by earthquake data in the Basin and Range Province (Stein and Barrientos, 1985) and the Aegean rift (Jackson, 1987), Gulf of Suez rift (Ziegler, 1992b).

The structural style of rifts in the upper crust is may be influenced by the lithological composition of the down-faulted pre-rift sediments, as well as syn-rift deposited sediments.

(i) Halite and also some shales may give rise to the development of multi-level extensional detachment faults (Jarrige et al., 1990; Jarrige, 1992) and can become sole-out levels for the secondary fault systems, caused by gravitational instability of the accumulated sediments.

(ii) Ramping of extensional faults can give rise to complex deformation patterns in hanging-wall blocks, involving folding and the development of secondary tensional fault systems (McClay and Scott, 1991; McClay, 1989)

(iii) Displacement along deep-seated faults can be dissipated and attenuated upwards in clays and thick salt layers, giving rise to the development of local forced folds (flexures) over the leading edges of the fault blocks (Withjack et al., 1990).

(iv) Faulting and tilting of the basin floor, causing differential sediment loading of thick salt layers, commonly triggers their halo-kinematic deformation (Geil, 1991; Ziegler, 1992b). Such examples of salt mobilisation are commonly observed:

- pre-rift salts: Permian in North Sea (Hospers et al., 1988; Ziegler, 1990)
- syn-rift salts: Triassic-Jurassic in Grand Banks area (Balkwill and Legall, 1989) or Devonian Dniepr-Donetz graben (Kabyshev et al., 1989; Chekunov et al., 1992)
- post-rift salts: Late Aptian Gabon Shelf (Teisserenc and Villemin, 1990) or Compos basin in Brazil (Guardado et al., 1990).

2.3 Analog models of rift systems

The development of knowledge in rift-genesis required detailed studies of the structural architecture of rifts. In recent years many geologists conducted research on the progressive development of extensional fault systems in sedimentary basins. Based on these studies and observations of palaeo- and modern rifts in nature, scientists tried to simulate in the laboratory, the brittle extensional deformation of sedimentary rocks in the upper crust. Scaled analogue models became a useful method of understanding stereo-geometrise and kinematic histories of rifts (e.g. McClay, 1990a, 1990b; McClay and White, 1993; Higgs and McClay, 1993). Based on the experimental study McClay and White (1993) described three dimensional analogue models of orthogonal and oblique rifting as follows:

(i) Orthogonal rifting

In an orthogonal rift system, the zone of rifting was oriented at 90° to the direction of extension. The extension resulted in a series of asymmetric rift grabens, which developed along the rift axis. As stretching inreased, there evolved the rift border faults at each margin of the rift. The rift marginal faults developed as a system of long faults, parallel to the rift zone and perpendicular to the extension vector. The intra-rift faults are straight and relatively short, propagating along the strike, forming strongly developed overlapping antithetic fault systems. There developed distinct extensional sub-basins, separated by transfer zones. In a late stage of the rift development the rift margin faults had coalesced. The intra-rift system developed into relay ramps, which are overlapping zones perpendicular to the direction of the extension (Figure 2.5). Strike slip faults were not observed.

A horizontal section through the rift model is shown in Figure 2.6. The rift model shows long, straight rift border faults and long intra-rift faults oriented perpendicularly to the direction of the extension. There is a very distinct main half-graben border fault, which continues along the whole model whereas the antithetic faults on the opposite margin are strongly segmented with relay ramps joining each segment. The intra-rift faults are relatively straight but strongly segmented with joining relay ramps. In areas where relay ramps developed bedding of the pre-rift and syn-rift layers is at a high angle to the fault traces.

(ii) Oblique rifting

The extensional oblique rifting model (at 60°) is presented in Figure 2.7. The extension produced the rift border faults, which developed adjacent to the moving margin of the rift. The border faults are segmented and parallel to the overlying zone of stretching. The intra-rift fault system forms an en-echelon pattern with individual faults parallel or sub-parallel to the extension direction. These faults are slightly curved, concave towards the direction of the extension. The system of intra-rift faults developed into overlapping and antithetic faults which propagate along strike. Three distinct extensional sub-basins developed. These sub-basins are separated by transfer zones which accommodate a fault systems with one dip polarity merging into another fault systems with opposite dip polarity. With progressing extension the strongly segmented rift marginal faults had coalesced. The intra-rift system faults developed into distinct patterns oriented at high angles to the extension.

As McClay and White (1993) report a similar evolutionary progress of rift border and intra-rift fault systems was observed in other oblique rift experiments. Strike slip faults were not observed.

Based on McClay and White (1993) experimental research the general characteristics of the extensional rifts can be summarised as follows:

- The rift systems are characterised by asymmetric grabens with one dominant rift border fault.
- Symmetric grabens developed where asymmetric half-grabens of opposite polarities overlap.
- The rift marginal faults show planar geometry, whereas intra-rift faults may also curve slightly.
- The intra-rift faults form domino style systems which are antithetic to the rift margin faults.
- The polarities of the half-graben may switch along the strike in the zones where an accommodation zone of intersecting conjugate faults is created. This plane strain zone of coeval

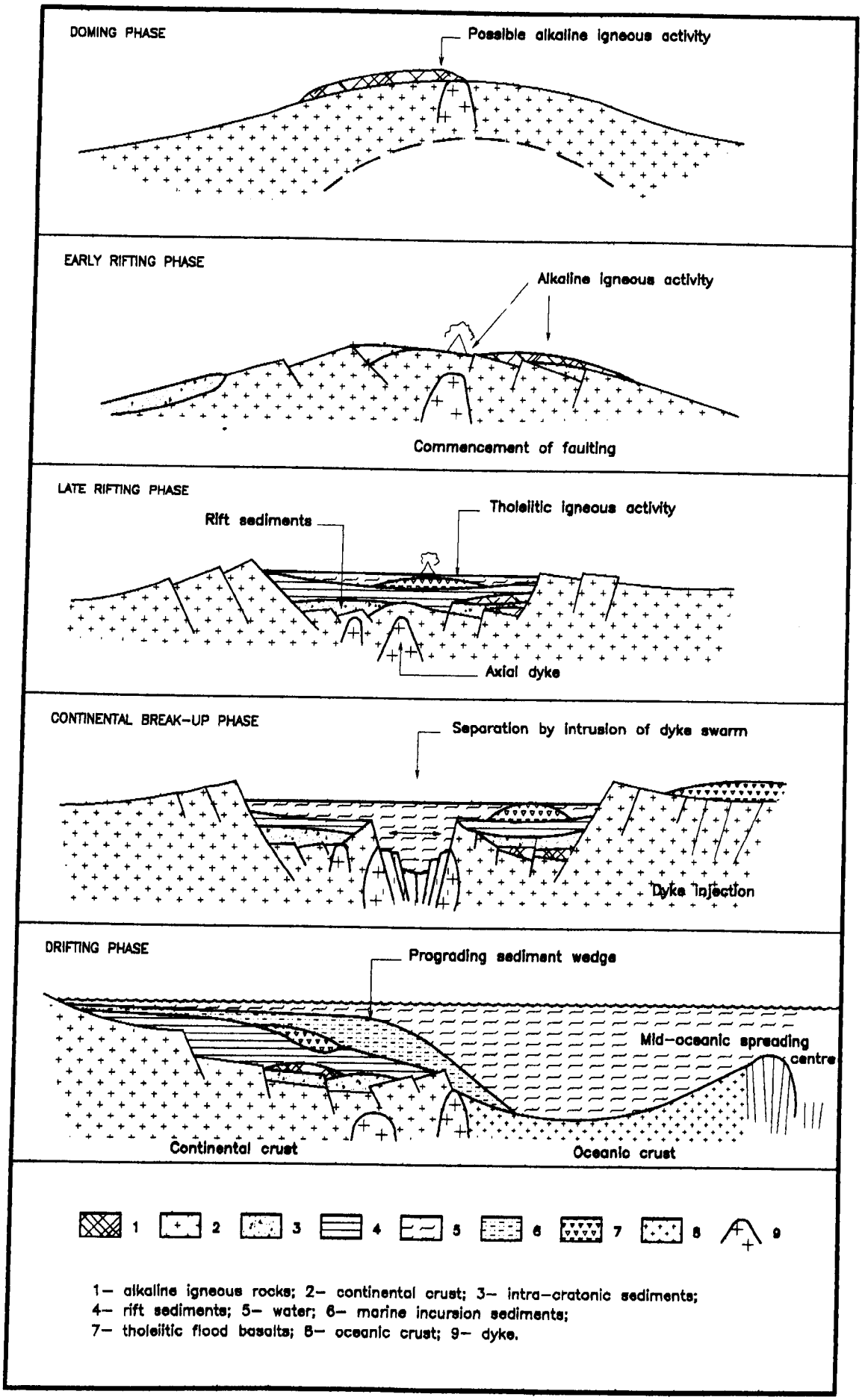

Figure 2.8 Stages in the evolution of a rift system. After Gunn (1984).

conjugate faulting creates a symmetric graben and facilitates the polarity switch without development of strike-slip or oblique transfer faults.

2.4 The rifting stages

The sequence of geodynamic processes associated with rifting have been extensively discussed in geological literature. In many references the synthesis of rifting attempted to encompass the tectonic, igneous, sedimentological and geophysical aspects of this process. Some authors simplified the whole process, assuming that rifting occurs in a series of characteristic stages (Falvey, 1974; Schuepbach and Vail, 1980; Ramberg and Spjeldanaes, 1978; Salveson, 1978; Gunn, 1984; Ziegler, 1992b). For example Gunn (1984) describes the mechanism of rifting in five following stages (Figure 2.8):

(i) Doming phase

The actual rifting is preceded by pre-rift domal uplifts of the crust which is considered to arise from a wedge of mantle material rising towards the Earth's surface. The doming structures may have large extend, as for example the oval-shaped Kenya uplift which is 1000 km long and 300-400 km wide with surface elevation in the order of 3.4 km (Girdler et al., 1969; Fairhead, 1976). Gravity profiles across such features show broad negative anomalies (Darracott et al., 1973; Burke and Whiteman, 1973).

The pre-rifting stage is characteristically associated with alkaline (igneous) magmatic activity which could precede the doming process (Bott, 1981). Burke and Dewey (1973) place the volcanic centres along the crest of the uplifts.

Fluvio-deltaic and shallow marine sedimentation may occur in the prior-rift stage (Falvey, 1974) in the depressions laying over the crest of the uplift (Bhattacharji and Koide, 1978). Such depressions may be manifestation of extension and thinning of the crust above the mantle plume and they are an unfaulted precursor to the rift. The sediments in such structures unconformably overlay the older pre-existing crust.

As a result of doming in the brittle upper crust which overlays the ductile lower crust, a series of tensional cracks develop (Bott, 1981), often forming sets of parallel fault graben systems (Logatchev et al., 1978). Developments of such faults indicates the Early Rift Stage (Gunn, 1984).

(ii) Early rifting phase

According to Battacharji and Koide's (1978) modelling the final effect of the upward movement of the wedge of the mantle material is crustal rupture along two major fault sets dipping $30^{\circ} - 60^{\circ}$. These faults originated on the apex of the mantle wedge. The fracture zones cause the collapse of the central part of the domal uplift and the formation of graben structures which frequently form 'triple junctions' (Burke and Dewey, 1973). Such grabens are strongly faulted and surrounded by sets of parallel faults which sometimes flank smaller grabens or half grabens. Fractures due to adjacent

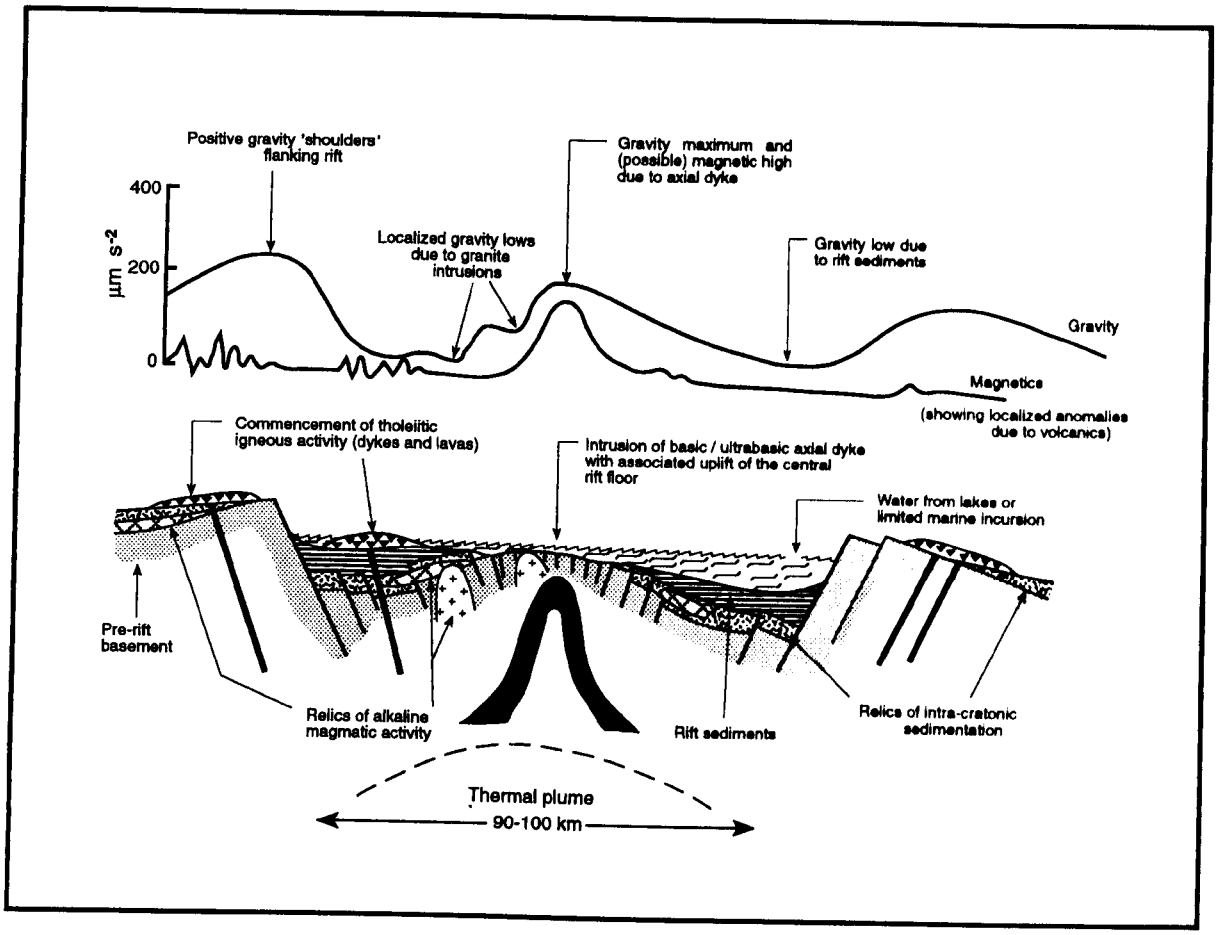

Figure 2.9 Theoretical section of a mature rift. After Gunn (1984).

crustal domes may link up to form elongated sinuous rift systems often exhibiting 120° curves in their traces.

The central main graben (which usually is approximately 60 km wide) becomes the locus for alkaline igneous activity. However, there are examples of rifts with much broader extensions on both side of the rift axis of the alkaline lavas and associated volcanics (Kenya Rift in Williams, 1978 or Baker et al., 1978).

The depressed central part of the rift may be filled with substantial volumes of lava and pyroclastic material. The subsidence of the fault bounded graben is expressed on the surface by strong topographic depression. The sedimentation style changes and becomes the onset of the rift valley phase as defined by Falvey (1974).

(iii) Late Rifting Phase

During the late rifting phase the general subsidence around the central main graben is possibly caused by cooling, pressure relief resulting from igneous activity and rift formation or metamorphism in the crust (Falvey, 1974). The subsidence allows rejuvenation in sedimentation which produces an unconformity, referred to by Falvey (1974) as the 'rift-onset unconformity'.

The characteristic sedimentary facies of the depressed region is continental and deltaic but also shallow marine. Incursions may occur, and evaporates may be present. Movement along the faults during deposition and continued subsidence control the thicknesses of the sediments.

Alkaline igneous activity continues during this stage of sedimentation but appears to progressively change in style. A detailed study of the Permian Oslo Graben, which became a non-active rift, since the Late Rifting Phase (Ramberg and Neumann, 1978), shows that erosion of the sediment cover has exposed sequences of alkaline igneous rocks, forming the floor of the graben. Ramberg and Spjeldanæs (1978) distinguished various magmatic activities for the area which change from volcanics, fissure eruptions, central volcanoes (ring type intrusions), cauldron collapse, basic and ultrabasic plugs to major granite batholithic emplacement. Mitchell and Garson (1976) observed that carbonatities appear to be preferentially located in rifts.

Geophysical evidence suggests that the final stage of the rift development is associated with the intrusion of an axial dyke of a dense, magnetic (basic or ultrabasic) material in the centre of the rift (Figure 2.9). Darracott et al. (1973) modelled such dykes for the East African Rift. The presence of axial dykes beneath more ancient rifts was deduced from the existence of axial gravity highs. For instance Ramberg (1976) proposed such dykes for the Oslo Graben; Cratchley and Jones (1965) suggested such an interpretation for the Benue Rift in Nigeria. These dykes are the ultimate result of the upwelling of mantle material.

Seismic reflection studies of the Rio Grande Rift (Brown et al., 1980) show that fault bounded domal uplift occurs under a thick sediment cover in the central down faulted part of the graben. The possible explanation for this effect is an axial dyke emplacement which is regarded as the final stage

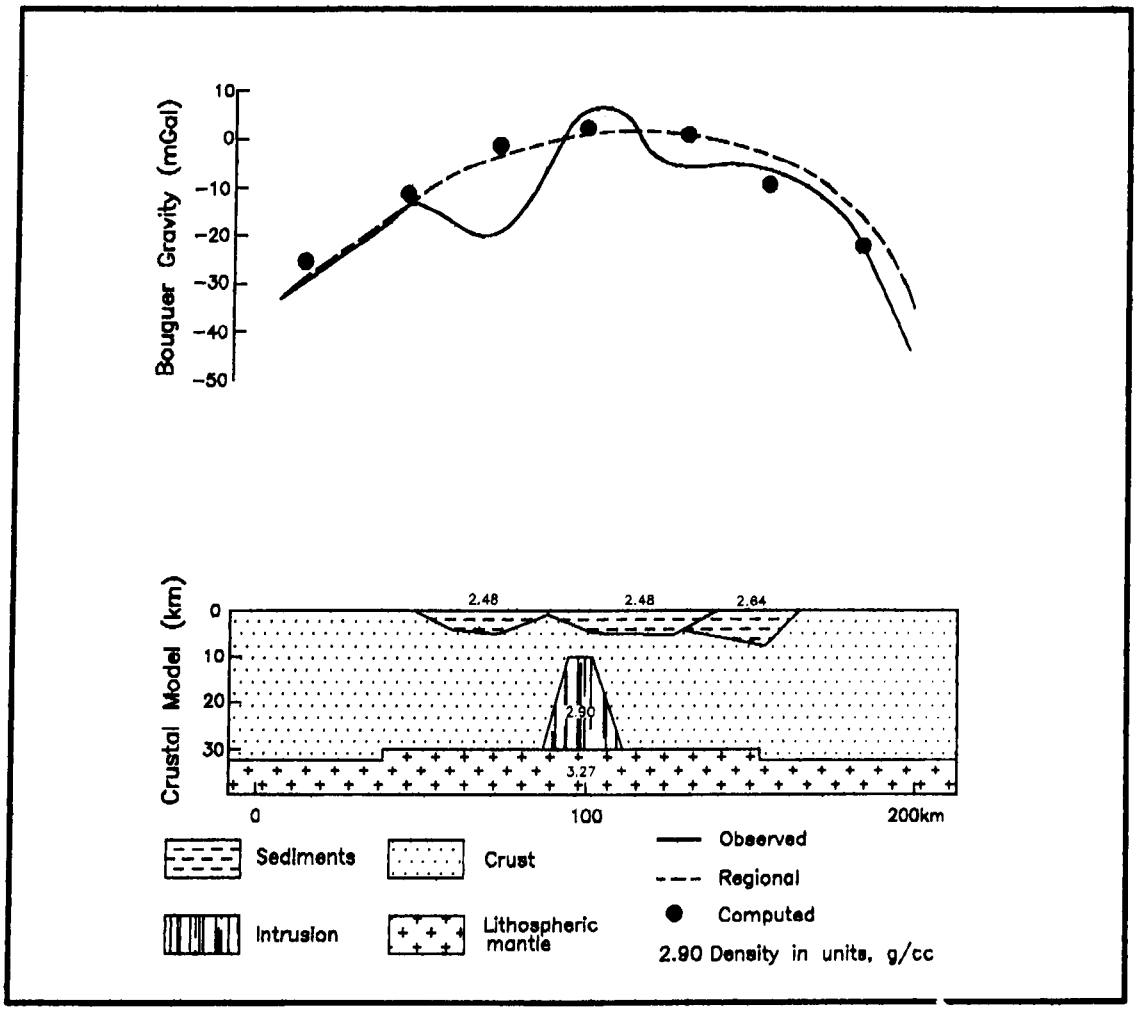

Figure 2.10 Interpretation of regional gravity profile across the Benue Trough. After Ajayi and Ajakaiye.

of an upwelling of dense basic/ultrabasic mantle material, accompanied by crustal thinning beneath the graben. The axial dyke progressively pushes apart the continental crust forming the floor of the graben. The intrusion of the axial dyke may cause doming of the basement and in-rift sediments, which may appear as two separate basins within the rift. The Benue Trough is a classic example of such a scenario (interpretation of gravity profile across Benue Trough in Figure 2.10; after Ajayi and Ajakaiye, 1981).

(iv) Continental break-up phase

The next stage of the rift development is the complete separation of the continental crust by an upwelling wedge of basic/ultrabasic rocks and the formation of the oceanic crust. The separation of the continental crust may be aborted on one of the triple junction arms before progressing beyond the Late Rifting Phase. Sedimentation within such a failed rift continues with sediment transfer along the axis of the rift with deltaic deposition into the new ocean.

The separation of the rift valley floor characteristically occurs along the axial topographic high of the main graben, as a result of the upward intrusion of an axial dyke, which is probably bisected during the splitting event. Rabinowitz (1974) suggests that magnetic anomalies, which occur on both sides of the Atlantic Ocean, are associated with parts of an axial dyke. Other supporting evidence, suggesting that separation occurs along the axial dyke and the upwelled basement in the centre of original graben, comes from the work of Schuepbach and Vail (1978). They observed basement highs on the outer edges of opposing continental shelves of the Atlantic Ocean.

Simultaneously with the initiation of the crustal break-up tholeiitic igneous activity may commence (Falvey, 1974; Vine and Hess, 1970; Dietz and Holden, 1970). This phase of magmatic activity is characterised by dyke intrusions into tensional fissures and extensive basalt flows (Girod, 1978). There are discussions and disagreements concerning the change from alkaline stage to tholeiitic phase. Some authors (Burke and Whiteman, 1973; Falvey, 1974) are in favour a natural progression in the development of rift systems, but others (e.g. Le Bas, 1971; Bailey, 1974) claim that alkaline activity is limited to intercontinental rifts which have not attained the crustal separation stage. In their opinion the rifting process leads to the creations of oceans, whereas, the activation of tholeiitic magmas is an entirely different process.

Veevers (1974) reports, from drill holes on the rifted continental margin of Western Australia, Permian alcalic igneous rocks as well as younger, Late Jurassic to Early Cretaceous, tholeiitic igneous rocks which intruded after a separation. The early stage of the development of the Atlantic margin in Brazil (Herz, 1978) appears to be associated with alcalic igneous activities. Barberi and Varet (1978) observed geochemical changes of the igneous activity in the Afar Triple Junction; in the part of the rift which reached the continental separation stage tholeiitic igneous activity has developed, but in areas where the rift development is less advanced, magmatic processes become more alkalic. The geochemical character of the volcanic rocks in the southern Kenya Rift shows a temporal transition from strongly alkaline pre-rift igneous activity to the less alkaline character of those associated with rift itself (Baker et al., 1978).

The splitting of a rift is marked by a 'break-up unconformity' (Falvey, 1974) which indicates rapid marine transgression with onlapping sand and progradation of sediment into the continent. The marine sediments which dominate and have just formed a continental shelf contain mainly limestones, marls and prodeltaic shale. The marine transgression is a result of the general subsidence which is a continuation of the downwarping stage commenced during the Late Rifting Phase. The explanation of this general subsidence, involved, various theories including lithospheric cooling and crustal thinning, gravity loading or crustal creep (e.g. Bott, 1979; Ziegler, 1992b).

(v) Drifting phase

The progressive emplacement of the axial dyke finally caused the separation of two graben halves and the formation of the oceanic crust. Different crust segments which spread at different rates create transform faults, which may cause offsets in the line of spreading centres and in the line of separation. With time the subsidence of the continental shelf diminishes, and therby the marine regression is initiated (Falvey, 1974). The progradation may cause the outbuilding of the continental shelf beyond the original edge of the continental crust (classic 'Atlantic Style' passive margin).

Interpretation of seismic data by Falvey and Mutter (1981) shows growth faults indicating that vertical adjustment occured on the continental margins long after the separation of the continents. The tholeiitic magmatic activities connected with those tensional adjustments may still continue after continental break-up. As Gunn (1975, 1984) suggests, volcanic activities related to the split of the Gondwana, on the south-eastern margin of the Australian continent, have continued until Holocene.

The remnants of the axial high of the original rift may be buried under younger sediments and may not correspond to the continental edges as defined by the continental slope. These 'outer highs' (Schuepbach and Vail, 1978) are evident in the seismic reflection sections (Falvey and Mutter, 1981), and may be traced from the gravity. Beneath the outer portion of the outer high there occur remnants of the axial dyke sometimes forming 'continental edge magnetic anomalies'. Several examples have been observed on different continents: the East Coast Magnetic Anomaly of the Eastern United States (Rabinowitz, 1974; Behrendt and Kiltgord, 1980); the magnetic anomaly on the eastern rift margin of the Tasmanian and Bass Strait area of Australia (Gunn, 1975); the Magnetic Trough of Southern Australia, which some scientists have interpreted to be a reversely magnetised body (Talwani et al., 1978, Gunn, 1984).

2.5 Case history - study of the continental rift basins

In the following sections of this chapter geological evolution and characteristic geophysical signature of the several major rift systems will be briefly discussed.

Since the early Cretaceous, two major rift systems have developed within the African continent, the Tertiary to the Recent rift system of East Africa and the Cretaceous to the early Tertiary rift system of West and Central Africa. Both systems are the result of extensional tectonics, but they appear to be tectonically different. The East African Rifts have characteristic uplift and strong

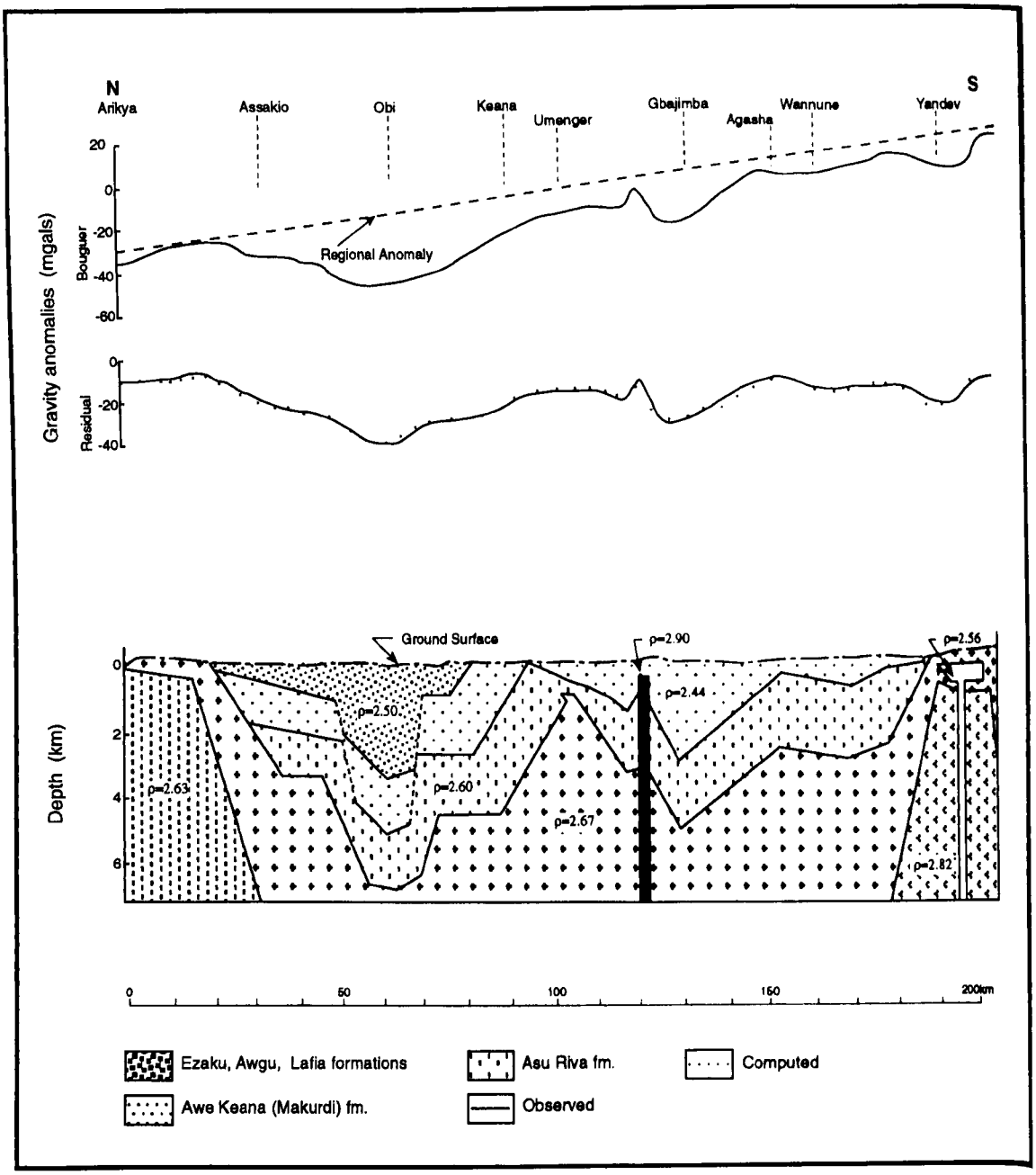

Figure 2.11 Interpretation of detailed gravity profile across the Benue Trough. After Ajayi and Ajakaiye (1981).

volcanism, wheras subsidence and sedimentation are features of the West Africa. Based on three examples, the Benue Trough, the Dead Sea Rift and Red Sea Rift, geological evolution of the African Rift System will be discussed.

The geological and geophysical characteristic of two other rifts, the Baikal Rift and the North Sea rift system, will be also briefly discussed.

The comparison of the Polda rift with described below observed or interpreted features of these five well known and intensivelly studied rift systems may permit to draw conclusions concerning origin and structure of the Polda rift.

2.5.1 The Benue Trough

The Benue Trough of Nigeria is a failed arm of a triple junction, which did not develop beyond the initial extensional phase that lasted about 30 Ma (Albian to Santonian). A triple junction centred on the Niger delta has two arms which developed into the Equatorial Shear Zone and the South Atlantic (Bonatti and Crane, 1984), while the third failed arm is the Benue Trough. The linear Benue depression which points ENE forks into a northern trough.

The trough is a 500 km long feature trending in SW-NE direction and occupies the eastern half of central Nigeria. This feature has an abnormal width (130km – 200km) when compared with, the width (50km ± 15km) normally associated with rift valleys. There are some other peculiarities of the trough, which distinguished this structure from typical rifts; sediments within the trough are folded parallel to the axis of the trough (Wright, 1968, 1970).

The origin of the Benue Trough is a controversial subject. Over the years, there have evolved several theories, from a rift, with or without plate tectonic concept (King, 1950; Wright, 1968, 1970; Grant, 1971; Burke et al., 1972; Olade, 1975) to a geosyncline (Lees, 1952) and a combination of both (Cratchley and Jones, 1965). The evolution of the rift is contemporaneous with the opening of the South Atlantic Ocean during the Cretaceous.

Ajayi and Ajakaiye (1981) based on the interpretations of the gravity data along two north-south profiles, have considered the Benue Trough to consist of two parallel rifts separated by axial ridge, which partly explains the abnormal width of the trough (see Figure 2.11). The crust below the central axis thinned enough to enable the local injection of upper mantle material into the shallow basement, along or near, the central axis of the trough. However, the rifting tension ceased prior to the stage when the asthenosphere reached the bottom of the thinned crust. The Benue Trough did not reach the separation stage of the continental crust and the creation of the oceanic crust, as for example in the Red Sea Rift.

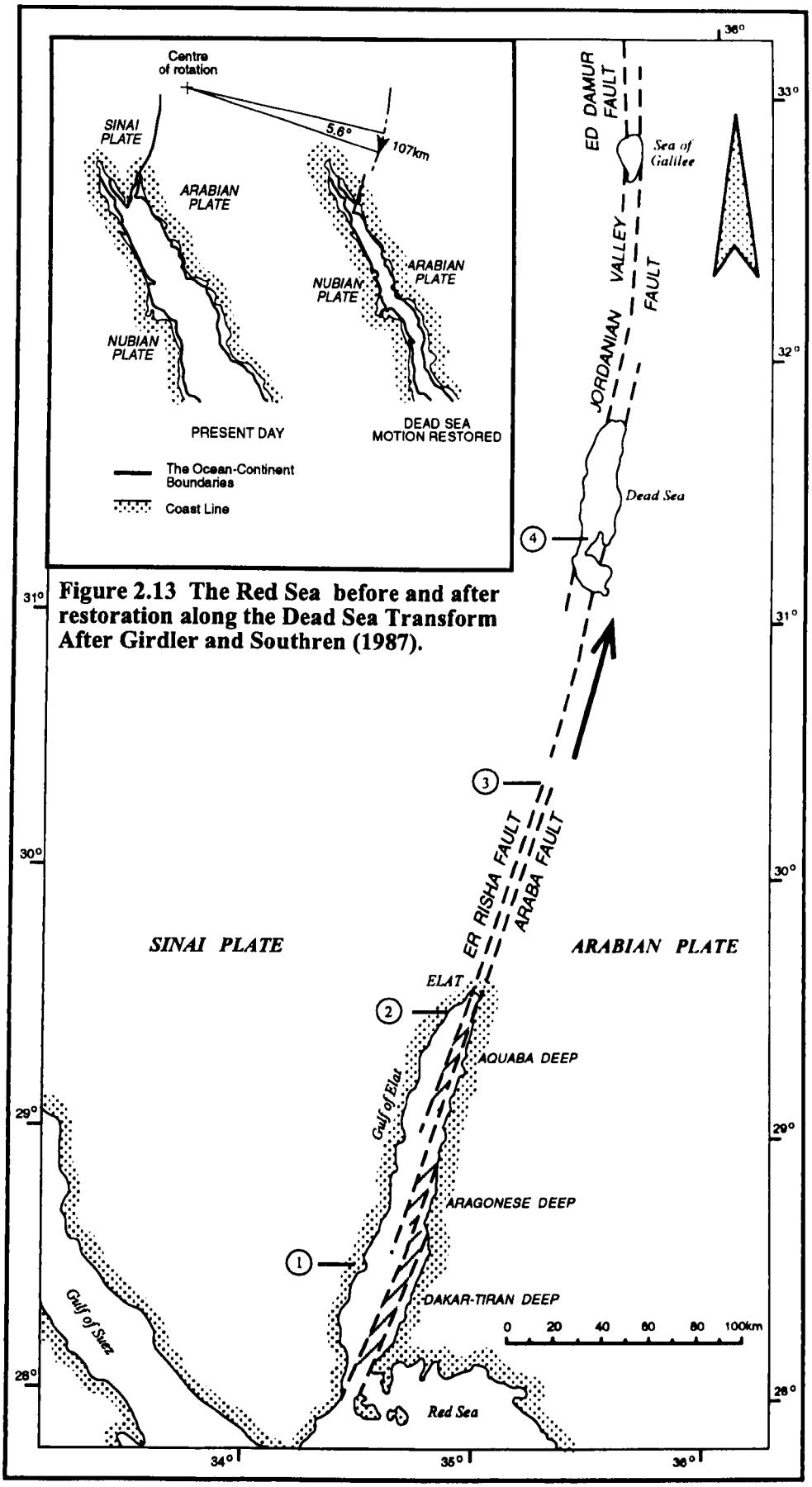

Figure 2.13 The Red Sea before and after restoration along the Dead Sea Transform After Girdler and Southren (1987).

Figure 2.12 The Dead Sea Transform Fault System. After Girdler (1991).

2.5.2 The Dead Sea Rift

The Dead Sea Rift and the Gulf of Aquaba lies along a lineament that separates two lithospheric plates, the Arabia Plate and the Sinai Block of the African Plate (Figure 2.12). The transform plate motion along the Dead Sea Rift indicates that Arabia rotates anticlockwise with respect to Sinai, opening the Red Sea to the south-east and causing the mountainous zones of compression and uplift collision zone to the north-east (Figure 2.13; Girdler, 1990). The seismity and the satellite imaginary (Girdler, 1990) show the Dead Sea Transform might extend beneath the Mediterranean Sea, to join the collision zone east of Cyprus (Girdler, 1991a).

The Dead Sea Transform is a system of en echelon faults, often offset westward. In the overlap areas appear a series of pronounced rhomb-shaped depresions refered to as pull-apart basins. The Dead Sea Basin is one of such depressions. The motion along the transform faults is a left-lateral shear with total horizontal displacement of 107 km (Quennell, 1958). According to Quennell (1958, 1983) this horizontal displacement took place in two stages, with the first 62 km in the early Miocene and the second 45 km since in the Plio-Pleistocene and is still continuing. Additional evidence of the strike-slip movement along the rift comes from interpretation of large east-west magnetic anomalies truncated by the Dead Sea rift; if Arabia is restored southward relatively to Sinai slightly over 100 km, these magnetic anomalies become continuous (Hatcher et al., 1981).

The seismic reflection studies (Rotstein et al., 1991) in the Jericho area, north of the Dead Sea, shows that in this part of the Dead Sea Transform, there is a zone of intense deformation, not just a distinct fault plane. The transform fault dips westerly, away from the rift, suggesting that it may have a reverse-faulting component. There is evidence of local compression immediately north of the Dead Sea, but there are also some indications that the compressional field characterises the north-western part of the Dead Sea Basin. Along the Dead Sea Transform lie younger fold structures which are associated with it (Kalia Monocline, Jericho Anticline; See Figures 1-3 in Rotstein et al., 1991).

The crustal structure of the Dead Sea Rift has been studied by seismic surveys (Ginzburg et al., 1979a, 1979b, 1981; El-Isa et al., 1986, 1987a, 1987b; Prodehl and Mechie, 1991). Deep seismic refraction studies of the crust and the upper mantle in the rift zone (Figure 2.14) show crustal thinning underneath the rift together with the presence of a velocity transition zone in the lower crust, just above the crust-mantle discontinuity (Ginzburg et al., 1981). The sedimentary cover ranges in thickness between 1.5 km and 5.5 km, the crystalline basement underneath having a velocity of 5.9-6.2 km/s. At a depth of 15-19 km an intermediate bouhdary between the upper and the lower crust can be traced (velocities 6.5-6.7 km/s). The crust-mantle boundary is interpreted as a of approximately 8 km thick transition zone between depths of 25.5-27 km and 33-35.5 km depth (velocity in upper-most mantle beneath the transition zone is 7.9-8.1 km/s). Within the uppermost mantle at a depth of 54-55 km a boundary occurs, below which the velocity is 8.5-8.6 km/s (Prodehl and Mechie, 1991).

In the Gulf of Elat the crust beneath the rift thins considerably to the south. The observed thinning is some 8 km, but the crust reaches a thickness of 35 km near Elat and only 27 km thickness at a distance of 160 km south of Elat (Figure 2.14; Ginzburg et al., 1981). The rift and its immediate

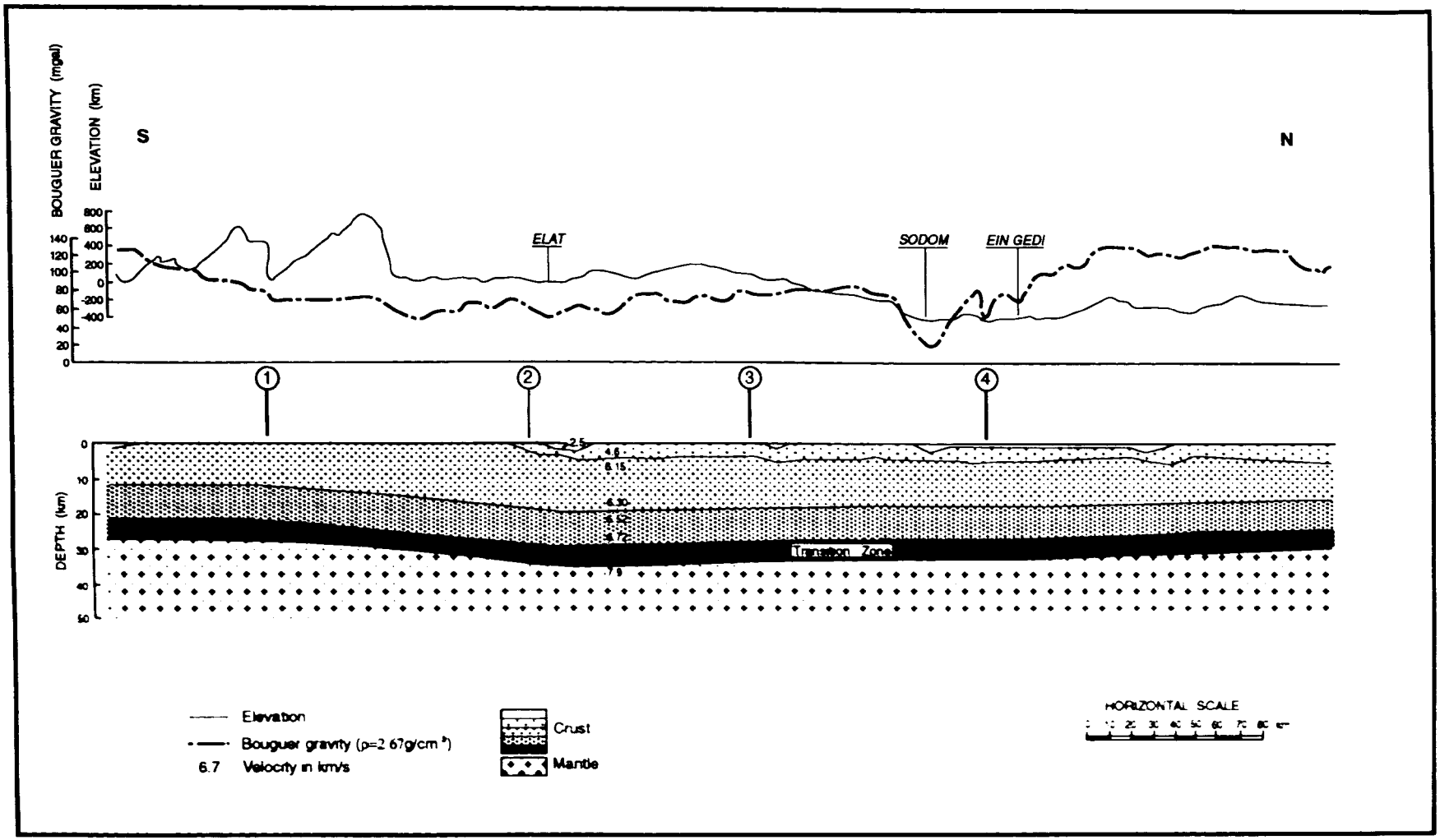

Figure 2.14 Interpretation of North-South gravity profile across the Dead Sea - northern Sinai. After Ginzburg et al. (1981).

surroundings are underlain by a thinner than usual crust. The crustal thickness varies from 30 to 40 km immediately west of the rift, but on the eastern flank the crust thickens about 60 km east of the rift boundary (Ginzburg et al., 1979a, 1979b; El-Isa et al., 1986, 1987a, Prodehl and Mechie, 1991). To the east of the rift the crust-mantle transition zone decreases in thickness to approximatelly 5 km (Prodehl and Mechie, 1991).

The crustal thinning and the presence of the velocity transition zones are interpreted, as the result of the existence of an upwelling zone underlying the rift. The intrusion of upper mantle material into the lower crust, along a narrow active zone, possibly represents the initial stage of the geodynamic process, which have been active further south in the Red Sea since early times (Ginzburg et al., 1979a, 1979b, 1981) .

2.5.3 The Red Sea Rift

As already discussed the Red Sea and its two northern branches, the Suez rift and the Dead Sea transform, were formed during the Cainozoic times. The separation of the Arabian and the African plate opend the Red Sea between them, while in the north, the plate movement was taken up by the opening up of the Suez rift, and the Dead Sea Transform (Freund, 1965; Joffe and Garfunkel, 1987).

The evolution of the Northern Red Sea, and its relation to the Gulf of Suez and the Dead Sea shear zone, are crucial in understanding the geotectonic processes in the Red Sea region. Rihm et al., (1991) based on the results of several seismic profiles across both flanks of the Red Sea Rift suggest that the main crustal feature of the Northern Red Sea and adjacent regions is a fundamental asymmetry of the region. This asymmetry is expressed by the presence of a different type of crust on both flanks of the trough (Figure 2.15(a)). The western flanks show oceanic crust within only 20 km off the African coast, while the eastern flank is underlain by a typical continental crust. The seismic data indicate rapid thinning of the continental crust towards the coast (Makris, 1983). Interpretatation of the gravity profiles across the Red Sea Rift (Girdler and Southren, 1987; Girdler, 1991) incorporated with evailable borehole data and seismic data shows possible location of the ocean-continent boundary.

As shown in Figure 2.15 (a) there are significant differences in the shape of the continent-ocean transitions on both flanks (Rihm et al., 1991). The Arabian margin represents a typical example of a stretched passive continental margin. This margin, which shows attenuation of the continental crust extends almost into the centre of the Red Sea. It shows the significant feature of rotated basement blocks (mapped, based on their gravity signature by Gaulier et al., 1988) and considerable stretching and thinning. On the other hand, the crust on the African margin appears to thicken towards the escarpment and the change to oceanic crust becomes very abrupt (Figure 2.15(b)).

The asymmetry in the Northern Red Sea is regarded by Rhim, Makris and Möller (1991) to be the expression of strike-slip processes in the initial stages of Red Sea evolution. The strike-slip motion in the early stage of Red Sea origin led to substantial differences and asymmetry of further

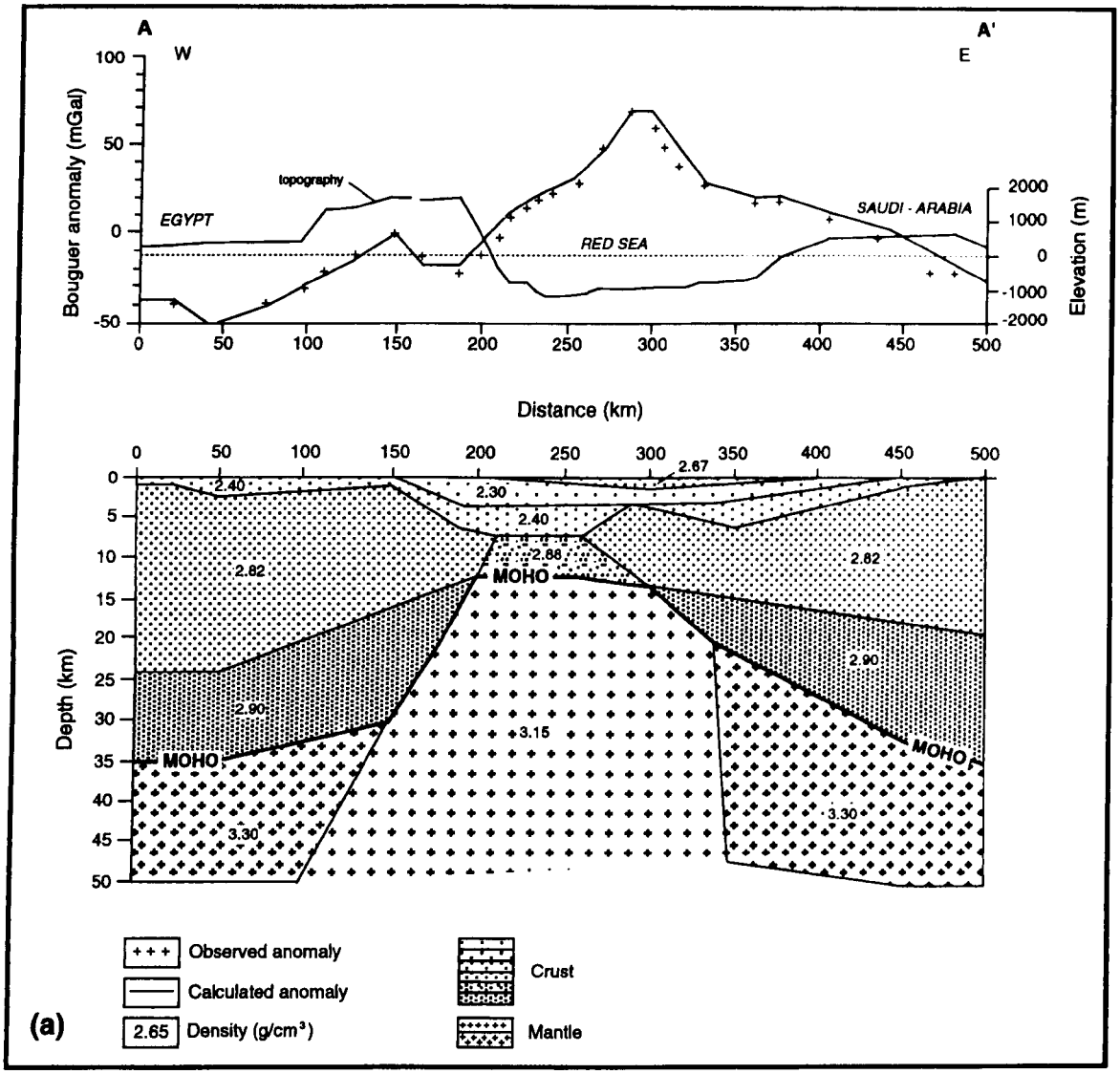

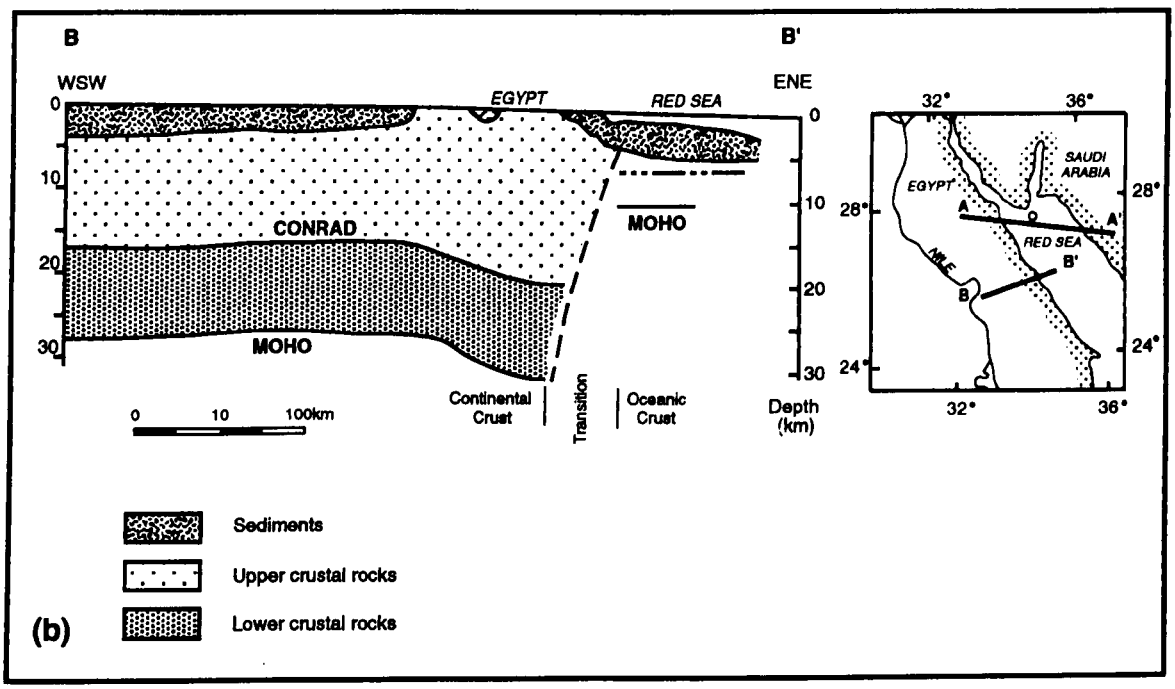

Figure 2.15 Passive continental margin - the Red Sea. After Rhim et al. (1991).

development. A crucial stage in these processes was the nucleation and early oceanisation of pull apart basins on the western Red Sea flank, which allowed the plates to separate without having a definite pole of rotation (Makris and Rhim, 1991). The Arabian plate thus moved away after initial separation, without further stretching on the African side.

Densely spaced seismic and magnetic profiles off the shore of Saudi Arabia (24°N) provided new information on the crustal structure of the northern Red Sea. In addition to the NNW trend representing the general Red Sea orientation, another three structural trends have strongly influenced the crustal development within the trough.

An observed NNE-SSW trend (gravity map presented by Makris et al. (1991b)) corresponds to the Dead Sea - Aquaba sinistral wrench fault system, which is active at present. Initiation of the motion occurred at 16 to 14 Ma and the annual horizontal shift along the Dead Sea fault ranges from 0.5 to 1 cm/year (Bayer et al., 1988; Ten-Brink and Ben-Avraham, 1989). The NNE trends of Aqaba orientation control the break-up of the continental crust.

Some structures of WNW to NW orientation can also be observed across Red Sea. They correlate with the direction of the Najd Shear Zone in Saudi Arabia (Dixon et al., 1987) and in the Egyptian Eastern Desert (Sultan et al., 1988). This trend indicates that a pre-Red Sea major fault system had a strong influence on the mechanism of rifting that controls the present day deformation (Dixon et al., 1987; Makris and Rihm, 1991; Makris et al., 1991).

The pre-existing zones of weakness of the E-W to NE-SW trends, which are parallel to the Central African Fault Zone (Garson and Krs, 1976; Guiraud et al., 1985; Schandelmeier and Pudlo, 1990) strongly influenced the opening of the Red Sea basin and the generation of different crustal types within it (Makris and Rihm, 1991; Egloff et al., 1991). Coutelle et al. (1991) showed that pre-existing continental structures of this orientation control the development of the Red Sea deeps, which is ongoing.

The crust of the eastern flank of the Red Sea, as determined seismically and as discussed above (Makris et al., 1983; Rihm et al., 1991; Makris and Rihm, 1991), is composed of the stretched continental crust, which is often less then 12 to 16 km thick. Areas of crustal dislocation, fracturing and opening are confined in an en-echelon array of wrench fault systems which are accompanied by intensive magmatism. The magnetic anomalies, the bathymetry and thermal regime express this process. Sea-floor spreading is producing classical linear magnetic anomalies in the southern Red Sea (Allan, 1970; Girdler and Styles, 1974; Roeser, 1975; Hall et al., 1977; Richter et al., 1991). The northern part of the Red Sea has not been stretched enough to produce a continuous system of fractures that will gradually permit the initiation of linear and continuous spreading. These results provide evidence for the dominance of different stress processes during different stages of evolution of the northern Red Sea (Richter et al., 1991).

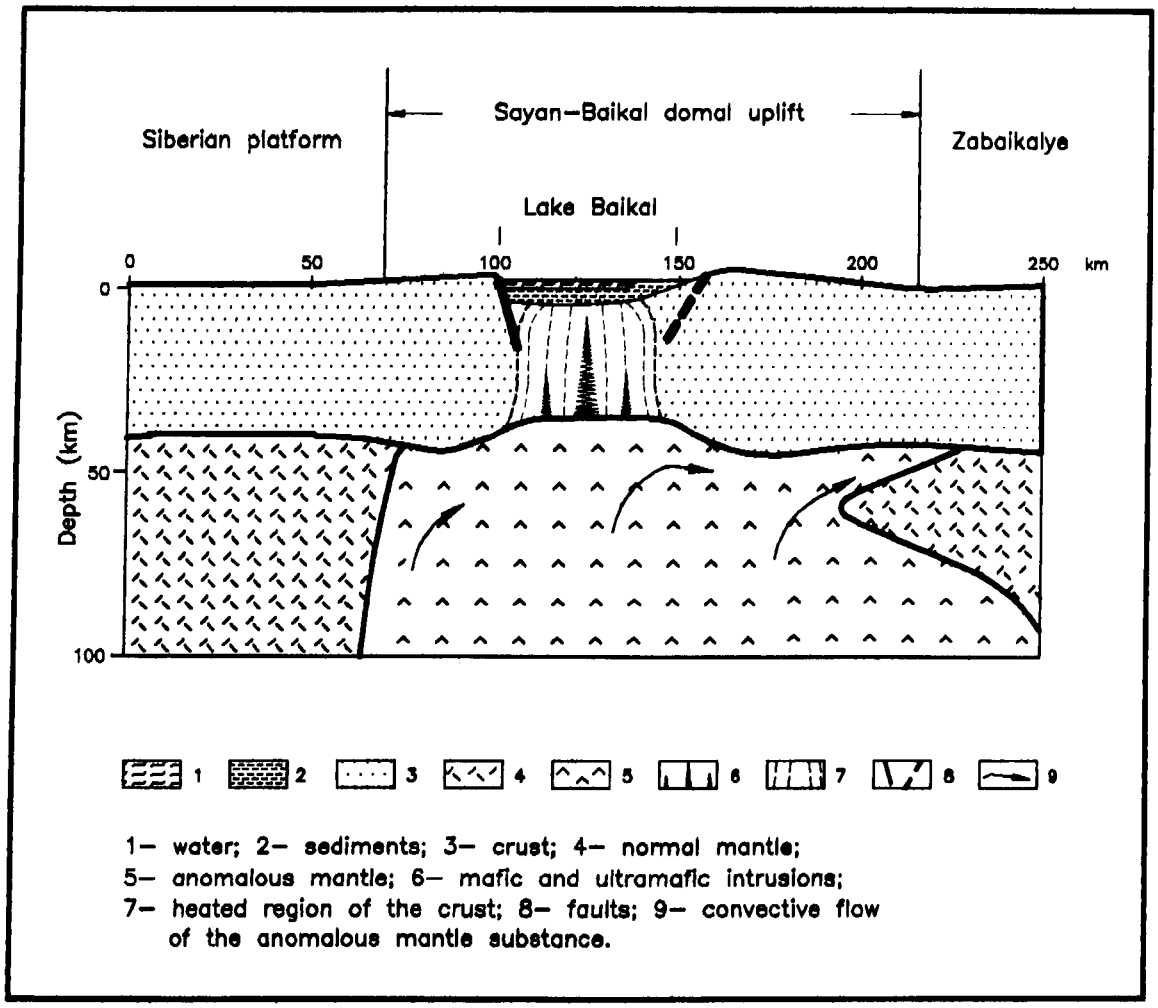

Figure 2.16 The Baikal Rift. After Logatchev (1978).

2.5.4 The Baikal Rift

Neotectonic history of the Baikal Rift explains the pattern and the distribution of rift faults and valleys, which result from an interaction of the basement structure with regional extension due to the domal uplift of the lithosphere. The regional extension in the crust also leads to dispersion of the rift valleys in the areas where marginal faults are oblique to the general strike of the rift zone and to the regional extension vector. In such regions displacements along the faults are of strike-slip type, and depressions occur in en-echelon arrangement (Logatchev et al., 1978).

Geophysical evidence indicates thinning and attenuation of the crust of the Baikal depression. The depth to the base of the crust in the Baikal rift zone varies between 34 and 46 km. The shallowest depth was registered in the deepest part of the Baikal depression and the greatest beneath the surrounding mountains (Logatchev et al., 1978). In addition to the anomalous upper mantle layer beneath the Baikal rift zone, the data from the seismic station in East Siberia allowed the detection of the existence, in the upper mantle beneath the vast South Siberian and Mongolian mountain region, of an extra-large body of anomalous low-velocity mantle. This large scale anomalous mantle region (Figure 2.16) has a lower boundary descended to 300-700 km below the rift zone and adjacent mountain areas (Logatchev et al., 1978).

2.5.5 North Sea rift system

The tectonic framework of NW Europe has its origin in Ordovician-early Devonian times of the Iapetus Ocean closure. In Norway this led to a NW-SE collision of the Laurentian and Fennoscandian Shields, whereas, in Britain occurred the complex accretion of Precambrian continental blocks and islands arcs onto the North American craton (Coward, 1990). Subsequent tectonic episodes reactivated existing basement lineaments. There is, in the region of the North Sea and the Atlantic Margin west of the Shetlands, an important SW-NE trending structure, reflecting reactivation of the Caledonian thrust. Prominent NW-SE lineaments are possibly related to a diffuse transform zone between Fennoscandian Shield and the accreted terrains in the Central and Southern North Sea.

During the Devonian post-orogenic collapse of the Caledonides, a major sinistral translation between the Laurasia and Fennoscandia Shield took place. In the Northern North Sea this caused the rapid subsidence of pull-apart basins (Midland Valley, Orcadian Basin) in which several kilometres of sediments was deposited (Old Red Sandstone). The evolution of the British Isles in early Carboniferous, was controlled by the north-south extension along a series of NW-SE and NE-SW striking faults, located along the Caledonian weakness. From the Namurian (early Upper Carboniferous) onwards, crustal stretching stopped and broad regional subsidence was initiated.

The closure of the Proto-Tethyan Ocean, south of Britain, and the subsequent collision of Laurasia and Gondwana, resulted in the intra-plate stress transmission into the next orogenic event - the Variscan orogeny. This caused extensive deformation, resulting in uplift and folding of the hanging walls of the main extensional faults in the East Midlands area. During latest the

Carboniferous-early Permian, NW Europe was transected by a late Variscan post-orogenic systems of conjugate shear faults, which, in the North Sea, triggered wide-spread magmatism and deformation of the sedimentary fill of the Variscan forland basins.

In NW Europe the wrench faulting and volcanic activities decreased towards the end of Autunian. The broad Permian basins began to subside during the Saxonian, presumably as a response to the decay of thermal anomalies, which were induced during the Stephanian-Autunian wrench faulting phase.

On the 'boundary' of Permian and Triassic, rifting activity accelerated in the Norwegian-Greenland Sea area and in the Tethys domain. By the early Triassic in NW and Central Europe, a stress regime developed, which caused differential subsidence of a complex set of multi-directional grabens and troughs (Steel and Ryseth, 1990). Although the prime extensional direction was east-west, many of the fault-bended grabens formed along reactivated Caledonian trends. Triassic sedimentation and syn-depositional faulting triggered diapiric deformation of the Zechstein salts during the middle to late Triassic.

During the Lower to the Middle Jurassic the Central North Sea became uplifted, and this was accompanied by the extrusion of a large volcanic complex at the triple junction between the Viking, Central and Moray Firth-Witch Ground Grabens (Latin et al., 1990). Volcanics displayed the bimodal mafic-felsic alkaline geochemical character typical for intracratonic rifts. As a result of thermal updoming, erosion products (recycled Triassic sandstones), were deposited in adjacent grabens as major deltaic complexes (the hydrocarbon-bearing Brent Group in the Viking Graben; Richards, 1990).

Accelerating crustal extension in the North Sea accompanied sea-floor spreading in the Central Atlantic during Kimmeridgian to Berriasian-Valangian times. This led to major fault blocks rotation and salt diapirism in the Northern Sea area.

In the Southern North Sea crustal distension was accommodated by reactivated NW-SE dextral oblique-slip faults along which differential subsidence occurred.

In the Central and Northern North Sea areas rifting ceased during the late Cretaceous and thermal subsidence prevailed, possibly resulting in the onset of oil generation in the graben axes. Igneous activity increased along the Faeroe-West Shetland and mid-Norway rift zones and culminated during the Paleocene in major volcanic events that affected large areas of the Arctic-North Atlantic borderlands. Doming, centred over NW Scotland, resulted in large-scale erosion and shedding of clastics into the deep-water basins of the Central and Northern North Sea thermal sag (Milton et al., 1990; Harding et al., 1990). Subsequent compression, during the Oligocene, partly destroyed old traps and created new traps. Simultaneously a second phase of inversion affected the Sole Pit and triggered salt diapirism in the Central Graben.

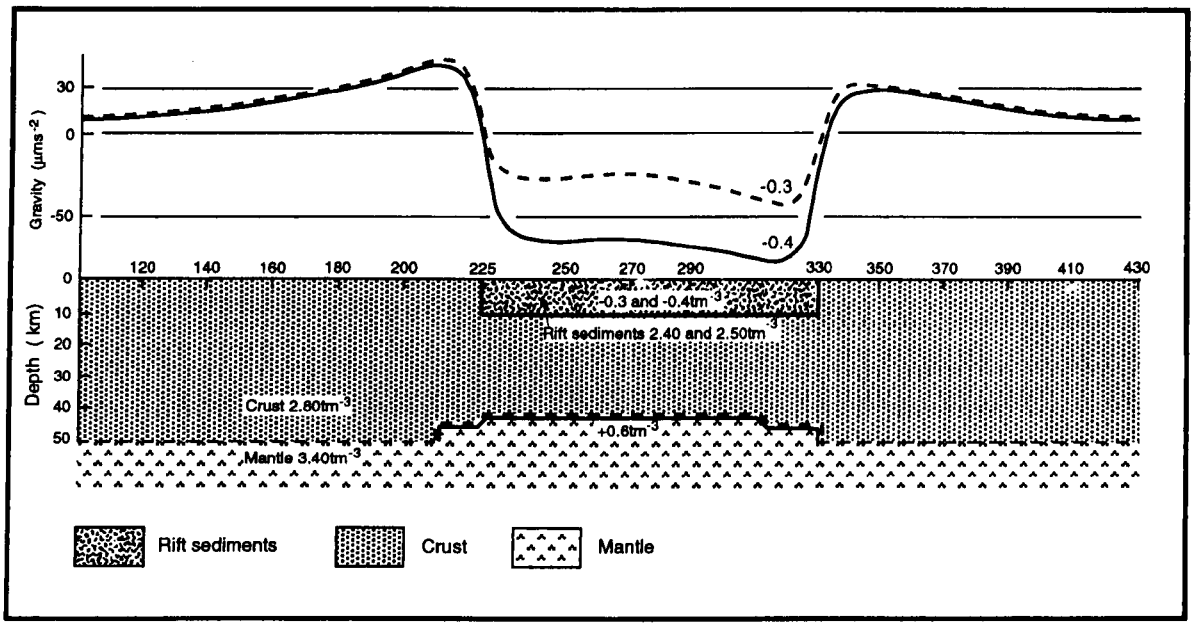

Figure 2.17 Theoretical gravity anomaly over rift structure. After Gunn (1984).

2.6 Gravity and magnetic signature of the rift structure

The following section of the Chapter 2 shows several examples of observed gravity and magnetic characteristics of the active rift systems of the East Africa and ancient rift structures from the Central and West Africa. The compilation of only gravity and magnetic signature of the various rifts and omitting discussion of seismic observations across rift's zones was dictated by the fact that, in the Polda rift area the onshore seismic data is of a very poor quality and seismic survey data which covers offshore part of the Polda rift was not available for author to study and present in this thesis.

Geophysical signatures of the rifts may be enclosed in a wide range of possible responses. Examples of gravity results over rifts given by Burke and Whiteman (1973) and Darracott et al. (1973) show that initial uplift and young rift systems exhibit broad gravity lows due to the low density material which causes the crustal doming. The sedimentary rift infill may be responsible for the local gravity low located over the central rift. Since an axial dyke develops, a gravity high will be superimposed along the centre of the graben, and depending how close to the surface the dyke rises, its positive gravity may overprint any gravity lows due to sediment infill. The gravity high due to the axial dyke may be affected by the additional anomaly caused by the occurrence of the dense volcanic rocks within the central graben.

Gunn (1984) points out one gravity characteristic of rifts, which is not widely appreciated. It is the combined effect of a sharp gravity negative, due to the low density of the sediments within the rift, which is superimposed on a broad gravity maximum, due to the thin continental crust occurring beneath the rift. The combined effect causes a gravity anomaly of the form, as shown in Figure 2.17. Gunn (1984) used for modelling of this gravity anomaly the rift dimensions of the Dniepr Don aulacogen defined, based on the seismic refraction studies conducted by Hall (1976). The model of the gravity field of the Rio Grande Rift proposed by Birch (1982) similar to Dniepr Don rift exhibits occurrence of the positive gravity 'shoulders' not directly overlying high density material.

2.6.1 The East African Rift System

The East African Rift System (Red Sea, Gulf of Aden and the Eastern Rift) represents the three stages of the evolution of an ocean. Whereas, in the Red Sea and the Gulf of Aden, the separation of the continental lithosphere is completed, in the Eastern Rift the plates they do not appear to be separated, though there may be extension and thinning of the lithosphere beneath the rift zone. The three branches of the East African Rift System present characteristic broad negative gravity anomalies with superimposed axial positive anomalies. The width and amplitude of the positive anomaly is dependent on the extend to which the axial intrusives zone has developed (Darracott et al., 1973).

The nature of the gravity field characteristic for the rift zone in East Africa is well established (Figure 2.18; Darracott et al., 1973). The gravity anomalies and the geological model of the lithosphere and asthenosphere for a section at the latitude of Lake Magadi (1.8°S) represents the

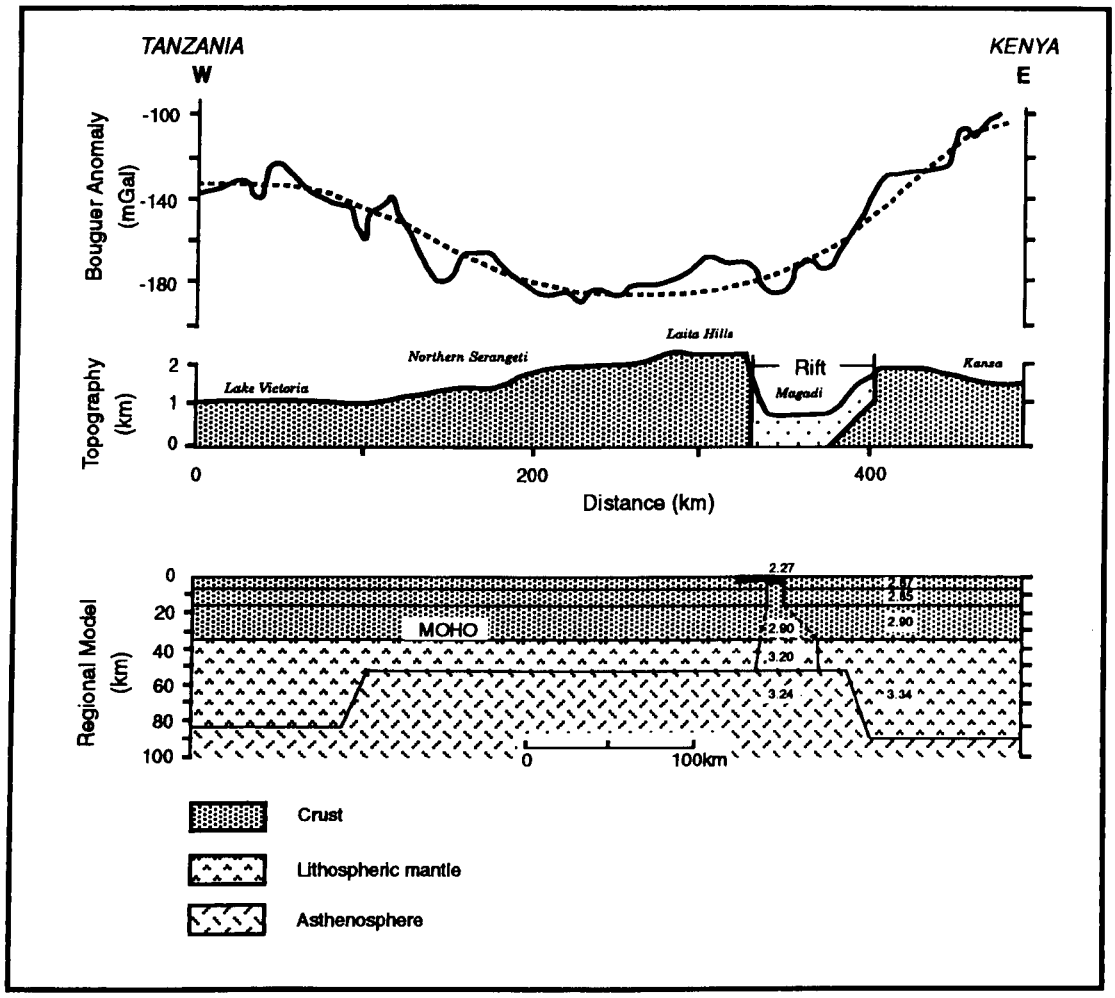

Figure 2.18 Interpretation of the gravity profile of Lake Magadi (1.8° S). After Darracott et al. (1972).

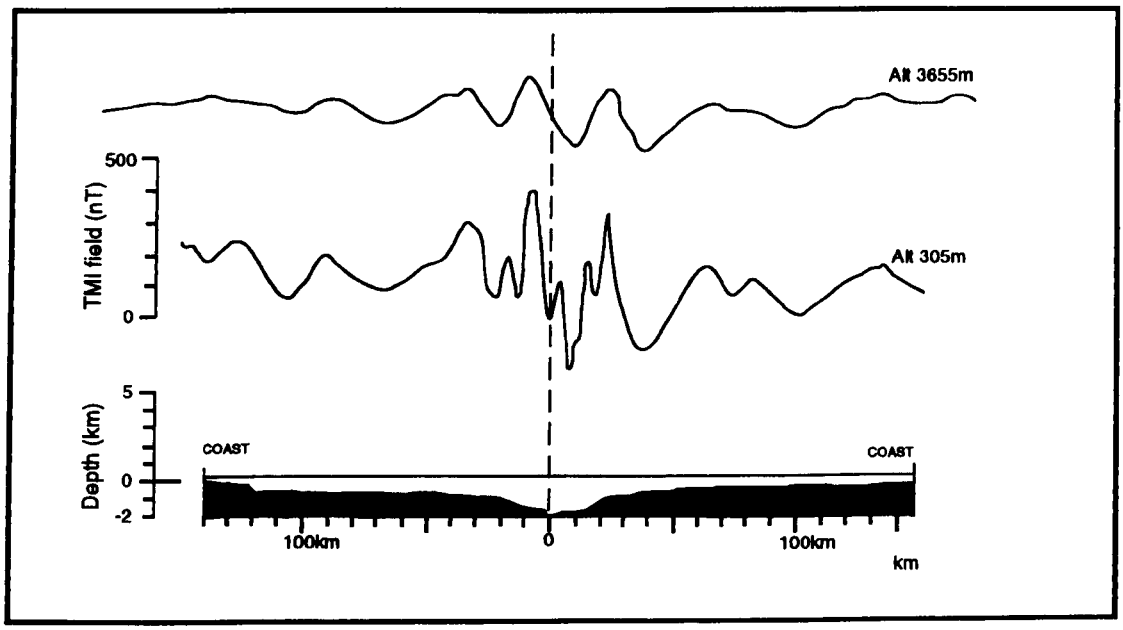

Figure 2.19 Aeromagnetic anomalies across the Red Sea (18° N). After Darracott et al. (1972)

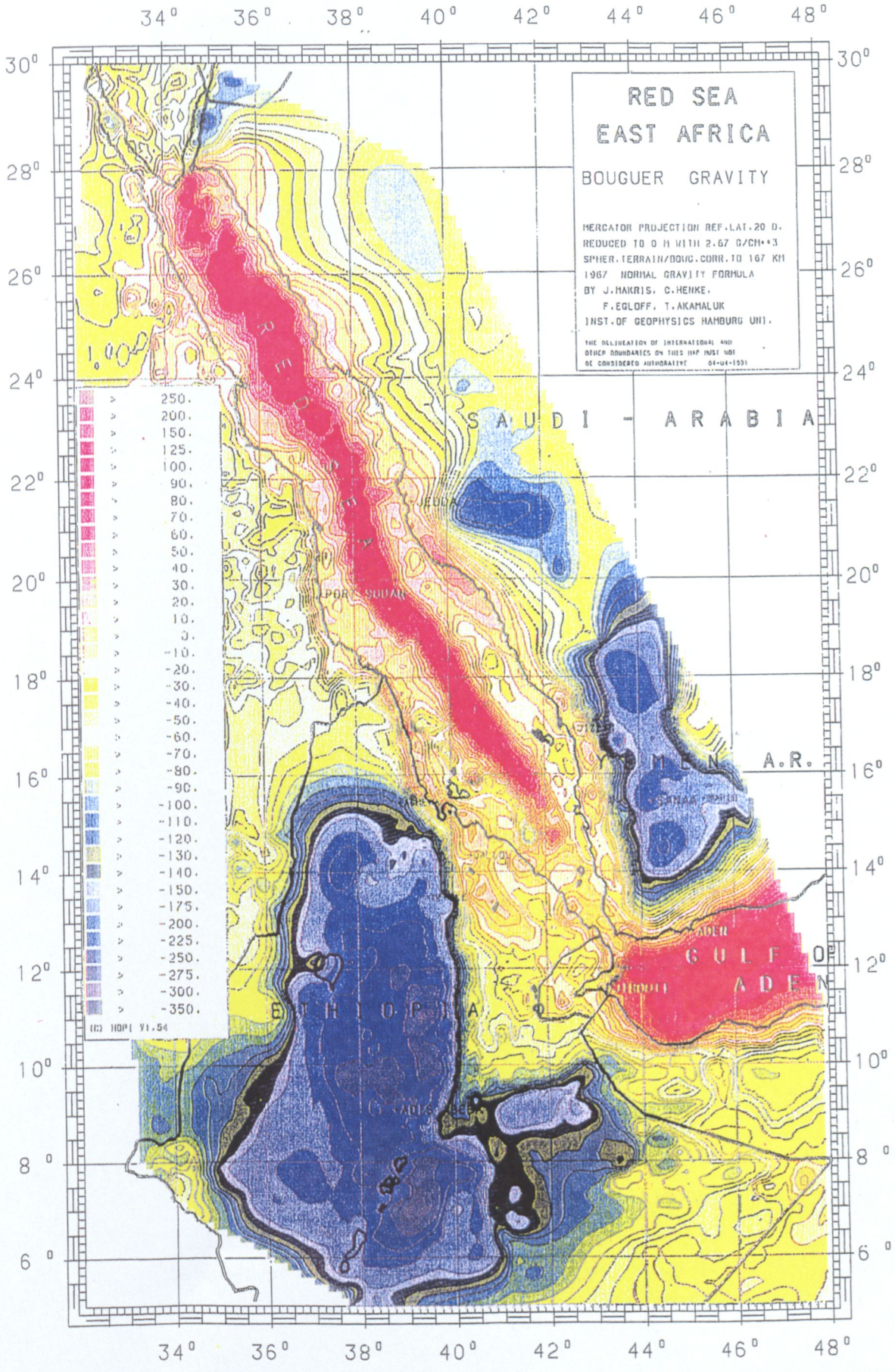

Figure 2.20 Bouguer gravity contour map of the Red Sea Rift. After Makris et al. (1991a)

typical situation for such a rift system; i.e. the broad regional (a long wavelength) negative Bouger anomaly with a superimposed smaller positive anomaly over the Eastern Rift axis (Figure 2.18). This gravity profile is typical of the Gregory Rift in Kenya and Ethiopia, and the Red Sea and Gulf of Aden. In East Africa, the negative anomaly has a width of up to 1000 km and a maximum amplitude of -150 mGals. The gradients are small which may suggest that the light material causing the anomaly is at considerable depth and has a small density contrast with the surrounding rocks (Darracott et al., 1973). This anomaly has been interpreted by Girdler et al. (1969); Baker and Wohlenberg (1971), to be due to the lower density asthenosphere replacing the upper lithospheric mantle (gravity contrast -0.12 mGal).

(I) The Red Sea Rift

The study by Darracott et al. (1973) of the Kenya Rift indicates that axial dykes can give prominent magnetic anomalies. The magnetic anomaly profiles across the Red Sea (Figure 2.19) show sea-floor spreading anomalies over the axial trough.

Cochran (1983) provided an excellent example of the magnetic effect of an axial dyke on the Red Sea Rift, which he interpreted as undergoing increased extensional opening towards the south. The TMI map of the rift shows a series of isolated magnetic highs aligned along the central rift axis in the north, but towards the south these anomalies start closing up until they become a continuous axis, thus illustrating the progressive stages of axial dyke development. Gunn (1984) and others suggest that the dyke is initially expressed by isolated intrusions and that, as the dyke comes closer to the surface, it forms a continuous magnetic sheet.

Makris et al. (1991a) have presented recompiled gravity data of the Red Sea and East Africa (Figure 2.20). The maximum Bouguer gravity values ($> 100mGal$) are located over the median troughs of the Red Sea and Gulf of Aden.

(II) The Dead Sea Rift

Geophysical characteristics of the Dead Sea Rift described and reported by Folkman (1981) were defined as the result of a combined analysis of aeromagnetic and gravity data, covering the rift zone and adjacent areas. The following major regional gravity features were observed:

- Bouguer gravity values increasing towards the Mediterranean, and from south to north, caused by crustal thinning under the Coastal Plain (Ginzburg et al., 1979b), and by lateral lithological variations within the crust (Folkman and Bein, 1978);
- a gradient towards the rift zone with negative Bouguer values over the rift, caused by young sedimentary fill;
- a gravity low over the Coastal Plain and the Continental Shelf, caused by the low density sediments filling the Neogene sedimentary basin;

Within the rift zone four distinct gravity lows occur over the major depressions (the Hula basin, the eastern portion of the Sea of Galilee, the Dead Sea and the northern Gulf of Elat).

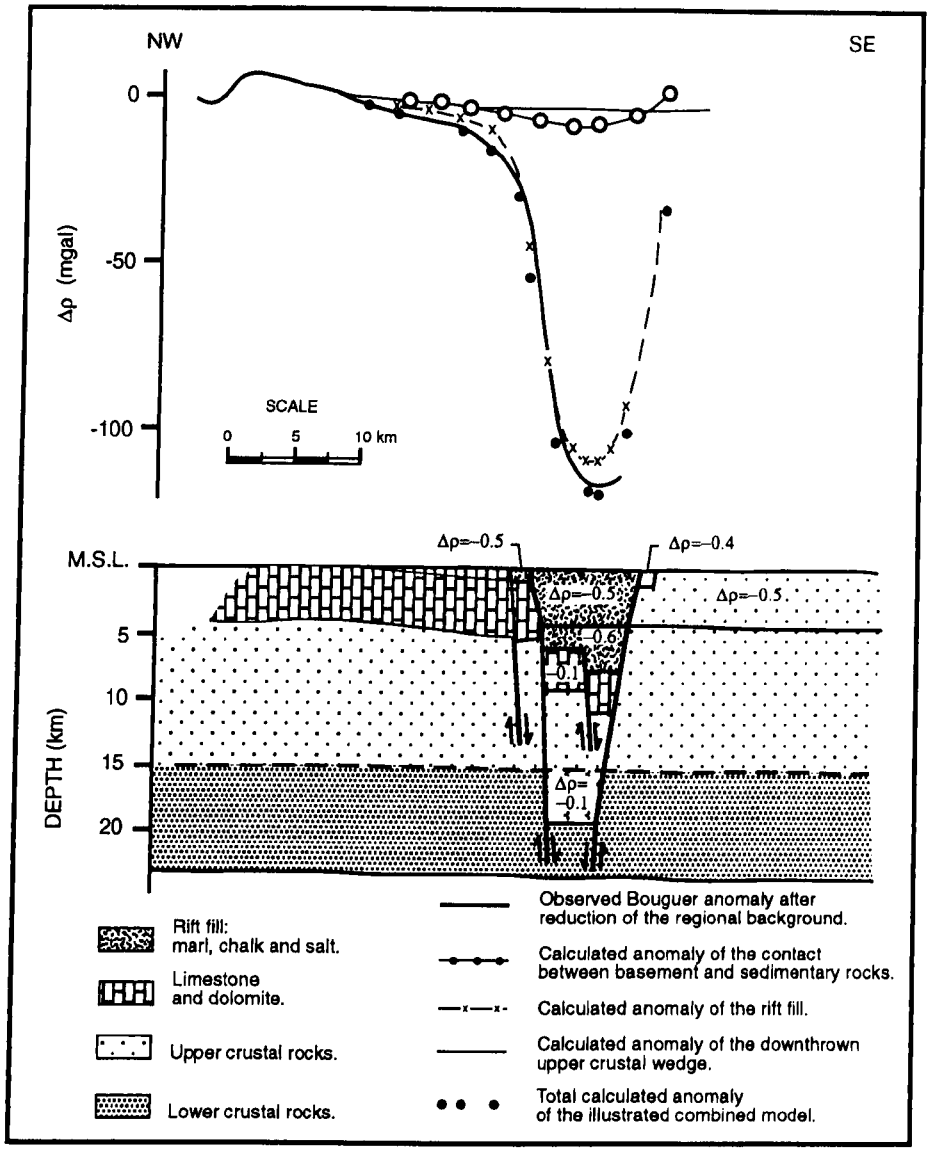

Figure 2.21 Interpretation of the gravity anomaly of the Dead Sea. After Folkman (1981).

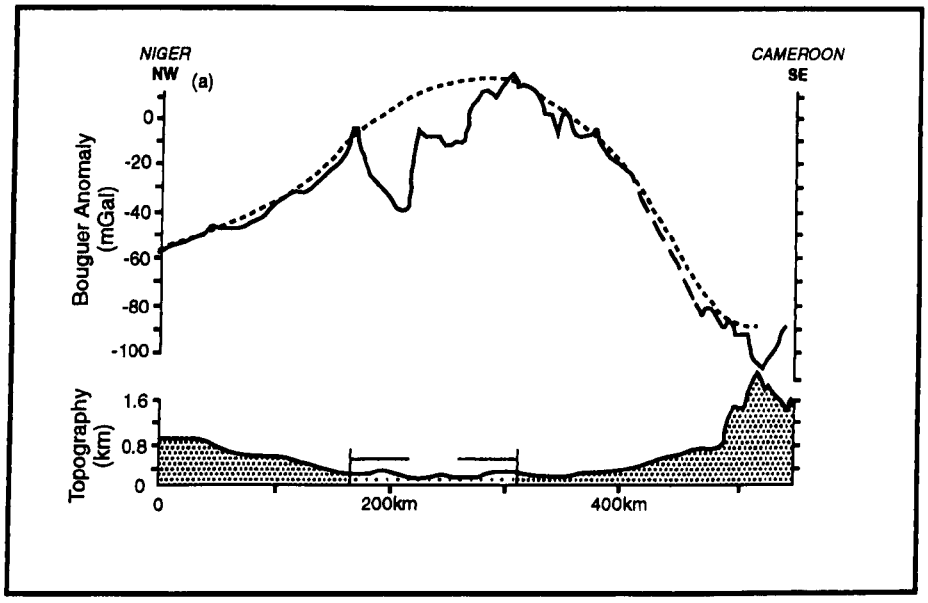

Figure 2.22 Bouguer gravity anomaly and surface topography of the Benue Trough. After Fairhead (1986).

Magnetic anomalies, indicative of shallow igneous rocks, characterised the northern portion of the Dead Sea Rift. Some of the anomalies show reverse magnetisation, while others are normal. The southern portion of the rift is magnetically smooth, except for an anomaly which is probably, in the opinion of Folkman (1981), related to a transversal fault system, rather than to the rift.

As Folkman (1981) reported, the results of a combined analysis of aeromagnetic and gravity data covering the Dead Sea- Jordan rift zone and adjacent areas does not show similarities with other portions of the East African rift system, which are associated with significant crustal thinning (Girdler, 1978). However, this study shows two different deep structural models:

- across the northern and central portion of the rift zone the crustal thickness and the character of the upper mantle remain unchanged
- the Gulf of Elat, the southern portion of the rift may be underlain by an anomalous, low-density upper mantle.

Low negative gravity anomalies (-115mGal) within the rift zone delineated depressions, separated by structural highs. Folkman (1981) interpreted the Dead Sea depression to be filled by 7.5 km of young sediments (Figure 2.21). In outside part of the rift thickness of the sediments was based on interpretation of magnetic field.

2.6.2 The West and Central Africa rift systems

Gravity studies (Browne and Fairhead, 1983; Fairhead, 1988; Fairhead and Green, 1989) of the West and Central Africa rift system show that these structures are associated with broad regional positive Bouguer anomalies located symmetrically over each basin. These anomalies are up to 450 km wide with an amplitude up to 80 mGal (Figure 2.22).

Refraction and reflection seismic studies across the Yola rift indicate at least 11 km of crust thinning (Stuart et al., 1985). Three dimensional gravity modelling over the Benue Trough indicates that the 150 km wide crustal zone thinned to 18 km (Fairhead and Okereke, 1988). Superimposed on the regional positive gravity anomalies are smaller negative Bouguer anomalies, which are due to sediments and referred to as residual anomalies (Fairhead and Green, 1989).

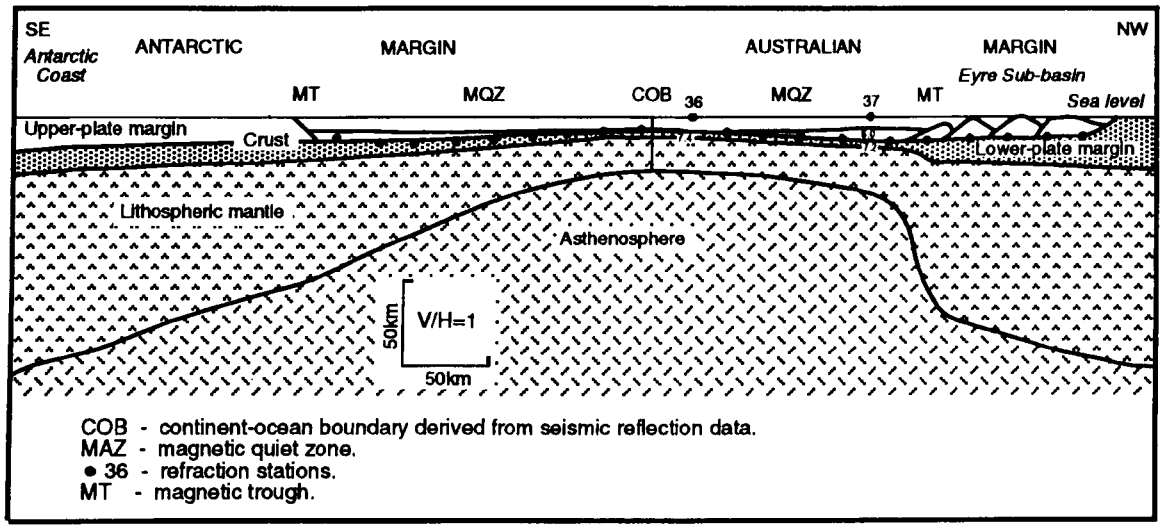

Figure 2.23 Detachment model from Eyre Terrace to Wilkes Land, Antarctica. After Etheridge et al., (in press).

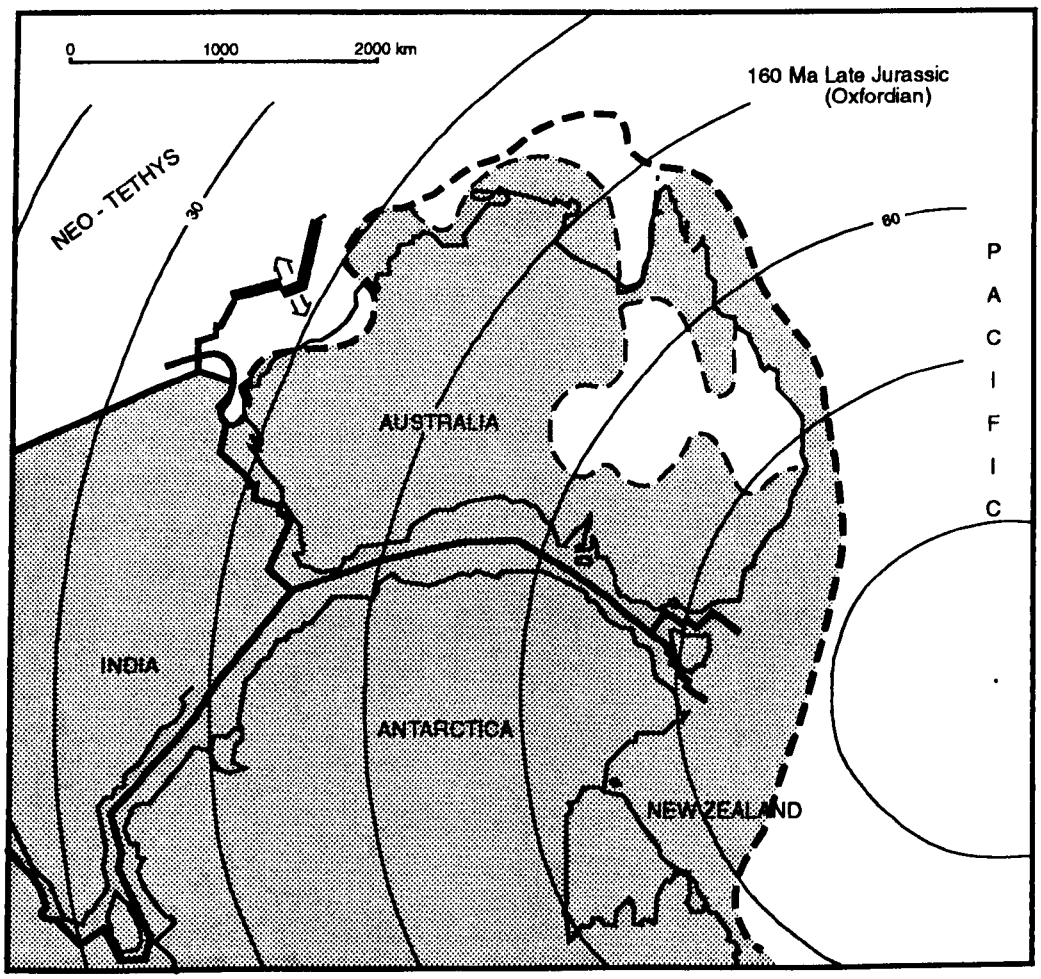

Figure 2.24 Australia, India and Antarctica in the Late Jurassic (160 Ma). After Veevers et al., (1991).

2.7 Tectonic development of the Southern Australian Rift System; break-up of the Gondwana super-continent

The Australian continent has not always been an island isolated from the other continents by vast oceans and oceanic crust. In terms of the geological time table it was not long ago - a little over 100 million years, that Australia was part of the much larger 'super-continent' Gondwana, and was connected to Antarctica along the present southern margin. In Jurassic, the middle part of southern Australian continent was juxtaposed to Wilkes Land and George V Land, including Commonwealth Bay (Figures 2.23 - 2.25).

The geological matching of the southeastern Australia and adjacent Antarctica, in the Gondwana context, has long been postulated (e.g. Sproll and Dietz, 1969; Smith and Hallam, 1970; Von der Borch, Conolly and Dietz, 1970; Griffiths, 1971; Weissel and Hayes, 1971; Weissel et al., 1977; Oliver, 1972) and broadly reported (e.g. Oliver et al., 1983; Veevers and Eitrreim, 1988; Veevers et al., 1990; Flötmenn et al., 1993; Sheraton et al., 1993; Flötmenn and Oliver, 1994). Flötmenn and Oliver (1994) pointing similarities in the evolution of late Proterozoic-early Palaeozoic mobile belts flanking the southeastern Australian and adjacent Antarctic craton margins. The matching structural imprints support other geological evidence for former juxtaposition of these two cratons. Reconstruction (Veevers and Eitrreim, 1988; Veevers, 1990) of the Australian and Antarctic plates which fit along their margins, is resulting in many common geological signatures (Flötmenn et al., 1993; Flötmenn and Oliver, 1994). For example, in the late Archaean to earliest Proterozoic hypersthene gneiss, amphibolite and granitoid gneiss at Commonwealth Bay on the north-eastern margin of the Antarctica, are comparable and considered to be possibly equivalent to rocks of a similar age on the southern Eyre Peninsula, located in the middle of the southern margin of the Australian continent (Oliver et al., 1983).

The eastern, western and southern margins of the Australian continental plate are very much like the Atlantic seaboards of Africa and North and South America, passive continental margins. The northern Australian margin of Papua New Guinea and south of the Indonesian island chain, is an active major subduction zone (volcanically and seismically) where the Australian continental plate is converging with the Pacific and the Eurasian plates.

The southern margin of the Australian continent is a tectonically stable, divergent, passive, continental margin, extending for 4000 km from the Perth Basin in Western Australia to the Tasman Plateau in the south-east. This part of the Australian plate is a stable region of the crust interrupted only by relatively minor epeirogenic movements, especially along ancient fractures. The southern margin has been affected by Jurassic-Tertiary rifting and sea-floor spreading which was initiated in the mid-Cretaceous and continues to the present day (Figure 2.24). The broad zone of the southern margin of the Australian continental plate is dominated by the Mesozoic rift system referred to as a 'Southern Rift System' (SRS).

The interpretation of the break-up history of Australia and Antarctica is constantly under review. New information and methods for determining the real time and the reconstruction of the sequential phases of the break-up history, have resulted in several hypotheses.

Initially a relatively simple model of the classical passive margin associated with the fragmentation of the Gondwana continent was adopted (Sproll and Dietz, 1969; Smith and Hallam, 1970; Griffiths, 1971; Willcox, 1978). A propagating east-west rift valley, was considered to have stretched from the south-west of Western Australia to Tasmania in the south-east. Such a tectonic setting led to the formation of several related extensional basins from the Early Cretaceous onwards, including the Eyre Sub-basin, GAB Basin, Duntroon Basin, and Otway Basin. These basins were considered to be underlaid by Early Cretaceous infra-rift sediments, which directly overlay the basement complexes of the Precambrian Albany-Fraser Province and Gawler Craton in the GAB, and Palaeozoic sediments of the Tasman Orogen in the Tasmanian region (Willcox and Stagg, 1990).

Weisel and Hayes (1972) originally dated the break-up of continents as Palaeocene. However, the age of initiation of drifting was revised when Cande and Mutter (1982) re-modelled the sea-floor spreading magnetic anomalies and concluded that the break-up event actually commenced in the early Upper Cretaceous (Cenomanian), and was followed by a period of slow ocean floor spreading which, since the Eocene, has become fast spreading and has continued at this rate until the Recent.

Hence, by the late eighties an established concept was that Australia had separated from Antarctica by lithospheric extension between the mid-Jurassic (> 160 Ma) and mid-Cretaceous (96 Ma). Subsequently the opening of the south-east Indian Ocean evolved in three stages of sea-floor spreading. Cande and Mutter (1982) suggest that:

- stage one occurred at a slow half-rate < 4.4 mm/year sea-floor spreading on a separation azimuth of 335° until magnetic anomaly A21 time (96-49 Ma),
- stage two at an intermediate half-rate 10 mm/year until anomaly A20 time (49-44.5 Ma),
- stage three at a fast rate 20 mm/year on a separation azimuth of 360° to present.

Veevers et al. (1990) confirmed the previously reported results, except for the reinterpretation of the oldest anomalies. They described the phase of slow spreading as being characterised by:

- jumps of the spreading ridge to the Australian continent-ocean boundary between 131.25°E and Tasmania to accommodate the south eastward offset of the line of separation between Tasmania and Antarctica, and
- variable azimuth of spreading isochrones within individual spreading segments, as, for example, from 90°±5° between 129°E and 130°E (an angle of 65° between separation and spreading azimuth) and 75° and 80° between 130°E and 131.75°E (an almost orthogonal 80°).

Veevers et al. (1990) observed similarities in the relation between spreading and separation azimuth in the southern margin of Australia and the Gulf of Aden, where sea-floor spreading between Arabia and Somalia started 4.5 Ma ago and followed a stage of continental extension that dates from 30 Ma ago (Hempton, 1987). The spreading half-rate of 10 mm/year is similar to that of the intermediate stage of spreading between Antarctica and Australia. The separation azimuth, defined by

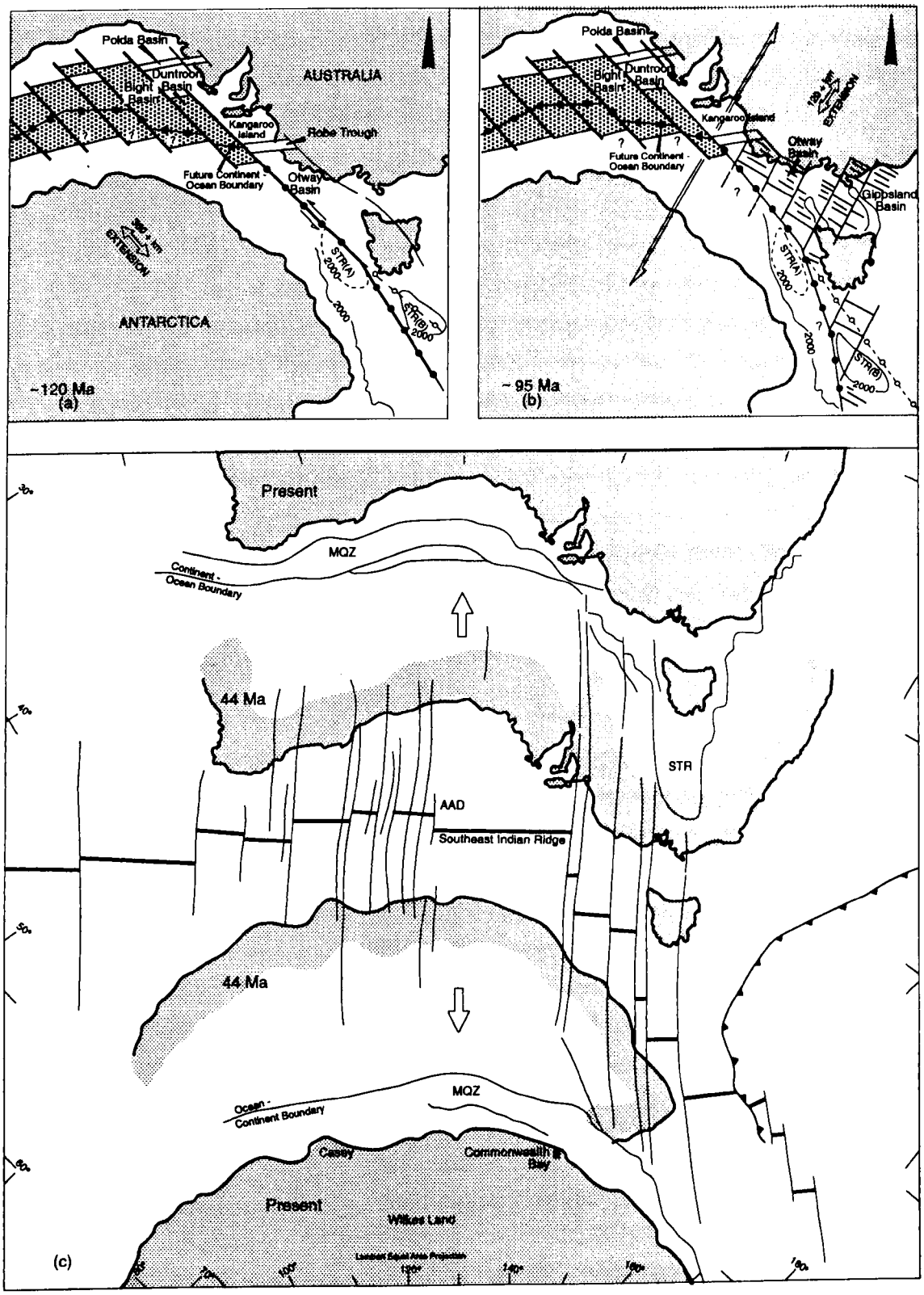

Figure 2.25 The southern Australian margin in relation to Antarctica. After Willcox and Stagg (1990).

the transform faults, is 210°. It subtends an angle of 77°±5° with the isochrone azimuth in the area east of 47.5°E, and 55°±5° to the west. This sharp change of the azimuth is interpreted as the response of a slow-intermediate (10 mm/year) spreading system to confinement between continental margins now only 90 km apart, whose boundaries are oblique to the separation azimuth. The variable oblique angles between the azimuth of spreading and separation off the southern margin of Australia are likewise attributable to the narrow space between the continental margins reaching no more than 500 km after 45 Ma of slow spreading (half-rate < 4.4 mm/year). In the stage of fast spreading that followed, the pattern of spreading was apparently unaffected by the already widely separated margins, and ridge jumps were negligible, except in the Australian-Antarctic discordance (Weissel and Hayes, 1974; Vogt et al., 1983). Instead, the main irregularity was the asymmetric spreading (Weissel and Hayes, 1972) that brought the South-East Indian Ridge relatively closer to Antarctica.

With the recognition of the detailed pattern of slow spreading in the Great Australian Bight, together with the identification of ridge jumps to the Australian continent-ocean boundary east of 131°E, Veevers et al. (1990) established a clearer understanding of the influence of the oceanic crust on the structure and subsidence of the late Cretaceous and early Cainozoic continental margin.

Willcox and Stagg (1990) proposed a comprehensive history of the formation of the southern margin. Based on the seismic and magnetic profiles they reconsidered the location of the continent-ocean boundary previously established by Veevers and Eittreim (1988). Figure 2.25 present Willcox and Stagg's scheme of the formation of the southern margin, which comprises the three periods of continental extension, during which the Australian and Antarctic plates were joined or were in partial contact, and two periods of continental drifting.

Within the region of the Great Australian Bight, the computed value of the pre-late Jurassic extension is 360 km in a NW-SE direction (Figures 2.25). In conclusion Willcox and Stagg suggest that the extension resulted in the formation of the extensional Eyre Sub-basin, Great Australian Bight Basin, Duntroon Basin, possibly the Robe Trough and was related to the modification of pre-existing, much older structural features, within the Polda Trough. These authors also postulate that a major left-lateral strike-slip fault-zone extended through the Otway Basin, passed between Tasmania and the South Tasman Rise and led to formation of the strike-slip Sorell Basin and NE margin of the South Tasman Rise. The Bass Basin and Tamar Graben areas of northern Tasmania were also affected by this strike-slip movement.

During the Early Cretaceous (post-Neocomian) a major change in the stress field regime occurred. A NNE-SSW extension initiated origin and development of Gippsland and Bass Basins, and enhanced development of the Otway and Sorell Basins of south-eastern Australia. In the region between the Australian mainland and Tasmania this extension was about 120 km. As shown in Figure 2.25 the pre-Late Jurassic and Early-Cretaceous phases of extension were almost orthogonal what is perhaps responsible for a complex structure of the South Australian Rift System.

According to Stagg and Willcox (1992), the age of separation of Australia and Antarctica can be determined by the identification of sea-floor spreading of magnetic

anomalies adjacent to the margin, or by extrapolation of the spreading rate/time span between the oldest identified anomaly and the continent-ocean boundary (COB) as interpreted from magnetic and single-channel seismic data. The most recent estimate of the age of the Gondwana break-up, using this model, is 95±5 Ma in the Cenomanian. However, identification of the oldest magnetic anomalies, formed during the early phase of slow drift between Australia and Antarctica is fragile, particularly between south-west Australia and central Great Australian Bight (GAB).

The South Australian Rift System includes a number of basins, sub-basins, troughs, and embayments which have different structural style and orientation. Stagg et al. (1993) recognised within the South Australian Rift System several structural zones, which align major basement offsets, which are likely to be caused by independent normal faults. They suggest, that as these normal faults propagate along strike as the extension increases, offsets are accommodated.

These increased stress and 'accommodation' zones, develop into transform faults (Etheridge et al., 1988; Stagg et al., 1993). In well known major rifted margins, such as the Atlantic margin of North and South America, or the Grand Banks of Alaska, these 'accommodation' zones or transform faults are used to subdivide the margin into a structural units i.e. basins, grabens, etc.. Based on several such zones, the western part of the Australian Southern Rift System has been divided into a number of structural units: the Great Australian Bight Basin (or Ceduna Sub-basin or Ceduna Depocentre), Eyre Sub-basin, Recherche Sub-basin, Duntroon Basin, Denman and Eucla Basins, Bremer Basin, and the Polda Trough. The Polda Trough on land is a relatively small structure, but because it is part of the much larger system and might involve Proterozoic basin as well as Mesozoic-Tertiary basin, it is necessary to consider a wide range of geology and this is done in the following chapter.

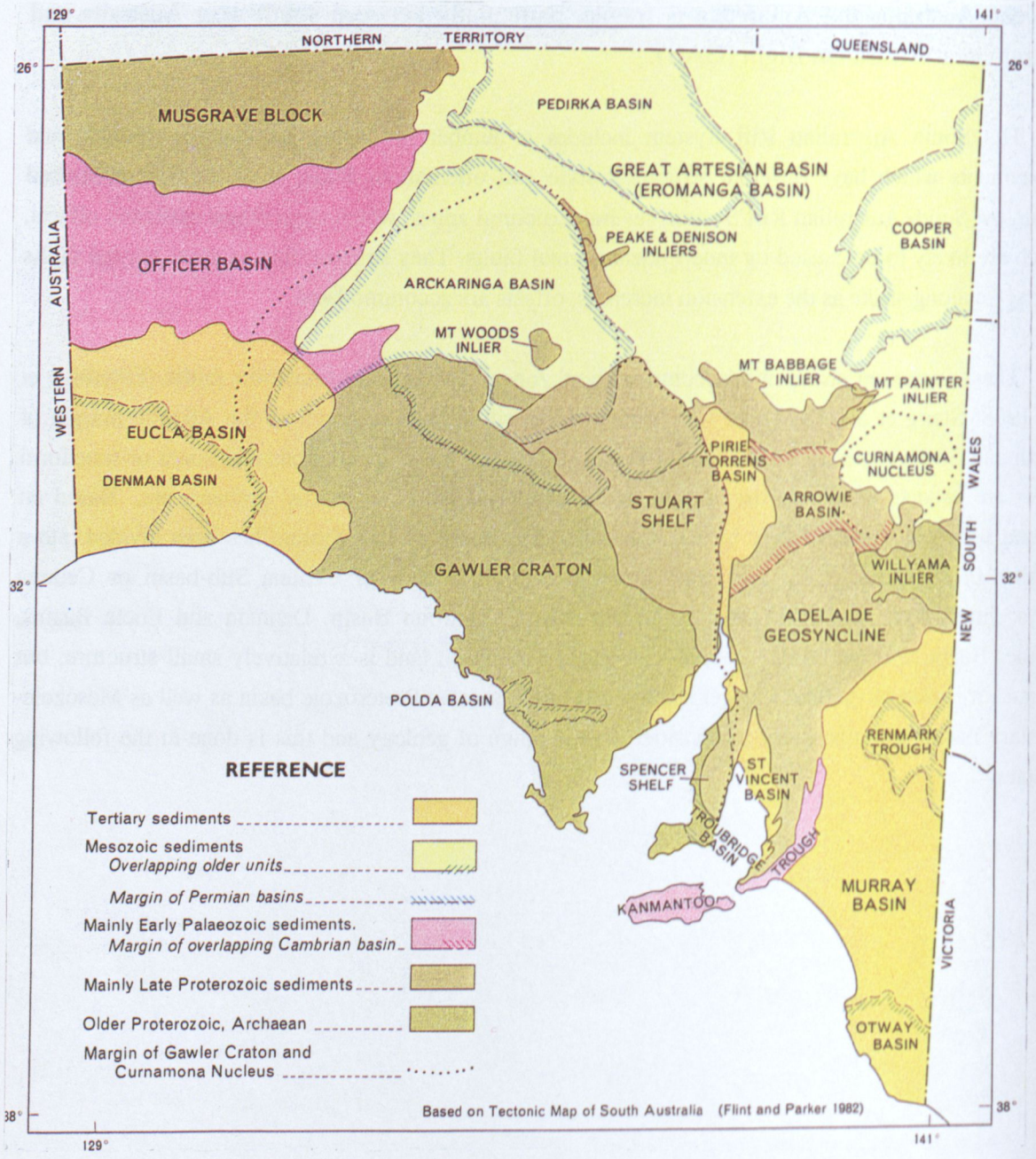

Figure 3.1 Geological provinces of South Australia.

Chapter 3

Geological setting of the Polda Trough

3.1 Introduction

The Polda Trough is a narrow east-west trending structure 50 km wide and 350 km long located on the southern Gawler Craton. It extends in the east from the central Eyre Peninsula and westwards to the continental margin in the Great Australian Bight. The surface imprint of the Polda Trough cannot be seen on either remote sensing images or aerial-photographs and is not visible to geologist in the field, as the whole area is covered by a thick Quaternary sediments. The presence of this structure and its geology is known from drill hole data and geophysics only.

This chapter contains the three following sections:

- regional geology with a focus on the southern part of the Gawler Craton;
- detailed lithological description of the stratigraphic units which form basement and sedimentary successions preserved or deposited within the trough;
- review of the existing concepts concerning the origin, evolution and structure of the Polda Trough.

3.2 Regional setting of the Polda Trough

The main elements of the geology of the central part of southern Australia consist principally of the rocks

- of Early to Middle Precambrian age forming stable cratons: Gawler Craton, Musgrave Block, Curnamona Nucleus, Willyama, Mount Painter and Mount Babbage Inliers, and
- the Neoproterozoic to Early Palaeozoic tectonic provinces: Amadeus Basin, Officer Basin, Adelaide Geosyncline, Tasman Fold Belt, Peak and Denison Inliers, and
- several Phanerozoic sedimentary basins, among which the principal are: the Palaeozoic Arkaringa Basin, Pedirka and Cooper Basin, the Mesozoic Eromanga Basin, the basins of the Australian Southern Rift System of Late Mesozoic to Cainozoic and the Tertiary Murray Basin (Figure 3.1).

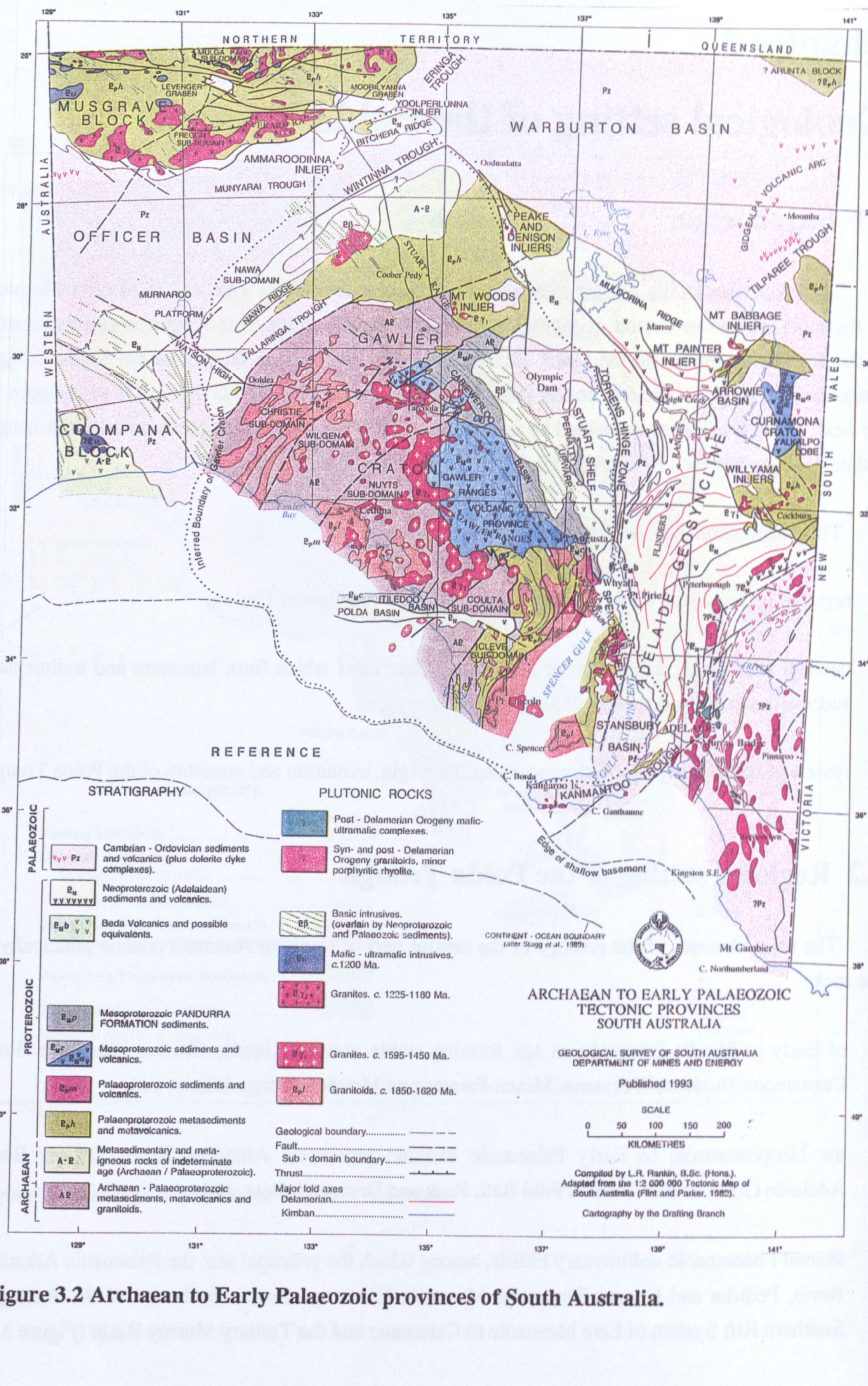

Figure 3.2 Archaean to Early Palaeozoic provinces of South Australia.

3.2.1 Boundaries of the Gawler Craton Province

The Gawler Craton, which is a part of the Australian Precambrian shield, is a major tectonic province occupying the central part of the region in which the Polda Trough occurs. The description of the tectonic evolution of the Gawler Craton and detailed stratigraphy and lithology of the succession is drawn predominantly from Preiss (1987), Fanning et al. (1988), Parker and Lemon (1982), Parker et al. (1985), Webb et al. (1986), Parker (1993), Flint and Rankin (1991), and Flint (1992).

The boundaries of this stable crystalline basement are clearly defined in the east by the Torrens Hinge Zone and the continental shelf to the south. The northern and western edges of the craton are under the cover of thick Neoproterozoic and Phanerozoic sediments and therefore are not clearly defined. To the north, the Craton is flanked by the Mesoproterozoic Musgrave Orogenic Domain and to the west by the Albany-Frazer Province fold belt of similar age (Rutland et al., 1981; Webb et al., 1986).

According to Flint and Parker (1982) the northern edge of the Gawler Craton extends at least to the Wintinna Trough with possible continuation beneath the Officer Basin, where it is substantially depressed and thinned (Figure 3.2). The marginal Neoproterozoic and Lower Palaeozoic zone of the sedimentary cover was deformed during the Palaeozoic; therefore the underlying basement is excluded from the Gawler Craton province (Parker, 1993). The western boundary of this shallow crystalline basement is established based on well defined gravity and magnetic features (Thomson, 1980; Flint and Parker, 1982). To the east, part of the Gawler Craton is covered by relatively undeformed Adelaidean and Early Palaeozoic sediments (Figure 3.3). It is referred to as the Stuart Shelf and Spencer Shelf respectively in the south-east (Figure 3.1; Sprigg, 1952; Thomson, 1969a, 1969b). According to Parker (1993) the Archaean rocks of the Gawler Craton may extend to the east under the Adelaide Geosyncline.

3.2.2 Tectonic evolution of the Gawler Craton

The tectonic evolution of the Gawler Craton occurred in three major megacycles of complex deformation, metamorphism and plutonism (Fanning et al., 1988).

- The oldest (2700 to 2300 Ma) basement rocks of the Gawler Craton are Late Archaean metasediments and metavolcanics followed by Palaeoproterozoic plutons, metamorphosed during the Sleafordian Orogeny.

- An initial basin and platform sedimentation, which occurred from 1950 Ma to 1700 Ma was followed by broad spectrum plutonism, metamorphism, volcanism and the Kimban Orogeny deformation (1820 to 1580 Ma; Webb, 1979; Webb et. al., 1982).

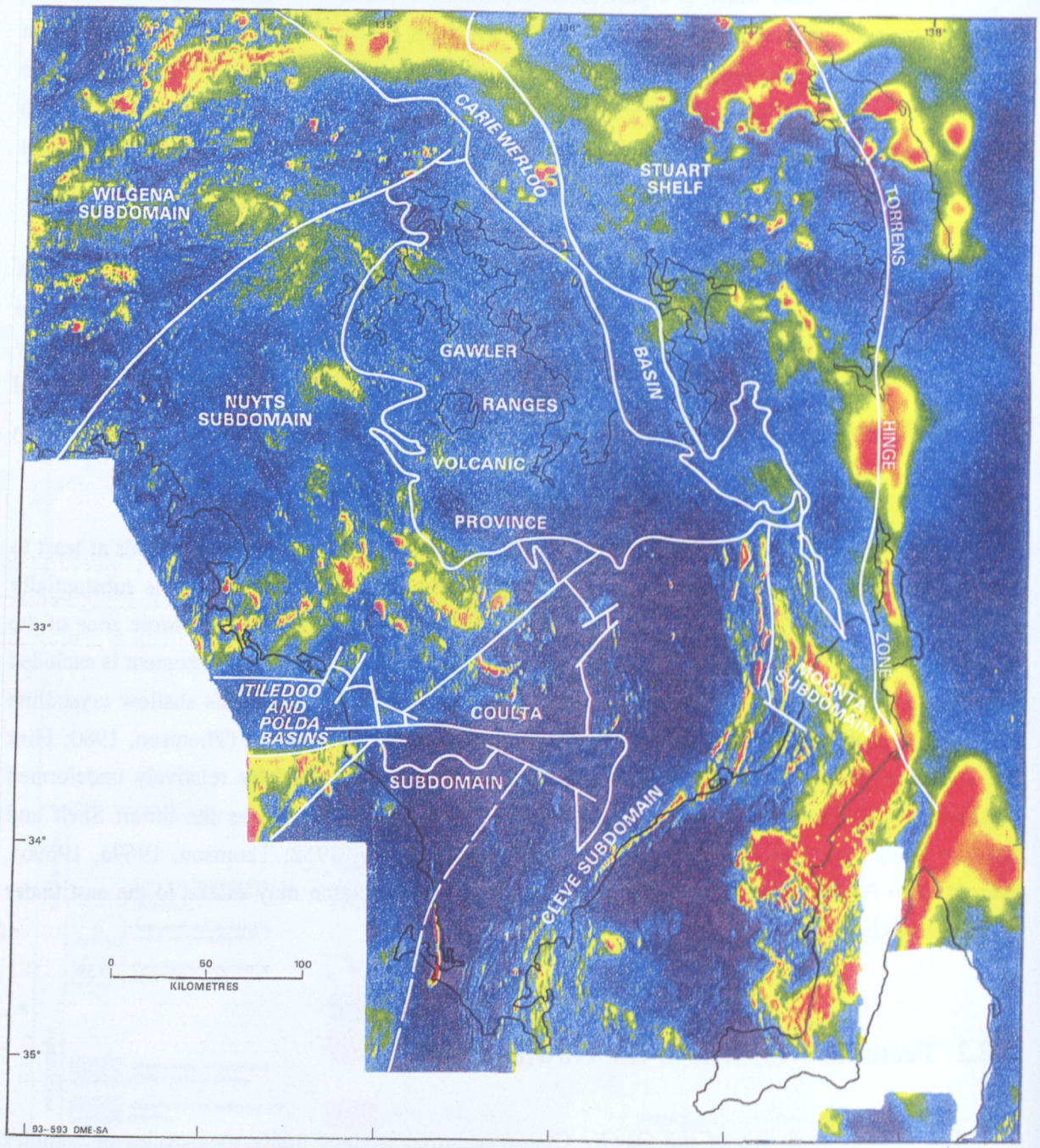

Figure 3.3 Tectonic subdivisions of southern Gawler Craton superimposed on total magnetic intensity image. After Parker (1993).

– The last cratonic megacycle, dated from 1650 to 1450 Ma, has a significantly different tectonic character. Relatively undeformed sediments and felsic volcanics form the flat cover of the north-eastern part of the Gawler Craton. The Gawler Range Volcanic Province which consists of those felsic volcanics (1600 to 1590 Ma) is known as one of the biggest acid volcanic provinces in the world. An orogenic acid magmatism included also large granite plutons of the Hiltaba Suite which accompanied volcanism or were intruded shortly after; about 1590 to 1580 Ma. A broad belt of the Hiltaba Suite granites surrounds the Gawler Range Volcanics. During the last period of tectonic evolution of the craton the Wartaken 'Event' (Thompson, 1969) occurred 1500 to 1450 Ma. This deformation (WD_1) which has also been referred to as D_4 of the Kimban Orogeny (Parker et al., 1988), affected, throughout Eyre Peninsula, basement schists and gneisses. The evidence of this deformation is found in the form of crenulations, kink fold bands, irregularly spaced macro- and mesoscopic fracture zones, major lineaments, quartz veins and cross-folding (Parker, 1993). In the Cowell-Cleve region (Kimba Geological Map, 1:250,000) kink bands are oriented east-west and northwest-southeast. The east-west oriented fractures and shear zones are evident in the Middle Camp area, and major lineaments and cross-folding of similar orientation are present in the Middleback Range.

The region of the crystalline basement has not been substantially deformed or remobilised since 1450 Ma, which was the final stage of cratonisation (Parker and Lemon, 1982; Parker, 1990; Parker, 1994). When consolidation of the craton was completed subsequent sedimentation had a platformal character.

3.2.3 Tectonic Subdomains of the Gawler Craton

The Gawler Craton is subdivided into several tectonic regions or Subdomains of a different structural, metamorphic and stratigraphic character (Parker, 1990). The tectonic boundaries are not clearly defined, often because of poor exposure, therefore, they are often placed along major linear magnetic features. These geophysical lineaments reflect major faults, shear zones (significant for location of the Polda Trough) or boundaries of major rock units within the cratonic crust (Figure 3.3; Parker, 1990). This situation is likely to change significantly as a result of the wide ranging detailed aeromagnetic surveys flown in 1993/94.

The tectonic framework of the southern Gawler Craton on the Eyre Peninsula and Yorke Peninsula is outlined in five major tectonic subdivisions: Coulta, Cleve, Moonta, plus Gawler Ranges and Stuart Shelf. These are illustrated in Figure 3.3 (Parker and Lemon, 1982).

– ***The Coulta Subdomain*** (Thompson, 1980) is a major cratonic area which contains outcrops of Late Archaean and Palaeoproterozoic basement known as the Sleaford Complex (Parker and Lemon, 1982; Thompson, 1980; Webb et al., 1982; Cooper et al., 1976; Webb and Thompson, 1977).

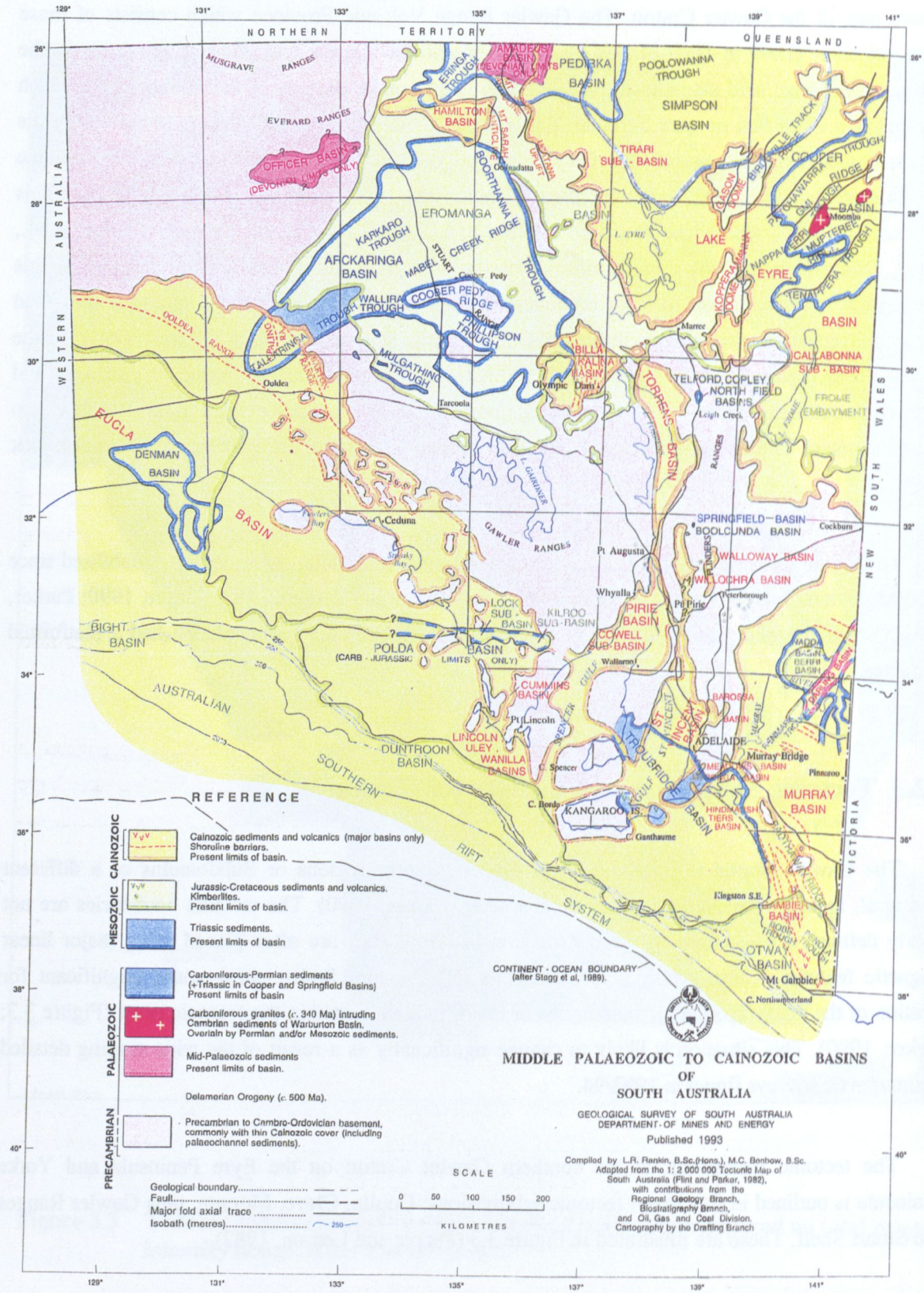

Figure 3.4 Middle Palaeozoic to Cainozoic basins of South Australia.

- ***The Cleve Subdomain*** is a major Palaeoproterozoic to Mesoproterozoic fold belt or 'mobile zone' which extends along eastern Eyre Peninsula to York Peninsula.

- ***The Moonta Subdomain*** is located east of the Cleve Subdomain and extends towards the north under the Stuart Shelf to the Peak and Denison Inliers (Parker, 1993). This subdomain is composed mainly of syn-Kimban Orogeny acid volcanics and clastic sediments metamorphosed and deform by late-Kimban and subsequent tectonic events. Lincoln Complex granitoids and remnants of Hutchison Group metasediments comprise the basement of the volcanics which are overlain by a succession of clastics, the Wandearah Metasiltstone.

- ***The Gawler Range Volcanics Province*** consist of acid volcanics of Mesoproterozoic age (Blissett, 1975; Giles, 1977; Branch, 1978, Stuart, 1990; Parker, 1994) which are outcropping in the central-east region of the craton forming a nebulous ellipsoidal zone. This province overlays the older Cleve and Coulta Subdomains.

- ***The Stuart Shelf*** is not considered as a 'sensu stricto' tectonic unit of the Gawler Craton but as a region of Neoproterozoic to Cambrian platformal sedimentation developed upon the existing craton.

- Towards the south there is part of the Gawler Craton known as ***the Spencer Shelf*** that is also covered by Adelaidean and Cambrian sediments (Sprigg, 1952a; Thomson, 1969b).

The Coulta Subdomain and the north Christie Subdomain are both composed of Archaean to earliest Palaeoproterozoic rocks. Their similarity suggests that they originally formed one large Archaean province which was extended across the Wilgena and Nuyts Subdomains and possibly to the north through the Nawa Subdomain, possibly west to the Coompana Block and perhaps even south across Commonwealth Bay in Antarctica (Figure 3.3; Parker, 1993). The original protolith of the craton (Parker, 1993) on which the younger tectonic units were superimposed was moderately deformed during later Palaeoproterozoic events, but does not contain larger volumes of younger Proterozoic metasediments, volcanics or intrusives. This distinguishes these two areas from the Wilgena, Nuyts and Cleave Subdomains.

Late Palaeoproterozoic to Mesoproterozoic sediments outside the Gawler Range Province are represented by the Pandura Formation of the Cariewerloo Basin, the Subdomain of the Gawler Craton (Figure 3.2; Cowley, 1991a; Cowley and Martin, 1991) and the Blue Range Beds (maximum age 1590 Ma) deposited in the Itiledoo Basin (Flint and Rankin, 1991).

Since the Mesoproterozoic, the Gawler Craton has remained stable with only thin, often wide spread, continental sediments being deposited during the Neoproterozoic, Cambrian, Permian, Mesozoic and Cainozoic (Figure 3.4; Parker, 1990).

CAINOZOIC	Quarternary	Holocene		
		Pleistocene		Bridgewater Formation
	Tertiary	Pliocene		
		Eocene		Poelpena Formation - Tep
MESOZOIC	Jurassic			Polda Formation - Jup Kimberlites
PALAEOZOIC	Permian			Coolardie Formation - CPc
PROTEROZOIC	Neoproterozoic			Kilroo Formation - Pc
	Mesoproterozoic		Hiltaba Suite	Calca Granite - Pγh Phenocrystic Adamellite Granite - Pγb
				Blue Range Beds
	Palaeoproterozoic		Lincoln Complex	Dolerite Dykes - $P\beta_2$ Muscovite-bearing granite - Pγa Carappee Granite - Pγg Granite - Pγm Undiferentiated Granitic Gneiss - Phl
			Hutchison Group	Bansanquet Formation - Pb Yadnarie Schist - Phy Upper Middleback Jaspilite - Phm_2 Cook Gap Schist - Phc Lower Middleback Jaspilite - Phm_1 Katunga Dolomite - Phc Warrow Quartzite - Phn
ARCHAEN			Sleaford Complex	Dutton Suite
				Carnot Gneisses

Table 3.1 Stratigraphic column of the rock units at the Polda Trough area.

3.3 Litho-stratigraphy of the Polda Trough

There are limited outcrops in the study area which is totally covered by Cainozoic sediments. The stratigraphy of the Polda Tough is mainly known from the drill holes, and there are only four holes which intersected sequence of Mesozoic, Palaeozoic and Precambrian sediments: *Columbia-1*, *Mercury-1*, *Colton-1* and *CRA 83KD1A*. Only one drill hole, *CRA 83KD1A*, is onshore.

The stratigraphic sequences of the rock units associated with the Polda Trough are shown in Table 3.1.

3.3.1 Archaean

The Coulta Subdomain, which is a basement of the western and central onshore Polda Trough, is composed predominantly of Archaean to earliest Palaeoproterozoic rocks.

The whole graben is underlain by the Late Archaean to Palaeoproterozoic rocks of the Gawler Craton known as **the Sleaford Complex**. The Sleaford Complex is composed of two distinct units: ***the Carnot Gneisses*** and younger sequence of the granitoide suite, ***the Dutton Suite.***

(i)The Carnot Gneisses

The Carnot Gneisses are composed of thinly layered garnetiferous quartz feldspatic gneisses often intercalated with thin layers of leucogneiss, biotite gneiss, hypersthene bearing felsic gneiss and basic granulite. Hypersthene gneisses also appear as distinct mesolayers. The gneisses in the Cape Carnot area yield an isochrone age of 2412±72 Ma.

(ii) The Dutton Suite

The Dutton Suite is comprised of the Whitby granite and gneissic Kiana Granite which outcrop on the south-west Eyre Peninsula and on the offshore islands. They are the intrusive equivalents of the Carnot gneisses, outcropping along the western side of the Peninsula and have an isochrone age of 2334±109 Ma.

3.3.2 Palaeoproterozoic

The rocks succession of the Cleve Subdomain, which is a Palaeoproterozoic fold belt, overlie Archaean and very early Proterozoic basement, on the eastern side of the Eyre Peninsula. This Palaeoproterozoic fold belt is composed of folded, high-grade metamorphic rocks (***Hutchison Group***) derived mainly from clastic shallow marine sediments, iron formations, carbonates, mafic and also to a lesser extent acid volcanics (Parker and Lemon, 1982). The metasediments were intruded by numerous granitoids (***Lincoln Complex***) during major deformation and metamorphism of the Kimban Orogeny. These Palaeoproterozoic rock units compose the surrounding basement of the eastern-onshore part of the Polda Trough.

(I) Hutchison Group

The Sleaford Complex is unconformably overlain by the lower member of the Hutchison Group, the Warrow Quartzite. The Hutchison Group is a sequence of highly deformed and metamorphosed mixed clastic and sedimentary rocks which range in age from late Archaean through to Palaeoproterozoic. This sequence possibly represents a number of cyclic transgressions and regressions either across the shelf or within a major basin deepening towards the eastern side of the peninsula. Deposition was terminated by the Kimban Orogeny which deformed and metamorphosed the sequence to upper amphibolite facies, this event being the final before cratonisation of the Gawler Craton.

- **Lithology of the Hutchison Group**

The Hutchison Group is a succession of metamorphosed mixed clastic and chemical sedimentary rocks, consisting of calc-silicate and quartzite (***Warrow Quartzite***) carbonate (***Katunga Dolomite***), banded iron formation (***Lower and Middleback Jaspelite***) and schist (***Cook Gap Schist and Yadnarie Schist***). ***The Bosanquent Formation*** also is included in the Hutchison Group.

(i) Warrow Quartzite - P*hw*

The Warrow Quartzite is the basal unit of a Hutchison Group. At its base occurs well banded calc-silica gneiss (P*hd*). The unit consists of alternating layers 50-350 mm thick of white dolomitic marble (with minor muscovite and microcline) and diopside-microcline-quartz-muscovite-dolomite calc-silicate. In thin section the calc-silicate bands are medium grained and granoblastic to granoblastic-elongate. Diopside is inter-grown with quartz, with optical continuity between the grains of diopside which suggests that they were originally coarse-grained porphyroclasts 10-15 mm wide. The Warrow Quartzite outcrops at Toolgie Hill (southern margin of the Polda Trough), Callis Hill and Dark Peak (northern margin of the Polda Trough) and in a number of small exposures located easterly from the Polda Trough. It is a medium to coarse-grained massive quartzite. Locally cross-bedding is preserved. The Warrow Quartzite grades upwards from massive and muscovite-feldspar rich quartzite near the base, to flaggy, coarse-grained, sugary quartzite with numerous pelitic interbands near the top. The Warrow Quartzite probably represents an arcosic sand sequence, grading from fluvial in the west to marginal-marine in the east (Cowell to Cleve). The marine transgression was directed westwards onto the Coulta Subdomain (Parker and Lemon, 1982).

(ii) Katunga Dolomite - P*hk*

The Katunga Dolomite overlies locally the Warrow Quartzite, and contains massive grey, pink and white dolomitic marble, occasionally silicified and altered to opalite, with minor layers of fine-grained quartzite and calc-silicate gneiss. The Katunga Dolomite which varies in thickness and is absent in many localities, comprises a series of metamorphosed shallow marine carbonate and marble beds.

(iii) Lower Middleback Jaspilite - Phm_1

The bended iron formation of the Lower Middleback Jaspilite overlies and inter-fingers with the Katunga Dolomite, but also directly overlies Warrow Quartzite. This unit is well exposed towards the east of the Polda Trough marginal-end, especially in the Cleve Council pits. It contains silicate-facies iron formation consisting of recrystallised chert and graphitic chert with a low iron content. The banded iron formation, which grades into and is locally interlaid with the overlying Cook Gap Schist, represents a period of marine chemical sedimentation.

(iv) Cook Gap Schist - P *hc*

In the Cleve Uplands, east of the marginal-end of the Polda Trough, this unit is locally known as the Mangalo Schist. The radiometric age of this unit is dated 1688±76 Ma (Rb-Sr). The bottom layer of the schist is gradational from the Lower Middleback Jaspilite and Katunga Dolomite or even from the Warrow Quartzite. The unit consist of well layered and foliated quartz-veined, semi-pelitic biotite-muscovite-garnet schist and gneiss, with local minor quartz-feldspar psammitic interbeds. Within the schist, well foliated, multiply deformed and concordant amphibolite bodies ($P\beta_1$) are common. Textures vary from fine grained and schistose, to massive and medium, to coarse grained. Coarse hornblende grains are randomly orientated, while the finer grained crystals commonly form a strong mineral lineation. According to Parker (1978) amphibolite has a chemical composition consistent with a quartz-tholeiitic basalt and may, therefore, represent either basaltic volcanics synchronous with sedimentation or basic intrusive sills. Alternatively, the amphibolite bodies (which are best exposed in the Mangalo Creek, east of the Polda Trough) may represent metamorphosed calcareous sediments.

In the Cockabidnie Reservoir, almost on the north-east corner of the Polda Trough, there is local magnetite-rich gneiss and calc-silicate bands inter-layered with schist. Some of these carry anomalous base-metal concentrations. Cook Gap Schist has gradational contact with the overlaying Upper Middleback Jaspilite.

(v) Upper Middleback Jaspilite - Phm_2

This unit is also locally known as the Mt. Shannon Iron Formation. In the Mangalo Creek, east of the Polda Trough, the unit grades from the semi-pelitic Cook Gap Schist into massive to poorly banded, reddish pink to grey dolomite plus crenulated mica schist. These pass upwards into inter-layered cherty quartzite and medium to fine-grained pink-white dolomite. The quartzite is fine grained, laminated and varies from grey to red with jaspilite bands 5-30 mm thick (Parker et al., 1988). Rocks recovered from the drill holes (CRA and Shell, 1985b) in the region of Cockabidnie Corner, which is a north-east corner-margin of the Polda Trough, include banded calc-silicate and quartz-magnetite gneiss. The unit also combines brecciated, cherty and ferruginous quartzite, graphitic schist, dolomite and quartz-grunerite-cummingtonite-magnetite gneiss.

The iron formations represent a period of marine transgression and chemical sedimentation (Parker and Lemon, 1982).

(vi) Yadnarie Schist - *Phy*

The Yadnarie Schist was only recognised east of the Polda Trough marginal-end, in the Cleve Uplands (Kimba Geological Map, 1:250,000). The minimum thickness of this unit is at least 1000m; the upper contact is not exposed. The unit consists of fine-grained muscovite-biotite-quartz-feldspar schist. The Cook Gap Schist and Yadnarie Schist are similar in outcrop appearance, but, the Yadnarie Schist has a greater proportion of muscovite, and amphibolite is absent. An outcropping weathered Yadnarie Schist sub-unit (*Phyp*) in the Campoona-Cockabidnie Corner area, north-east of the Polda Trough eastern margin, consists of iron-stained, quartz-sericite banded metasiltstone with sericite aggregates replacing sillimanite porphyroblast, with minor interlayered quartz-magnetite gneiss. The Yadnarie Schist has a characteristic light to dark grey banded appearance. This unit represents a second major period of regression.

(vii) Bosanquet Formation - *Pb*

This stratigraphic unit was only recognised in one location on the entire Gawler Craton, a five kilometres square zone east of Carappee Hill, therefore, its presence in the basement underlying Polda Trough sediments is not certain (Kimba Geological Map, 1:250,000). U-Pb isotopic radiometric dating place this unit at an age of 1845±9 Ma (Rankin et al., 1988). This formation consist mainly of large crystals of rhyodacite containing abundant microcline and quartz phenocrysts within a recrystallised matrix of quartz, feldspar and biotite. The succession represents a period of contemporaneous acid volcanism and carbonate sedimentation with considerable conglomerate input. The rock geochemistry of volcanics within the Bosanquet Formation is dissimilar to other Palaeoproterozoic volcanics of the Gawler Craton. The contact of the Bosanquet Formation with Upper Middleback Jaspilite is ambiguous.

The combined geochronology and geochemistry evidence suggest that the Bosanquet Formation was deposited either as part of the Hutchison Group in a restricted area, or, represents a distinct younger episode of vulcanism and sedimentation older than the Myola Volcanics in the Whyalla region (Rankin et al., 1988). The similarity of some calc-silicate beds inter-layered with volcanics to those in the banded iron formation suggests affinity with the Hutchison Group.

- **Tectonic framework of the Hutchison Group**

Palaeoproterozoic sediments of the Gawler Craton are best exposed on the eastern Eyre Peninsula in a major Palaeoproterozoic to Mesoproterozoic fold belt or mobile zone known as the Cleve Subdomain of the Gawler Craton. Within the western part of this fold belt, the sediments were highly deformed and metamorphosed forming a series of complexes, elongated, dome-and-basin shaped structures trending NE-SW but swinging around to N-S on northern Eyre Peninsula. Such tectonic setting is clearly visible just towards the east and north-east of the eastern margin of the Polda Trough (Kimba Geological Map 1:250,000). These structures were developed during an orogenic event about 1500-1450 Ma known as the Kimban Orogeny. During this major period of complex deformation, metamorphism and plutonism three events have been recognised:

- regional metamorphism and schistosity formation D_1
- overturned isoclinal folding D_2
- upright, open folding and mylonitisation D_3.

A later but much weaker deformation known as a Wartaken Event (Thomson, 1969a, 1969b) occurred about 1500-1450 Ma.

(II) Lincoln Complex

The upper part of Palaeoproterozoic is represented on the Gawler Craton in the vicinity of the Polda Trough by a series of syn-Kimban Orogeny granite and granitic gneiss and also minor mafic intrusives, with a complex relationship of intrusion through the Kimban Orogeny (Parker et al., 1988). These rocks outcrop around the eastern end of the Polda Trough. Some of the members of the Lincoln Complex were intersected in drill holes north-east from the Talia Caves (Kimba Geological Map, 1:250 000). The following successions of the Lincoln Complex stratigraphic unit are distinguished in the region surrounding the Polda Trough:

(i) Undifferentiated Granitic Gneiss - Pl

This unit includes fine to medium-grained orange to grey, well foliated quartz-feldspar-biotite, granitic gneiss, massive to foliated medium-grained granite and microgranite, migmatite gneiss, aplite and quartz-feldspar-muscovite-garnet-tourmaline pegmatite.

The well foliated granitic gneiss is considered to have been granite injected either *pre-* or *syn-*D_1 of the Kimban Orogeny, and subsequently imprinted with a variable intensity foliation (S_{1-2}). The gneiss is probably equivalent to Minbrie Gneiss (Parker, 1983).

East of the marginal-end of the Polda Trough, in the Gam Valley to High Bluff area, granite and granitic gneiss intrude the Hutchison Group. Schist has been migmatised, and both schist and iron formation occur as rafts within the gneiss. It is possible that partial melting of Hutchison Group metasediments at a greater depth was the source of some of the granite and gneiss. Interlayering with and migmatisation of the Warrow Quartzite by quartz-feldspar-muscovite granitic gneiss are seen within the drill-core from the Campoona Syncline-Cockabidnie Corner area, north-east marginal corner of the Polda Trough (Kimba Geological Map, 1:250 000; CRA and Shell, 1985a).

The Undifferentiated Granitic Gneiss were injected throughout the Hutchison Group metasediments and are either tectonically or intrusively intercolated with Archaean garnet gneiss (*APsg*) near 'Windzel', about 30 km NNE from the Polda Trough.

(ii) Granite - Pγm

A pink to grey, medium grained quartz-feldspar-biotite granitic gneiss is well exposed in several outcrops, distributed NNE of the Polda Trough (Kimba Geological Map, 1:250 000); for example near the Balumbah railway siding where it intrudes the Undifferentiated Granitic Gneiss.

The granite contains abundant pegmatite veining, and more gneissic varieties contain garnet. The weak to moderate intensity foliation suggest that the granite was intruded during the D_2 tectonic event of the Kimban Orogeny, making it an equivalent to the Middle Camp Granite (Parker 1978, 1983).

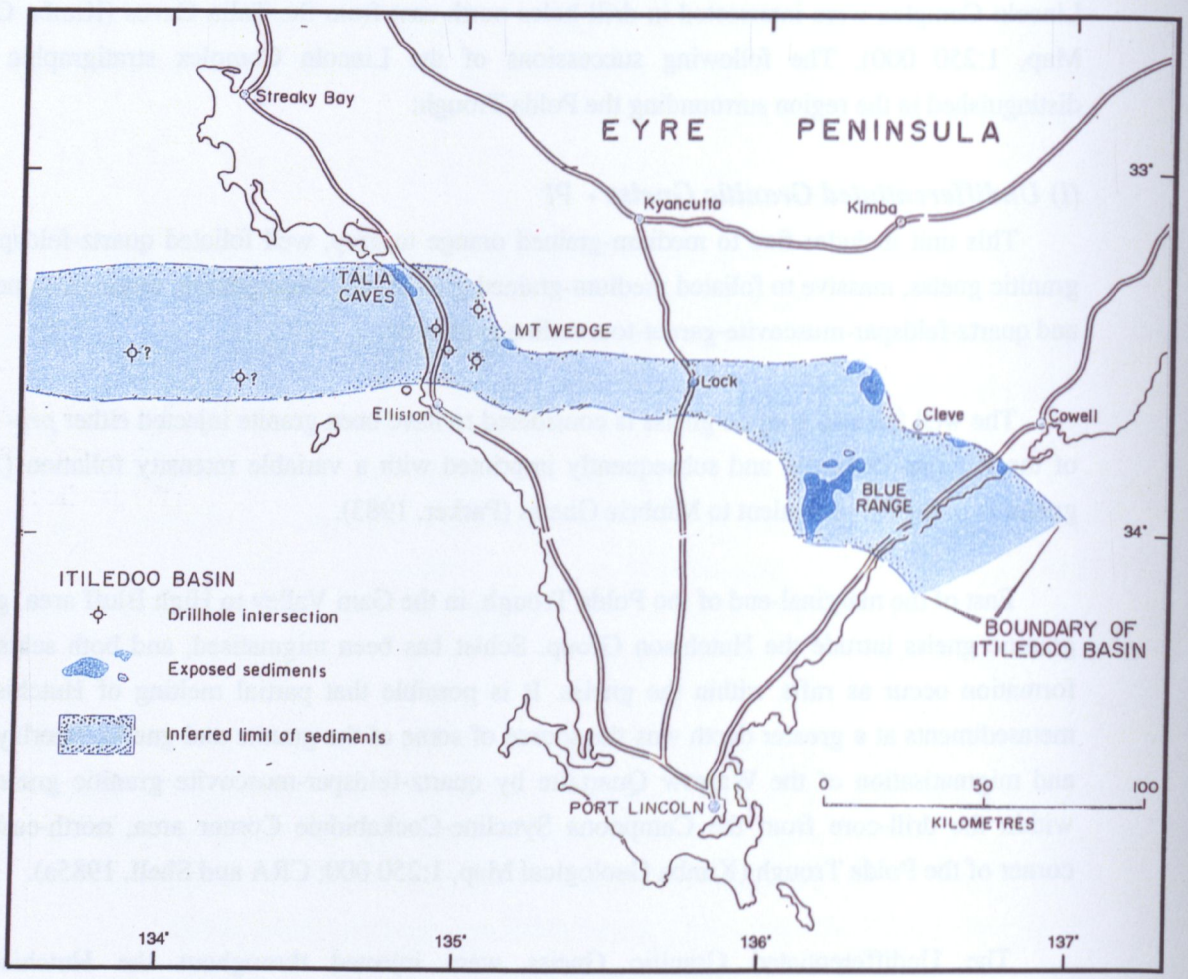

Figure 3.5 Distribution of the Itiledoo Basin. After Flint (1992).

(iii) Carappee Granite - $P\gamma g$

This unit forms an inselberg of Carappee Hill, and also occurs on the western flank of the Dark Range and Caralue Bluff, which is immediately north of the north-east marginal corner of the Polda Trough (Kimba Geological Map, 1:250 000). This granite is relatively homogenous, consisting of tabular microcline megacrysts up to 20 mm in length with a fine to medium grained matrix of quartz, feldspar and biotite. The granite is in contact with the Warrow Quartzite on the eastern flank of the Darke Range.

The U-Pb zircon isotopic data indicate an age of 1689±59 Ma for the Carappee Granite, with evidence of a high percentage of radiogenic lead loss from the zircon grains (Flint et. al., 1988a). This age is slightly younger then the U-Pb age of 1738±68 Ma obtained for the Middle Camp Granite (Fanning, 1987) and the Carappee Granite is, therefore, interpreted to have been intruded during the period spanned by D_2 and D_3 tectonic events of the Kimban Orogeny.

(iv) Muscovite-bearing Granite - $P\gamma a$

This is a massive to weakly foliated, coarse-grained, cream to pink microcline-quartz-plagioclase-muscovite-garnet granite. The granite is best exposed in the Poornamookinie Creek as sills intruding the Warrow Quartzite. This unit is probably equivalent to the Carpa Granite outcropping near Elbow Hill (Parker, 1983). It intruded the Hutchison Group before or during an early stage of the D_3 event of the Kimban Orogeny. Two generations of pegmatite occur within the granite :

- garnetiferous pegmatite synchronous with granite intrusion, and later
- coarse grained, tourmaline-bearing pegmatite with sharp intrusive contacts.

(v) Dolerite Dykes - $P\beta_2$

North of the town of Cleve and also in the drill hole *PAC ZN1* to *PAC ZN5* (Kimba Geological Map, 1:250 000), narrow north-east trending, fine-grained plagioclase-pyroxene-hornblende dolerite dykes discordantly intrude both the Cook Gap Schist (P *hc*) and concordantly the amphibolite ($P\beta_1$) of the Hutchison Group. The dykes locally have a weak foliation, and are intensively chloritised. The age of the intrusions is uncertain but is estimated as $post-D_3$ and about 1600 Ma (Parker et al., 1988).

3.3.3 Mesoproterozoic

Mesoproterozoic rocks unconformably overlie the Hutchison Group and are represented by ***the Blue Range Beds***. Unlike the older rocks they are not highly metamorphosed.

(I) Blue Range Beds

The Blue Range Beds occur in outcrops and drill holes in the vicinity of the presently known Polda Trough structure. The extent of the depositional basin is unknown. The known distribution of this formation is limited to the areas shown in Figure 3.5, which were interpreted by previous workers to be a part of the large Mesoproterozoic basin, known as the Itiledoo Basin. Figure 3.2 presents the generally accepted distribution of the Mesoproterozoic rocks in South Australia. The Itiledoo Basin is

usually described as '... a major elongated east-west trough containing up to 2500 m of sediments deposited in a braided stream-alluvial fan environment... Flint (1993)'.

The Blue Range Beds were probably also intersected in some of the drill holes in the vicinity of Mount Wedge (*Mucka Cuddla-1* and *WF8*). This formation was commonly considered to be more extensive below the Polda Trough.

Fluvial sediments, deposited unconformably on the Archaean to Palaeoproterozoic basement consist dominantly of unmetamorphosed sandstone and conglomerate (Flint and Parker, 1981).

These unmetamorphosed arenites outcrop in several areas on the central Eyre Peninsula and the Mount Wedge and Talia Caves area on the west coast (Geological Map Kimba and Elliston, 1:250,000). The deposition of the Blue Range Beds occurred either synchronous with or after intrusion of the Hiltaba Suite (Flint, 1992).

The sediments in the Mount Wedge and Talia Caves area (north-west edge of the onshore Polda Trough) are gritty to gravelly, coarse-grained sandstone and medium coarse-grained arkosic sandstone. Fine-grained sandstone, siltstone and silty shale horizons are occasionally present (Flint, 1992, 1993).

Near the 'Ningana' homestead, the basal conglomerate is not exposed, but round quartz cobbles up to 0.2 m diameter are common as residuals (Parker et al., 1988). The lowest unit exposed is a pebbly conglomerate with subrounded to rounded quartzite clasts, overlain by interbedded granular conglomerate and sandstone. The conglomerate is poorly sorted, with abundant granules in a detrital quartz, feldspar and mica matrix.

At Blue Range, sandstone is more dominant and better sorted, and is medium to very coarse grained with sub-angular to surrounded arcosic matrix.

Low angle trough and planar cross-beds with foresets up to 0.5 m high are ubiquitous, and graded bending is common. Overturned forset, sandstone dykes and slumped bedding occur also (Flint and Parker, 1981).

The thickness of the Blue Range Beds is unknown. Drill holes evidence shows 401 m of preserved sediments in SADME *Newland-1*, 14 m in *Colton-1*, 151 m in *Mercury-1* and 467 m of clastics intersected in *Columbia-1* (Gatehouse, 1981a; McClure 1982a, 1982b). Flint (1992), based on the interpretation of seismic profiles in the offshore section, infers that the true total thickness of the Blue Range Beds is approaching 2500 m.

The interpreted age and nomenclature of the sediments has varied considerably, but the unconformable basal contact with the Hutchison Group, and the presence of the rhyolite (possible Gawler Range Volcanics) pebbles in conglomerate near Talia Caves, indicate a maximum age of

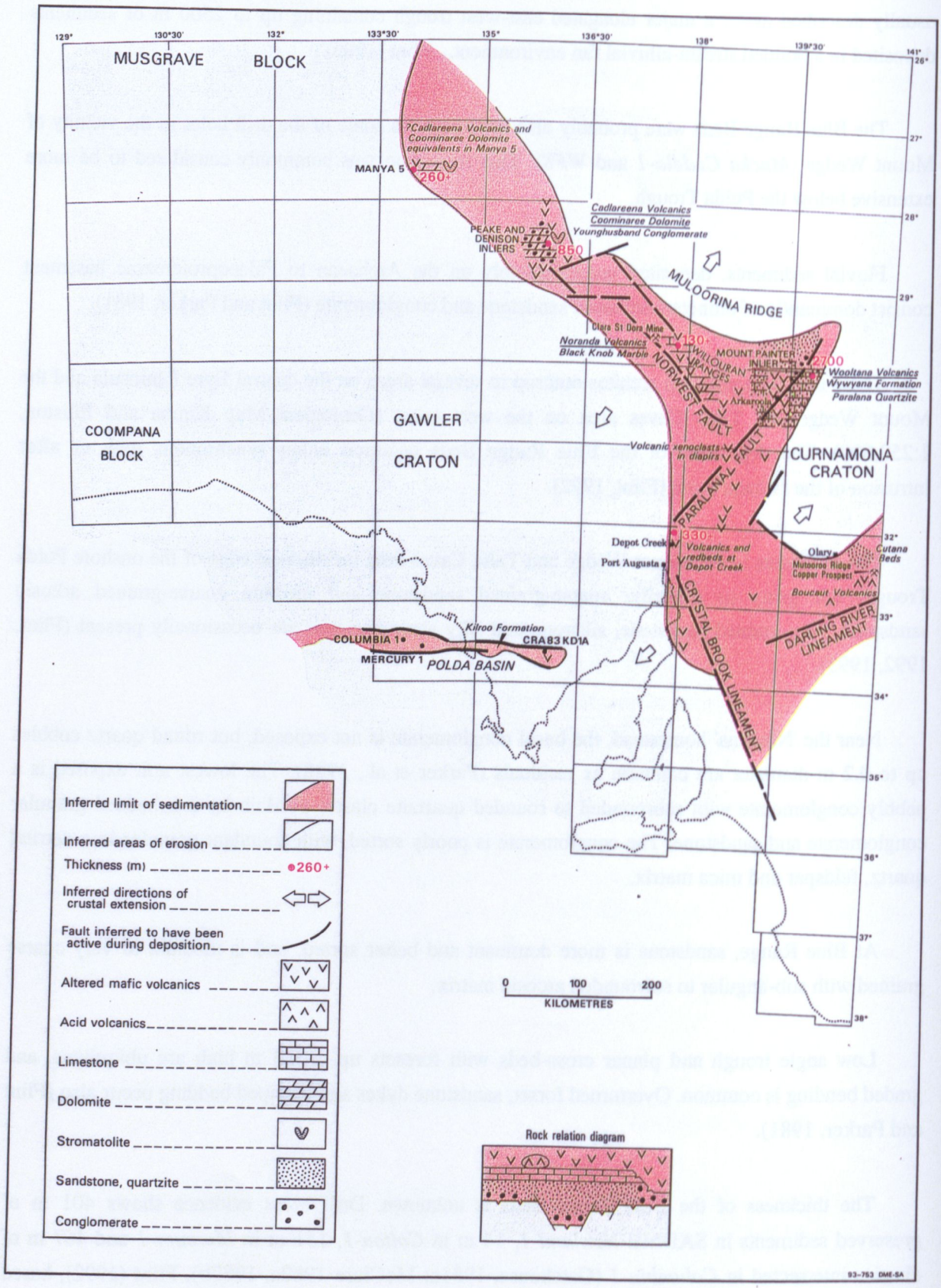

Figure 3.6 Inferred limit of the Kilroo Formation. After Preiss et al. (1993).

about 1590 Ma, which is synchronous with the Gawler Range Volcanics (Flint, 1989). No contacts have been observed between the Blue Range Beds and granite bodies of the Hiltaba Suite.

The Blue Range Beds have been correlated with the Mesoproterozoic Corunna Conglomerate of the Moonabie Range, and also correlation with the Pandurra Formation is suggested (Flint and Parker 1981).

(II) Hiltaba Suite

Granite of the Hiltaba suite which was emplaced after the Kimban Orogeny, is represented in the study area by two major varieties: ***Phenocrystic Adamellite Granite*** and ***Calca Granite*** and its lithological equivalents.

(i) Phenocrystic Adamellite-Granite - Pγb

The massive phenocrystic granite and adamellite, with large pink potassium-feldspar phenocrysts and white-green plagioclase outcrops offshore on several islands south of the Polda Trough. Numerous exposures are also visible on the Eyre Peninsula, north of the Polda Trough.

Radiometric age (Rb-Sr) of the offshore samples was recorded as 1572±229 Ma and 1550-1585 Ma (Webb et al., 1982). The isotopic age of the granite from the drill-core from *Wudina-1* was dated as 1519±67 Ma with initial ratio 0.7058±0.0082 (Webb et al., 1986).

(ii) Calca Granite - Pγh

Characteristically red to pink, massive coarse-grained granite and adamellite with veins of pegmatite and aplite outcrop offshore on the southern flank of the Polda Trough on Flinders Island, Waldegrave Island and several other small islands (see Elliston Geological Map, 1:250 000). The Calca Granite litho-stratigraphic unit is named after the geographic location of the major outcrops of this rock in the Calca region, which is the most western part of the Eyre Peninsula on the northern flank of the Polda Trough. The Calca Granite is an equivalent type to the Hiltaba Suite granite at Hiltaba H.S. in the Yardea region. The radiometric age was dated as 1456±26 Ma (Rb-Sr).

3.3.4 Neoproterozoic - Kilroo Formation - *Pc*

The oldest unit confined entirely to the Polda Trough is the Kilroo Formation of Neoproterozoic age. The unit is not exposed and is generally overlain by Carboniferous to Permian glacial diamictite, the Coolardie Formation.

The deepest onshore stratigraphic borehole, *CRA 83KD1A* (total depth equal 1398.2 m), drilled on the eastern part of the Polda Trough, intersects 792.9 m of flat-laying sediments and volcanics defined as the Kilroo Formation (Flint et al., 1988b). Flint et al. (1988b) suggest a probable correlation of this formation with the rock unit which was intersected in the stratigraphic hole *Colton-1* (110.0-124.65 m) located about 100 km to the west of the *CRA 83KD1A*. This formation is also correlated with rock units intersected in two offshore wells: Columbia-1 (771.0-1701.0 m) and *Mercury-1* (886.0-3100.0m; Figure 3.6; McClure, 1982a, 1982b; Rankin, 1993).

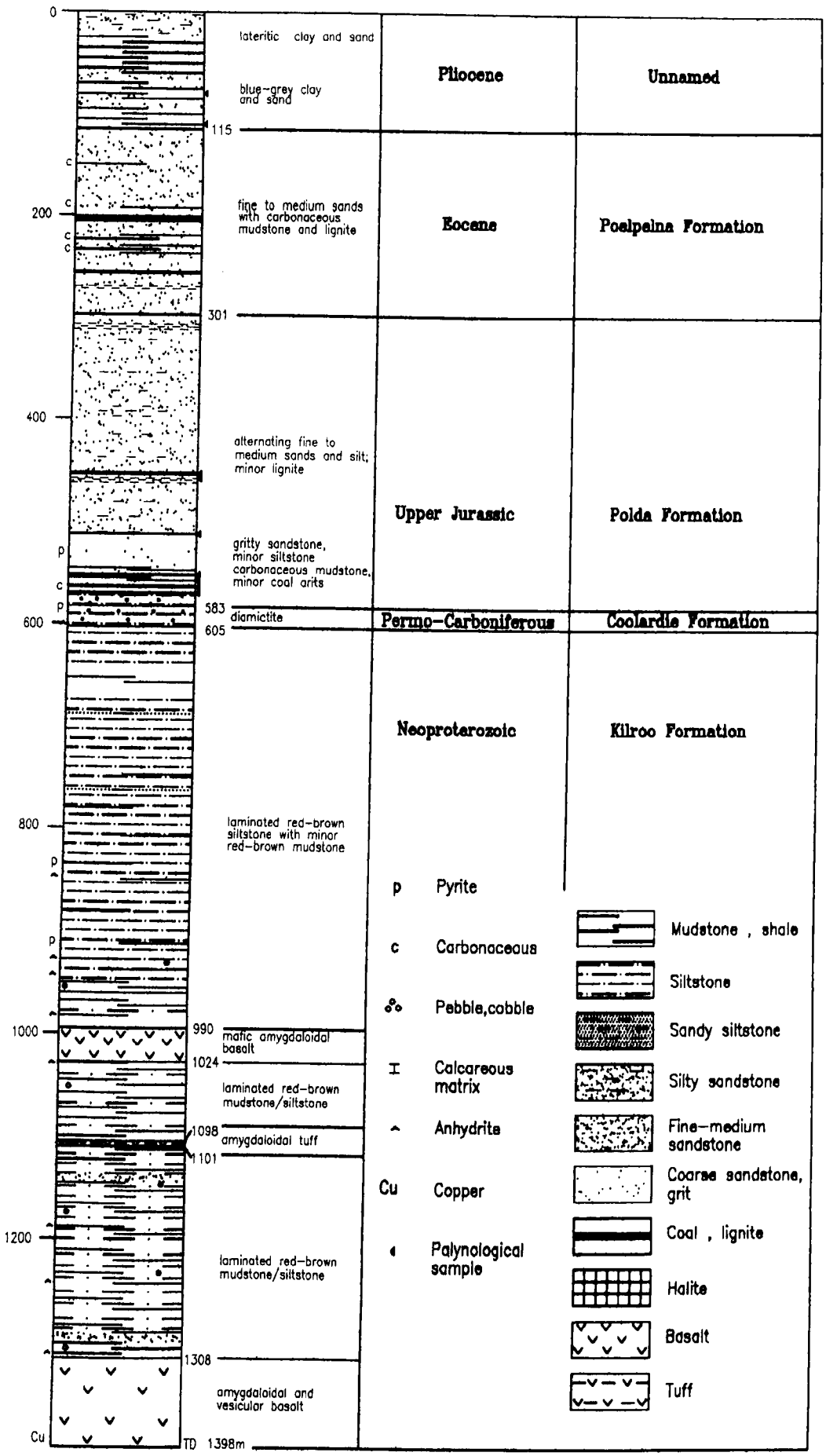

Figure 3.7 Lithostratigraphic log of hole CRA 83KD1A.

Based on the drill hole data, the Kilroo Formation was interpreted to be wide spread throughout the deeper sections of the basin (Flint, Fanning and Rankin, 1988). The thickness ranges from at least 793 m in *CRA 83KD1A* to possibly 2214 m in *Mercury-1* assuming the offshore red-beds are correlational with onshore Kilroo Formation. The formation consists of mixed clastics, evaporites and volcanics. In *CRA 83KD1A*, two horizons of multiple amygdaloidal basalt flows and one thin andesite crystal tuff are interbedded with three intervals of clastic sediments. The clastics sediments are reddish brown laminated siltstone and mudstone with minor sandstone with thin laminations, and graded bedding. The sediments contain abundant detrital quartz, feldspar and mica. Additionally aggregates, layers and veins of anhydrite are common.

The basalts are medium to coarse grained with sub-ophitic plagioclase laths, clinopyroxene, pseudomorphosed olivine and opaques within a very fine-grained, altered, chloritic matrix. Amygdales up to 10 mm in diameter are abundant at the top of the multiple volcanic flows, consisting of chlorite, or chlorite rims with centres of calcite and large clusters of radiating prehnite.

A 2.6 m thick andesite crystal tuff contains pumice and glass shards, angular fragments of quartz and feldspar in a chlorite-calcite-opaque matrix. Within the tuff, ellipsoidal amygdales are common; constituent minerals are chlorite, calcite and anhydrite.

There are no volcanics found in *Columbia-1* and *Mercury-1*, but similar laminated reddish brown mudstone is associated with medium grained sandstone, carbonate-cemented sandstone and siliceous siltstone. Evaporites also occur, particularly in *Mercury-1* which contains a 1707 m of massive halite with minor siltstone interbeds.

The base of this formation is ambiguous; it is possibly present in *Columbia-1* and *Mercury-1* where brecciation, silicification and discontinuity in bedding orientation suggest a stratigraphic break between the red-brown clastics and underlying white quartzose sandstone. It was postulated by Rankin (1993), that the lower sandstone may represent a continuation of the Kilroo Formation or an older sedimentary unit, the Blue Range Beds. In the hole *CRA 83KD1A*, the top of the Kilroo Formation is disconformably overlaid by glacigene diamictite of the late Palaeozoic Coolardie Formation.

The environmental scenario in which sedimentation of the Kilroo Formation occurred is described as an intracratonic graben or rift valley with predominantly basic volcanism contemporaneous with sedimentation in the fluvial, playa-lake system under arid, terrestrial conditions. According to Rankin (1993) such association may suggest that the Polda Trough was a tectonically active intracratonic rift graben with associated volcanism.

(I) Geochronology

Radiometric dating by K-Ar isotope analysis was carried out on plagioclase and clinopyroxene minerals from five amygdaloidal basalt samples from *CRA 83KD1A*, two from the upper basalt layer and three from the lowermost basalts (Flint et al., 1988b).

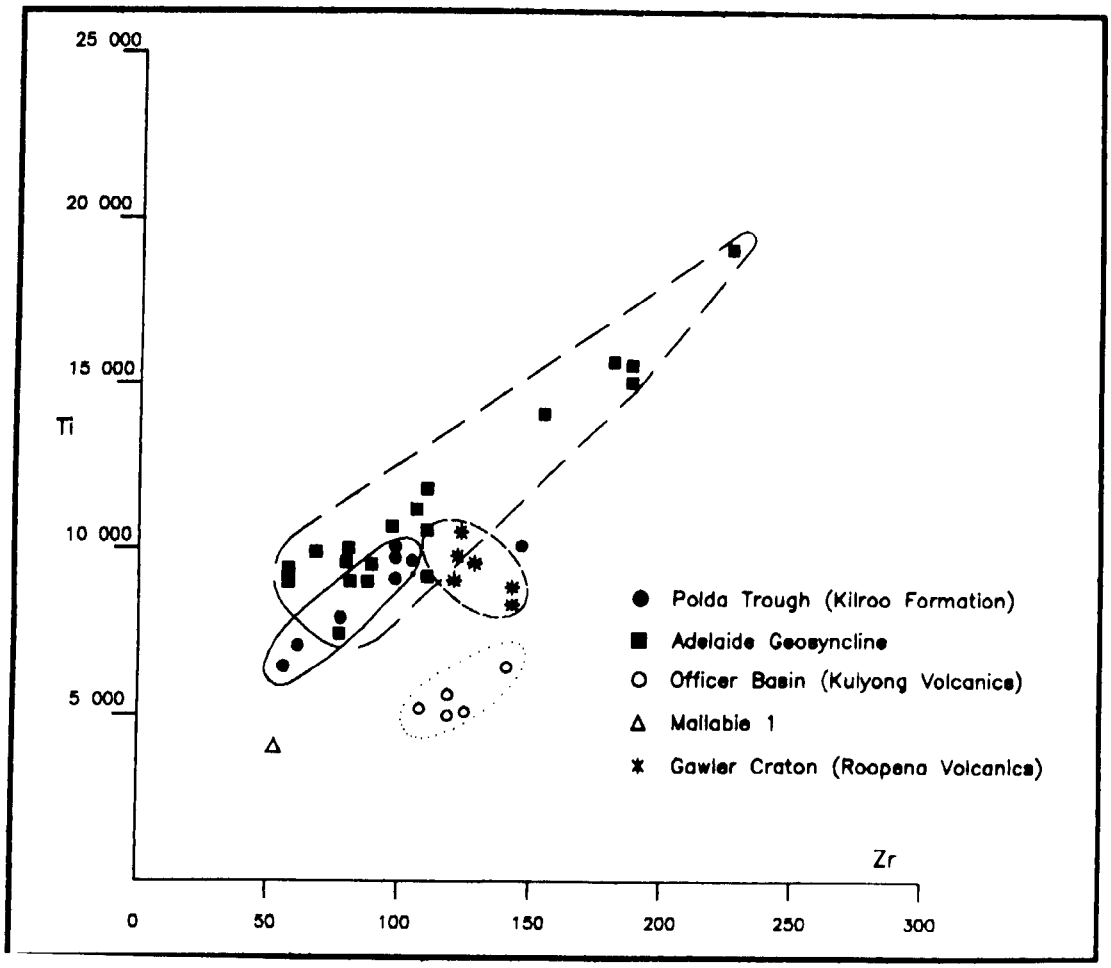

Figure 3.8(a) Comparison of Ti/Zr ratio of basic volcanics in South Australia. After SADME.

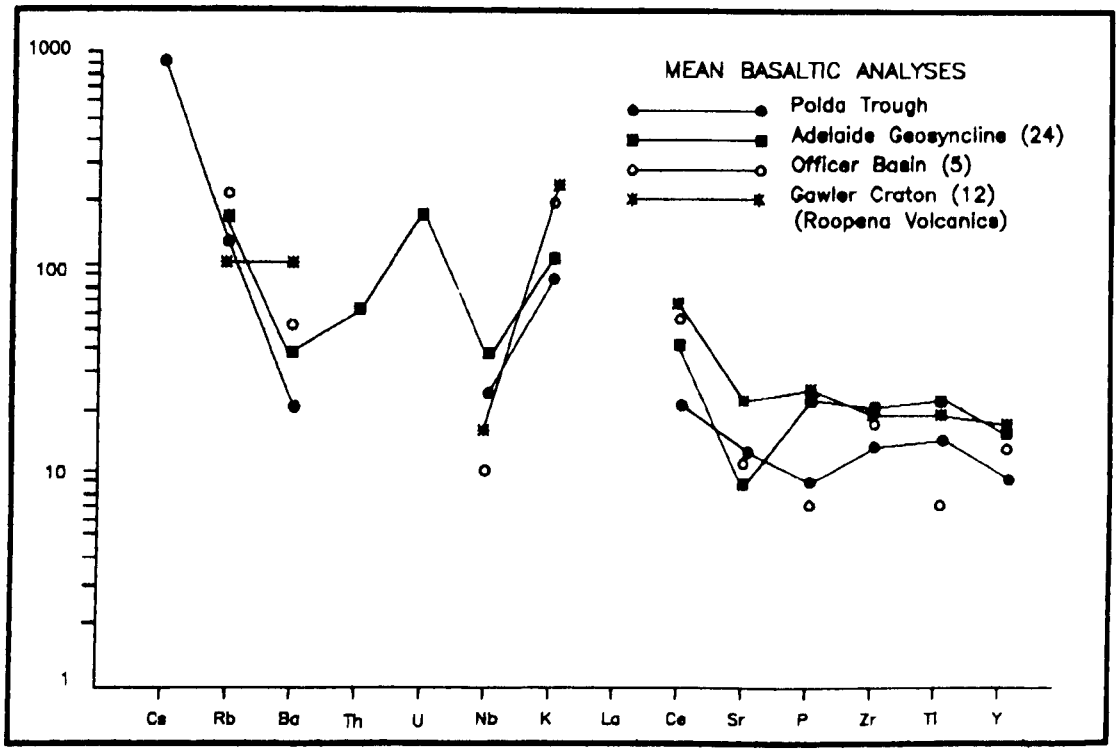

Figure 3.8(b) Trace element composition of volcanics from the Polda Trough, Adelaide Geosyncline, Officer Basin and Gawler Craton. After SADME.

- The pyroxene age range from 884±97 Ma to 235±15 Ma (K content is abnormally low). The spread of clinopyroxene ages suggests that the clinopyroxene grains did not remain closed systems to K and Ar after crystallisation.

- The plagioclase K-Ar ages of 768±9 Ma and 764±42 Ma provide better estimates of the minimum age of crystallisation for the basalts than clinopyroxene ages.

The plagioclase ages are similar to the age of the Rook Tuff in the Willouran Ranges of the Northern Adelaide Geosyncline. The Rook Tuff formed simultaneously with early Adelaidean sedimentation and has a U-Pb zircon age of 802±10 Ma (Fanning et al., 1986). Base on this similarity with the Rook Tuff, collectively, K-Ar isotopic ages imply that evaporitic red beds and inter-layered amygdaloidal basalts of the Kilroo Formation in the eastern Polda Trough are also Neoproterozoic (Adelaidean) rather than previously assumed Palaeozoic age (McClure, 1982a, 1982b; CRA Exploration Pty Ltd, 1984).

(II) Geochemistry

The results of the silicate and trace element analysis of nine basalt samples from *CRA 83KD1A* (Figure 3.7) were compared with the geochemistry of assumed Cambrian amygdaloidal basalts of the Kulyong Volcanics from the Officer Basin (4742 RS 1-5; Flint, Fanning and Rankin, 1988), altered basalt of unknown age from drill hole Mallabie-1 on the eastern Nullabor Plain (5034 RS 1), amygdaloidal basalts from the Stuart Shelf and basal successions in the Adelaide Geosyncline (6333 RS 45, 6334 RS 94-99, 6434 RS 1-10, 6041 RS 161-164, 6737 RS 1167-1169) and altered basalts of the Mesoproterozoic Roopena Volcanics (6332 RS 476-487).

On the Pearce and Cann (1973) Ti/100-Zr-3Y triangular diagram, often used to determine the tectonic setting of basalts, the plot of the basalts from both the Polda Trough and Adelaide Geosyncline indicates the 'within the plate basalts'. Analyses of the Kulyong Volcanics from the Officer Basin, plotted on this diagram, indicate the 'volcanic-arc basalt' type (Figure 3.8(a)).

On the chondrite-normalised diagram (Figure 3.8(b) showing the mean basaltic analyses), the basalts from the Polda Trough and Adelaide Geosyncline show a similar pattern, but with the former having consistently lower chondrite-normalised values. Sr, which is a relatively mobile element, is the only exception. The Kulyong Volcanics and Roopena Volcanics exhibit very different patterns which are also illustrated in the Ti- Zr discrimination diagram (Figure 3.8(a)). Geochemical similarities between basalts from the Polda Trough and the Adelaide Geosyncline are further supported.

A comparison of basalt from Mallabie-1 to other volcanics is inconclusive, probably due to the high degree of alteration in the only sample, which may also not be representative.

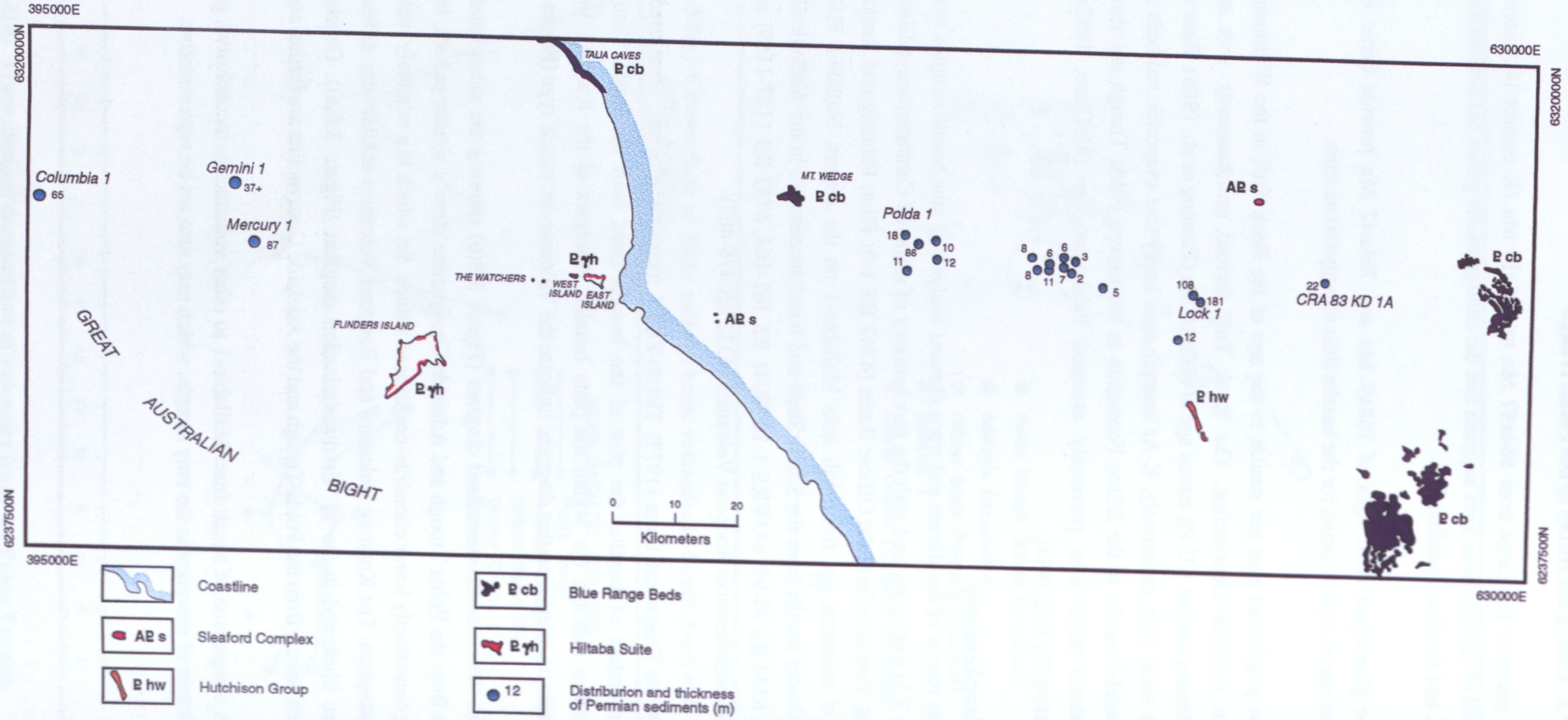

Figure 3.9 Extent of the Coolardie Formation.

3.3.5 Palaeozoic - Coolardie Formation - *CPc*

The glacigene sediments of the Coolardie Formation of Permo-Carboniferous age form a wide spread veneer in the Polda Trough. This sequence marked a prominent unconformity with the underlying red-bed sequence of the Neoproterozoic Kilroo Formation.

The Coolardie Formation does not have surface exposure, and its occurence is known only from drilling. Figure 3.9 shows the distribution of drill holes which intersected Permian sediments. Only the partial thickness of this sequence is known. The thickest sections are in *Lock-1* and *Polda-8*, where respective thicknesses of 181 m and 108 m were recognised.

The Coolardie Formation is interpreted as a series of glacially derived diamictite beds and other sedimentary units. Brown, grey, green and white diamictite, mudstone, sandstone and siltstone beds are characteristic for this formation. Palynology of core samples collected from drill hole *Lock-1* (Cooper et al., 1982; Kwitko, 1982) correlate this unit with the lower Tamarrian stage of the Permo-Carboniferous of Tasmania (Clark and Farmer, 1976; Truswell, 1978) and locally correlate this formation with the Cape Jervis Formation and basal Stuart Range Formation of the Arckaringa Basin.

The Palaeozoic sediments were also intersected in the offshore part of the Polda Trough in two wells: *Mercury-1* (65 m), and *Columbia-1* (87 m). This sequence consists of siltstone, claystone, and conglomerate and is correlated as a diamictite with the Coolardie Formation recognised onshore.

There is a significant break in the sedimentary succession at the top of the Coolardie Formation, as a highly weathered and kaolinised horizon forms at the top of this Late Palaeozoic unit.

3.3.6 Mesozoic

The Mesozoic is represented in the study area by sediments of the Upper Jurassic Polda Formation and kimberlite intrusions of Jurassic age.

(I) Polda Formation - Jup

The Polda Formation is a fluvial to lacustrine sequence (Harris and Foster, 1974; Gatehouse and Cooper, 1982) intersected in numerous drill holes across the Polda rift (Figure 3.10). The Polda Formation is also known from surface exposures which are located on the eastern margin of the Polda rift in the vicinity of the town Kielpa (Figure 3.10; Kimba Geological Map, 1:250,000).

Lithology of the Polda Formation in principal is grey, brown and black clayey sand, grey carbonaceous silt, and clay beds with inter-layered lignite and coal. Clastic detritus includes muscovite, weathered feldspar and igneous and metamorphic fragments.
Gatehouse and Cooper (1982) distinguished three lithological units within the Polda Formation:

- upper unit; dark brown to grey, medium to coarse-grained sandstone with minor pyrite and clay;

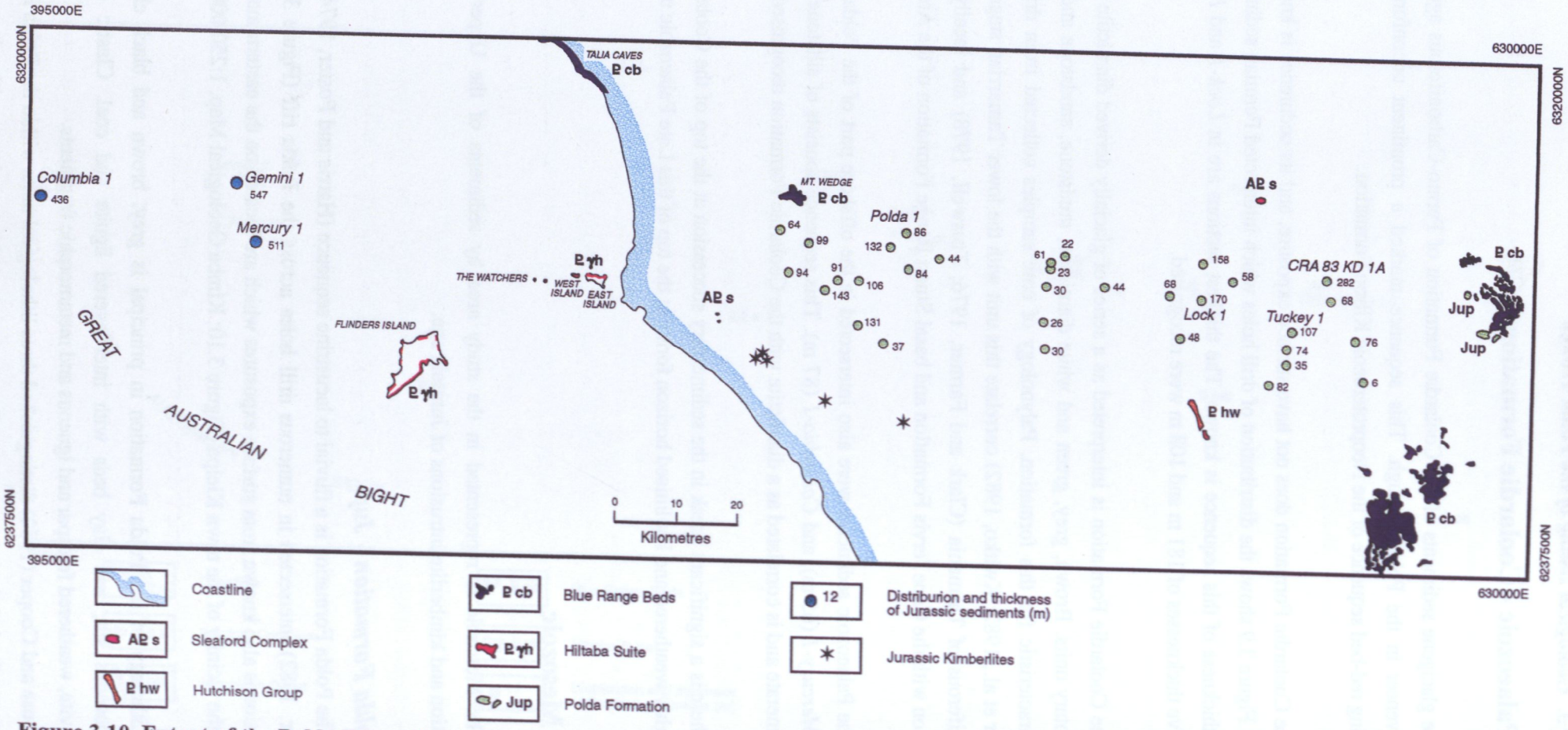

Figure 3.10 Extent of the Polda Formation.

- middle unit; dark grey to black carbonaceous claystone with interbeds of siltstone, lignite and sandstone;
- lower unit; grey sandstone, siltstone and claystone.

Gatehouse and Cooper (1982) noted that occurrence of this sequence changes greatly between drill holes with the sandy interval at the top of the basal unit absent in several holes, the middle carbonaceous claystone unit ranging greatly in thickness and lignite content, and the upper sandstone removed by erosion in many areas prior to deposition of Tertiary sediments. Lignite seams of the Lock Coal Deposit occur only in the middle carbonaceous unit.

Palynological studies by Harris (1964) and Harris and Foster (1974) of the drill-core and cuttings of the lignitic clays have shown that these are of Upper Jurassic age. Microfloral assemblages obtained were characterised by abundant pollen of the genus ***Tsugaepollenites*** and the spore ***Contignisporites cooksonii (Balme) Dettmann***. Palynological investigations established correlation with the Late Jurassic microflora of Evans (1966) which indicates that this unit is slightly older then the Jurassic of the Eromanga Basin. Harris and Foster indicated from the pollen distribution that there appear to have been four major arboreal advances during sedimentation, implying shrinkage of marshland in response to climatic changes.

About 450-500 m of the Upper Jurassic Polda Formation was intersected offshore in two wells, Mercury-1 and Columbia-1.

Strong unconformity marked the upper section of the Polda Formation with the overlying base of the flat-laying Tertiary section.

(II) Jurassic kimberlites in the Polda Trough region

On the southern flank of the central part of the Polda Trough five kimberlite were discovered by Stockdale Prospecting Ltd. in the early nineties (Figure 3.10). The exploration program for diamonds was based on aeromagnetic survey data and covered a large section of the main trough at its northern and southern margins.

The petrographic studies of the loam samples and drill chips indicated a wide spread of kimberlitic indicators (e.g. kimberlitic garnets, ilmenite, chromite, chrome diopside) recovered from Quaternary, Tertiary and Jurassic units, which act as secondary source horizons. The primary hosts were detected from magnetic anomalies at five sites: *SH08, SH09, SH13, MH1, MH14* (Stockdale Prospecting, 1992a, 1992b, 1992c, 1992d).

Based on the petrological descriptions reported by Stockdale Prospecting (1992a, 1992d), the kimberlitic rocks intersected by drilling are classified as follows:

- *SH08* - a porphyric, hypabysal facies kimberlite breccia with an indistinctly segregated groundmass texture. Mineralogically it is classified as a contaminated phlogopite - monticellite kimberlite.

- *SH09* - a probable crater facies, altered phlogopite monticellite kimberlite.

- *SH13* - possibly a crater facies volcaniclastic kimberlite. Mineralogically the sample is an altered monticellite kimberlite due to its pelletal nature.

- *MH1* - a pelletal tuffaceous (monticellite) kimberlitic breccia.

- *MH2* - a highly altered macrocrystic hypabyssal facies - monticellite kimberlite

The ion-microprobe $^{206}Pb/^{238}U$ analysis of the perovskite grains (4 samples) separated from the kimberlite resulted in a weighted mean age Ma191±17 Ma, i.e. Early Jurassic time (Stockdale Prospecting, 1992a). One sample indicated slightly older $^{206}Pb/^{238}U$ age at ~250 Ma (Stockdale Prospecting, 1992a). Two kimberlitic indicators were recovered from the Proterozoic grits, as described in Stockdale exploration progress reports submitted for SADME.

3.3.7 Tertiary - Poelpena Formation - *Tep*

Overlying the Polda Formation within the Polda Trough are Middle-Late Eocene fluvial sediments of the Poelpena Formation

There are no outcrops of Tertiary sediments in the Polda Trough, but they are known from a large number of drill holes, which were drilled during hydrogeological investigations carried on in the area or exploration for coal. This unit consists mainly of grey, poorly sorted sands and clays of Middle Miocene age and Middle Eocene unit, the Poelpena Formation.

This formation appears to be restricted to the Polda Trough itself and the marginal areas. It is absent on the southern edge of the trough. Estimated thickness of the sediments is greater than 200m. It contains coarse, grey, dark grey and brown sands, highly carbonaceous sands and lignite

3.3.8 Quaternary

Thin veneers of Quaternary sediments mask the underlying Archaean-Palaeoproterozoic basement on the edges of the rift and cover with a thick blanket of younger succession of rocks deposited within the Polda Trough. The Bridgewater Formation predominantly consists of sand, clay interbeds, off-white calcrete and carbonate-cemented aeolianite and is of Pleistocene age. The aeolite forms the coastal cliffs on the western side of Eyre Peninsula, consisting of large dune-size cross-beds containing comminuted shell fragments in a micrite cement. The calcrete varies in form from intraclast breccia to nodular, massive and laminated calcrete. Overlying the Bridgewater Formation in the north-west to the south-east of Eyre Peninsula are Pleistocene-Holocene longitudinal and parabolic dunes and sands spreads of the *Wiabuna Formation* and *Moornaba Sand.*

3.4 Review of the hypothesis concerning structure and evolution of the Polda Trough

3.4.1 Brief history of exploration

Initially an onshore part of the analysed structure was referred to as the Polda Basin and offshore as the Elliston Trough. The Polda Basin was defined as a ground water basin (Jack, 1912) and later was found to contain Mesozoic and older sediments (Harris, 1964; Wopfner, 1969).

The existence of the deeper structure was first recognised offshore by aeromagnetic survey data (Hammons, 1966) and since referred to as the Elliston Trough. The continuation of the Elliston Trough landward into the Polda Basin was proposed by Rowan (1968) on account of east-west trending gravity lows. These gravity lows were interpreted as a part of a graben beneath the Polda Basin.

Smith and Kammerling (1969) suggested that the Elliston Trough contained a thick sequence of Cambrian and/or Jurassic-Cretaceous sediments. The term Polda Trough has been applied to both the offshore Elliston Trough and its onshore portion (Parkin et al., 1969), but in some publications the term Polda Basin was still used to describe only the onshore portion of the trough (Harris and Foster, 1974) or was even exclusively applied to Mesozoic-Cainozoic sediments only (Nelson, 1974; Gerdes, 1986). In some publications, the eastern end of the eastern (onshore) Polda Trough is referred to as the Lock Sub-basin.

(I) Onshore exploration

In 1953 an aeromagnetic reconnaissance survey was flown by the Bureau of Mineral Resources over the Eyre Peninsula. The principal aim of this survey was to provide geological information required for regional mapping and for iron ore exploration. Aeromagnetic data recorded along the flight line spacing of 1.6 km and altitude of 460 m were used to prepare TMI contour maps at 1:63,360 and 1:250,000 scales for regional mapping purposes.

In 1967 a refraction seismic survey (12km) - the Colton traverse on the west coast of Eyre Peninsula was conducted. After ten years, in 1977, a stratigraphic drill hole *Colton-1* was drilled to a depth of 120 m and intersected the Mesoproterozoic Blue Range Beds.

Regional gravity survey done by SADME in 1968 delineated the onshore extension of the Elliston Trough. As a result of the gravity survey the Kilroo Sub-Basin located towards the east of Lock has been identify. An east-west trending gravity low was found to be assocciated with the Tertiary-Jurassic Lock Sub-Basin in which coal was later discovered.

Since 1968, geophysical and geological exploration become more intensive in this region. A variety of geophysical methods has been used, including gravity, aeromagnetic and groung magnetic, electrical, seismic and radiometric surveys. Numerous holes have been drilled, including *Polda-1* (172 m), *Tuckey-1* (213 m), *Lock-1* (369 m), *CRA 83KD1A* (1398 m). However, none of the drill holes

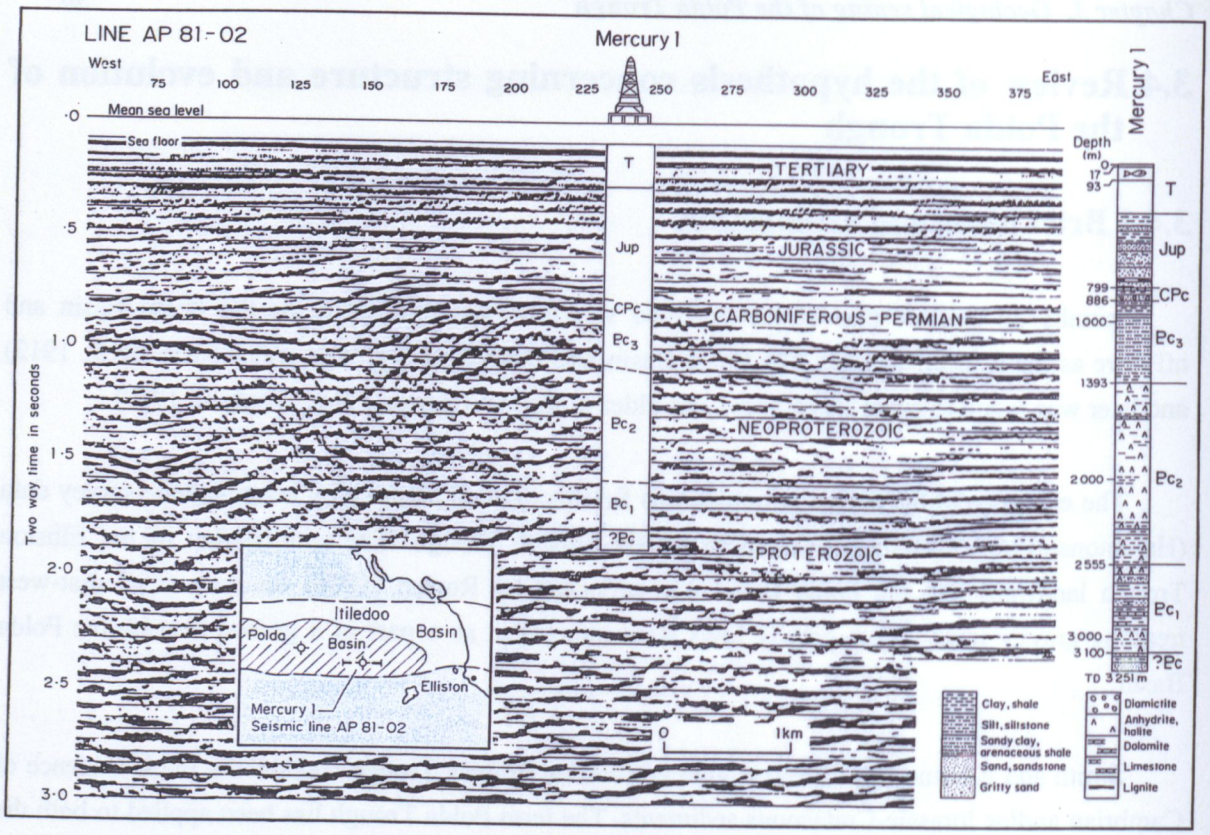

Figure 3.11 Seismic profile line AP 81-02 and drilling results from Mercury-1. After Flint (1992).

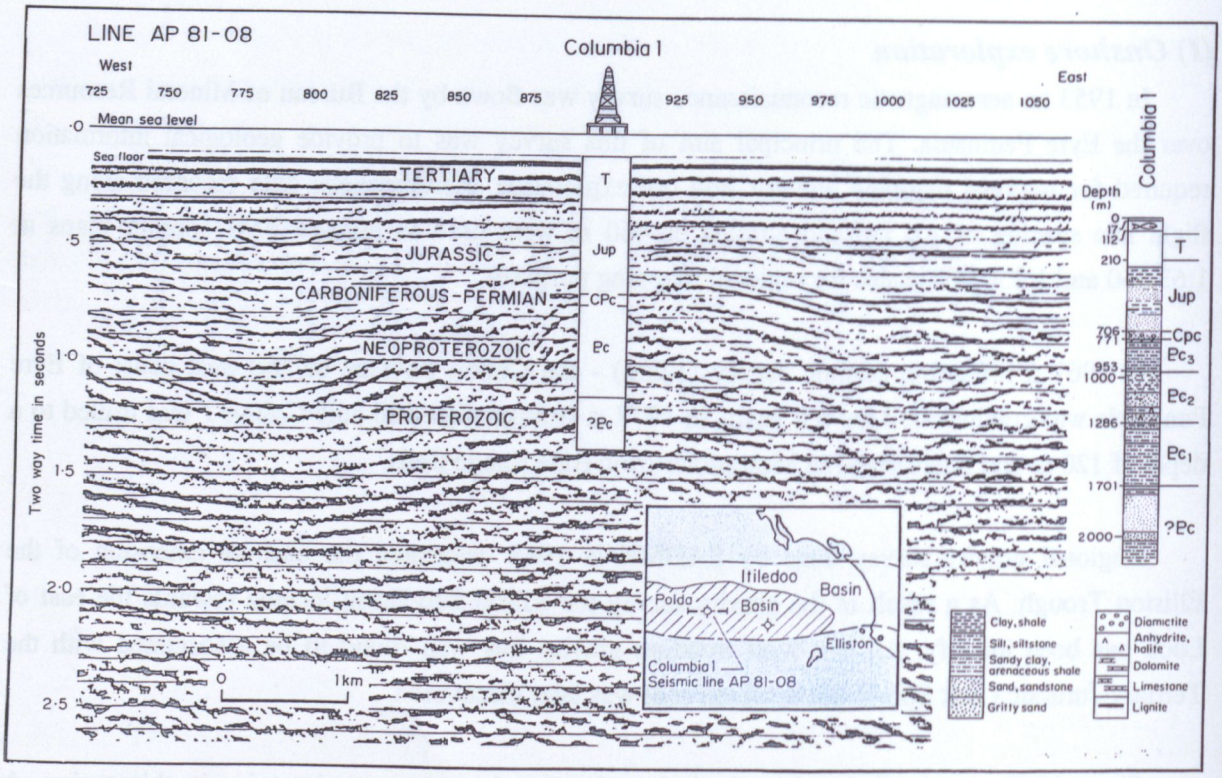

Figure 3.12 Seismic profile line AP 81-08 and drilling results from Columbia-1. After Flint (1992).

have intersected Palaeoproterozoic or Archaen basement within the trough. Only one hole *CRA 83KD1A* is sufficiently deep to extend beyond Permian sediments.

More detailed account of geophysical surveys conducted in the study area will be given in Chapter 4.

(II) Offshore exploration

The following is a brief summary of exploration in the offshore part of the Polda Trough, which was, as mentioned, first recognised as a geological entity in 1966, following an aeromagnetic survey flown for Shell Development (Australia) and Outback Oil.

Approximately 2100 km of reflection and refraction seismic data was shot by Shell in a 1966-1969 survey. Bridge Oil conducted two further seismic surveys in 1970-1971 along 2131 km lines. In 1975 Outback Oil drilled a well *Gemini-1* to a depth of 894 m. Outback Oil carried out a detail aeromagnetic survey in 1978. In 1980-81, Australian Occidental shot a further 3213 km of relatively good quality seismic data and subsequently drilled two exploration wells *Mercury-1* and *Columbia-1* (1981-82) to depths of 3251 m and 2168 m respectively (Figures 3.11 and 3.12). Both wells were plugged and abandoned being considered dry holes. Since then, exploration in the offshore part of the Polda Trough has been dormant, with the exception of 7 reflection seismic lines recorded in the western end of the trough by the Bureau of Mineral Resources in 1986.

Stagg et al. (1991), based on the main geological units identified in the offshore part of the Polda Trough, in *Mercury-1* and *Columbia-1* wells, identified and mapped several seismic horizons and intervals. The stratigraphic characteristic and geological significance of those mapped seismic reflectors Stagg et al. (1991) describe as follow.

- Horizon *b* marks the top of the crystalline basement; there is difficulty in confidently picking up this horizon;

- Horizon 1*p* marks intra-Neoproterozoic, a fairly strong, continuous reflector. It can be mapped with higher confidence than basement over most of the trough except in areas of intense deformation in the central basin (out-of-the-plane reflections due to high dips), and also where post-horizon 1*p* salt mobilisation occurred;

- Horizon *pc* marks the top of Precambrian Kilroo Formation. This reflector is the most prominent basin-wide unconformity between the highly oxidised red-beds of the Kilroo Formation and the overlying glacigene Permian Coolardie Formation;

- Horizon *t* marks the base of the Tertiary; this is a major unconformity separating shallow marine sediments of Tertiary age from underlying terrestrial sediments of the Upper Jurassic Polda Formation. This reflector is often masked by a water bottom multiple.

Based on the above seismic reflectors Stagg et al. (1991) recognised the following seismic intervals:

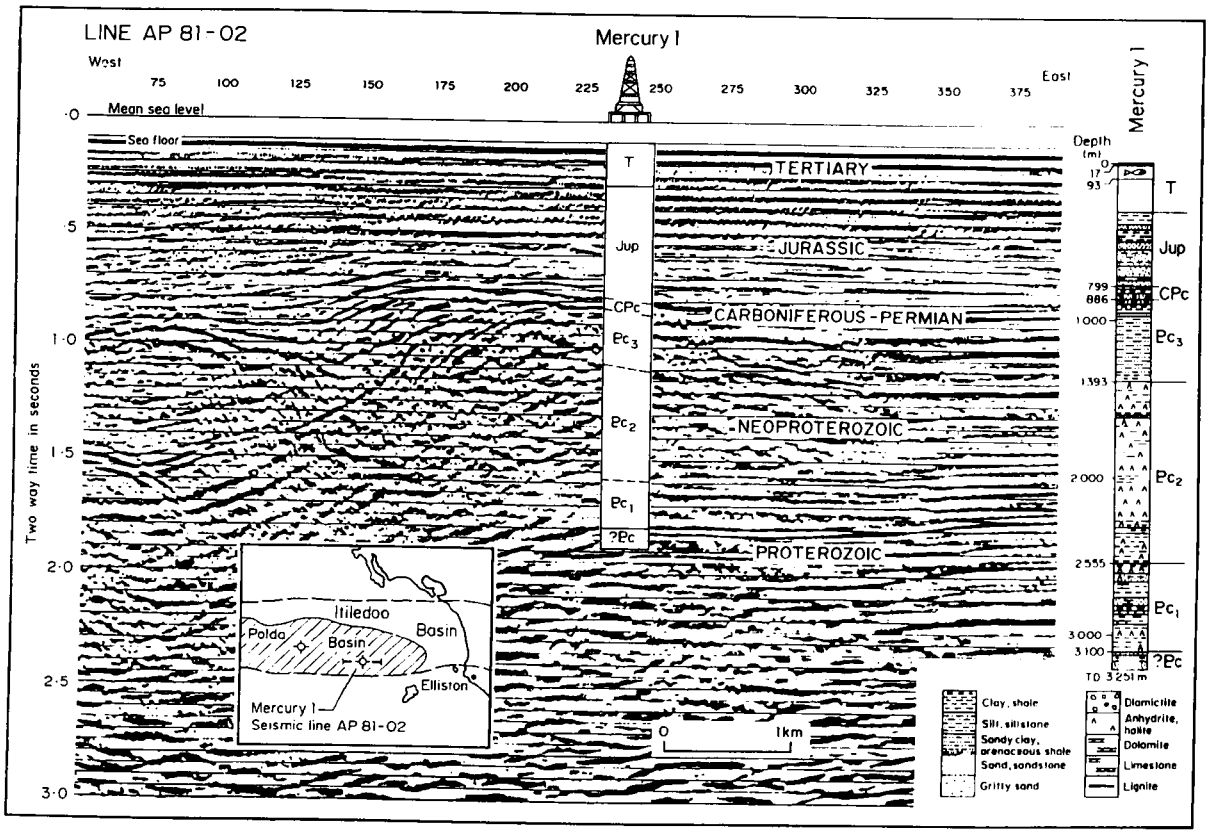

Figure 3.11 Seismic profile line AP 81-02 and drilling results from Mercury-1. After Flint (1992).

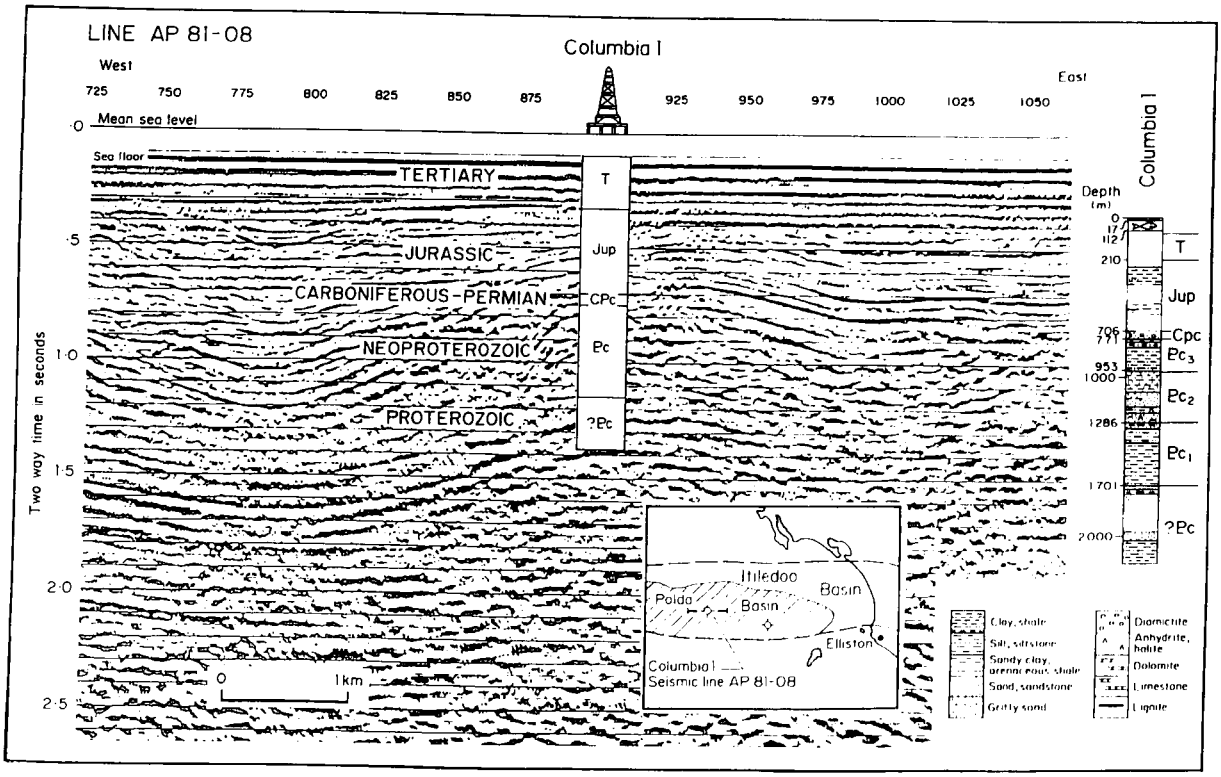

Figure 3.12 Seismic profile line AP 81-08 and drilling results from Columbia-1. After Flint (1992).

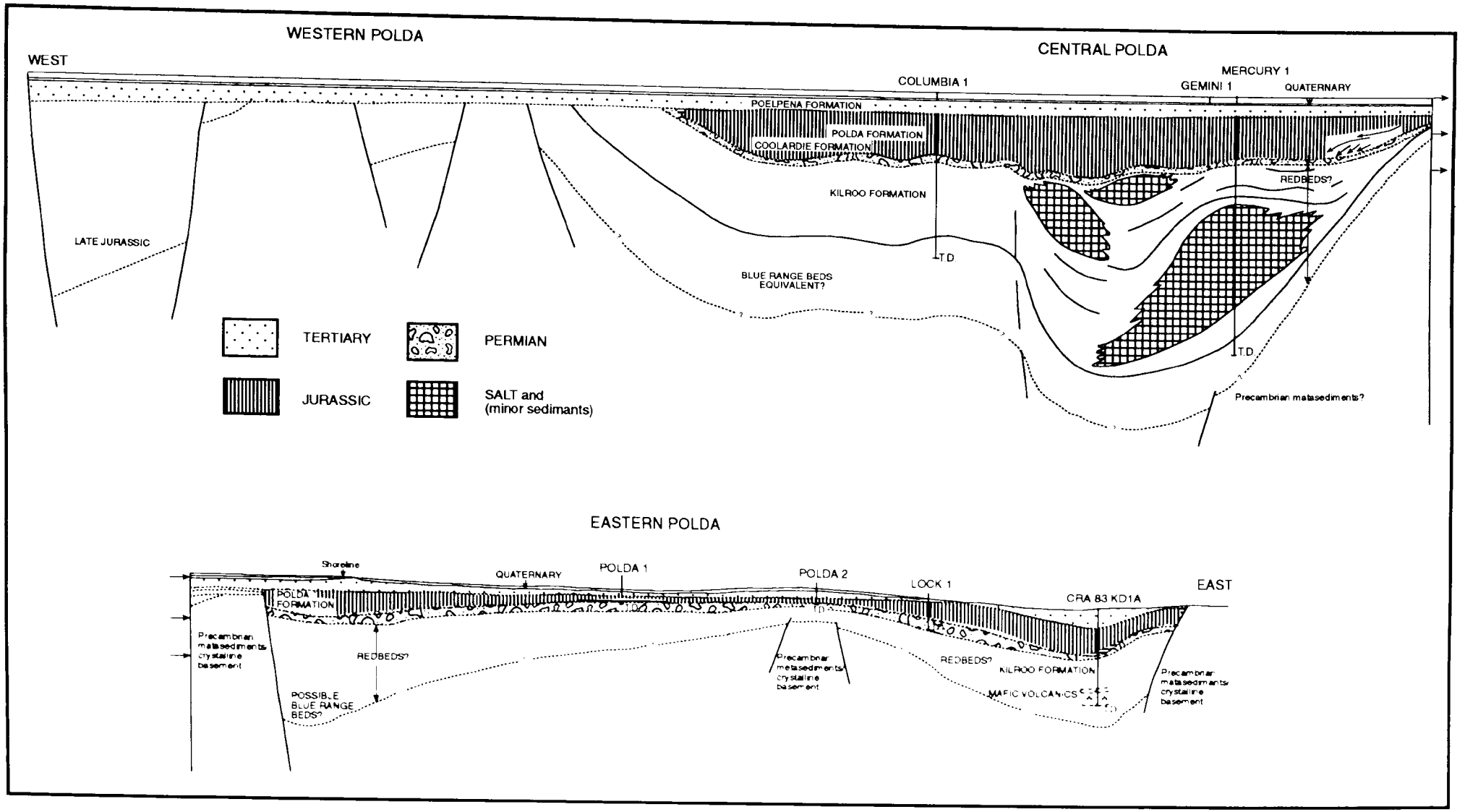

Figure 3.13 Longitudinal geological section of the Polda Through. After Stagg et al.(1991).

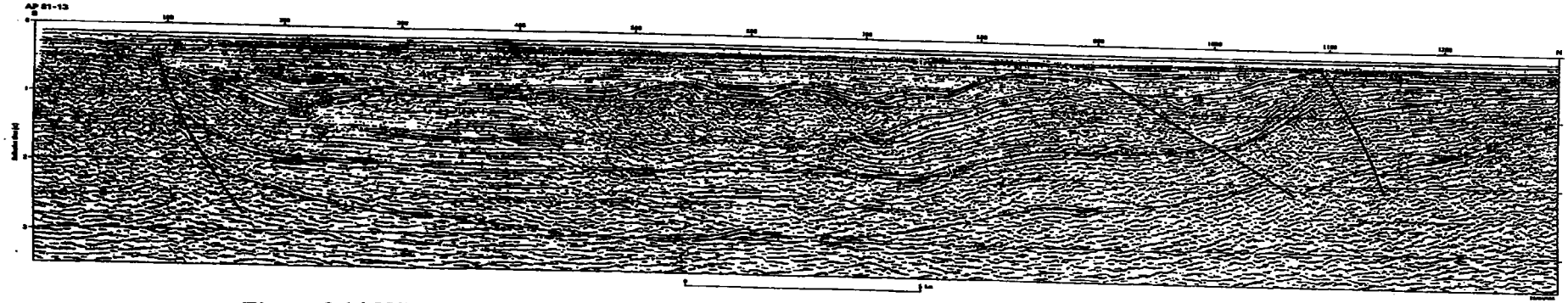

Figure 3.14 NS seismic cross-section of the offshore Polda Trough. After Stagg et al. (1991).

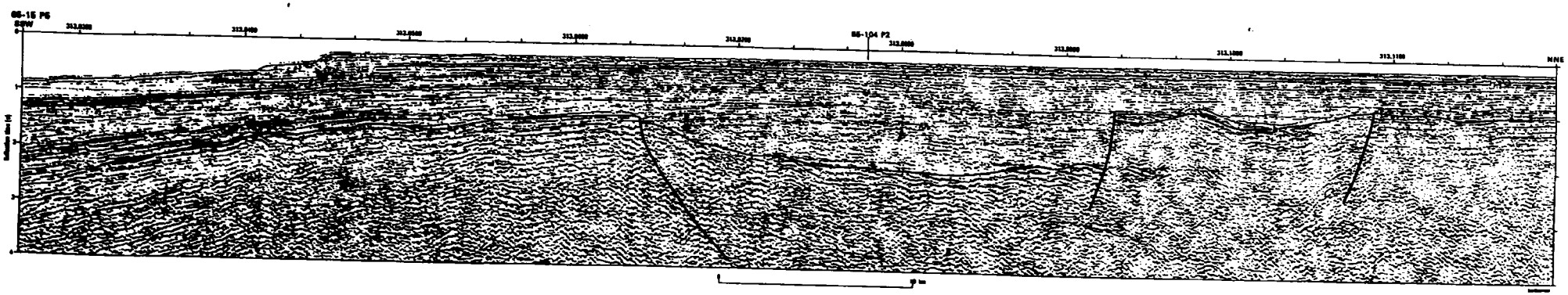

Figure 3.15 SSW-NNE seismic cross-section of the offshore Polda Trough. After Stagg et al. (1991).

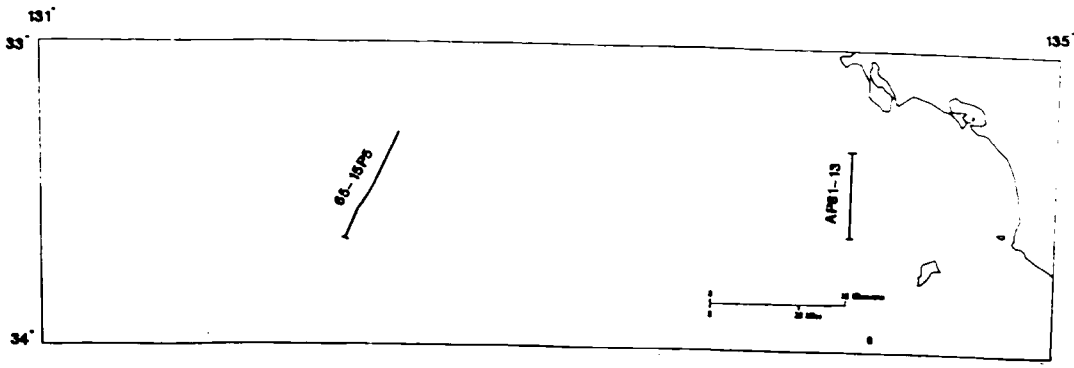

hydrocarbons. As Stagg et al. (1991) show on the longitudinal section this portion is separated from the eastern and western Polda Trough by a faulted shallow basement at a cross trend to the main structural grain (Figure 3.13).

The structure of the western Polda Trough is poorly defined, because of limited geophysical data. The western marginal-end of the trough was assumed to be in confluence with the Ceduna Sub-basin of the Bight Basin (Stagg et al., 1991). It was pointed out that the extension of the east-west Polda Trough trends across the northern margins of the Ceduna and Eyre Sub-basins. This may suggest that these Mesozoic features may be underlain by older Polda Trough sequences (Stagg et al., 1991).

The north-south seismic sections interpreted by Stagg et al. (1991) shows difference in the structural character between the western and central Polda Trough (Figures 3.14 and 3.15). The western part of the trough appears to be a simple graben with fault-bounded northern and southern margins (Figure 3.15). Stagg and his co-authors observed that ENE-WSW trend of the major interpreted faults is approximately parallel to the basin forming trend in the Eyre Sub-basin to the west. Therefore, they propose, that the western part of the trough, formed during the Jurassic-Cretaceous lithospheric extension, prior to the break-up of Australia and Antarctica, and hence contains mainly Mesozoic sediments. Their interpretation of the seismic section across the central part of the trough (Figure 3.14) shows a more complex northern margin and a relatively simple southern boundary marked by a symmetrical, normal fault system. They describe the northern margin as a combination of a monocline with normal and wrench faulting with some reverse faults. They interpreted this structure as a half-graben, hinged to the south, and fault-bounded to the north. While both flanks show an east-west trend, the observed strong NW-SE offset was suggested by these authors to be due to an interpreted accommodation zone extending from the Duntroon Basin. Also, according to Stagg et al. (1991) the area of shallow and complex-structured basement at the junction of the western and central Polda Trough may be a continuation of the East Duntroon Accommodation Zone located to the south-east (Figure 3.16).

Gerdes (1986) re-examined aeromagnetic survey data flown for SADME in 1953-1955, and calculated the depths to the magnetic basement based on the 'half maximum slope' technique. He distinguished two magnetic horizons:

(1) Shallow magnetic sources which he correlated with weakly magnetic intraformational units of the Polda Trough. According to his estimates such magnetic sources are present just below the Jurassic coal sequences. These shallow sources were interpreted '... as numerous horizontal sheets, occurring as a series of ferromagnetic remnants of either:

- a fractured sheet of basaltic material, where the anomalies reflect multiple edge effects; or
- numerous isolated events within a narrow stratigraphic level and/or band. (Gerdes, 1986)'

(2) Major magnetic bodies at depth which were correlated with magnetic units of the Hutchison Group or late Archaean metamorphics.

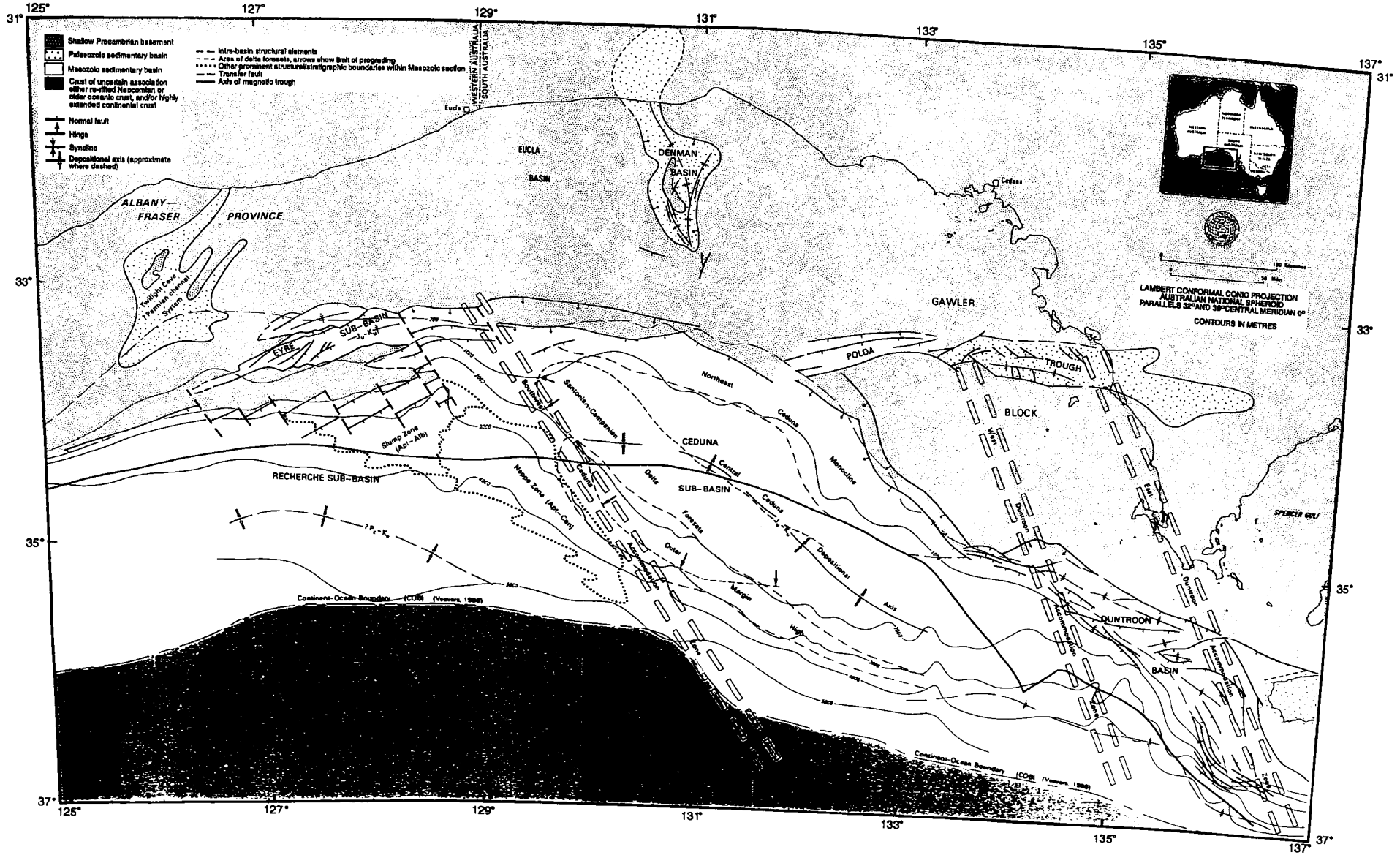

Figure 3.16 Tectonic elements of the South Australian Rift System. After Stagg et al. (1991).

Figure 3.17 includes gravity countours and magnetic basement contours constructed by Gerdes (1986). The map shows an east-west trending trough with a maximum depth to the magnetic basement at 2.4 km. Gerdes (1986) noted two distinct sub-basins located south of the gravity lows, and the presence of discontinous east-west fracture zones dislocated by NE-SW oriented fractures. In his opinion a fracture zone marked X-Y in Figure 3.17 which is located on the western edge of the structure interpreted as a N-S horst, separates the sub-basins and terminates the offshore graben.

Nelson et al. (1986) compiled and re-interpreted the aeromagnetic survey data over the Elliston Trough being the offshore extension of the Polda Trough, as well as the onshore infrabasin refered to as the Polda Basin. This interpretation is presented in Figure 3.18. Nelson et al. (1986) noted that the map constructed shows a series of sub-basins arranged in east-west en-echelon pattern, with incremental displacement to the south, at the eastern end of the trough (Figure 3.18). The oval shaped depocentres (reaching depths of 300 m) were interpreted to be separated by north-south basement swells. Interpretation of several seismic refraction lines shot across the Elliston Trough indicated consistency with the interpretation of the magnetic basement. Nelson and others (1986) also interpreted, based on the depth to the magnetic basement map, the existence of two fault systems as possibly related to wrenching; the synthetic and antithetic sets trending in a NE-SW and NW-SE direction. Nelson et al. suggest that the structures of this age range have protected and preserved the Blue Range Beds onshore.

(II) Genesis of the Polda Trough

In the past several different hypotheses concerning the origin of the Polda Trough have been published. Understanding of the history of origin and evolution of this geological feature has been changing over time as more geological information from drilling and geophysical surveys have been obtained.

The initial explanation of the origin of the Polda Trough was perceived (Fraser, Tilbury, 1979) before the older stratigraphic units were detected. Therefore, prior to the detection of the Palaeozoic and Proterozoic sequences, the Polda Trough was understood to be a tensional feature resulting from the break-up of the Gondwana super-continent during the Jurassic-Tertiary. However, since the presence of the Mesoproterozoic Blue Range Beds in both drill holes, as well as in onshore outcrops (Mt. Wedge, Talia Caves, Rudall area) was recognised, (Flint, Parker, 1981) and more seismic, magnetic and gravity survey data became available, the concept of the Polda Trough history was modified. It became accepted that Polda Trough had a much earlier origin and that this geological feature originated in the Proterozoic (e.g. Flint and Rankin, 1991; Flint, 1992; Rankin, 1993).

The early hypothesis associated the Polda Trough with rifting prior and during continental dissection, and it was suggested, that it was possibly an aulacogen. Among supporters of such an option are Flint, Fanning and Rankin (1988b) who discussed the possibility of the Polda Trough as an aulacogen; '...Some, but not all, features of the Polda Basin are consistent with it being an aulacogen of the Adelaide Geosyncline. Aulacogens are "elongated basins ...closely associated with geosynclines, from which they branch and penetrate far into the craton" ... (Preiss, 1987). Typically the mouths of aulacogen merge with the geosyncline, however, the Polda Basin and Adelaide Geosyncline are

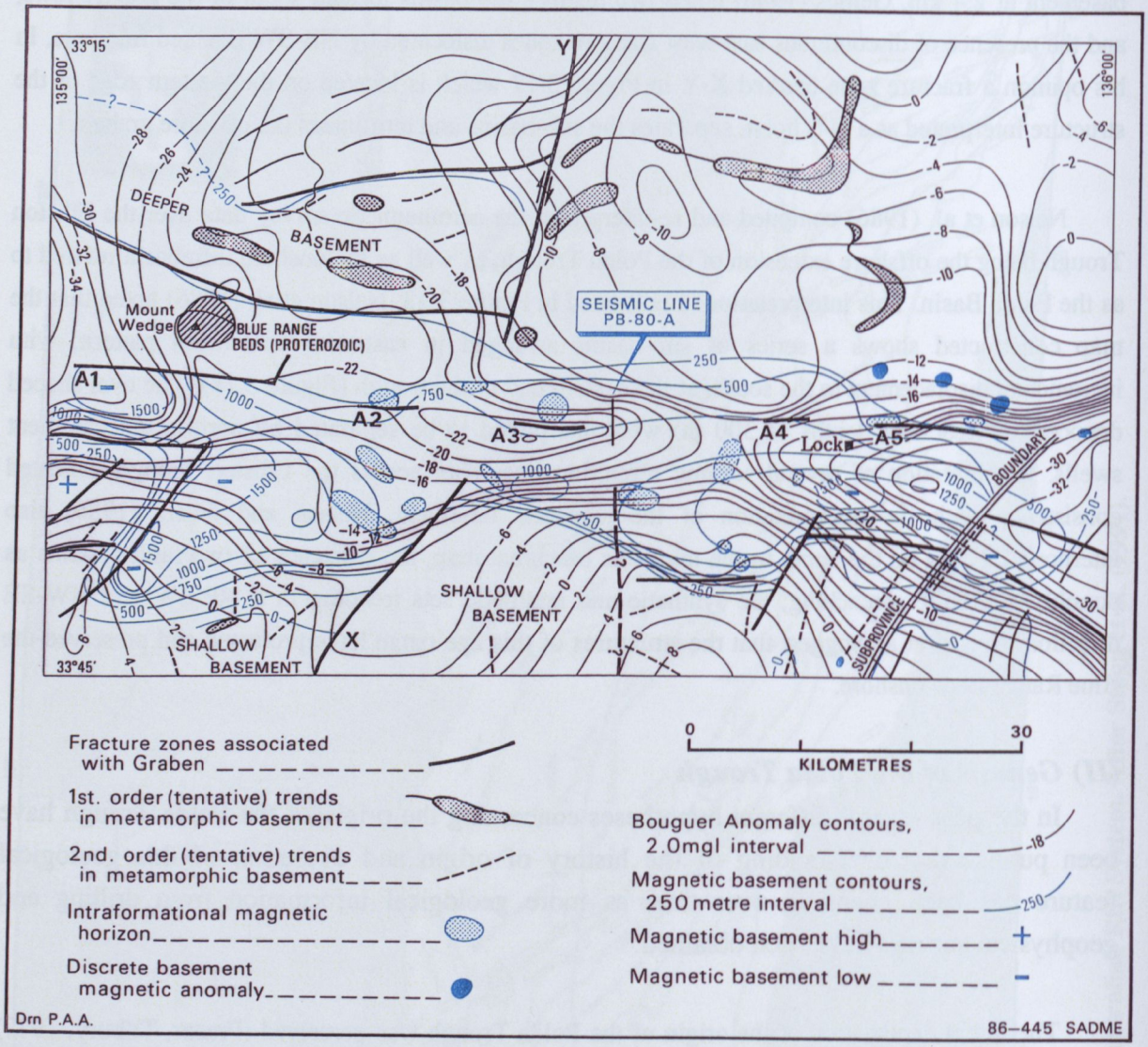

Figure 3.17 Contours of Bouguer gravity field and depth to the magnetic basement over the onshore Polda Trough. After Gerdes (1986).

disjoint and the corresponding portion of the geosyncline lacks any early Adelaidean, rift-related sediments.'.

Crabb, Gerdes and Nelson (1985) support the concept of an origin of the trough being associated with rifting during lithospheric extension preceding continental break-up and during the time-span of actual separation of Australia and Antarctica. They imply the possibility of a triple branch junction which developed at this zone of crustal weakness during the break-down of the Gondwana continent.

Among several hypotheses explaining the geological evolution of the Polda Trough the most comprehensive one is the review by Nelson, Crabb and Gerdes (1986). They suggest (based on the previous work of Thompson (1970), Lambeck (1984), and Veevers (1984) and the interpretation of seismic, gravity, magnetic and drilling data) the Proterozoic origin of the basin with structural overprint by Mesozoic rifting. These authors (Crabb et al., 1985; Nelson et al., 1986) proposed the following reconstruction of the Polda Trough tectonic history.

In the opinion of Nelson et al. (1986) the Polda Trough originated as a crustal downwarp during the same Proterozoic regime that gave rise to the family of basins that also includes the Ngalia, Amadeus, and Officer Basins of central Australia (Figure 3.19). It has been suggested by these authors, that the Polda Trough '...can be regarded as a compressional intracratonic trough, overprinted by transform movements and followed by rifting and extension associated with Mesozoic continental breakup. (Nelson et al., 1986)'. They implied that the affiliation of the Polda Trough with those other central Australian Palaeozoic sedimentary basins, which are characteristically east-west elongated forming a parallel series of basins and basement highs (Figure 3.19), is supported by the presence of thick deposits of halite which was intersected in the offshore wells and initially interpreted as salt swells on the seismic sections.

Lambeck (1984) has proposed a mechanical model to explain the structure and the evolution of the Amadeus, Officer and Ngalia Basins of Central Australia. This family of basins is of considerable interest, because their evolution cannot be ascribed to conventional basin formation mechanisms, neither based the thermal models (Sleep, 1971) nor stretching models of McKenzie (1978b). The foreland basin models of Price (1973) and Beaumont (1981) are also inappropriate. The principal objection to the thermal and stretching history is the lack of isostatic equilibrium of the basins, whilst the foreland basin model does not explain the continuous evolution of the basins over a time span of several hundred million years. The main assumptions of Lambeck's mechanical model state, that the continental crust has been in a state of compression since the Neoproterozoic. Lambeck's model was developed on the supposition that intracratonic basin formation is determined by the balance of the compression and the buoyancy forces, and on the assumption that the crust is subject to initial surface loading and visco-elastic forces. In this model the effects of erosion during uplift modify the balancing forces. The proposed model does not require magma emplacement and it considers the lithosphere as a viscoelastic plate being subjected to irregular loads in Neoproterozoic time, causing some deflections which increase with time, according to the various forces and plate properties. The uplift rates are a function of increase of bending stress, and gravity sliding become important, the basement being thrust over the basins. This would have occurred early in the Cambrian, corresponding to the

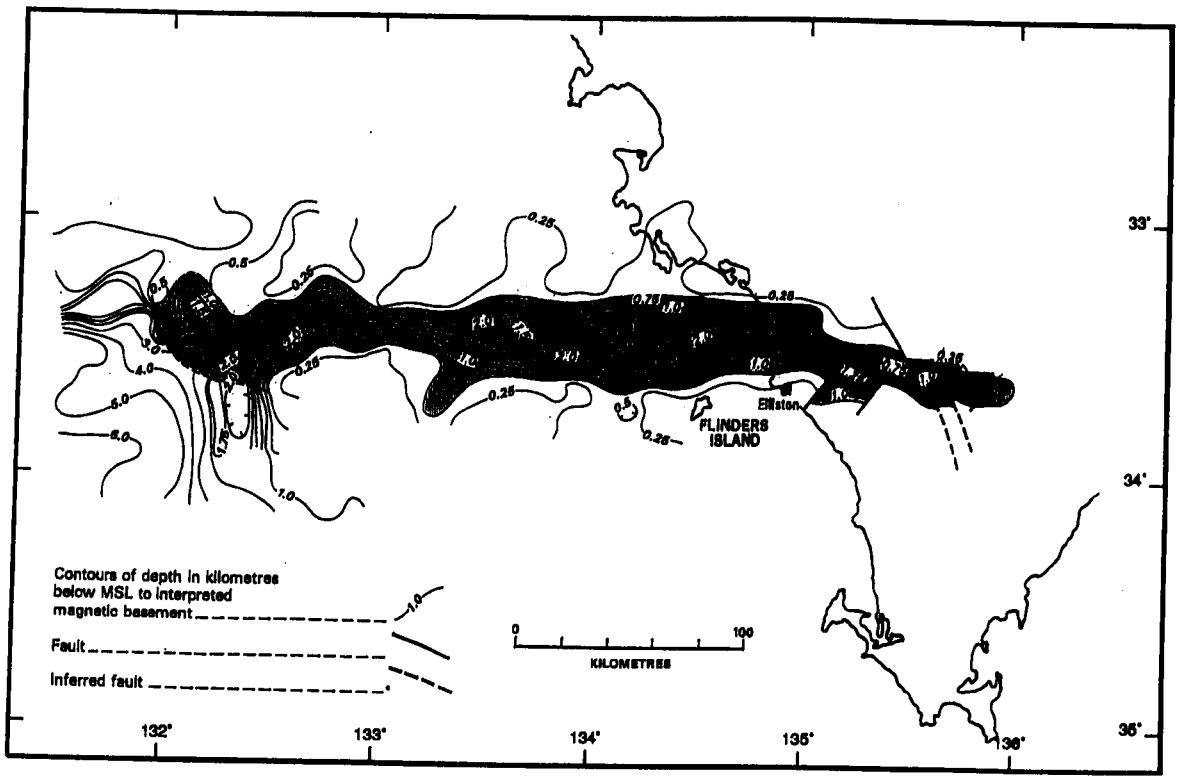

Figure 3.18 Depth to magnetic basement in the Polda Trough by Nelson et al. (1986).

Petermann Orogeny. According to this model, it can predict a further significant deformation in the southern Arunta in Late Palaeozoic time, corresponding to the Alice Springs Orogeny and the final stages of the Ngalia Basin formation. The mechanical model proposed by Lambeck predicts the structure of the continental crust that corresponds to the pattern of geophysical anomalies. The gravity anomalies observed in central Australia are quasi-linear in an east-west trending direction (Figure 3.20), where the strong negative Bouguer anomalies correspond to the basins and the positive anomalies correspond to the regions of exposed basement.

During the Petermann Orogeny (Austin and Williams, 1978; Veevers, 1984), dated at ca 600 Ma (Wells et al., 1970; Forman and Shaw, 1973; Austin and Williams, 1978) and ca 580 Ma (Thompson, 1970) the fundamental stress regime was changed over the whole Australian continent. Veevers (1984) suggests a dextral shear (about the pole to the north-east) which resulted in plate divergence and the initiation of pull-apart basins, such as, the Bonaparte and perhaps the Boorthana Trough with a NNW-SSE orientation. Nelson et al. (1986) considered that in the case of the Polda Trough, regional change of the stress regime led to a transform overprint on an already established east-west elongated feature. Nelson et al. (1986) and subsequently Stagg et al. (1991) interpreted, in the seismic sections, those transform elements within the Polda Trough as wrench fault structural assemblages.

(II) Depositional history of the Polda Trough

Nelson et al. (1986), based on the analogy with the central Australian basins, and adopting Lambeck's mechanical model described above, suggested that sedimentation in the Polda Trough originated in the Mesoproterozoic and was followed by shallow water sedimentation during the Adelaidean (850-650 Ma) with similar sedimentation in the Adelaide Geosyncline and the central Australian basins, which may have been parts of a larger area of Neoproterozoic deposition along an eastern margin. They suggested that since the Proterozoic, at least four or maybe even five periods of sedimentation, separated by periods of erosion have occurred in the Polda Trough. In their opinion major erosional unconformities in the typical stratigraphic column of the Polda Trough are well defined on the seismic sections and are inferred to correspond to major orogenic episodes. Cooper and Gathehouse (1983) suggested that sedimentation within the trough was initiated in the Proterozoic and only occurred during such periods of tectonic instability. They considered the fluviatile Blue Range Beds as the basal succession, although Nelson and others (1986) regard it to be subject to discussion.

As mentioned, the age of the red-beds sequence encountered in the offshore wells *Mercury-1* and *Columbia-1* is problematic. Some authors imply that this offshore detected red-beds sequence is possibly an equivalent of recognised onshore Neoproterozoic Kilroo Formation, others suggest correlation of its lower unit with Mesoproterozoic Blue Range Beds onshore and Nelson et al. (1986) imply that the red-bed sequences may be of Lower Palaeozoic age.

Stagg et al. (1991) assumed that sedimentation of the red-beds continued through the Neoproterozoic with the introduction of evaporites and that the original sedimentation was initially basin-wide. They suggest that successive salt mobilisation has entirely changed the distribution of the deposition. In their opinion, salt mobilisation continued over a long period of time, possible in two phases. They suggest that the first and major mobilisation phase took place prior to the deposition of

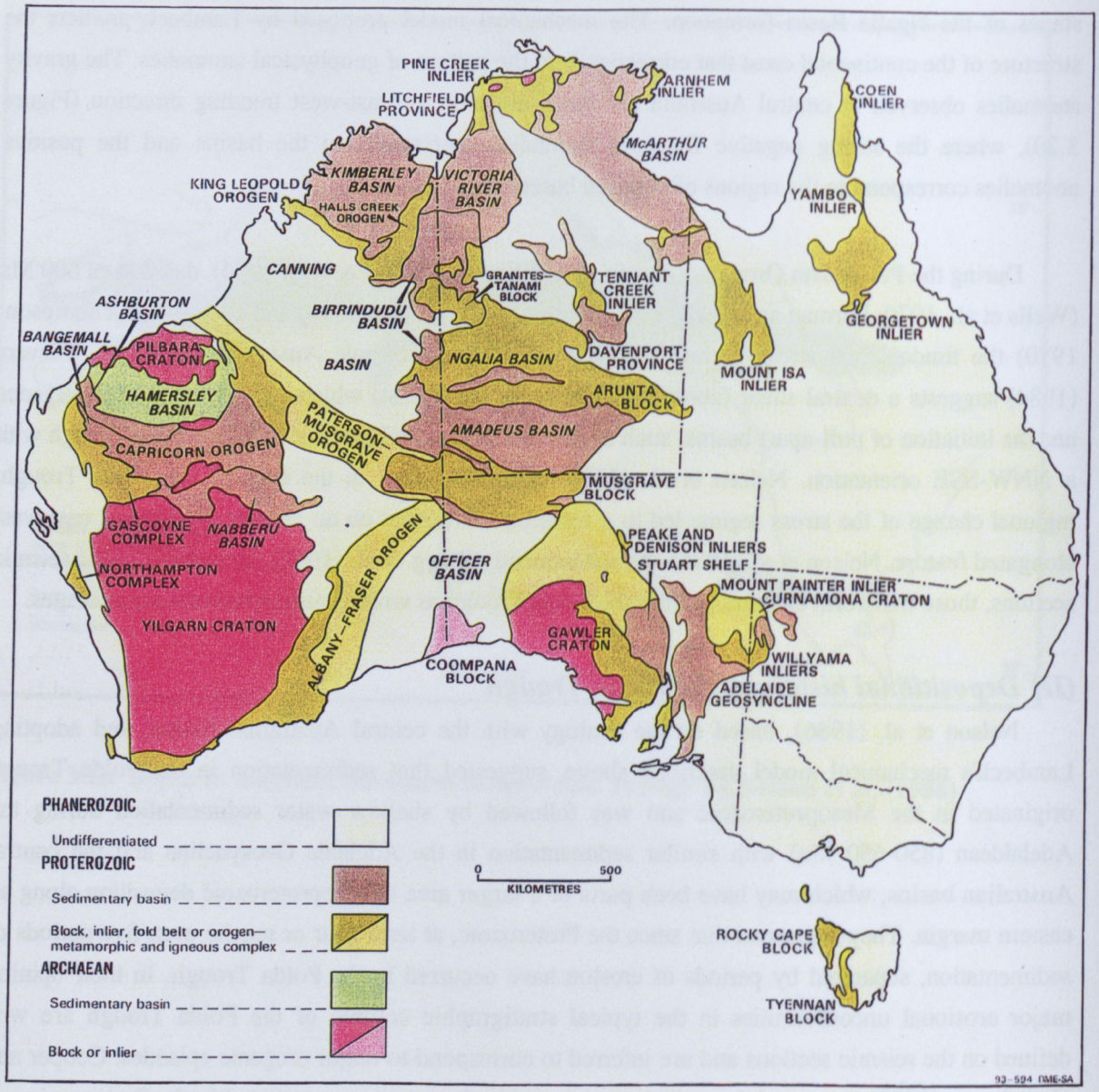

Figure 3.19 The major Archaean and Palaeoproterozoic provinces of Australia. After Parker et al. (1993).

the Permian Coolardie Formation, since, they interpreted most of the relief at the top of the Kilroo Formation (horizon $1p$) as salt-induced and the structural highs are strongly eroded. The structure, within the overlying Coolardie Formation and also Upper Jurassic Polda Formation, is also suggested by these authors as due to salt movement. Therefore, they conclude that mobilisation continued during the deposition of these units.

In the opinion of Stagg et al (1991) the deposition of the Neoproterozoic Kilroo Formation was followed by a major basin-wide erosional hiatus until the glacigene sedimentation of the Carboniferous-Permian Coolardie Formation commenced. They distinguished a major unconformity on the seismic sections which separates the sequence of the red-beds from the Upper Palaeozoic glacigene Coolardie Formation. Late Palaeozoic diamictite formed a uniformly thin (~100 m) veneer, which correlates with glacigene sediments of the St Vincent and Arckaringa Basins (Nelson et al., 1986). Stagg et al. (1991) suggest that the Upper Jurassic Polda Formation was deposited in the structural lows in the Kilroo Formation or Coolardie Formation reaching a locally significant thickness of 1500 m with an average value of 700-800 m. The Polda Formation when intersected in the wells, shows: fluviatile character, low-relief westwards prograding foresets which imply that the formation also originated in a shallow lacustrine environment. Stagg et al. (1991) suggest the possible correlation of this succession with the oldest syn-rift sediments of the Ceduna and Eyre Sub-basins, and subsequent indication is that it is the major sedimentary fill of the western part of the Polda Trough.

In the entire trough, no younger Mesozoic sediments have been penetrated. Based on the interpretation of the seismic data, it was concluded, that there is total absence of the Cretaceous (Stagg et al., 1991). The Upper Jurassic deposition within the Polda Trough was terminated and there occurd a major erosional unconformity. Stagg et al (1991) observed a similar hiatus in the outer parts of the Ceduna and Eyre Sub-basins, where both troughs and adjacent basement are covered by a thin layer of Tertiary carbonates and sand.

The literature review presented in Chapter 3 shows many controversy concerning origin and evolution of the Polda Trough. The new facts, and the interpretation of results of research forming a part of this thesis, has shed more light on the understanding of the structure and origin of the Polda Trough. Detailed analysis and new hypothesis are presented and discussed in Chapter 4.

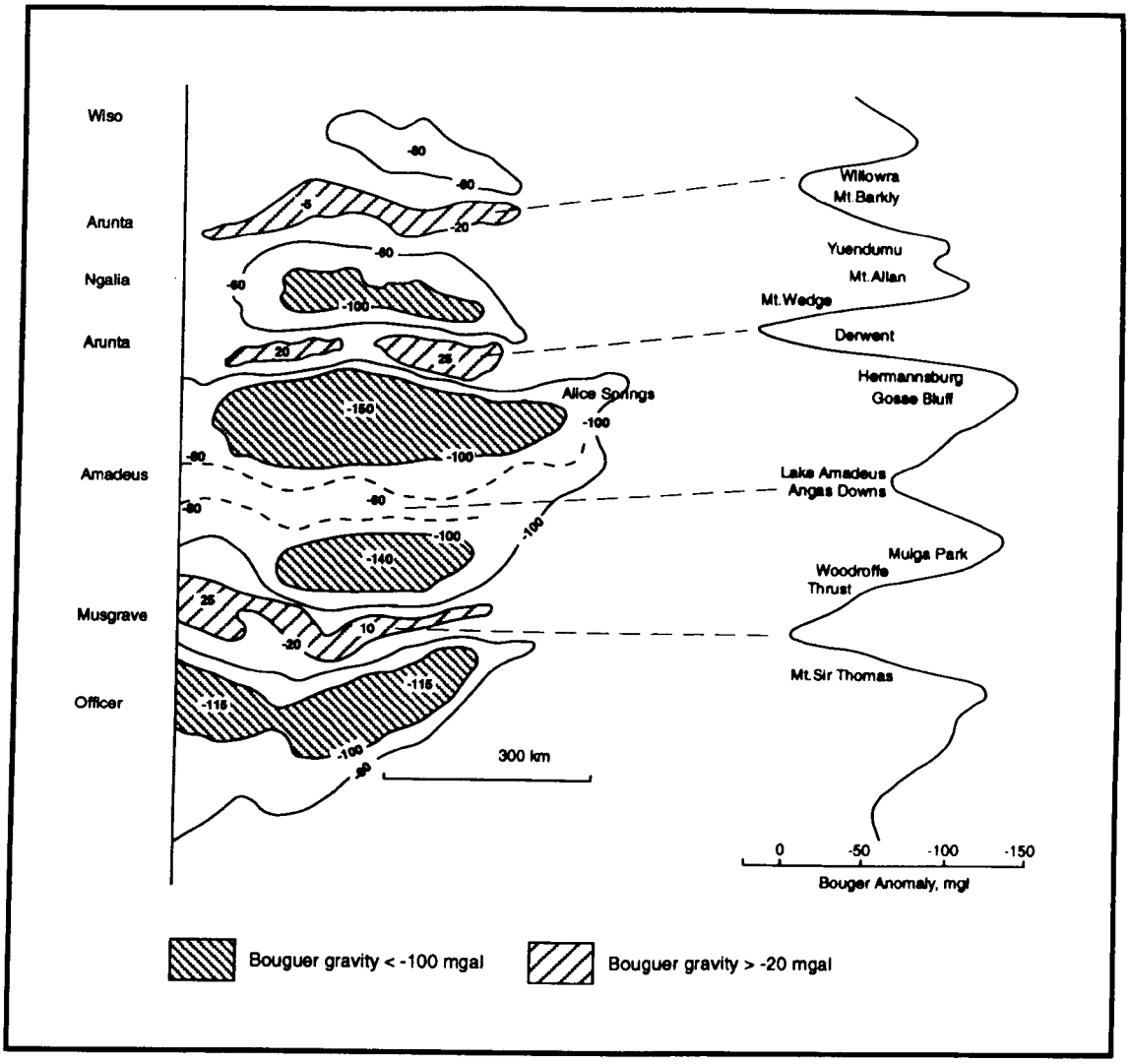

Figure 3.20 Regional gravity field of central Australia. After Lambeck (1981).

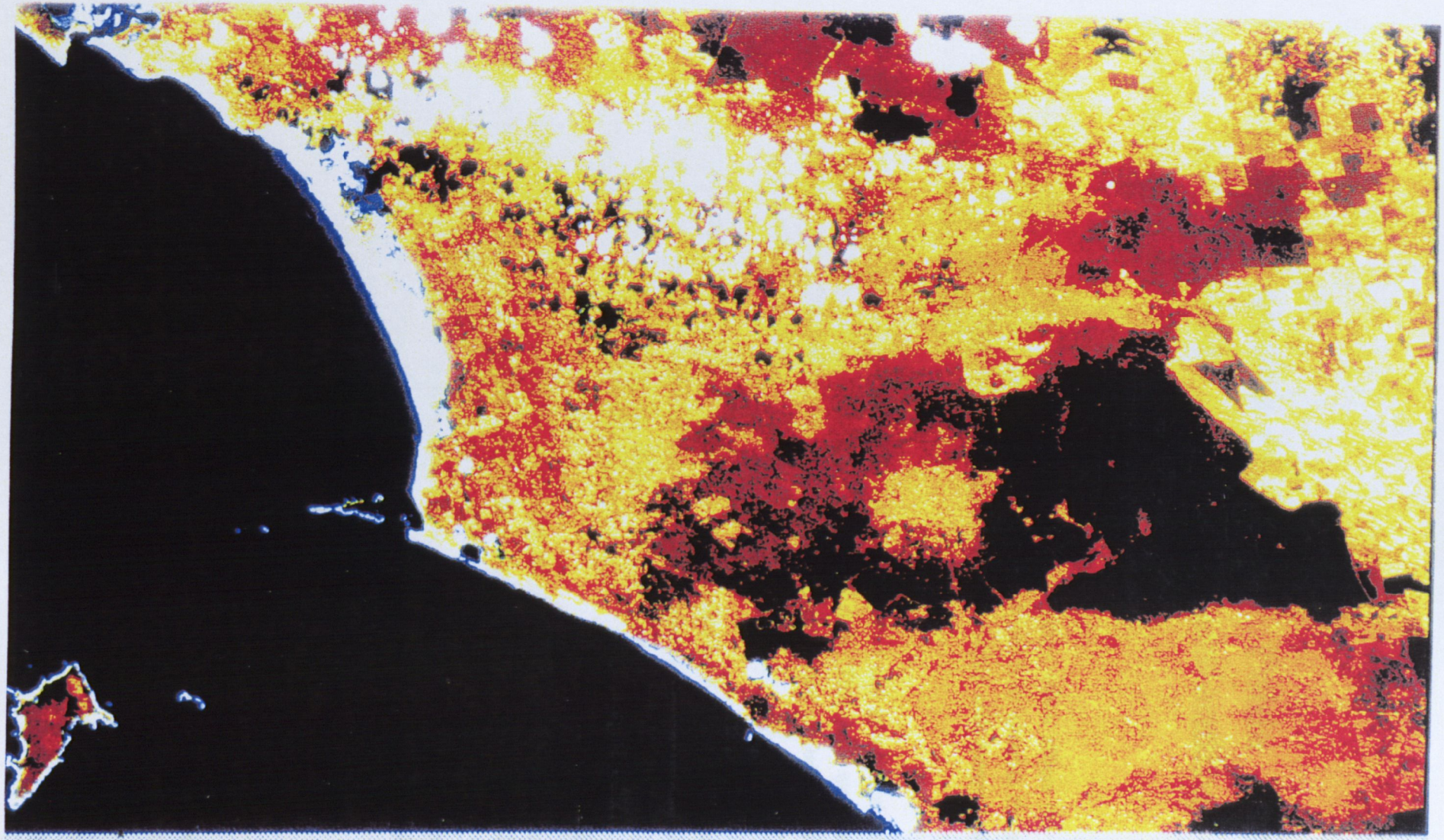

Plate III Satellite image of the Polda Trough area.

Chapter 4

Geophysical results from the Polda Trough and implications for understanding the geology

The Polda Trough is part of a more extensive tectonic feature which affects the whole of Southern Australia. The aim of the research presented in this thesis is to establish the geological history of the Polda rift by an integration of the geological information with interpretation of the geophysical data and a comparison with other rifts.

This research is restricted to an interpretation of the geological and geophysical data in the office, because due to an injury the author is unable to do field work. This thesis would have been rather different if the author were able to do geophysical surveying. In the following indications of possible ground surveys are mentioned.

A discussion of geological processes which occur in the earth's interior and are responsible for the origin of rifts, together with the geophysical signature of the major rift systems has been presented in Chapter 2. A detailed description of the lithology of each stratigraphic unit which has been recognised in the study area has also been introduced in Chapter 3.

The results of research presented in the following sections of Chapter 4 provide information used for delineation of the shape, interior structure, the origin and geological evolution of the Polda rift. A brief summary of the geophysical data used in this study will be introduced in Section 4.1. This is followed by a section concerning the physical properties of rocks occurring in the research area. A detailed analysis and interpretation of the available geophysical data, integrated with known geological information of the onshore Polda rift, is presented in Section 4.3.

4.1 Geophysical surveys used for interpretation

Over the years, the Polda Trough has been explored for coal, hydrocarbons, water, potash, uranium and diamonds. The exploration was based mainly on geophysical surveys followed by drilling, as the central-and the western part of Eyre Peninsula are totally covered by Quaternary sediments. In the this section a brief review of the geophysical surveys relevant to the research reported in this thesis will be presented.

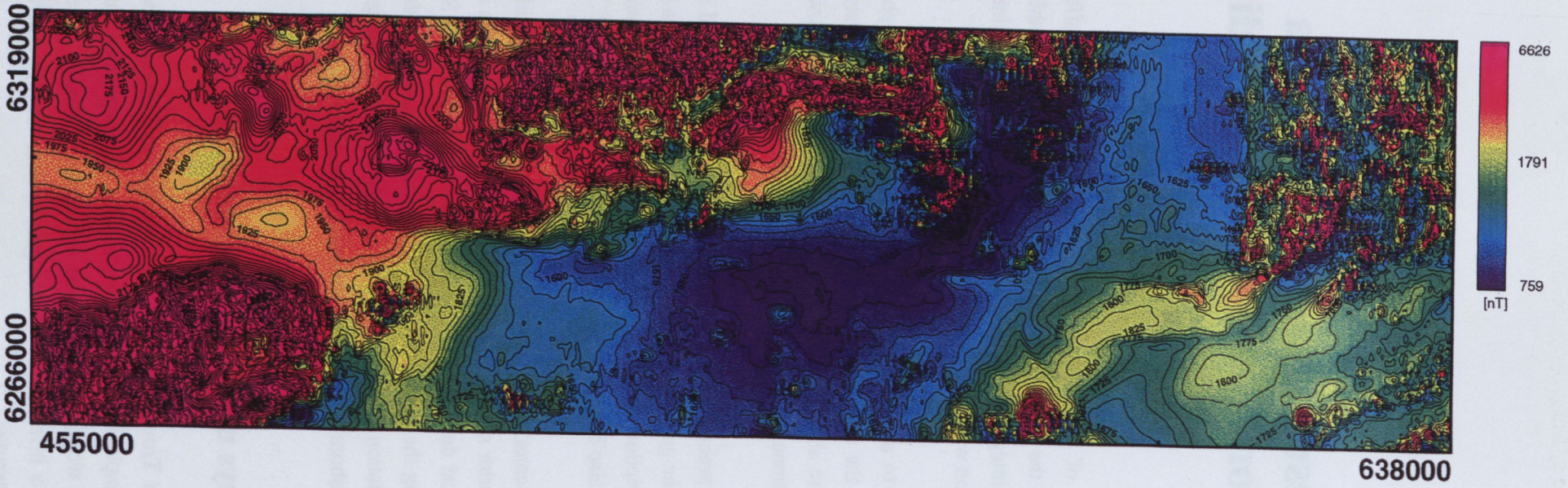

Figure 4.1 Total magnetic intensity field across the Polda Trough. Colour image with superimposed contours at 25 nT interval.

4.1.1 Aeromagnetic survey data

In 1987/88 a new airborne magnetic survey was flown by BMR and SADME over the central-east Eyre Peninsula. The east-west flight lines were 1 km apart on land and 2 km offshore; the north-south tie lines spacing was 5 km. The flying height was 80 m above ground.

This high quality airborne magnetic data is the major tool used for the detailed study of the eastern end of the Polda Trough (Figure 4.1). The processing and interpretation of this magnetic survey data was the major concern of this research.

This part of Chapter 4 summarises the procedure of data processing and lists the maps and other forms of presentation prepared, during the course of the research presented in this thesis, to obtained final or intermediate results.

The processing, analysis and presentation of the 1987/88 aeromagnetic survey data over the Polda Trough area involved a considerable amount of computing, which was carried on Vax and Unix computers.

The following is a list of the data processing done by the author as a part of the research presented in Chapter 4.

- Preparation of the located data for gridding, including correction of data-errors.
- Gridding and contouring of the magnetic data (TMI, vertical gradient and reduction to the pole).
- Preparation of digital image maps with directional filtering.
- Upward continuation of the TMI and presentation in the form of contour maps.
- Profile data processing (smoothing and filtering of TMI and vertical gradient data).
- Preparation of stacked profiles of TMI, vertical gradient and square root of the vertical gradient for both north-south tie lines and east-west flight lines.
- Forward modelling of the magnetic profiles from the western and eastern part of the Polda Trough and across its southern margin.

4.1.2 Gravity survey

The Polda Trough area has been covered by a regional gravity survey on land, as well as a marine gravity survey. Several short lines with closely spaced stations were also surveyed on land.

(I) Regional gravity survey

In the period 1956 to 1961 the Exploration Geophysics Section of the South Australian Department of Mines and Energy (now MESA) conducted a regional gravity survey on widely spaced stations, located along railway lines and main highways. From 1967 to 1976 a more uniform network of stations, with nominal spacing of four miles (about 7 km), was conducted by SADME together with the BMR (now the Australian Geological Survey Organisation). The station location map of Eyre Peninsula is shown in Figure 4.2.

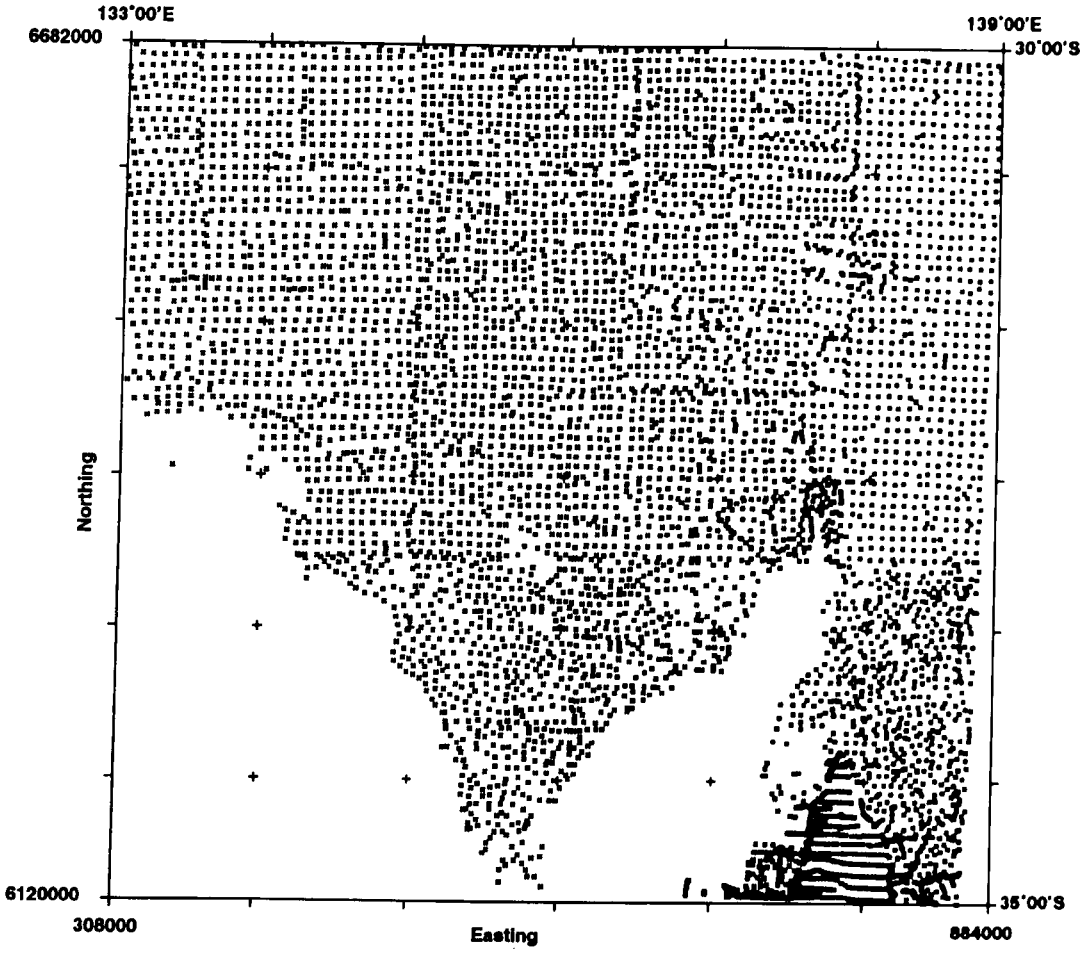

Figure 4.2 Location map of gravity stations - Eyre Peninsula.

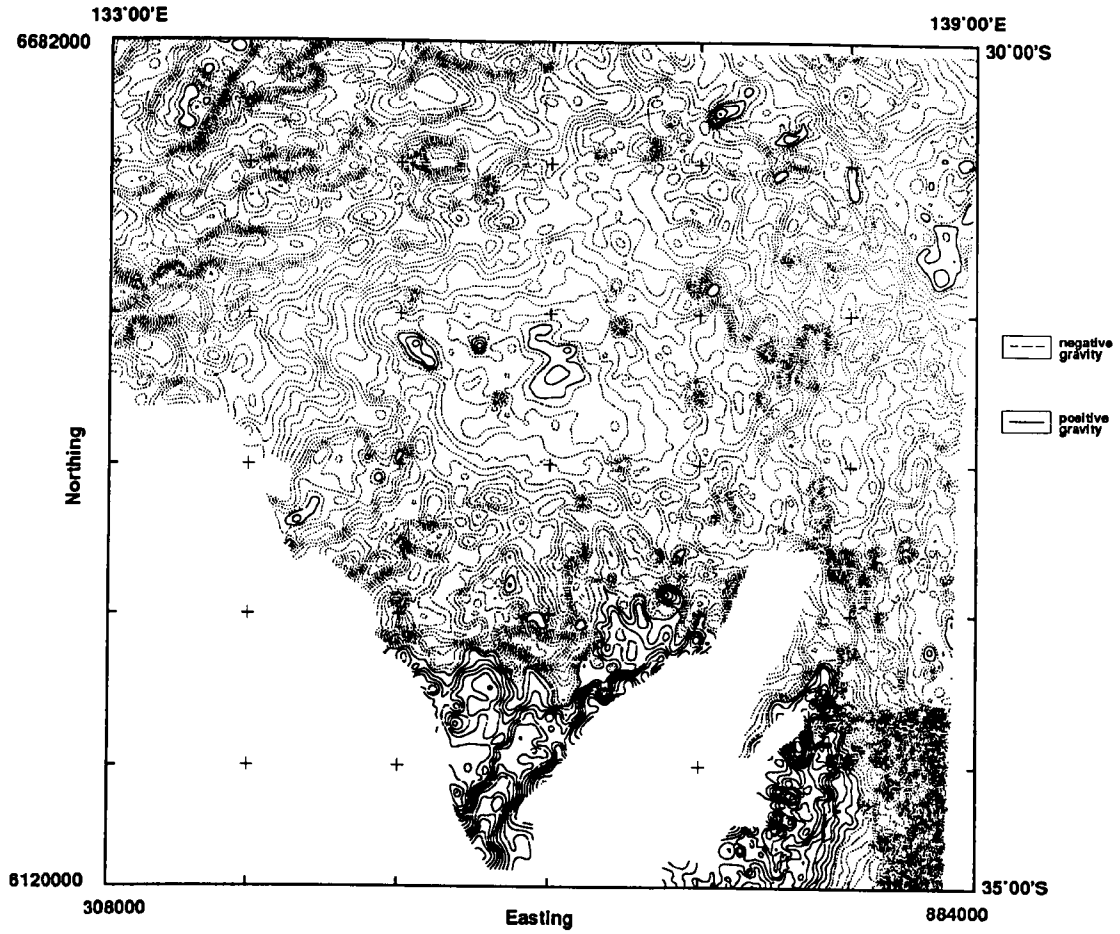

Figure 4.3 Bouguer gravity map - Eyre Peninsula. Contour interval 3 mgal.

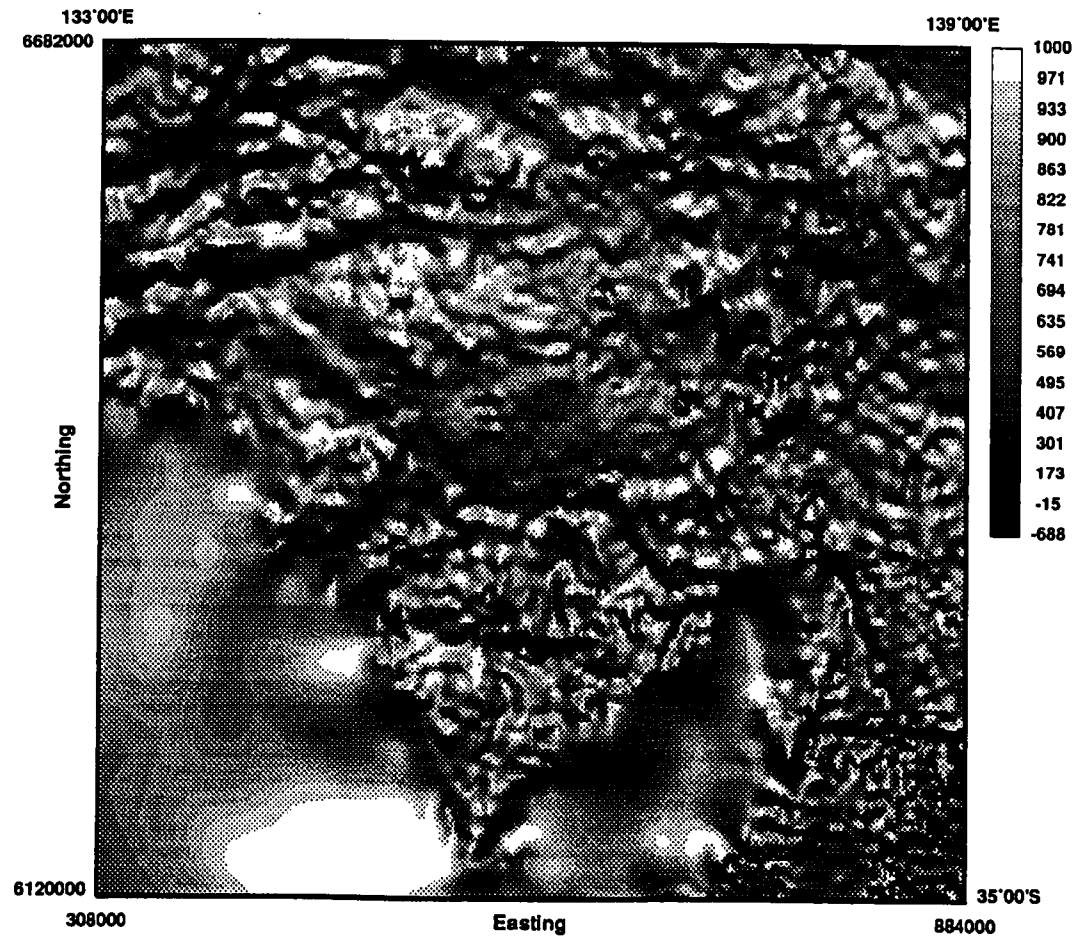

Figure 4.4 Shaded relief image of Bouguer gravity - Eyre Peninsula.

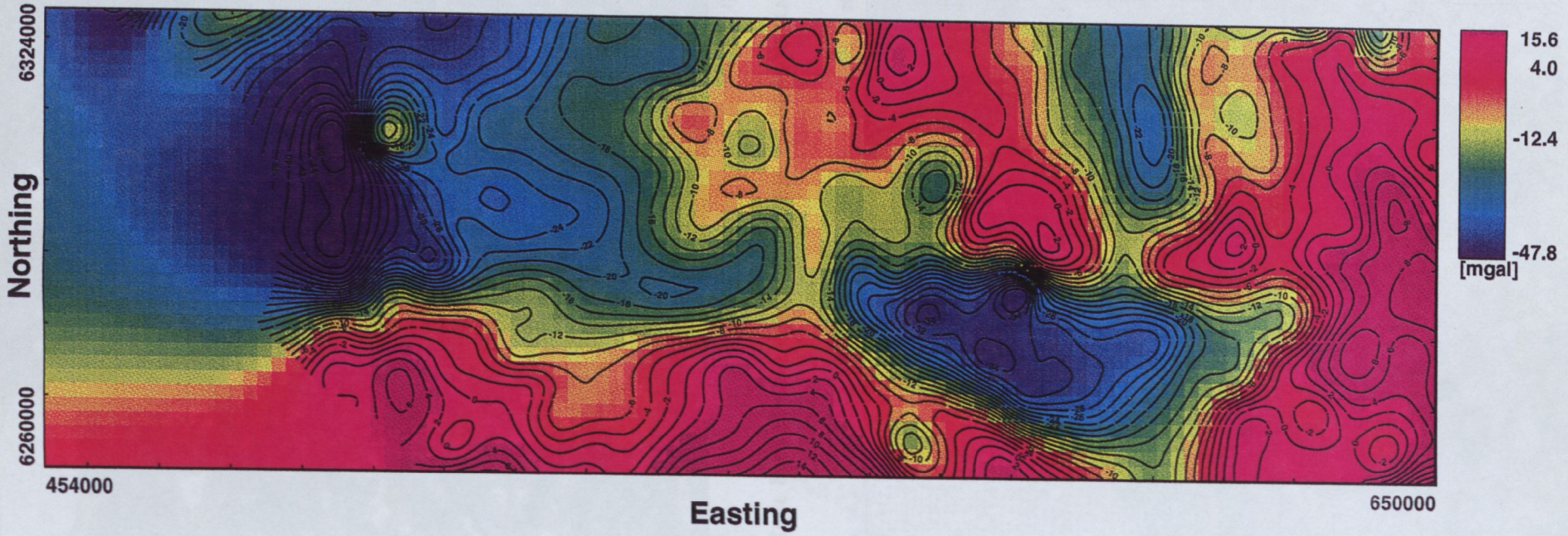

Figure 4.5 Bouguer gravity field across the Polda Trough. Colour image with superimposed contours at 2 mGals interval.

The standard gravity field in reference to an ellipsoid was computed using the Geodetic Reference System formula:

$$G = 978049(1 + 0.0052884\sin^2\varphi - 0.0000059\sin^2 2\varphi)$$

where φ is the latitude of the station and the gravity field units are in milli-gal (mgal) or $10\mu\ m/sec^2$.

Bouguer gravity anomalies, Δg, were computed at mean sea level with the assumption of an average crustal density of $2.67 g/cm^3$. The terrain corrections were neglected; as this area has a relatively flat topography and the error introduced is therefore very small.

The observed gravity data covering the State of South Australia was processed and transformed into a grid format, with a grid spacing of $2km \times 2km$. This data is presented in form of a 1:2,000,000 contour map (Figure 4.3) and, on the same scale, several grey scale images with various illumination parameters (azimuth, elevation angle, scale factor). An example of a shaded relief image of the Bouguer gravity over Eyre Peninsula is shown in Figure 4.4

In Figure 4.5 the colour image with superimposed contours of the Bouguer gravity across the Polda Trough is shown. The spacing between the observation stations of the regional gravity data is too large for a detailed interpretation of the relatively narrow Polda Trough structure.

(II) Gravity profiles

Several north-south oriented gravity traverses transect the study area. As indicated in Figure 4.6 the majority of these profiles are too short as they cover only part of the gravity anomalies. Most of the profiles provide information about the northern margin of the Polda Trough only. The results of the interpretation of the gravity profiles together with the interpretation of the regional gravity survey are integrated with the interpretation of the aeromagnetic survey data and geological information. The significance of this will be discussed in the following sections of this chapter.

4.1.3 Seismic survey

As mentioned in Chapter 3, in the onshore part of the Polda Trough a seismic survey was commenced in 1967 after discovery of the Elliston Trough. The Colton refraction seismic traverse of 12 km length, located on the west coast of Eyre Peninsula covered and verified the onshore extension of the Elliston Trough (Coppin, 1967). The survey quality revealed refractor velocities indicating a high speed basement at 690 m with some records also suggesting greater depth.

To assist in the evaluation of the coal potential of the Polda Basin a seismic refraction survey was conducted in 1976. Two discontinuous traverses were shot, one along the Lock-Tuckey road and a second along a NW-SE track north of Mt. Wedge (Figure 4.7).

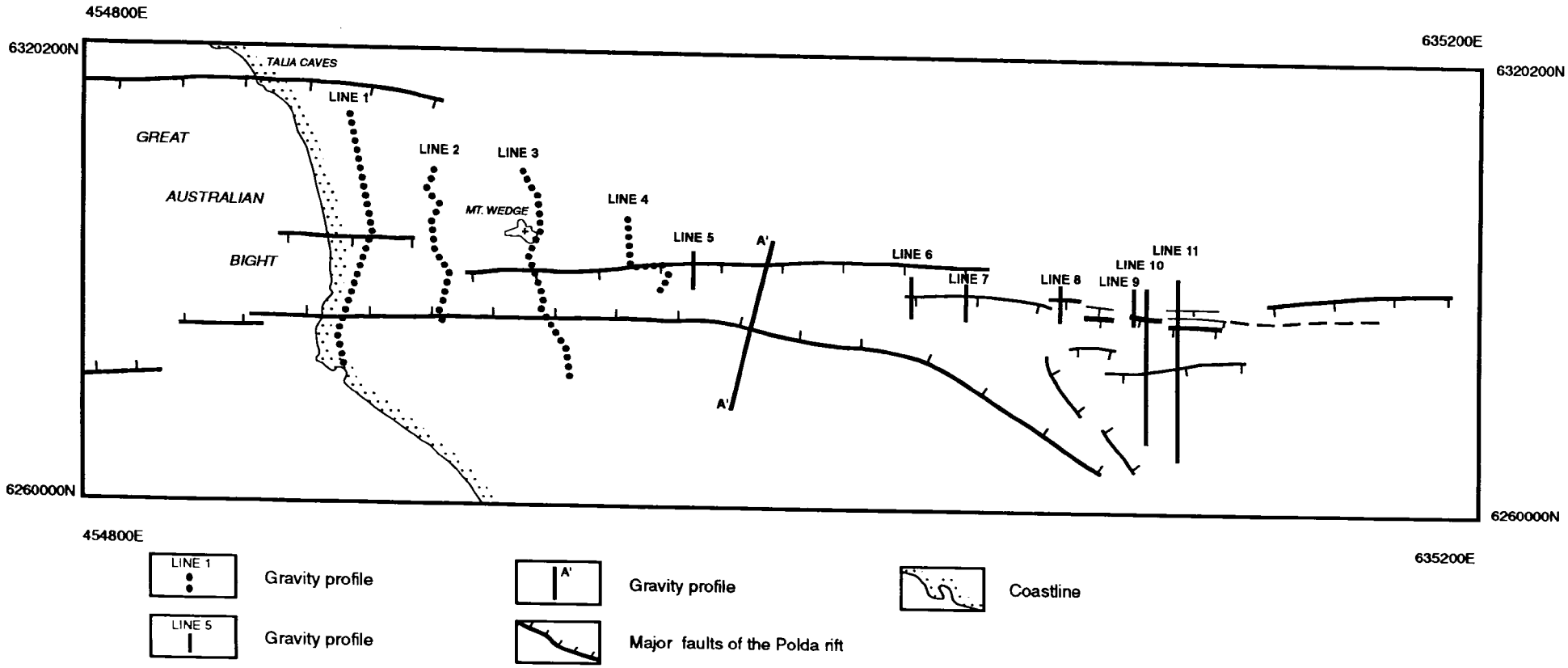

Figure 4.6 Location of gravity traverses across the Polda Trough.

Gerdes (1983) interpreted the reflection seismic section *PB-80-A* (Figure 4.8) surveyed by SADME in 1980. His interpretation was based on geological data from 4 drill holes together with additional data from a multiple uphole shot and an expander spread (Gerdes, 1983). According to Gerdes (1983), there are five reflection horizons which indicate internal sedimentary structures, possible facies changes, or perhaps the result of the data processing.

In the eastern end of the Polda Trough a seismic reflection line *PB83-001* was surveyed and processed (non migrated) by SADME in 1983 (Figure 4.7; SADME, 1983).

4.2 Physical properties of rocks and minerals occurring in the research area

The important aspect of the interpretation of geophysical data is assessment of the geological significance of geophysical anomalies. To minimise the ambiguity inherent in interpretation of the potential fields, it is essential to known as much as possible about the petrophysical properties of rocks occurring in the study area.

4.2.1 Magnetic susceptibility

A significant part of the research presented in this thesis is connected with analysis of the magnetic anomalies caused by a rocks at great depth, down to the Curie point surface. Magnetic properties of rocks in the lower crust and possibly upper mantle are determined based on laboratory studies of xenoliths from the lower crust and the upper mantle (Wasilewski et al., 1979; Wasilewski and Mayhew, 1982; Haggerty and Toft, 1985; Toft and Haggerty, 1988), and a detailed magnetic analysis of tectonically uplifted terrains (Fountain and Salisbury, 1981). The results of the study of the deep crust as well as discussion of the basal depth of the magnetisation (based on the literature review) are included in Chapter 5 and Chapter 6.

This section summarises the magnetic properties of rock samples from the Polda Trough. The information provided allows interpretation of the anomalies governed by the magnetic sources that are distributed in the upper few kilometres of the earth's crust.

The susceptibility values used for the modelling of the magnetic anomalies were based on:

- literature review for magnetic properties of rocks and minerals occurring in the research area
- susceptibility measurements of drill core samples from the stratigraphic holes: *CRA83KD1A, Polda-1, Lock-1*. The sediments are non-magnetic.
- susceptibility measurements of the samples representing the intrusives of the Hiltaba Granite Suite collected by SADME from the offshore islands within the Great Australian Bight south of the Polda Trough.

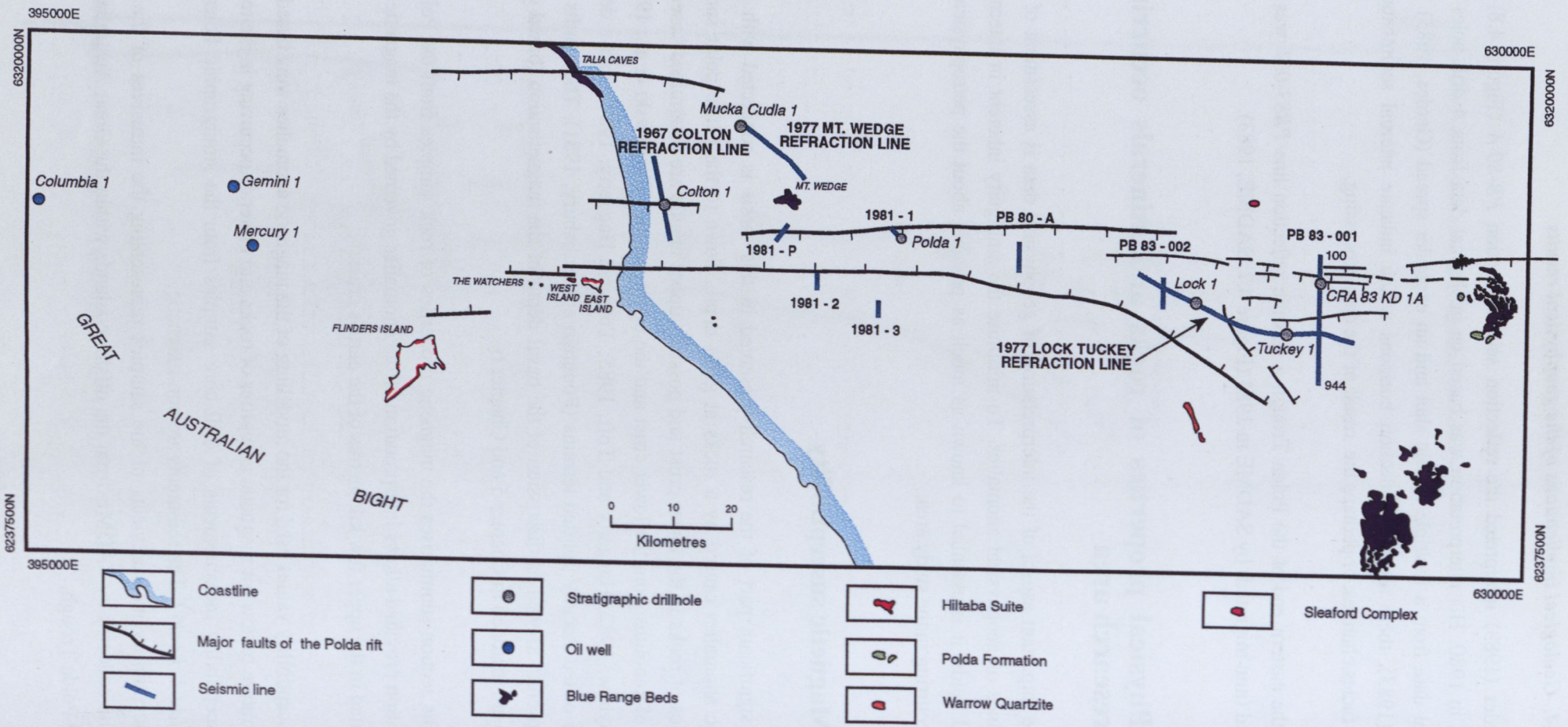

Figure 4.7 Location of seismic refraction traverses across the Polda rift. After SADME.

(i) Neoproterozoic Kilroo Formation .

The sediments of this formation are not magnetic, with most susceptibility values in the range of $5-30\times10^{-5}SI$. Sporadically red-brown hard siltstone is interbeded with thin, of up to a few tens of centimetres thick, dark bands containing fine-grained magnetite ($90-100\times10^{-5}SI$). In the hole *CRA83KD1A* magnetisation increases towards the contact of the sediments with the volcanics; in the zone from 1098 m to 1101 m where the sediments contain tuff, magnetisation becomes slightly stronger ($100-400\times10^{-5}SI$). Both layers of volcanics encountered in hole *CRA83KD1A* are strongly magnetic. The susceptibility of the upper basalt ranges from $1500-3250\times10^{-5}SI$ and the lower basalt shows stronger magnetisation. Most of the susceptibility readings are between $3500-5000\times10^{-5}SI$ with some values reaching over $7000\times10^{-5}SI$.

(ii) Permo-Carboniferous Coolardie Formation.

The magnetisation of the Coolardie Formation is very weak.; susceptibility varies in the range $100\pm300\times10^{-5}SI$, with sporadic higher values above $700\times10^{-5}SI$.

4.2.2 Density of rocks

The determination of the density contrast between the basement rocks and the sediments, which are preserved or deposited in the Polda Trough, is of prime importance in the interpretation and study of the gravity field. All of the sedimentary units, together with the underlain basement rocks, can be sampled from the drill cores only. There are no outcrops of rift fill sediments with the exception of exposed Jurassic rocks on the eastern margin of the Polda rift. Outcrops of surrounding and underlying basement are very limited, except for the Mesoproterozoic Blue Range Beds, which are exposed on the eastern end of the rift and in the vicinity of Mt. Wedge and the Talia Caves immediately north of the northern margin of the rift, close to the coast line.

Several samples of the granites, representing the Mesoproterozoic Hiltaba Suite, were collected by SADME on the offshore part of the rift from Flinders Island, Waldegrave Island, the Watchers, the Ward Islands and the Pearson and Veteran Isles (Elliston Geological Map, 1:250,000,000 for locations).

The density contrast of the sediments, extrusive and basement rocks of the Polda Trough are obtained from direct measurements of the rock samples, an interpretation of the density borehole logs and also from a review of previous research and exploration conducted in this area (e.g. McPharlin, 1980; CRA, 1981, 1982A, 1982B, 1983, 1985, Capon, 1984). Density of $2.7g/cm^3$ was used for gravity modelling of the basement rocks.

The specific gravity values for a rock unit, representing basement and sediments in the study area are based on core samples of the stratigraphic hole *CRA 83KD1A* (total depth equal 1392 metres), and several shallower drill holes (*Polda-1, Polda-2, Polda-3, Polda-6, Polda-8, Polda-9, Polda-10, Polda-12, Polda-21, Polda-6, Tuckey-1, and Lock-1*) drilled by SADME. The measured density values for different stratigraphic units were calculated as a weighted average of the core

samples. The density of a total of 420 samples were measured. The full details of the measurements and the calculated average density values have been lodged with MESA.

(i) Mesoproterozoic Blue Range Beds.

McPharlin (1980) reports density values determined from drill core samples from the *Colton 1* drill hole and described as 'Mt. Wedge grit'. The average drill core density was calculated as $2.25 \pm 0.18 g/cm^3$. McPharlin (1980), based on five samples collected near the Talia Caves and from the Mount Wedge area, established the average density as $2.42 \pm 0.05 g/cm^3$. He suggests that the bulk density in situ should not exceed $2.5 g/cm^3$ assuming less than 10% porosity.

(ii) Neoproterozoic Kilroo Formation.

Detailed sampling (core samples from the hole *CRA83KD1A*) and density measurement of the Kilroo Formation indicate that the density of the sediments in the upper part of the hole is noticeably less than in the lower part. The top sequence of the red siltstone/mudstone has an average density of $2.45 g/cm^3$ (40 samples). The middle section has a density of $2.63 g/cm^3$ (13 samples), and the bottom interval has an average density of $2.68 g/cm^3$ (36 samples). The average density of the top basaltic layer is equal to $3.08 g/cm^3$ (10 samples); the density of the bottom 90 m of volcanics averages $2.87 g/cm^3$ (44 samples).

The average density inferred from the density log equals $2.54 g/cm^3$ for the top 100 m.

i) Permo-Carboniferous Coolardie Formation.

The average density of this formation which is represented by a coarse diamictite equals $2.29 g/cm^3$ on the moisture free basis (30 core samples from 4 drill holes).

(iv) Jurassic Polda Formation.

The average density of Jurassic rocks in the Polda rift, measured from the drill-core samples is on the moisture free basis 1.89 g/cm^3.

(v) Tertiary sediments.

The average density of the Tertiary sediments is *1.82* g/cm^3 (23 samples from 5 holes). For assumed porosities of 10% and 20%, average density equals 1.93 g/cm^3 and 2.02 g/cm^3 respectively.

4.3 Geological implications of the geophysical studies of the Polda Trough

As the aim of this thesis is to understand the structure and evolution of the onshore Polda Trough, it is essential to build an overall view of the basin by establishing what are the known facts, and what are only interpretation concepts in both the onshore and offshore parts of the trough.

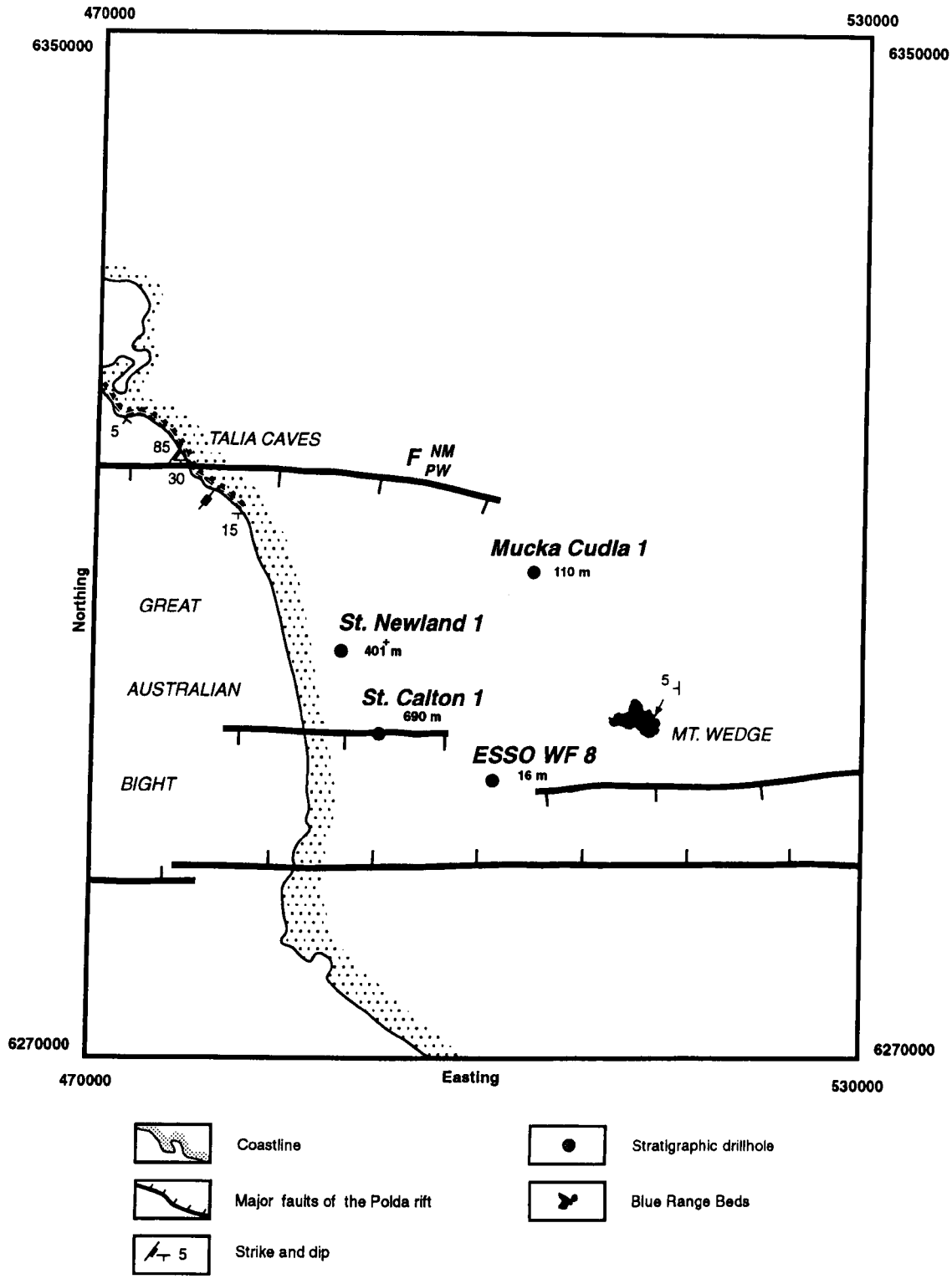

Figure 4.8 Itiledoo Basin West - geological evidence.

4.3.1 The Blue Range Beds of the Mesoproterozoic

The Mesoproterozoic unconformably overlies the Hutchison Group and is represented by the formation of unmetamorphosed arenites, assigned to the Blue Range Beds (see Section 3.2.3 part I). In the past, the structural setting of these arenaceous sediments was delineated as the Itiledoo Basin '...a major elongate east-west trough containing up to 2500 m of sediments...' (Flint, 1993). The distribution of the Mesoproterozoic rocks in South Australia, recently published by SADME (1993), also shows the Itiledoo Basin as a continuous, several hundred kilometres east-west elongated structure.

The Mesoproterozoic Blue Range Beds (BRB) are exposed in several areas on the central Eyre Peninsula and also on the west coast (see Geological Map Kimba, Elliston and Whyalla 1:250,000). The surface exposures of the Blue Range Beds are located in three different regions in relation to the Polda Trough. The Blue Range Beds outcrops are located along the Talia Caves and in the Mount Wedge area on the western coast of Eyre Peninsula and will be referred as the Itiledoo Basin West. The Blue Range, Verran Hill and Sheok Hill outcrops, which are located on the south-eastern flank of the Polda Trough, will be described as the Itiledoo Basin South-east, and the Blue Range Beds exposed immediately on the eastern end of the Polda Trough, will be referred to as the Itiledoo Basin East.

The Blue Range Beds are also exposed about 50 km eastwards from the eastern margin of the Polda Trough, at Point Gibbon area (Whyalla Geological Map 1:250,000). This occurrence of the Blue Range Beds will be shown at maps of the Itiledoo Basin South-east.

(I) Itiledoo Basin West

(i) New observations derived from the geophysical and geological interpretation

The identification of the geology and structure of the Blue Range Beds is based on two outcrops at Mount Wedge and the Talia Caves and four drill holes: *Newland-1*, *Colton-1*, *Mucka Cudla-1*, *ESSO WF8*. As marked in Figure 4.9, the Blue Range Beds which are exposed in the Mount Wedge area, dip very gently $5°W$ whereas in the Talia Caves, they dip $5°SW - 20°S$ with the exception of several high angles of dip in the area where the Blue Range Beds are transected by the northern boundary fault F_{PW}^{NM} of the Polda Trough.

Drill hole data covers only the upper contact of the Blue Range Beds with the Tertiary. Only hole *ESSO WF8,* intersects 71 m of Jurassic sediments overlying the Blue Range Beds. The hole is located on the faulted northern margin of the Polda Trough. Contact with underlying older basement was not encountered in any of the drill holes. Drill hole *Newland-1* intersected 401 m of the Blue Range Beds sediments.

During the Colton reconnaissance seismic survey (Coppin, 1967, drill hole *Colton-1*) a presumably crystalline basement refractor (*4900 m/sec*) was revealed at a depth of 690 m. Drilling intersected the Blue Range Beds below 110 m, hence the probable total thickness of this unit does not exceed 600 m.

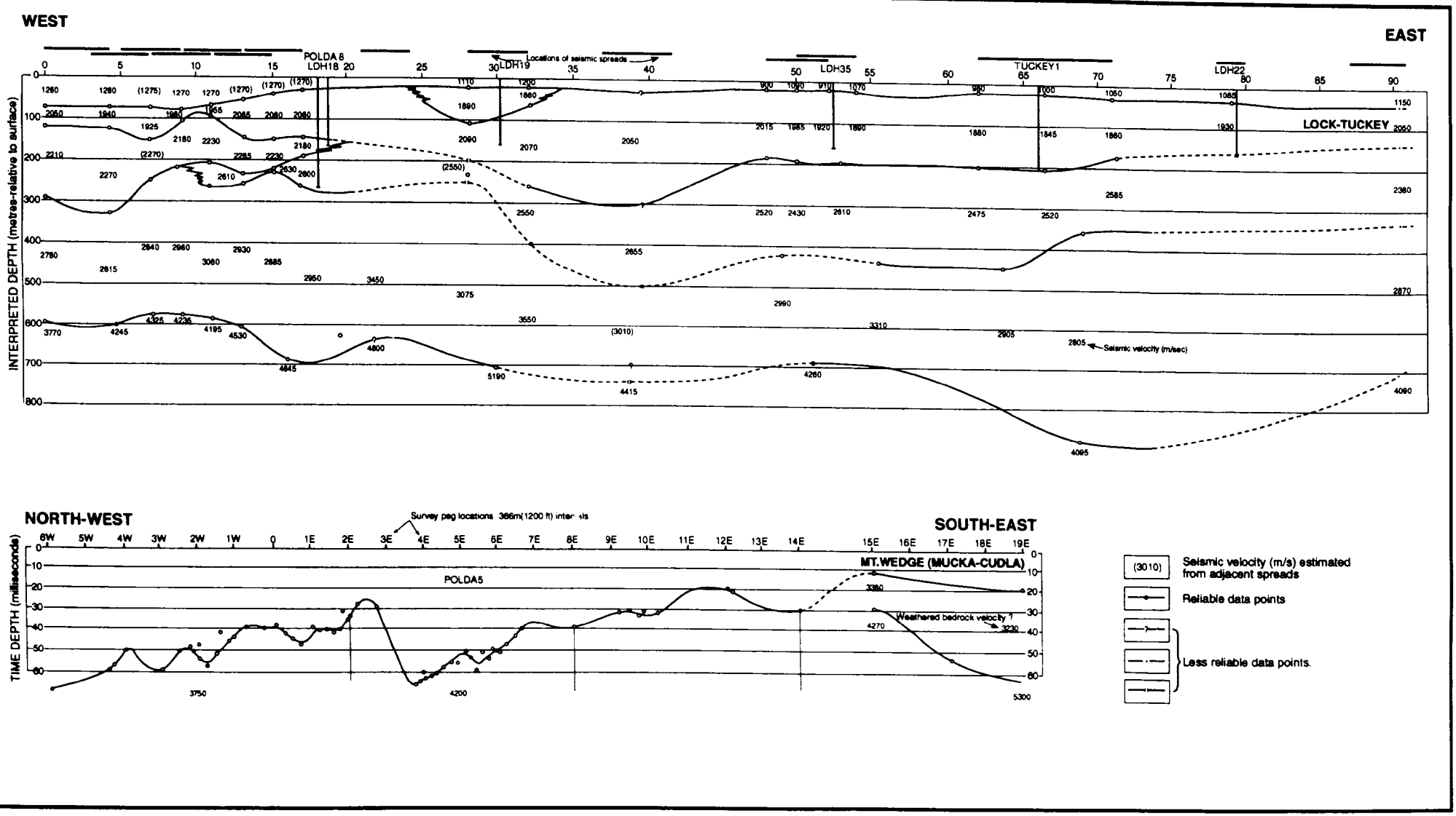

Figure 4.9 Lock-Tuckey and Mount Wedge refraction lines. After SADME.

Seismic refraction investigations in the Polda Basin (Figure 4.6) were carried out by SADME in 1977 as part of coal exploration. On the time-depth section produced from the Mt. Wedge line data, it can be seen that the bedrock dips shallowly westwards. It is probably faulted in the vicinity of peg 3E (see Figure 4.9). Subsequent drilling (*Mucka Cudla-1* and *Polda-5*) showed that the bedrock consists of Mount Wedge grits.

The Blue Range Beds are non-magnetic sediments. McPharlin (1980) reports very low susceptibility measurements based on the drill hole core (*Colton-1*).

Except for the two outcrops mentioned above, the whole area is covered by a thick layer of Tertiary and Quaternary sediments. Towards the north-east and east in a distance of less than 20 km from Mount Wedge, several drill holes (*P3, P2, CRA81LRM53-55* and, *51*) intersected 30-40 m of Tertiary underlain by Archaean basement, which is exposed further north. As there is limited drill hole data, the aeromagnetic and gravity survey data provide key information concerning the structural setting, extension and thickness of the Blue Range Beds sediments.

Important information about the structural setting of the Blue Range Beds is provided from the aeromagnetic data. Figure 4.10(b) shows the major structures interpreted from the aeromagnetic map (Figure 4.10(a)). These are marginal faults of the narrow east-west trending Polda Trough. A major east-west fault structure (F_{PW}^{NM}) is located towards the north. The fault F_{PW}^{NM} is a normal fault with the direction of dip towards the south. Near the Talia Caves gently dipping Blue Range Beds are exposed on both sides of the fault F_{PW}^{NM} (see Figure 4.10). It is to be noted that the position of the very steeply dipping strata of the Blue Range Beds coincides with the position of the F_{PW}^{NM} fault. The fault F_{PW}^{NM} can be traced offshore, where it obviously controlled the Mesozoic rifting. Thus it is clear that the movement along the F_{PW}^{NM} fault is post-deposition of the Blue Range Beds. There is no obvious evidence that this fault is older than the Blue Range Beds. The Blue Range Beds are preserved in the upthrow side of the boundary fault F_{PW}^{NM} showing that the Polda rift was not essential in preserving the Blue Range Beds from erosion. This geological interpretation, inferred from geophysical investigations, provides critical evidence for relating the Blue Range Beds to the Polda Trough.

(ii) Interpretation of geophysics

(a) Magnetic signature

The aeromagnetic map shows magnetic rocks at depths of about 500 m at both outcrops and also at the location of drill hole *Newland-1* (Figure 4.10). There are alternative explanations for the presence of a shallow magnetic sources:

1. Shallow magnetic basement with irregular surface configuration, such as shown in Figure 4.11(a). This may be due to erosion or, as Figure 4.11(b) presents, due to graben-like fault structures within the older basement.

2. The Blue Range Beds may perhaps contain magnetic material (Figure 4.11(c)). However there is no record of magnetic material in the Blue Range Beds and where the Blue Range Beds are thickening, there are no observed shallow magnetic anomalies.

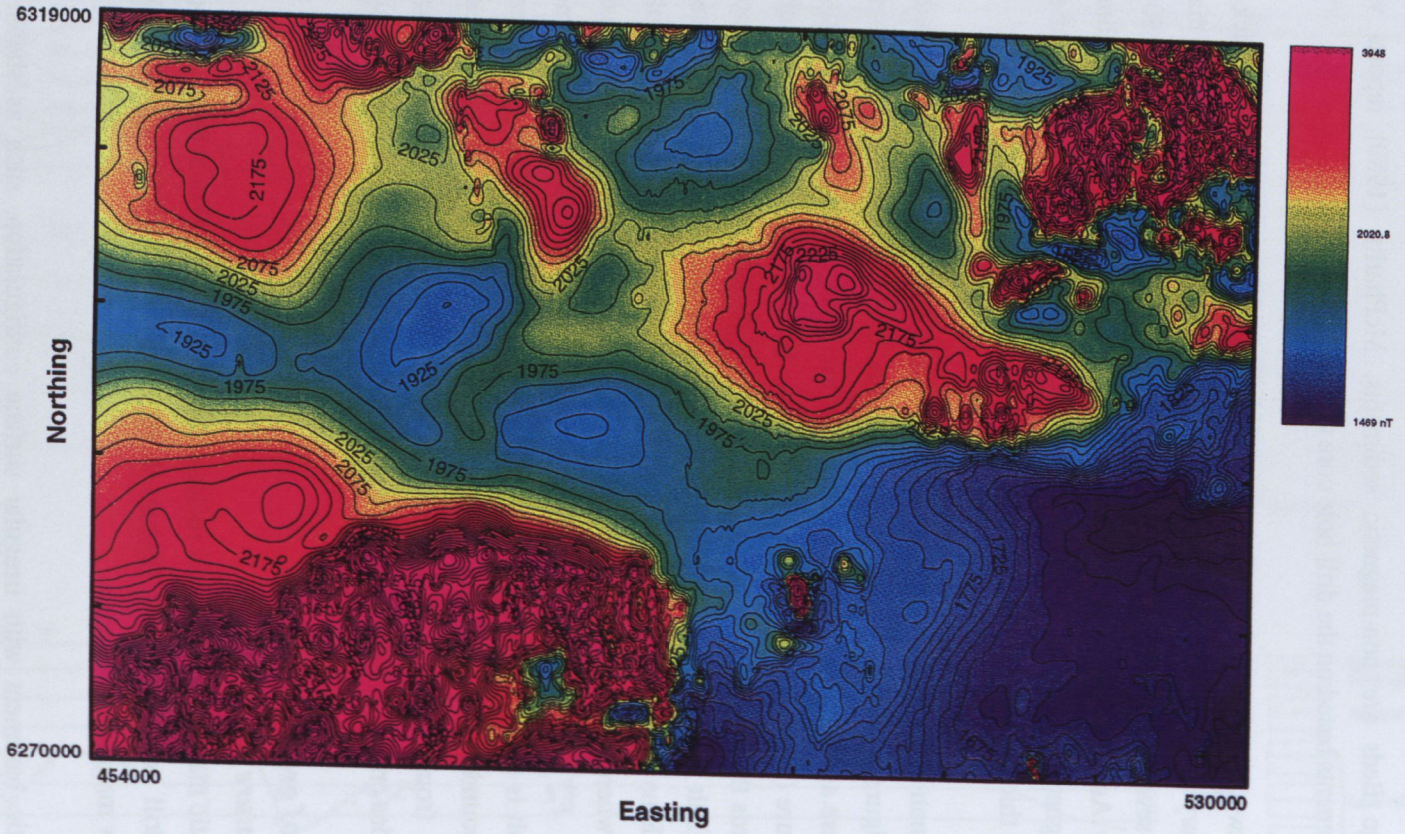

Figure 4.10(a) Itiledoo Basin West - Colour image of total magnetic intensity field with superimposed contours at 25nT interval

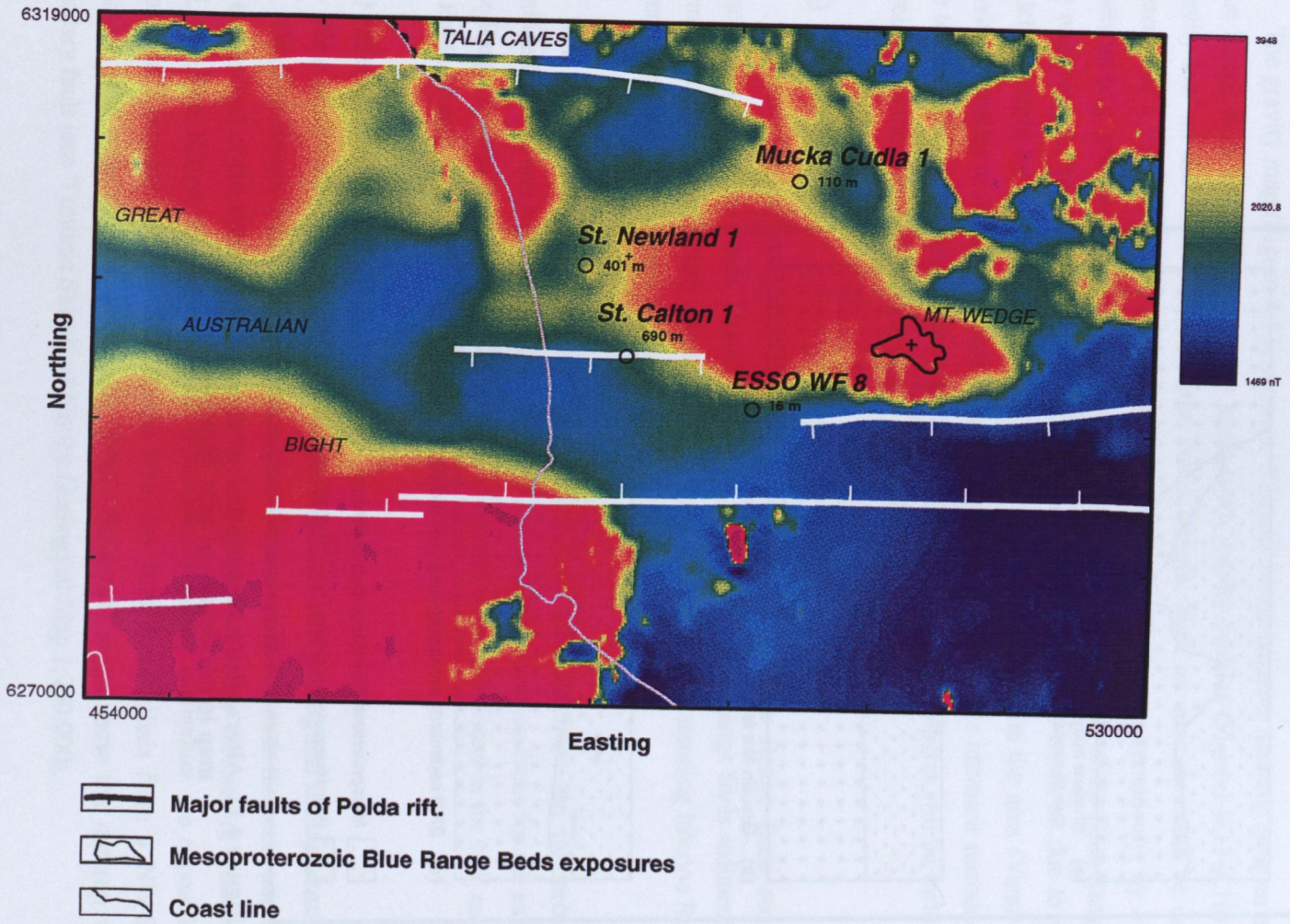

Figure 4.10(b) Itiledoo Basin West - Total magnetic intensity colour image showing also surface exposures and drillholes intersecting Mesoproterozoic Blue Range Beds.

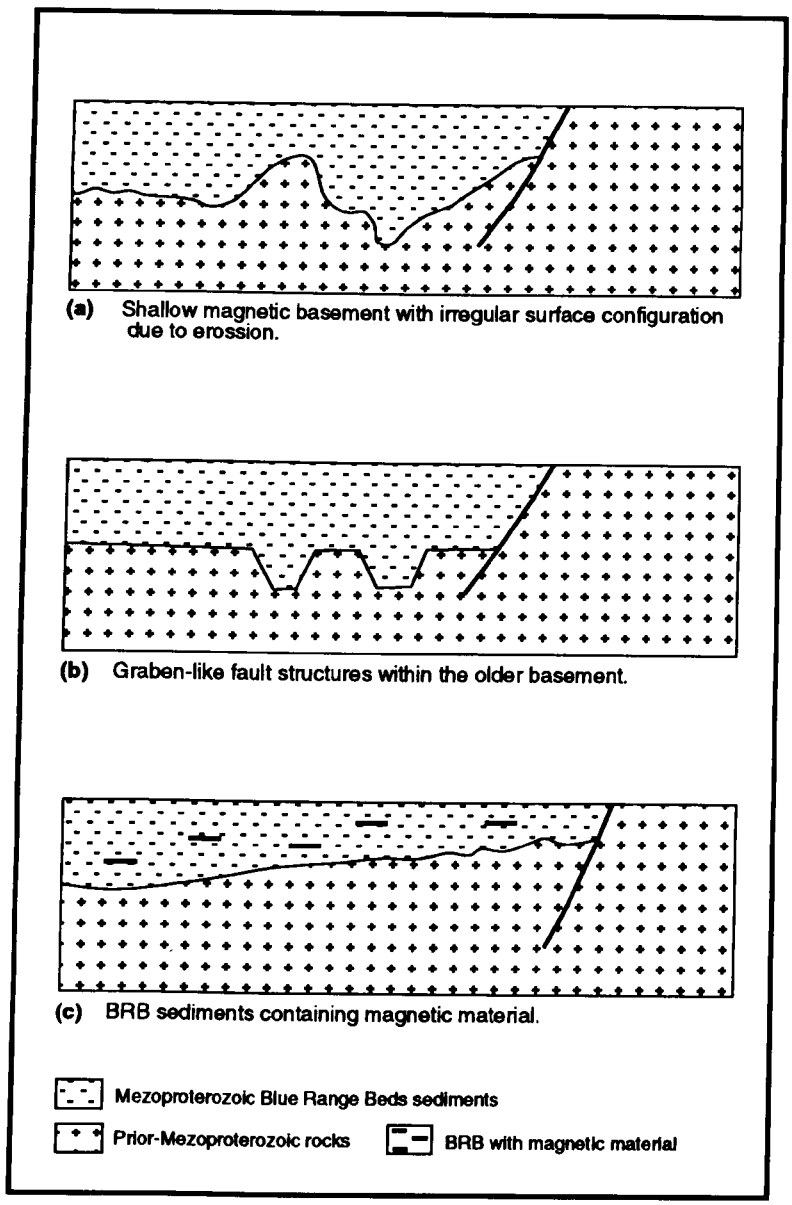

Figure 4.11 Alternative interpretations of the aeromagnetic map in the vicinity of hole *Newland-1*.

The TMI map shows areas where the magnetic field appears to be smoothed. These could indicate the deeper basement, but it is also probable that these areas of smoothed magnetic field are due to non-magnetic basement. A similar area of smooth TMI is observed in the central part of the Polda Trough region where it is known that its shallow basement is not magnetic.

(b) Gravity signature

The gravity map (Figure 4.12) shows a *40mgals* broad negative anomaly over an area were the Blue Range Beds are deposited. Three north-south gravity profiles (Figures 4.13-4.16) indicate the 'gravity low' on the northern flank of the Polda Trough. Such an anomaly could be caused by the presence of a very thick layer of low density Blue Range Beds, or alternatively, by a low density basement (e.g. granite intrusion of $2.65 g/cm^3$) covered by a thin layer of the Blue Range Beds. The big negative gravity anomaly with isolated patches of magnetic high could be due to country rock which is caught by a low density granite. There are other examples in the area (Venus Bay) where gravity anomalies of *-40 mgals* occur. These are perhaps due to granite intrusion surrounded by highs due to an aureole of scarns. Presence of these two large negative anomalies will be further addressed in relation to the deep crustal study found in Chapter 6.

(iii) Conclusions

The currently accepted model (Flint, 1993) is that the Blue Range Beds sediments were preserved in the 'proto- Polda Trough' structure, and that the Blue Range Beds sediments underlying Permian, Jurassic and Tertiary sequences are present in the east-west trending Itiledoo Basin which is several hundreds of kilometres long (Figure 4.17).

The maximum thickness of the Blue Range Beds obtained from the interpretation of the combined gravity and seismic data is less than 600 m, and there is no evidence for the existence of the Blue Range Beds in the continuous Itiledoo Basin, except where it is found in the NW onshore part of the Polda Trough and in the eastern end of the rift.

(II) Itiledoo Basin South-east

(i) New observations derived from the geophysical and geological interpretation

The Blue Range Beds are extensively exposed on the surface towards the south and south-east of the eastern end of the Polda Trough where the topography is slightly elevated at Verran Hill, Sheok Hill, and Blue Range. The series of unmetamorphosed pebbly sandstones are exposed in a gently dipping (*8°*) sequence. In the Blue Range area, the Blue Range Beds form a NW-SE synclinal structure with beds dipping *8°SW* and *8°NE*. Structural maps show the outcrop with a west boundary fault (see 'Tectonic Sketch' of Kimba Geological Map 1:250,000).

Drilling control in this area is limited. Only hole *PNC803-1* intersected 63 m of the Blue Range Beds covered by 49 m of Cainozoic sediments. The additional information is provided by magnetic and gravity data, which will be described in the following section.

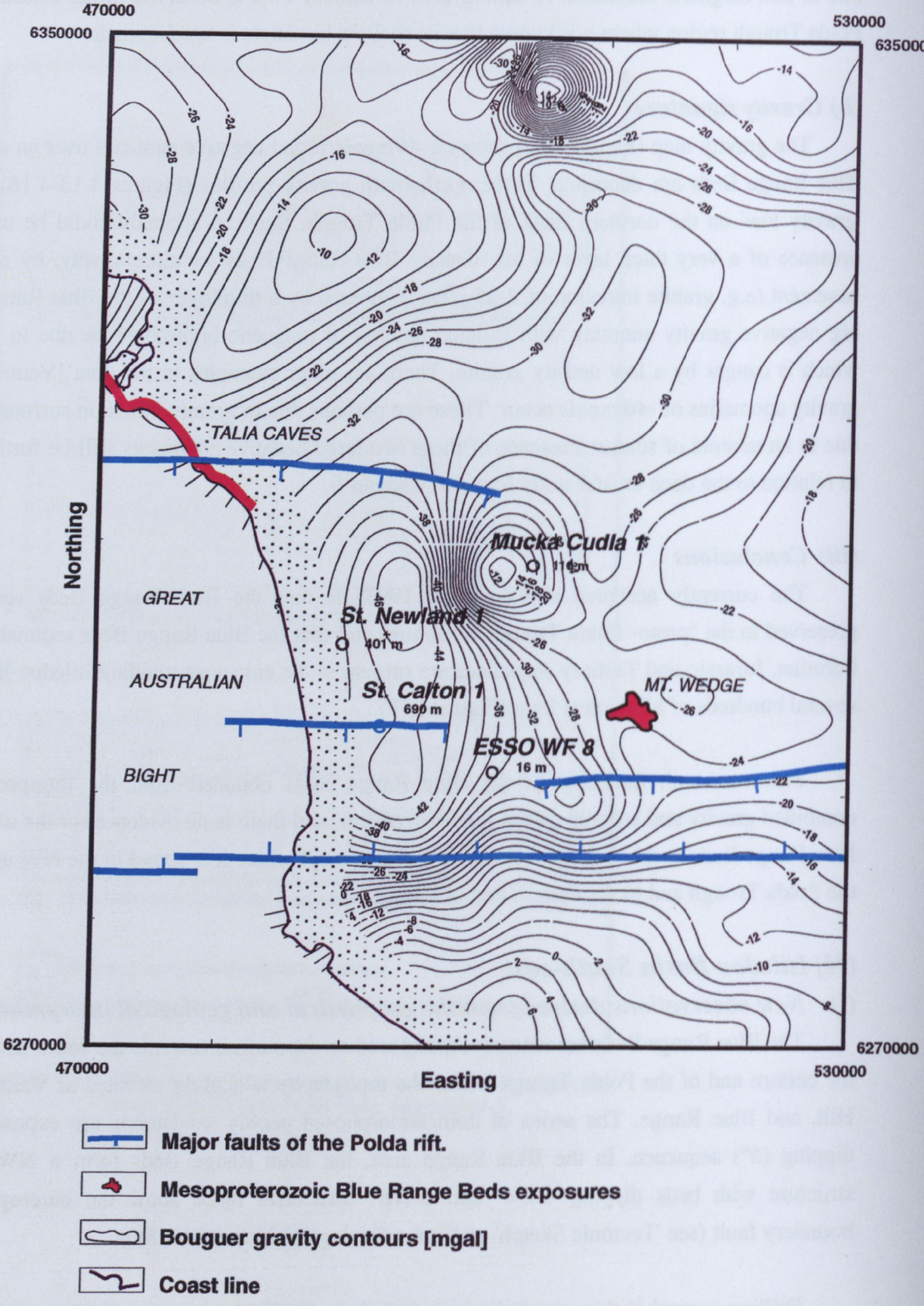

Figure 4.12 Itiledoo Basin West - Bouguer gravity map. Contours interval 2 mgal.

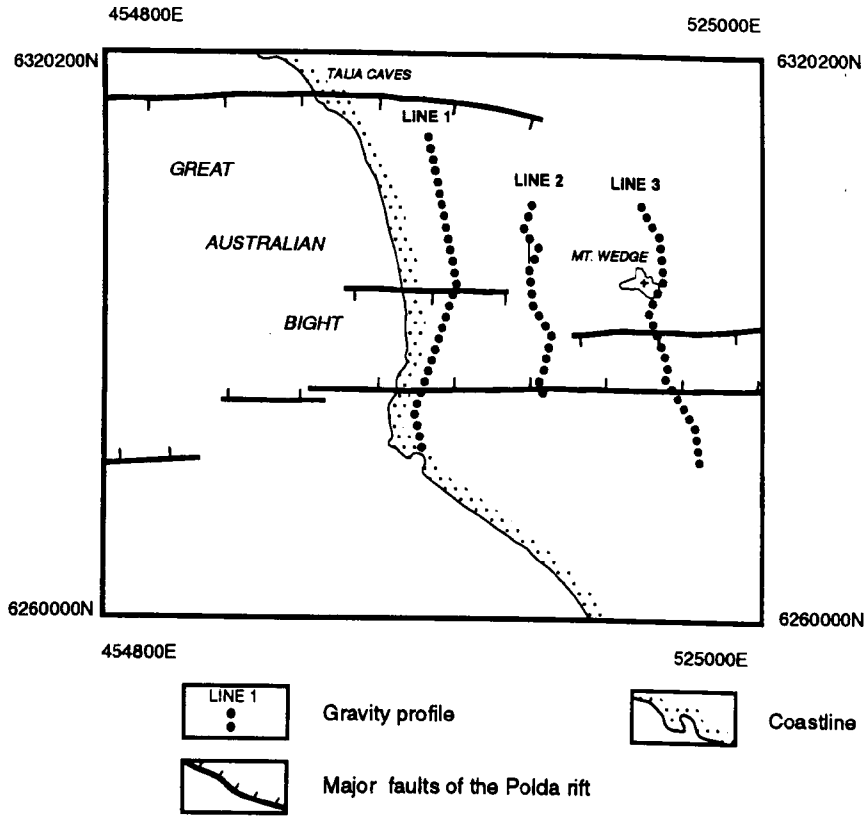

Figure 4.13 Itiledoo Basin West - location of the gravity survey profiles.

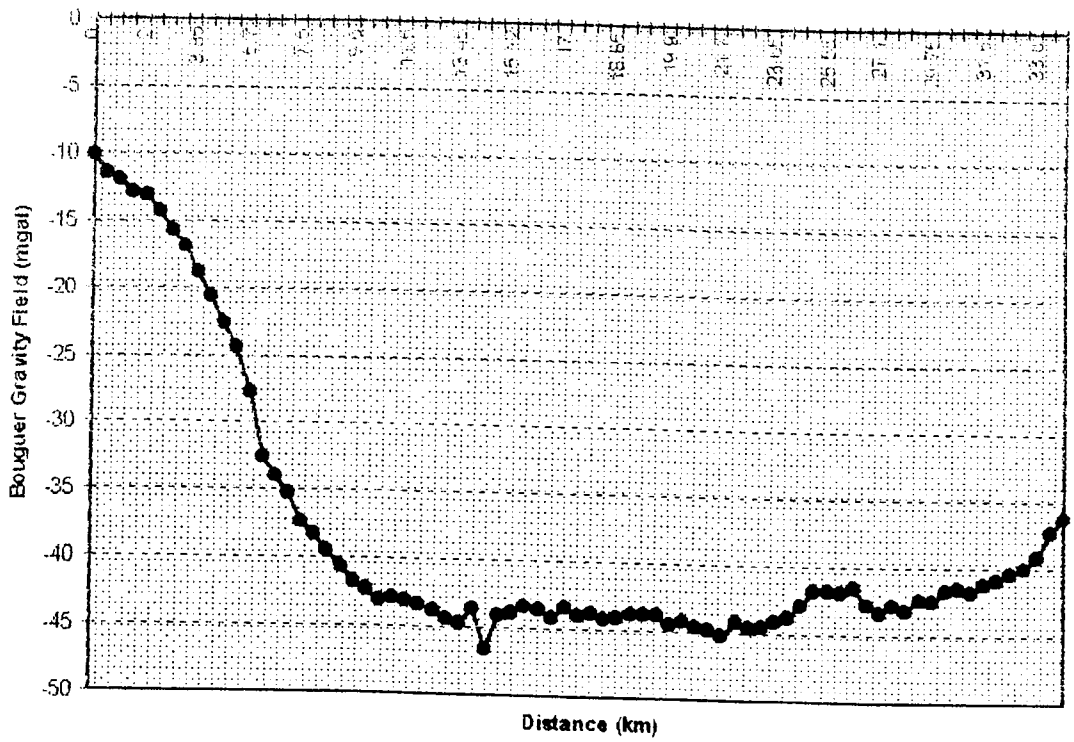

Figure 4.14 Itiledoo Basin West - Bouguer gravity prifile - 'Line 1'

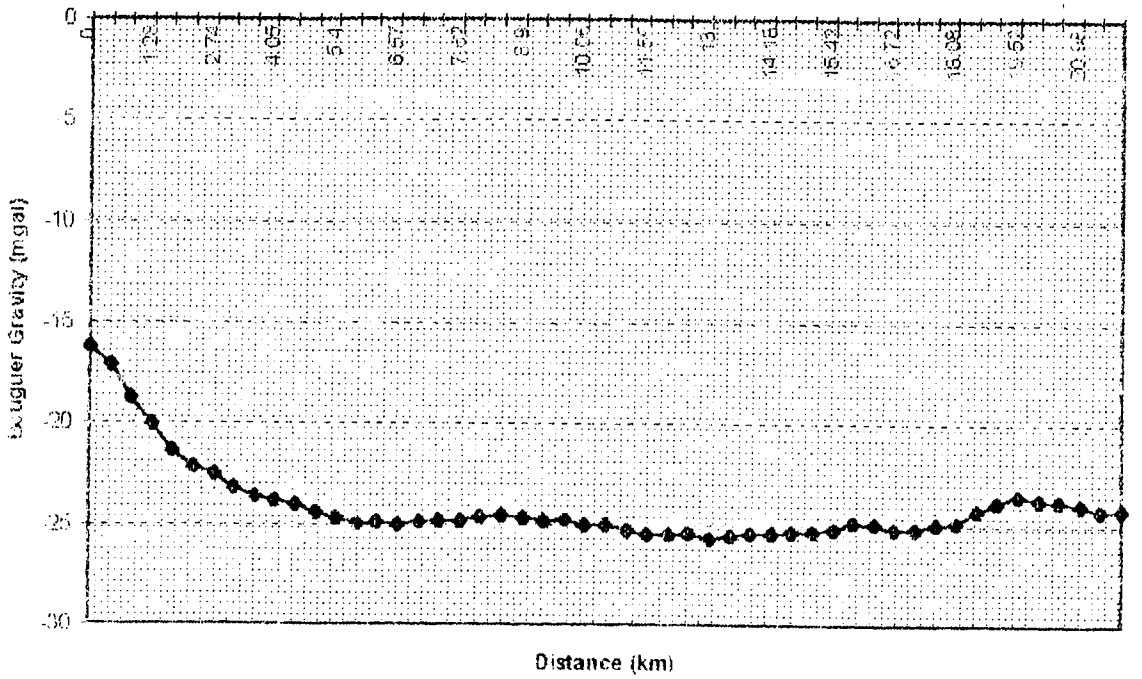

Figure 4.15 Itiledoo Basin West - Bouguer gravity prifile - 'Line 2'

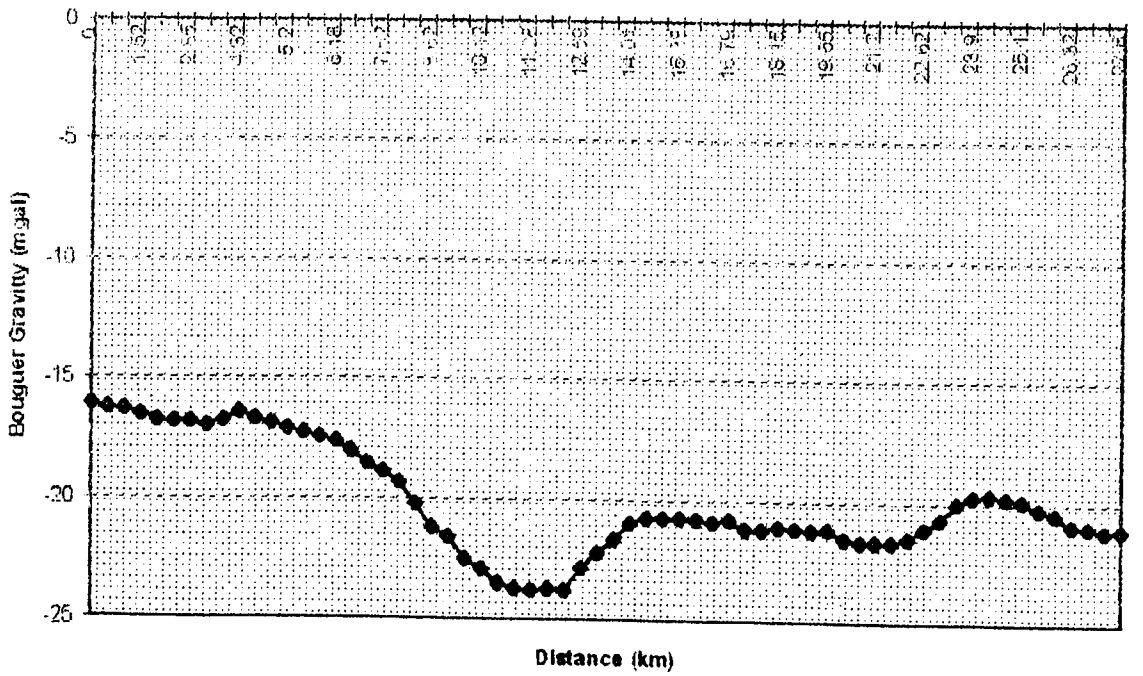

Figure 4.16 Itiledoo Basin West - Bouguer gravity prifile - 'Line 3'

(ii) Interpretation of geophysics

The configuration of the magnetic field anomalies is consistent with the boundaries of the Blue Range Beds established on geological evidence. The basement rocks are magnetic whereas the Blue Range Beds sequences are non magnetic; there is an evident north-south fault boundary on the western side of the outcrop of the Blue Range Beds (Figures 4.18-4.19).

There is no evidence of the presence of shallow magnetic rocks within the Blue Range Beds depositional boundaries established from the magnetics.

Three small magnetic anomalies shown in Figure 4.18 (A_1^{IB}, A_2^{IB}, A_3^{IB},) were used to determine the depth to the underlying magnetic basement. The depth of the underlying basement appears to be about 700 m.

In this part of the study area, the only available gravity data is a low resolution regional SADME survey, which was based on a spacing of 7 km. This consequently excluded any possibility of detailed interpretation.

A gravity anomaly of *-8 mgals* approximately coincides with the exposure of the Blue Range Beds sediments. This gravity anomaly starts from the exposed contact between the Blue Range Beds sediments and older basement rocks of Cook Gap Schists *(P hc)* which contain schists grading into gneiss (Figure 4.20). By constructing a geological section from the observed dip, the thickness of the Blue Range Beds can be as much as 1 km and assuming the density contrast between the Blue Range Beds and basement as $0.2 g/cm^3$ ($Sg_{BRB} = 2.5 g/cm^3$; $Sg_{bas} = 2.7 g/cm^3$) such a gravity anomaly could be explained. As the wide spacing of the gravity stations makes detailed interpretation impossible, it can only be observed that the gravity gradient on the north-south trending western edge implies a fault with the eastern side downthrown. The north-south gravity anomaly (Figure 4.20) on the western side of the outcrop, is consistent with the faulted boundary marked on the tectonic maps of this area.

(iii) Conclusions

The interpretation of the gravity field does not indicate the east-west fault boundaries of the Itiledoo Basin, which had, in the past, been claimed to exists (e.g. Flint, 1993). Based on the existing facts and the interpretation of geophysics, it is difficult to conceive that the Blue Range Beds depositional setting was an early east-west graben. On the contrary, the Blue Range Beds sediments appear to have been deposited in a platformal environment similar to the Stuart Shelf structural setting and have been preserved in a shallow fold.

(III) Itiledoo Basin East

(i) New observations derived from the geophysical and geological interpretation

Exposure of the contact between the Palaeoproterozoic basement rocks and unconformably overlying Mesoproterozoic sediments of the Blue Range Beds can be followed along the eastern end of the Polda rift. The Blue Range Beds are exposed in a series of thin sheets about 4 km long within the

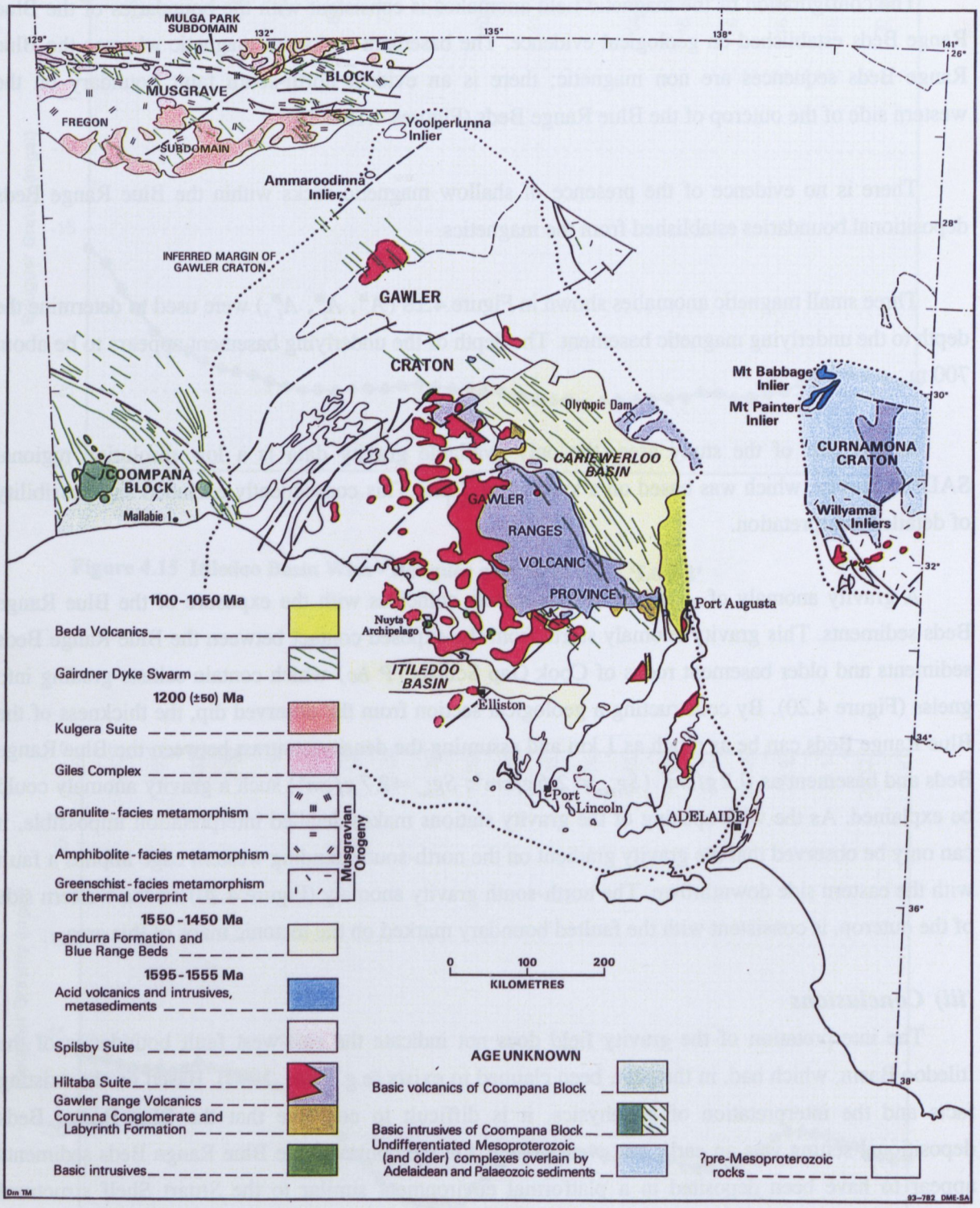

Figure 4.17 Distribution of Mesoproterozoic rocks in South Australia. After Flint et al. (1993).

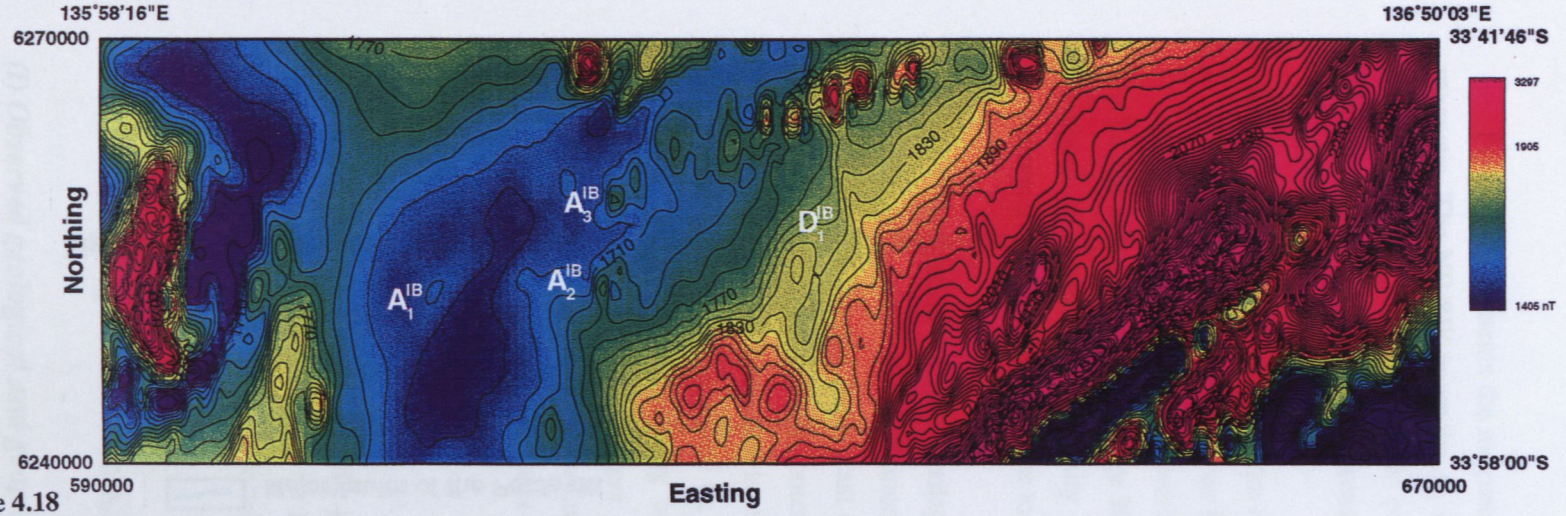

Figure 4.18

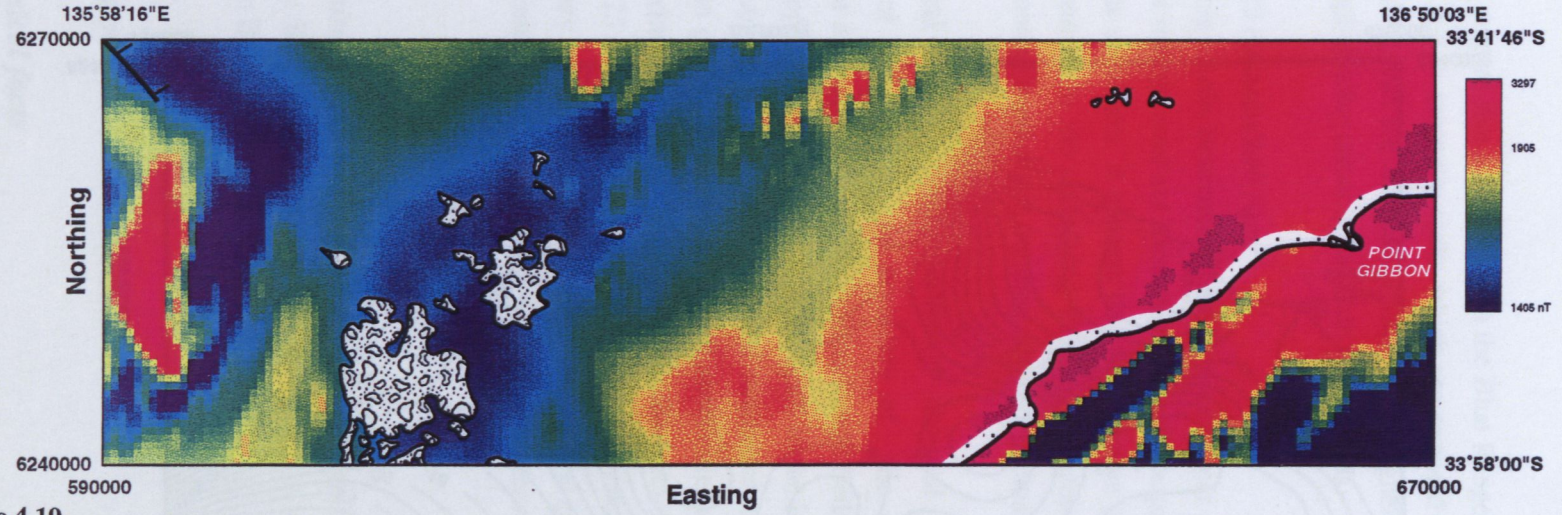

Figure 4.19

Major faults of the rift Mesoproterozoic Blue Range Beds exposures Coast line

Figure 4.18 Itiledoo Basin South-east: Image of TMI with contours at 15 nT interval showing location of magnetic anomalies A_1^{IB}, A_2^{IB}, A_3^{IB}.

Figure 4.19 Itiledoo Basin South-east: Image of TMI field with superimposed exposures of Mesoproterozoic Blue Range Beds and major faults of the Polda rift.

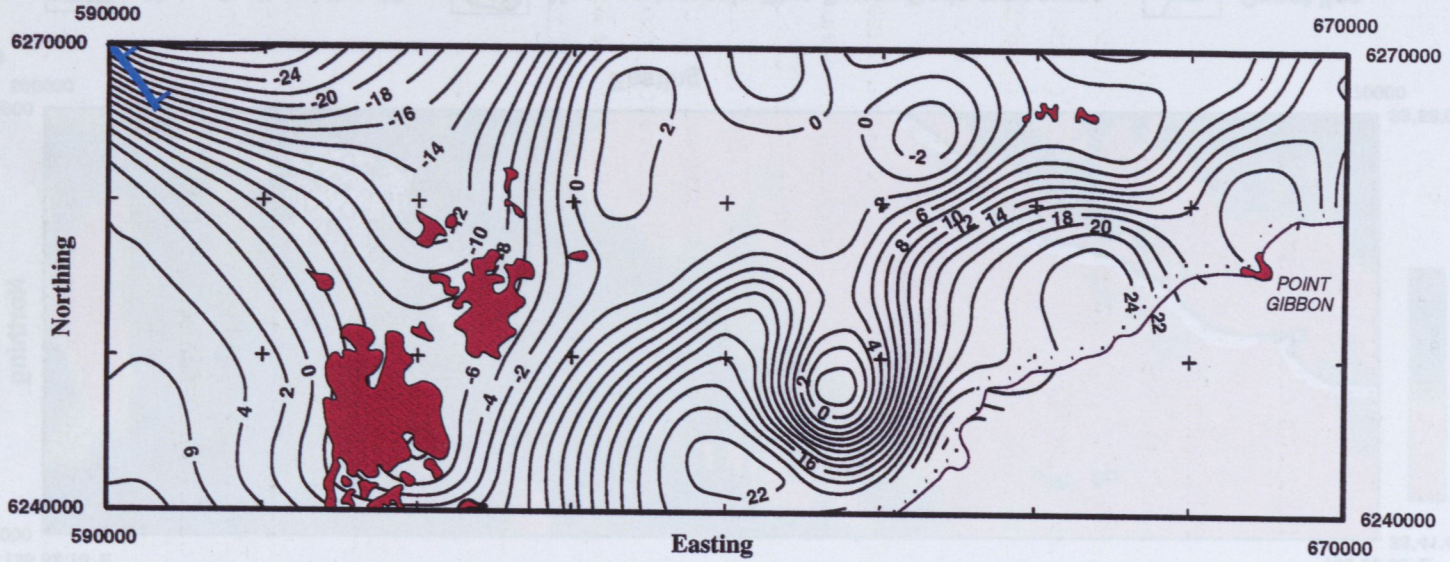

Figure 4.20 Itiledoo Basin South-East - Bouguer gravity map. Contours interval 2 mgals.

Tertiary sedimentary cover. The Blue Range Beds sediments dip towards the west with much steeper angles than elsewhere (*15°* to *45°*). From geological field observation it appears that these sequences are preserved in the fold structure and the subsequently calculated thickness of the Blue Range Beds is about 1500 m. The gravity anomaly of about 10 mgals indicates a density contrast of about $0.15 g / cm^3$

Figure 4.21 presents the magnetic map of this area on which the Blue Range Beds appears non magnetic. The NE-SW anomaly A'_{IB} is due to magnetic rocks which are exposed at the surface and where the Blue Range Beds are in contact with the magnetic rocks. This magnetic anomaly can be followed southwards below an increasingly thicker cover of the Blue Range Beds.

The gravity map presented in Figure 4.22 indicates two facts:

- To the west of the exposed Blue Range Beds, basement probably goes deeper. However the large spacing between gravity observation stations does not allow any detailed interpretation.
- To the east of the Blue Range Beds sediments, it appears that the negative gravity anomaly of about 10 mgals, due to density contrast in the underlying Palaeoproterozoic rocks, continues. Alternatively, this could be due to another north-south trending negative anomaly (Figure 4.22).

The integration of the geological evidence and information obtained from geophysical interpretation, enables the definition of the south-eastern boundary of the Blue Range Beds sediments. In the Itiledoo Basin East the eastern boundary of the Blue Range Beds is clearly defined in the northern part, by extended outcropping contact with basement rocks. In the Itiledoo Basin East, from the west, a fault boundary is established from the gravity and magnetics and also geological information. From the east, based on the gravity data and geological observations, (contact with the Cook Gap Schist and outcropping basement in the close vicinity) the Blue Range Beds boundary trending NNE is definite. As Figure 4.23 shows these two sections could be joined and the eastern Blue Range Beds depositional boundary can be marked. Certainly, there is no support for the proposition that the Blue Range Beds form a continuous deposit which was preserved in the east-west graben.

(ii) Conclusions:

In summary, it appears that the geological evidence and information provided by geophysics are not supporting the current model of the Blue Range Beds deposition within the east-west trending, several hundred kilometres long, Itiledoo Basin (e.g. Rankin et al., 1993).

4.3.2 The Neoproterozoic Kilroo Formation (onshore)

(i) Observed geological and geophysical facts

The Neoproterozoic rocks of the Kilroo Formation are known only from drilling. This formation was intersected in hole *CRA83KD1A* located in the middle of Eyre Peninsula, and two offshore wells *Columbia-1* and *Mercury-1* located about 170 km to the west (Figure 3.6). The lithology of the Kilroo Formation was described in detail in Section 3.2.4. As discussed in Chapter 3 the correlation

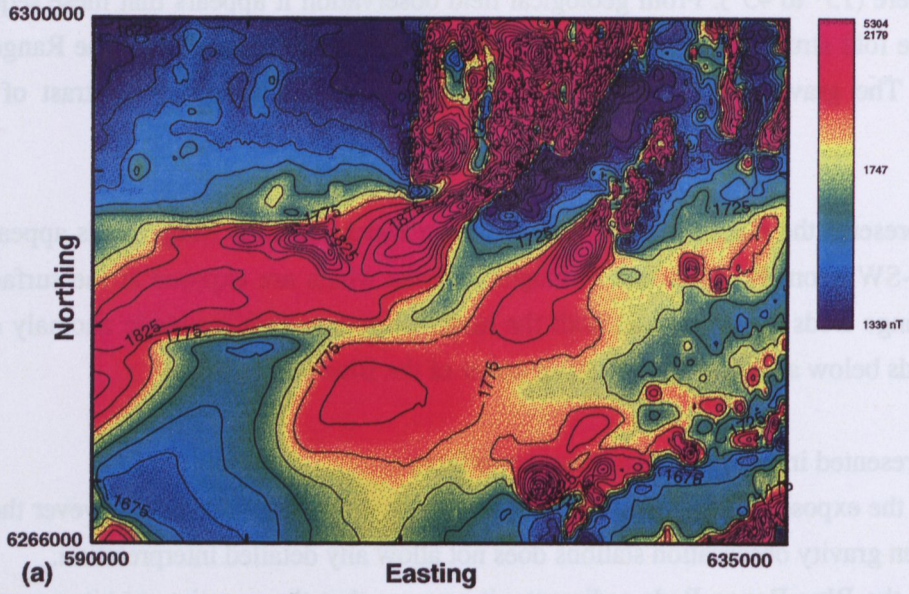

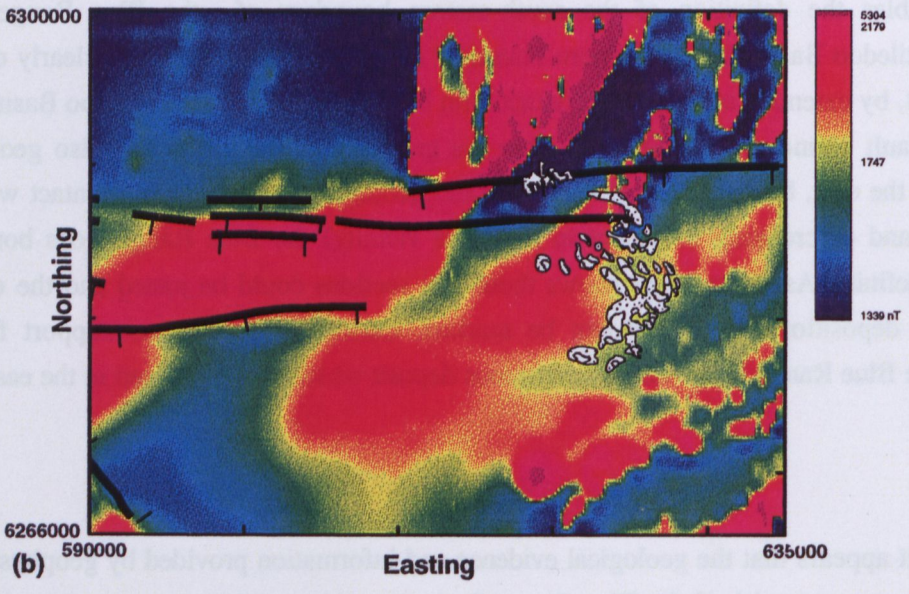

Figure 4.21 Itiledoo Basin East: (a) Colour mage and contours of TMI, (b) Colour image of TMI with surface exposures of Mesoproterozoic Blue Range Beds and major faults of Polda rift.

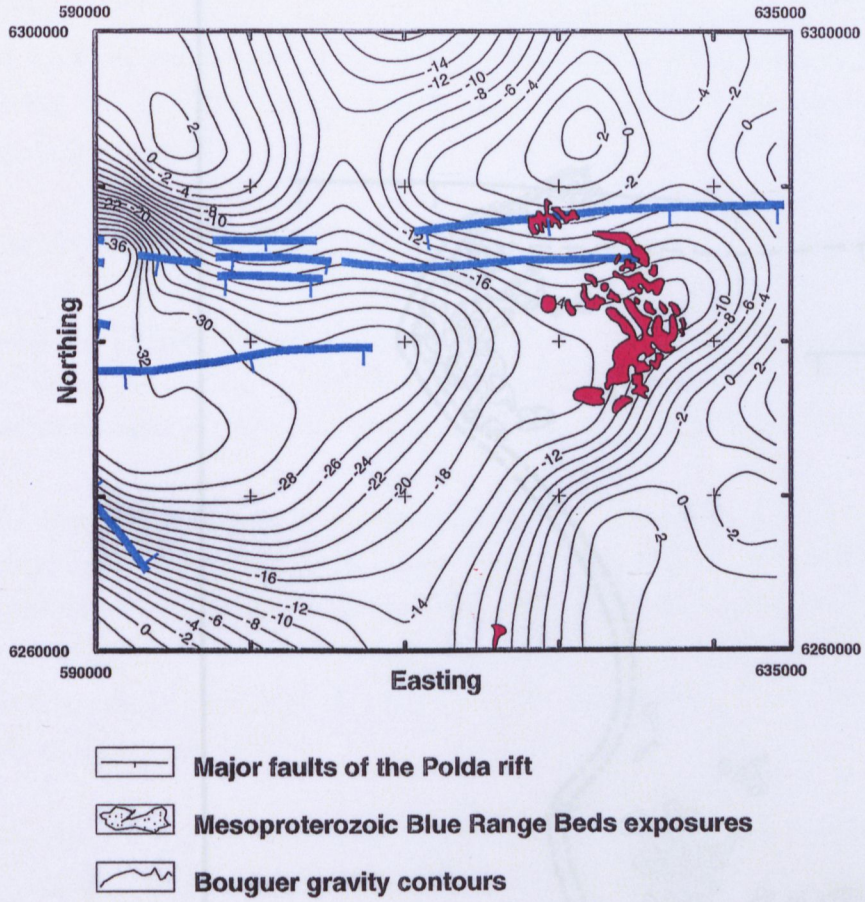

Figure 4.22 Itiledoo Basin East - Bouguer gravity map. Contour interval 2 mgals.

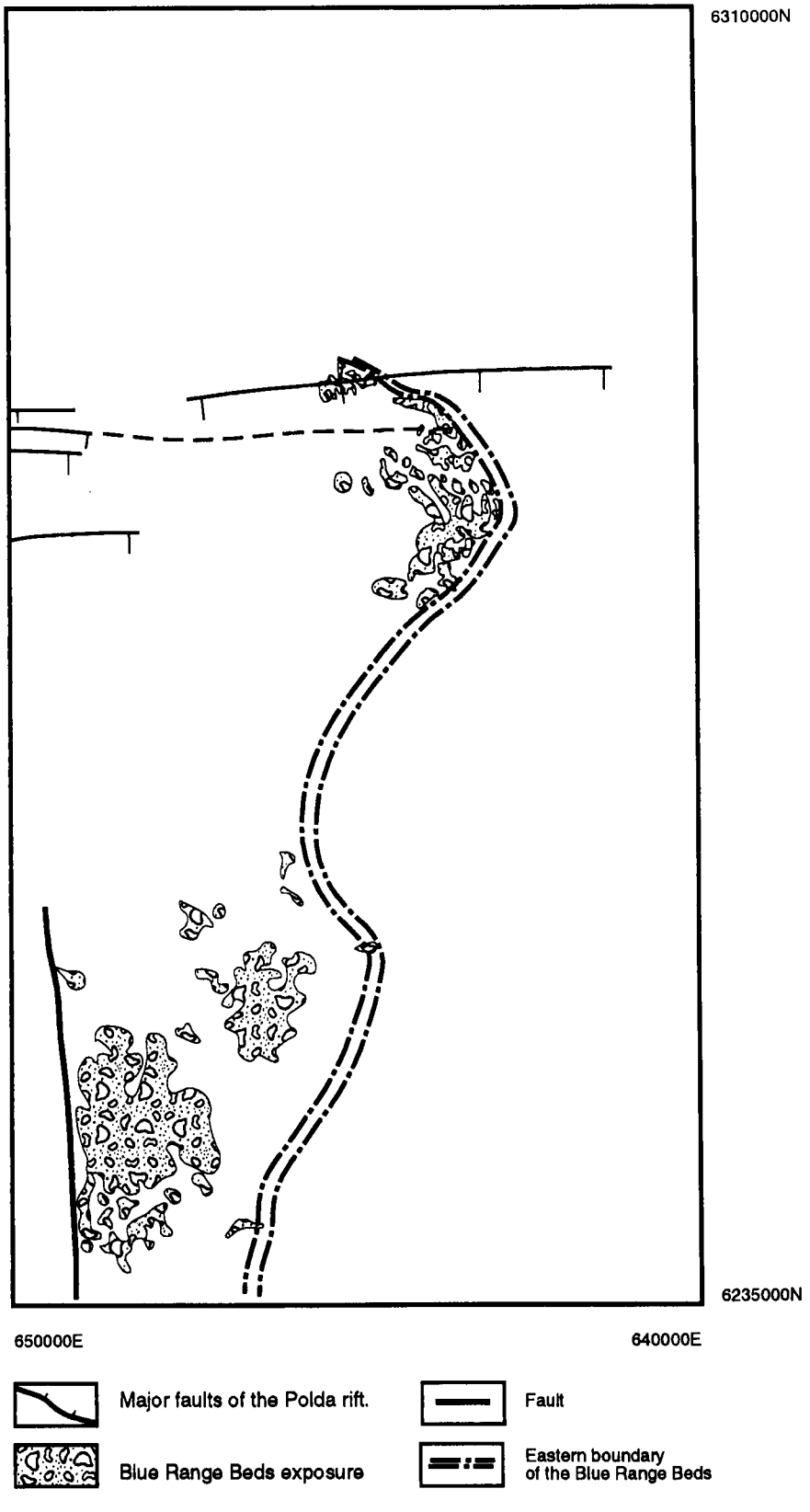

Figure 4.23 Itiledoo Basin South-East and East - Eastern boundary.

between the stratigraphic columns of two offshore wells and an onshore stratigraphic hole is not simple.

The hole *CRA83KD1A*, which is located at the eastern end of the Polda Trough, comprises three intervals of clastic sediments, two zones of amygdaloidal basalt and one thin bed of andesite crystal tuff (Figure 3.7). This hole was drilled on the seismic reflection line *PB83-001* at shot point 338 (Figure 4.24). A well velocity survey, which was conducted among standard downhole geophysical logs at drill hole *CRA83KD1A*, produced a good correlation between seismic velocity and geological formations (Figure 4.25).

Based on the mineralogical and petrographical evidence, Pontifex (1984) interpreted the depositional environment of these sequences as one of broad mature streams, possibly of an ephemeral type, crossing a system of playa lake back swamps, or saline flood plains, with sporadic intercalated basaltic flows. Most of the sediments were derived from a metamorphic area of probably low-grade metasediments (quartz-biotite-muscovite±chlorite±microcline) with sparse shallow water carbonate.

As discussed in Section 3.2.4 radiometric dating carried out on basalt samples, did not give a consistent age range. The results range from $235 \pm 15Ma$ to $884 \pm 97Ma$. Two age values $768 \pm 9Ma$ and $764 \pm 42Ma$, are comparable with the age of the early Adelaidean Rook Tuff in the Willouran Ranges (Fanning et al., 1986). This evidence was used to imply that these evaporitic red-beds interlayered by two zones of volcanics in the eastern Polda Basin were also considered to be Adelaidean (Flint et al., 1988b).

The specific gravity of sediments and volcanics of the Kilroo Formation were discussed in Section 4.2. An average density of each lithological unit was used for the modelling and interpretation of the gravity profiles surveyed in the vicinity of the hole *CRA83KD1A*.

As shown in Section 4.2 the sediments of the Kilroo Formation are not magnetic, (very low susceptibility of $5 - 30 \times 10^{-5} SI$) with sporadic slight increase of the magnetisation of thin magnetite-rich bends of siltstone. Two layers of basalt detected in hole *CRA83KD1A* show a strong magnetic signature (Section 4.21).

(ii) Geophysical interpretation

Geological information is restricted to one hole and thus it is very difficult to align this to the geophysical surveys.

The interpretation of the seismic reflection line *PB83-001*, according to the time versus depth graph, indicates that the reflection horizon marked in Figure 4.24 as blue, represents the upper layer of volcanics intersected in hole *CRA83KD1A* at the depth interval 979.75-1013.75 m. The reflection horizon marked in red in Figure 4.24 indicates an unconformity between the Neoproterozoic Kilroo Formation and the Permian diamactite of the Coolardie Formation, which was intersected at 572.75-594.75 in *CRA83KD1A*.

The Kilroo Formation sediments are not magnetic, showing only very low susceptibility values over thin layers with an increased magnetite content. As the top basaltic layer is only 24 m thick, its contribution to the magnetic anomalies is insignificant, but as the total thickness of the lower layer of the volcanics is unknown (more than 100 m), there is certain ambiguity concerning the source of the magnetic anomalies rising out from depths 1700-2400 m. As geological information is limited, the long wavelength anomalies are assumed to reflect the structure of the underlying rocks. It is difficult to recognise the effect of the volcanic lavas overprinted on the signature of the underlying basement.

4.3.3 The Coolardie Formation of the Permo- Carboniferous

Palaeozoic rocks are represented by only one sedimentary succession, the Coolardie Formation of Carboniferous-Permian time which was deposited after a period of glaciation. The glacigene sediments are known from drill holes only. Glacigene sediments were encountered in several drill holes on the onshore part of the basin (Figure 4.26) and in all three wells drilled offshore. Detailed lithology of the Coolardie Formation is described in the Section 3.2.5.

The bottom contact of the Carboniferous-Permian Coolardie Formation with the underlying Neoproterozoic Kilroo Formation has only been encountered in one hole (*CRA83KD1A*), located at the eastern end of the Polda Trough. The unconformity between these two formations was also intersected in *Mercury-1* and Columbia-1 (*Gimini-1* is too shallow) at depth of 886 m and 771 m respectively. The upper stratigraphic boundary, which is observed in all drill holes, is an unconformity between this Palaeozoic unit and the Jurassic Polda Formation.

The Coolardie Formation was deposited on the strongly eroded Neoproterozoic Kilroo Formation after a 300 Ma hiatus. Drilling shows that the Late Palaeozoic sediments were found within the trough boundary in several locations. None of the drill holes located outside the trough, as defined by the magnetic survey data, intersected Permian rocks (Figure 4.26). This observation, that Permian is preserved only within the narrow trough comes from the interpretation of the 1987/88 aeromagnetic survey, which defines the boundary faults of the Polda rift accurately for the first time.

The coarse diamictite of the Coolardie Formation has a density of *2.38 g/cm³* (Section 4.2.2) and an average thickness of 20 m. Assuming that a density contrast between basement rocks and sediments of the Coolardie Formation is *0.3 g/cm³*, this will produce an anomaly of only *0.012 mgal*. Such an effect cannot be seen on the gravity map or section.

The sediments of the Coolardie Formation are very weakly magnetic (Section 4.2.1).

As mentioned in Chapter 3 the palynological study of the samples collected from the drill holes *Lock-1* (Cooper, 1980) and *P8* (Cooper et al., 1982), allowed correlation of the Coolardie Formation with the Lower Tamarian stage of the Permo-Carboniferous of Tasmania (Clark and Framer, 1976; Truswell, 1978), and also correlation of this unit with the Cape Jervis Formation of the Troubridge Basin and the Boorthanna Formation and basal Stuart Range Formation of the Arkaringa Basin. As

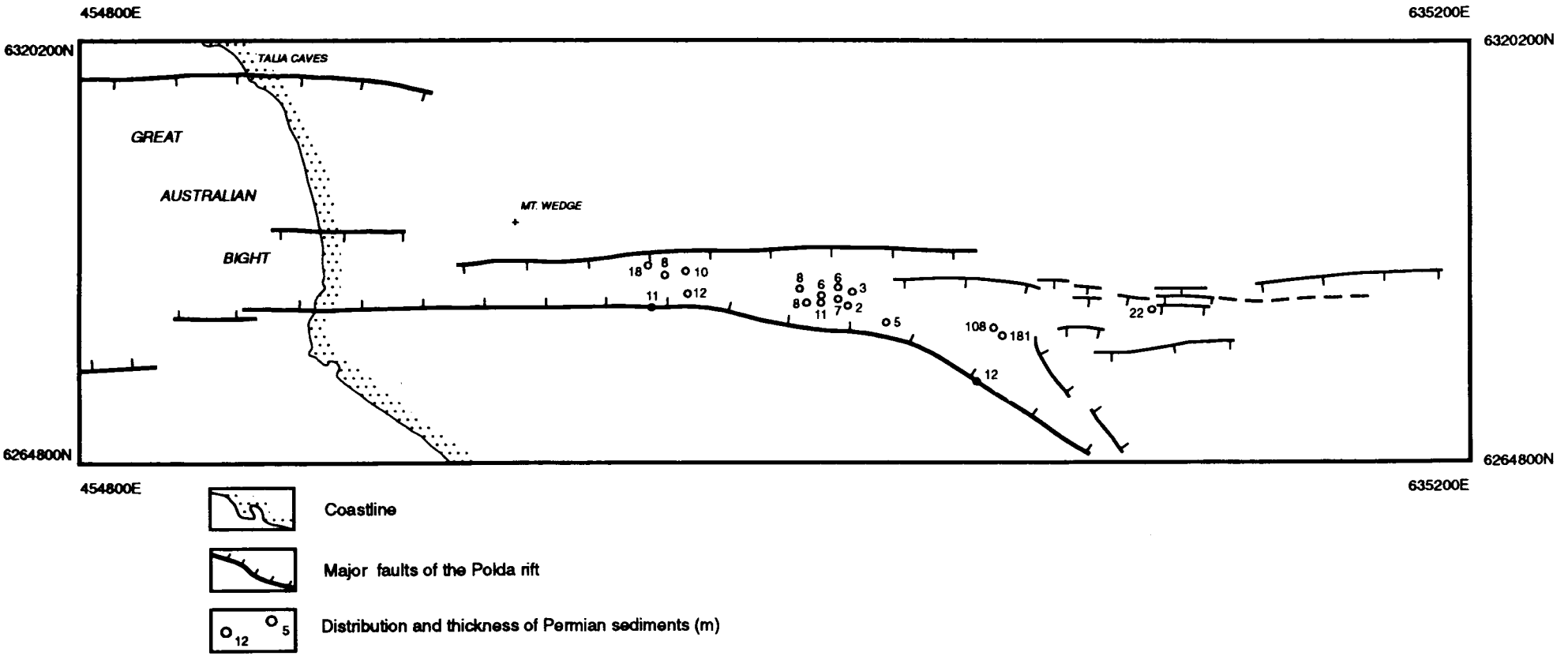

Figure 4.26 Distribution and thickness of the Coolardie Formation.

the Permian sediments found between the rift faults are not apparently different from rocks of similar age occurring in other areas, the Coolardie Formation has been preserved by the faulting and consequently the Polda Trough structure is younger than the Permian sediments.

From drill holes it is known that the greatest thickness of Permian sediments is 181 metres; the thickest layer of the diamictite was intersected at the depth of 188 m in the stratigraphic hole *Lock-1*.

Depth determinations made from the magnetic data indicate that the magnetic basement in these areas is relatively shallow, i.e. not greater than 500 m, so that there is no great thickness of Permian sediments present.

4.3.4 Jurassic

(I) The Polda Formation

(i) Observed geological and geophysical facts

Jurassic rocks are known from several drill holes as well as surface exposures at the eastern margin of the trough (Figure 4.27). Preserved sediments do not always represent a full type section of the Polda Formation. In some holes, the sandy interval at the top of basal unit is absent with the middle section containing carbonaceous claystone and lignite seams in a range of thickness. The top unit of sandstone, in many areas, was completely removed by erosion prior to the deposition of Tertiary sediments.

Figure 4.27 shows the distribution and thickness of the Jurassic rocks in the study area. The northern margin of the Polda Trough marks the depositional boundary of the Polda Formation. The southern margin of this unit extends towards the south of the narrow, east-west trough in which the thickest section of the Polda Formation has been preserved.

The Jurassic Polda Formation contains wide spread coal seams within the Polda Trough; however, economically recoverable coal is only known from the east-west elongated small deposit (10 km long and 1-2 km wide) located about 15 km west of the town of Lock in the central part of the onshore Polda rift. The coal is shallow and can be recovered by open cut mining. .

According to the geological investigations completed by The Electricity Trust of South Australia (ETSA), the Lock Coal Deposit contains Jurassic and Tertiary coal seams (Springbett, 1980). Jurassic coal occurs within the limits of the narrow east-west trending graben structure, thinning to the east and west of the deposit but continuing beyond the area delineated by ETSA (Figure 4.28). The southern and northern coal margins are better defined. To establish the economic potential of the Lock Coal Deposit ETSA carried out detailed geological and geophysical investigations including the following:

- 136 drill holes; all geophysically logged;
- refraction seismic -1978 (coal extension);

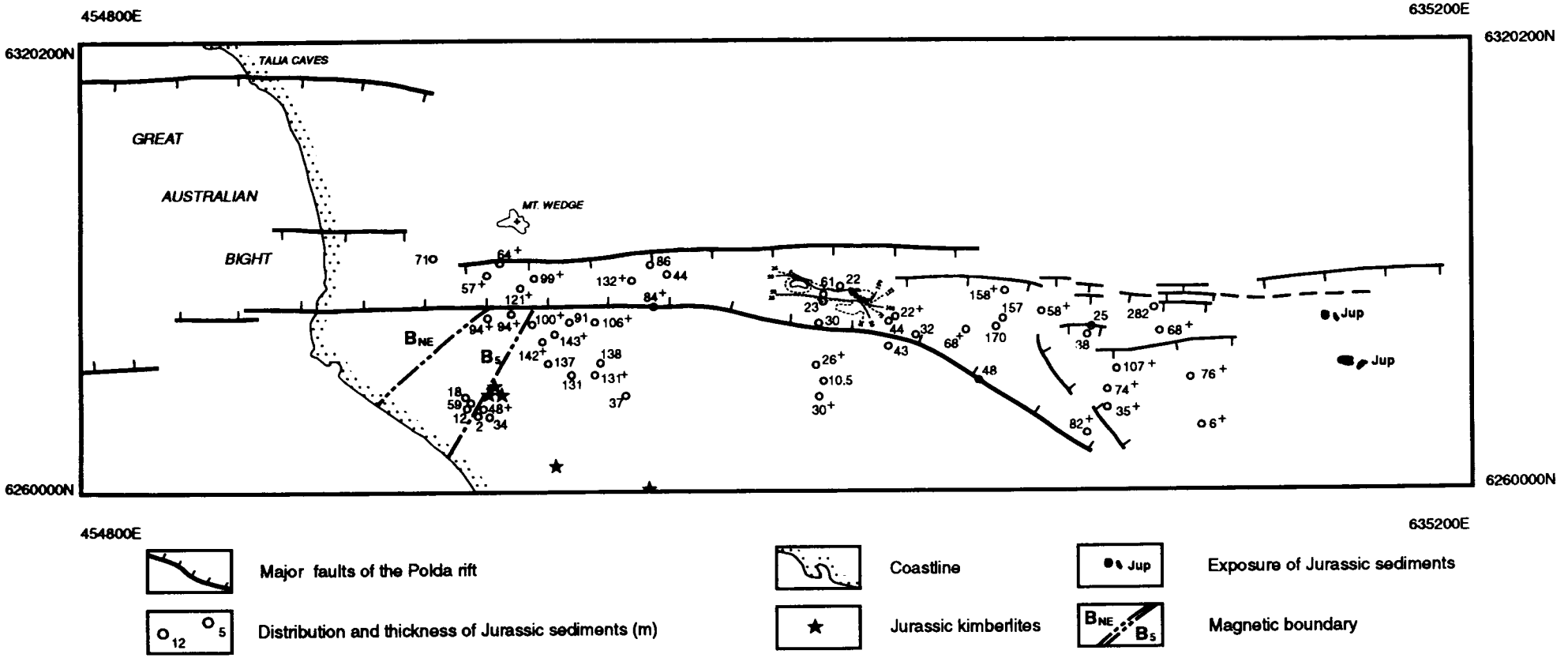

Figure 4.27 Distribution and thickness of the Polda Formation and kimberlite intrusions of Jurassic age.

- detail gravity carried out in conjunction with the 1978 drilling program to assist in the hydrogeological evaluation of the area;
- a trial high resolution reflection seismic traverse -1980 by SADME.

Cumulative coal thickness reaches a maximum of 17 m. In the eastern and western parts the cumulative thickness of the deposit locally exceeds 15 m. Coal occurs predominantly in a single zone, which commonly does not contain laterally consistent individual seams; most seams are 0.5 m to 2.0 m thick with maximum individual intersection of 6 m. Seams vary from flat to gently dipping (2°-5°). The western portion of the Jurassic coal is overlain by flat, poorly defined, Tertiary coal seams, which are thick and consistent. The maximum cumulative Tertiary coal thickness exceeds 15m.

Drilling and other investigations (Harris and Foster, 1974; Kwitko, 1982) have shown that coal still continues towards the west and east (but that mining economically is not viable). As reported by Springbett (1980), at the Lock Coal Deposit the thickness of the formation varies considerably in east-west and north-south direction. As shown in Figure 4.28, in the western (over 100 m) and eastern (greater than 175 m) part the thickness of the Polda Formation is much greater than in the centre of the deposit. Extensive drilling data in the region of the Lock Coal Deposit shows that the thickness of the Polda Formation does not decrease in the eastern and western end of the coal occurrence. At the north-south cross-section the formation has a lens shape with increasing thickness, from 25 m in the southern and northern ends to 100 m to 150 m towards the centre. The greatest thickness (175 m) of the Polda Formation sediments recorded, occur in the north-west corner of the Lock Deposit.

(ii) Interpretation of geophysical data and geological implications

Based on information from the existing drill hole data and geophysics, it appears that the thickest Jurassic sediments were deposited within the east-west trending narrow trough over a distance of at least 70 km (510000 mE - 580000 mE).

In the eastern end, the half-graben structure is bounded from the north by an east-west trending fault, from the west by a north-west striking fault and from the east by a monoclinal slope dipping to the west (Figure 4.28).

Jurassic rocks only occur south of the northern margin of the Polda Trough. Figure 4.27 presents the major structural features of the Polda Trough and also sites where the Jurassic sediments were recognised. The drilling data show that the Polda Formation has a maximum thickness of 200 m. The thickness of this formation cannot be much greater in this zone (except in the east-west trending deep narrow trough) because, as Figure 4.29 shows, there is a shallow non-magnetic basement. Polda Formation sediments are not magnetic. Depths of the magnetic rocks, estimated from the magnetic anomalies A_1^{PC}, A_2^{PC} and A_3^{PC} shown in Figures 4.30(a)-(c) are about 300 m.

The shallow depth to the basement within the central part of the Polda Trough has also been confirmed by drilling.

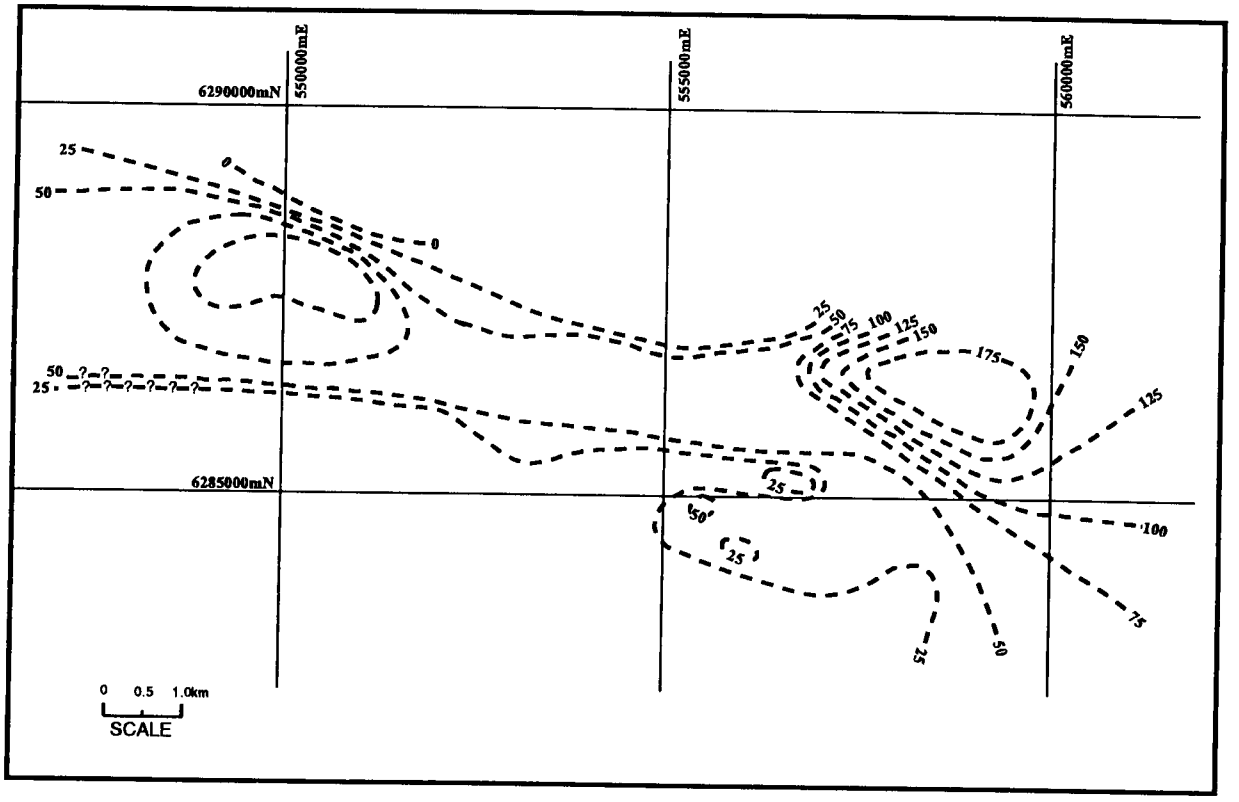

Figure 4.28 Thickness of the Polda Formation in the Lock Coal Deposit. Contour interval 25m.

Five gravity traverses surveyed by CRA in 1980 as part of the exploration for coal show that the fault zone at the northern margin has a decreasing total throw from over 2.2 km in the traverse across CRA83KD1A to less than 100 m, going westwards towards the Lock Coal Deposit from the eastern end of the basin. Estimates of the down-throws were calculated based on the assumption that the density contrast equals $0.45\,g/cm^3$ (see Figure 4.4).

McPharlin (1980) has presented an interpretation of the north-south gravity profile located to the west of the Lock Coal Deposit, which is line A-A' shown in Figure 4.31. This gravity profile was surveyed and interpreted by SADME as part of the investigations connected with the Lock Coal Deposit. The interpreted model indicates a presence of 2500 m of Mount Wedge grit. As Figure 4.32(a) shows this interpretation was based on the assumption that the Mount Wedge grit of density $2.47\,g/cm^3$ is covered by a thin layer (less than 200m) of low density ($2.1\,g/cm^3$) sediments. There is no geological information provided, such as surface exposure or drill hole log, which would indicate presence of the Mount Wedge grit in this area.

Examples of a new interpretation of the gravity profile A-A' are presented in Figure 4.32(b-c). Several different geological models, representing different density contrasts between the basement rocks and the sediments preserved within the Polda Trough, have been considered. As Figure 4.32(b) shows, for a 'single model' with an average value of density contrast, between basement rocks and the rift's sedimentary infill, $\Delta\ \rho = 0.40\,g/cm^3$, the computed depth to basement in the deepest part of the trough is about 1270 m. A similar 'single model', but with density contrast $0.31\,g/cm^3$, indicates the basement at a depth exceeding 1900 m. Figure 4.32(c) shows a 'single model' with density contrast $0.23\,g/cm^3$ and depth to basement of 2590 m. The density contrasts are based on the density values obtained for the core samples from several drill holes and a density log of the stratigraphic hole *CRA83KD1A* located in the eastern end of the basin (see Section 4.2.2).

Two 'double models', i.e. each model contains two sedimentary layers of different density contrast, have been also considered. In both models the first 600 m has density contrast of $0.5\,g/cm^3$, and the bottom layers respectively have $0.16\,g/cm^3$ and $0.25\,g/cm^3$. The density contrasts applied for the 'double-models' are also dependent on the assumed thickness of the Phanerozoic and Proterozoic sediments within the trough. The depths of the basement obtained from the 'double-models' are 2300 m or 1500 m.

All models indicate a similar internal structure of the basin. From the north, a set of step faults bound a narrow and deep trough. The Lock Coal Deposit is located within the rift on the northern step between faults with downthrow towards the south. This step between the faults is only a few hundred metres wide and relatively shallow (300 m). Located south of this step there is a deeper part of the rift which consists of a deep, but very narrow (approximately 6 km wide) main trough (Figures 4.32(b-c) and 4.33). The depth to the basement, within the main narrow trough, was computed from gravity modelling.

The position of the fault bounding the main narrow trough from the south, which is based on the interpretation of the gravity data (profile A-A'), coincides with the position of the southern boundary

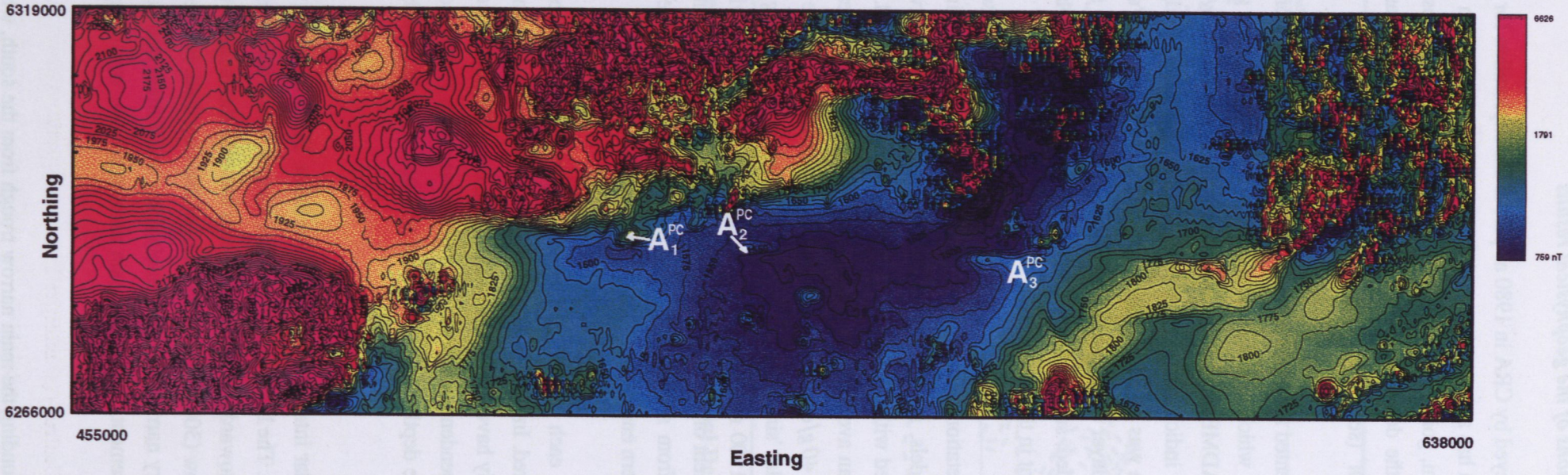

Figure 4.29 Polda Trough - Colour image and contours of total magnetic intensity field. Contour interval 25 nT.

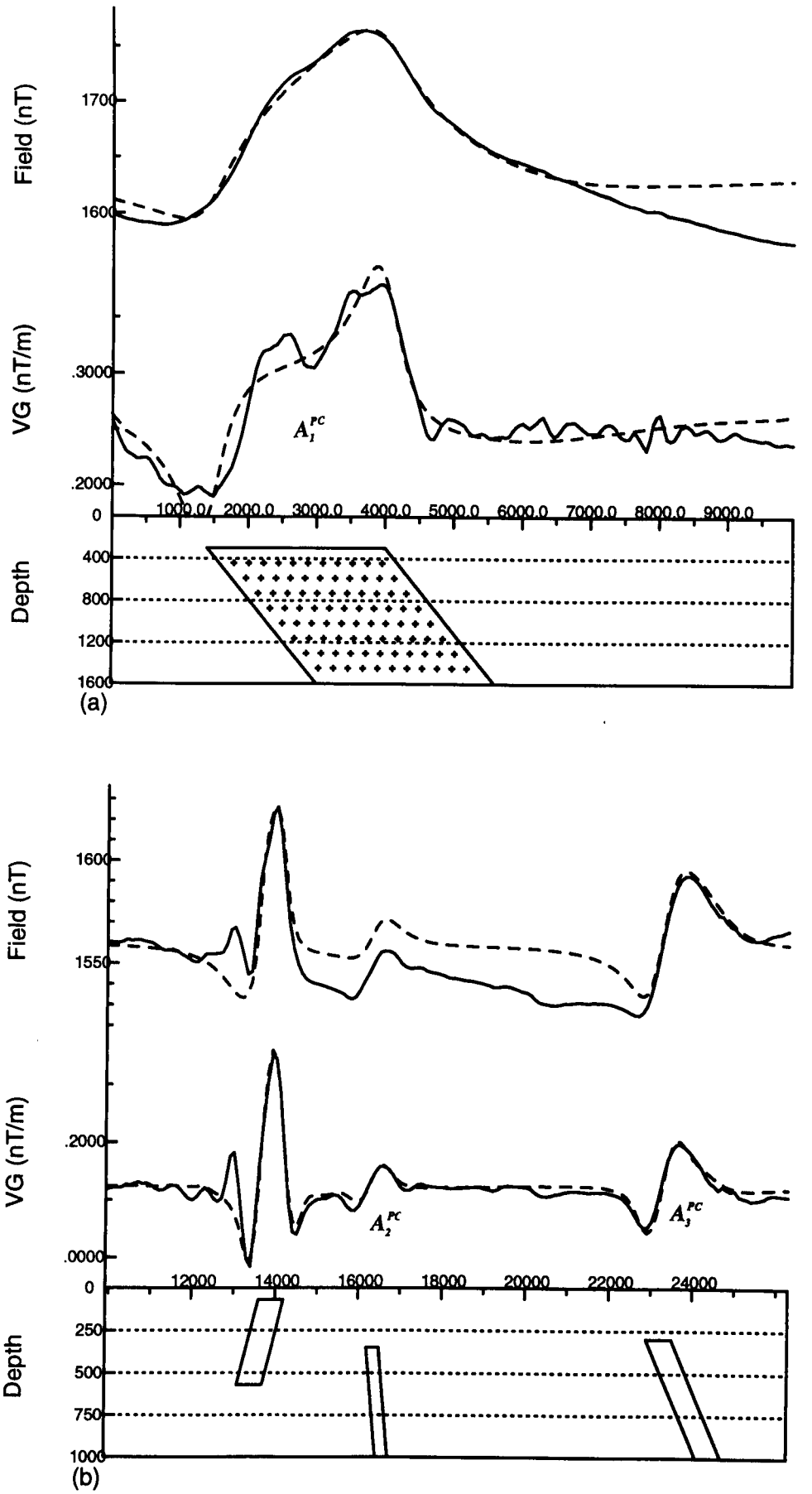

Figure 4.30 Polda Central - (a) Interpretation of magnetic anomaly A_1^{PC}
(b) Interpretation of magnetic anomalies A_2^{PC}, A_3^{PC}.

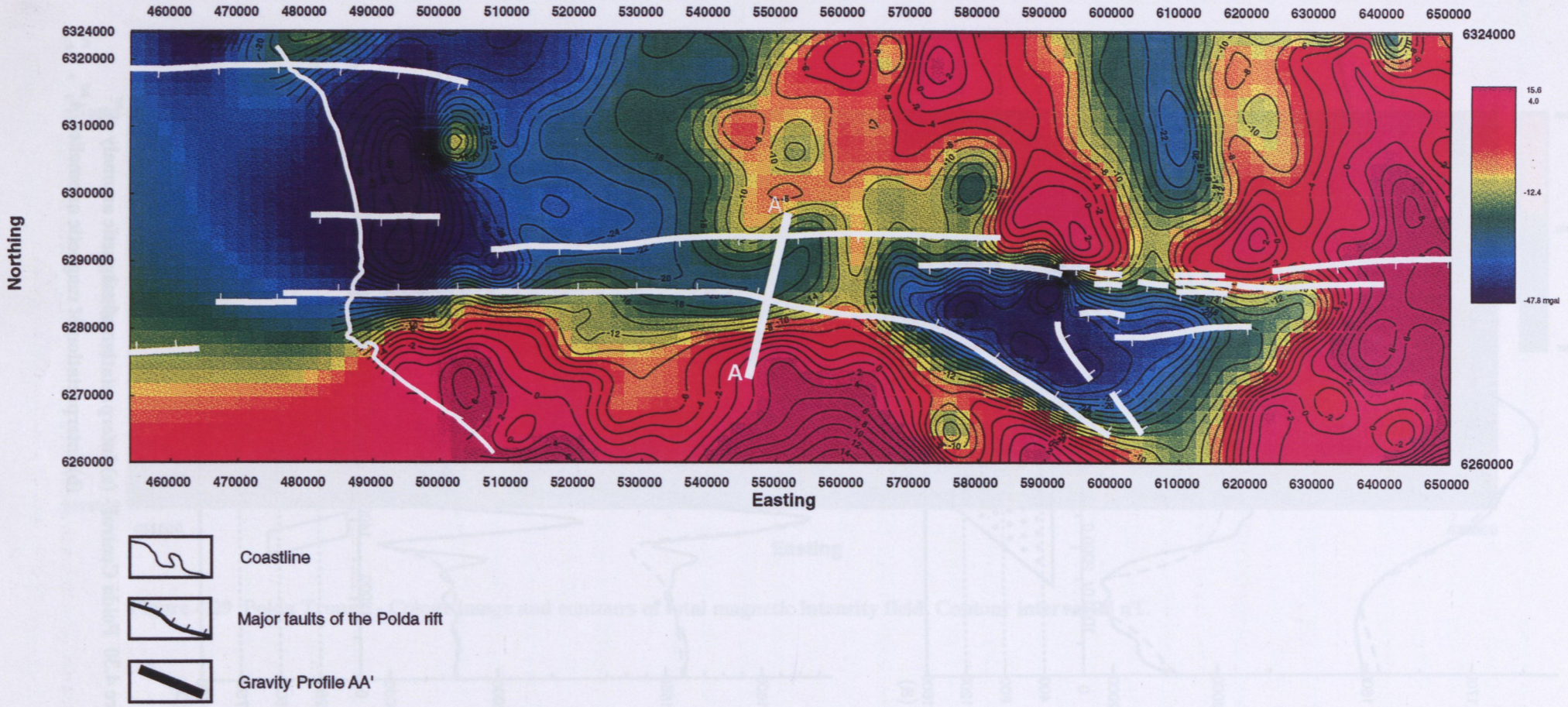

Figure 4.31 Polda Trough - Bouguer gravity image with contours at 2 mgal interval.

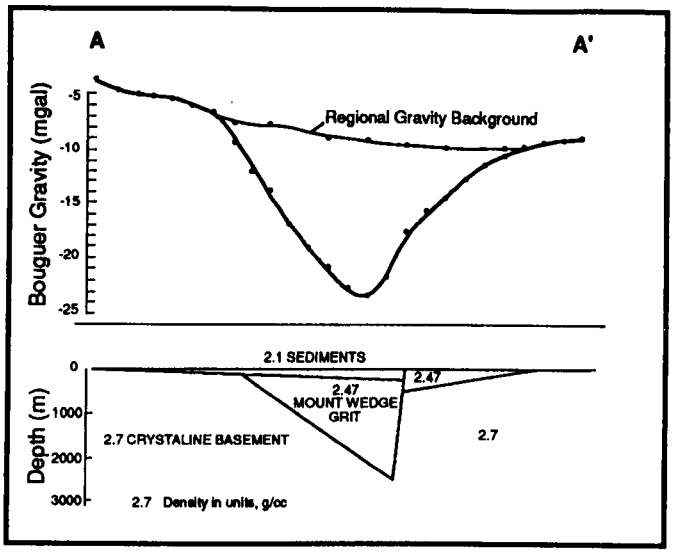

Figure 4.32(a) Interpretation model of gravity line AA' by McPharlain. After SADME.

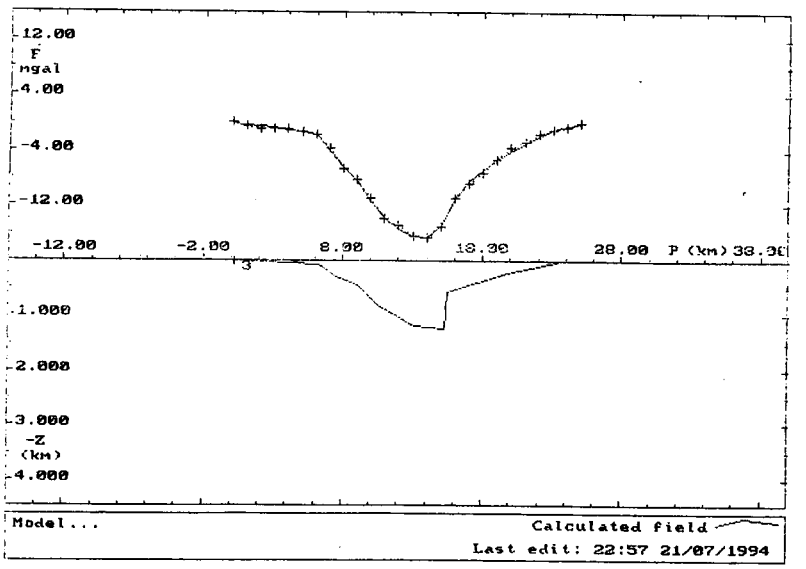

Figure 4.32(b) Alternative interpretation of gravity profile AA' applying density contrast of -0.4g/cm³.

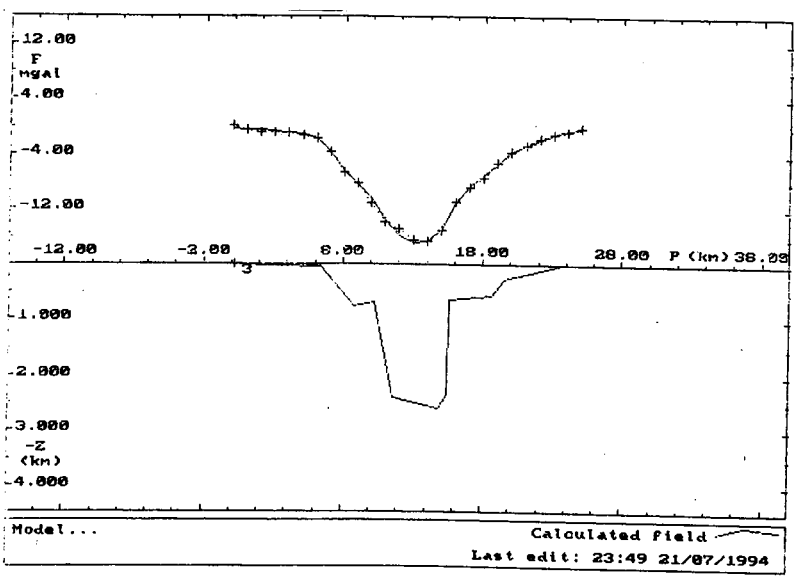

Figure 4.32(c) Alternative interpretation of gravity profile AA' applying density contrast of -0.23g/cm³.

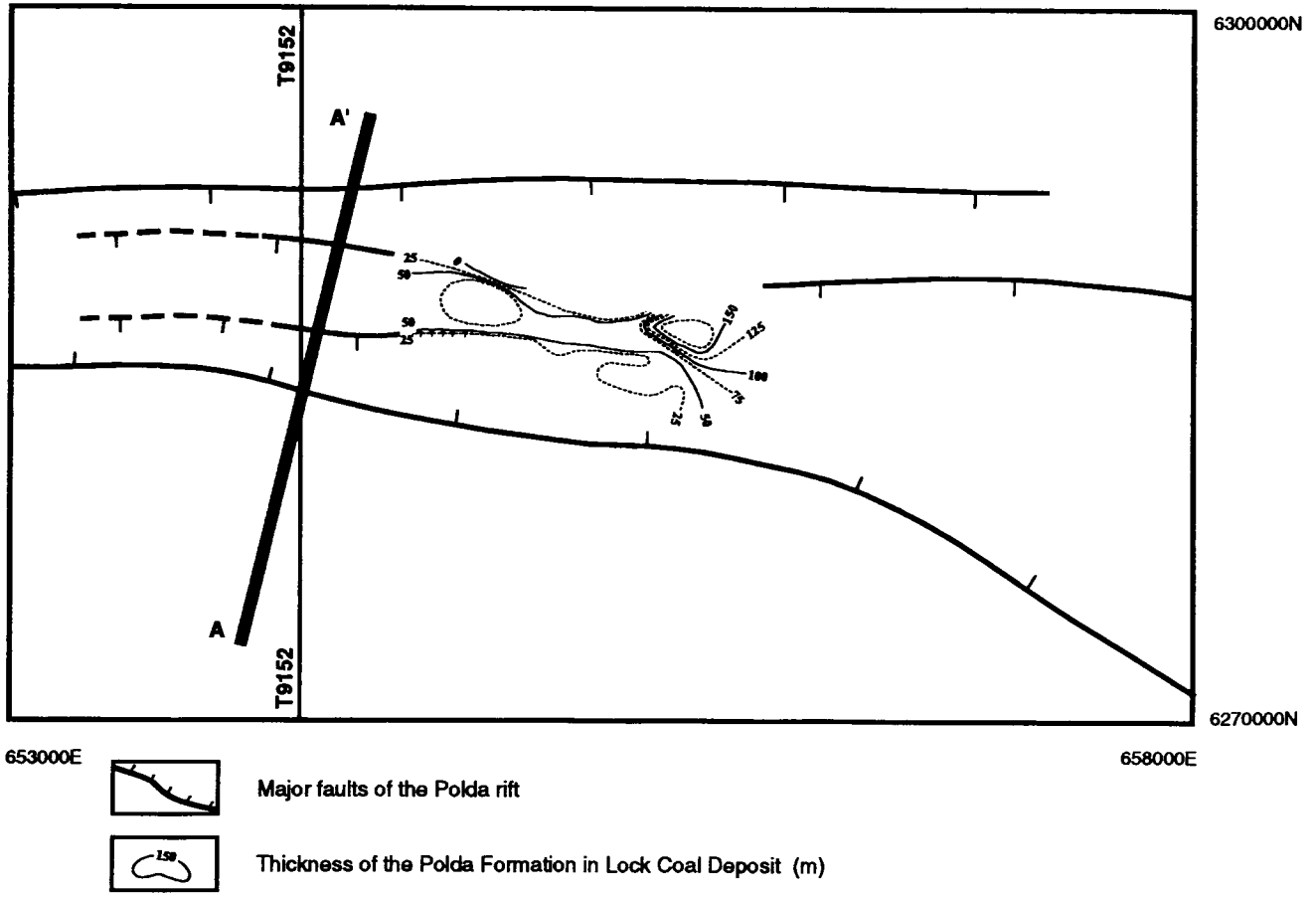

Figure 4.33 Interpretation of areomagnetic tie line T9152 and gravity line AA' across the Ploda Trough.

of the rift interpreted from magnetics. This structure is visible on the TMI field contour map (Figure 4.29).

The interpretation of the A-A' gravity profile shows the complex internal structure of the rift. In plan view it can be seen that there are two interacting en echelon troughs which are part of a relay ramp structure (Figure 4.33).

(iii) Conclusions concerning sediments in the Polda Trough

In plan view, it appears that, in the central part of the Polda rift, (Figure 4.33), the narrow east-west trough becomes shallower towards the west and continues towards the eastern end of the rift. In the vicinity of the Lock Coal Deposit the trough is approximately 300 m deep. The Lock Coal Deposit lies on a step between two faults which downthrow to the south. To the south of the deposit and sub-parallel to it, a relatively narrow but much deeper (1.2 km to perhaps more than 2 km) main trough is located.

The large negative gravity anomaly at the eastern end of the Polda Basin coincides with the position of the eastern NNW-SSE trending half-graben and westwards (up to longitude 560000 mE) with part of the east-west trending trough. Located east of this point is the Lock Coal Deposit, where relatively thick Jurassic sediments are preserved in the narrow east-west striking, fault-bound structure. As mentioned, the thickness of the Jurassic rocks east and west of the Lock Coal Deposit does not change significantly. Thus the relative gravity highs in the vicinity of the Lock Coal Deposit are probably due to density contrast within the basement rocks below.

The interpretation of the gravity profile A-A' indicates the presence of a deep narrow trough filled with 1200 m of sediments (Figure 4.32(b-c)).

The basin at the eastern end is much deeper than the one in the central part. East of the zone of the NW-SE oriented steep magnetic gradient, the depth to the top of the Jurassic rocks is greater than elsewhere, and also the thickness of this formation is greater. Two holes, located within the zone of the NW-SE steep magnetic gradient, intersected more than 150 m and 170 m of Jurassic rocks at very shallow depths (about 20 m). In the eastern end of the basin (eastern NNW-SSE half-graben), only one hole *CRA83KD1A* intersected the entire Polda Formation (282 m).

In the area of the eastern half-graben, the magnetic map indicates a deep magnetic basement. As shown in Figure 4.21, a major fault structure F_{PE}^{EW} of WSW-NEN orientation, dislocates magnetic basement; the southern side of the half-graben has been down-faulted. Based on the magnetic anomaly *BH1-U*, the magnetic basement has been established to be at a depth of 1700-1760 m on the footwall of the fault F_{PE}^{EW} (Figure 4.35). The modelling of the magnetic anomalies *BH2* and *BH1-D*, both located south of the fault F_{PE}^{EW}, indicates depths of the magnetic basement at 2300-2400 m.

The interpretation of the magnetic survey data suggests that the southern part of the eastern half-graben is approximately 700 m deeper than the northern portion. The lithology of the stratigraphic

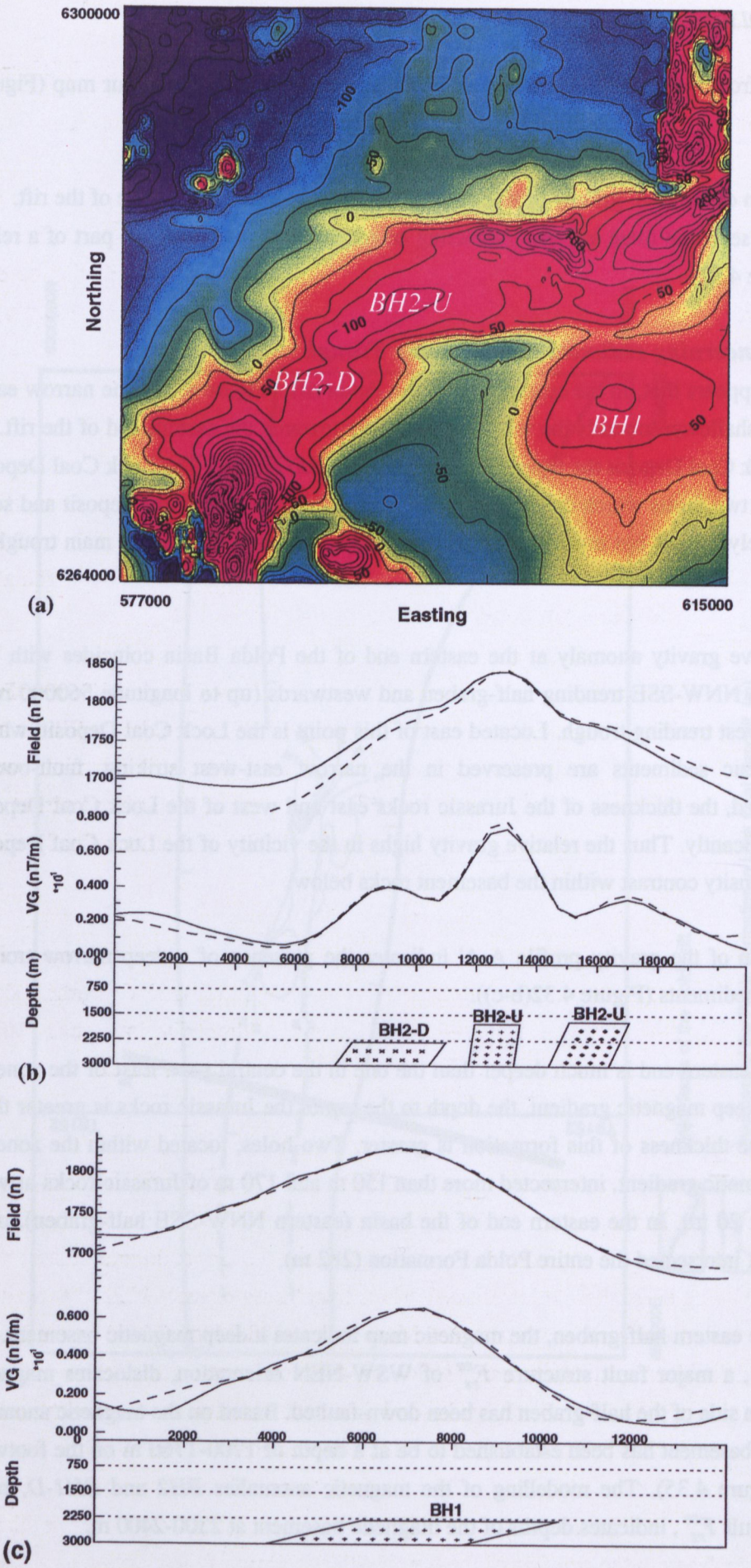

Figure 4.34 Polda East - (a) TMI image showing anomalies used for depth estimates. (b) Interpretation of magnetic anomalies BH2-U and BH2-D. (c) Interpretation of magnetic anomaly BH1.

hole *CRA83KD1A*, which was drilled on the northern part of the half-graben, suggests possible magnetic sources, which perhaps contribute largely to the observed magnetic field (see Section 3.2.4).

(II) Volcanics in the Polda Trough

The two basaltic layers which were intersected by drilling (at 1000 m and 1300 m depth) are both strongly magnetic. The top basalt layer is too thin to have a significant contribution to the observed TMI field, but the bottom basalt layer (at least 100 m thick) may mask a greater depth of sediments.

(III) The kimberlites in the Polda Trough region

(i) Observed geological and geophysical evidence

Jurassic kimberlites occur on the southern margin of the Polda Trough. These kimberlitic intrusions have been located at five sites: *SH08, SH09, SH13, MH1, MH14* (Figure 36; Section 3.2.6 part (II)). Kimberlites were found, based on a detailed ground magnetic survey, as all are associated with small magnetic anomalies (Figures 4.37-4.38).

Kimberlites are also known from five other locations in South Australia (Figure 4.39): near Port Augusta at El Alamein, Eurelia, Terowie, near Cleve and Truro. The radiometric dating (Rb-Sr and K-Ar) of kimberlitic rocks of the Terowie and Eurelia areas indicated that these intrusions were emplaced in the mid-Jurassic, approximately $170 \pm 2Ma$ ago (Stracke et al., 1979; Ferguson et al., 1979; Black et al., 1993). The kimberlite at Cleve (Wyatt et al., 1991) represents slightly older magmatic activity, about $180 \pm 3Ma$.

The location of three kimberlites (*SH08, SH09, SH13*) coincide with the magnetic boundary *B5*, which is a major crustal feature reaching the lower part of the crust (see Chapter 6 in which deep crustal structures under the Polda rift are discussed). The other two kimberlite intrusions (*MH1, MH14*) are located south of the Polda rift along the line sub-parallel to its east-west extension.

(ii) Relation of the kimberlites to the Polda rift

It is widely accepted (see Dawson, 1986) that kimberlite magmatism on the global scale is mainly confined to the old, stable cratonic areas. Kimberlite activity took place at numerous points in the geological time scale between the Precambrian and Tertiary, but the Upper Jurassic/Cretaceous activity was the major epoch of kimberlite intrusion. Various hypotheses connect kimberlite activity with contemporaneous tectonic activity, as proposed by Milanovsky and Malkov (1980) on the global scale or as shown by England and Houseman (1984) on the continental scale. Some authors postulated links between the intrusion of kimberlite and hot spot activity, or to shallow angle subduction of crustal material on account of a K and LILE enriched mantle from which kimberlite would be derived (Venturelli et al., 1984). Many scientist tend to associate kimberlite magmatism with crustal thinning and plate motion. The Mesozoic intrusion of kimberlite in Brazil, Angola, South Africa and Liberia coincides with the opening of the South Atlantic Ocean following the continental break-up along one rift arm of the triple junction centred approximately on Rio de Janeiro; the Brazilian kimberlites in the Alta Paranaiba area follow one of two failed rift arms of this triple junction (Herz, 1977).

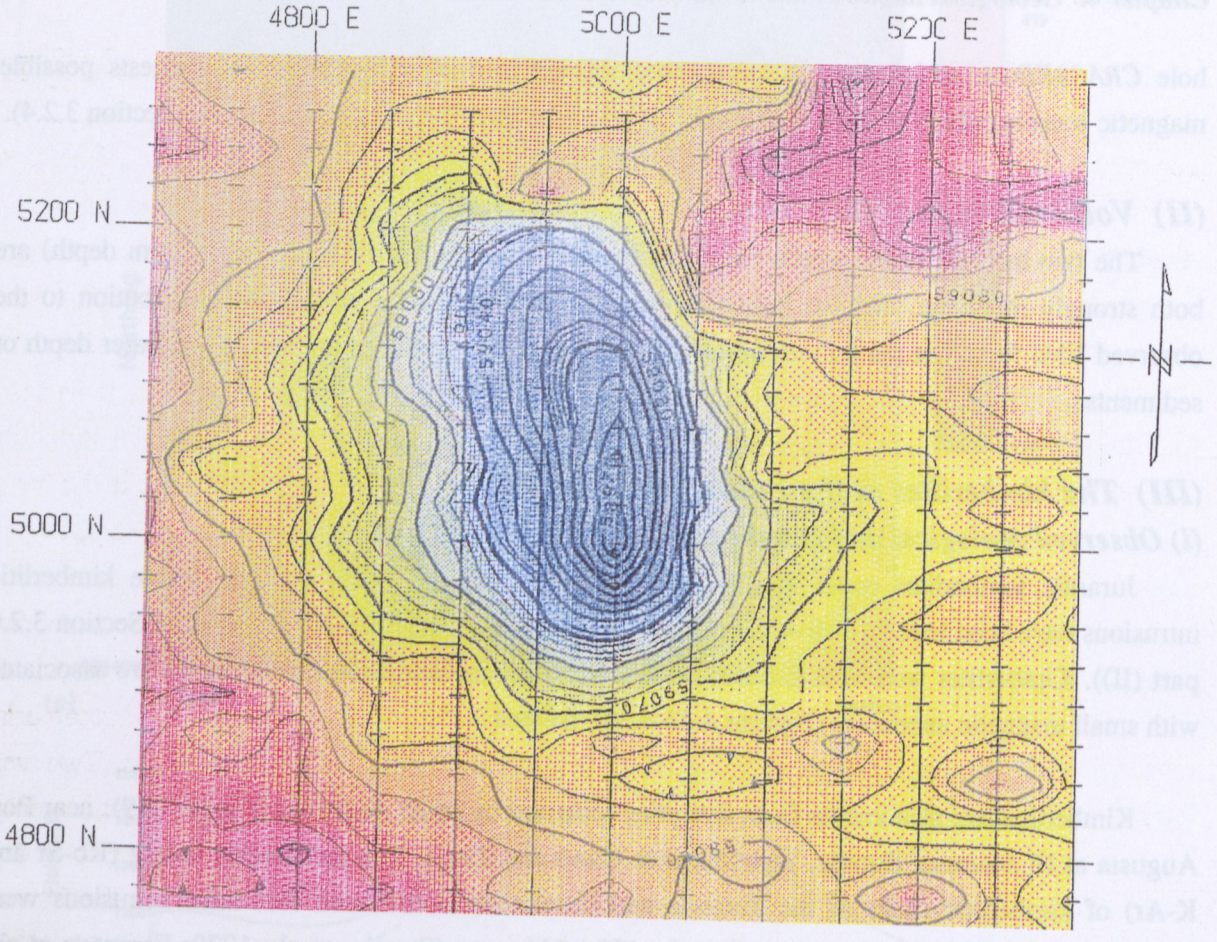

Figure 4.35 Ground magnetic survey - anomaly SH08. After Stockdale (1991).

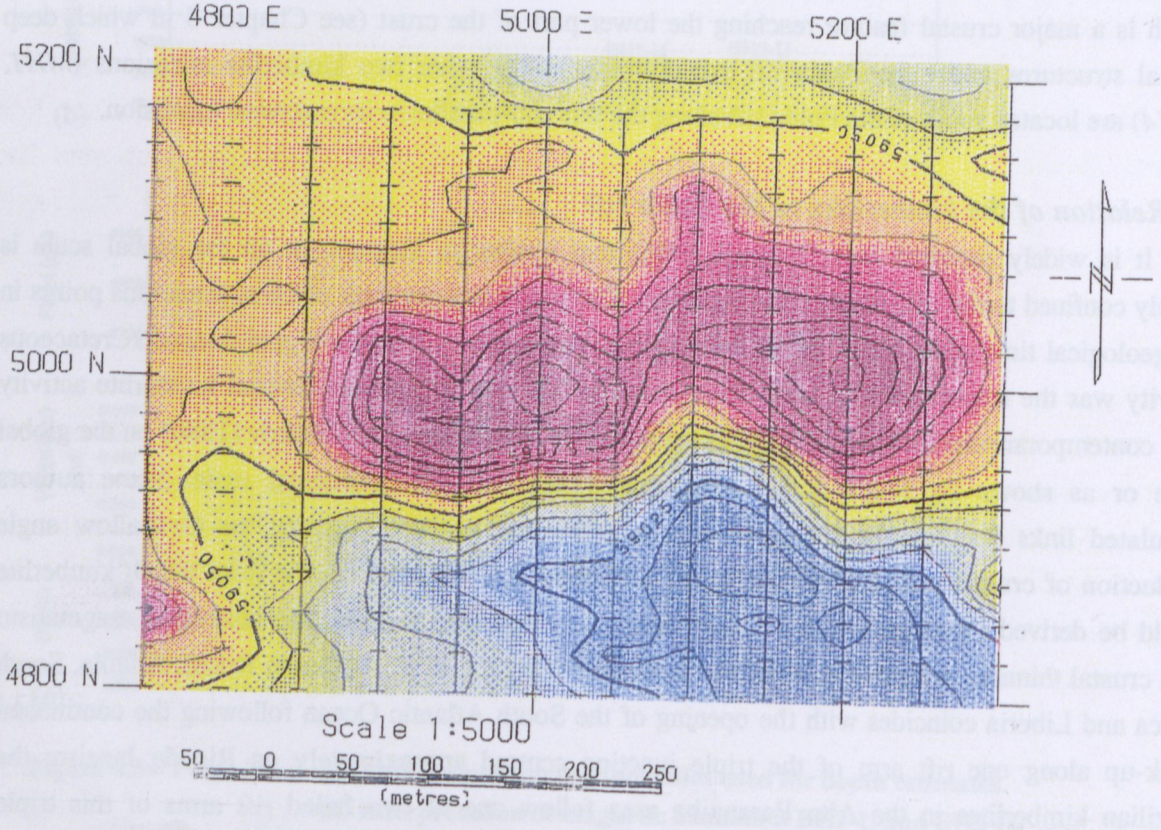

Figure 4.36 Ground magnetic survey - anomaly SH13. After Stockdale (1991).

Foden et al. (1995, in press) described the geochemical evolution of lithospheric mantle beneath the south-eastern part of South Australia based on the analysis of records of mafic magmatism which occurred in this region from the Neoproterozoic to the Quaternary. They identify the influence of major geological events such as rifting, which resulted in the development of the Pacific passive continental margin and the Delamerian Orogeny (Adelaidean-Cambrian). Theses authors postulated an hypothesis concerning the genesis of the magma being a source of the basalts, kimberlite and lamprophyres intruding the south-eastern edge of the Gawler Craton and a several hundred kilometres wide zone east of it since the Neoproterozoic. According to their postulates and also personal discussion with J. Foden, the origin and presence of the kimberlite occurring in the vicinity of the southern margin of the Polda rift could be similar to the origin of other mafic intrusions occurring in this part of the world. A brief summary of Foden and others (1995) findings is presented below.

Neoproterozoic to early Cambrian rifting of the Australian - East Antarctic Craton containing Archaean to Palaeoproterozoic rocks, result in the development of the Pacific passive margin; the Tasman Line (Veevers, 1984) defines the eastern margin of the exposure of Australian Precambrian cratonic rocks. This rifting event was accompanied by intensive magmatic activities. Two very distinct mafic magma suites were identified, a continental tholeiite suite which resulted from melting of the asthenospheric depleted mantle, and an alkaline series which show geochemical signature (low Zr/Nb, K/Nb, K/La, Rb/Ba and high Zr/Y) and also Nd-isotopic composition similar to the Jurassic kimberlite and the Quaternary alkalic suites present in this part of the globe (a number of localities along the Tasman Line from north-west New South Wales to South Australia and Tasmania). There is also observed a similarity in the range of T_{DM}^{Nd} values (0.5-0.8 Ga) which coincides with those of the enriched lherzolite xenoliths from western Victoria (O'Reilly and Griffin, 1988). These geochemical similarities provided support for the hypothesis postulated by Foden et al. (1995) that incompatible element enrichment of the sub-continental lithospheric mantle

> ...took place in the late Neoproterozoic (800-550 Ma), possibly in developing rift systems which formed the present margin of the eastern edge of the Australian craton (the Tasman Line). The enrichment may in fact essentially delineate 'fossil' rift zones. The enrichment zone has subsequently been sampled during successive events ranging in age from the latest Neoproterozoic and Cambrian to Jurassic and Cainozoic.

It is probable that the kimberlites which intruded the southern margin of the Polda rift in the Jurassic are samples of mafic magmas derived from the asthenosphere causing enrichment of the lithosphere in the late Neoproterozoic. This asthenospheric magma was placed within the lithosphere in the magma chamber at depth where temperature is not less than 800°C. During the Jurassic, when lithospheric extension followed by break-up of Australia and Antarctica took place, kimberlite formed from the enriched magma intruded crust and reached the surface. Such a scenario is illustrated in Figure 4.40 constructed after Wyllie (1986).

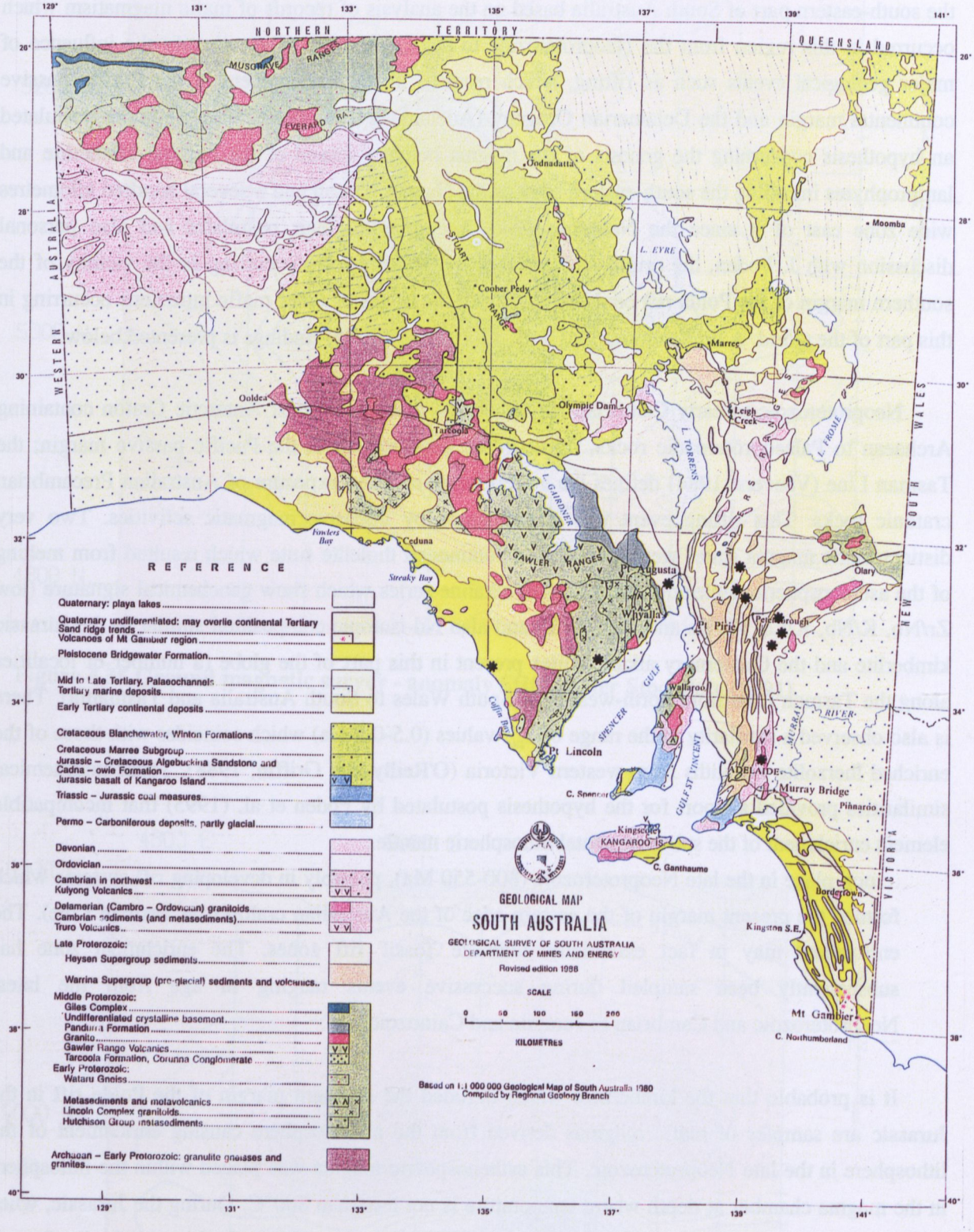

Figure 4.37 South Australian kimberlitic intrusions.
*** Kimberlite**

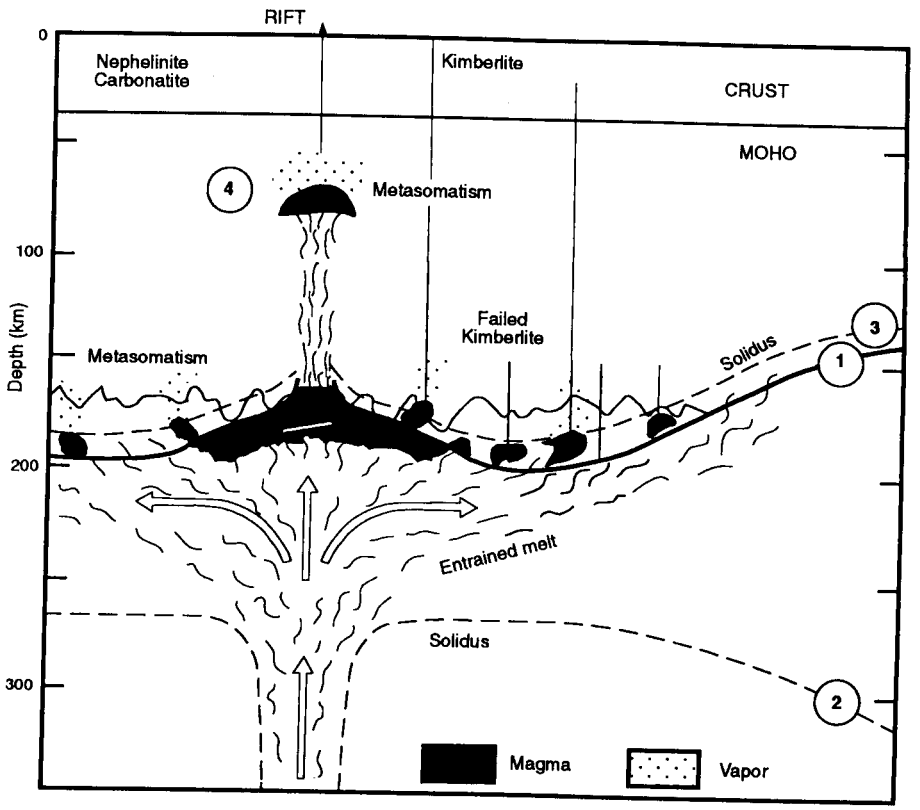

Figure 4.38 Magmatic processes responsible for kimberlitic intrusion. Upper mantle section with thinning of the lithosphere beneath a rift zone. After Wyllie (1986).

4.4 Summary

The presence of the Permian Coolardie Formation, only within the east-west narrow trough, supports the concept that the rift originated in Mesozoic time, when Gondwana was breaking apart and prior-rifting doming took place, followed by graben formation, in which Permian and older sediments were down faulted and preserved from erosion. Erosion removed all remnants of older sediments, except a few isolated spots, where the oldest Blue Range Beds were left.

The presence of the kimberlite pipes intruded in the Polda Trough region at Jurassic time provides indirect evidence of the processes occurring at the depth of the lithosphere-asthenosphere boundary which could be related to the uprising magma plume responsible for initiation of rifting in this part of the Gondwana continent.

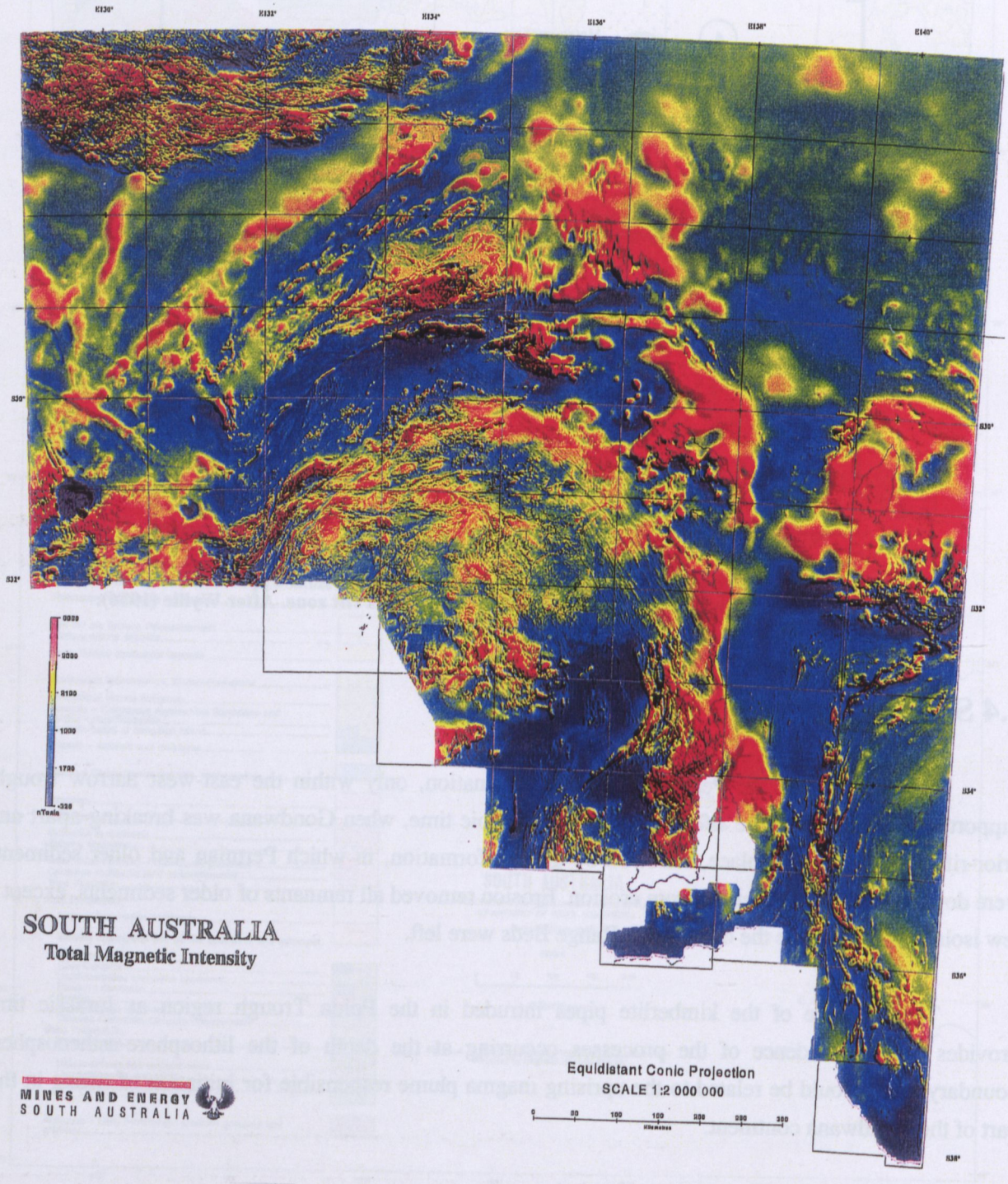

Figure 5.1 Total magnetic intensity image of South Australia.

Chapter 5

Spectral Analysis of Total Magnetic Intensity

The broad scale nature of aeromagnetic surveys over an area of unknown stratigraphy requires analysis of very large data sets. The main objective of the interpretation of an aeromagnetic survey is either to provide a preliminary estimate of the thickness of the non-magnetic overburden overlying the magnetic basement or to establish the distribution of magnetic bodies within the basement. The distribution and characteristics of the anomaly patterns suitable for depth analysis are usually limited. Conventional depth estimate methods, which analyse individual anomalies, utilise only some parts of the data, and thus a great deal of information is not fully utilised.

Even if magnetic rocks are exposed at the surface there are possibly other magnetic sources beneath them and the investigation of these has been the main aim of the application of the energy spectra analysis of TMI on the Gawler Craton. The average depth of those magnetic surfaces are obtained from the analysis.

A significant part of the analysis of the magnetic field presented in this thesis is either an application of the energy spectral analysis method or application of other techniques which are relevant to the results obtained from the spectral studies. As the energy spectrum analysis was applied to the large data sets to detect changes in the magnetic crust and possibly in the upper mantle, it is therefore necessary to set out in some detail theoretical aspects of the applied method, its principles and its limitations, so that the geological implications of the computational results can be understood. The fundamentals, principles and properties of this method are included in Appendix A; application of the method to simple model data is presented in Appendix B.

5.1 Application of energy spectral analysis to the TMI gridded data

Energy spectrum analysis provides a technique for quantitative studies of complex and large aeromagnetic data sets. The application of this method, for an interpretation of gridded aeromagnetic data is not enough on its own and needs to be an integral part of the interpretation process in obtaining geological information on the regional scale. The energy spectrum of the magnetic data provides the characteristics of the data structure and the combined information on the anomalies' parameters i.e. frequencies and wave-lengths involved, together with the directions and the trends of the magnetisation.

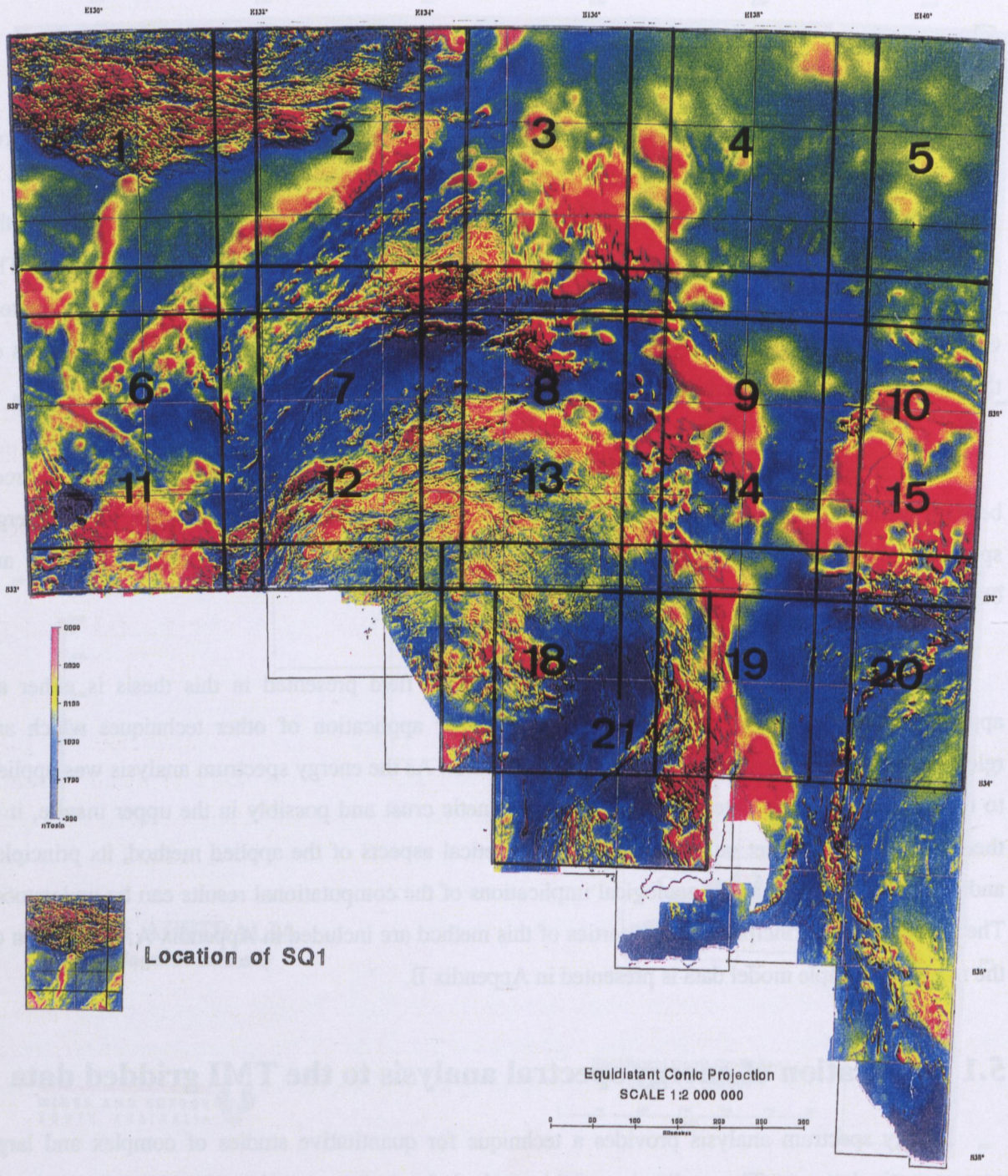

Figure 5.2 Total magnetic intensity image of South Australia. Location of 300x300km blocks over which energy spectra of TMI field was computed.

By plotting of the logarithmic radial energy spectrum against the radial frequency, the slopes of the linear segments which correspond to separate depth ensembles are obtained and provide parameters used for the design of numerous filters (downward and upward continuations, optimum-matched filtering, wavelength filtering, 'compensation smoothing filtering').

The results of the quantitative studies combined with anomaly separation and average depth estimation, have been widely reported in geophysical journals. Spectral analysis of potential field data has been applied to relatively small regions in several countries including Canada (Spector and Grant, 1970), United States (Bhattacharyya and Leu, 1975; Connard et al., 1983), Brazil (Gasparini et al., 1979), Germany (Hahn et al., 1976) and Japan (Hansen et al., 1983). On a larger scale, this method was used in China (Hou and Shi, 1985; Hou, 1989) and India (Negi et al., 1983; Negi and Agrawal, 1986; Pal at al., 1979; Rao et al., 1992) for both gravity and magnetics, to determine the crustal thickness or its magnetic inhomogeneity. However, to obtain reliable regional geological interpretation and to study the structure of the deeper crust, based on the potential field, requires that the energy spectral method is applied to high quality data sets on relatively large area blocks. Such high quality magnetic data sets are not widely available on all the continents.

5.1.1 Data processing and computation of the logarithmic radial energy spectrum of the TMI grid data of the whole of South Australia

Research presented in the following sections has been possible because of the availability of good quality total magnetic intensity gridded data over an area covering the State of South Australia ($129^\circ E - 141^\circ E$ by $26^\circ S - 39^\circ S$). Regional total magnetic intensity data was produced from the surveys conducted by Australian Geological Survey Organisation (AGSO), Mines and Energy, South Australia (MESA) and Delhi Petroleum over a period of nearly thirty years. This data set has recently been digitised and reprocessed by MESA and the new properly levelled data in a gridded form became available for analysis and interpretation (Figure 5.1). The grid spacing is 0.005° of latitude and longitude. The grid was generated based on the flight lines being $1.6km$ apart. This is true for most of the State, with the north-eastern corner, covering the Cooper Basin, Simpson Basin and western part of the Pedirka Basin, being an exception. There the flight lines are $7km$ apart, and additional levelling problems occur.

(I) Data preparation

As the TMI State grid data was written in the earth's geographical coordinate system, to enable a relatively quick analysis of the magnetic map covering the area of approximately 1.3 million square kilometres, it was necessary, at the initial stage of this project, to assume that the geographical latitudinal and longitudinal degrees are both equal to $100,000m$. This assumption while permissible on the macro scale, neglects the curvature of the earth and treats the latitude- and the longitude-axes as a perpendicular coordinate system. Hence, the grid cells (gc), being equal to 0.005° along the latitude- and longitude-coordinates, are equal to $500m$ along an equivalent $x-$ and $y-$axis, respectively.

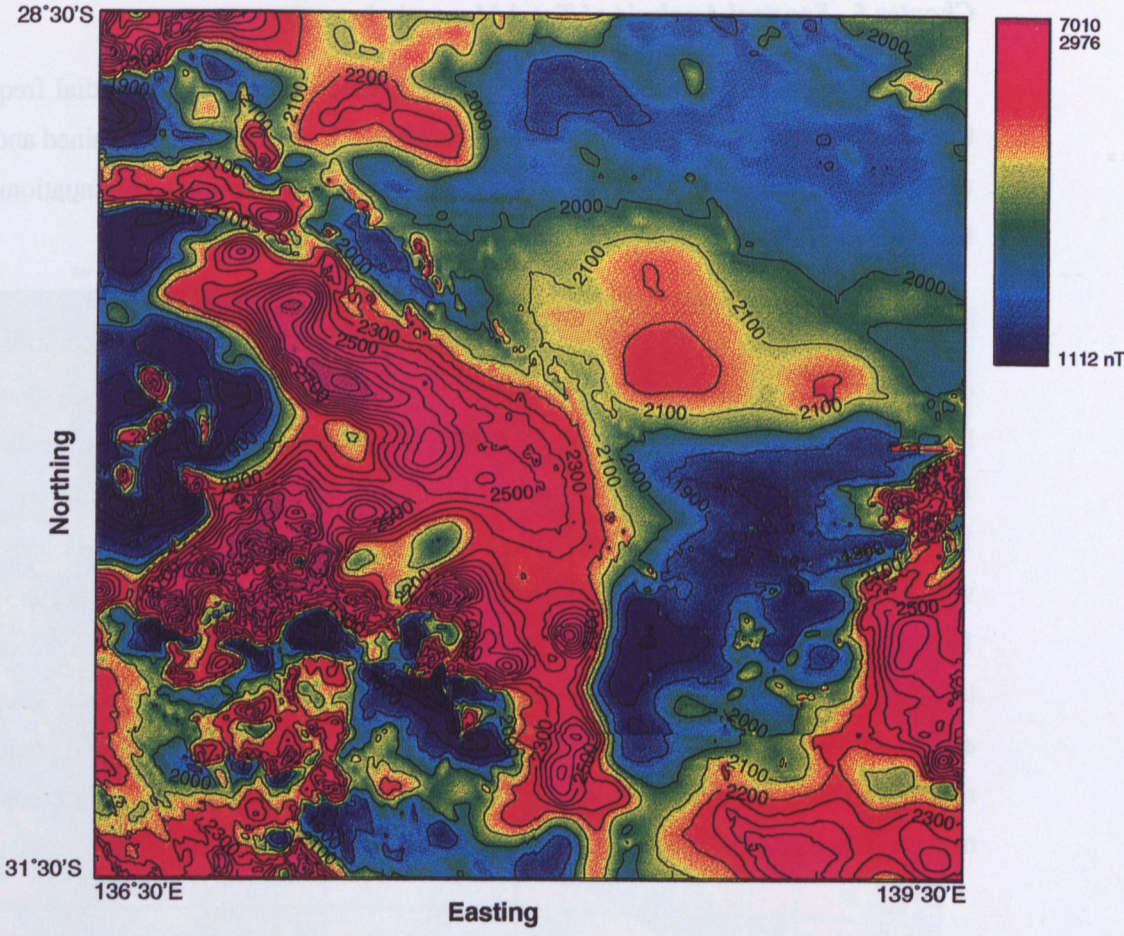

Figure 5.3 Colour image with contours of TMI over 300x300km block - SQ9.

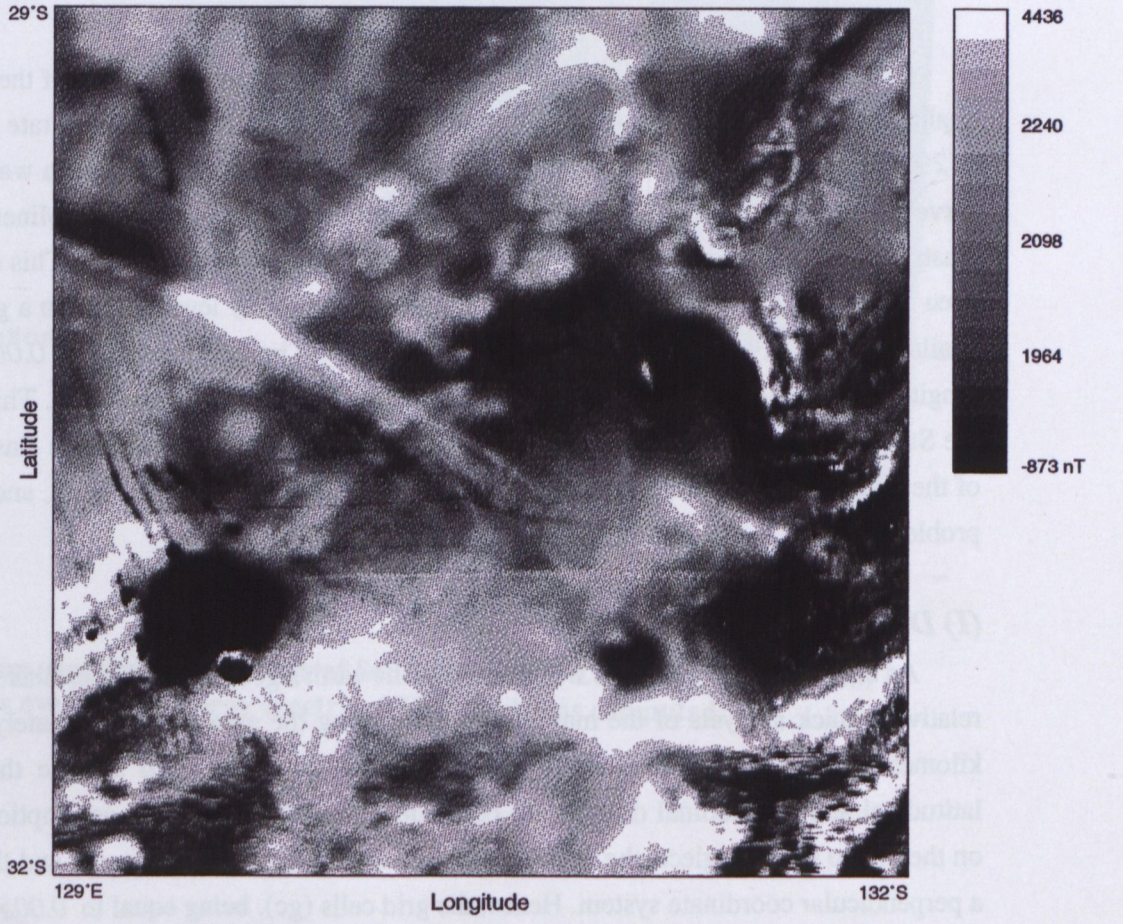

Figure 5.4 Total magnetic intensity grey image over 300x300km block - SQ11.

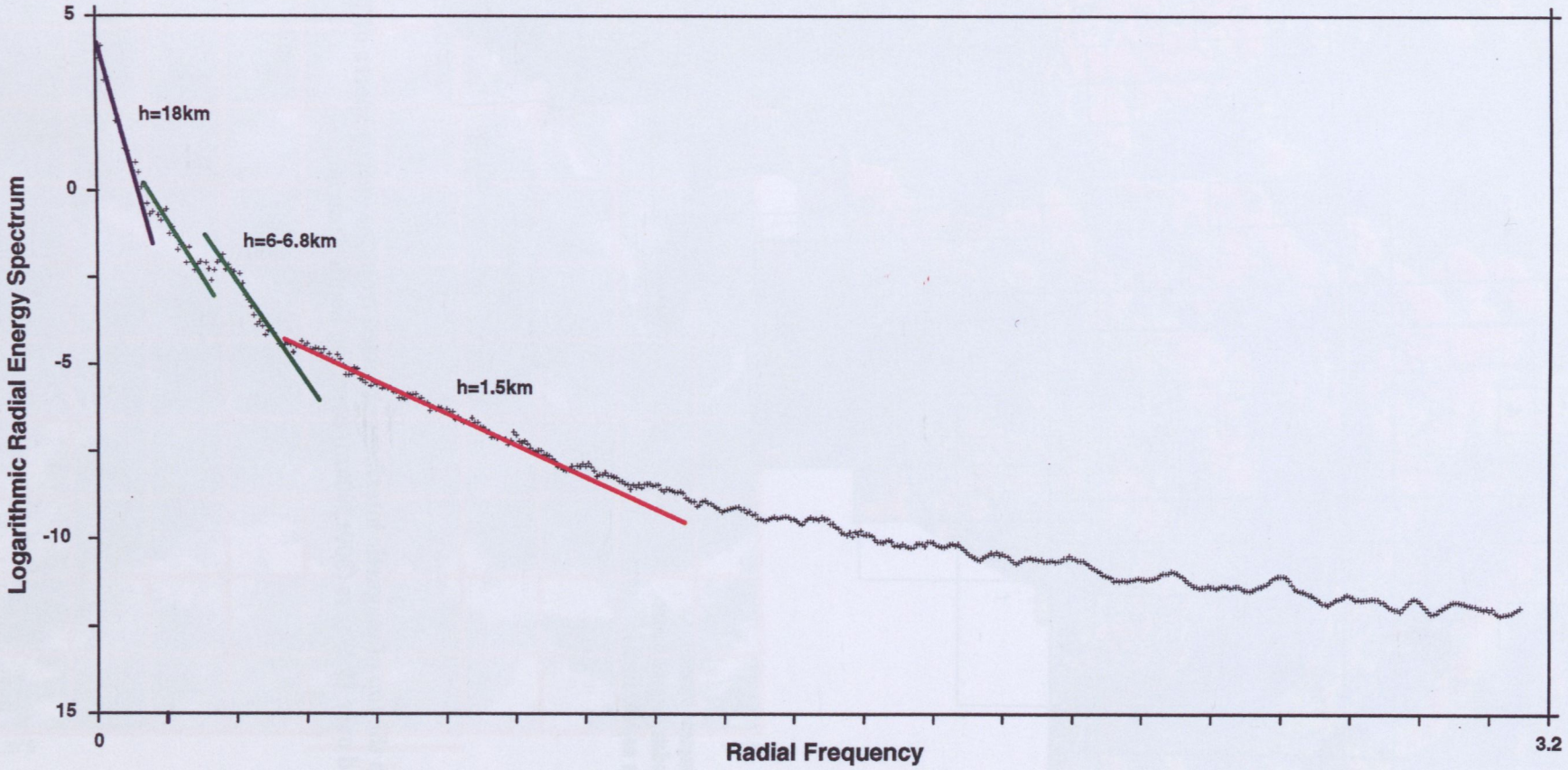

Figure 5.5 Interpretation of logarithmic radial energy spectrum of TMI computed over 300x300km block SQ11.

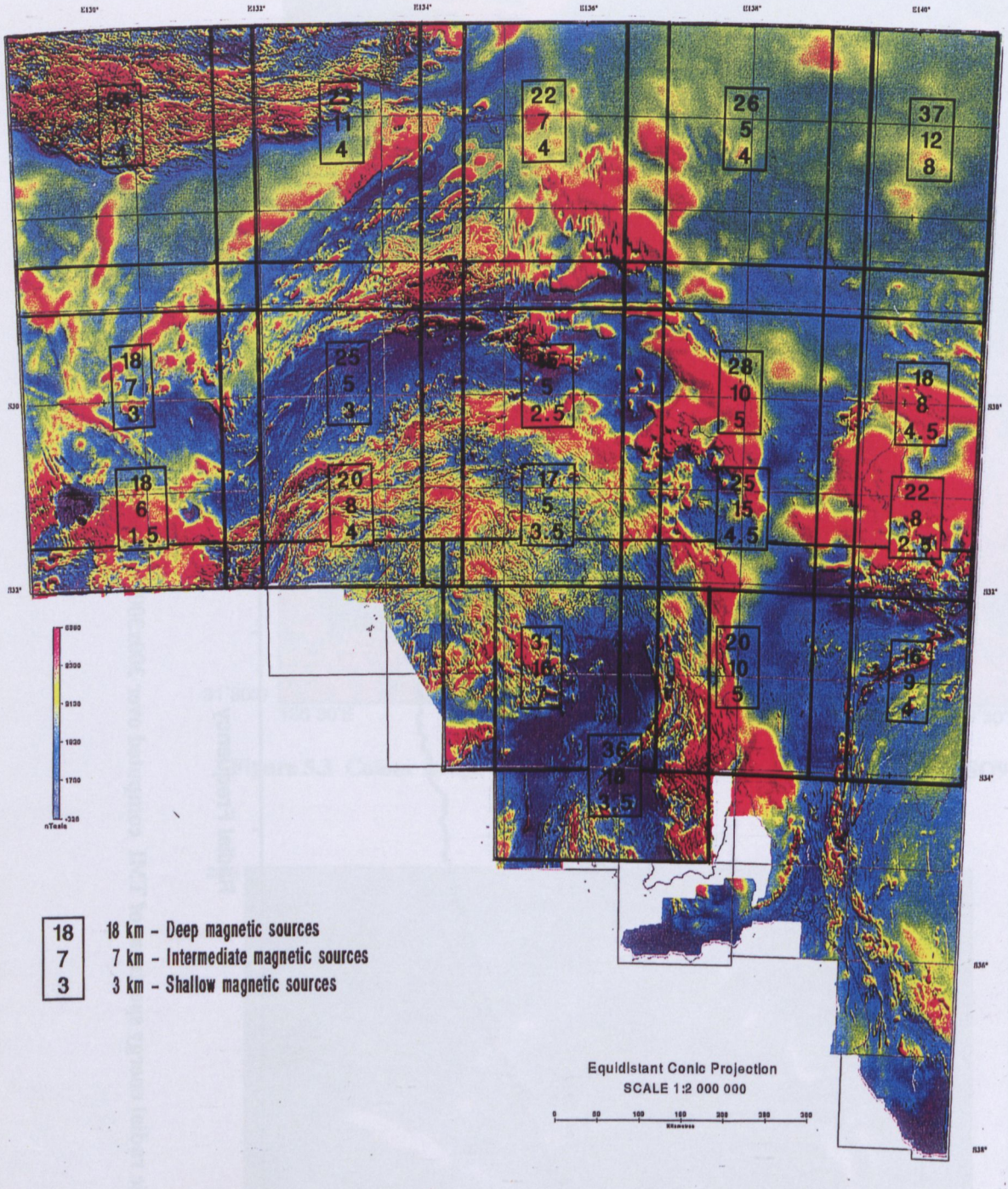

Figure 5.6 Depths to the top of magnetic interfaces obtained from the energy specra of TMI computed over 19 blocks (300x300km) covering South Australia.

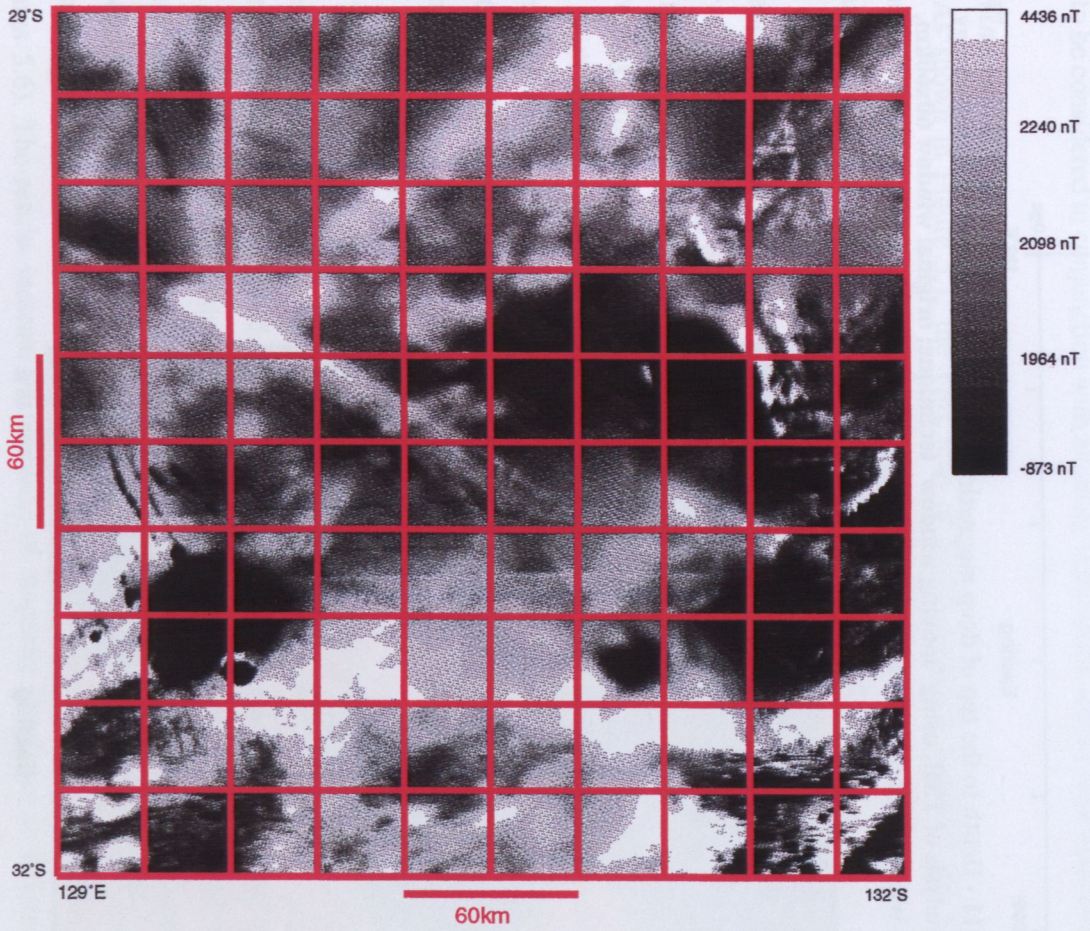

Figure 5.7 Total magnetic intensity grey image of 300x300km block - SQ11 with superimposed 60x60km 'moving window' designed for energy spectra analysis. Each window overlaps by 50% along x- and y-axis.

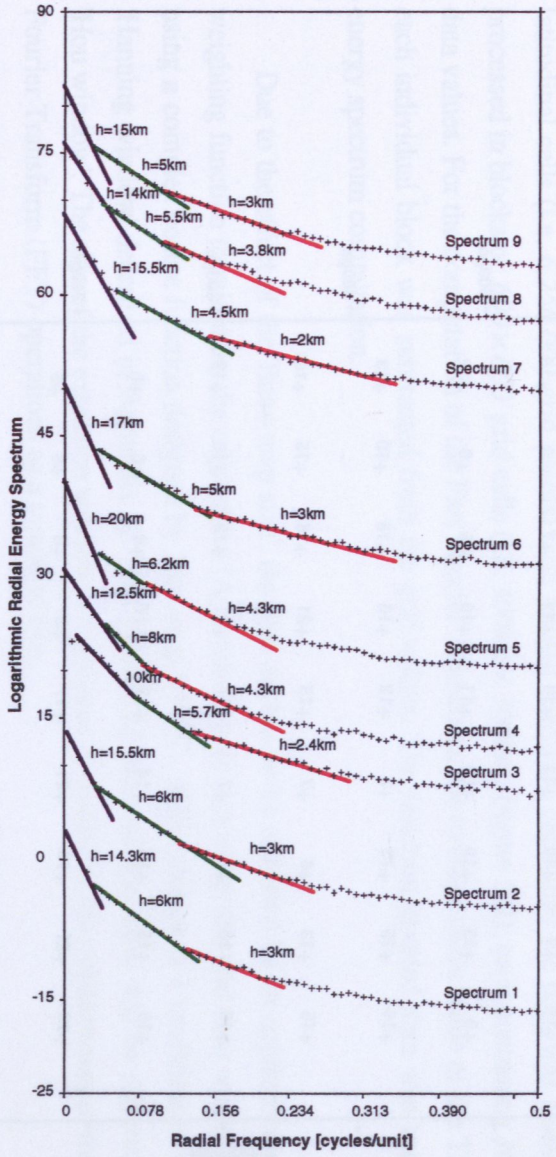

Figure 5.8 Log-radial spectra of TMI computed using 60x60km 'moving window' with extension 128x128km.

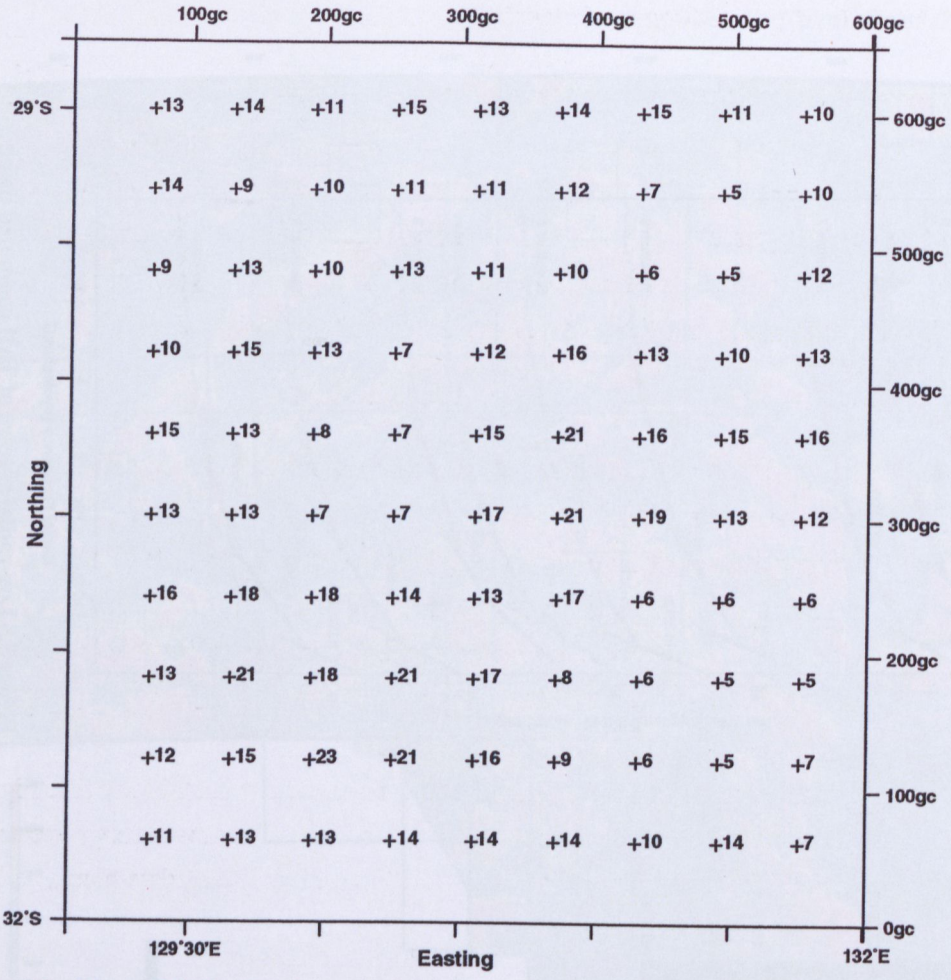

Figure 5.9 **Block SQ11 - Depth to the top of deep magnetic sources computed by applying energy spectra analysis of TMI, using 'moving window' technique; original window 60x60km, extension window 128x128km. Cross indicates centre of 60x60km window.**

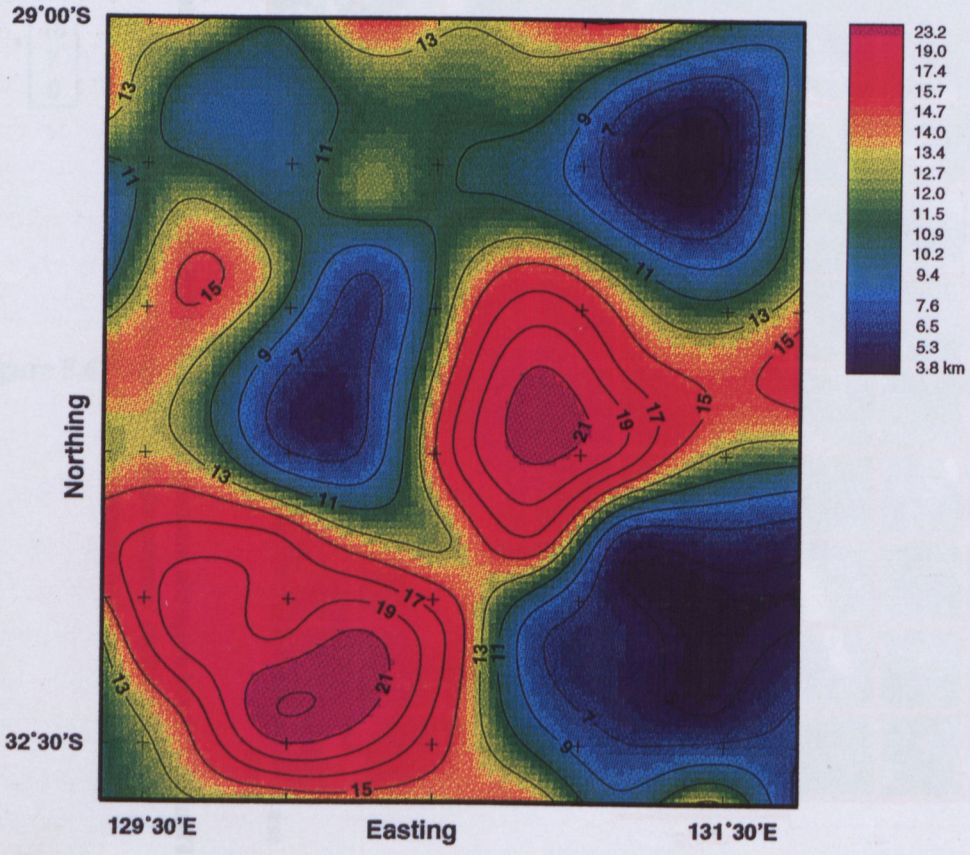

Figure 5.10 **Contours and colour image of depth values shown at Figure 5.9. Contour interval 2km.**

(II) Calculations procedure of the energy spectrum

Because of the very large size of the original grid file, i.e. *2401* longitudinal cells by *2601* latitudinal cells (i.e. *6,250,000* grid points), and limited hardware capacities the data was stored and processed in blocks of 600×600 grid cells (i.e. $300km \times 300km$; Figure 5.2), each containing *36,000* data values. For the computation of the Fast Fourier Transform, the average mean value of the TMI of each individual block was subtracted from the grid values. The resultant gridded data was used for energy spectrum computation.

Due to the effect of the 'finite map size', the data set has to be extended by an application of the weighting function to minimise the edge effect (Appendix A). In this study the grid data was extended using a complex cosine function designed by Hou et al. (1977). This function is a modification of the 'Hanning window' described in Appendix A. This process of data extrapolation will be referred as a 'Hou window'. The size of the extension window is calculated according to the requirements of the Fast Fourier Transform (FFT) operations as a power of two.

Contour maps and grey image maps of the TMI field were generated for each block (i.e. Figure 5.3 and 5.4) since the interpretation of the depth values obtained from the log-radial energy spectrum need to be considered in conjunction with anomaly distribution within each analysed data block.

(i) Window $300km \times 300km$

As shown in Figure 5.1, the TMI map of South Australia indicates the presence of shallow magnetic sources e.g. in the Musgrave Block and Gawler Craton, and magnetic rocks at much greater depths e.g. below the Officer and Eromanga Basins. However, even if magnetic rocks are exposed, there are possibly other magnetic sources beneath them. Initially the energy spectral analysis of TMI was applied to $300km \times 300km$ squares, which showed that the greatest depth obtained was of the order of 25 km. Twenty one squares overlapping each other by *50km (100gc)* along both easting and northing have been computed. Referring to the Figure 5.2, areas covered by individual blocks are accordingly termed $SQ1, SQ2, SQ3, ..., SQ21$. The block size, each covering about $90,000km^2$ of the map, with the exception of the *SQ5*, *SQ10*, *SQ15* and *SQ20*, was chosen mainly to obtain preliminary indications of the distribution of major magnetic horizons and an indication of the variation of the Curie point isotherm within the crust underlying different geological provinces of South Australia.

The radial energy spectrum was computed and its logarithm was plotted versus radial frequency values for each block using original window size $600gc \times 600gc$ with an 'extension window' of $1024gc \times 1024gc$ size (Figure 5.5; Appendix A and B). Using a manual 'pencil and ruler' technique, each spectrum was divided into segments delineated by the best fitted regression straight line. The slope of each linear segment designates the approximate average depth of an ensemble of the bodies (Appendix A). At least three distinct straight line segments were interpreted for each energy spectrum graph (Figure 5.5). The depths to the deep, medium and shallow magnetic sources have been recorded (Figures 5.6). The results indicate the presence of magnetic interfaces at different levels within the crust of South Australia.

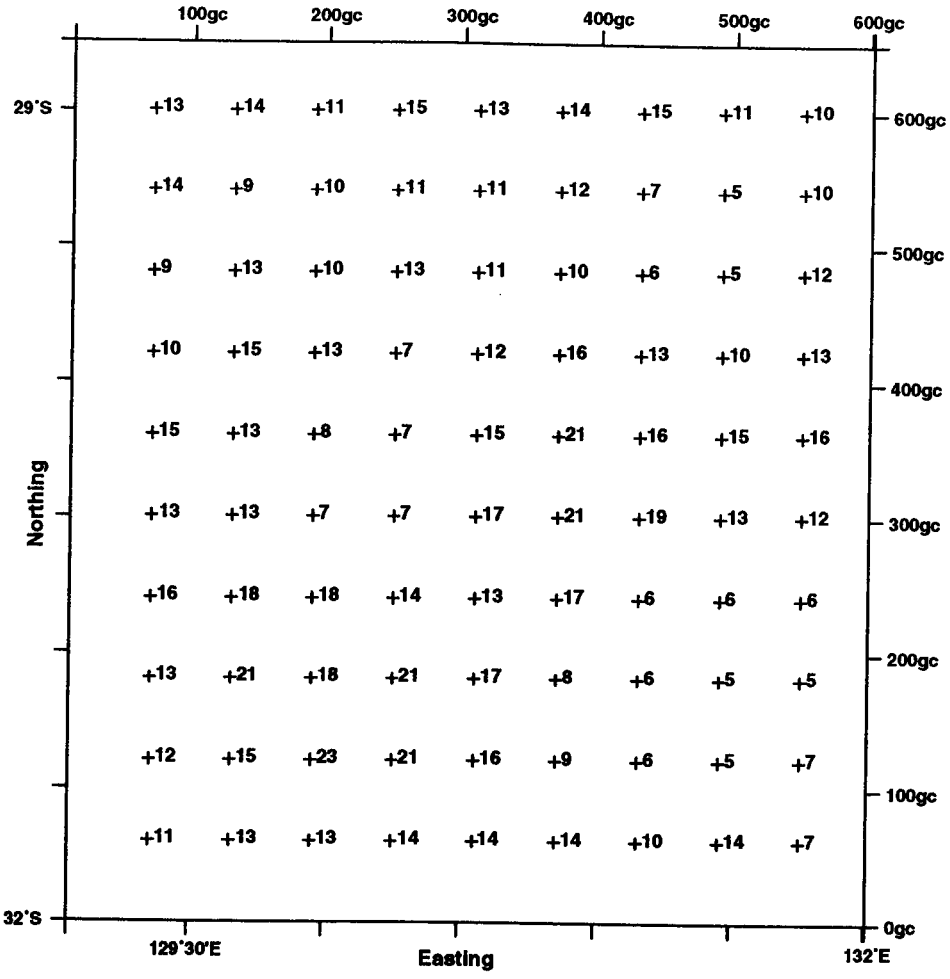

Figure 5.9 Block SQ11 - Depth to the top of deep magnetic sources computed by applying energy spectra analysis of TMI, using 'moving window' technique; original window 60x60km, extension window 128x128km. Cross indicates centre of 60x60km window.

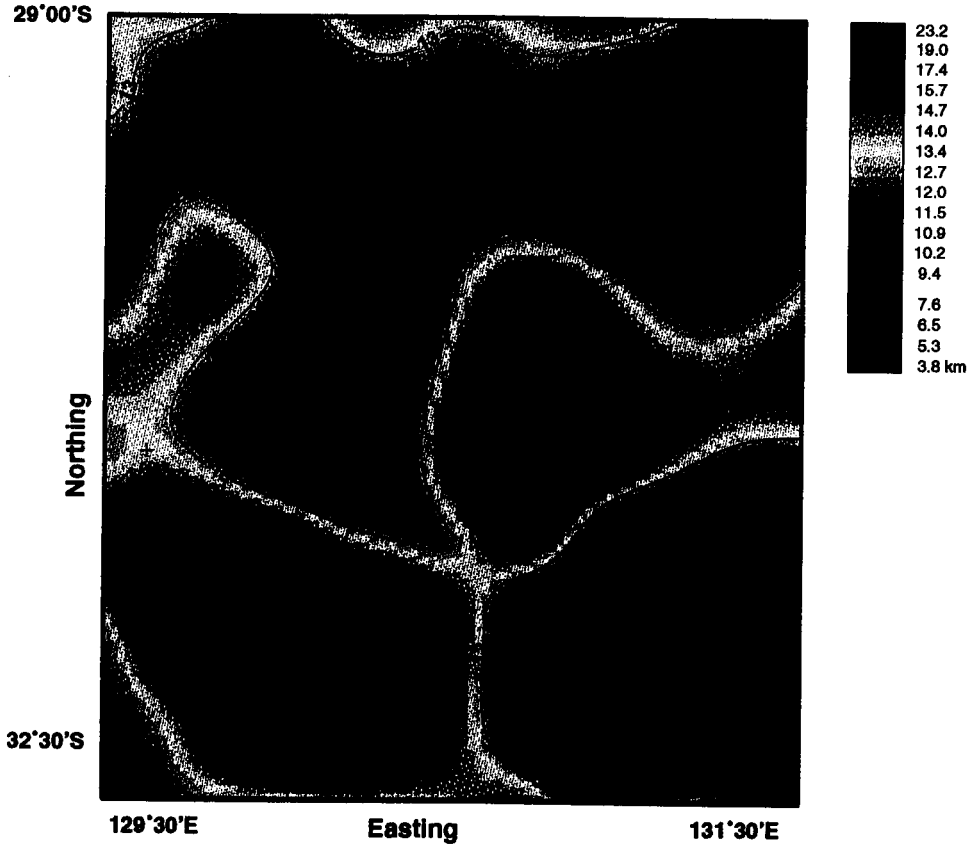

Figure 5.10 Contours and colour image of depth values shown at Figure 5.9. Contour interval 2km.

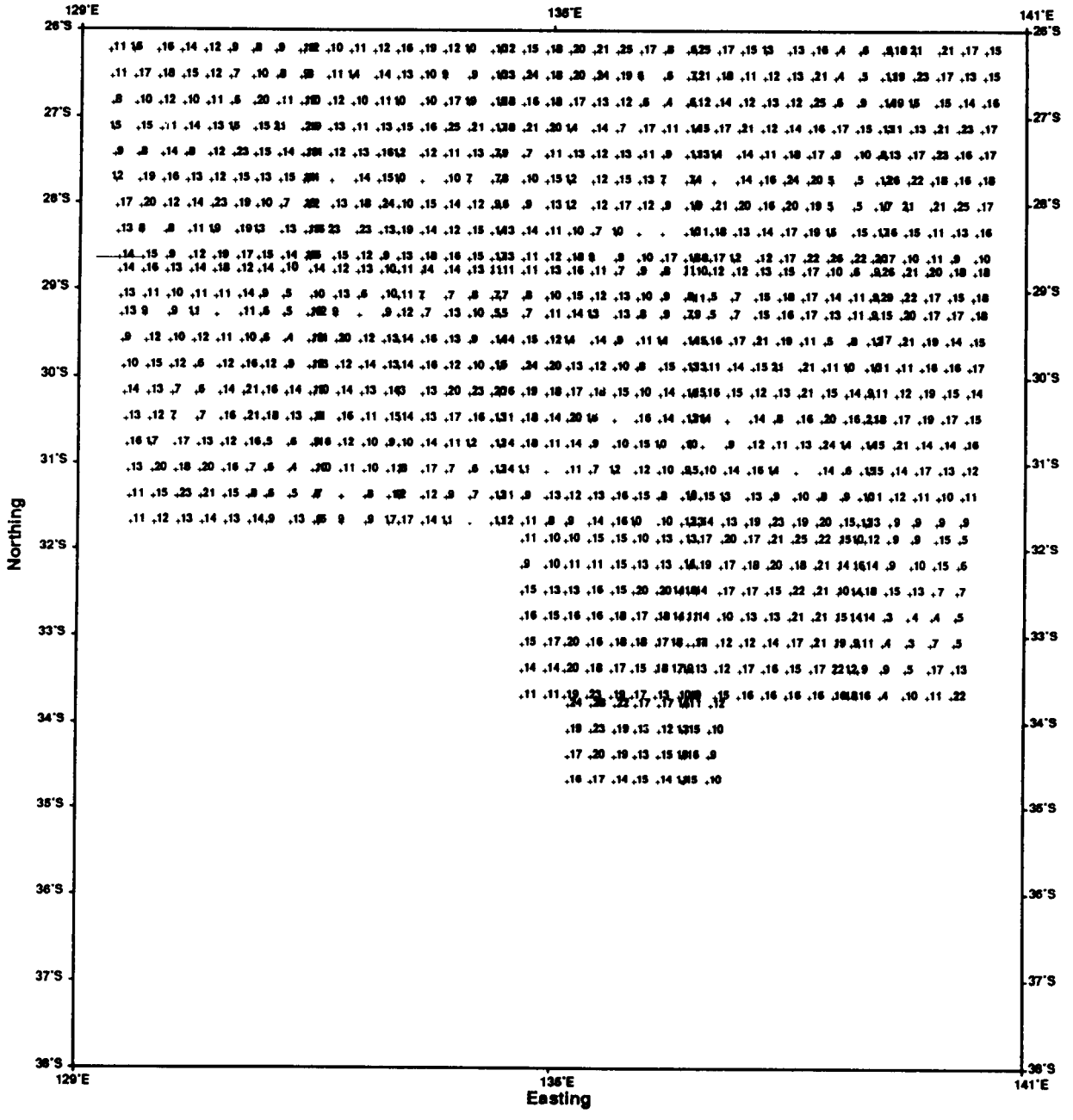

Figure 5.11 South Australia - Average depth to the top of deep magnetic sources computed by applying spectra analysis of TMI using 'moving window' technique. Original window 60x60km. Extension window 128x128km. Cross indicates centre of the window. Simple conic projection with central meridian 135°00'E was applied.

(ii) Window 60km×60km

To obtain more detailed information about the structure of the deep crust the energy spectral analysis method has been applied to approximately *2,000* data-blocks using a smaller window size, based on TMI grid $1km \times 1km$ ($0.01^\circ \times 0.01^\circ$). As Shi (1993) indicates, the maximum depth detected from the spectral analysis of TMI (also gravity) is not greater than forty percent of the size of the original window. To obtain the average approximations of the depths to the top of the different magnetic sources within the crust of South Australia, four different sizes of the 'original window' were analysed: $40km \times 40km$, $60km \times 60km$, $80km \times 80km$ and $120km \times 120km$. Based on the results obtained, the $60km \times 60km$ size of the 'original window' was chosen to compute energy spectra over the whole State of South Australia. The energy spectrum depth estimates were then inferred from the squares of observations each containing about *16,000* magnetic field values, with the 'extension window' size of $128km \times 128km$.

To speed up computation procedure and to optimise informative output and minimise the effect of the anomalies' distribution within the 'original window', the area of the State was 'scanned' by a $60km \times 60km$ window with an overlap of fifty percent along both $x-$ and $y-axes$ (Figure 5.7). This technique is referred to as 'the moving window' (Shi, 1993). Examples of energy spectrum graphs computed over *SQ1* are included in Figure 5.8.

All magnetic interfaces detected by this research are beyond the depth of direct observation, therefore, attention has first been directed to the deepest boundary, as it was thought that this would be the simplest and possibly the least ambiguous. Estimated values of the approximate average depths to the top of the deepest magnetic sources (DMS) within the crust were plotted in the centre of each spectral window (see Figure 5.9 showing example from *SQ11*). These depth values represent different magnetic interfaces, and the colour image and contour map of the deep magnetic sources was constructed for each of $300km \times 300km$ blocks, based on the $2km \times 2km$ grid (Figure 5.10). Integrated depth values over the whole of South Australia are shown in Figure 5.11. The colour image with superimposed contours at *2 km* interval is presented in Figure 5.12.

5.1.2 Application of spectral analysis method to the 1987/88 survey aeromagnetic data of Eyre Peninsula

(I) Introduction

The aeromagnetic survey flown in 1987/88 over Eyre Peninsula is of higher quality than that available for the whole of the state (Chapter 4). To distinguish this survey from that of the state grid (Section 5.1.1), it will be referred to as the high resolution aeromagnetic data. These magnetic data were analysed using the energy spectral method to solve two separate problems:

- structure of the underlying crystalline basement where the nature of magnetic boundaries is uncertain, and
- thickness of sediments within the Polda Trough.

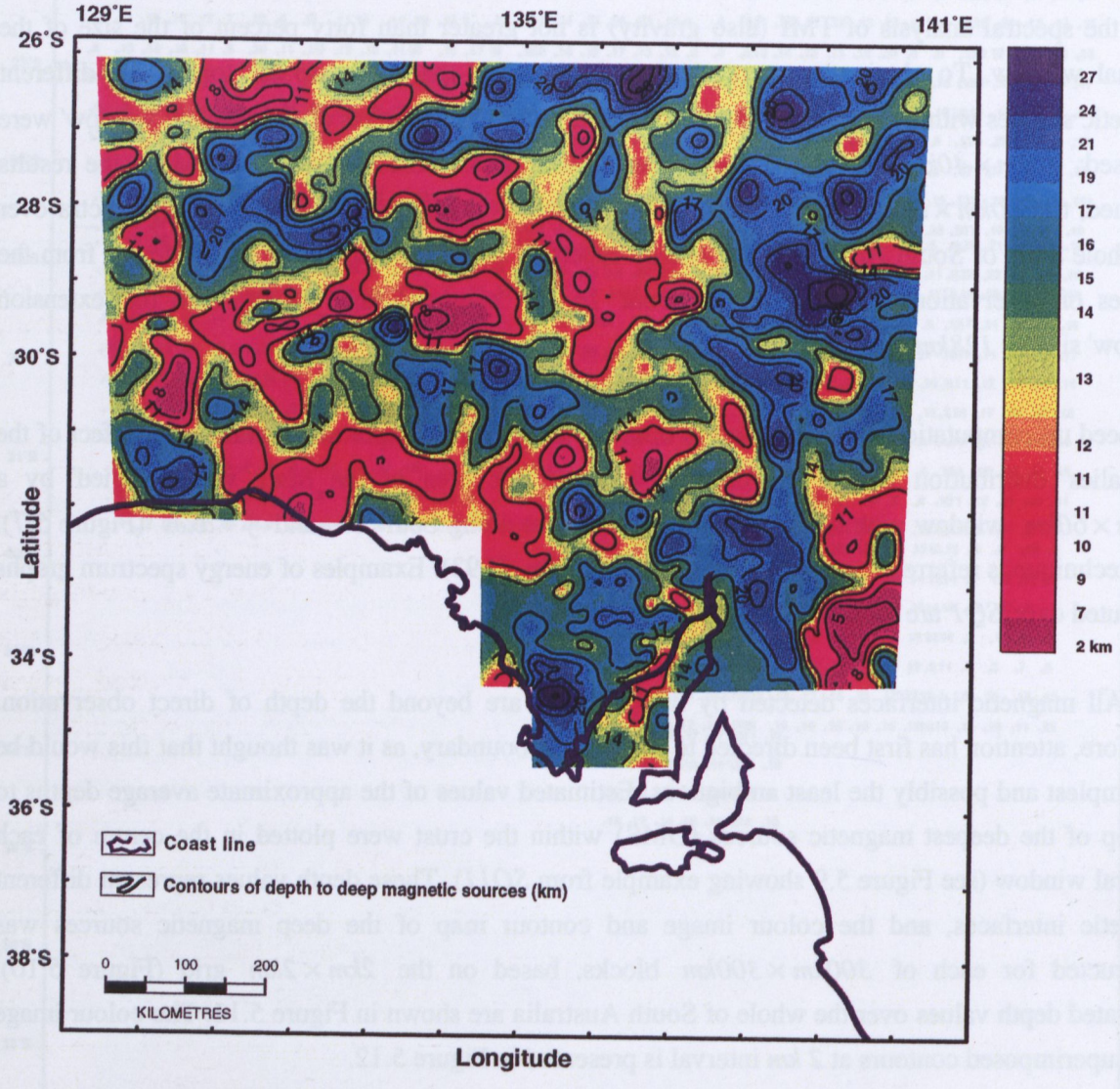

Figure 5.12 Depth to the top of deep magnetic sources obtained by applying spectral analysis of TMI field of South Australia. Logarithmic radial energy spectra computed using 'moving window' technique: original window size 60x60km, extension window 128x128km, depth contour interval 2km.

As discussed in Chapter 4, the 1987/1988 high resolution aeromagnetic survey has covered 25-30 km of the offshore part of the Polda rift and its extension on land. The data were collected along the east-west flight lines, being one kilometre apart in the onshore section and two kilometres apart over the ocean. The details of this aeromagnetic survey are presented in Section 4.1.2. These new data were gridded using a $200m \times 200m$ grid spacing in contrast to the state grid data with a $500m \times 500m$ or $1km \times 1km$ sampling interval.

Because the structure of the Polda Trough varies significantly along its length, the area was divided into three parts: Polda West, Polda Central and Polda East (Figures 5.13-5.15). In the western and eastern part of the study area, thick non-magnetic sediments overlie a strongly magnetic basement. Separation of high frequency components (mainly the effect of surface noise), from lower frequency anomalies was undertaken in order to study the response of deeper sources (the basement and beneath) and determine the thickness of the sediments in various parts of the rift and to detect the structure of magnetic basement.

As described in Chapter 4, in the Polda Central region the main trough becomes a relatively narrow structure, often only 4-5 km wide, with shallow highly magnetic metamorphic basement rocks on the northern side of the rift and weakly magnetic basement rocks covered by non-magnetic sediments up to 300 m thick on its southern flank. According to the principles of the energy spectral analysis method (Appendix A), and considering that flight line spacing is 1 km, spectral analysis cannot produce reliable results in estimating the thickness of the sediments in this part of the rift.

The distribution of anomalies within the data block may influence the energy spectrum, and consequently the estimated depth values (Appendix A). Therefore, this problem should be carefully considered because, as Cowan and Cowan (1993) point out '...analysis of spectra covering more than one magneto-tectonic province, i.e. not homogeneous, may produce averages which are not found in either province...'. In the south-western corner of Figure 5.13, which shows the TMI field of Polda West area, there occurs a complex of high frequency anomalies caused by shallow, or outcropping granites of the Hiltaba Suite. These highly magnetic intrusive rocks occur on the southern margin of the Polda West. The northern margin of the rift which contains the non-magnetic sediments is in contact with shallow, highly magnetic basement rocks. In this area the rift zone is a relatively wide structure. The spectral windows were selectively designed within the rift margins, where the magnetic anomalies are due to the magnetic basement underlying Polda Trough sediments.

(II) Data preparation and processing for depth determination by spectral analysis

In Polda West the energy spectral analysis method was applied to gridded magnetic data ($200m \times 200m = 1gc$) using the 'moving window' technique (75% overlap). To be able to detect thickness of the non-magnetic sediments the $80gc \times 80gc$ i.e. $16km \times 16km$ window with extrapolation array of $128gc \times 128gc$ ($25.6km \times 25.6km$) was used (Figure 5.16).

(ii) Thickness of sediments in the Polda rift

The results of the spectral analysis of high resolution magnetic data over the Polda Trough give the following:

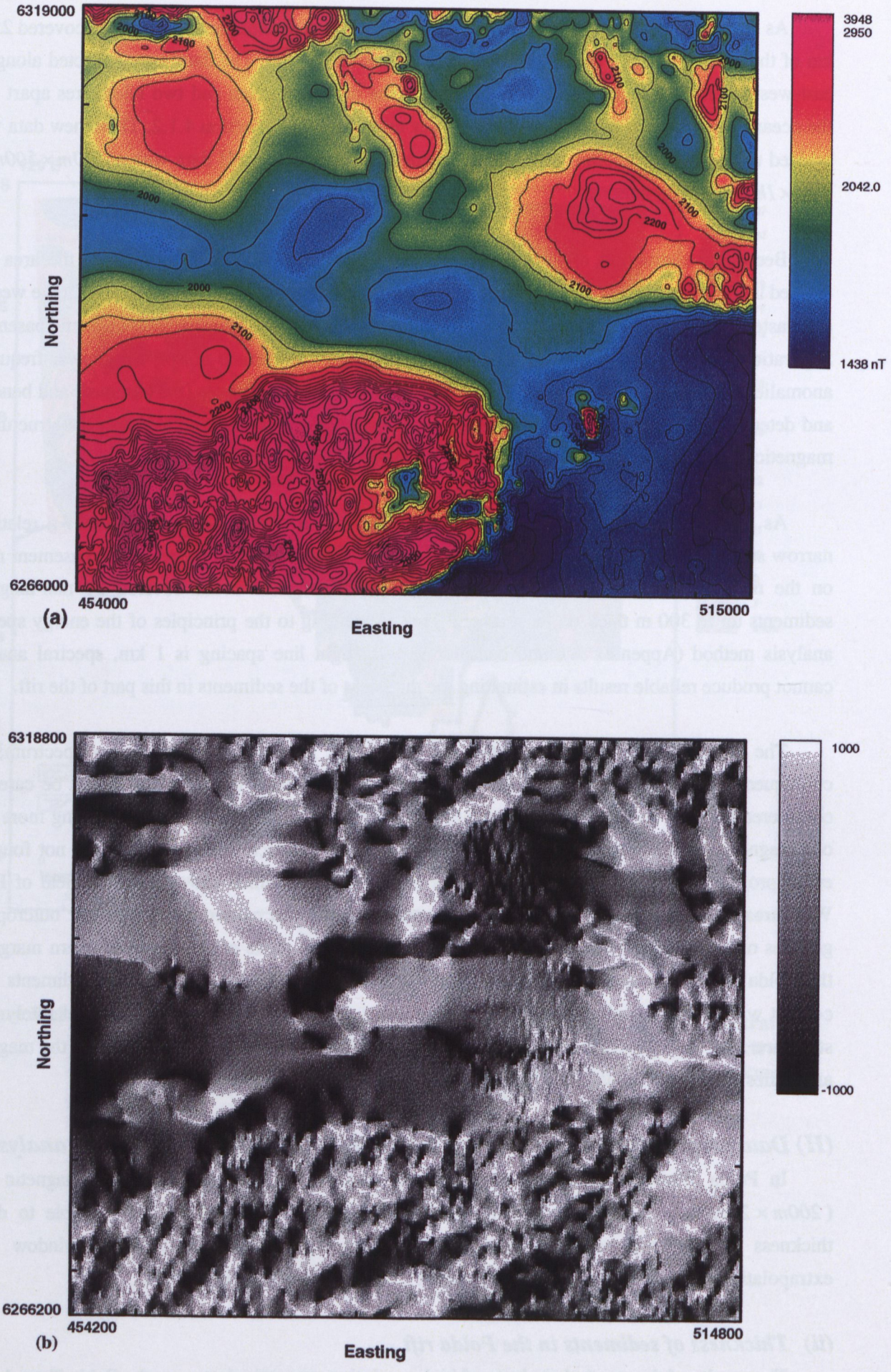

Figure 5.13 Polda West - Total magnetic intensity field: (a) Colour image with contours at 50nT interval (b) Shaded relief. Elevation angle 0°, azimuth 135°, slope factor 0.001. TMI grid cells 200x200m.

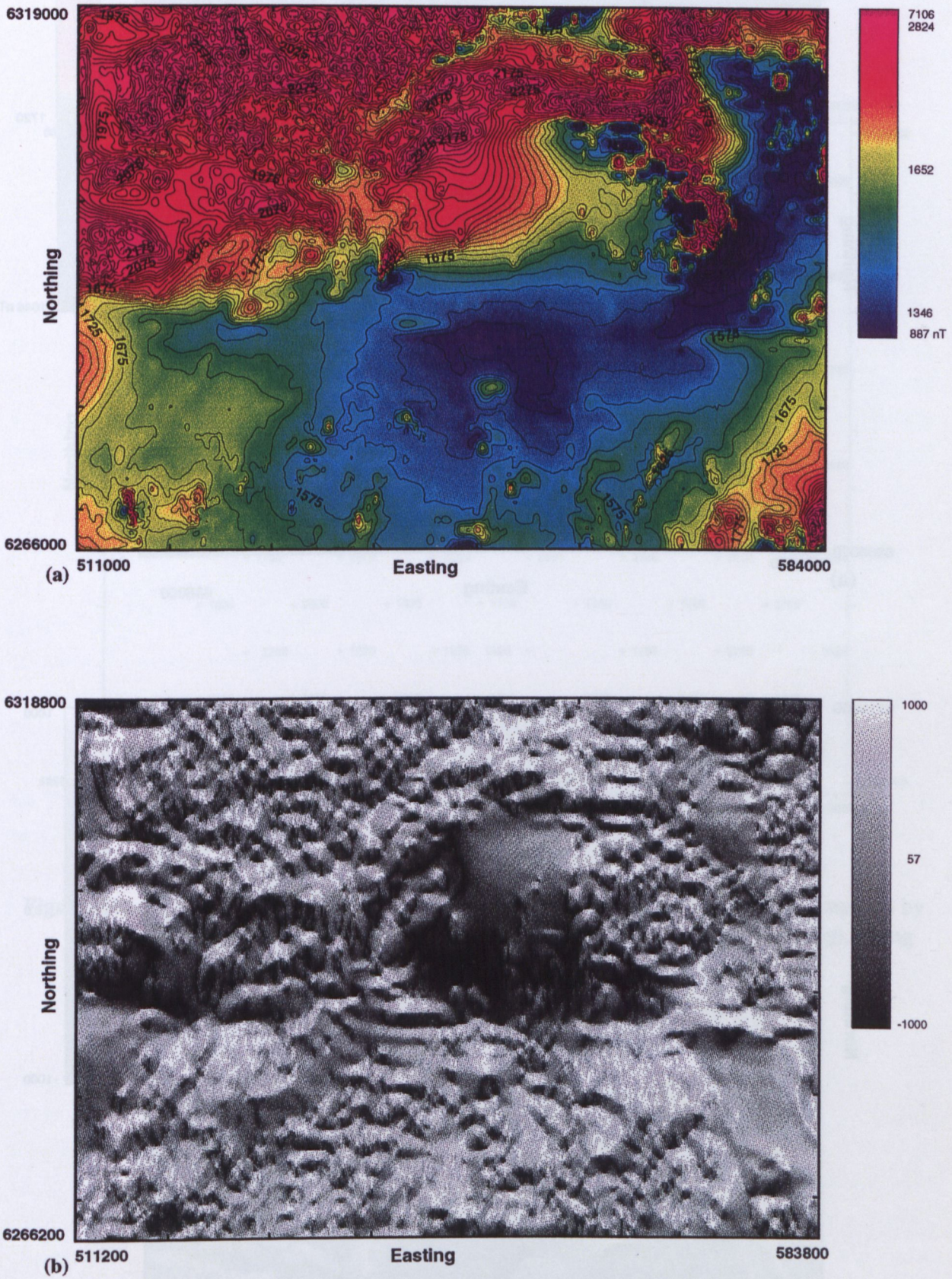

Figure 5.14 Polda Central - Total magnetic intensity field: (a) Colour image with contours at 25nT interval (b) Shaded relief. Elevation angle 0°, azimuth 0°, slope factor 0.001. TMI grid cells 200x200m.

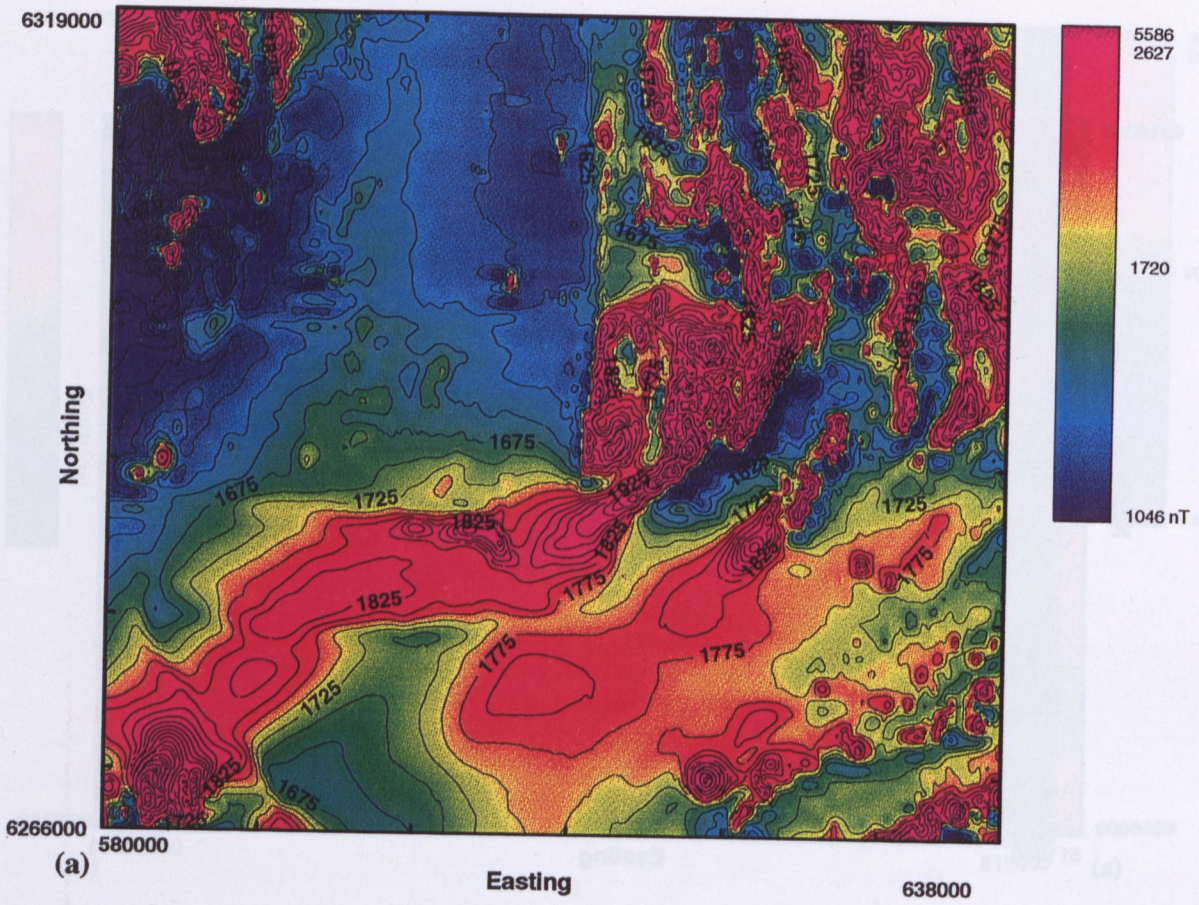

Figure 5.15 Polda East - Total magnetic intensity field: (a) Colour image with contours at 50nT interval. (b) Shaded relief. Elevation angle 0°, azimuth 0°, slope factor 0.001. TMI grid cells 200x200m.

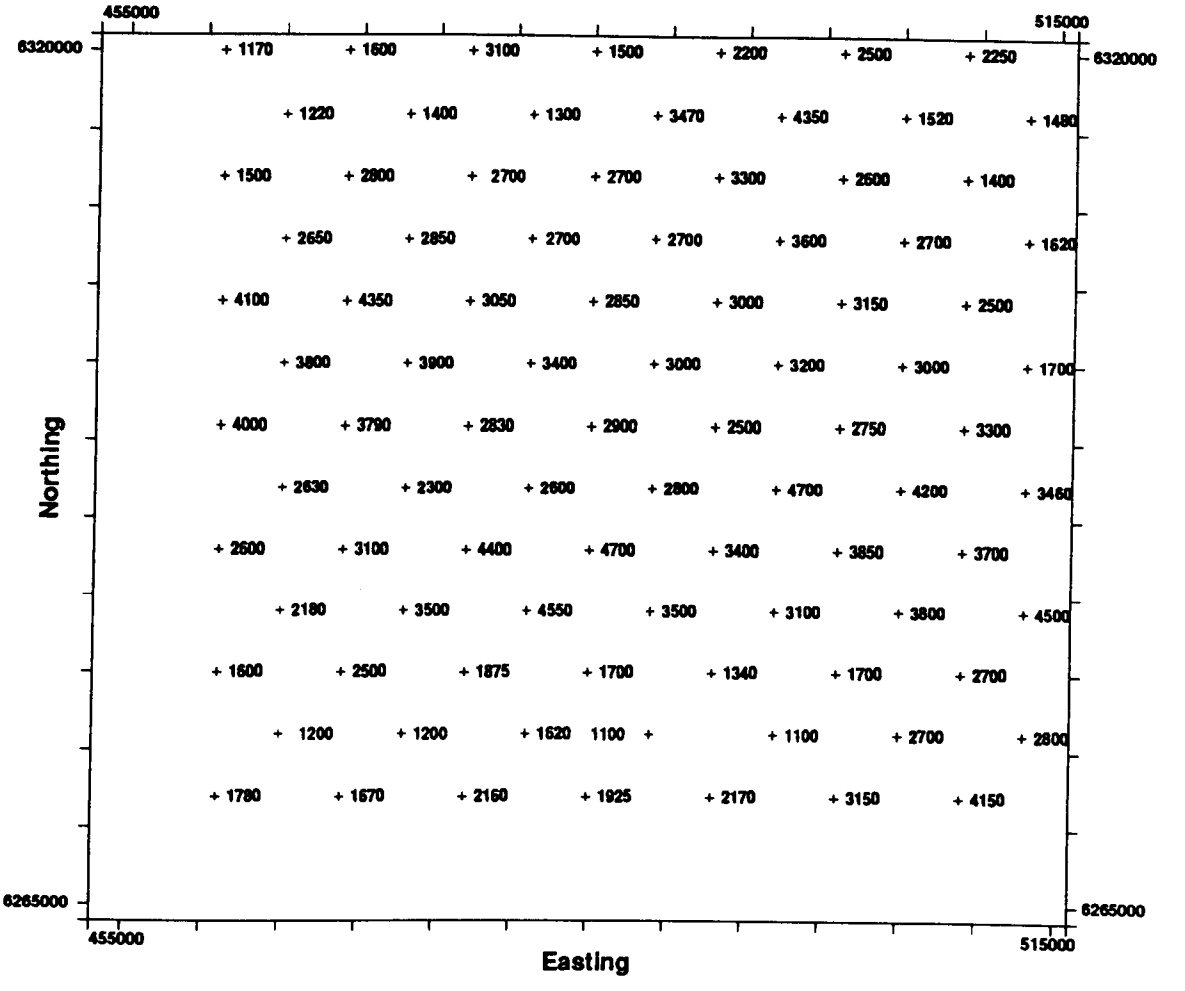

Figure 5.16 Polda Trough - western part. Depth to the top of magnetic sources computed by applying energy spectra analysis of TMI field (200x200m grid spacing), using 16x16km 'moving window' with extension array 25.6km.

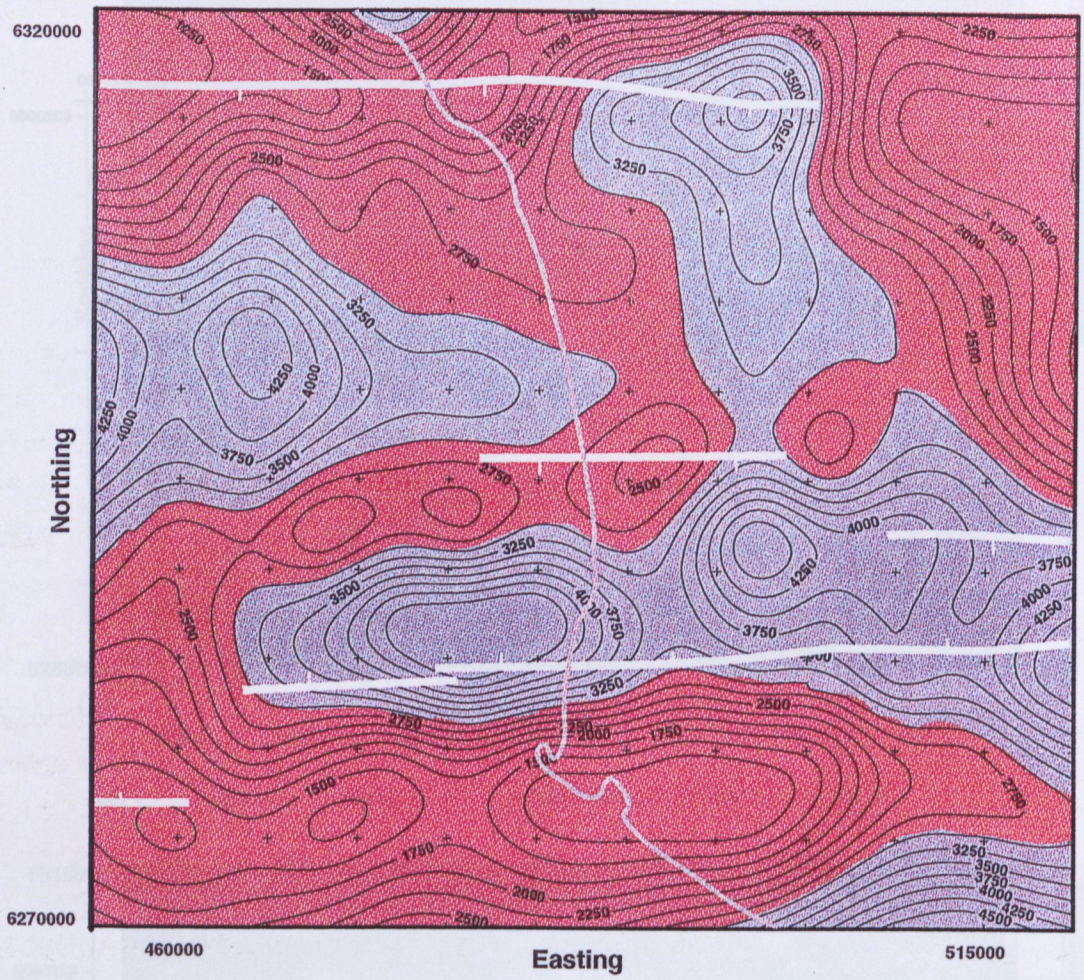

Figure 5.17 Polda Trough - western part. Contours of the depth to the top of magnetic sources as described at Figure 5.16 with superimposed major faults of the Polda rift. Contour interval 250m.

(a) Thickness of sediments in the Polda West area

The map constructed shows two east-west trending basement troughs separated by a parallel ridge, which is interpreted as a relay ramp. As Figure 5.17 shows these structures are in an en echelon setting. Such a pattern suggests that the northern rift continues offshore towards the west, whereas the southern trough continues towards the east as a narrow onshore extension of the Polda rift (Figures 5.17 and 4.26). The dividing ridge represents the position of the relay ramp (Chapter 2; Figure 2.5) which is a characteristic structure of rifts and is responsible for change of polarity of the internal half grabens. A similar interior structure has also been detected in Polda Central in the vicinity of the Lock Coal Deposit (Chapter 4). As discussed in Chapter 2, such relay ramps are characteristic structural features of rifts and are observed for example in the East African Rift System. They have been proven to exists in rifts by analog sand-box modelling which simulates development of the rift's structure (McClay, 1993). The maximum thickness of sediments indicated within the northern magnetic trough exceeds 4200 m, and in the southern part of the rift it is greater than 4600 m. It is slightly shallowing towards the east where the deepest section is 4300 m. The magnetic ridge is about 2600 m deep. The northern margin of the deep magnetic northern trough coincides with the position of the basement fault F_{PW}^{NM} (Chapter 4).

(b) Thickness of sediments in the Polda East area

This is an area where the data quality was barely adequate to solve the problem presented. It would have been more satisfactory to have data with more closely spaced flight lines. The depth to magnetic basement at the eastern end of the rift was obtained from spectral analysis and confirmed by forward modelling of several magnetic anomalies (Figure 5.15). Both techniques indicate several depth values. The forward modelling results (*1.7km – 2.4km*) are shown in Figure 4.34. The spectrum computed for the square covering the entire Polda East area (Figure 5.18) indicates depths of *3.4 km, 2.8 km* and *1.4 km*. The depth of *3.4 km* possibly represents the depth to the basement (total thickness of the sediments including two basaltic layers), while depths of *2.8 km* and *1.4 km* may reflect highly magnetic basaltic lavas which were detected by drilling (hole *CRA 83KD1A* intersected volcanics at a depth of *1.3 km*; Chapter 3).

(III) Concluding remarks concerning the structure of basement and thickness of sediments in the Polda Trough

The results of spectral analysis of high resolution aeromagnetic data confirm previous interpretations, giving the same order of thickness of the sedimentary cover as is obtained from the refraction seismic survey and standard depth estimation methods from magnetics. These results also provide better definition of the internal structure of the Polda West area. The configuration of the sub-basins in the Polda West become clearer. This interpretation of the Polda rift structure is an integrated result of that inferred from the basement topography map constructed from the energy spectrum results (Figure 5.17), and the general understanding of the structure and evolution of rifts which was discussed in Chapter 2. This understanding of the internal structure of the rift may bring some benefits for the future exploration for coal and hydrocarbons in the Polda rift. Due to the absence of any available geological information, geophysical analysis is the only tool which can be used to build a structural model of this part of the rift.

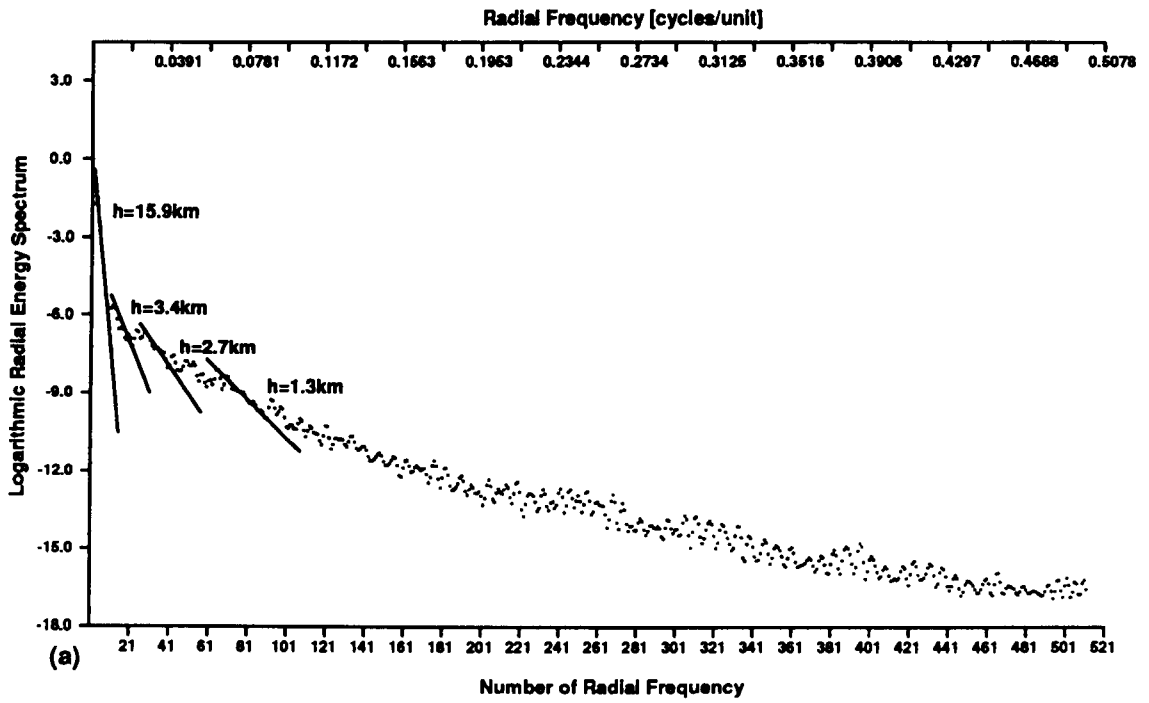

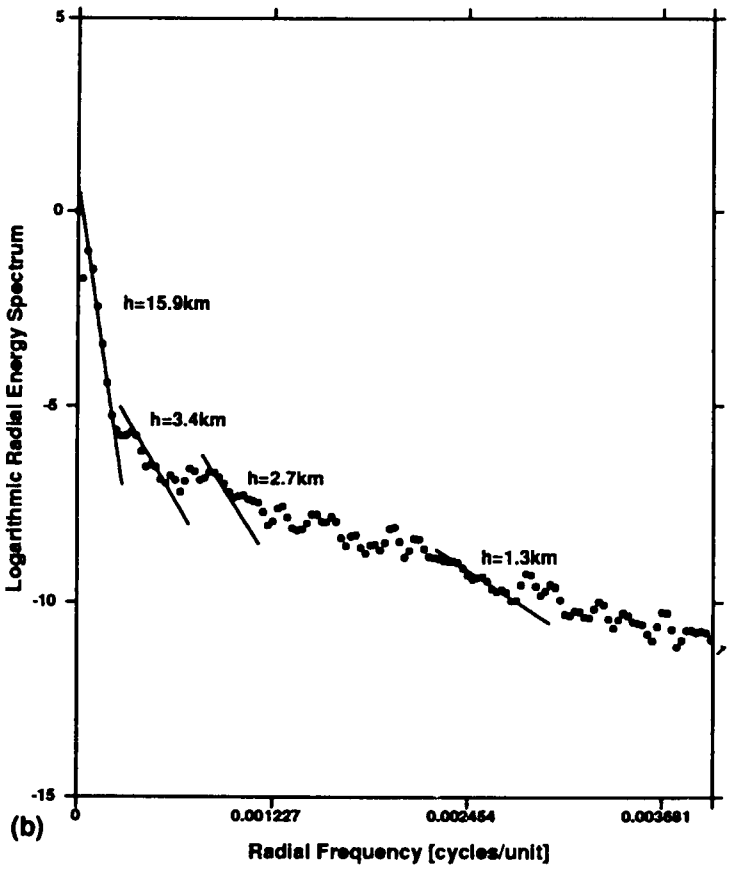

Figure 5.18 Polda East - Logarithmic radial energy spectrum of TMI. Original map size 50x50km, extension window 200x200km, TMI grid spacing 200x200m.
(a) Full spectrum
(b) Detail of the spectrum showing low frequency zone.

5.2 Deep crustal studies based on geophysical methods in South Australia

The Australian continental crust is *35-45 km* thick with well defined Moho discontinuity separating it from the upper mantle (Bolt et al., 1958; Doyle and Everingham, 1964; Hawkins et al., 1965; White, 1969; Thomas, 1969; Stewart, 1972; Denham et al., 1972; Simpson, 1973; Finlayson et al., 1974; Mathur, 1974; Shackleford and Sutton, 1981; Finlayson, 1984; Greenhalgh et al., 1989; Lambeck and Penney, 1984; Lambeck and Burgess, 1992; and others).

The structure of the crust and upper mantle in South Australia has been studied over the decades. The following seismic-related investigations providing information from the deeper parts of the crust and upper mantle have been conducted in South Australia:

- refraction studies from quarry and mine blasts (Finlayson et al., 1974; Shackleford and Sutton, 1981);
- analysis of the P-wave travel times for large regional earthquakes (White, 1969) and local earthquakes (Stewart, 1972);
- determination of the dispersion characteristics and the crustal P-wave velocities for surface waves traversing the Australian continent (Thomas, 1969);
- analysis of teleseismic residuals in correlation with heat flow (Cleary, 1967; Stewart, 1972; Cleary et al., 1972);
- computation and study of the teleseismic P-wave residuals using nuclear explosions and distant earthquakes;
- seismic tomography which mapped lateral velocity variations within the crust using earthquake records (Greenhalgh et al., 1989);
- teleseismic travel-time analyses (Lambeck and Penney, 1984; Lambeck and Burgess, 1992);
- study of the distribution and the focal depth patterns of earthquakes in South Australia (Greenhalgh et al., 1986a, 1986b);
- the micro-earthquake surveys undertaken primarily to map active faults provided information on upper crust velocities (Greenhalgh et al., 1989);

and a recently shot deep seismic sounding in the Officer Basin (AGSO, 1993; see Figure 5.25).

Geomagnetic variation studies which have been conducted in the Gawler Craton and Adelaide Geosyncline of South Australia revealed the existence of electrical conductivity anomalies within the crust (White and Milligan, 1984; White and Polatayko, 1985; White and Milligan, 1986; Milligan and White, 1988; Milligan, 1989; Milligan et al., 1990). The anomalous zones have been detected in two distinctly different geological regimes and are referred to in the literature as: the Southern Eyre Peninsula anomaly within the Gawler Craton and the Flinders anomaly within the Adelaide Geosyncline (e.g. White and Milligan, 1984). The conductivity anomaly identify on the southern Eyre Peninsula follows the major structural trends in the Precambrian basement of the Gawler Craton. According to Milligan et al. (1990) this anomalous conductivity zone delineates the boundary between non-conductive Archaean crystalline basement to the west (Coulta-Subdomain) and the Proterozoic metasediments of the Hutchison Group to the east (Cleve Subdomain). The presence of an anomalous conductive body at a depth of 25 km has been suggested (Milligan et al., 1990). It has also been

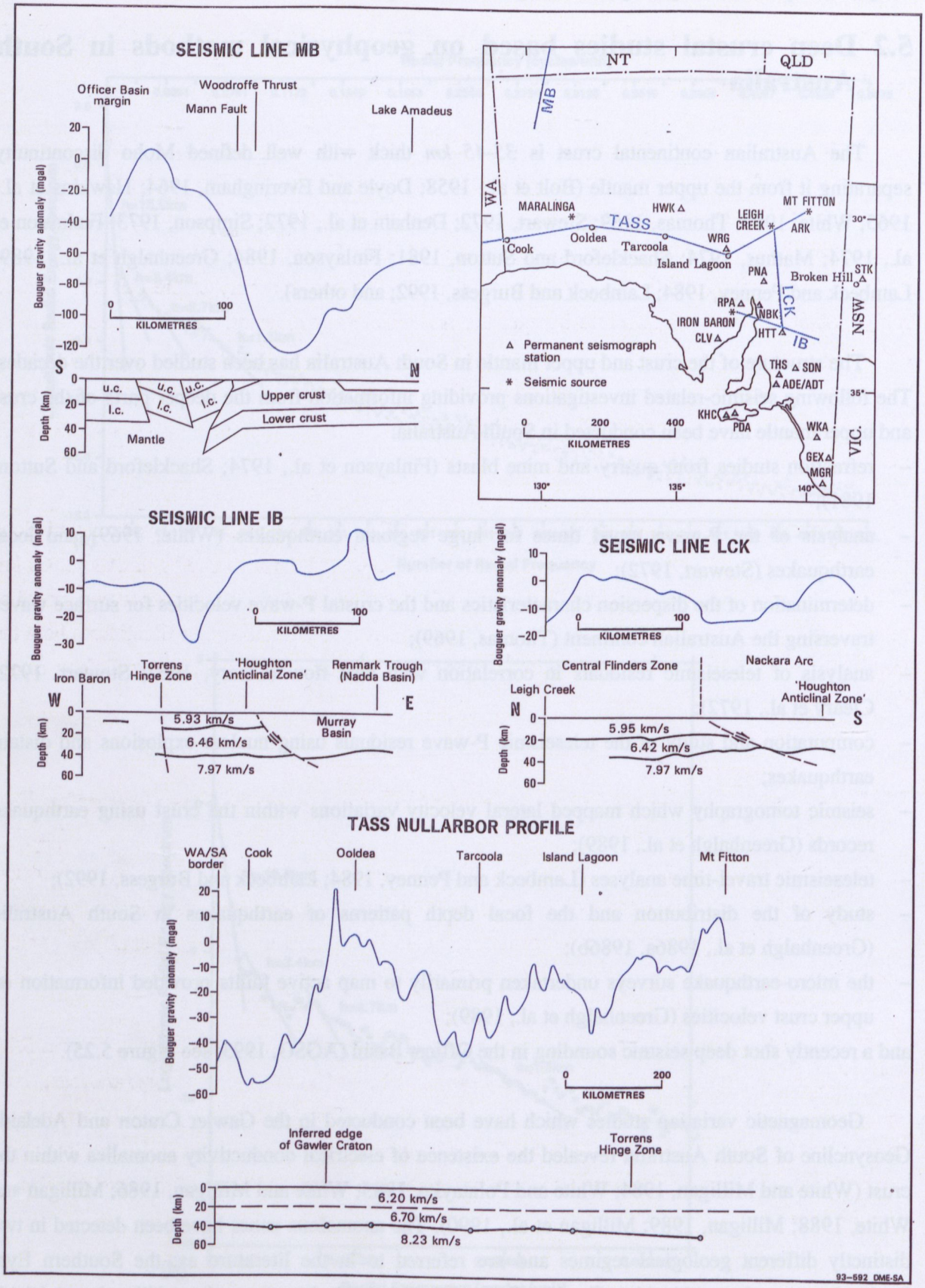

Figure 5.19 Crustal thickness estimates and crustal structures of South Australia. After Finlayson et al. (1974), Greenhalgh et al. (1989), Lambeck and Burgess (1992).

suggested that there may be another conductive body 26 km wide at depth of 10 km (White and Polatayko, 1985; Milligan and White, 1988; Milligan, 1989).

At present there is not enough evidence for reliable determination of the crustal thickness across South Australia. An average depth to the Moho is assumed to be 38 km with substantial shallowing up to a depth of 10 km around the southern continental margin (Parker, 1993). However, recently reported results of the deep crustal studies in the Adelaide Geosyncline and in central Australia indicated major heterogeneities in deep crustal structure beneath relatively stable cratonic blocks. Lateral variation in crustal structure beneath the Adelaide Geosyncline has been detected based on seismic refraction profiles by Shackleford and Sutton (1981). Greenhalgh et al. (1989) who reinterpreted seismic profiles in conjunction with analysis of local earthquake data, have distinguished two crustal layers: an upper crust 15-20 km thick and a lower crust with depth to the Moho varying between 30 km to 40 km (Figure 5.19).

In central Australia Lambeck and his co-authors (1988, 1992) identified major lateral variations of the entire crust and the upper mantle. The crustal slabs extend down to depths of at least 60 km (Figures 5.20 and 5.21). Lambeck and Burgess (1992) postulate similarities in the structural model of the crust and upper mantle between the Musgrave Block and the southern Arunta Block from both the teleseismic evidence and deep crustal seismic reflection data (Lambeck et al., 1988; Goleby et al., 1989, 1990).

5.3 Interpretation of Deep Magnetic Sources map of South Australia.

The interpretation of deep magnetic sources (DMS) map of South Australia focused on two main aspects: (i) the character of the crust under the Polda rift, and (ii) an understanding of a nature of the non-rifted crust. It was considered necessary to look further afield to establish typical characteristics of the crust in the stable cratonic regions and rift zones.

The boundary determined from the energy spectral analysis of TMI and shown in Figures 5.11 and 5.12 is the deepest recorded boundary but it may not always be the same boundary; at this stage of the research not enough is known to be sure. The geophysical interpretation and geological meaning of the results obtained by this research are not final (Boyd et al., 1993; Kivior et al., 1993; Kivior and Boyd, 1995). At this stage, the research is producing new facts about a region of the crust previously little known.

A very important question requiring early attention is the nature of the magnetic boundaries detected. Identification would be facilitated by comparison with any deep seismic sounding. An interpretation of the DMS map of South Australia in correlation with other geophysical survey data and known geological information will be discussed in the following sections and also in Chapter 6.

An integration of the regional structural information, the interpretation of the existing seismic profiles together with the magnetic and gravity data allowed the interpretation of some of the major

magnetic interfaces detected by spectral analysis of TMI and shown on the DMS map of South Australia.

The contour map of DMS detected by energy spectral analysis (see Section 5.12) shows a specific characteristic over the different tectonic regimes. As already mentioned, at the north-east corner of the State, that is over the Cooper Basin magnetic data is of a poor quality with flight line spacing of 7 km. Thus this region of the DMS map was neglected. However, it is clear that major NE-SW faults running across the central-eastern part of the continent (they can be seen on the gravity map of Australia) correlate with the position and direction of major deep crustal features at the north-western part of the DMS map. The energy spectrum results show that the central part of the state, i.e. the Gawler Craton region has less variation in depth than the Adelaide Geosyncline, the Musgrave Block or Officer Basin (Figure 5.12).

5.3.1 The Musgrave Block

The Musgrave Block, which is a major tectonic regime of Australia, consists mainly of the Mesoproterozoic crystalline basement which is flanked by the Neoproterozoic and Palaeozoic basins. The TMI map of the Musgrave Block indicates that magnetic anomalies are strongest over the basement complexes and quiet over the Neoproterozoic and Phanerozoic basins (Figure 5.23). Major fault structures are clearly visible. East-west trending, south verging thrusts flank the southern margin of the Musgrave Block. Figure 5.22 shows the deep underlying structures:

- the ENE striking ridge, marked by stars;
- the flanking lows on the Gawler Craton.

The Musgrave Block is an area of great interest in studies of the crust in Australia because of the large range of gravity values and, in particular, the extensive ENE striking gravity ridge (see Figure 5.24). The spectral analysis results show a well defined boundary at a depth of *11 km* which lies south of the gravity high. This feature has a strike length of about *250km* and width of about *40km*. The fact that the position of the magnetic ENE ridge does not coincide with the gravity anomaly suggests that the boundary dips towards the north. This indicates that the structure is similar to the one postulated to explain the AGSO Deep Seismic Sounding and gravity profile across the southern edge of the Arunta Block, which is *200km* to the north of the Musgrave Block in the Northern Territory (Figures 5.20 and 5.21). There is an indication of similarities between the structural styles of these two areas. The teleseismic studies by Lambeck and others (1984, 1992) indicate major changes in the depth of the Moho discontinuity in this region. Teleseismic results show that Musgrave Block is bounded by south verging thrusts at the southern margin and north verging thrusts at the northern margin (Figure 5.21). The Arunta section also shows south verging thrusts. It has been postulated by Lambeck et al. (1984) that the Musgrave Block has a core of elevated Lower Crust. Interpretation of two north-south deep seismic sounding profiles shot across the Officer Basin also indicates large thrust faults. As shown in Figure 5.25, on both seismic profiles, the marked depths of magnetic interfaces detected be spectral analysis of TMI correspond to seismic reflection horizons. Such correspondence is very significant for further employment of the spectral analysis method to detect this kind of flat

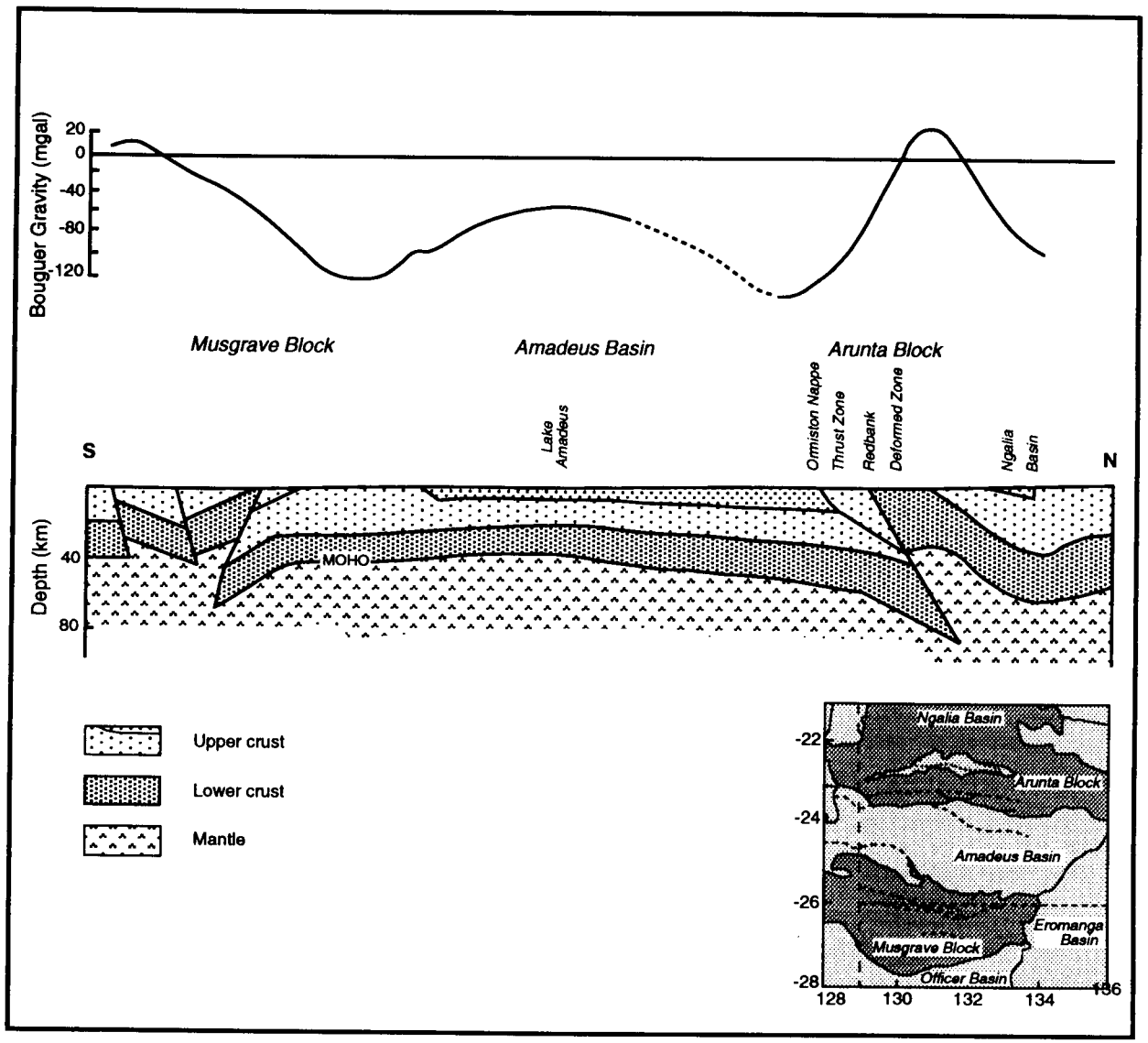

Figure 5.21 Cross-section of crustal structure across the Musgrave and Arunta Blocks and the Amadeus Basin as derived from teleseismic travel time analyses. After Lambeck et al.,1988; Lambeck and Penney, 1984; Lambeck and Burgess, 1992.

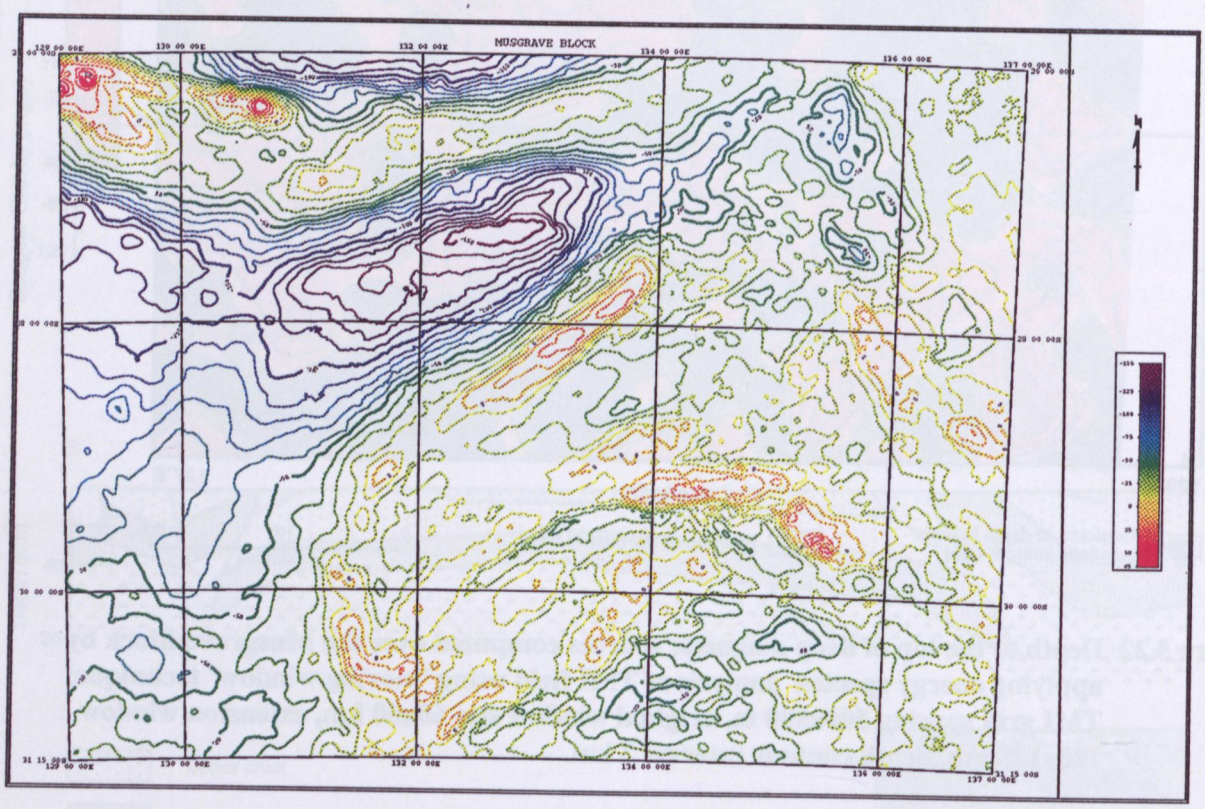

Figure 5.24 Bouguer gravity contour map of the Musgrave Block.

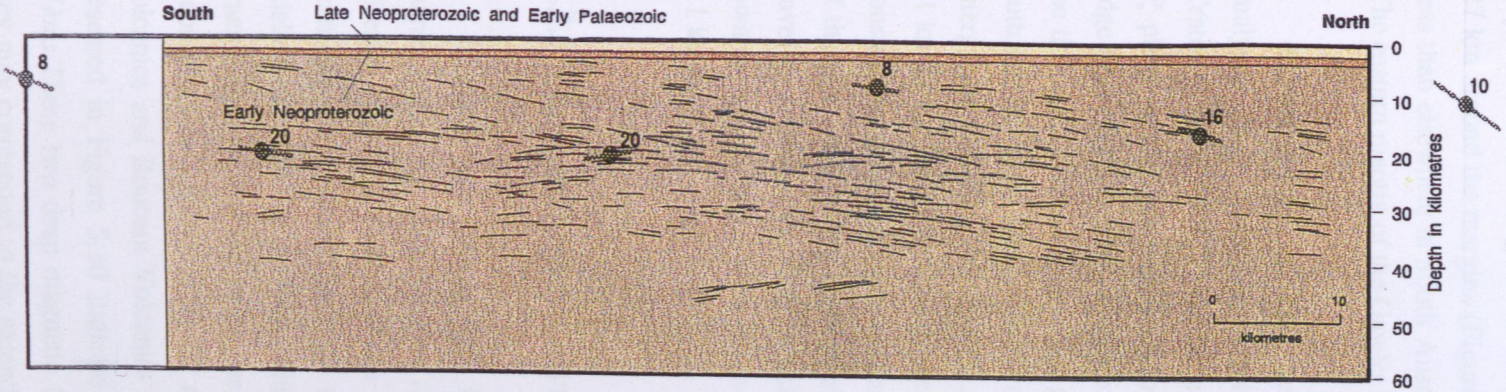

(a) Line 6 - showing mid-crustal trusts with magnetic horizons.

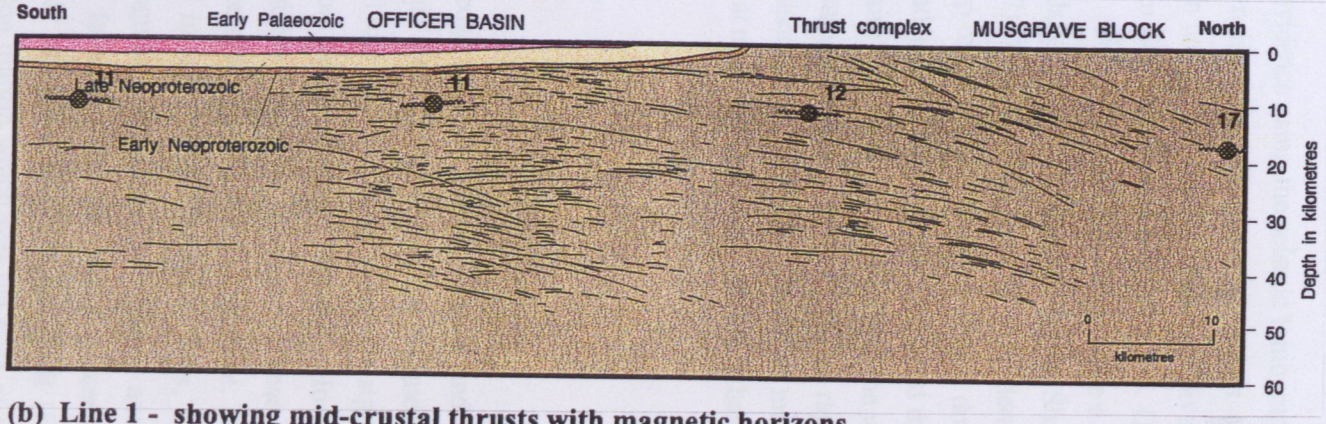

(b) Line 1 - showing mid-crustal thrusts with magnetic horizons.

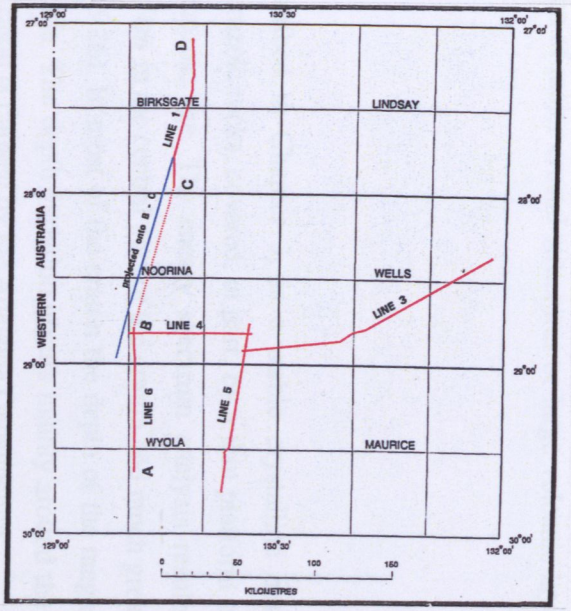

(c) Seismic lines location plan

20 Depth to the top of Deep Magnetic Sources inferred from spectral analysis of TMI

Figure 5.25 Officer Basin - Deep Seismic reflection sections with superimposed magnetic boundaries detected by energy spectra analysis of TMI.

surfaces which may be an indication of major crustal structures or large volcanic layers buried under thick sedimentary cover.

5.3.2 The Gawler Craton

The Gawler Craton, as described in Chapter 3, is a stable crystalline basement province comprising Archaean to Mesoproterozoic rocks, covered, in part, by a thin platform of sediments and regolith of Neoproterozoic to Cainozoic age. The energy spectrum analysis results show shallow depths within the range of $5km - 15km$ in the central part of the craton and much greater depths up to 27 km around the margins (Figure 5.26). In most of the craton the depth of the magnetic layer varies less than elsewhere in South Australia. The depth variation occurs mainly around the Craton margin. The eastern margin of the Gawler Craton is flanked by the Adelaide Geosyncline.

Greenhalgh et al. (1989), based on earthquake evidence using the seismic tomographic technique analysed crustal velocities over the Adelaide Geosyncline and adjacent eastern part of the Gawler Craton (Figure 5.28). They also carried out time-term analysis of local earthquake travel time for the P_n phase to map the variations in crustal thickness in South Australia (Figure 5.27). On the eastern edge of the Eyre Peninsula approximately at $33°30'S$ and $137°E$ their results indicate a low value on the time-term contour map which possibly corresponds to a relatively shallow Moho (Shackleford and Sutton, 1981) and high crustal velocity (Figure 5.27). On the DMS contour map derived from the energy spectral analysis (Figure 5.26), depth to the top of the deepest magnetic source does not exceed 11 km in the area. There are more coinciding facts and analogy between the DMS and time-term map constructed by Greenhalgh and his co-authors. As Figure 5.27 shows immediately to the west of region of the thin crust on the mid-eastern coast of Eyre Peninsula seismic studies indicate rapid change of travel-time (from 1.5 to 5.0) which may be due to thickening of the crust. The DMS map also shows towards the west a presence of the magnetic interface at much greater depth (19 km) than on the coast (11 km).

5.3.3 The Adelaide Geosyncline

The Adelaide Geosyncline is a rift on the edge of the Gawler Craton and has specific characteristic features within the crust. In the Adelaide Geosyncline region, the magnetic field has a different character than over the Gawler Craton (Figure 5.29). Strong magnetic signature of the basement rocks is subdued by thick Neoproterozoic non-magnetic sediments. However, in the Adelaidean there are rocks which produce prominent magnetic horizons. These include the Braemar/Holowilena Ironstone, the Brachina Formation and the ABC Range Quartzite. There are also a considerable number of minor magnetic horizons. In addition the volcanic rocks, the Wooltana Volcanics and Boucaut Volcanics produce strong magnetic anomalies. The spectral analysis results presented in Figure 5.30 indicate two very distinct features with the depths between $19km$ and $27kms$.These two deep magnetic features are possibly offset by the Paralana Fault (Figure 5.31). They may correspond to the extended crust at the craton margin which was the edge of the continent

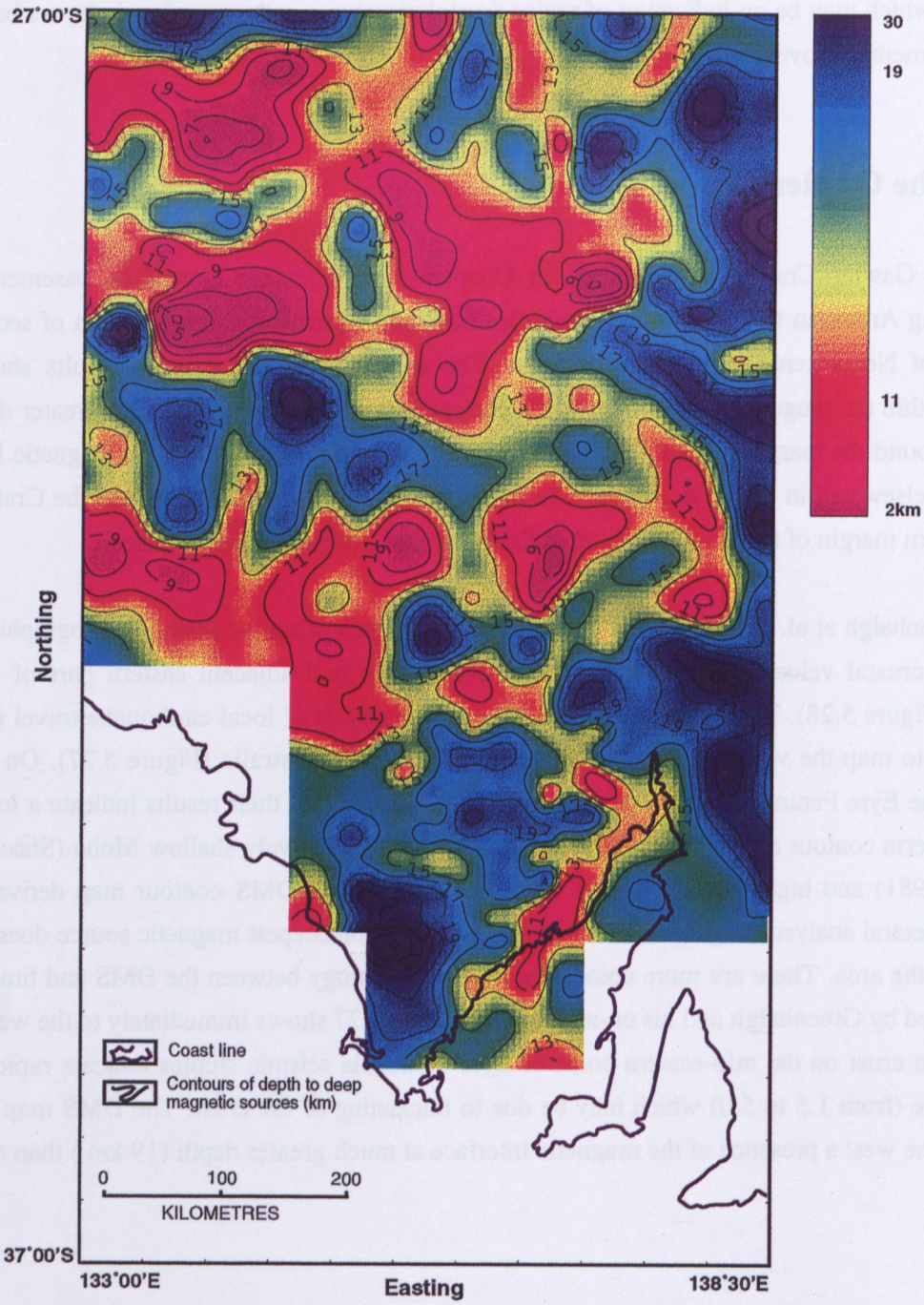

Figure 5.26 Depth to the top of deep magnetic sources obtained from the energy spectra analysis of TMI field of Gawler Craton. Logarithmic radial energy spectra computed using 'moving window' technique: original window size 60x60km, extension window 128x128km, depth contour interval 2km.

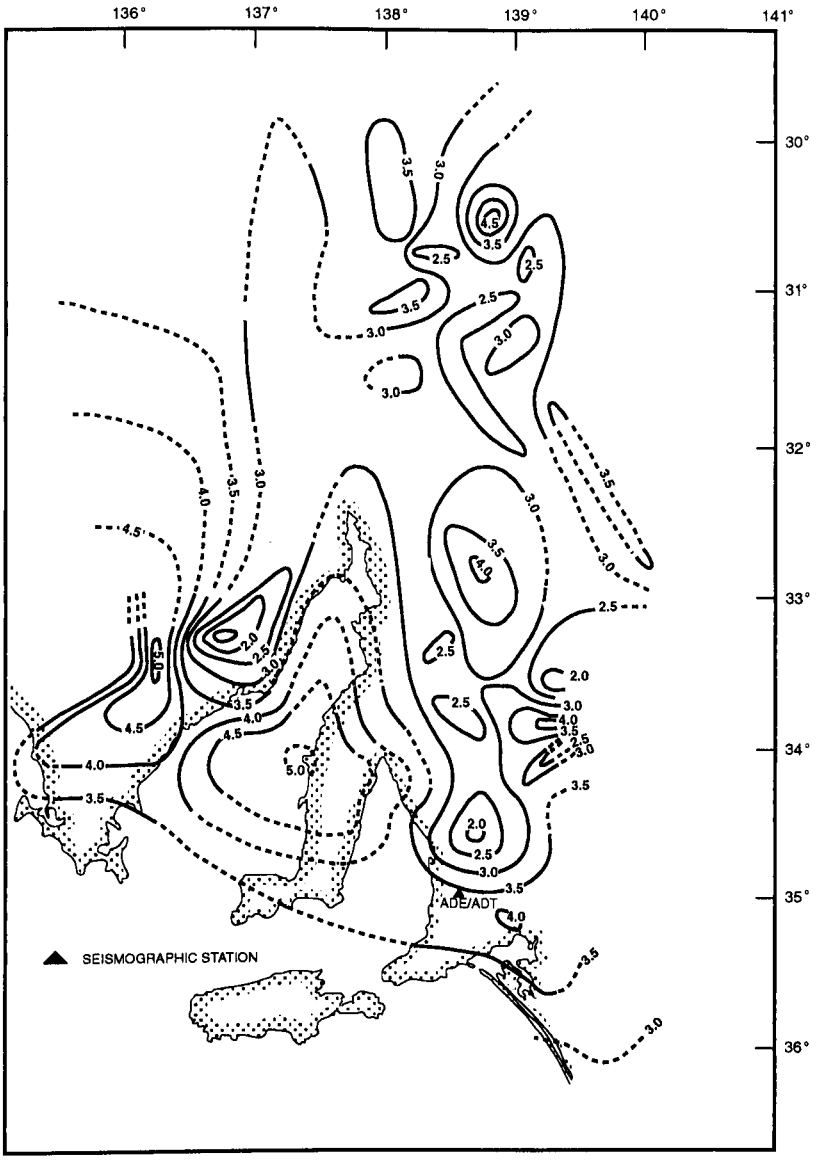

Figure 5.27 Time-term contour map of the P_n phase, deducted from analysis of South Australian earthquakes.After Greenhalgh et al.,1989.

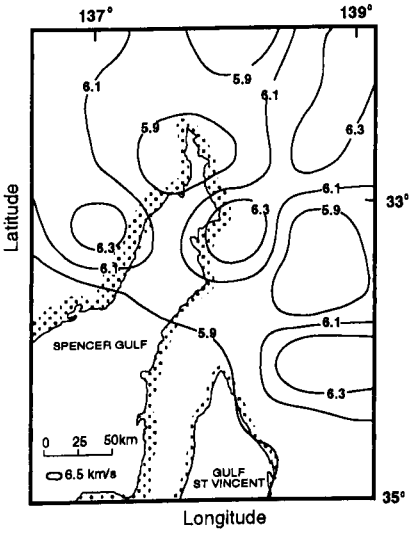

Figure 5.28 Crustal velocity tomogram obtained from earthquake data. After Greenhalgh et al.,1989.

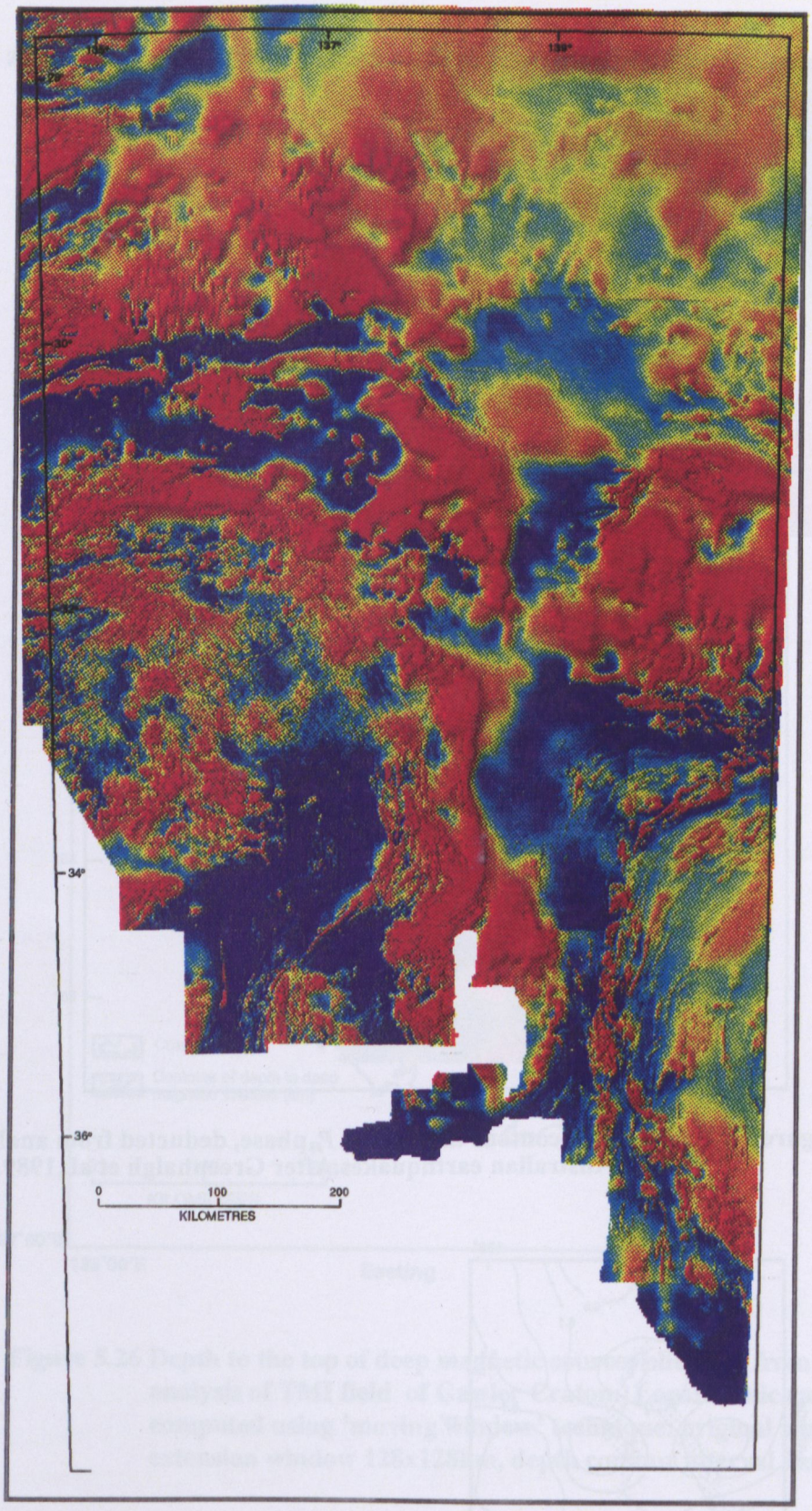

Figure 5.29 Colour image of TMI of the Adelaide Geosyncline.

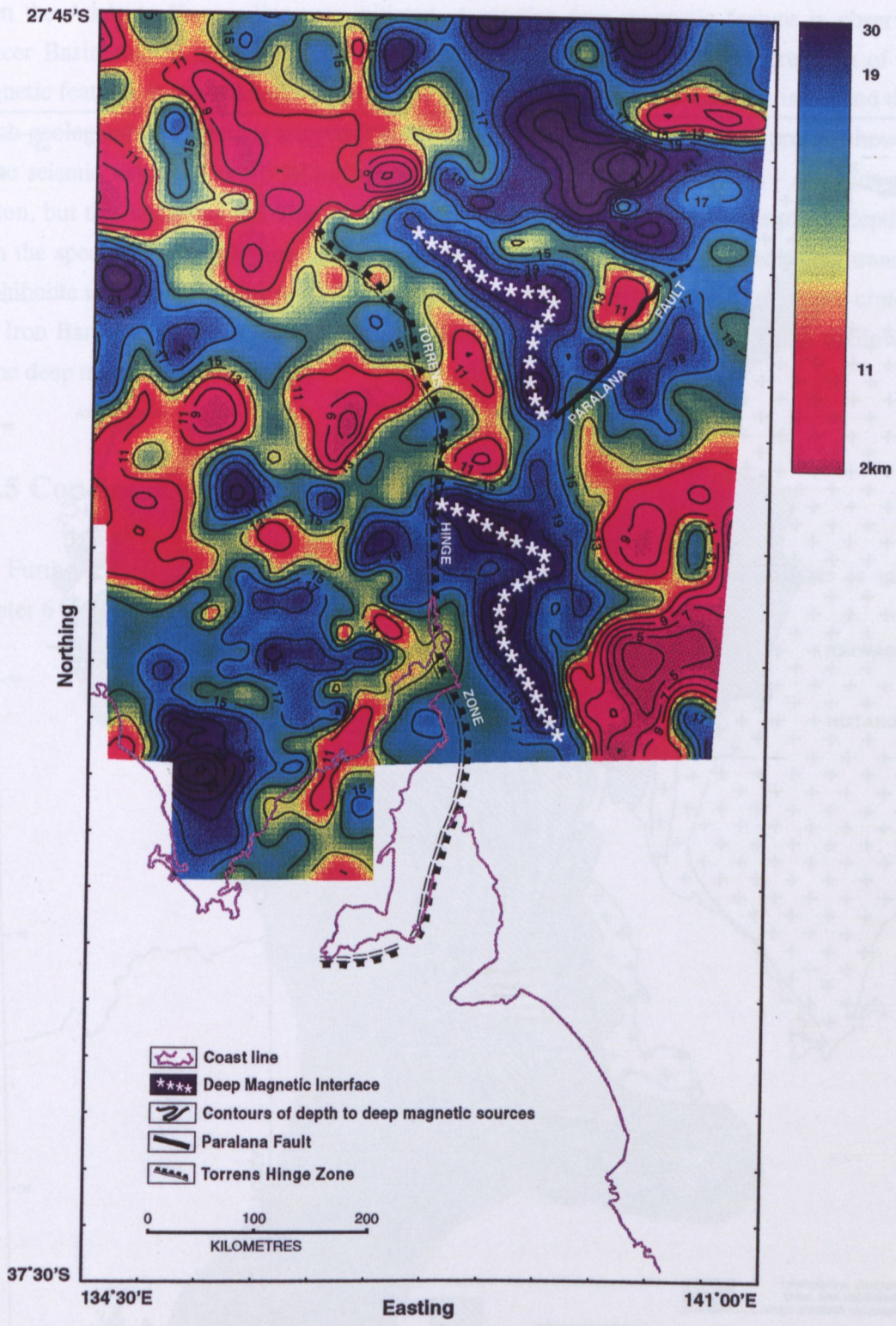

Figure 5.30 Depth to the top of deep magnetic sources obtained from the energy spectra analysis of TMI of Adelaide Geosyncline. Logarithmic radial energy spectra computed using 'moving window' technique: original window size 60x60km, extension window 128x128km, depth contour interval 2km.

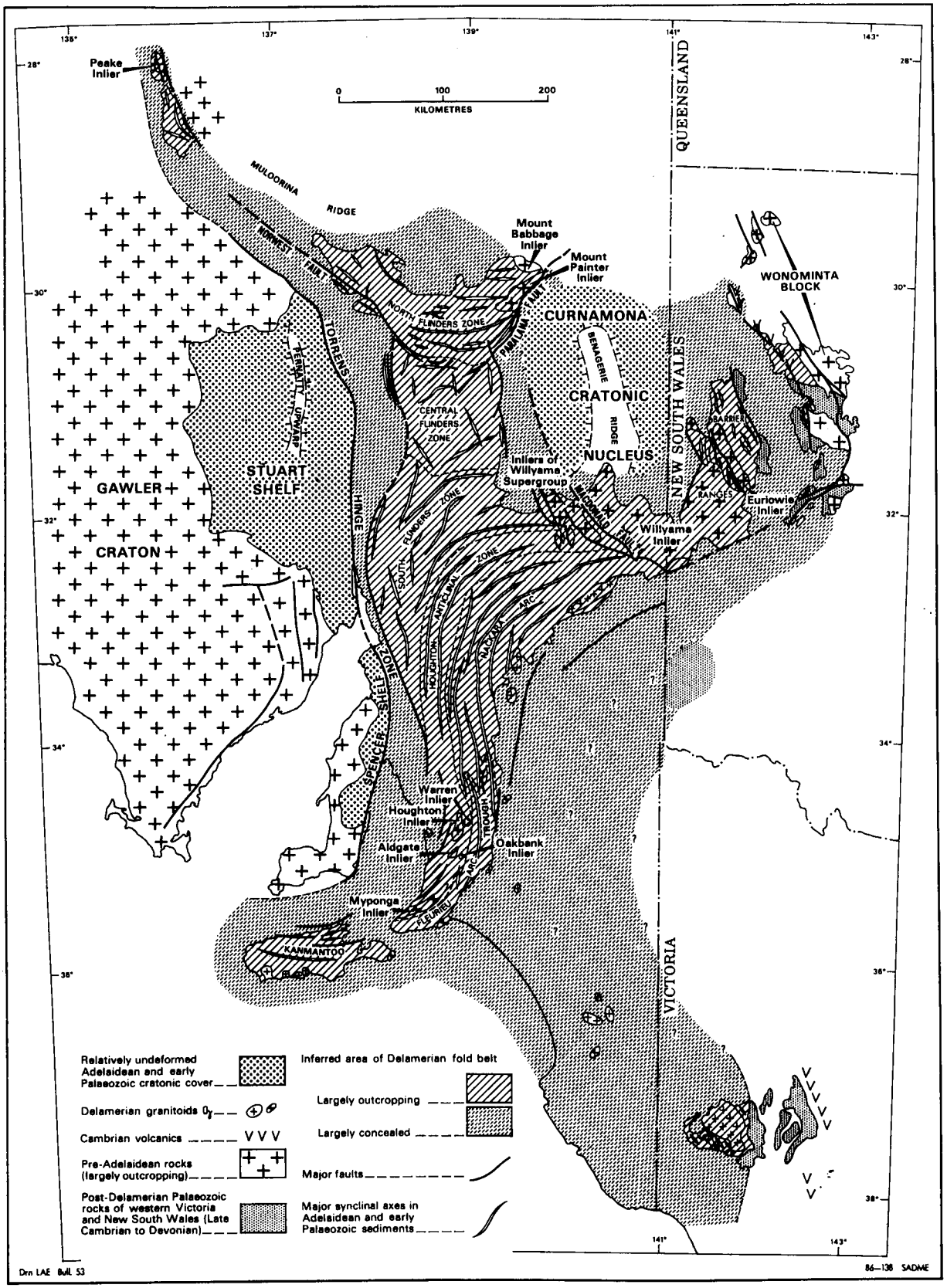

Figure 5.31 Structural elements of Cambro-Ordovician Delamerian fold belt - Adelaide Geosyncline. After Preiss et al. (1987).

when the Adelaide Geosyncline was initiated. A similar deep magnetic feature is observed on the Officer Basin side of the Gawler Craton (see Figure 5.12). Geological interpretation of these deep magnetic features in the Adelaide Geosyncline region is problematic, because it is beyond the depth at which geological observations are possible. The Iron Baron seismic refraction profile shows a change in the seismic velocity from $5.93\,km/sec$ to $6.46\,km/sec$ at a depth of $12km - 14km$ on the Gawler Craton, but this boundary is $10km$ deeper east of the craton. This corresponds to the depths obtained from the spectral studies (Figure 5.19). These deep magnetic horizons may indicate a transition from amphibolite to granulite facies or basic bodies which intruded the lower crust along the craton margin. The Iron Baron seismic profile does not extend sufficiently far east to relate to the shallower horizon on the deep magnetic sources map.

5.3.5 Concluding remarks

Further development of energy spectral analysis of TMI and crustal studies is taken up in Chapter 6 by linking it to work done in Canada, Europe and India.

Chapter 6

Interpretation of the regional magnetic field

Results of spectral analysis of the magnetic field across different geological provinces of South Australia presented in Chapter 5 show significant variation in thickness of the upper crustal layer. To obtain more information about the structure of the crust underlying the Polda rift, more detailed analysis of the regional aeromagnetic field of the south-eastern edge of the Gawler Craton, are presented and discussed in the following sections of this chapter. The interpretation is based on comparisons and analogy with deep crustal studies done on other continents, where interpretation of deep crustal structures from aeromagnetic survey data has been integrated with deep seismic sounding (DSS). The first part of this chapter reviews relevant research done in Canada, Ukraine and India, and is followed by a detailed account of the research carried on in the Polda rift. The second part of this chapter refers to the interpretation of results obtained in South Australia.

6.1 Background to crustal studies of the Polda Trough

The earth's magnetic sources are located in the crust and the outer core. The interior space between the Curie-temperature isotherm and the core-mantle interface is understood to have a non-magnetic nature except for weak magnetic fields caused by electrical currents (Shive et al., 1992).

The magnetic properties of the deep continental crust are investigated in two different ways: the satellite and the aeromagnetic data measured above the earth's surface yield information about the distribution of magnetic sources at depth; more detailed information is provided by laboratory petrological studies and measurements of magnetic properties of rocks that represent the deep crust. Both studies are well represented in the literature. However, there is dispute on the question of deep crustal magnetisation (e.g. Hall, 1974; Haggerty, 1978; Haggerty and Toft, 1985; Toft and Haggerty, 1988; Wasilewski et al., 1979; Wasilewski and Mayhew, 1982; Krutikhovskaya and Pashkevich, 1977, 1979).

The studies of the long wave-length magnetic anomalies obtained from the aeromagnetic and satellite magnetometer surveys, (wave length $\lambda \geq$ distance from the survey level to the lower crust) show that highly magnetic sources appear to exist deep in the crustal section at depths above the Curie-temperature isotherm (caused primarily by spontaneous magnetisation of titanomagnetite). The

Location	M* [A/m]	Depth extent [km]	Reference
Ukrainian and Baltic shields	>4	40-50	Krutikhovskaya and Pashkevich (1977, 1979)
British Columbia	3-5	30-40	Coles and Currie (1977)
Northwest Territories	4	16	Coles (1976)
British Columbia	5	24	Coles (1976)
Manitoba and Ontario	5	40	Hall (1974)
Northwestern Germany	2	various	Hahn et al. (1976)
Conterminous U.S.	2-6	20-55	Schnetzler (1985)
Southeaster U.S.	2	45	Ruder and Alexander (1986)
Utah	6	20-35	Shuey et al. (1973)
Kentucky	4	40	Mayhew et al. (1982, 1985b)
Fennoscandia	2	35	Elming and Törne (1976)
Sweden	3-5	10-23	Riddihough (1972)
Central African Republic	3	35	Regan and Marsh (1982)
Japanese Volcanic Arc	5	30	Segawa and Oshima (1975)
Broken Ridge	6	17	Johnson (1985)
Alpha Ridge	3	30	Taylor (1983)
Western Pacific	5	>15	LaBrecque et al. (1985)
Pacific and Atlantic basins	7	1	Raymond and LaBrecque (1987)
Lord Howe Rise	2	2	Frey (1985)
Aleutian arc	4	7	Clark et al. (1985)

*M: magnetization

Table 6.1 The magnetisation and thickness of the magnetic crust.

After Shive et al. (1992)

problem of the origin and nature of long wave-length geomagnetic anomalies has been widely discussed in the literature[1].

The relationship between long wave-length anomalies, the thickness of the crust and the depth to the Curie point isotherm surface (of magnetite) have been investigated in conjunction with deep seismic sounding surveys, and heat flow measurements and petrography of the deep crustal and the upper mantle rocks.

A major controversy concerns the attempt to estimate the basal depth of magnetic sources from magnetic anomalies; the problem is both mathematical and geological. The depth estimates and determination of the variations in the configuration of the Curie-temperature isotherms are usually attempted using either the shape of isolated magnetic anomalies (e.g., Bhattacharyya and Leu, 1977; Byerly and Stolt, 1977) or the statistical properties of the anomalies patterns (e.g., Shuey et al., 1977; Connard et al., 1983). As the majority of these studies were done in areas of elevated heat flow, such as the Cascade Range (Connard et al., 1983), the Japanese volcanic arc (Okubo et al., 1985) or the Basin and Range Province (Blakely, 1988), the depths to the Curie-temperature isotherm is relatively shallow (10-20 km). Mayhew (1985) developed a method to calculate the depth to the Curie-point isotherm using satellite data, which gives a good correlation with the estimates from aeromagnetic data in the Pacific North-west (Connard et al., 1983).

The literature review concerning the deep crustal study shows that our knowledge of the structure and composition of the lower continental crust is still very incomplete. Valuable new information could be obtained from an analysis of long wave-length anomalies. Shive et al. (1992) pointed out that '..recent compilations....emphasise a point made ...by Hall (1974); some long wave-length anomalies correlate with exposed upper crustal sources. This implies (1) that upper crustal magnetisation may be an important contributor to long wave-length anomalies and/or (2) that deep crustal structure may be reflected in surface geology. Patterns of anomalies with sources in the upper crust are often consistent over geological terrains and provinces...'.

Table 6.1 presents a brief compilation of the magnetisation and thickness of the magnetic crust from different places on the earth, inferred from long wave-length magnetic anomalies (Mayhew et al., 1985b, Shive et al., 1992). As this summary indicates, the methods and assumptions that underlay these determinations vary widely. All of these studies indicate that a relatively strong magnetisation (2-10 A/m; typically ~5 A/m) exists in the deep crust. Moreover, this strong magnetic signature extends either to the bottom of the crust or to the Curie temperature isotherm, whichever is shallower.

---

[1] **Note:** The shape and amplitude of the magnetic field anomalies measured by satellite magnetometers above the earth are dependent on the depth to causative sources. The long wave-length anomalies due to the crustal and core sources are usually distinguished by the common technique of spherical harmonic analysis. It is assumed that a crustal magnetic map could be constructed from the satellite data by subtracting a 13-degree spherical harmonic expansion derived from the same data (e.g. Cain et al., 1974; Langel and Estes, 1982; Lowes, 1966; Johnson and Mayhew, 1985), however, as Carle and Harrison (1982) showed, the long wave-length contribution from the core cannot be totally eliminated. It was suggested by Arkani-Hamed and Strangway (1985) and also independently concluded by Harrison et al. (1986), that the crustal portion of the magnetic field is limited to the high-degree harmonic expansion of order 19 and greater.

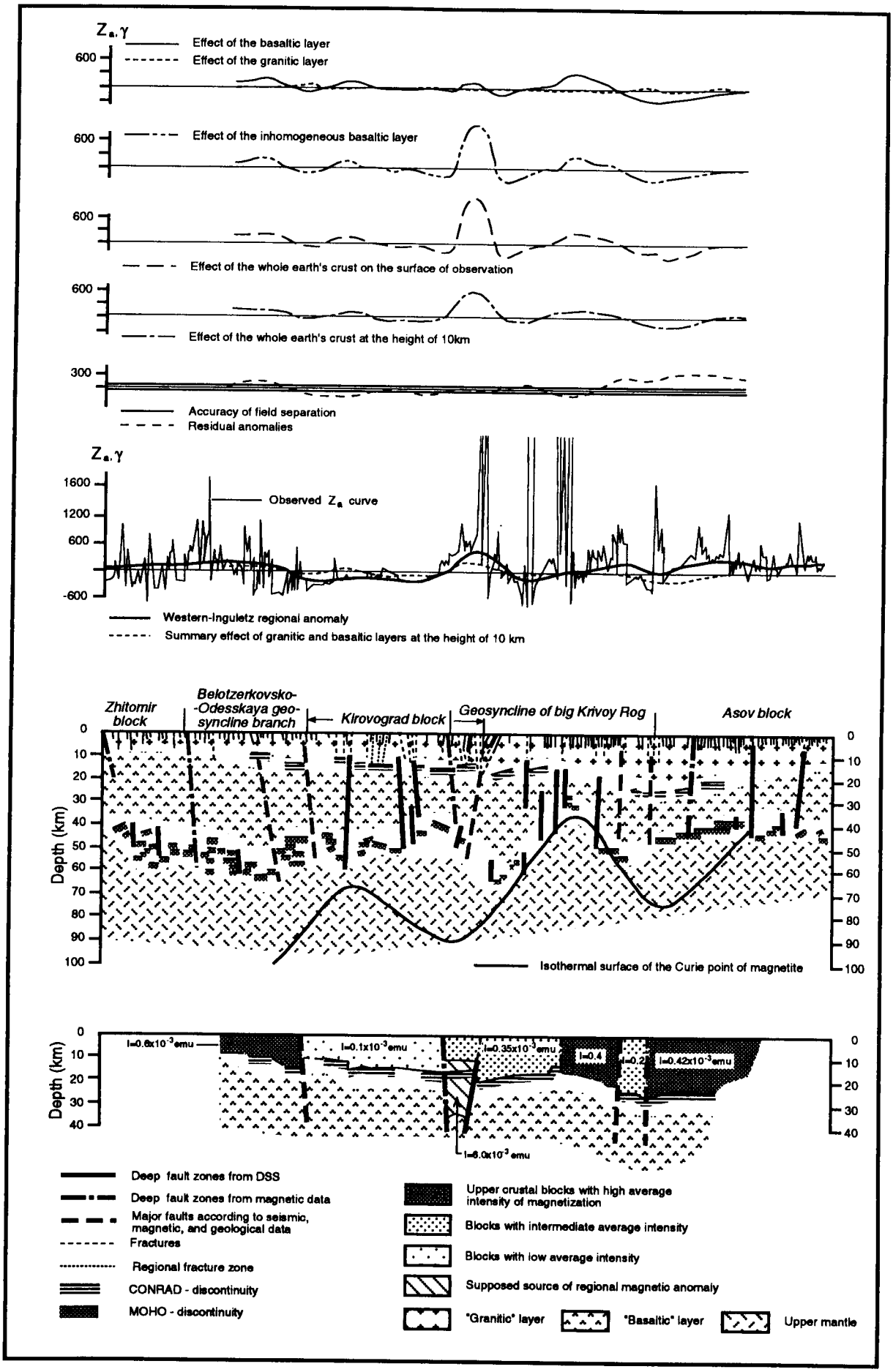

Figure 6.1 Magnetic model of the earth's crust under the Ukrainian Shield (DSS profile VIII) After Krutikhovskaya and Pashkevich (1977).

According to petrologic evidence (Shive et al., 1992) the long wave-length magnetic anomalies are probably produced by rocks that contain 5% or more magnetite by volume and are located above the *600°C* isotherm in the crust. Some authors consider the possibility that these anomalies may arise from some other strongly magnetic sources, which may play a significant role in the deep crust and the upper mantle, such as partially serpentinized ultramafic rocks containing metal (iron) alloys as the prime magnetic material with Curie temperatures in the range *620-1100°C* (Haggerty, 1978; Jordan and Frazer, 1975; Arkani-Hamed, 1988). The discrepancy between magnetisation intensities of lower crustal rocks and the source requirements for the lower crust from anomaly analyses is the most perplexing problem in studies of lower crust magnetisation.

Over the years various deep-crustal models have been proposed to explain the origin of long wave-length anomalies, these being: irregularities of the crust-mantle interface, undulations in the Curie point isotherm (Mayhew, 1985), undulations of an interface between mid- and lower-crustal layers (Hall et al., 1985) and lateral compositional changes (e.g. Krutikhovskaya and Pashkevich, 1977, 1979). Because of the inherent non-uniqueness of magnetic data and the absence of control it is difficult to decide which model might be the most favourable in any particular area.

Various models of the earth's crust have been developed based on the information obtained from independent sources. This includes seismic studies of the crustal structure (Hall, 1974; Mayhew et al., 1982, 1985a), heat-flow measurements (Shuey et al., 1973), gravity anomalies (Mayhew et al., 1982, 1985a; Shi, 1993), measurements of the magnetic properties of high-grade metamorphic terrains (e.g. Hall, 1968; Hall et al., 1979; Lidiak, 1974; Krutikhovskaya and Pashkevich, 1979; Mutton and Shaw, 1979), laboratory studies of xenoliths from the lower crust and the upper mantle (Wasilewski et al., 1979; Wasilewski and Mayhew, 1982; Haggerty and Toft, 1985; Toft and Haggerty, 1988), and detailed magnetic analysis of tectonically uplifted terrains (Fountain and Salisbury, 1981).

The problem of the basal depth of the magnetisation mentioned above, has been investigated by scientists from several countries, but the questions of the Moho being the deepest magnetisation boundary and the magnetic nature of the upper mantle still remain unsolved. Some scientists believe that the Moho discontinuity is the maximum basal boundary of magnetised crust e.g. Wasilewski, Thomas and Mayhew (1979) or Gasparini (1979). Other findings prove that the limit of lithospheric ferromagnetism can continue beneath the crust-mantle (e.g. Krutikhovskaya and Pashkevich, 1977; Toft and Haggerty, 1988). Briefly described below are examples showing discordance in the final results.

Toft and Haggerty (1988) analysed variations in magnetic, geochemical, density, and mineralogical properties (magnetic susceptibility and NRM) of a suite of granulite facies of a lower crustal xenolith from a kimberlite in the Shield of the West African Craton. The correlation of the temperature and pressure dependant crystallographic transition in magnetite and iron metal together with silicate equilibrium, oxidation states, and geothermal gradients included in a model of cratonic lower crust and upper mantle, constrains the deepest limit of the lithospheric ferromagnetism to 95 km. However, a limit of 70 km is considered by Toft and Haggerty to be the most reasonable for the West African Craton and for modelling Magsat anomalies over exposed Precambrian shields.

Zone	$F(\gamma)$	$M(km)$	$R(km)$	$LL(km)$	$t(km)$	
I	425	38	13	25	18	Kenora Block*
IIa	0	32	21	11	1	Englishn River Block*
IIb	-200	31	22	9	-2	Englishn River Block*
III	250	34	18	16	7	Red Lake Block*
IV	125	30	18	12	3	Area of uniform crustal structure
Va	200	33	18	15	6	Structure in the vicinity of the Nelson River lineament
Vb	10	34	20	14	4	Structure in the vicinity of the Nelson River lineament
Vc	60	31	15	16	8	Structure in the vicinity of the Nelson River lineament
Vd	250	34	18	16	7	Area to north and west of the Nelson River lineament
VI	150	31	-	-	-	Special area
VII	500	40	-	-	-	Special area
VIII	200	43	27	16	3	West-central Hudson Bay

* Fault blocks of the western Superior Province

F: the average values of magnetic field

M: total crustal thickness

R: thickness of the upper-crustal layer

LL: thickness of the lower-crustal layer

$t=M-1.5R$

Table 6.2 Intensity of the magnetic field and the thickness of the crust and sub-crustal layers. After Hall (1974).

According to Krutikhovskaya (1976) the Curie point isotherm of magnetite is always located below the Moho discontinuity (see Figure 6.1). Not only is the lower crust magnetic but a part of the upper mantle is as well. The reported depth to the Curie point isotherm often exceeds 50-60 km, but since the topography of the isothermal surface is mainly a repetition of the Moho topography, a question is raised as to the correlation between regional magnetic anomalies and the thickness of the crust. The data presented for the Ukrainian Shield indicate a temperature at a depth of 50 km, near the crust-mantle boundary, ranging from $416 \pm 50°C$ to $610 \pm 50°C$ for different blocks. Hence, this allows a considerable variation of depth to the Curie point isotherm of magnetite, showing the existence of magnetic inhomogeneities deep in the mantle (Krutikhovskaya and Pashkevich, 1977).

Wasilewski, Thomas and Mayhew (1979), in connection with a project concerning interpretation of global magnetic anomalies measured by the magnetometer satellite (Magsat - launched by NASA) in the earth's orbit at altitudes about $350km$, analysed mantle derived rocks and found that mantle xenoliths showed negligible levels of magnetisation. The petrographic and micro probe analyses confirmed a non-magnetic mineralogy. The geochemical deliberations combined with temperature and pressure influences on mantle xenolith magnetisation led Wasilewski et al. (1979) to the conclusion that the crust-mantle transition is a magnetic mineralogy transition, with refractory (non-magnetic) spinels in the mantle and FeTi spinels in the crust. The Moho discontinuity, which is a seismic derived boundary separating crust and mantle, is a compositional boundary. This hypothesis of Moho being a chemical discontinuity, with peridotites dominantly below the Moho and granulite metamorphic grade directly above the Moho along with minor amphibolites, pyroxenites, etc., is supported by several other authors; Meissner (1973), Ringwood (1975), Dawson (1977), Padovani and Carter (1977), McGetchin and Silver (1972), Eggler and McCallum (1974).

In the past attempts were made to establish possible connection between the long wave-length components of the regional anomalies and the structure of the earth's crust. Hall and Hajnal (1973) suggested that the thicknesses of the crustal layers are somehow related to the regional long wave-length anomalies ($\lambda > 100km$). The relationship between the long wave-length component of the magnetic field and the thickness of the crust was investigated on several Precambrian Shields. The results of such studies conducted for the Canadian (Hall, 1974), Ukrainian (Krutikhovskaya and Pashkevich, 1977), Baltic (Vogel and Lund, 1970; Krutikhovskaya, 1976), and African (Green, 1976) Shields are used to predict the topography of the Moho discontinuity and they are considered to be of great value in structural studies of the lower crust.

Hall (1974) studied long wave-length aeromagnetic anomalies, with wave lengths in the range $60km < \lambda < 4000km$, and deep crustal magnetisation in Manitoba and north-western Ontario. His analysis shows considerable correlation of long wave-length anomalies with broad features of deep crustal structures as derived from deep seismic sounding. Based on statistical analysis of the magnetic field and the thickness of the crust and sub-crustal layers (inferred from independent sources) Hall suggests that there is a considerable relationship between the intensity of the magnetic field and the crustal thicknesses. He found a linear relationship between the intensity of the magnetic field and depths to the Moho and to the boundary between the upper and the lower crustal layers (the Conrad discontinuity locally named the Riel discontinuity, Figure 6.2; Table 6.2), as well as to the thickness

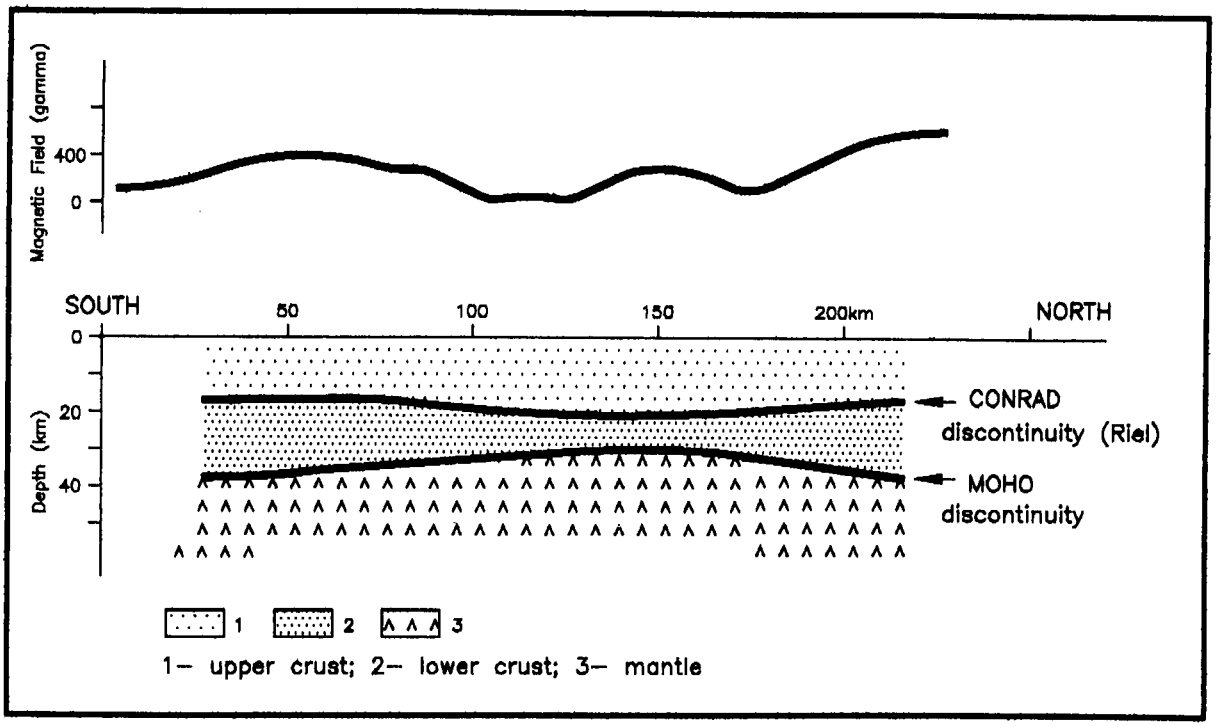

Figure 6.2 Crustal section with regional long wavelength anomaly field. After Hall (1974).

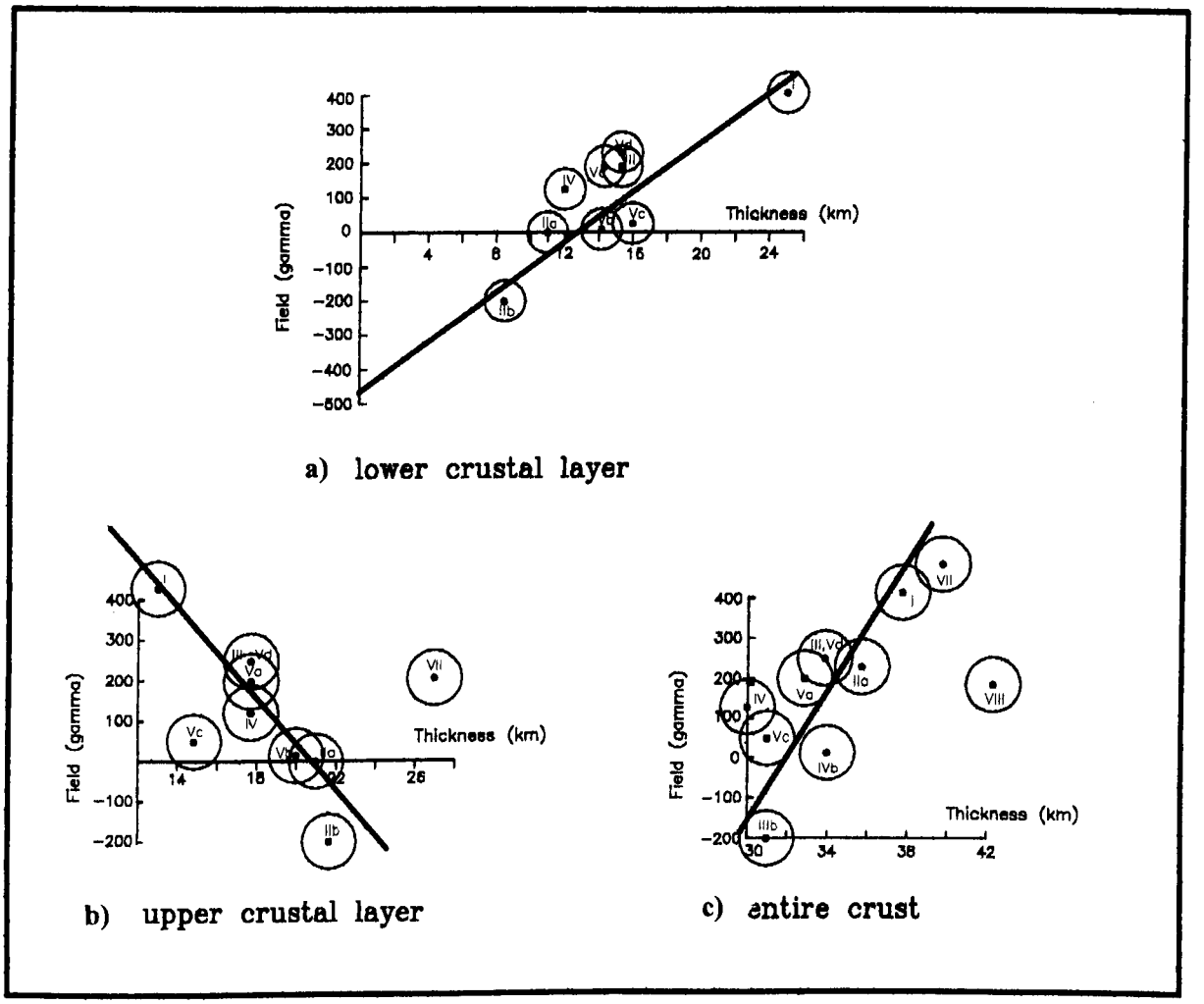

Figure 6.3 Canadian Shield. Plot of regional TMI vs crustal thickness. After Hall (1974).

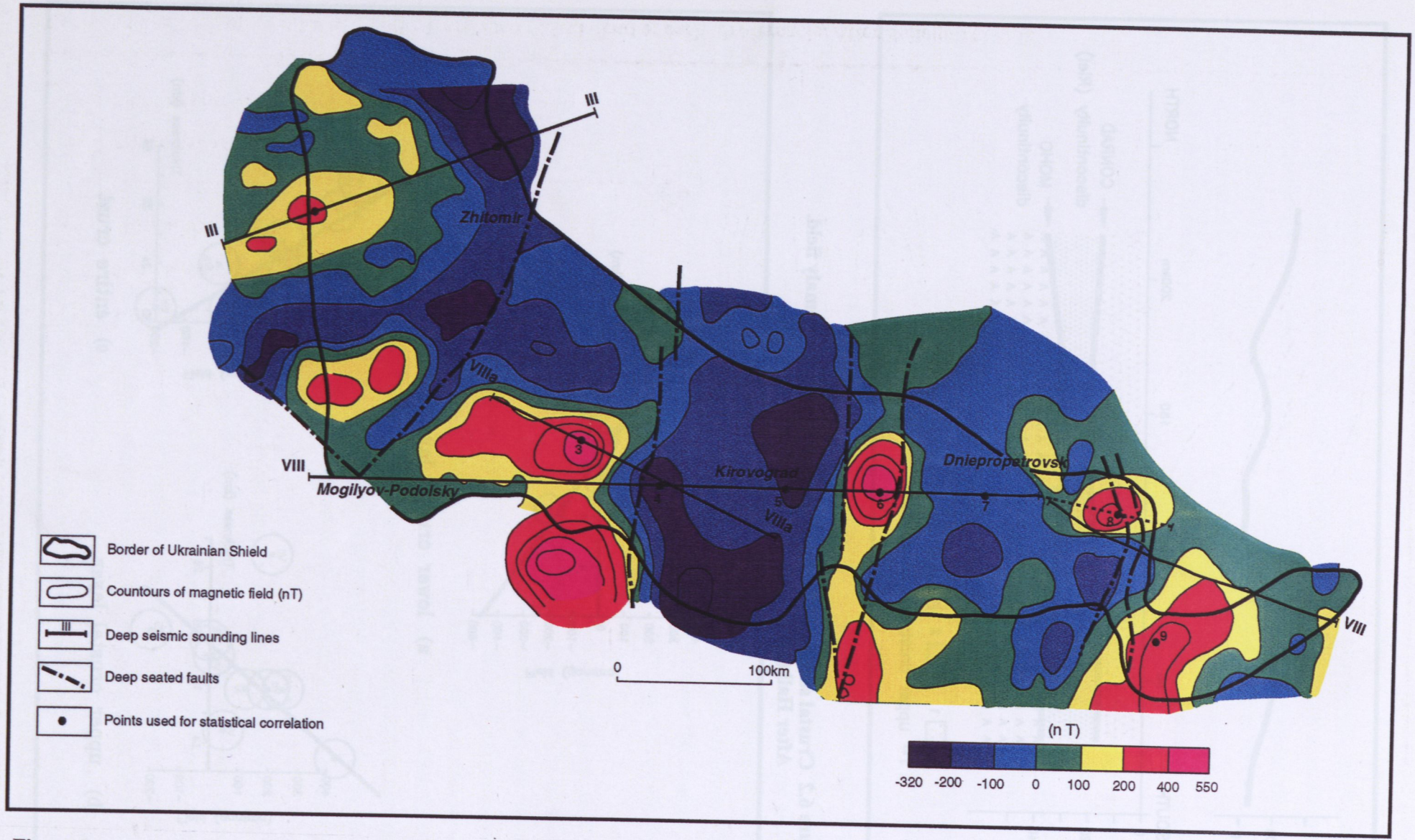

Figure 6.4(a) Regional magnetic anomalies above Ukrainian Shield. After Krutikhovskaya and Pashkevich (1979).

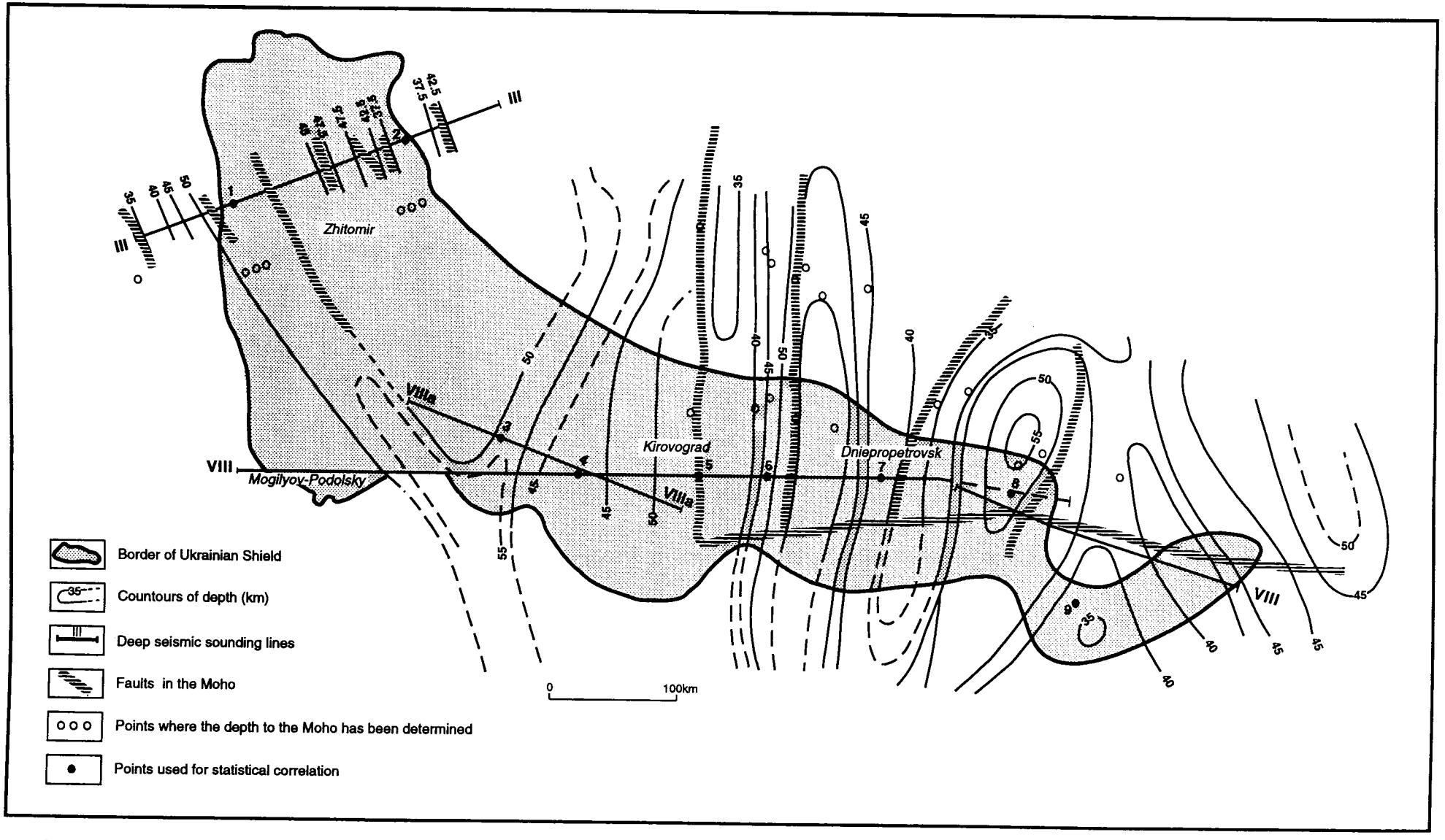

Figure 6.4(b) The Moho topography within the Ukrainian Shield - end of early Proterozoic. After Sollogub (1975).

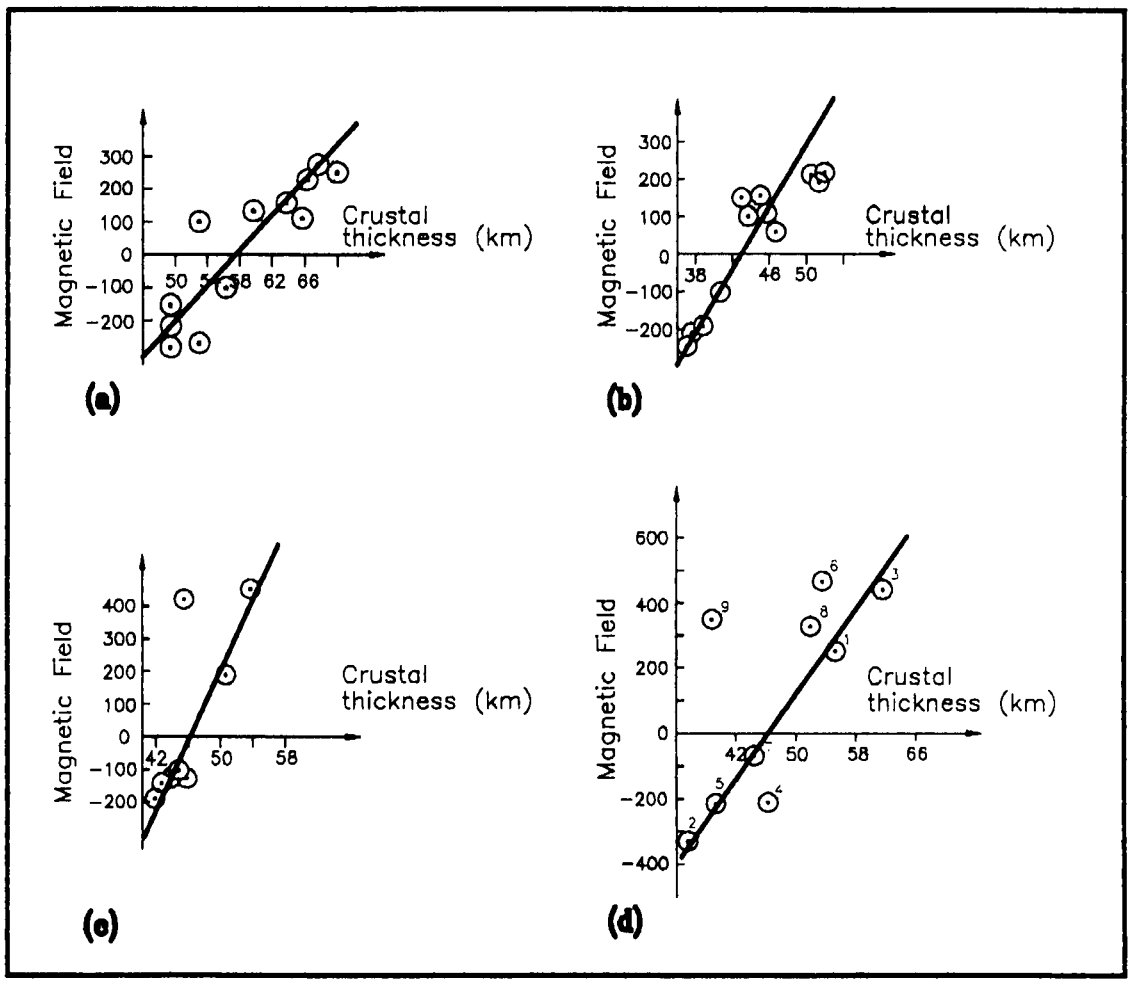

Figure 6.5 The correlation between the regional magnetic field and the crustal thickness for the Ukrainian Shield. After Krutikhovskaya and Pashkevich (1979).
(a) DDS lineVIII,
(b) SS line III,
(c) DSS line VIIIa,
(d) Whole area of Ukrainian Shield.

of the lower crustal layer. Hall's work indicates that the correlation of the regional component with thickness of:

- the upper crust is linear with negative slope (Figure 6.3(a));
- the lower crust is linear with positive slope (Figure 6.3(b));
- the crust is linear with positive slope (about $50\eta T/km$; Figure 6.3(c)).

Hall's studies also showed lateral inhomogeneity of the lower crust layer, with an intensity of magnetisation of $5.3 \times 10^{-3} emu/cc$, causing magnetic anomalies and a strong relationship to major features in surface geology. He examined two extreme models of deep crustal magnetisation: uniformly magnetised crustal layers, and lateral inhomogeneities.

Krutikhovskaya and Pashkevich (1977, 1979) worked on the same problem on the Ukrainian and Baltic Shields, and constructed magnetic model of the earth's crust. The Ukrainian Shield was chosen for the investigations as it is a most favourable geologic region. They separated the high-frequency component from the magnetic field related to the deep crust by upward continuation of the magnetic field (*2km x 2km* grid; subtracted values of $\pm 1000\ \eta T$ from the observed field) to a certain height. A height of 10 km was chosen as an optimum level for the field separation as the well known anomaly related to the iron-ore formations of the Krivoy Rog synclinorium has been totally suppressed at this height. The autocorrelation functions were computed for 0, 2, 6 and 10 km and show the presence of a long wave-length component in the anomalous magnetic field. Six positive regional anomalies with maxima up to $550\ \eta T$ and with wave-lengths from 60 to 300 km were found above the Ukrainian Shield (the attenuation rate with height was much smaller than the local anomalies). These anomalies were assumed to be produced by magnetised bodies at grater depths. The negative part of the field reaches $-340\ \eta T$ at certain locations.

Krutikhovskaya and Pashkevich (1977, 1979) reported that deep seismic sounding data and heat flow investigations were used to study the relationship between these long-wave-length anomalies and both the crustal thickness and the topography of the Curie isotherm of magnetite. The results show that, in the areas of the regional highs, the crust is characterised by a higher magnetisation of the basement rocks, a greater thickness (Moho subsidence) and the presence of strong seismic reflectors within the mantle (Figure 6.3). The uplifted parts of the Moho surface are located in low fields. As all the areas of a significant increase of crustal thickness are confined to zones of deep-seated faults, Krutikhovskaya and Pashkevich suggest that the magnetic highs are caused by highly magnetised rocks of basic and ultrabasic composition intruding into the fault zones (the areas of the most active interaction between the crust and mantle). But, on the other hand, the correlation of the magnetic anomalies with crustal thickness was also found for areas with uplifted Moho discontinuity. There are minor magnetic anomalies as the upper crust is relatively weakly magnetic.

The statistical correlation between the regional anomalies (the extremum value of magnetic field; Figure 6.4(a)) and the crustal thickness as derived from deep seismic sounding (Figure 6.4(b)) for the Ukrainian Shield (Krutikhovskaya and Pashkevich, 1977) is shown in Figure 6.5. The results are similar to those obtained by Hall (1974) for the Canada Shield (Figure 6.2).

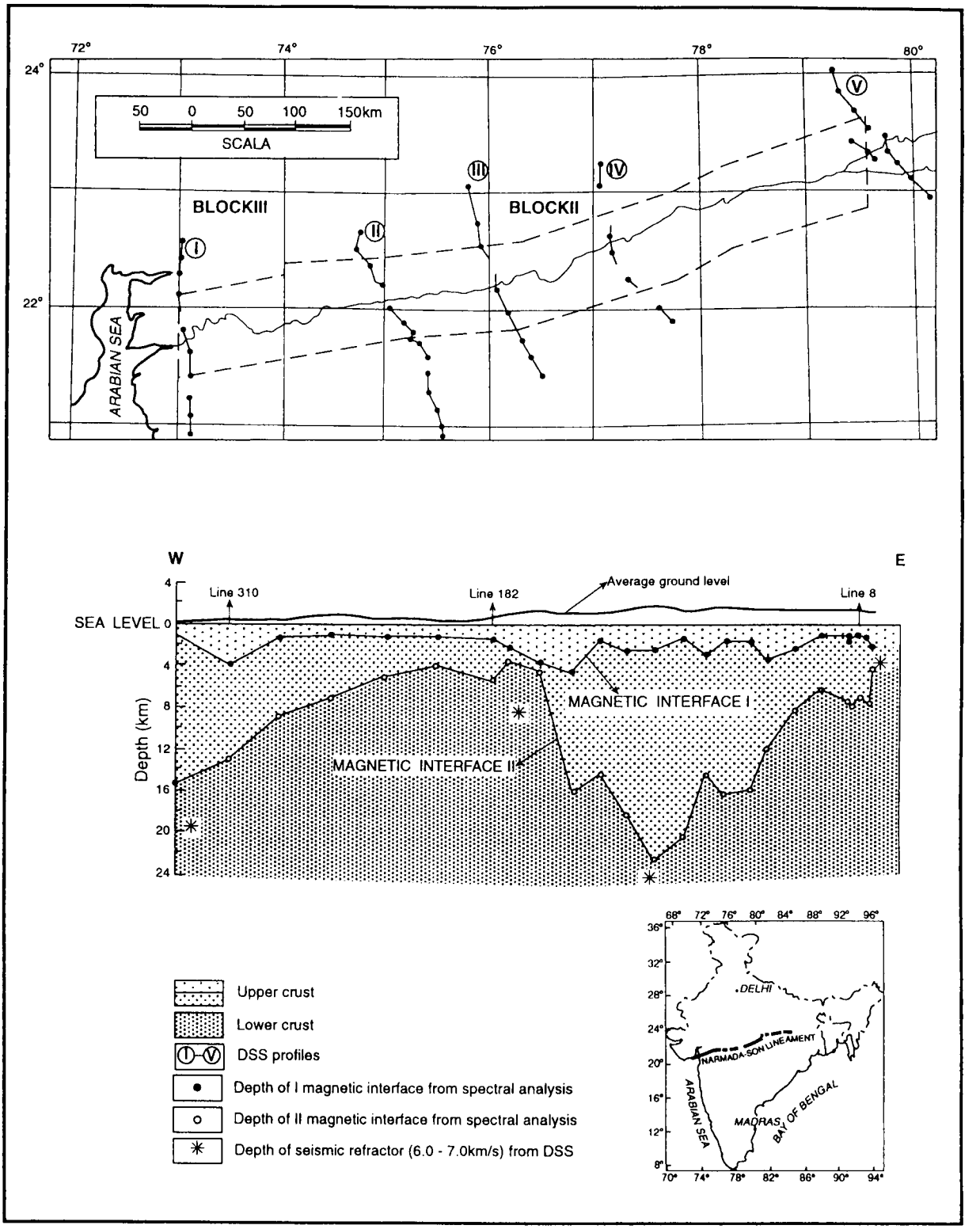

Figure 6.6 Normada-Son Lineament. Crustal cross section showing deep structure inferred from the spectra analysis of TMI and interpretation of DSS. After Rao et al (1992).

Based on the observed correlation between crustal thickness and regional magnetic field, Krutikhovskaya and Pashkevich (1977) constructed a model for the lower crust magnetisation effect with the lower boundary of the magnetised layer coinciding with the Moho surface. The lower crust is found to be inhomogeneous and 5-10 times more magnetic than the upper crust. Assuming (support from seismic velocity data) that if the upper part of the lower crust includes highly compact metamorphic acid rocks then the average magnetisation of strata below the Conrad discontinuity would not exceed 1.4×10^{-3} emu. Krutikhovskaya and Pashkevich suggest that the crust can only be composed entirely of basic rocks below 20-25 km.

In India a deep crustal study across the Narmada-Son Lineament based on spectral analysis of aeromagnetic data, and the interpretation of deep-seismic sounding (DSS) profiles show two distinct crustal layers (Atchuta Rao et al., 1992). Figure 6.6 shows the depths of seismic refractors indicating the upper-lower crust boundary which has been derived from the velocity of 6.0 km/sec of the upper crust and 7.0 km/sec of the lower crust. As Atchuta Rao et al. (1992) report spectral analysis of the aeromagnetic field along the north-south profiles indicate the presence of two prominent magnetic interfaces within the crust underlying the Narmada-Son Lineament:

- the upper interface with an average depth of 2 km (depths also supported by DSS) attributed to the magnetic basement (Interface I in Figure 6.6);
- the lower interface corresponding to the seismic velocity changes, which indicates significant change of the magnetic properties within the crust in the depth range from 4 km to 25 km (Interface II in Figure 6.6).

Atchuta Rao et al. (1992) observed that the east-west gravity profile along the Narmada-Son Lineament shows a significant drop in the regional gravity anomaly of about 40 mgals towards the eastern half. They interpreted this broad gravity 'low', together with inference drawn from aeromagnetic interpretation, to be due to thickening of the upper crust in the eastern part as compared to the western part. Apparently, this section of thicker upper crust corresponds to the Gondwana Graben which cross-cuts the Narmada-Son Lineament in a north-south direction.

The plot of the thickness of the upper weakly magnetic crustal layer (as derived from DSS) versus the intensity of the regional magnetic field, along the east-west profile along the Narmada-Son Lineament shows a similar trend to that obtained by Hall (1974) for the upper crustal layer under the Canadian Shield.

• Conclusion from literature study

The compilation of the known relationship between regional field and crustal thickness for several Precambrian Shields show linear trends with positive slopes, e.g. the low values of the regional long wave-length anomalies are indicating thinner crust whereas regional highs are indicators of the thicker magnetic crust. These correlations present a generalised characteristic of magnetisation for the earth's crust, pointing to a similarity of average magnetisation values for the crust under ancient shields, and are important for the interpretation of the spectral analysis of TMI in South Australia.

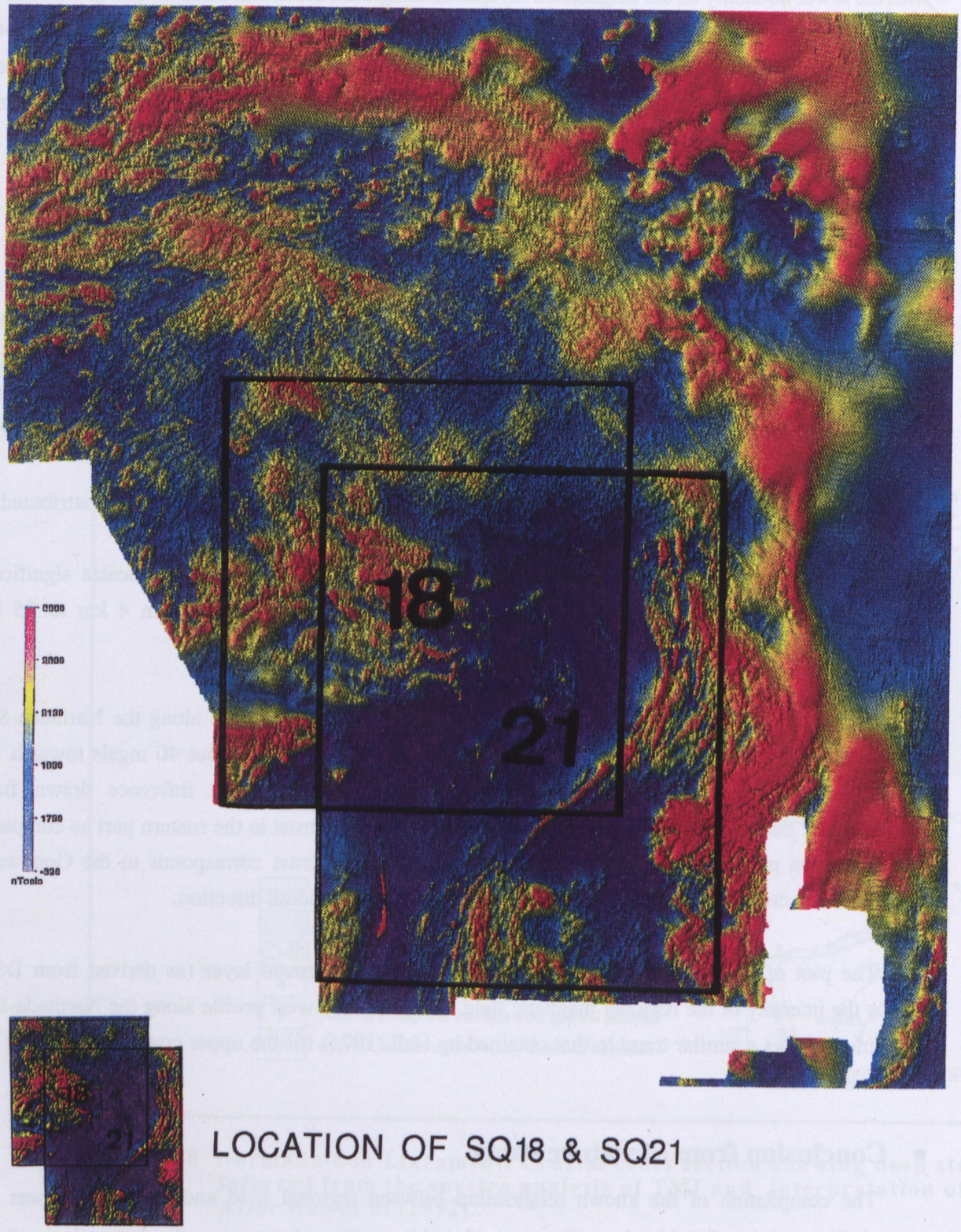

Figure 6.7 TMI image of southeastern Gawler Craton with location of SQ18 and SQ21.

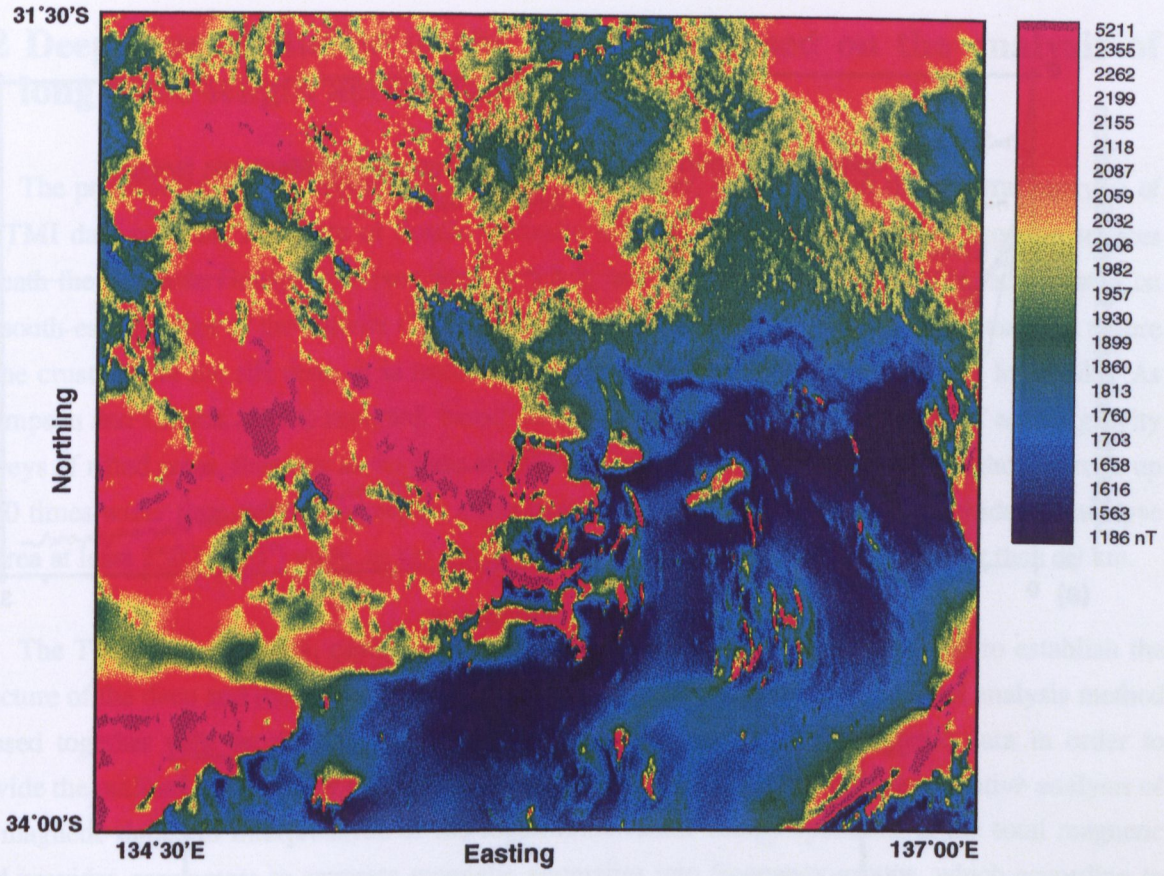

Figure 6.8 Total magnetic intensity image map of SQ18.

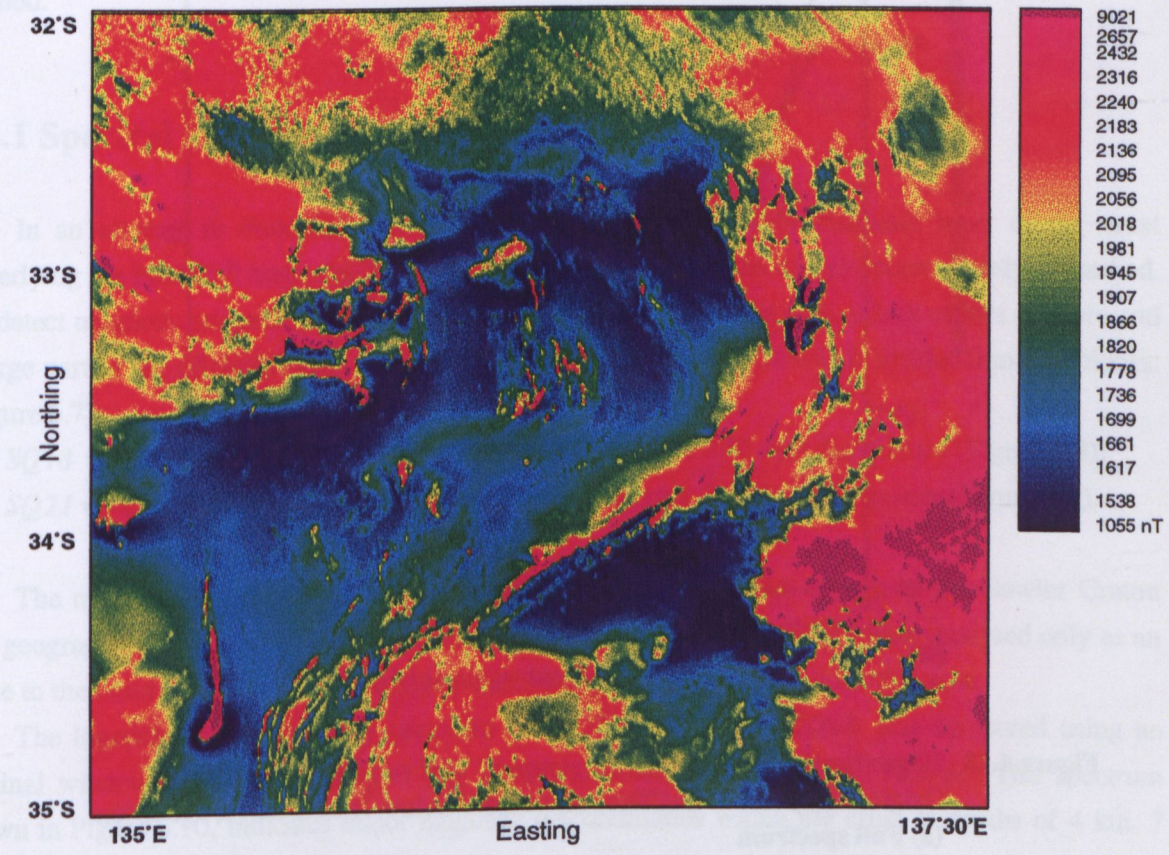

Figure 6.9 Total magnetic intensity field of SQ21.

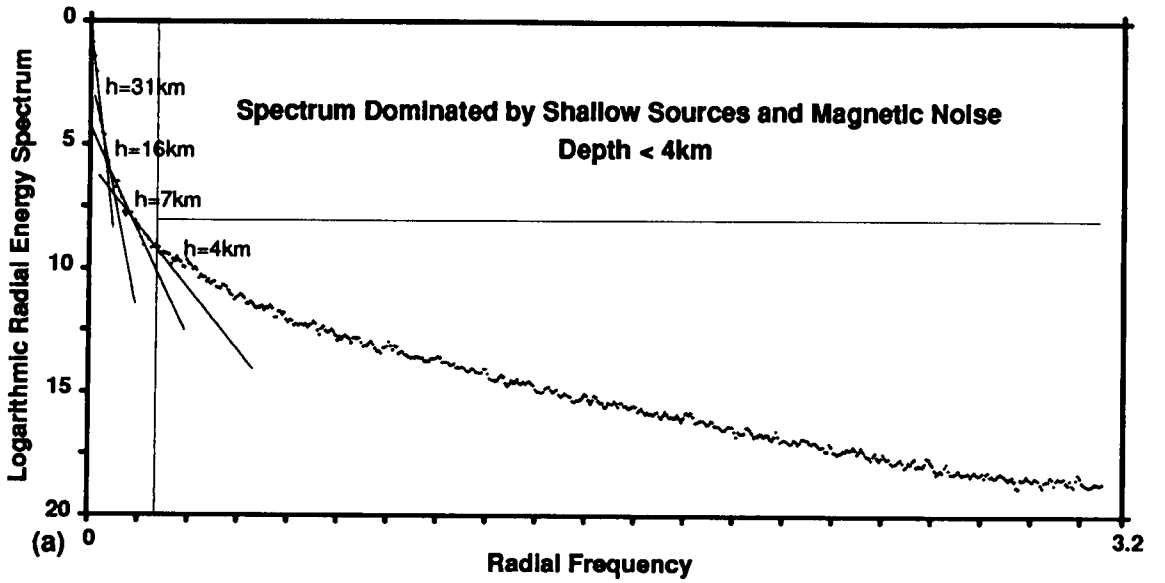

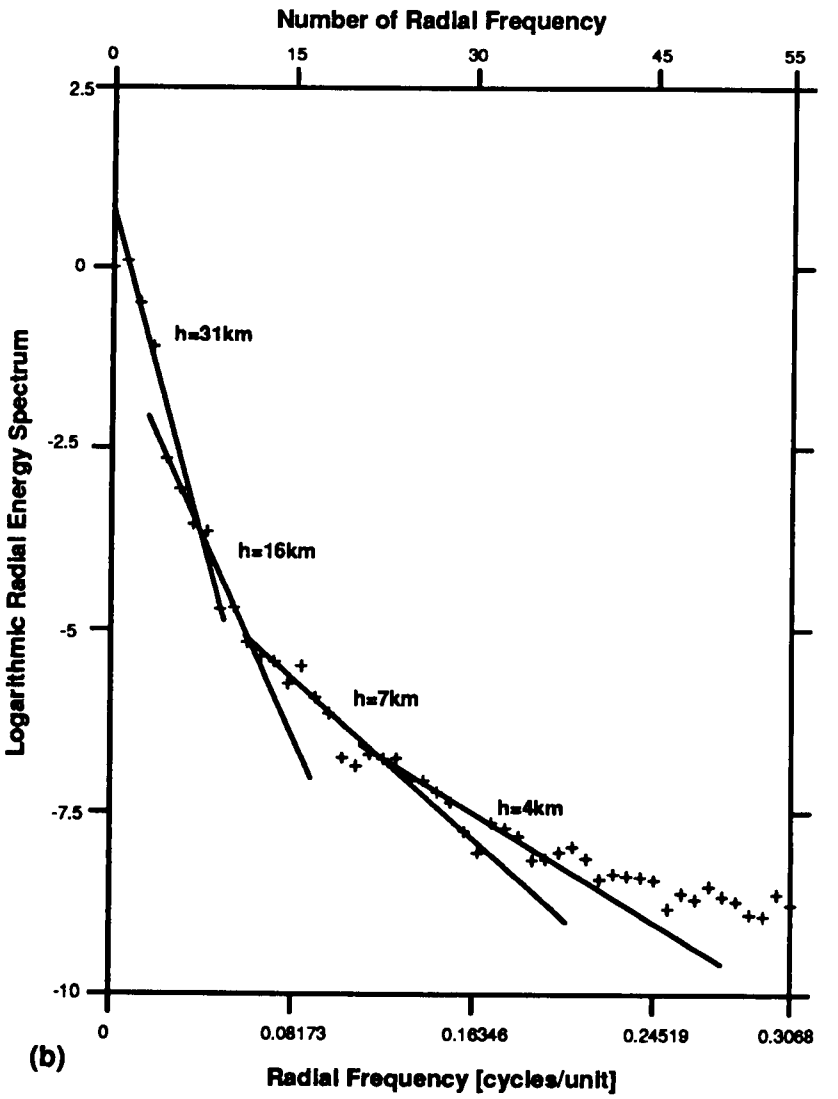

Figure 6.10 Logarithmic radial energy spectrum of TMI computed over SQ18.
Original map size 590x590gc, extension window 1024x1024gc, 1gc=500m.
(a) Full spectrum
(b) Low frequency part of the spectrum.

6.2 Deep crustal studies of the Polda rift based on the analysis of long wave-length aeromagnetic anomalies

The preliminary results, reported in the previous chapter, obtained from the spectral analysis of the TMI data covering the State of South Australia indicate the presence of deep magnetic sources beneath the Adelaide Geosyncline (see Section 5.2.2) and a very deep magnetic interface located on the south-eastern edge of the Gawler Craton, where the Polda rift is located. To understand the nature of the crust within the rift zone, it is necessary to establish what the non-rifted crust looks like. As Thompson and Gibson (1994) reported, based on teleseismic studies and the results of earlier gravity surveys of rifted areas, thinning at the base of the continental lithosphere occurs throughout a zone up to 10 times wider than the physiographic expression of the rift. Therefore, it was decided to analyse an area at least 250 km (3°) wide, as the maximum width of the Polda rift is not greater than 40 km.

The TMI state grid data, covering a large part of Eyre Peninsula, are analysed to establish the structure of the deep and the middle crust in the vicinity of the Polda rift. The spectral analysis method is used together with an anomaly separation technique to interpret aeromagnetic data in order to provide the outlines of the major deep crustal structures and also to carry on a quantitative analysis of the magnetic data. An interpretation of the logarithmic radial energy spectrum of the total magnetic field provides parameters to separate magnetic anomalies into frequency-groups, which according to the characteristic of the spectrum may be associated with different levels of the crust ('depth slice maps'). In order to delineate the shape of the magnetic sources and detect major faults or crustal lineaments the 'depth slice maps' are analysed using the vertical gradient and horizontal gradient method.

6.2.1 Spectral analysis of block-data

In an attempt to determine the thickness of the upper weakly magnetic layer of the crust underlying the Polda rift zone, the TMI field was analysed, using the energy spectral analysis method. To detect magnetic anomalies arising from the lower crust, the study area, which covers onshore and a large part of the offshore Polda rift with the surrounding Gawler Craton, is divided into two blocks: (Figure 6.7):

- *SQ18* which covers an area $250km \times 270km$ and contains *270,000* data values (Figure 6.8);
- *SQ21* which covers an area $300km \times 275km$ and contains *330,000* data points (Figure 6.9).

The main study area was *SQ18* located along the south-eastern margin of the Gawler Craton and geographically known as Eyre Peninsula. The magnetic data over *SQ21* were analysed only as an aside to the main study area and results are therefore only briefly reported for this area.

The logarithmic radial energy spectrum of the TMI data from *SQ18* was computed using an original window of $540gc \times 500gc$, and an extrapolated array $1024gc \times 1024gc$. The spectrum shown in Figure 6.10, indicates major magnetic discontinuities within the crust at depths of 4 km, 7 km, 16 km and 31 km.

6.2.2 'Depth slice' maps

Based on the characteristics of the energy spectral distributions, four frequency cut-offs: 0.03418, 0.01953, 0.01074 and 0.00781 cycles per sample interval, have been used to separate the long wave-length component from the total magnetic intensity field. These parameters (wave-length λ) have been applied to designe a low-pass filters to separate the anomalies caused by superimposed sources from different depths. The problem of anomaly separation and 'contamination' of the lower frequency zone by shallow but horizontally extended bodies is discussed in Appendix A. The 'depth slice' maps are constructed using the anomaly separation filtering technique described by Hou (1981) and Shi (1993). For each frequency cut-off, two different low-pass filters have been designed and tested for the separation of long wave length anomalies from the high frequency component and surface-noise. The parameters which have been used to compute the long wave-length magnetic field representing groups of anomalies arising from slices of the magnetic crust underlying the south-eastern Gawler Craton are described below. The parameters relate to those of Shi (1993).

- '$\lambda > 15km$'
  The low-pass filtered magnetic field with wave-length greater than 15 km is assigned to represent the magnetic signature of causative bodies seated deeper than 4 km within the crust; the frequency cut-off 0.03418 cycles/unit equals the wave length $\lambda = 15km$, (35 spectrum points); low-pass filter parameters: $\beta = 1600$, N=77, bell-shape with radial horizontal cross-section, FN=1 (Figure 6.14);

- '$\lambda > 25km$'
  The low-pass filtered magnetic field with wave-length greater than 25 km is assigned to represent the magnetic signature of causative bodies seated deeper than 7 km within the crust; the frequency cut-off 0.01953 cycles/unit equals the wave length $\lambda = 25.6km$, (21 spectrum points); low-pass filter parameters: $\beta = 1600$, N=45, bell-shape with radial horizontal cross-section, FN=1 (Figure 6.15);

- '$\lambda > 46km$'
  The low-pass filtered magnetic field with wave-length greater than 46 km is assigned to represent the magnetic signature of causative bodies seated deeper than 16 km within the crust; the frequency cut-off 0.01074 cycles/unit equals the wave length $\lambda = 46.5km$, (12 spectrum points); low-pass filter parameters: $\beta = 1600$, N=24, combination of a bell-shape filter with 'nearly' rectangular (Figure 6.16);

- '$\lambda > 64km$'
  The low-pass filtered magnetic field with wave-length greater than 64 km is assigned to represent the magnetic signature of causative bodies seated deeper than 31 km within the crust; the frequency cut-off 0.00781 cycles/unit equals the wave length $\lambda = 64km$, (9 spectrum points); low-pass filter parameters: $\beta = 1600$, N=17, the combination of a bell-shape filter with 'nearly' rectangular (Figure 6.17);

The 'depth slice' maps were also constructed for *SQ21* based on the characteristics of the energy spectral distribution.

6.2.3 Residual maps

The low frequency TMI data were subtracted from the original TMI field and subsequently the short wave-length magnetic field referred to as the residual field has been computed for each 'depth slice'. The residual fields generated by causative bodies present within the four upper crustal layers, defined above, are presented in Figures 6.18 - 6.21.

The 'dépths slice' maps and residual field maps indicate magnetic inhomogeneities within the upper crust (4 km and 7 km), the middle crust (16 km depth perhaps reflecting the Conrad discontinuity) and the lower crust or possibly even the upper mantle (magnetic signal arising from a depth greater than 31 km).

6.2.4 Application of the horizontal gradient method

The horizontal gradient method has been applied in the past to potential fields to delineate the boundaries reflecting changes in rock properties, lithological boundaries or rock magnetisation. Cordell (1979) used this technique to determine the position of suspected graben-bounding faults based on the maxima of gravity gradients associated with low-density graben fill. Dole and Jordan (1978) extended the horizontal gradient technique to magnetic data applying it directly to aeromagnetic data. Hou and Shi (1982) and also Cordell and Grauch (1985) applied this analysis to magnetic data, making use of the pseudo-gravity anomaly (Baranov, 1957). Shi (1993) applied the horizontal gradient method in conjunction with filtering techniques to gravity field anomalies to outline the shape of deep seated causative bodies using artificial models simulating a real geological situation.

By combining the results of depth estimations from spectral analysis and the information from the vertical gradient and four directional horizontal gradients of the long wavelength anomalies, Shi (1993) analysed the crustal structures of a region covering Eyre Peninsula in South Australia.

In this thesis the horizontal gradient method has been applied together with the filtering technique to analyse the aeromagnetic data in order to delineate shapes of the magnetic sources, trends of major structures and magnetic boundaries within the crust underlying the Polda rift (*SQ18*). To obtain information at different depth levels of the crust, the technique has been applied to each of the 'depth slice' maps e.g. the low-pass filtered magnetic data sets.

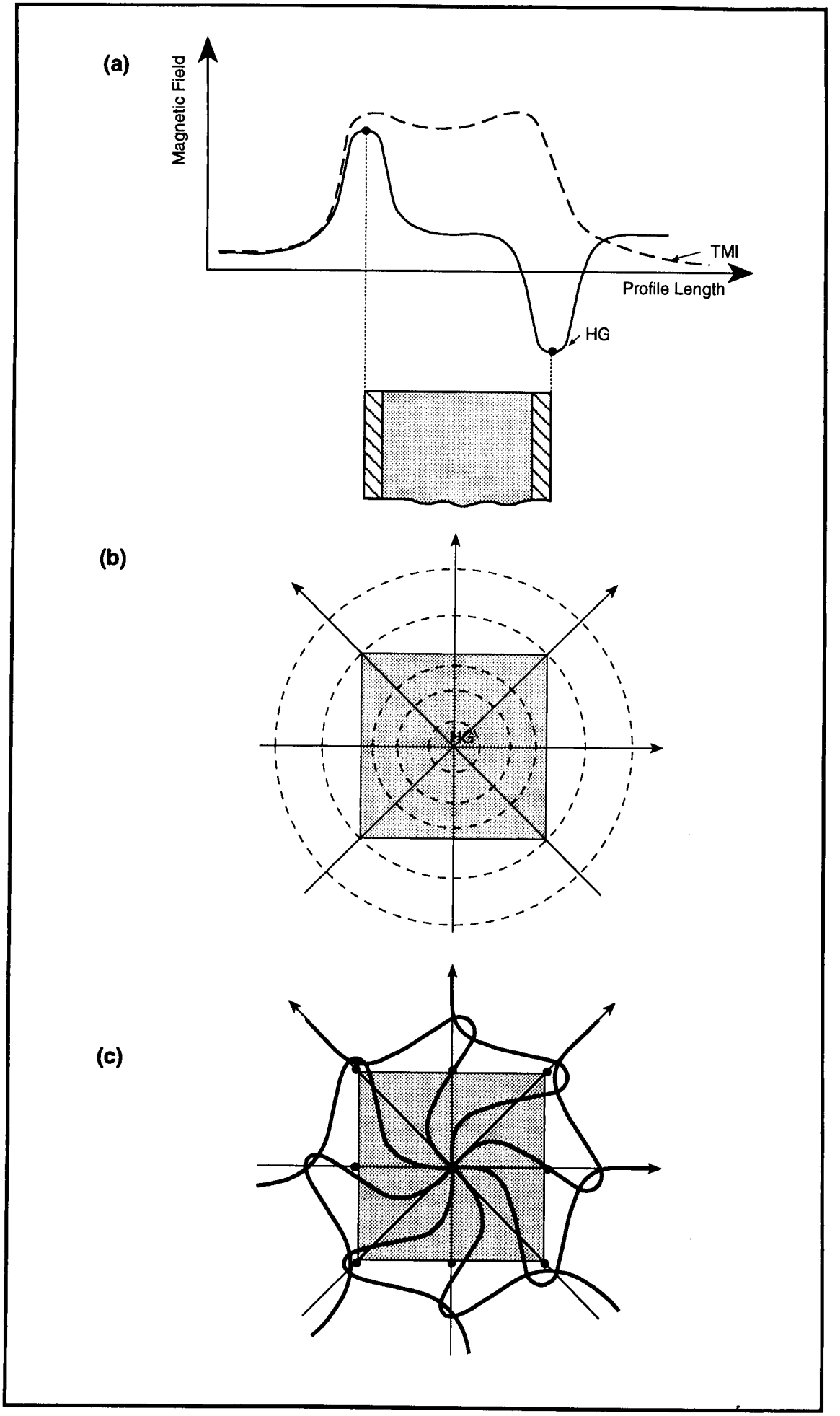

Figura 6.11 Delineation of the shape of the magnetic body on the magnetic map using horizontal gradient technique.

6.2.5 Calculation procedure and principles of the horizontal gradient technique (HGT)

This technique can be successfully applied to the interpretation of the broad magnetic anomalies caused by large bodies. However, it is necessary that, these data first be reduced to the pole.

The principles of the method are basic and well known. The direct meaning of the horizontal gradient technique, when applied to a magnetic field, is the computation of the difference between the values of an original magnetic field, caused by a large size body, and the values of the magnetic field caused by this body when shifted a small distance along the horizontal direction. As shown in Figure 6.11(a) the original magnetic field F(x,y) is caused by the dot-shaded body and the resultant magnetic field f(x,y) (the horizontal gradient) is caused by two thin cross-shaded dykes located on the margins of the original causative body and having opposite magnetisation.

The extreme values, i.e. the pairs of a minimum and a maximum value of the horizontal gradients of the magnetic (or gravity) anomaly can indicate edges of the broad causative sources along the directions of the computed horizontal gradients (Figure 6.11(b)). The maximum value (for positive anomaly and minimum if the anomaly is negative) of the vertical gradient of the magnetic anomaly can indicate the centre of the causative body. The centre of the causative body coincides also with the point in which all horizontal gradient profiles intersect (see Figure 6.11(b)). The position of this point can be located also from the contour map, as the joint point of the zero lines of the horizontal gradients (Figure 6.11(c)). The zero value of the vertical gradient (zero contour line) around the interpreted anomaly also indicate the boundary of the causative body (Hou and Shi, 1982; Cordell and Grauch, 1985; Shi, 1993).

6.2.6 Spectral analysis of the TMI field over *SQ18* using the 'moving window' technique

In the search for new, more detailed information about the thickness and structure of the rifted and non-rifted crust at different depth levels, the energy spectra are computed over the block *SQ18* using the 'moving window' technique with two different 'original windows' $50km \times 50km$ and $25km \times 25km$.

(i) The 'moving window' $25km \times 25km$

Each of the $25km \times 25km$ 'moving windows', which contains $2,500gc$ (data points), is expanded into a $64km \times 64km$ extrapolation array. The energy spectra are computed and interpreted for 419 'original windows'. Only the depths to the top of the deepest magnetic sources (DMS_{25x25}) are recorded. In Figure 6.12(a) are shown depth values rounded to the nearest integer. Figure 6.12(b-c) has been constructed based on the gridded row depth values obtained from the spectral analysis.

(ii) The ' moving window' 50km × 50km

The energy spectra of the magnetic field over the *50km × 50km* window are computed for 90 blocks (50% overlap along the x- and y-axis) covering *SQ18* (Figure 6.13(a); depths rounded to the nearest integer). Each *50km × 50km* data-block contains *10,000* data points which are extrapolated into a *128km × 128km* array. Interpretation has focused on the deepest boundaries ($DMS_{50\times50}$), which have been (non-rounded values) gridded and are contoured in Figure 6.13(b-c).

6.3 Interpretation of 'deep magnetic sources' maps of the Polda rift region and surrounding Gawler Craton

6.3.1 Deep magnetic sources map based on window *25x25 km* - $DMS_{25\times25}$

The deep magnetic sources map $DMS_{25\times25}$ (Figure 6.12(b)) map shows contours of the deepest magnetic horizon within the upper crust. There are several magnetic features which are related to major geological structures occurring in this area.

- Along the latitude *33°30'S* can be seen an east-west magnetic trough which coincides with the position of the Polda Trough. South of the east-west trending Polda rift are located deep magnetic sources, which could be a manifestation of the major listric fault dipping towards the south.

- A major crustal break which runs north-south is shown on this map. It appears that along the longitude *135°15'E*, between latitude *33°30'S* and *34°00'S* runs deep crustal feature (B_{NS}). There is a significant change in the depth values, on the eastern and western side of the observed boundary B_{NS}. As can be seen in Figures 6.12(a) and 6.12(b), moving from the south towards the north, these depth values change along the longitude *134°30'E*, as follows:

  – on the western side of the B_{NS} boundary, detected depths range between 10-13 km, whereas on the opposite site depth values are between 20-27 km,

  – 50 km towards the north along the boundary B_{NS} there appears a switch of 'depth polarity'; on the western side there are indications of magnetic rocks below 18 km whereas towards the east, estimated depth values are much shallower, not exceeding 12-14 km

  – further north, the switch of 'polarisation' occurs once again; the break is marked by shallower west side (~14 km) and deep-seated (~23 km) east side magnetic sources. These changes continue for the next 100 km north.

- In the SE quarter of the map $DMS_{25\times25}$ the dominant direction of the detected magnetic sources is NE-SW. Along the central axis of an area referred to as the 'huge magnetic low', *HML*, there runs a magnetic ridge (CR_{HML}) in the NE-SW direction showing interface at 8-10 km depths. The CR_{HML} on both eastern and western side is accompanied by two sub-parallel narrow magnetic troughs

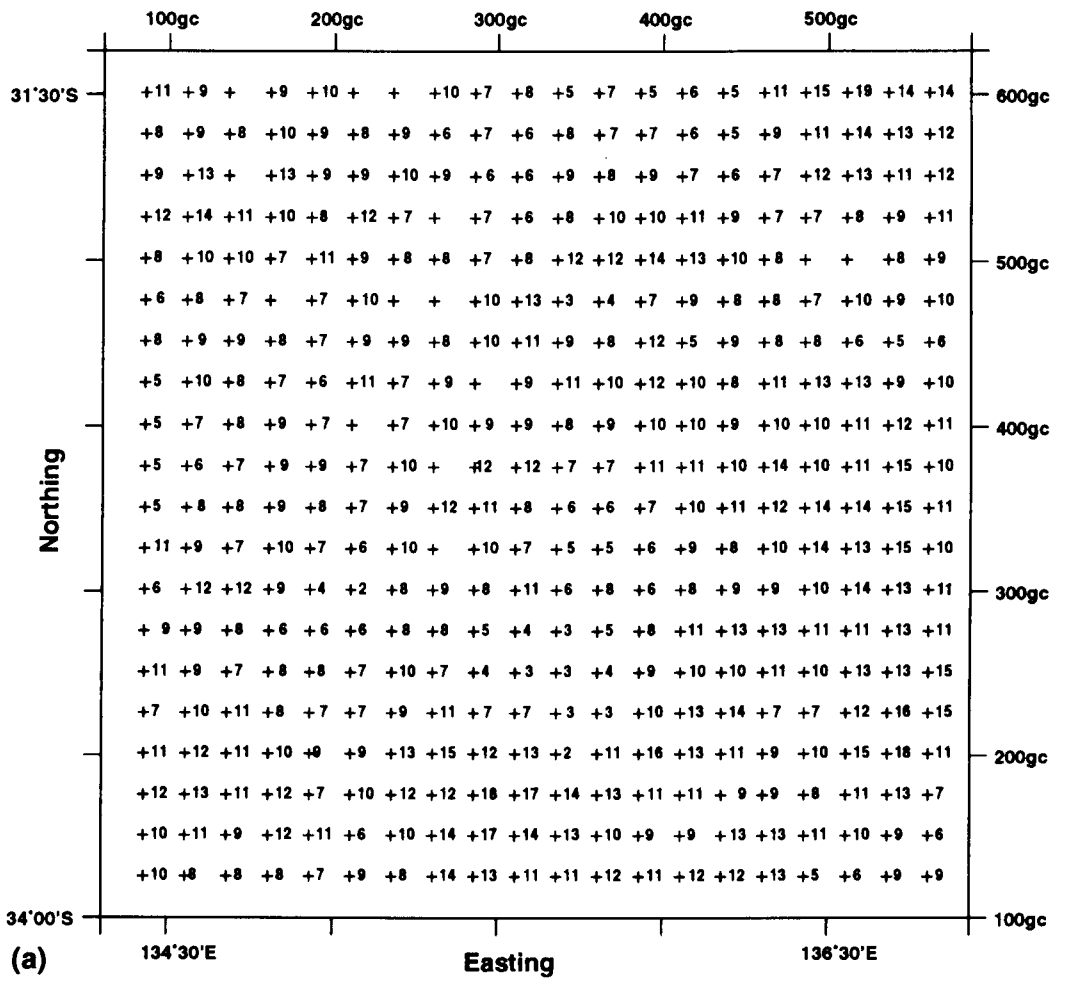

Figure 6.12 Depth to the top of deep magnetic sources computed over SQ18 by applying energy spectra analysis of TMI field (500x500m grid) using 'moving window' technique. Original window 25x25km (50x50 grid cells), extension window 64x64km.
(a) Depth value [km] with cross representing centre of 25x25km window
(b) Colour image and contours of depth [km].
(c) Image and contours of depth [km] with major tectonic features and boundaries.

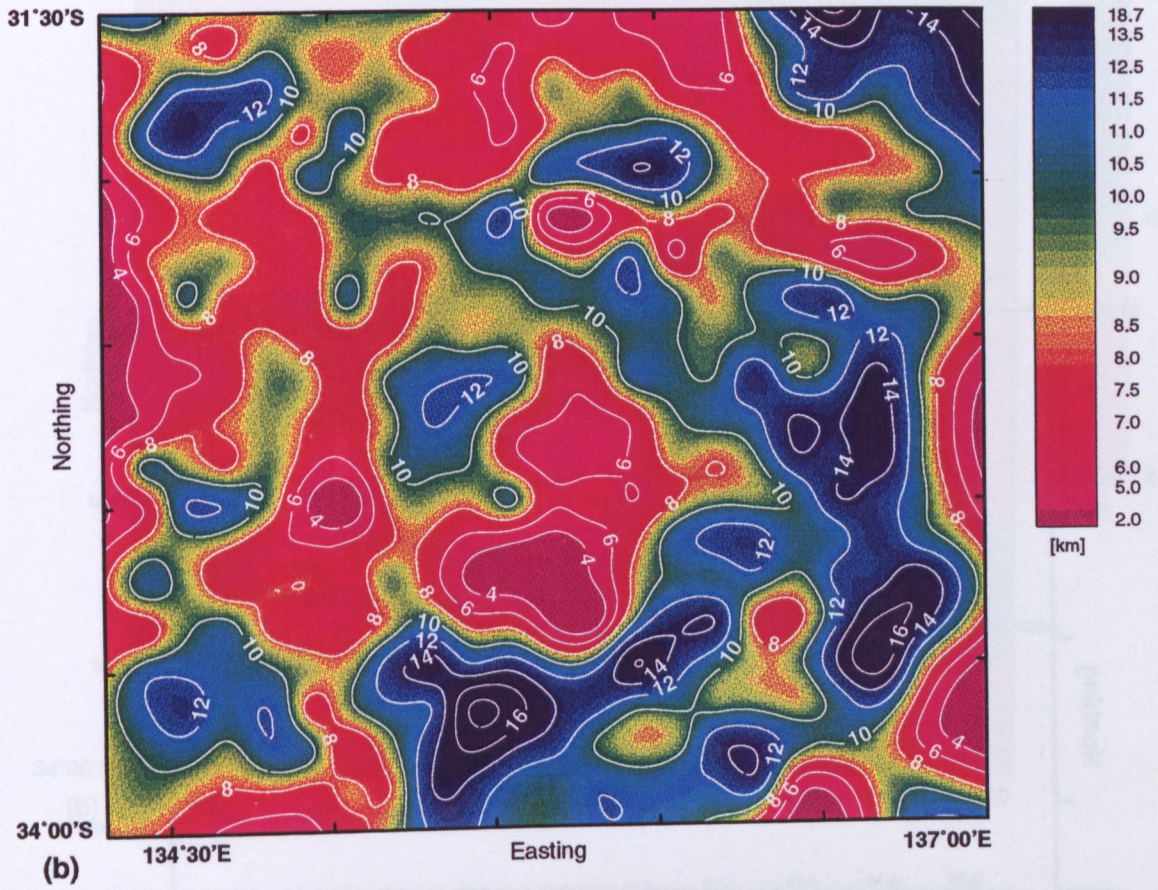

(b)

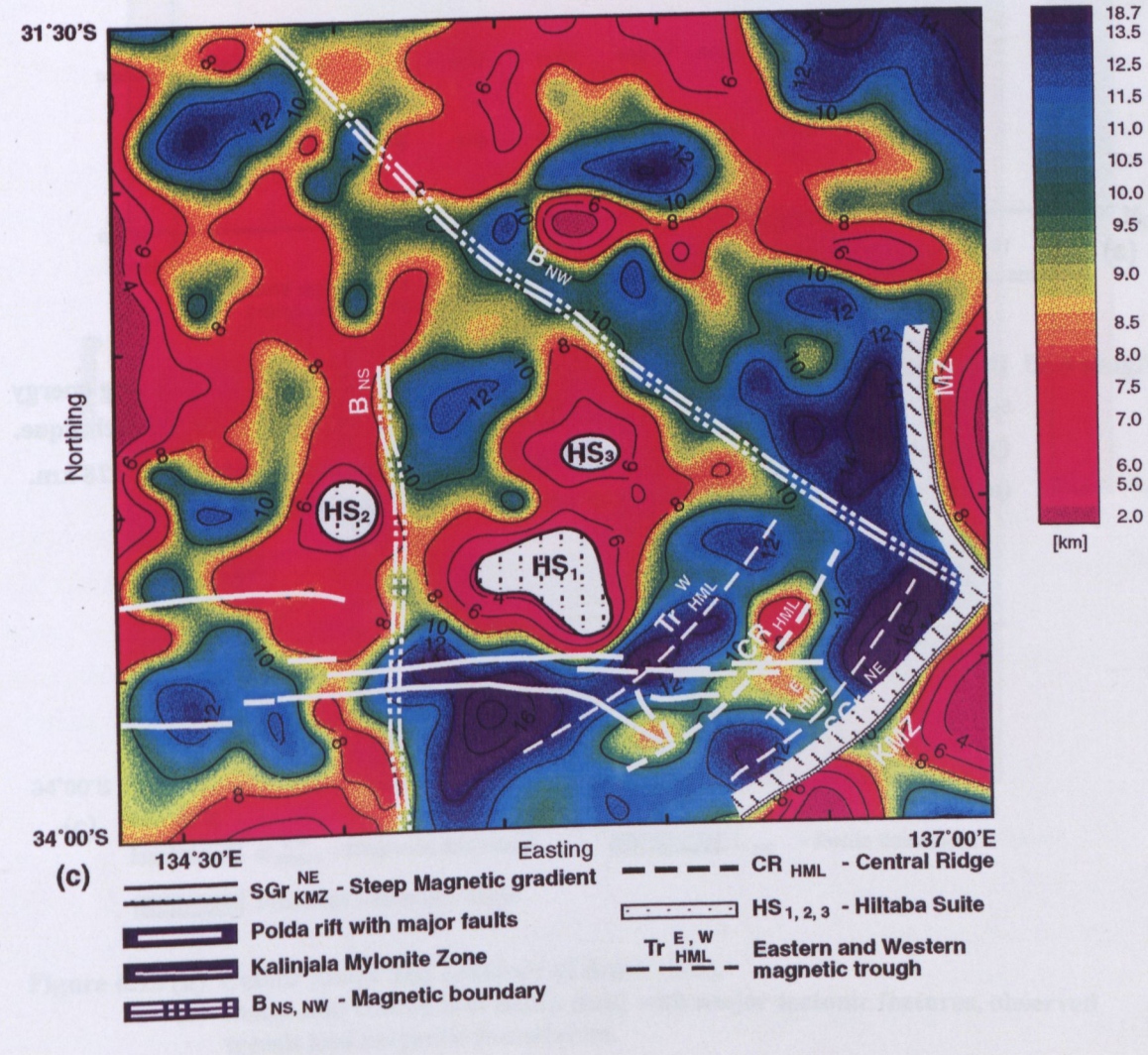

(c)

SGr NE KMZ - Steep Magnetic gradient

Polda rift with major faults

Kalinjala Mylonite Zone

B NS, NW - Magnetic boundary

CR HML - Central Ridge

HS 1, 2, 3 - Hiltaba Suite

Tr E, W HML Eastern and Western magnetic trough

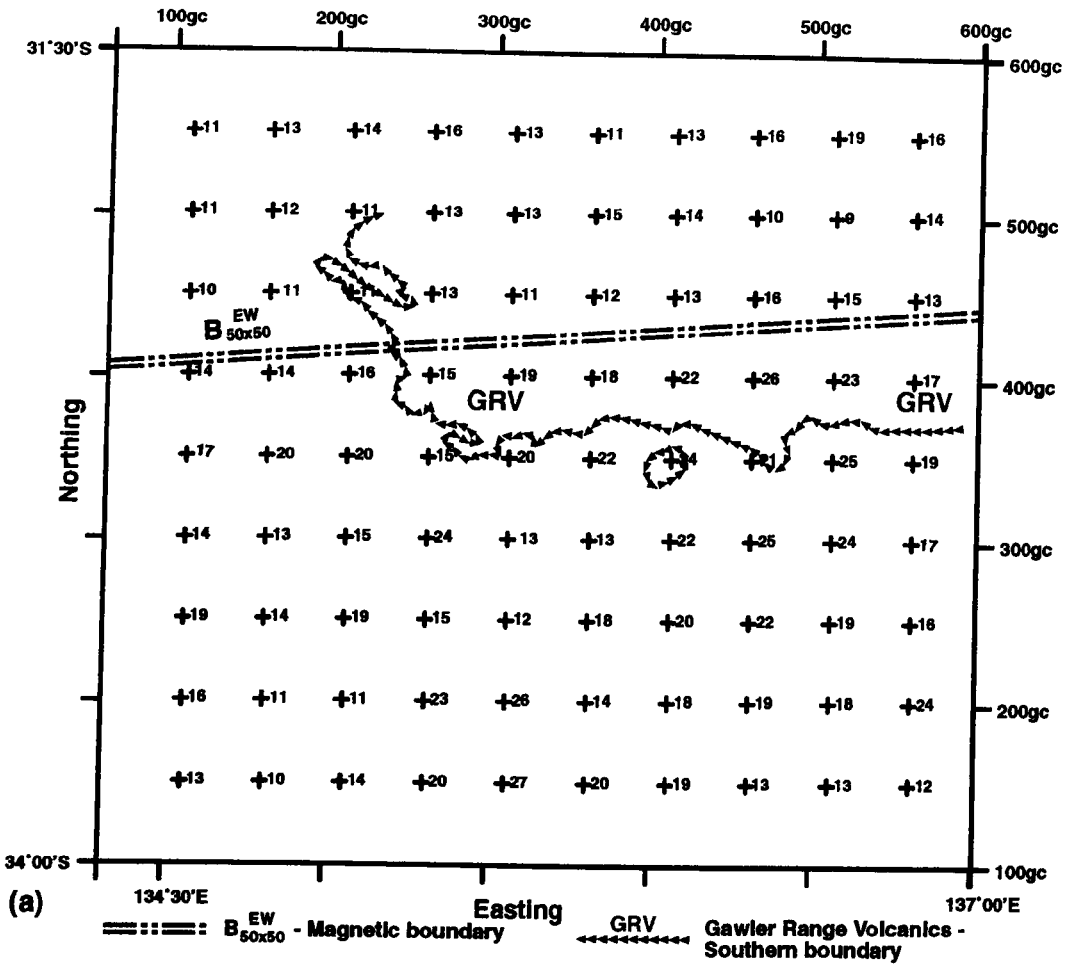

Figure 6.13 Depth to the top of deep magnetic sources computed over SQ18 by applying energy spectra analysis of TMI field (500x500 m grid) using 'moving window' technique. Original window 50x50 km (100x100 grid cells), extension window 128x128 km. (a) Depth value [km] with cross representing centre of 50x50km window

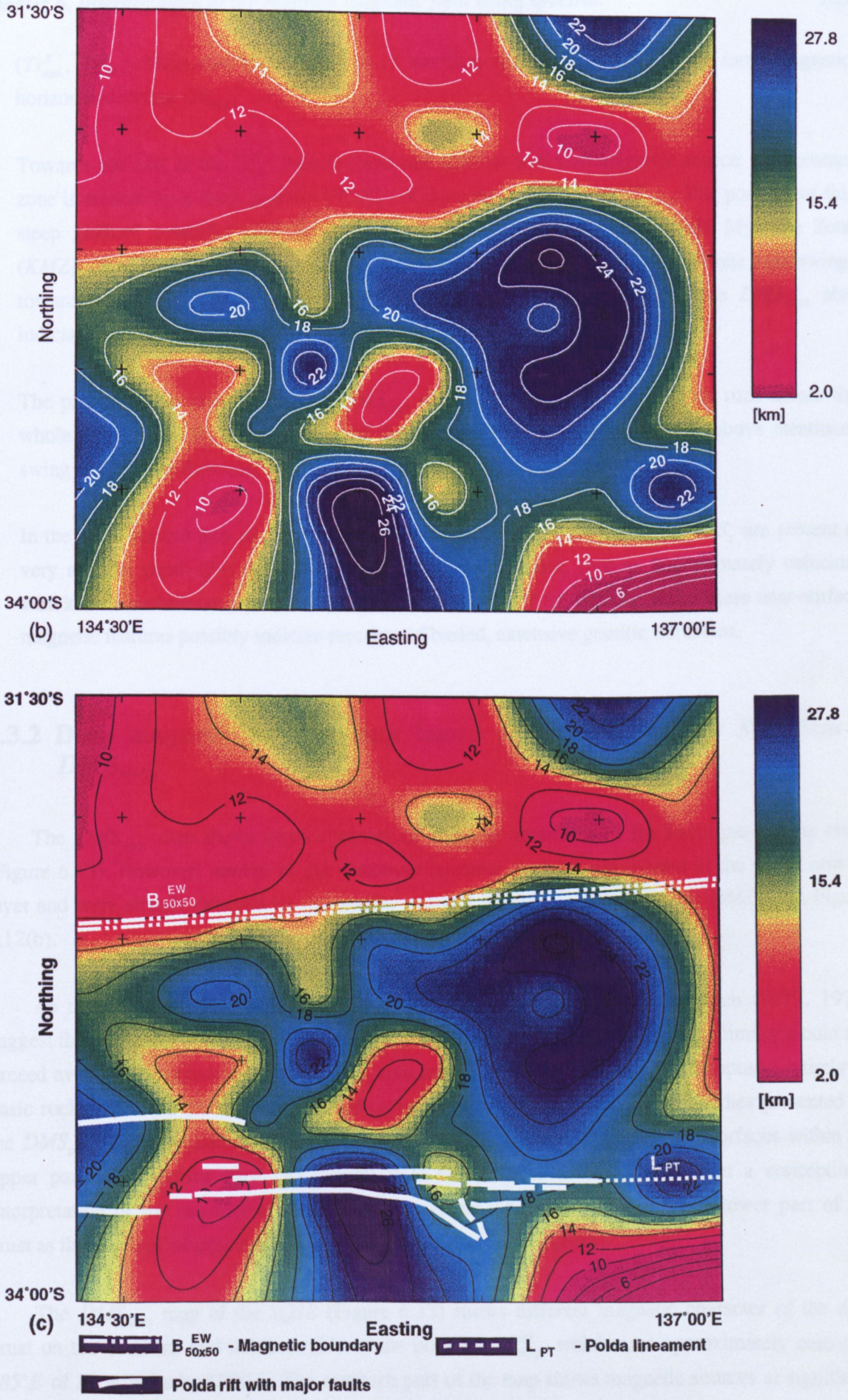

Figure 6.13 (b) Colour image and contours of depth [km].
(c) Image and contours of depth [km] with major tectonic features, observed trends and magnetic boundaries.

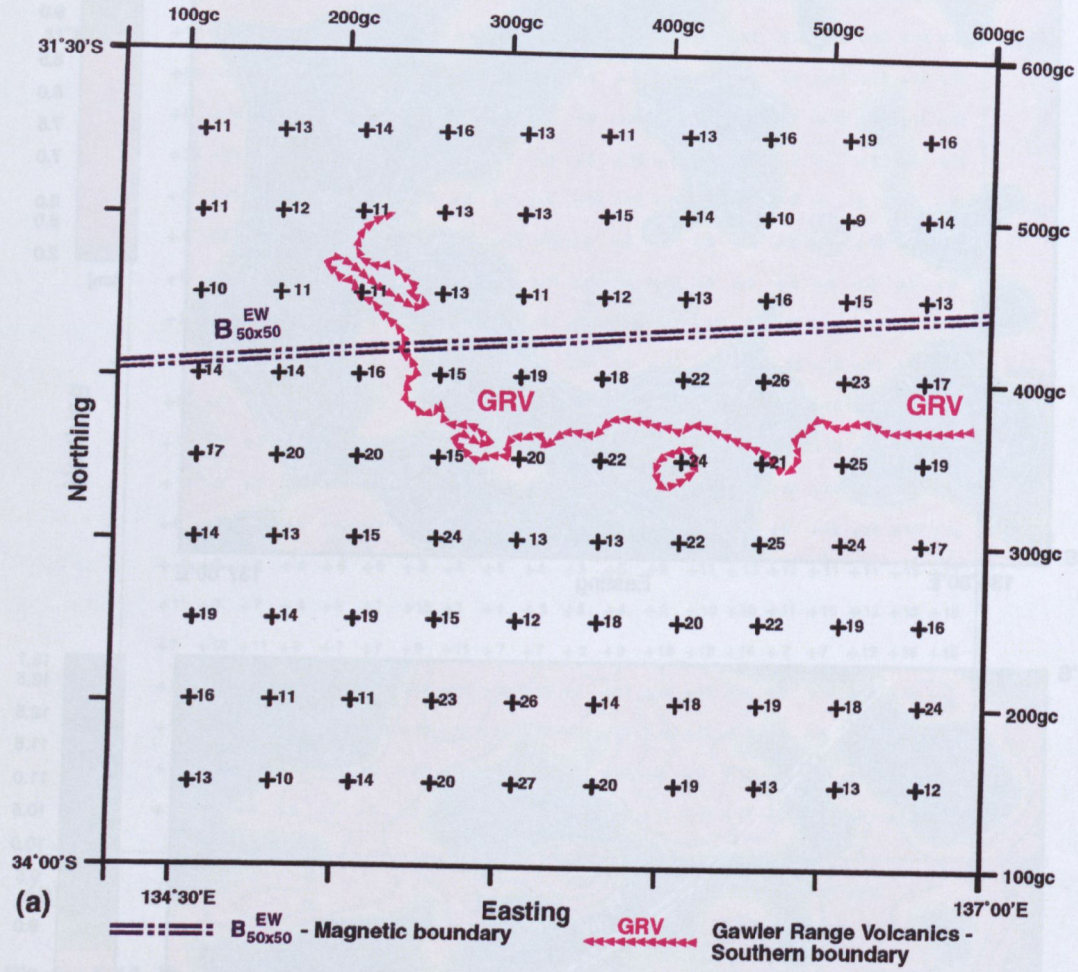

Figure 6.13 Depth to the top of deep magnetic sources computed over SQ18 by applying energy spectra analysis of TMI field (500x500 m grid) using 'moving window' technique. Original window 50x50 km (100x100 grid cells), extension window 128x128 km. (a) Depth value [km] with cross representing centre of 50x50km window

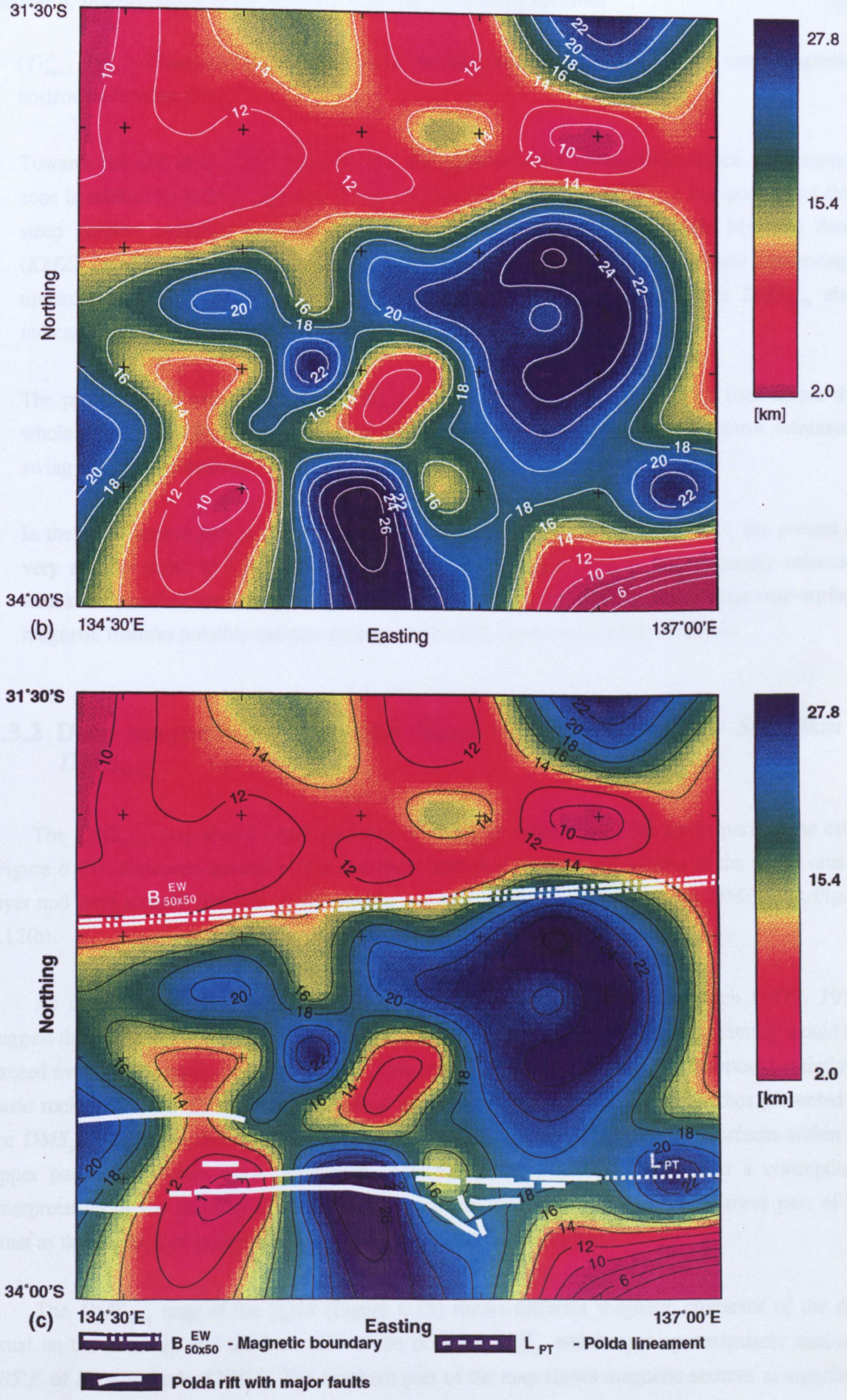

Figure 6.13 (b) Colour image and contours of depth [km].
(c) Image and contours of depth [km] with major tectonic features, observed trends and magnetic boundaries.

(Tr^{E}_{HML}, Tr^{W}_{HML}). These two features are 14-16 km deep and perhaps represent the same magnetic horizon underlying CR_{HML}.

- Towards the east of the Tr^{E}_{HML} there is large and shallow (4-6 km) magnetic source. The contact zone is marked by a steep gradient (SGr^{NE}_{KMZ}) of the contours on the $DMS_{25\times25}$. The position of this steep gradient coincides with the surface-mapped NE-SW oriented Kalinjala Mylonite Zone (*KMZ*). As shown on the tectonic map of South Australia, the strike of this mylonite zone swings towards the NNW-SSE at approximately longitude $136°50'E$. Contours of the $DMS_{25\times25}$ also indicate similar change of the strike direction.

- The pattern of the contours on the $DMS_{25\times25}$ shows a NW-SE structure which runs across the whole *SQ18* map (B_{NW}). Intersection of this feature with the *KMZ* marks the above mentioned swing in the strike direction.

- In the south-central part of the $DMS_{25\times25}$ the magnetic sources HS_1, HS_2 and HS_3 are present at very shallow depth (2-3 km). The position of these magnetic sources approximately coincides with known surface occurrences of the granitic intrusions of the Hiltaba Suite. These near-surface magnetic features possibly indicate presence of buried, extensive granitic intrusions.

6.3.2 Deep magnetic sources map based on moving window *50x50km* - $DMS_{50\times50}$

The $DMS_{50\times50}$ map shows depth contours of magnetic interfaces of the lower part of the crust (Figure 6.13). However, several of the shallower magnetic features are located in the upper crustal layer and were already detected by the smaller spectral window as shown on the $DMS_{25\times25}$ in Figure 6.12(b).

As mentioned in Section 6.1 of this chapter Krutikhovskaya and Pashkevich (1977, 1979) suggest that the upper part of the lower crust, e.g. the strata below the Conrad discontinuity would not exceed average magnetisation of 1.4×10^{-3} emu and that the crust can only be composed entirely of basic rocks below 20-25 km depth. Based on such an assumption the magnetic bodies presented on the $DMS_{50\times50}$ which are detected at a depth 20-26 km perhaps show magnetisation surfaces within the upper part of the lower crust. At present it is not possible to build more than a conceptional interpretation of the majority of the observed magnetic inhomogeneity within the lower part of the crust as there is lack of proper control by deep seismic sounding (DSS).

The $DMS_{50\times50}$ map of the *SQ18* (Figure 6.13) shows different magnetic character of the deep crust on the southern and northern side of the boundary $B^{EW}_{50\times50}$ which runs approximately east-west ($85°E$ of *N*) at latitude $32°30'S$. The southern part of the map shows magnetic sources at significant depths, often exceeding 20 km, whereas the northern region shows the presence of the much shallower magnetic sources at average depths of 11-14 km. The boundary $B^{EW}_{50\times50}$ approximately coincides with the southern margin of the Gawler Range Volcanics (GRV) and the position of the east-west running

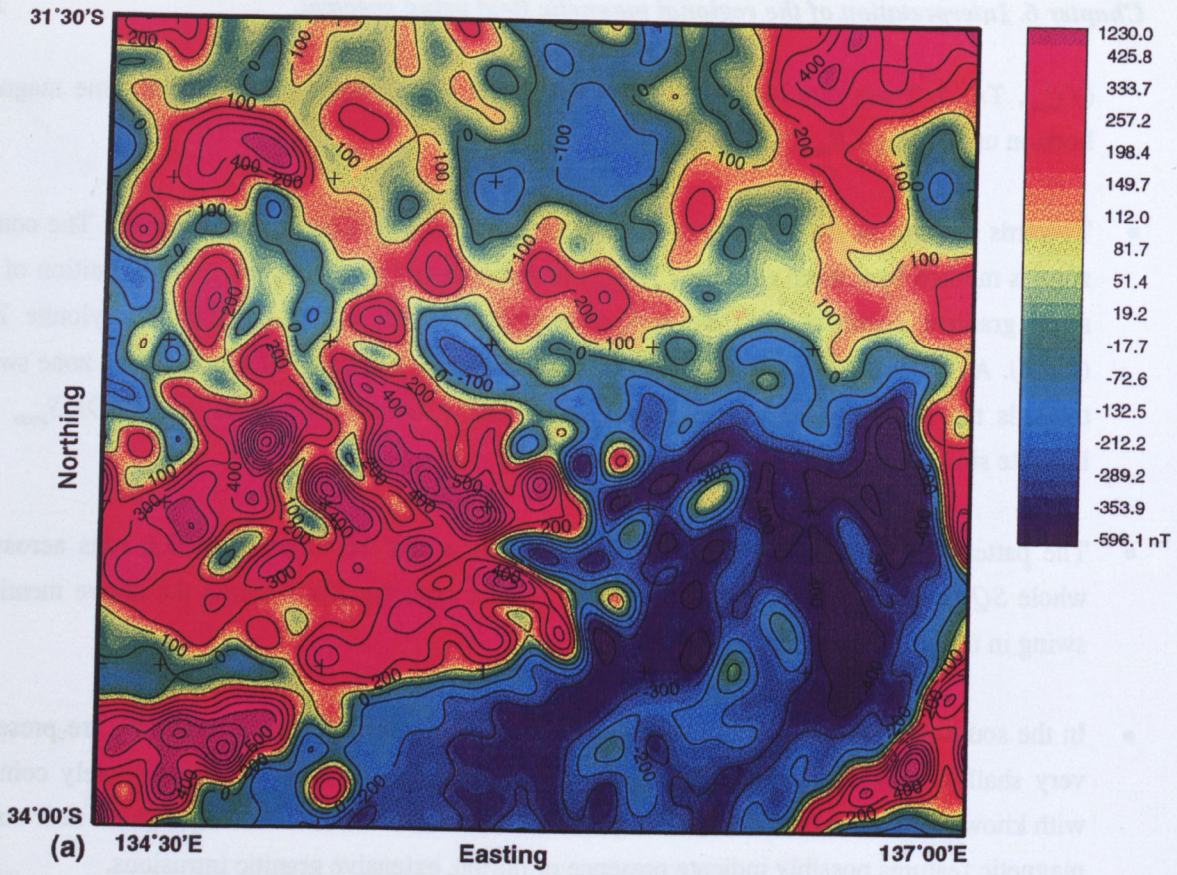

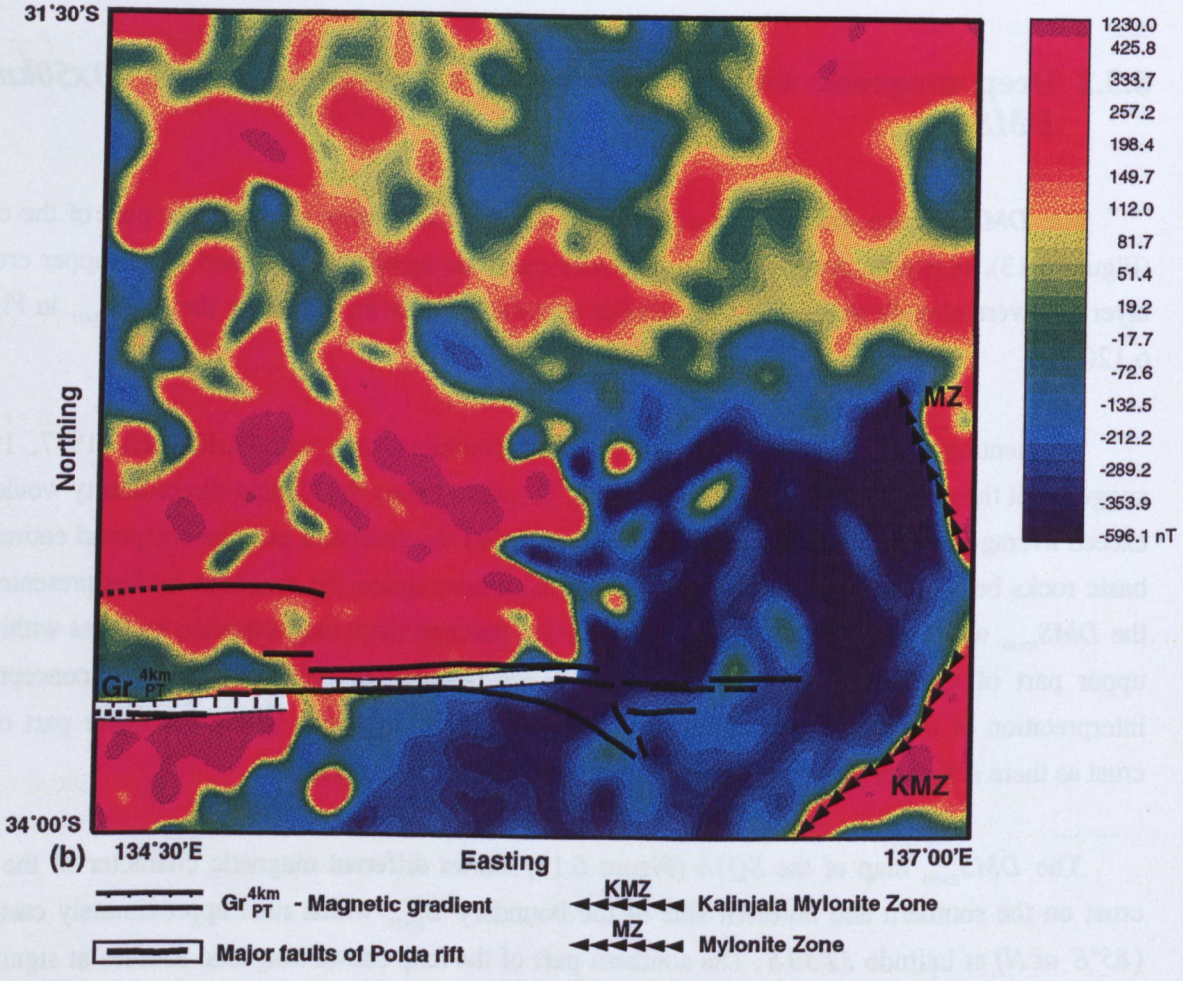

Figure 6.14 Long wavelength magnetic anomaly map of SQ18 - 'λ>15km':
(a) colour image with contours,
(b) colour image with major tectonic features and observed magnetic boundaries.

Uno Fault. As is shown in the interpretation sketch in Figure 6.13(a) the surface mapped southern boundary of the GRV is located south of the centres of the spectral windows located along latitude *32°30'S*. The depth values of the $DMS_{50\times50}$ shown in Figure 6.13(a) clearly indicate that towards the south of the *GRV* the magnetic sources were detected at depths exceeding 20 km, whereas north of the margin the magnetic surfaces are at much shallower depths (average 11-15 km).

In the region of the offshore part of the Polda rift between latitude *33°00'S* and *33°30'S* (south-western side of *SQ18*) a magnetic interface at depths greater than 19 km has been detected. This may be indicating thicker upper crust under the rift.

It is important to note that the whole *SQ18* area is dominated by two sub-parallel features, the Polda rift with extending lineament L_{PT} and the magnetic boundary $B^{EW}_{50\times50}$ located about 75-90 km towards the north.

6.4 Interpretation of 'depth slice' maps of the Polda rift region and surrounding Gawler Craton - *SQ18*

As discussed the anomaly separation techniques allow the study of the characteristics of the magnetic field in relation to the wave length and the crustal layers which contain the majority of the causative sources. The following observations concerning regional structures and crustal magnetic inhomogeneity have been noted.

6.4.1 The long wave-length magnetic anomaly map of *SQ18* -' $\lambda > 15km$'

The long wave-length magnetic anomaly map of *SQ18*, '$\lambda > 15$km ' shows the magnetic field due to sources at depths greater than 4 km (Figure 6.14). At the lower part of the Figure 6.14 along the latitude 33°30'S and between longitudes 134°15'E and 136°00'E, runs a steep east-west gradient (Gr^{4km}_{PT}), which coincides with the surface-mapped position of the offshore Polda rift as well as part of its onshore extension. The position of the magnetic gradient Gr^{4km}_{PT} is indicated by white strips in Figure 6.14(b).

6.4.2 The long wave-length magnetic anomaly map of *SQ18* - '$\lambda > 25km$'

The long wave-length magnetic anomaly map of *SQ18*, '$\lambda > 25$km , represents the magnetic field arising from causative sources located within the crust at depths greater than 7 km (Figure 6.15). On this map the surface-mapped position of the Polda rift coincides with a gradient Gr^{7km}_{PT} which is much stronger than Gr^{4km}_{PT} on the map '$\lambda > 15$km '. The east-west elongated magnetic low (anomaly A^{7km}_{PT} with central axis along latitude *33°30'S*) extending between *134°15'E* and *135°00'E*, indicates either thicker upper crust or a thinner entire crust underlying the offshore part of the Polda rift, which is about 23-30 km wide and at least 5 km deep in this section. The anomaly A^{7km}_{PT}, in comparison with the '$\lambda > 15$km ' map, is much broader and more dominant. The magnetic signature of the central and

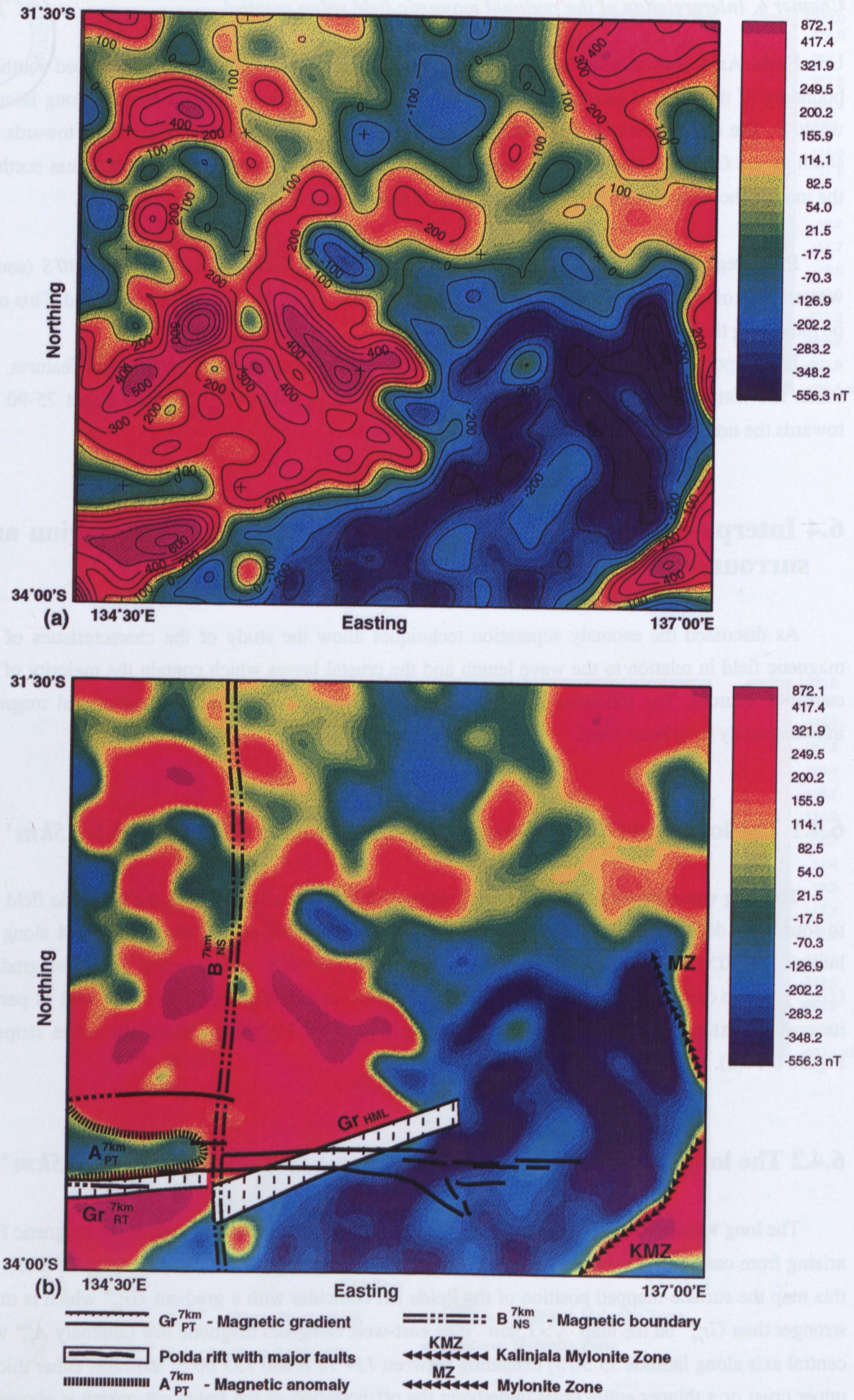

Figure 6.15 Long wavelength magnetic anomaly map of SQ18 - 'λ > 25km':
(a) colour image with contours,
(b) colour image with major tectonic features and observed magnetic boundaries.

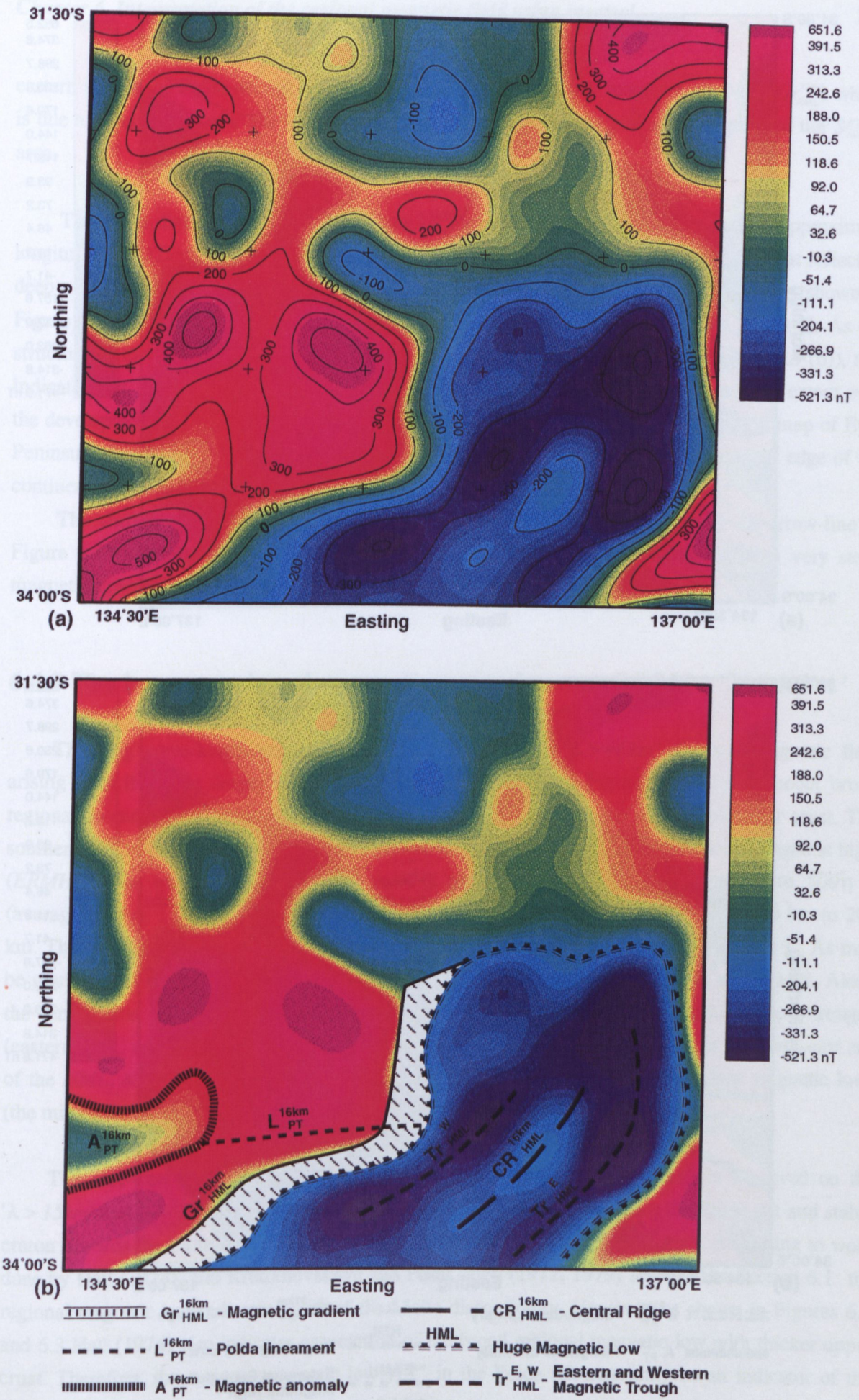

Figure 6.16 Long wavelength magnetic anomaly map of SQ18 - 'λ>46km':
(a) colour image with contours,
(b) colour image with major tectonic features and observed magnetic boundaries.

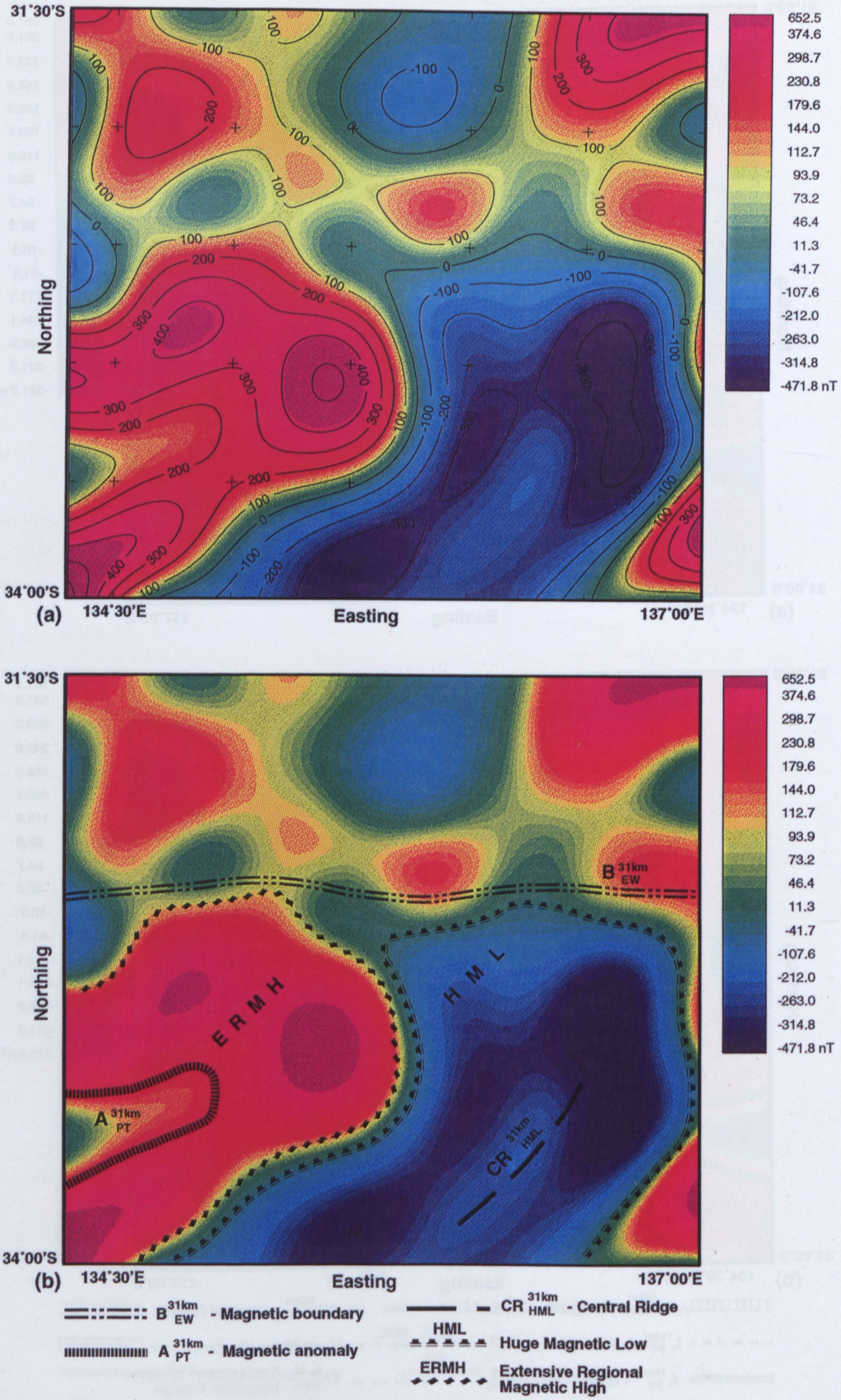

Figure 6.17 Long wavelength magnetic anomaly map of SQ18 - 'λ>64km':
(a) colour image with contours,
(b) colour image with major tectonic features and observed magnetic boundaries.

eastern part of the Polda rift is overprinted by a very strong NE-SW magnetic gradient (Gr^{7km}_{HML}) which is due to a huge magnetic low (*HML*) occupying the majority of the south-east quarter of the *SQ18* area.

There is a distinct north-south boundary (B^{7km}_{NS}) transecting the '$\lambda > 25$km' map at approximate longitude *135°00'E*. This magnetic boundary is not due to any error in the magnetic data but reflects a deep north-south crustal structure. This magnetic boundary is also observed on DMS_{50x50} shown in Figure 6.13 and is therefore a deep crustal feature; it is discussed in Section 6.4.2 Part II. As the structure of the Polda rift changes around the intersection with this boundary (Figure 6.15 (b)), this indicates that B^{7km}_{NS} could influence the development of the Polda rift and perhaps to a small extent even the development of southern margin of Australian continent. As shown on the geological map of Eyre Peninsula (Figure 6.22) several major faults trend in a north-south direction and cut the edge of the continent.

The surface-mapped position of the Kalinjala Mylonite Zone, indicated by an arrow-line in Figure 6.15(b), corresponds to the eastern boundary of the HML. It is marked by a very steep magnetic gradient and therefore is a deep crustal structure (Figure 6.15(a)).

6.4.3 The long wave-length magnetic anomaly map of *SQ18* - '$\lambda > 46km$'

The long wave-length magnetic anomaly map of *SQ18*, '$\lambda > 46km$' shows a magnetic field arising from the crust deeper than 16 km. The map presented in Figure 6.16 shows smooth broad regional anomalies indicating changes of rocks magnetisation within the middle and lower crust. The southern half of the map is occupied by the *HML* to the east and an 'extensive regional magnetic high' (*ERMH*) to the west. There are several positive regional anomalies with maxima up to *500*η *T* (average field of 1400 nT was subtracted from the TMI) and with wave-lengths from 60 km to 200 km. The negative part of the field includes lows, the minimum of which reaches – *500*η *T*. As may be seen, almost all of the regional low (*HML*) is located in the south-east quarter of the area. Along the central axis of the *HML* runs a magnetic ridge (CR^{16km}_{HML}) accompanied by two magnetic troughs (eastern TR^{E}_{HML} and western TR^{W}_{HML}) located on both sides in a sub-parallel pattern. In the north-east end of the *HML*, at latitude *32°30'S-33°30'S*, there is a north-south oriented set of deep magnetic lows (the minimum value of the magnetic field is less than – *520*η *T*).

The east-west oriented magnetic low A^{16km}_{PT} along latitude *32°30'S* which is observed on the '$\lambda > 15km$' and '$\lambda > 25km$', indicates difference between the crust underlying the Polda rift and stable craton towards the south and north of it, where strong magnetic highs are located. According to work done by Hall (1974), and Krutikhovskaya and Pashkevich (1977, 1979) reviewed in Section 6.1 the regional magnetic low indicates uplift of the Moho discontinuity. However, as shown in Figures 6.2 and 6.3 Hall (1974) also indicates association of the broad regional magnetic low with thicker upper crust. Therefore, the regional magnetic low A^{16km}_{PT} in the Polda rift zone may be an indicator of the thinning of the entire crust or the presence of thicker upper crust.

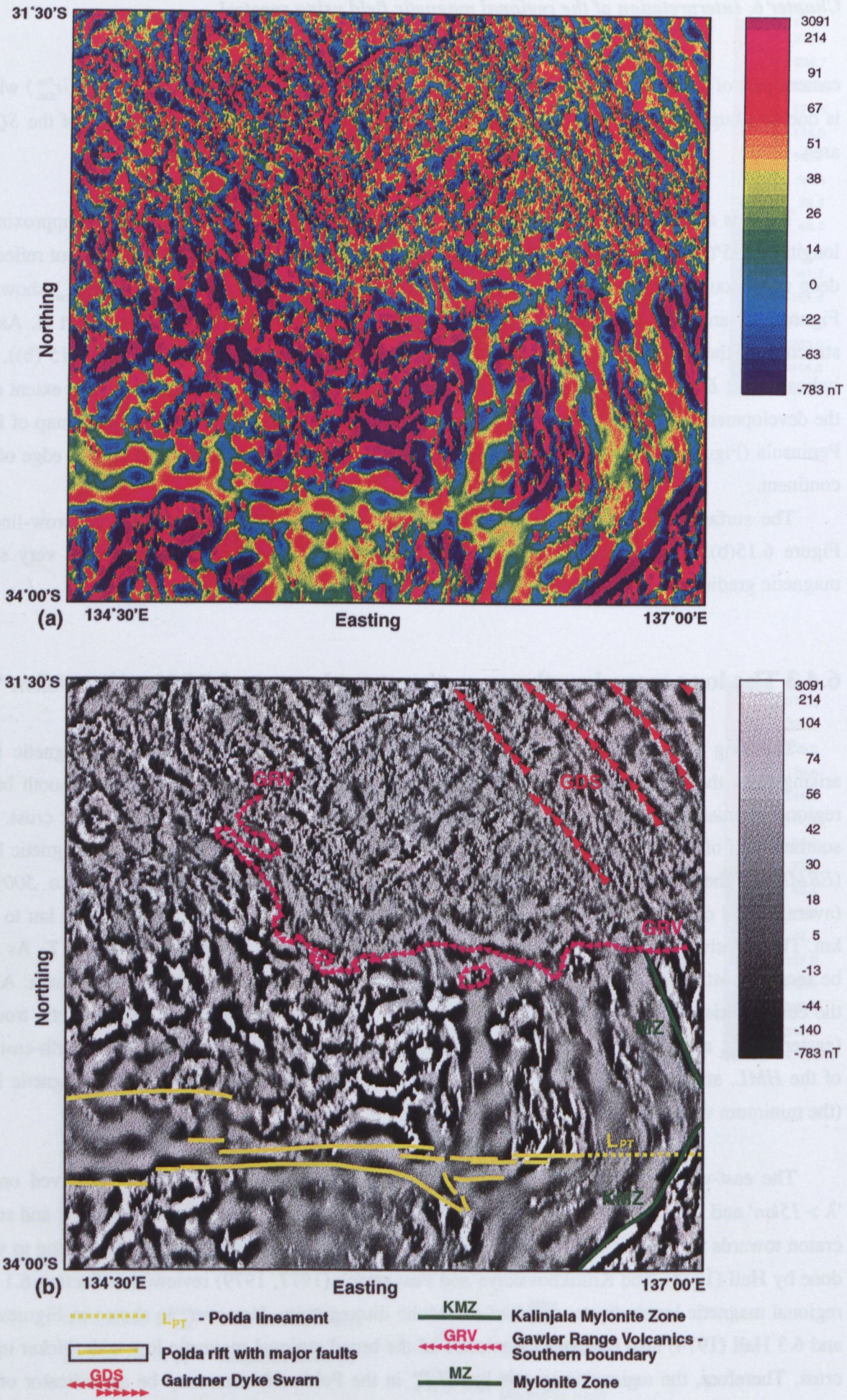

Figure 6.18 Residual magnetic field of SQ18 - 'λ<15km':
(a) colour image,
(b) grey image with major tectonic features and observed magnetic boundaries.

A very strong gradient Gr_{HML}^{16km}, due to *HML*, overprints the central and eastern zone of the Polda Trough, as the rift in this part is only a few kilometres wide. However, there is a prominent feature (L_{PT}^{16km}), running east-west which truncates the interior anomalies of the *HML*. This break in the anomaly pattern coincides with the position of the Polda Trough.

The north-south boundary B_{NS}^{7km} observed on the map '$\lambda > 25km$' can still be traced on the map '$\lambda > 46km$'.

6.4.4 The long wave-length magnetic anomaly map of *SQ18* - '$\lambda > 64km$'

The long wave-length magnetic anomaly map of *SQ18*, '$\lambda > 64km$', indicates magnetic characteristics of the lower crust or, perhaps upper mantle (see comment at page 92). On the map '$\lambda > 64km$' at latitude $32°30'S$ there is an east-west break in the anomaly pattern across the whole *SQ18* area (boundary B_{EW}^{31km}). To the north of this boundary there are a few randomly distributed broad anomalies, with one very strong high, located at the north-east corner of the *SQ18* map. The southern half of the '$\lambda > 64km$' map is dominated by two large and very smooth anomalies, each several hundred kilometres long:

- The NE-SW trending *HML*, with local anomaly amplitude greater than $800\eta\ T$. It seems that the magnetic low of such an extent may be a signature of the shallow topography of the Moho discontinuity over a very broad area. The central ridge (CR_{HML}^{16km}) observed on the '$\lambda > 46km$' map becomes a more subdued anomaly (CR_{HML}^{31km}) with maximum value $-\ 260\eta\ T$. The east-side low is not very strong, whilst the west-side still appears to be a strong broad anomaly (exceeding $-\ 470\eta\ T$). The north-south trending set of lows in the north-east end of the HML are a prominent internal feature (minimum field value is less than $-\ 400\eta\ T$) reflecting changes of the magnetization within the lower crust. In this region of the HML, the DMS_{50x50} map, shown in Figure 6.13, indicates that the weakly magnetic upper part of the crust is more than 26 km thick.

- The extensive regional magnetic high (*ERMH*) oriented more towards the ENE-WSW direction and located west of the *HML*; the centre of this *ERMH* is occupied by a broad east-west striking magnetic low (A_{PT}^{31km}), which as discussed, signals crustal changes within the Polda rift zone.

6.5 Interpretation of the residual magnetic field of the Polda rift region and the surrounding Gawler Craton, *SQ18*

6.5.1 The residual magnetic field of *SQ18* - '$\lambda < 15km$'

The residual magnetic field of wave-length '$\lambda < 15km$' is caused by magnetic sources located within the upper 4 km of the crust underlying the south-eastern Gawler Craton (Figure 6.18). The imprint of the Polda rift is very clear on the map '$\lambda < 15km$'. It appears that magnetic anomalies are truncated by an east-west lineament $L_{PT}^{<4km}$, which run across the whole *SQ18* map, for more than 70

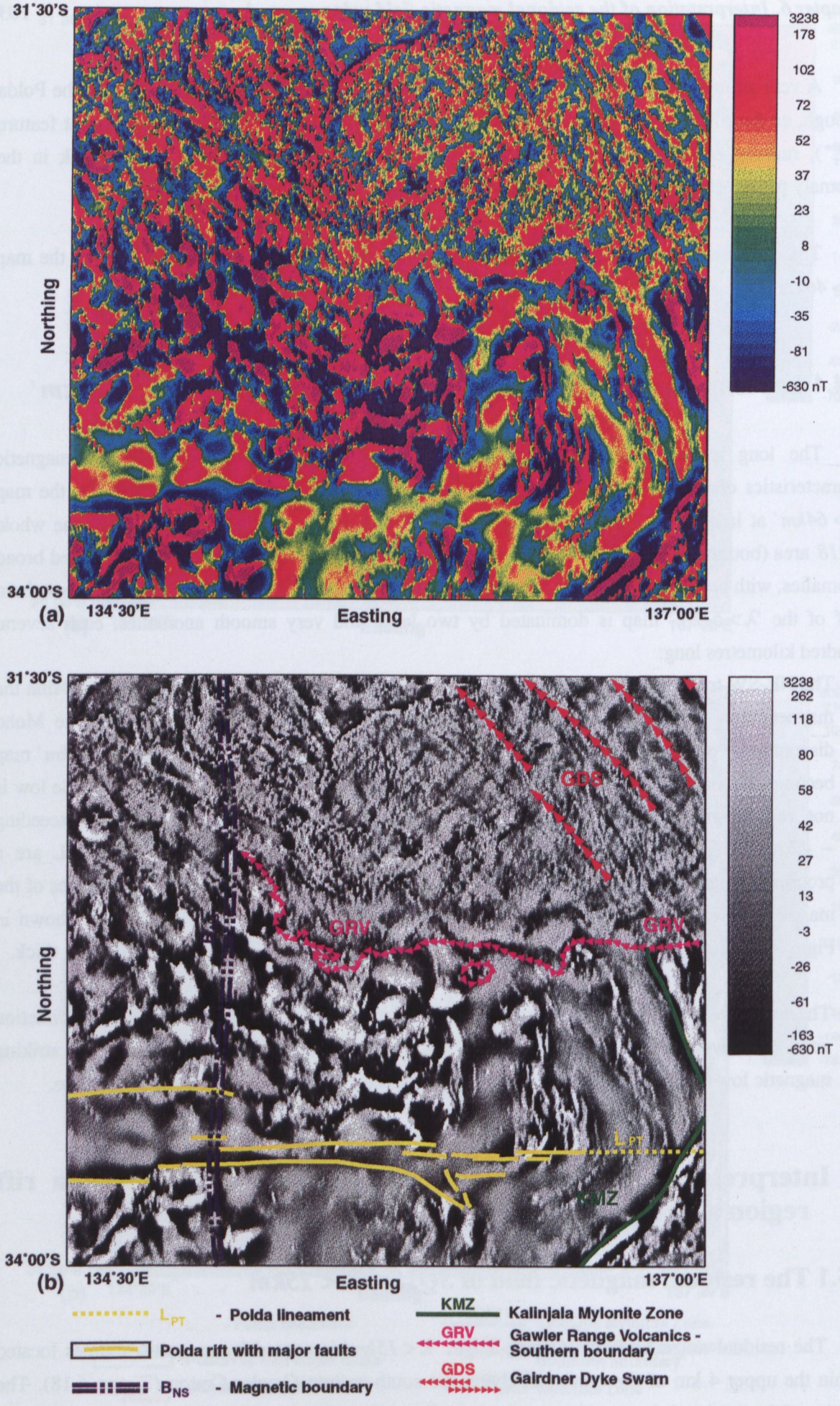

Figure 6.19 Residual magnetic field of SQ18 - 'λ<25km':
(a) colour image,
(b) grey image with major tectonic features and observed magnetic boundaries.

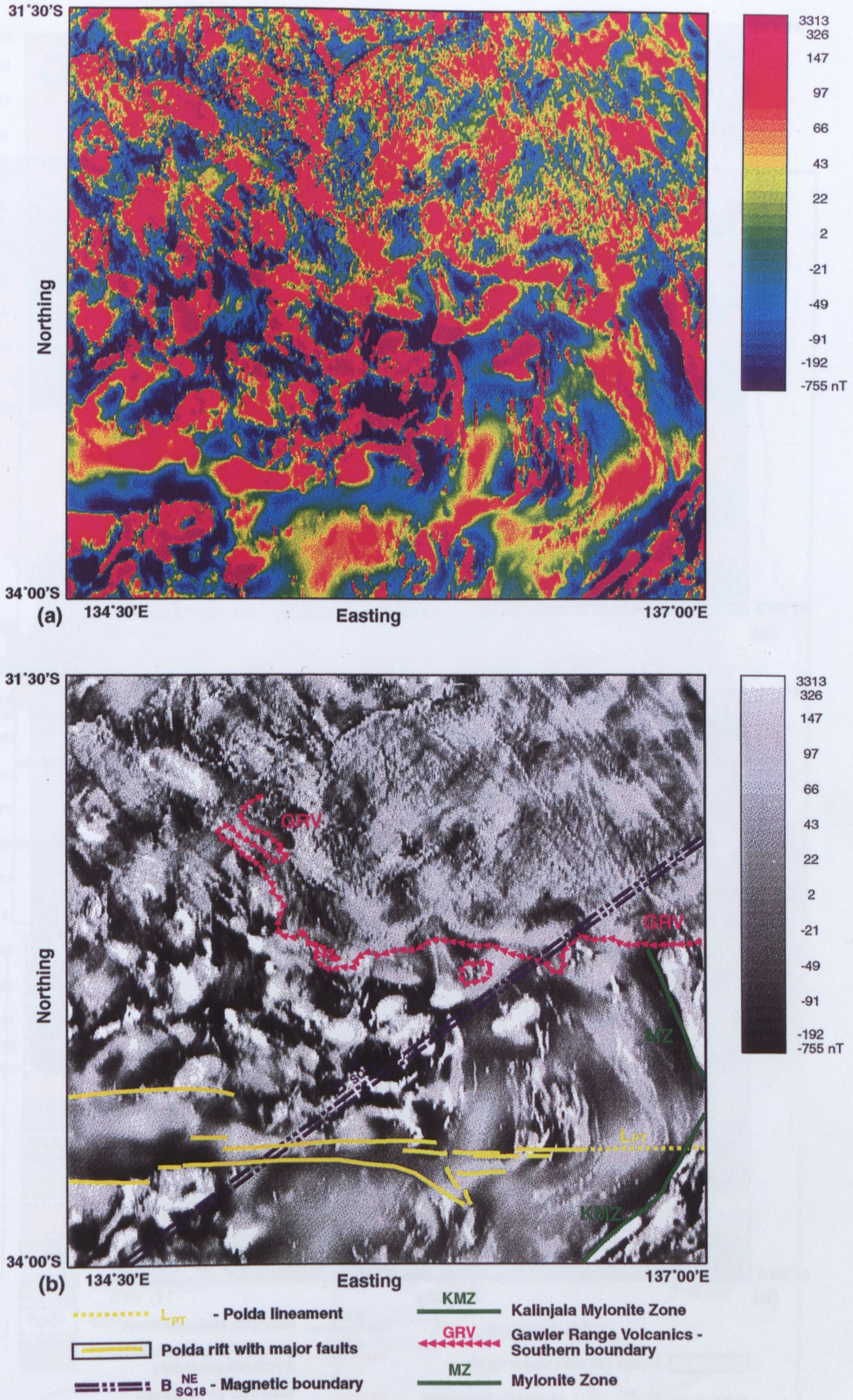

Figure 6.20 Residual magnetic field of SQ18 - 'λ<46km':
(a) colour image,
(b) grey image with major tectonic features and observed magnetic boundaries.

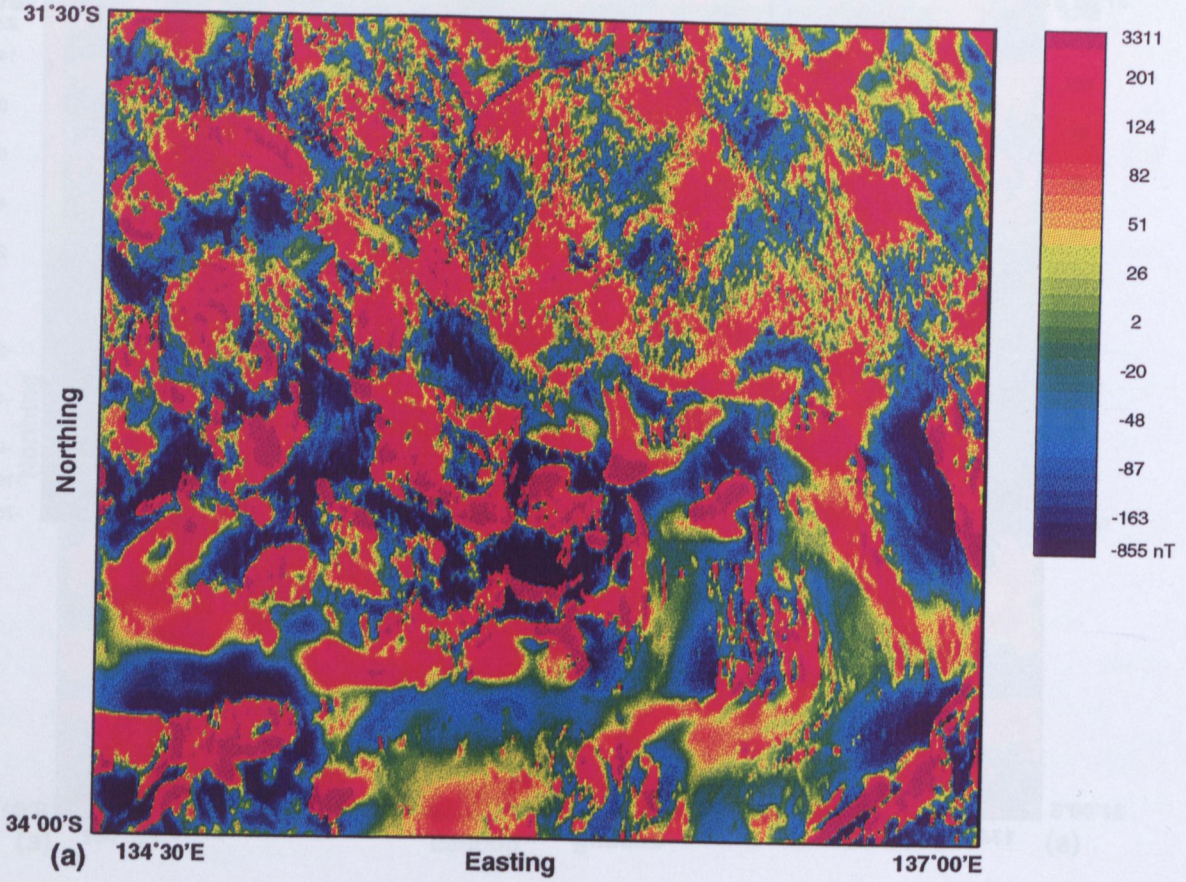

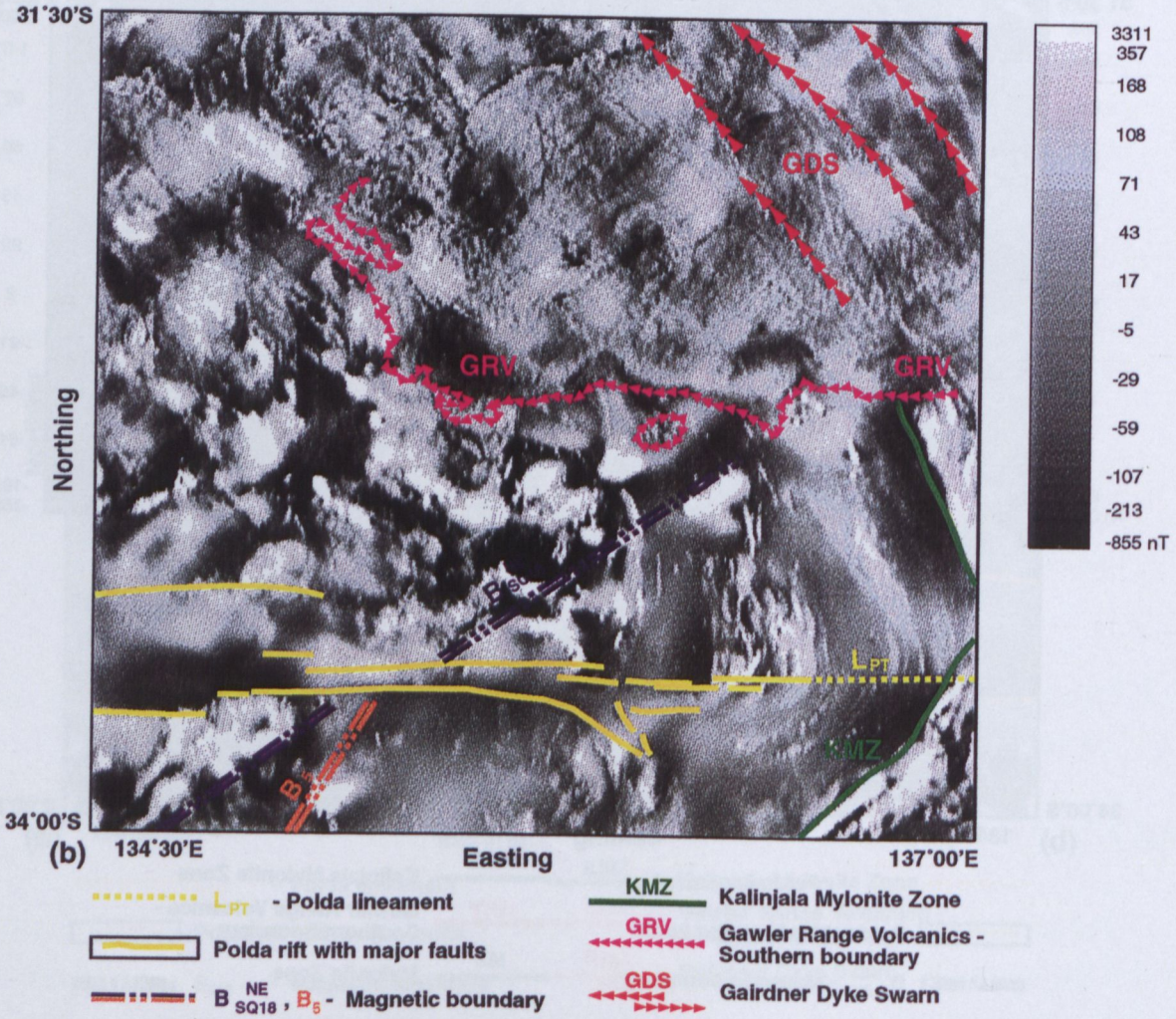

Figure 6.21 Residual magnetic field of SQ18 - 'λ<64km':
(a) colour image,
(b) grey image with major tectonic features and observed magnetic boundaries.

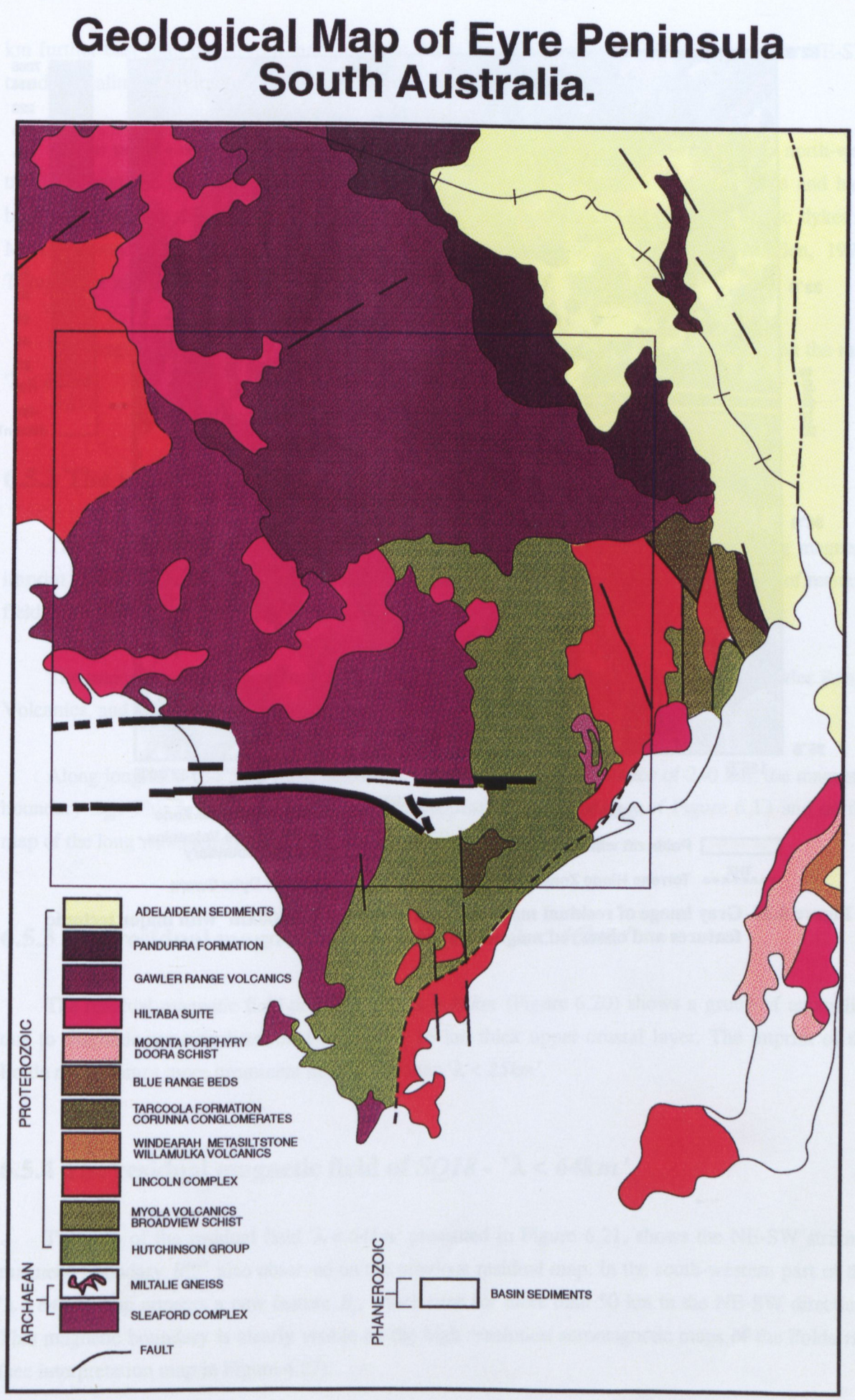

Fig.6.22 Geological map of Eyre Peninsula, South Australia.

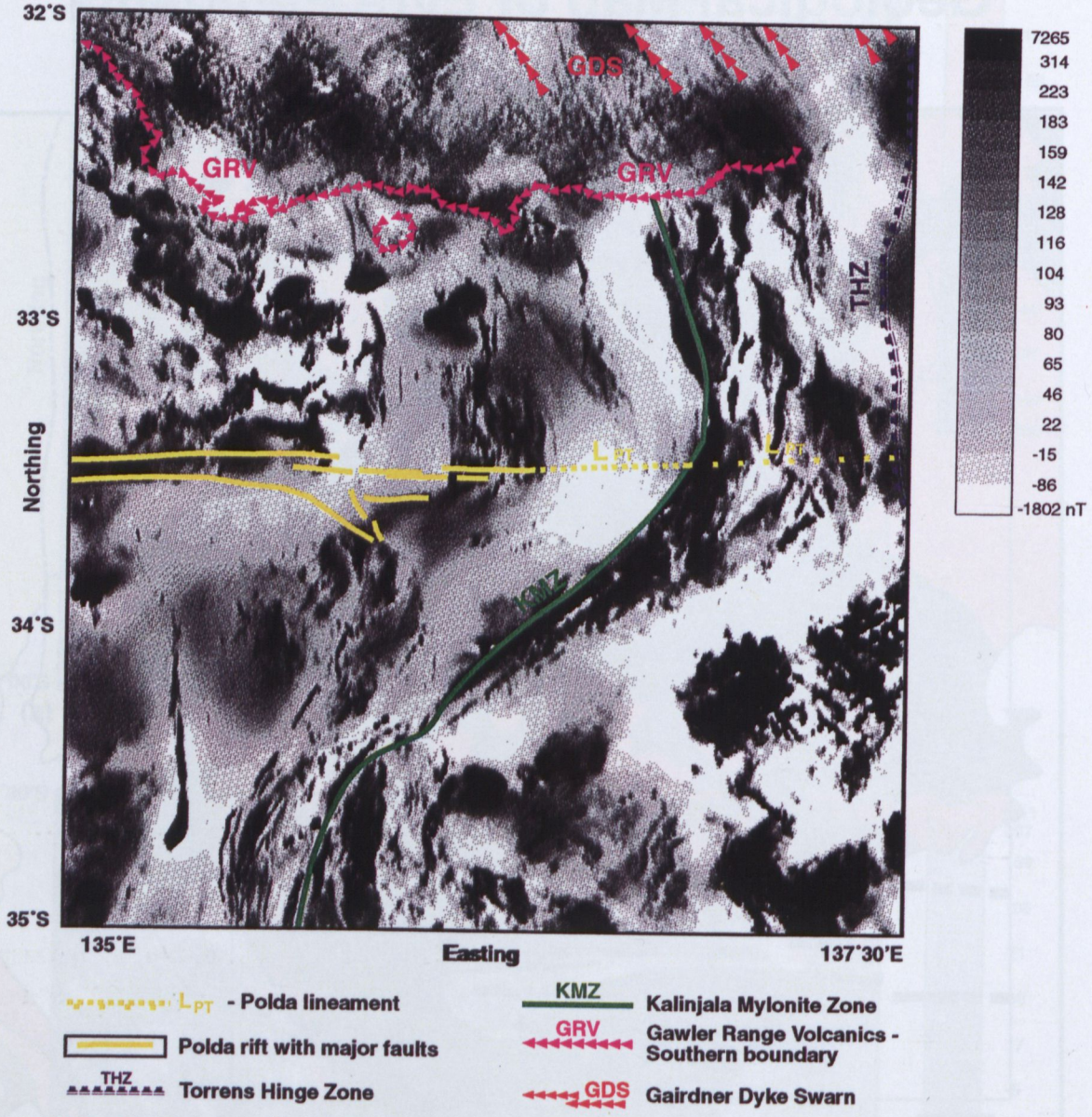

Figure 6.23 Grey image of residual magnetic field of SQ21 - 'λ <100km' with major tectonic features and observed magnetic boundaries.

km further east than the eastern-margin of the Polda rift. The lineament $L_{PT}^{<4km}$ truncates the NE-SW trending Kalinjala Mylonite Zone (*KMZ*) at the very eastern end of the '$\lambda < 15km$' map.

At the north-eastern corner of the residual field map '$\lambda < 15km$' run several linear north-west trending magnetic anomalies. These anomalies also appear on the surface magnetic maps and have been identified, by drilling, as subvertical, 30-50 m wide and up to 150 km long, mafic dykes of Mesoproterozoic age (the Gairdner Dyke Swarm; Goode, 1970; Gersteling and Maiden, 1975; Thomson et al., 1976; Rattigan et al., 1977; Parker et al., 1987).

The magnetic signature of the Gawler Range Volcanics (GRV) appears very clearly on the map '$\lambda < 15km$'.

6.5.2 The residual magnetic field of *SQ18* - '$\lambda < 25km$'

The *residual magnetic field of SQ18 with anomaly length* $\lambda < 25km$ *shows* a strong magnetic imprint of the Polda rift (Figure 6.19). The structural lineament $L_{PT}^{<4km}$, observed on the map of residual field '$\lambda < 15km$' marks a more prominent break in the pattern of anomalies.

The major structural features of the *SQ18* region, i.e. the Gairdner Dyke Swarm, Gawler Range Volcanics, and the Kalinjala Mylonite Zone, are very distinct.

Along longitude 134°50'S runs, across the whole *SQ18* over a distance of 240 km, the magnetic boundary B_{NS}. This is the same boundary which appears on the DMS_{50X50} of Figure 6.13 and on the map of the long wave-length magnetic field '$\lambda > 25km$' of Figure 6.15.

6.5.3 The residual magnetic field of *SQ18* - '$\lambda < 46km$'

The residual magnetic field of *SQ18* with $\lambda < 46km$ (Figure 6.20) shows a group of anomalies due to magnetic sources distributed within the 16 km thick upper crustal layer. The imprint of the Polda rift becomes more prominent than on the map '$\lambda < 25km$'.

6.5.4 The residual magnetic field of *SQ18* - '$\lambda < 64km$'

The map of the residual field '$\lambda < 64km$' presented in Figure 6.21, shows the NE-SW striking magnetic boundary B_{NE}^{SQ18} also observed on the previous residual map. In the south-western part of the '$\lambda < 64km$' map appears a new feature B_5, which runs for more than 50 km in the NE-SW direction. This magnetic boundary is clearly visible on the high resolution aeromagnetic maps of the Polda rift (see interpretation map in Figure 4.27).

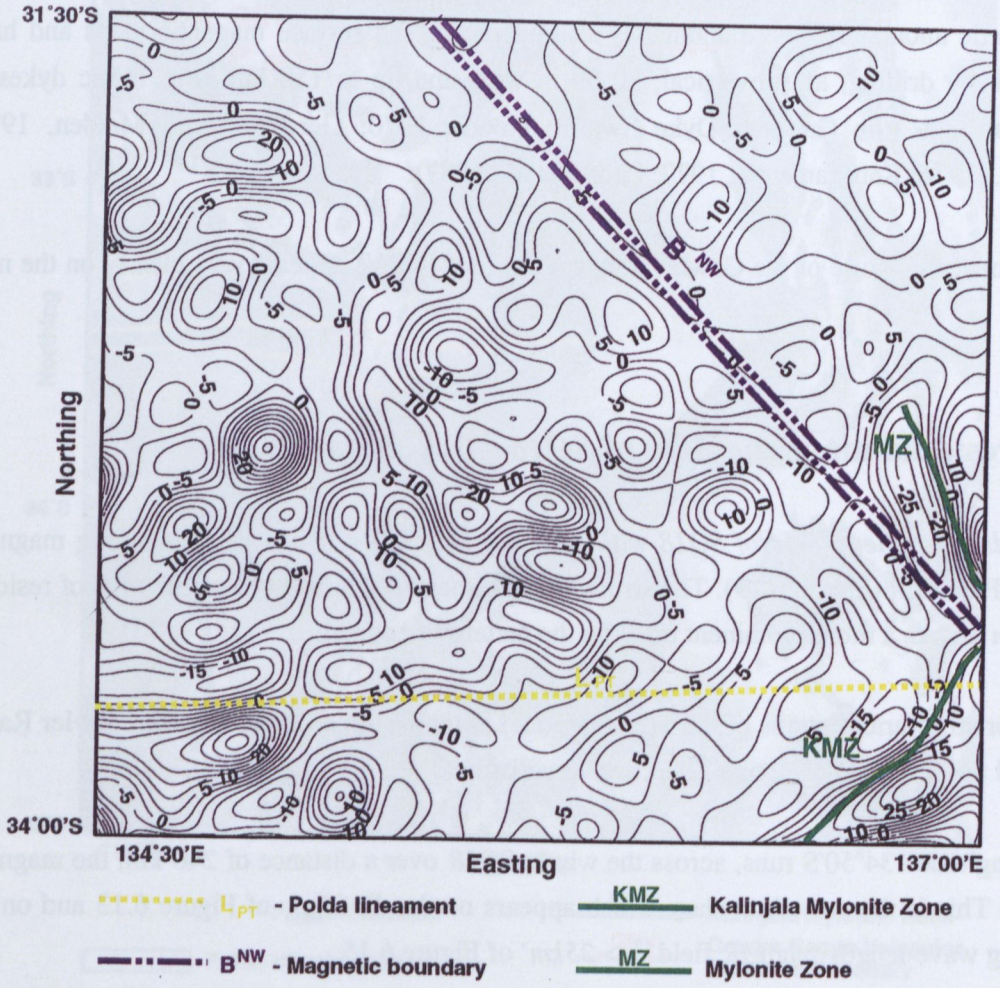

Figure 6.24 **Vertical gradient of filtered magnetic field of SQ18 - λ >25km'. Vertical gradient enlarged by a factor of 1000. Contour interval 0.005 nT/km.**

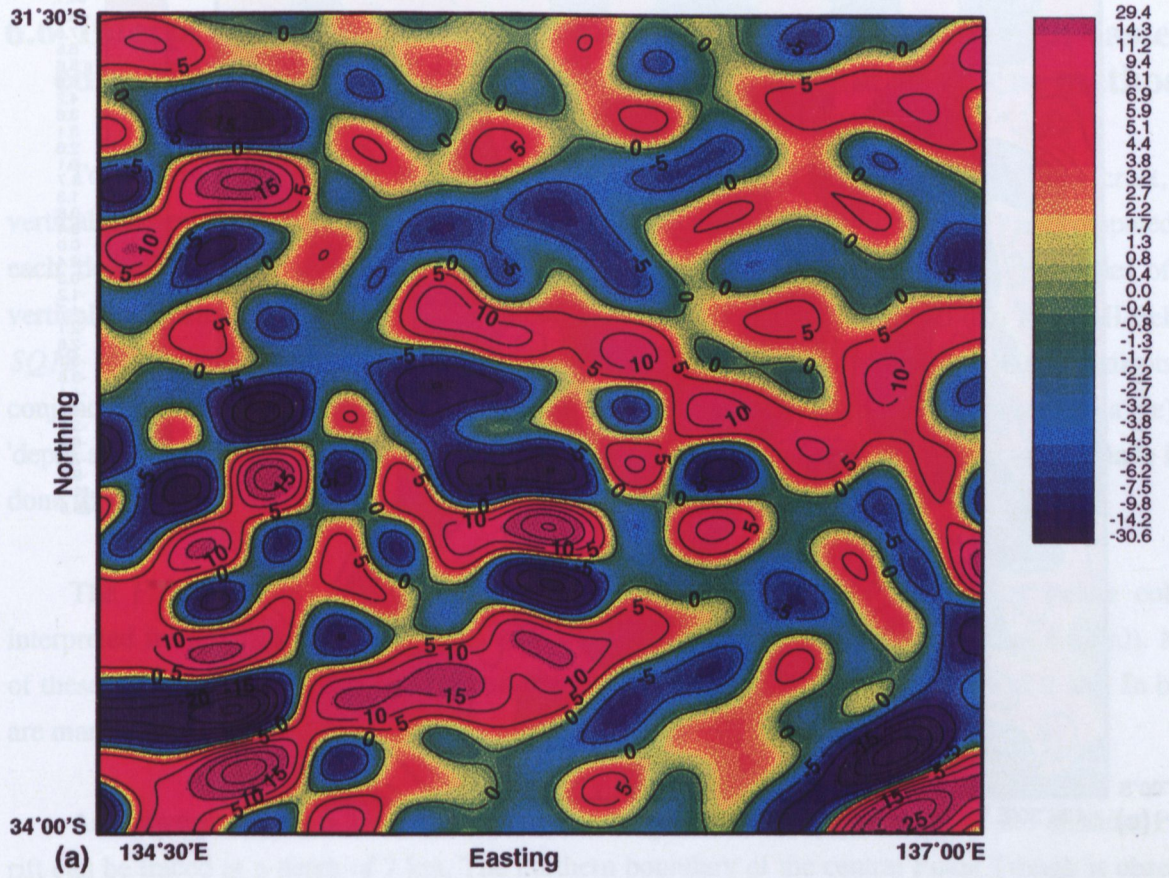

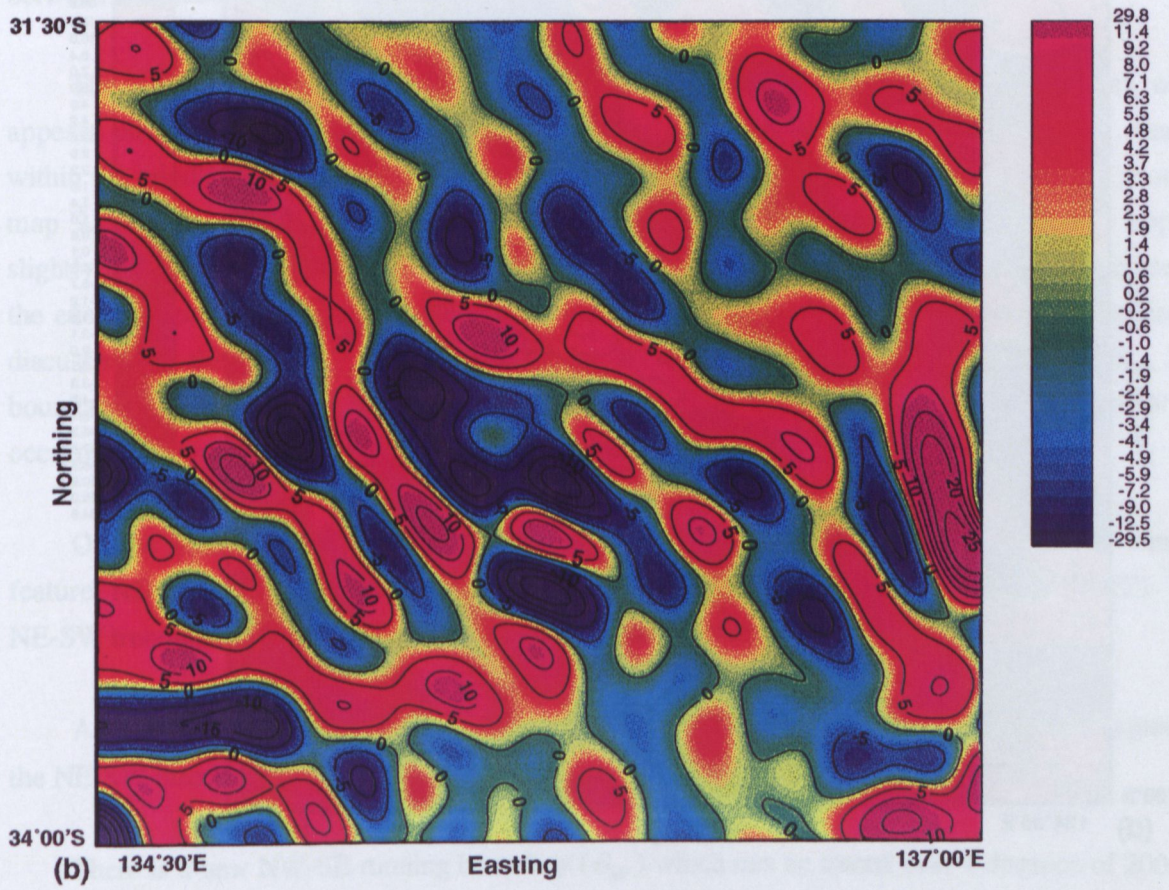

Figure 6.25 SQ18 - Horizontal gradient of low-pass filtered magnetic field 'λ>25km' computed at:

(a) azimuth of 0°

(b) azimuth of 45°

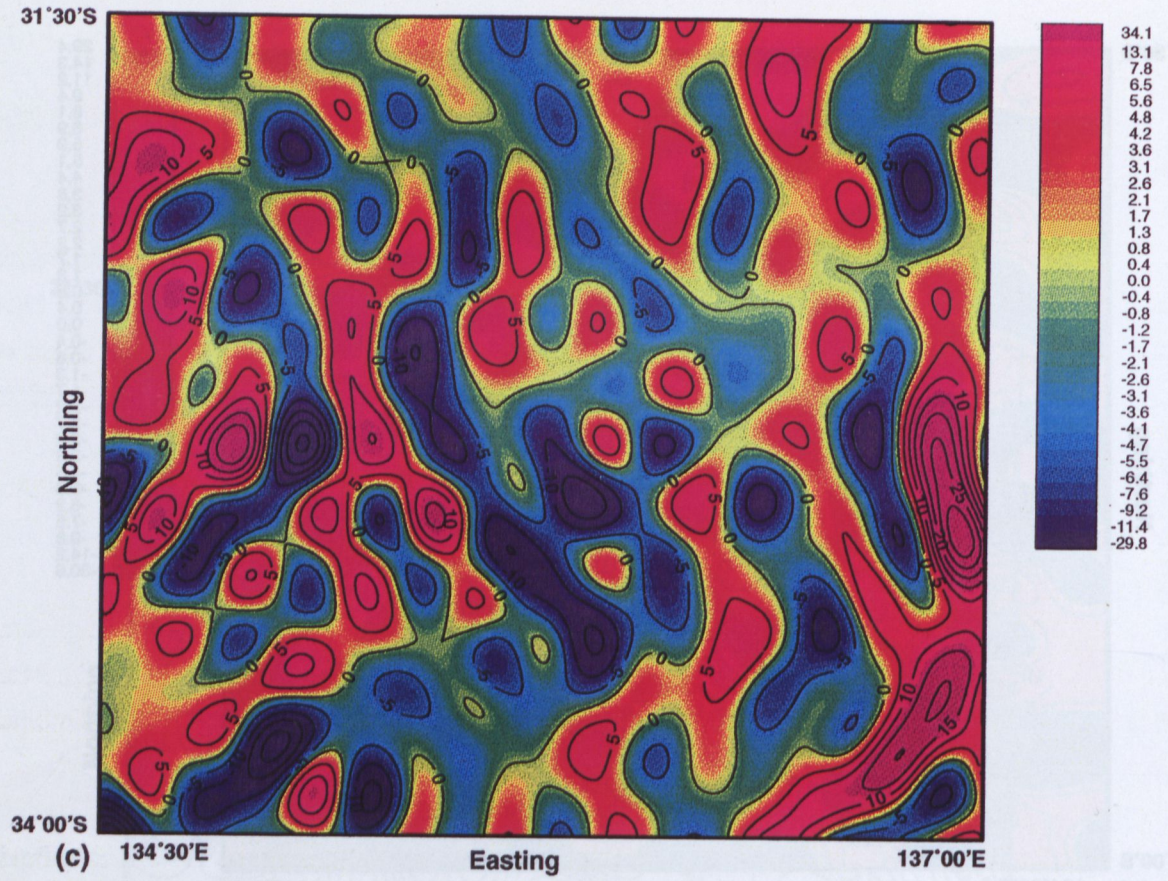

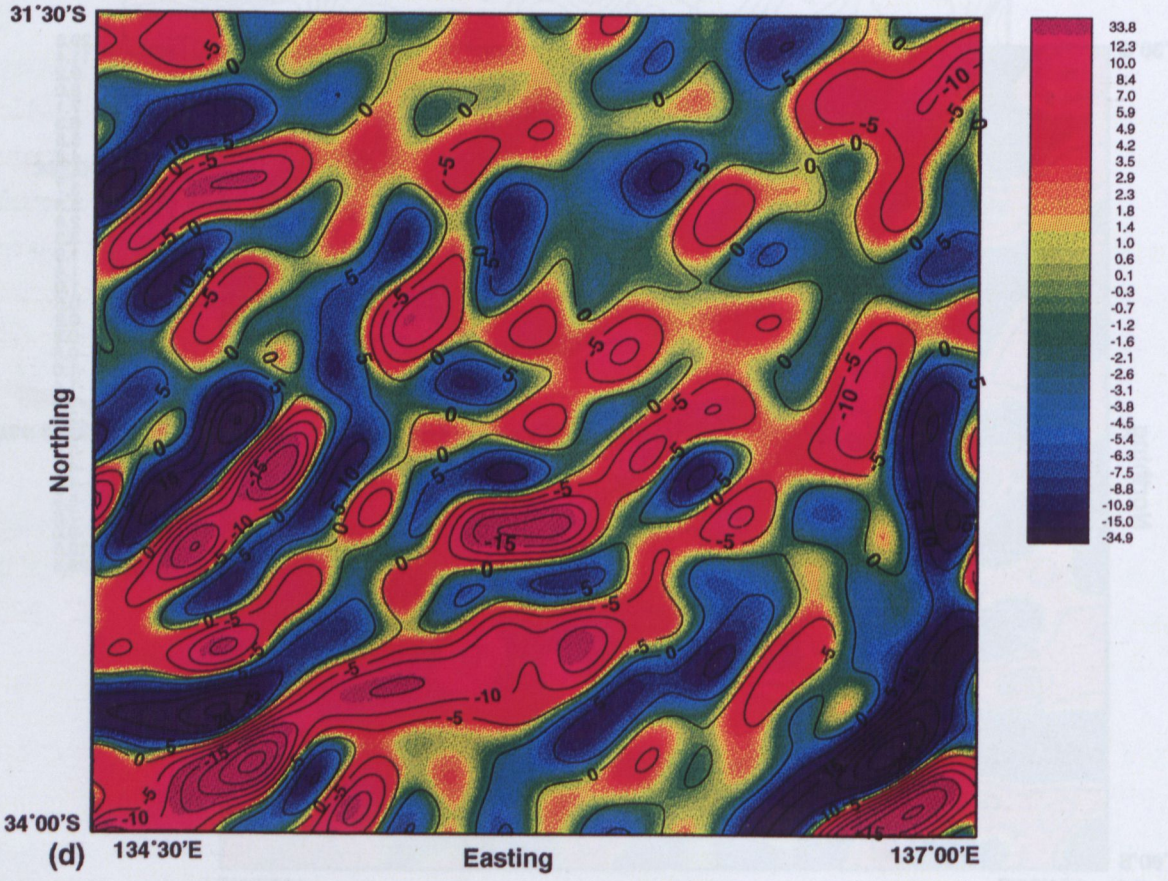

Figure 6.25 SQ18 - Horizontal gradient of low-pass filtered magnetic field 'λ>25km' computed at:

(c) azimuth of 90°

(d) azimuth of 135°

6.6 Interpretation of deep crustal structures of the south-eastern edge of the Gawler Craton using the horizontal gradient method

To analyse a distribution of large magnetic sources at different depths within the crust, the vertical gradient and the horizontal gradients in four directions: *0°, 45°, 90°* and *135°* are computed for each 'depth slice' map, i.e. for '$\lambda > 15km$', '$\lambda > 25km$', '$\lambda > 46km$' and '$\lambda > 64km$'. Examples of the vertical and horizontal gradients maps are included in Figures 6.24 and 6.25(a)-(d). The TMI field of *SQ18* was reduced to the pole. The results of interpretation of a set of horizontal gradients, in conjunction with a maximum value and the 'zero line' of the vertical gradient (Figure 6.26(a)-(e)) of 'depth slice' map '$\lambda > 25km$' are presented in Figure 6.27. The analyses and interpretation have been done for all 'depth slice maps'.

The Figure 6.27(b) shows outlines of the magnetic boundaries and bodies (white colour) interpreted from the group of anomalies with wave-length greater than 25 km (Figure 6.27(a)). Most of these anomalies are reflecting the crust's magnetic inhomogeneity below a depth of 7 km. In black are marked surface-mapped major faults of the Polda rift.

As shown in Figure 6.27(b) the east-west oriented southern fault-margin of the offshore Polda rift can be traced at a depth of 7 km. The northern boundary of the central Polda Trough is observed between longitudes *134°50'E* and *135°30'E*.

The N-S trending magnetic boundary (B_{NS}) at longitude *135°E* (easting of 200-220 gc), which appears on the 'low-pass' frequency map '$\lambda > 25km$' and also on the '$\lambda > 46km$' reflects changes within the middle crust, and does not appear on the surface TMI map or long wave-length anomaly map '$\lambda > 64km$'. On the deep magnetic sources map $DMS_{25\times25}$ (Figure 6.12) this boundary appears slightly towards the east, along longitude *135°15'E*. This is possibly due to the window size used in the energy spectrum analysis or could be an indication of an easterly dipping structure. As already discussed, on the $DMS_{25\times25}$ map changes occur is 'depth-polarity' along the boundary B_{NS}. This boundary may be a major N-S oriented deep crustal fault along which strike slip movement has occurred; this would account for the switch in 'depth-polarity'.

On the southeastern corner of the map shown in Figure 6.27(b), there is a NE-SW trending feature, reflecting deep crustal structure associated with the Kalinjala Mylonite Zone (*KMZ*). This NE-SW trending feature was also detected at the shallower depth.

A central ridge of the *HML* (CR_{HML}) is indicated by a 50 km long magnetic source, elongated in the NE-SW direction.

There is a new NW-SE running boundary (B_{NW}) which can be traced over a distance of 200 km, indicated by a dotted line in Figure 627(b). The boundary B_{NW} is very distinct on the vertical gradient of '$\lambda > 25km$' map presented in Figure 6.24.

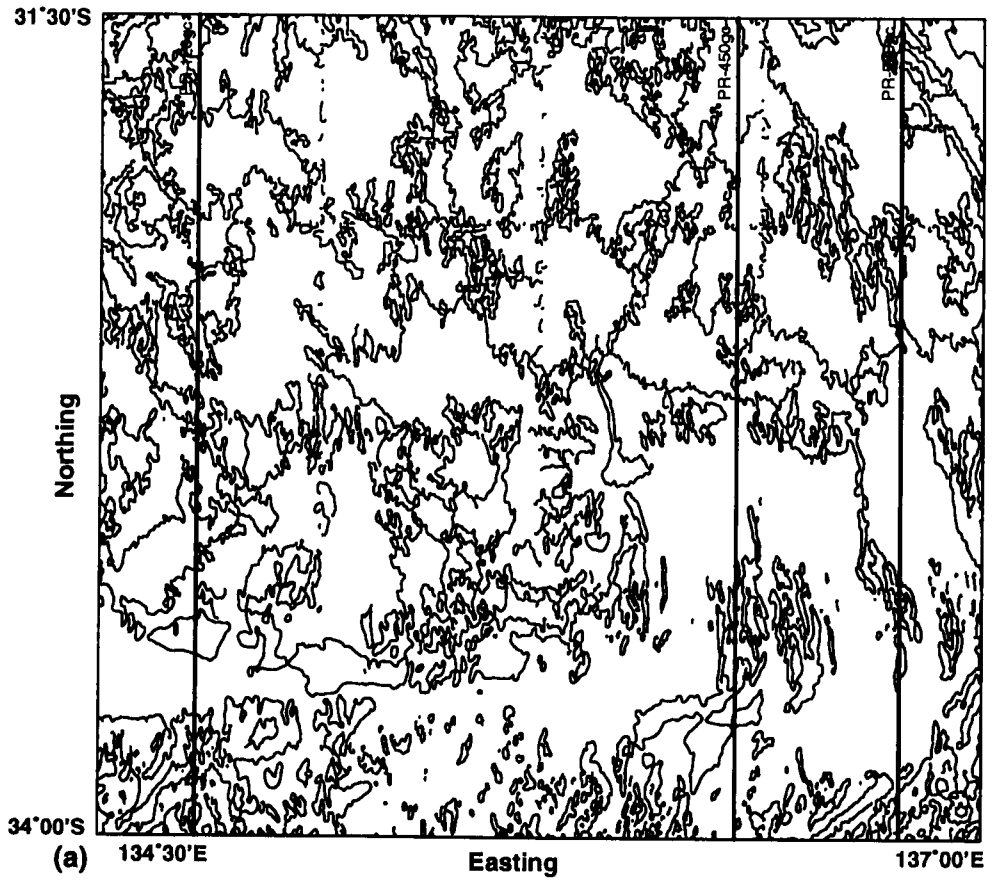

Figure 6.26 SQ18 - Location of the north-south crustal cross-sections presented in Figure 6.28 which are superimposed on the contour of the'zero line' of the vertical gradient of:

(a) total magnetic intensity field reduced to the pole

(b) long wavelenght magnetic anomalies - 'λ>15km'

(c) long wavelenght magnetic anomalies - 'λ>25km'

(d) long wavelenght magnetic anomalies - 'λ>46km'

(e) long wavelenght magnetic anomalies - 'λ>64km'.

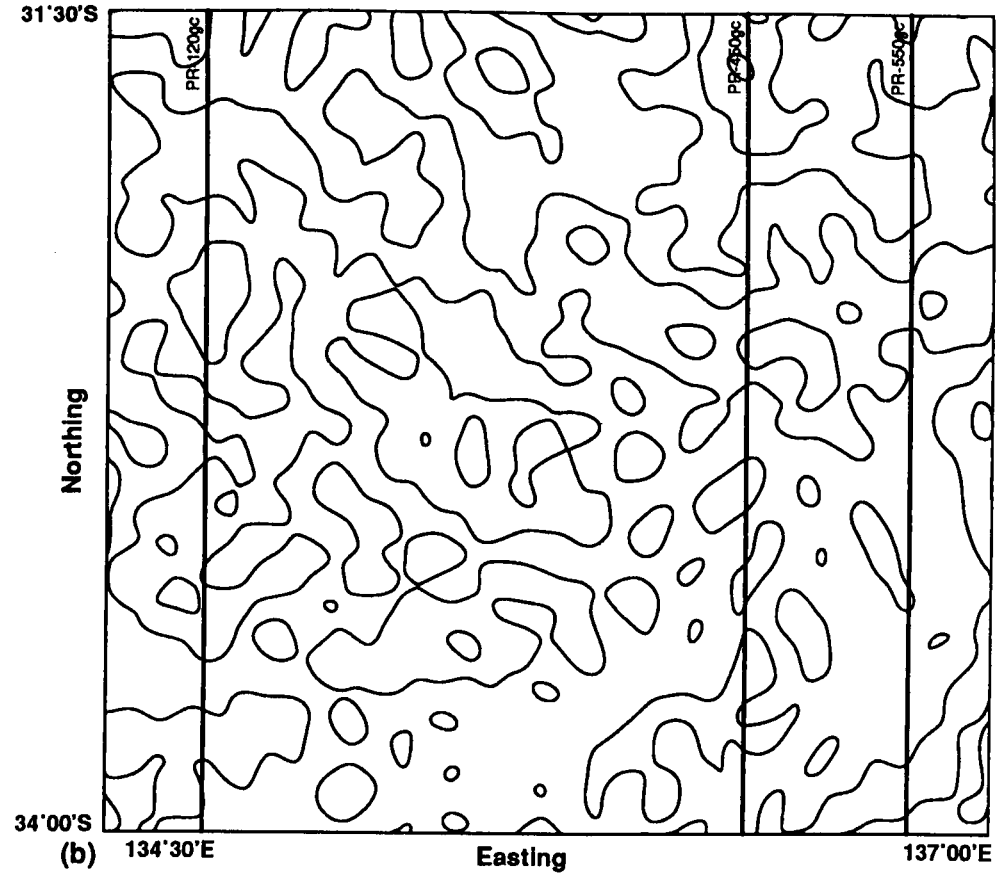
31°30'S
PR-120gc
PR-450gc
PR-550gc
Northing
34°00'S
(b)
134°30'E
Easting
137°00'E

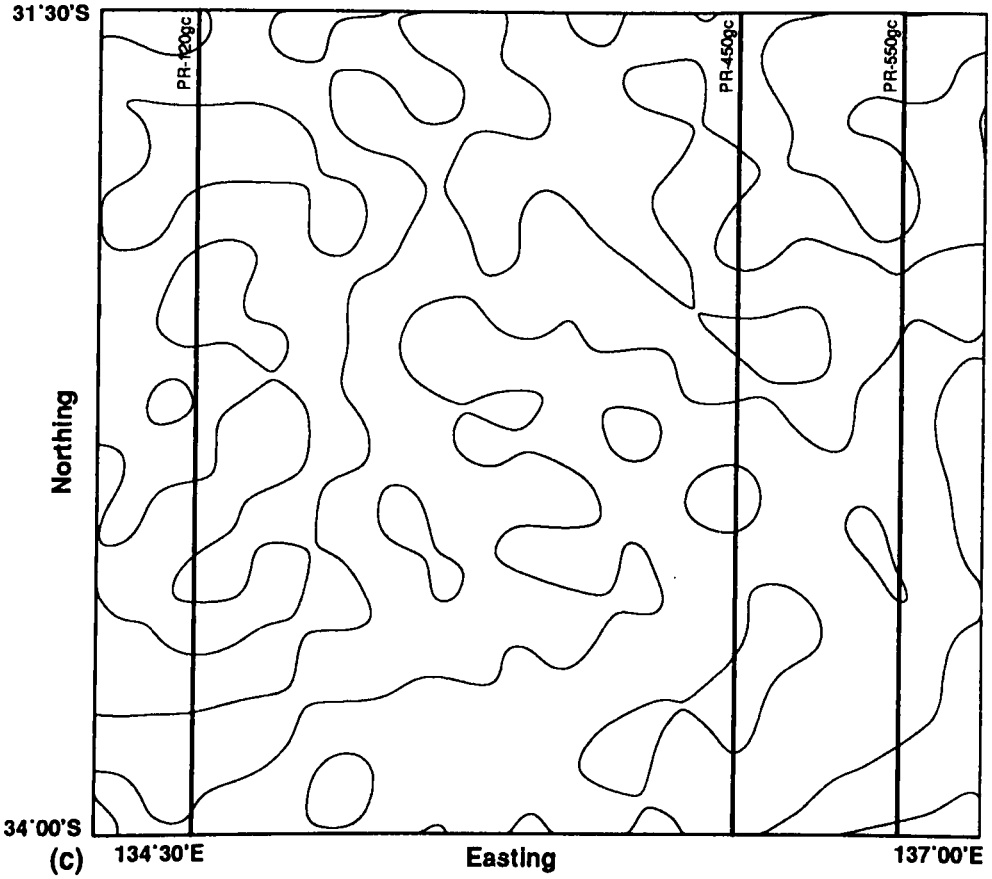
31°30'S
PR-120gc
PR-450gc
PR-550gc
Northing
34°00'S
(c)
134°30'E
Easting
137°00'E

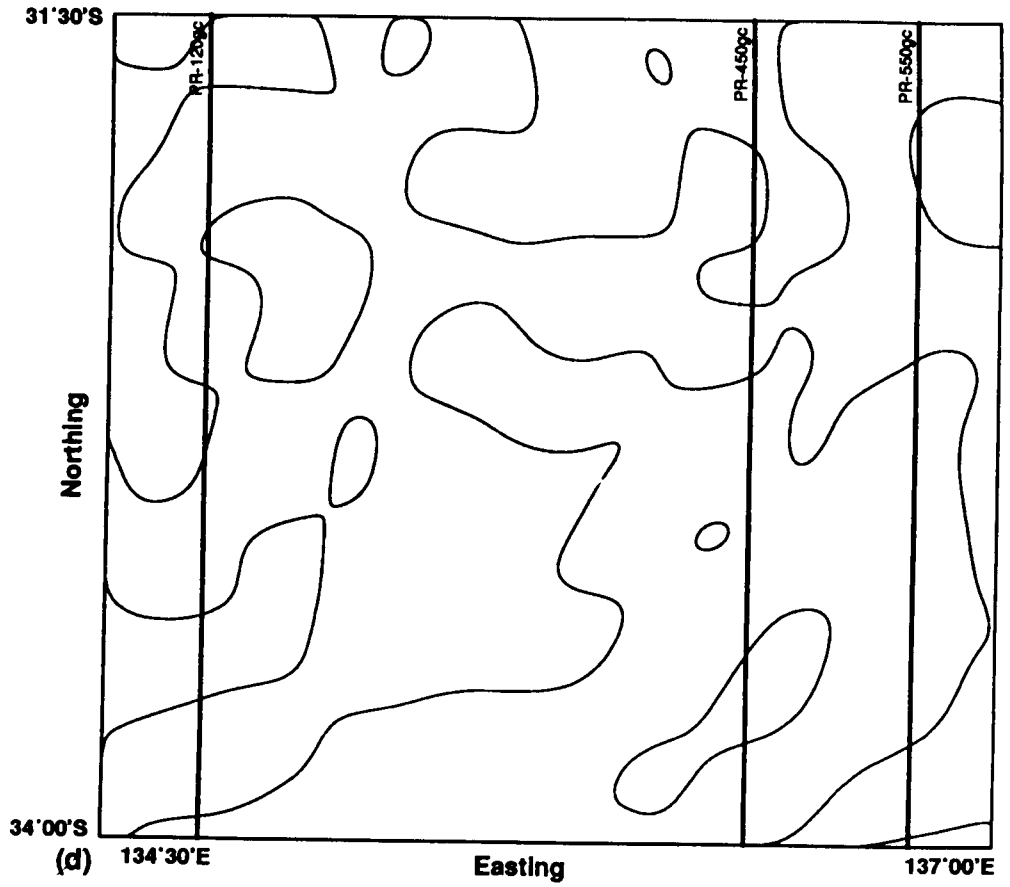
31°30'S
PR-120gc
PR-450gc
PR-550gc
Northing
34°00'S
(d)
134°30'E
Easting
137°00'E

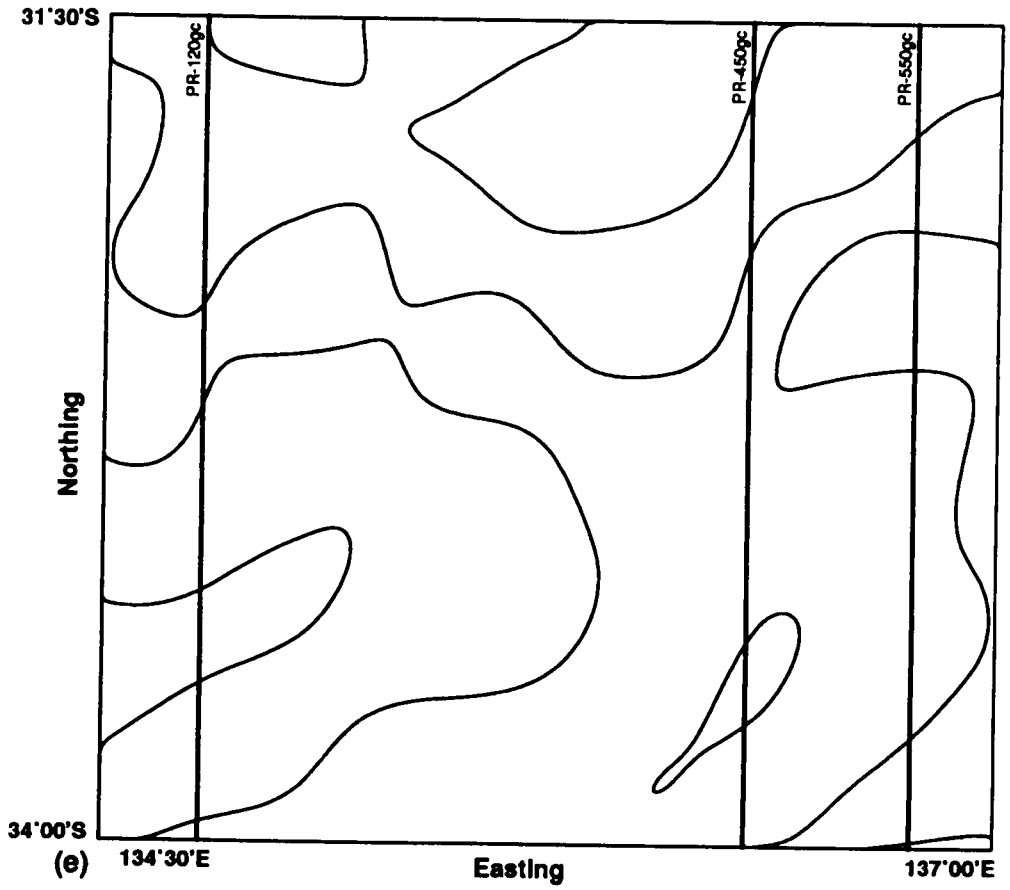
31°30'S
PR-120gc
PR-450gc
PR-550gc
Northing
34°00'S
(e)
134°30'E
Easting
137°00'E

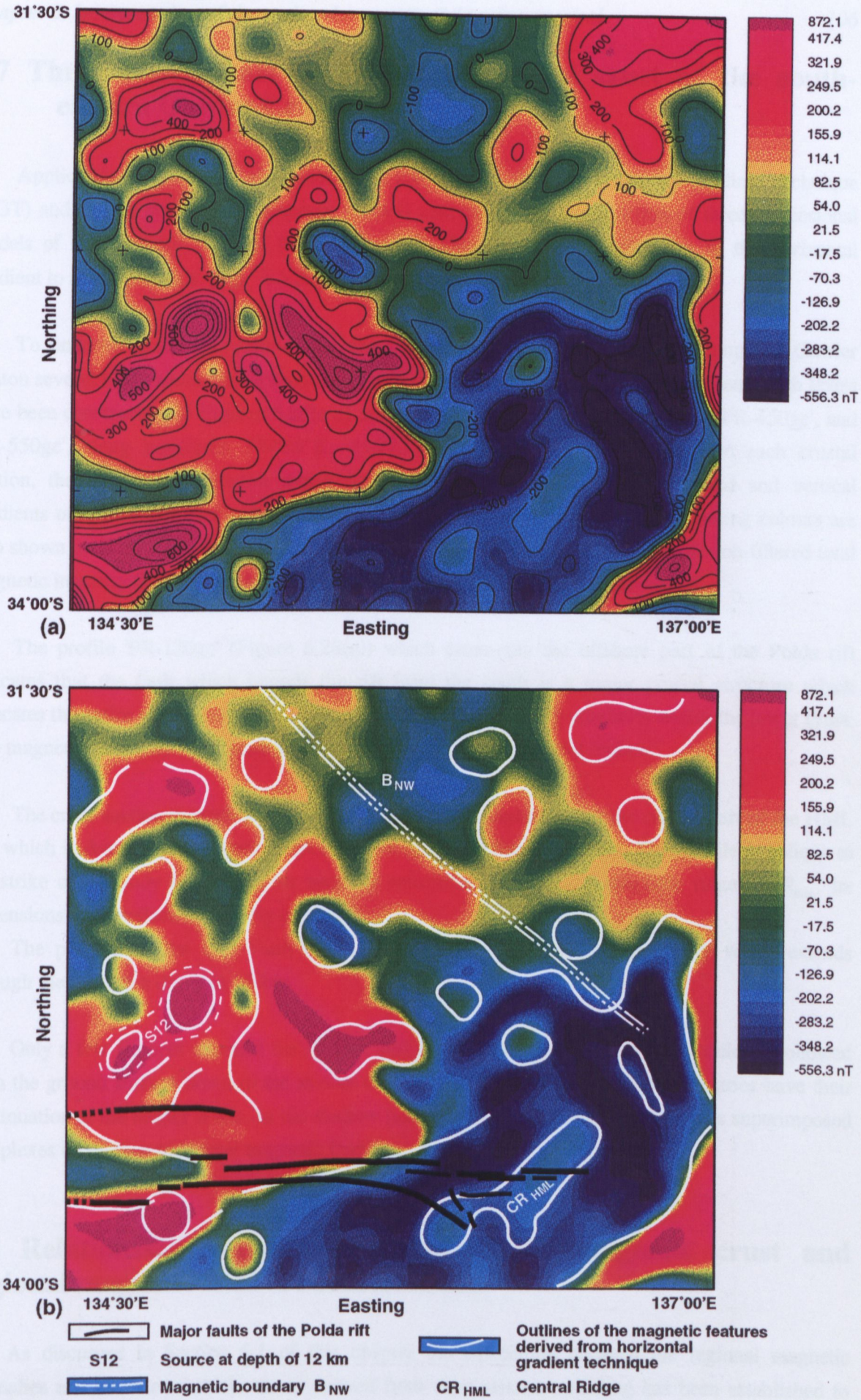

Figure 6.27 Long wavelength magnetic anomaly map of SQ18 - '$\lambda > 25$km':
(a) colour image with contours,
(b) colour image with outlines of the magnetic features interpreted based on the horizontal gradient technique.

6.7 Three dimensional model of magnetised crust of the south-eastern Gawler Craton.

Application of the 'depth slice' method in combination with the 'horizontal gradient' technique (HGT) and results obtained from energy spectral analysis enable construction of three dimensional models of the magnetic crust of the south-eastern Gawler Craton. Application of the horizontal gradient to the 'depth slice' map '$\lambda > 25km$' is illustrated in this section.

To understand the character of the crust underlying the Polda rift and surrounding Gawler Craton several north-south crustal sections showing magnetic boundaries at four different depth levels have been constructed. In Figures 6.28(a-c) are presented three profiles: 'PR-120gc', 'PR-450gc', and 'PR-550gc', along longitudes $134°36'E$, $136°15'E$ and $136°45'E$ respectively. On each crustal section, the magnetic boundaries which have been interpreted from the horizontal and vertical gradients of four 'depth slice' maps are marked in different colours. In the corresponding colours are also shown profiles of the four long-wave length magnetic fields. In red is shown the non-filtered total magnetic intensity field along each of the profiles (TMI with subtracted mean value).

The profile 'PR-120gc' (Figure 6.28(a)) which cross-cuts the offshore part of the Polda rift indicates that the fault which bounds the rift from the south is a major crustal structure which truncates the entire weakly magnetic upper crustal layer and possibly continues within the lower crust. The magnetic boundary B_3 appears to be a very prominent deep crustal feature.

The cross-section through the magnetic body which is located within the central part of the HML and which is detected at all depth levels is shown on the profile 'PR-450gc'. This profile is oblique to the strike of the body and causes an anomaly referred to as a central magnetic ridge CMR_{HML}. Its dimensions are therefore not clearly indicated.

The position of the Uno Fault coincides with the very prominent boundary which extends through the crust to a depth of 31 km.

Only a few features intersect the shallow and deeper crust: several interfaces could be followed from the ground surface down to the middle crust. Often it is not clear which boundaries have their continuation at the deeper levels, as the shallow layer of the crust consists of numerous superimposed complexes of smaller and larger magnetic bodies.

6.8 Relationship between thickness of the magnetic crust and regional magnetic field in South Australia

As discussed in Section 6.1 of this chapter the correlation between the regional magnetic anomalies and the crustal thickness as derived from deep seismic sounding has been established to exists for the Ukrainian Shield (Krutikhovskaya and Pashkevich, 1977), the Baltic Shield (Krutikhovskaya, 1976), the western part of the Canadian Shield (Hall, 1974), and appears to be present under the Indian subplate (Atchuta Rao, 1992). These relationships (Figures 6.3-6.7)

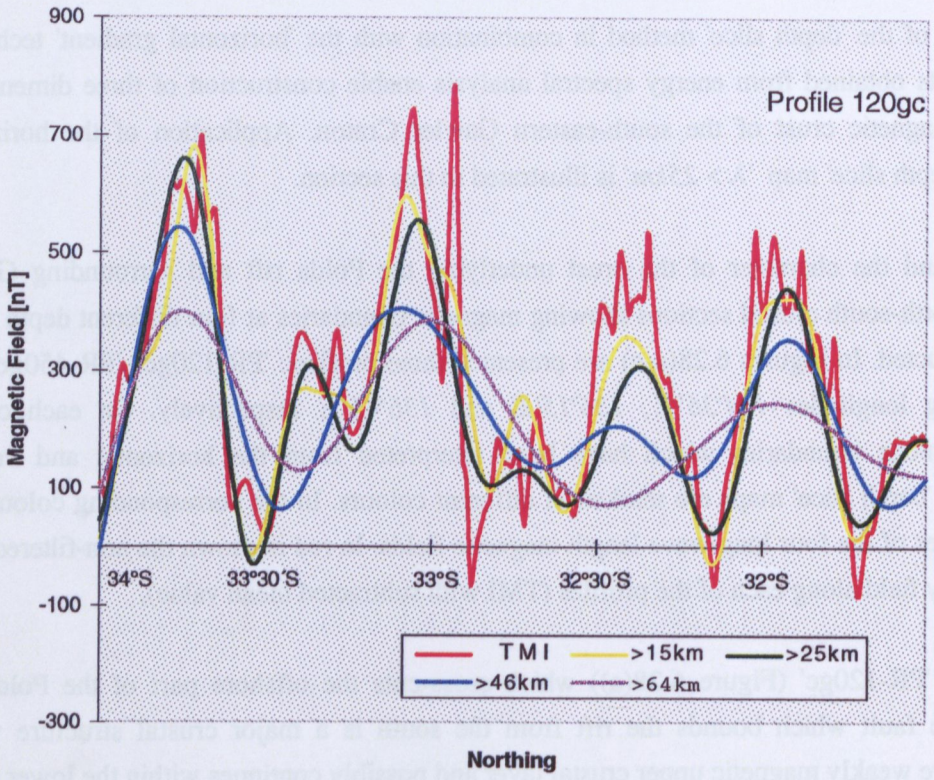

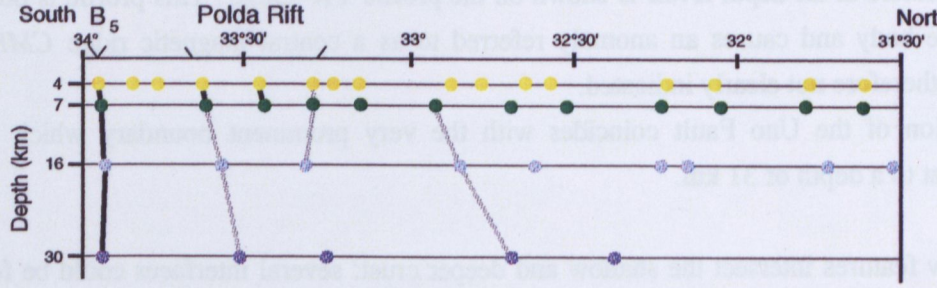

Figure 6.28(a) South-eastern Gawler Craton: Crustal cross-section PR-120gc/134°36'E.
(i) TMI and low-pass filtered magnetic field: 15km, 25km, 46km, 64km.
(ii) Magnetic boundaries inferred from the interpretation of 'depth slice' maps using horizontal gradient technique.

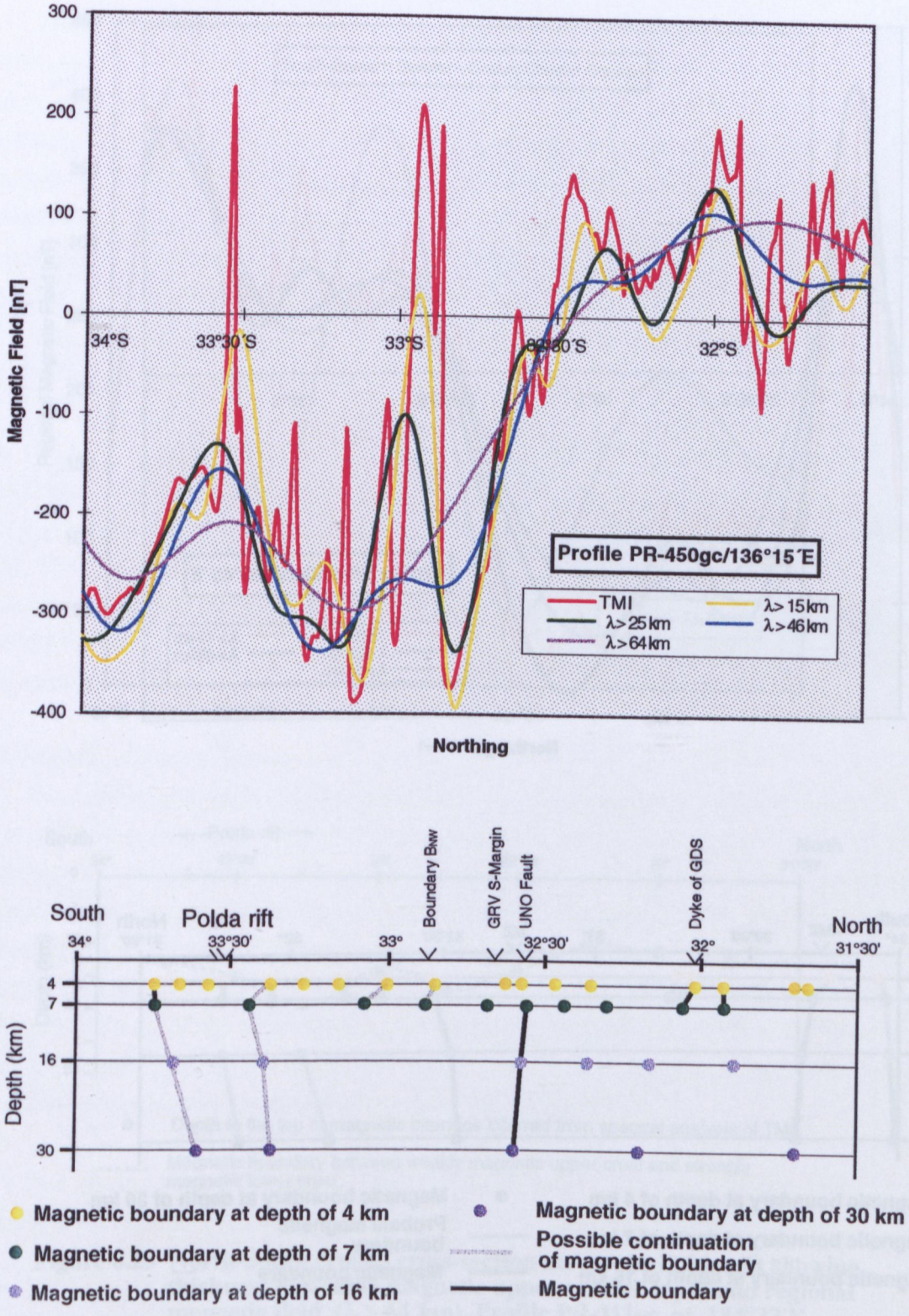

Figure 6.28 (b) North -South crustal cross-section: PR - 450gc at 136° 15' E.

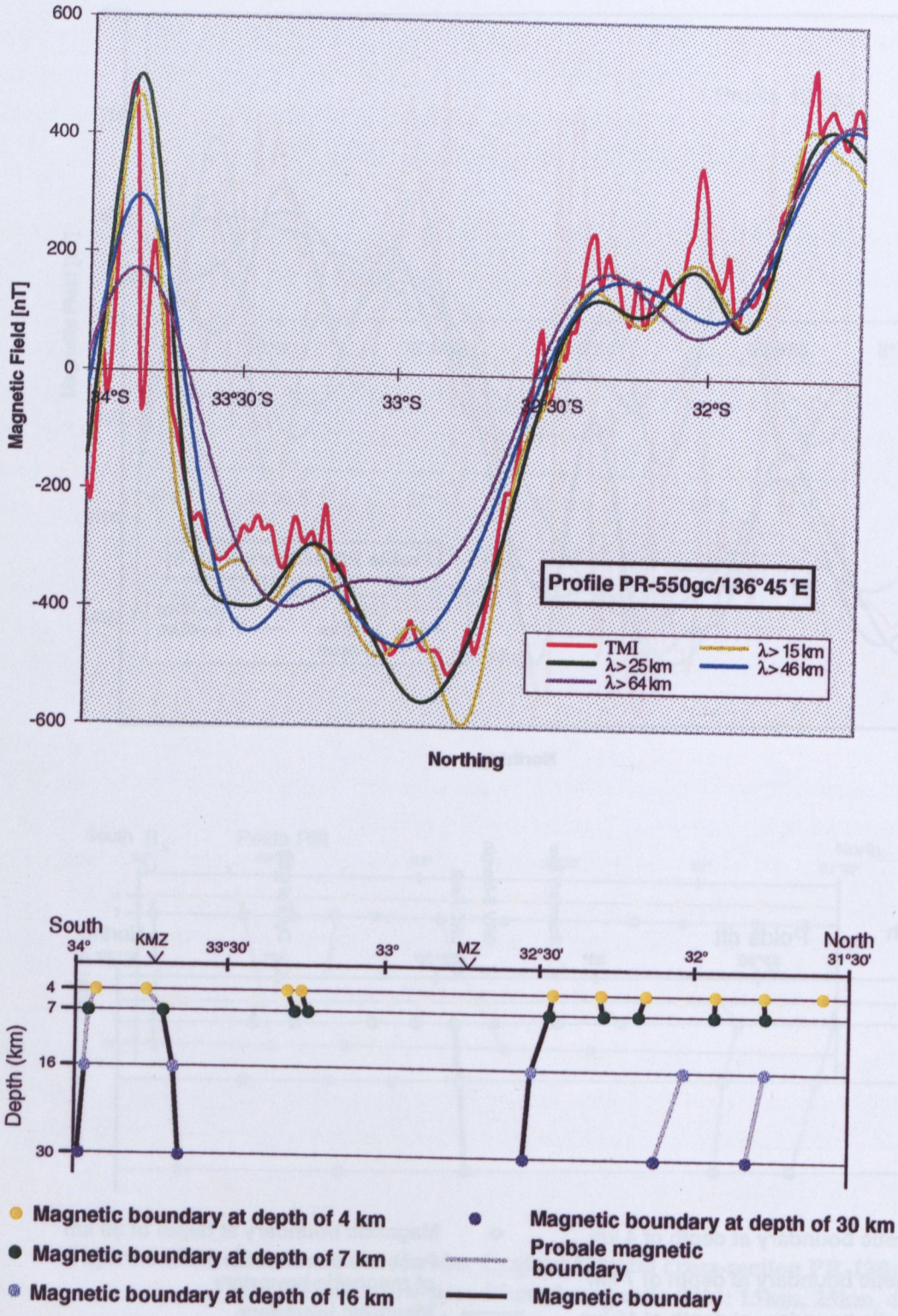

Figure 6.28(c) North -South crustal cross-section: PR - 550gc along 136° 45' E.

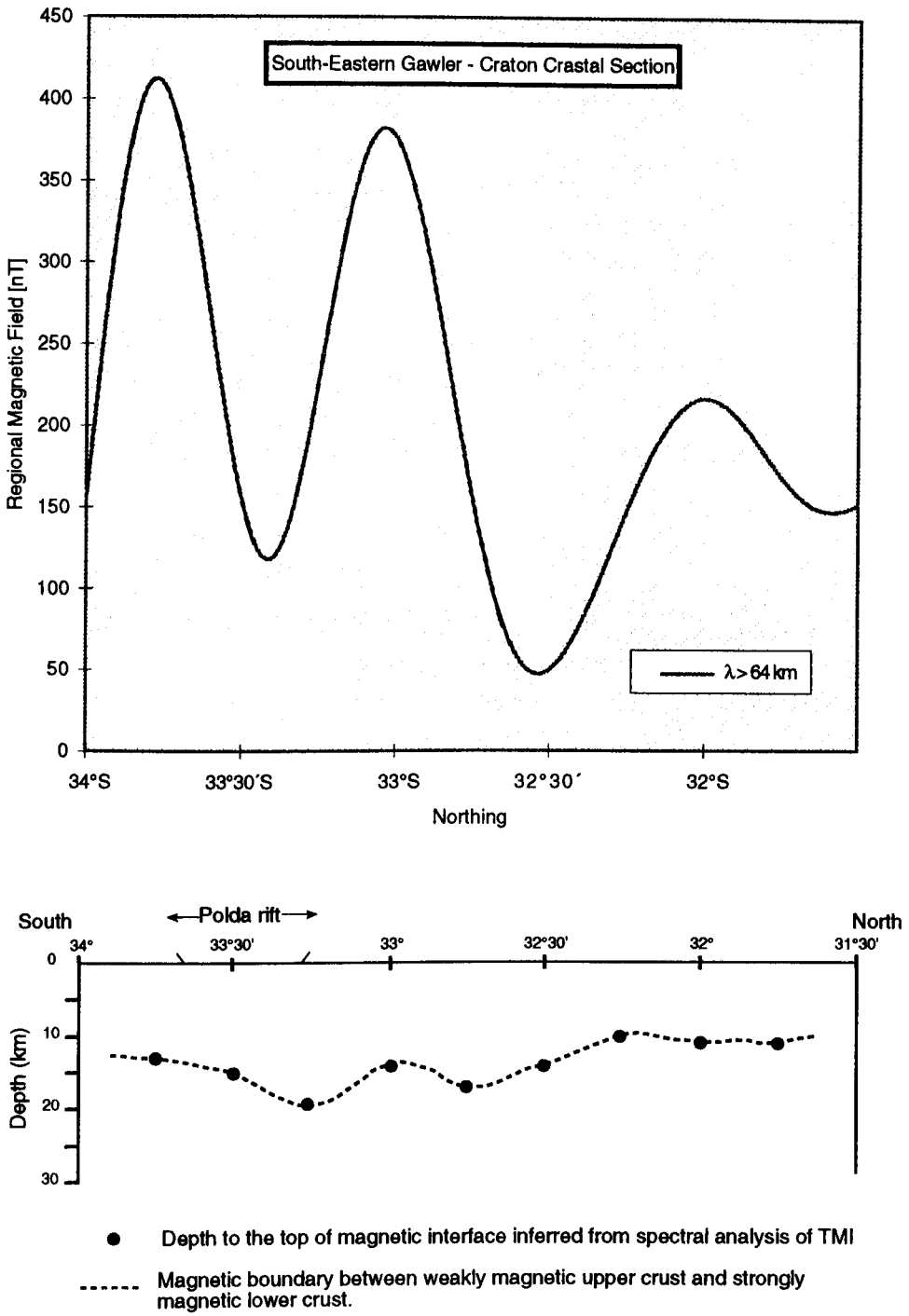

Figure 6.29 North-South crustal cross-section across the Polda rift showing thickness of weakly magnetic upper crustal layer and regional magnetic field ($\lambda > 64$ km). Profile PR-111gc at 134°32'E.

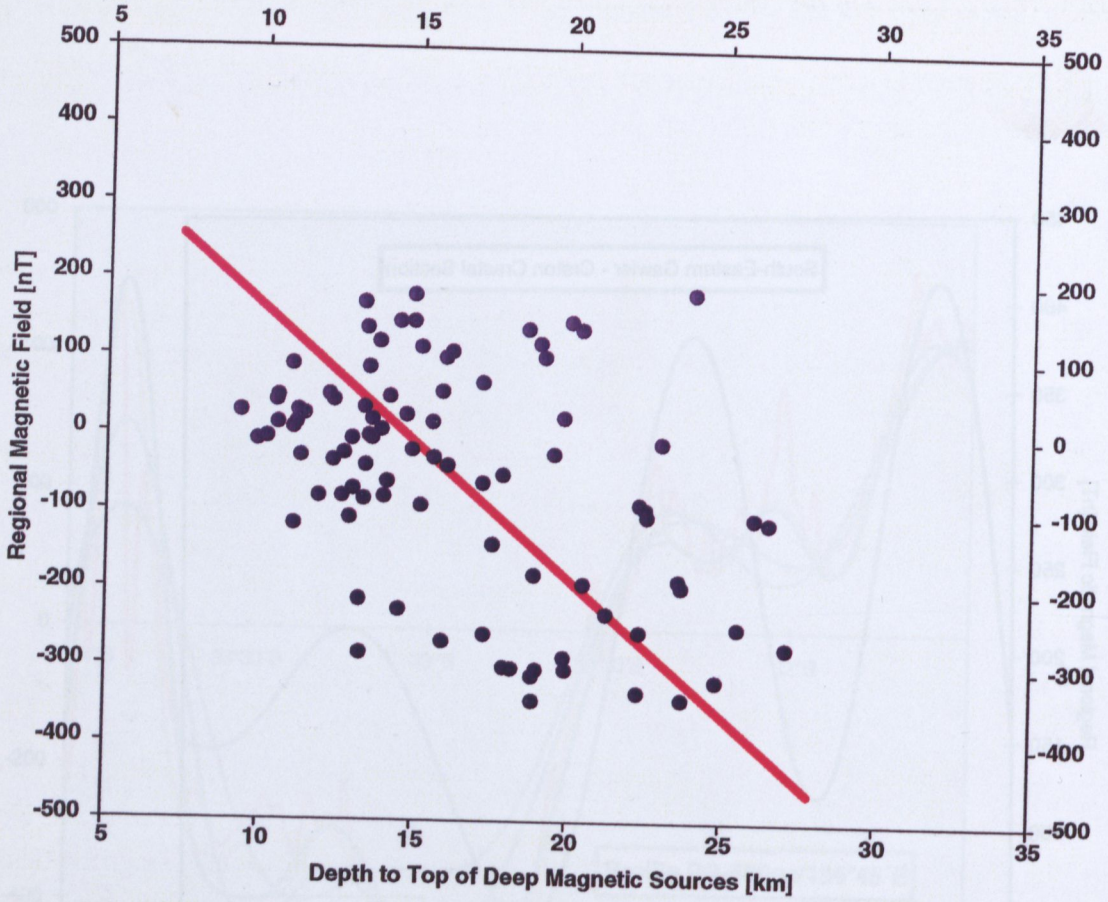

Figure 6.30 Statistical correlation between thickness of upper crustal layer and regional magnetic field at 10 km in southeastern Gawler Craton (SQ18).

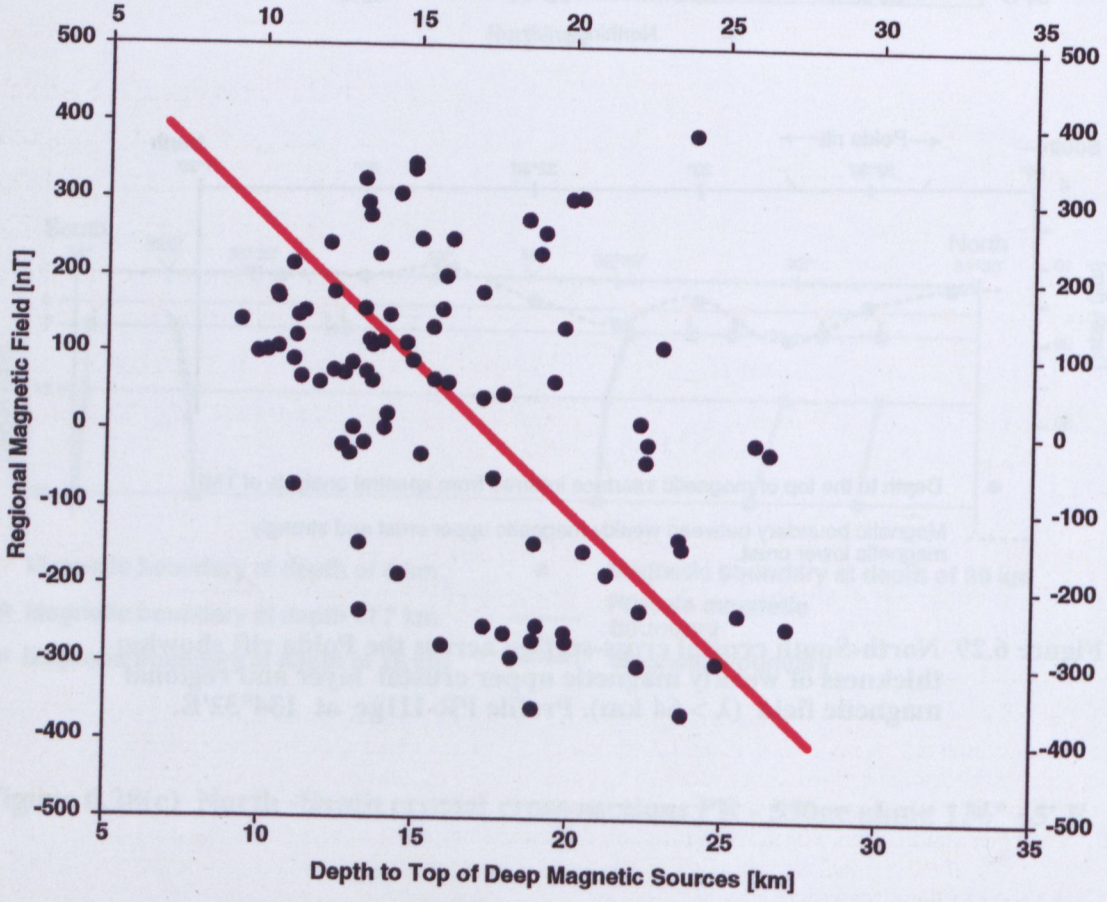

Figure 6.31 Statistical correlation between thickness of upper crustal layer and regional long-wave length magnetic anomaly field, 'λ >64km' across an area of SQ18.

generalise characteristic of magnetisation for the earth's crust and point to similarity of average magnetisation for the crust under cratonic regions.

Results obtained by Hall (1974) and those presented by Krutikhovskaya and Pashkevich (1977, 1979) suggest that a similar correlation may exists for the crust underlying the Polda rift. However, the crustal thickness could not be determined by deep seismic sounding as none exist in the area, the thickness of the crust had to be established in another way and the method chosen was energy spectral analysis of the TMI field (Figure 6.29). Moreover, to obtain additional confirmation of the relationship between the thickness of upper crust established by spectral analysis and the regional component of the magnetic field, the comparison between the Polda rift and Adelaide Geosyncline which is major rift structure has been done.

(i) South-eastern Gawler Craton

The thickness of the weakly magnetic upper crustal layer established from the energy spectral analysis of TMI using *50km x 50km* 'moving window' is shown at the $DMS_{50\times50}$ map, Figure 6.13. The thickness of the weakly magnetic upper crust is plotted versus average values of the long wave-length magnetic field '$\lambda > 64km$' in Figure 6.30 and versus 10 km upward continued field in Figure 6.31. The statistical correlation between thickness of the upper crust and regional magnetic field for both cases shows a linear character with negative slope. Similar results for the upper crust were found by Hall (1974) for the Canadian Shield, where thickness of the upper crustal layer was derived by deep seismic sounding.

(ii) Adelaide Geosyncline

To establish relation between regional field component and crust thickness under the Adelaide Geosyncline magnetic field was upward continued to 10 km to filter out high frequency component (Figure 6.32). As presented in Chapter 5 the thickness of the weakly magnetic upper crustal layer under the Adelaide Geosyncline has been detected by the energy spectral analysis using *60km x 60km* 'moving window' (Figure 5.30). The average values of the magnetic field at 10 km were computed for each of the spectral windows. Figure 6.33 shows statistical correlation between regional magnetic field and thickness of the upper crustal layer under the Adelaide Geosyncline. The obtained results show linear trend with negative slope ($35 - 40\eta$ *T/km*). Similar statistical relationship was found for the south-eastern Gawler Craton where the Polda rift is located.

This justifies that, Hall's (1974), Krutikhovskaya's and Pashkevich's (1977, 1979) conclusions about average magnetic field and crustal thickness can be applied to the Polda rift area[2].

---

[2] **Note:** The relationship between crustal thickness obtained from spectral analysis of TMI and intensity of regional magnetic field for both rift zones: Polda rift and Adelaide Geosyncline, which shows a linear trend is not simple to define, as both parameters are derived from the same observation. Graphs shown in Figures 6.30-6.31 and in Figure 6.33 include regression lines which are not properly mathematically described, as the direction of minimization is not simple to define. The regression lines have been fitted based on the assumed errors (Ludwig, 1980): 10% for crustal thickness and 1% for intensity of the regional magnetic field. Presented in Figures 6.30-6.31 and 6.32 graphs are result of a purely statistical approach to the discussed relationship, and using Ludwig's algorithm. The observed data-scatter could be reduced by elimination of certain data points. Such data-points are for example due to contamination of the low frequency zone in the energy spectrum by large and shallow magnetic bodies. However, this will not be addressed here. It will be a question to resolve in the future.

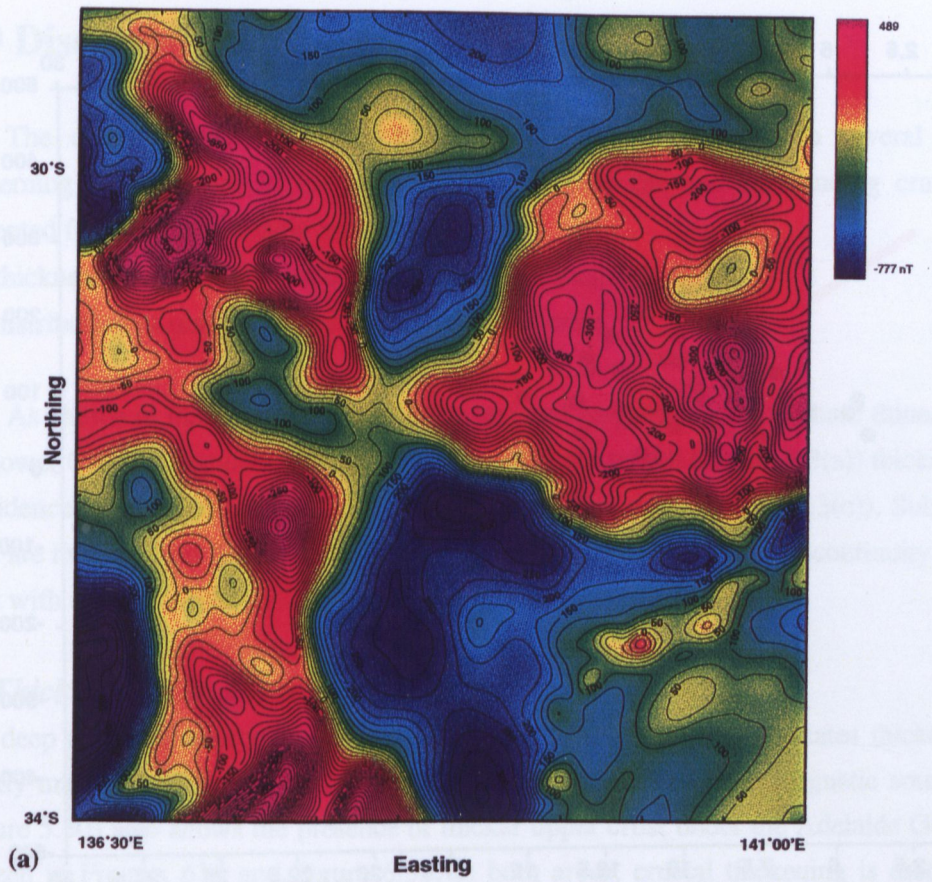

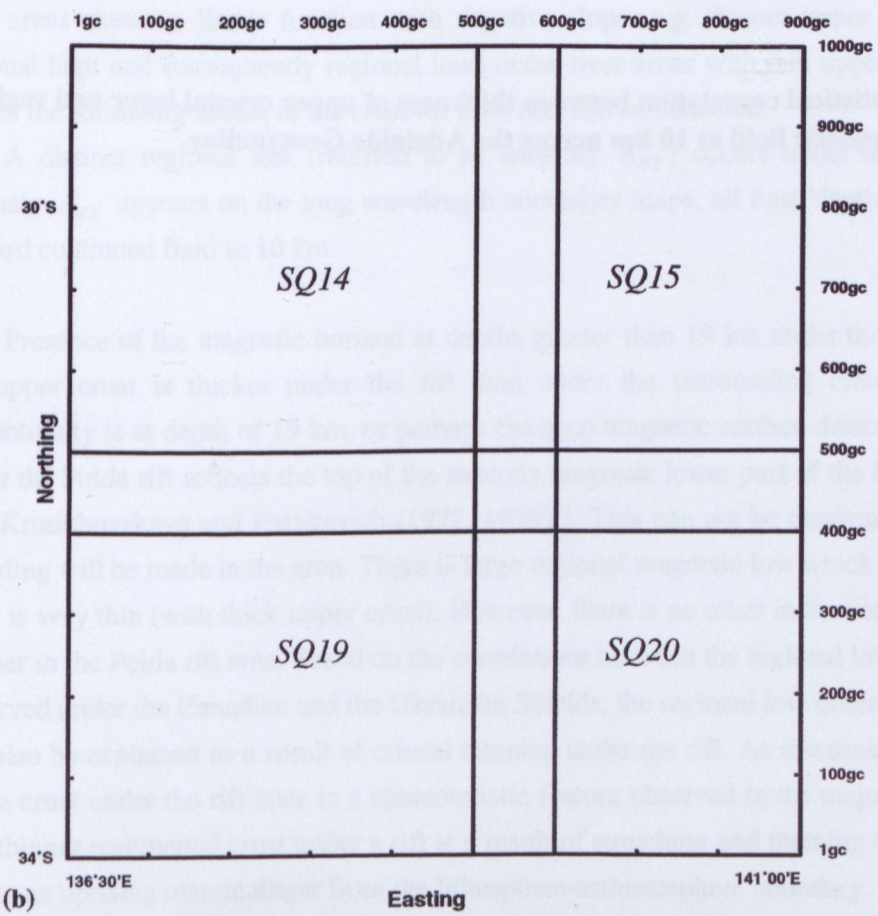

Figure 6.32 Adelaide Geosyncline - (a) Colour image with contours at 25nT interval of magnetic field upward continued to 10km. (b) Location plan of four blocks: SQ14, SQ15, SQ19 and SQ20. 1gc equals approximately 500 metres or 0.005°.

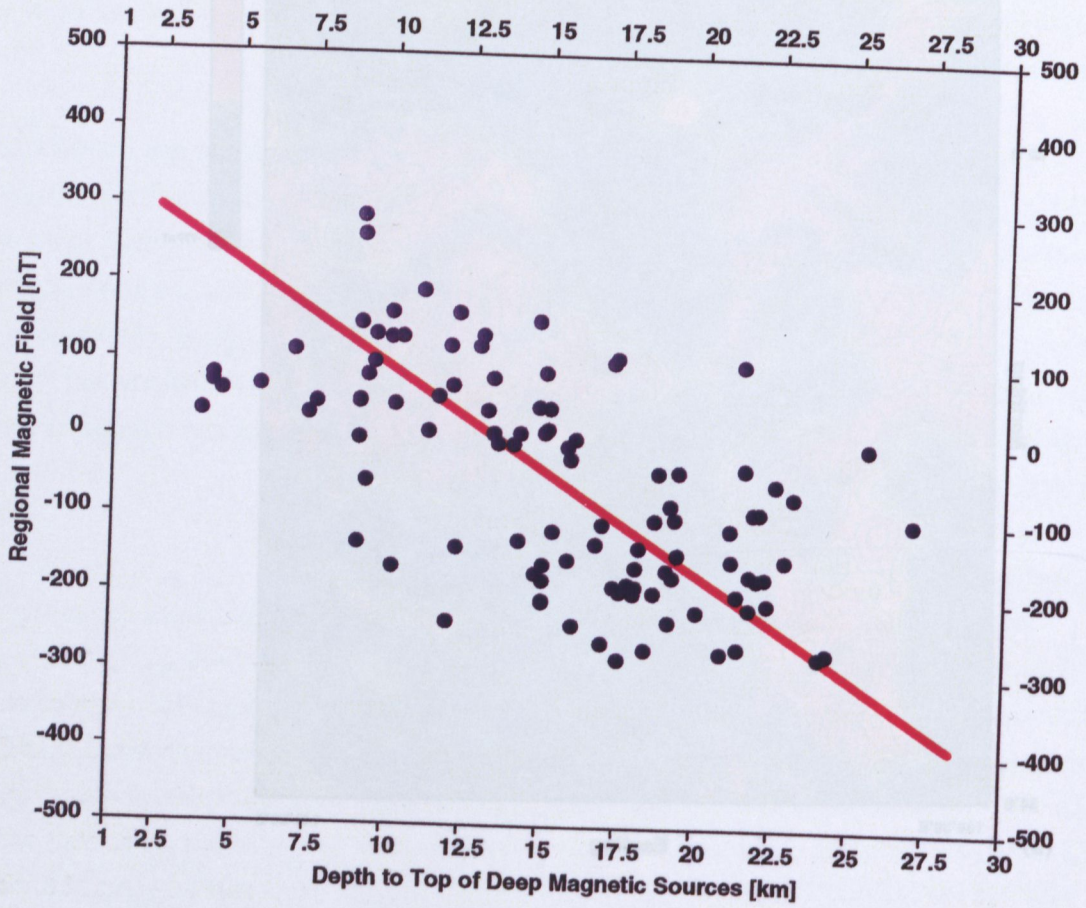

Figure 6.33 Statistical correlation between thickness of upper crustal layer and regional magnetic field at 10 km across the Adelaide Geosyncline.

6.9 Discussion of the results

The observations and results presented in this chapter lead to several final conclusions concerning the structure of the crust under the Polda rift and surrounding craton. The research presented focused on two main aspects:

- thickness of the upper crust computed from the magnetic field;
- distribution of magnetic boundaries within the crust.

As shown in the previous sections the regional magnetic highs indicate thinner upper crust e.g. shallower Conrad discontinuity, and according to Hall's model (Figure 6.3(a)) thicker lower crust with subsidence of the Moho discontinuity, and thicker entire crust (Figure 6.3(c)). Subsequently regional lows are indicators of thicker upper crust e.g. greater depth to Conrad discontinuity, and thinner lower crust with uplifted Moho, and thinner entire crust (Figure 6.2).

(i) Thickness of the upper crust

The deep magnetic sources map of *SQ18* DMS_{50X50} (Figure 6.13) indicates thickening of the upper weakly magnetic upper crustal layer under the Polda rift. The deep magnetic sources map DMS^{AG}_{60x60} (Figure 5.30) also shows the presence of thicker upper crust under the Adelaide Geosyncline. As can be seen in Figures 615 and Figure 6.35, in both areas, crustal thickening is associated with broad regional low. The statistical correlation between the regional field component and crustal thickness for both areas shows a linear function with negative slope, e.g. thinner upper crust is related to the regional high and subsequently regional lows occur over areas with thin upper crust. Based on these results the following model of the crust for both rifts can be deducted.

A distinct regional low (referred to as anomaly A_{PT}) occurs under the Polda Trough. This anomaly A_{PT} appears on the long wavelength anomalies maps, all four 'depth slice' maps and on the upward continued field to 10 km.

Presence of the magnetic horizon at depths greater than 19 km under the Polda rift implies that the upper crust is thicker under the rift than under the surrounding craton. Either the Conrad discontinuity is at depth of 19 km, or perhaps the deep magnetic surface detected by spectral analysis under the Polda rift reflects the top of the strongly magnetic lower part of the lower crust (see Section 6.1; Krutikhovskaya and Pashkevich (1977, 1979)). This can not be confirmed until a deep seismic sounding will be made in the area. There is large regional magnetic low which indicates that the lower crust is very thin (with thick upper crust). However, there is no other indication that the lower crust is thinner in the Polda rift area. Based on the correlations between the regional lows and shallower Moho observed under the Canadian and the Ukrainian Shields, the regional low observed under the Polda rift can also be explained as a result of crustal thinning under the rift. As discussed in Chapter 2 thinning of the crust under the rift zone is a characteristic feature observed in the majority of continental rifts. The thinner continental crust under a rift is a result of stretching and thinning of the whole lithosphere due to an uprising mantle diapir from the lithosphere-asthenosphere boundary.

(ii) Distribution of magnetic boundaries within the crust

A similar model can be applied to the Adelaide Geosyncline (terrain correction over the Flinders Ranges has not been applied to TMI data). Under this rift two very deep magnetic features (20-25 km; Figure 5.30) have been detected. The magnetic field upward continued to 10 km shows strong negative anomalies (Figure 6.35) over these two features. The thickness of the Adelaidean and Cambrian sediments (Section 6.2) filling this rift could be 10-15 km (Parker, 1993) than the deep magnetic features detected by spectral analysis could indicate thickness of upper crust. As discussed in Section 6.3 results of seismic studies conducted in this area by Shackleford and Sutton (1981) and Greenhalgh et al. (1989) show a two layered crust, with the Conrad discontinuity at a depth of 15-20 km. If this is true, then perhaps the spectral analysis of the TMI detected a strong magnetic interface within the lower crust.

In the area of the *HML* observed on the 'depth slice' maps, deep magnetic source were detected (Figure 6.33(b)). Based on the results obtained the following indications could be drawn:
-thick upper crust as $DMS_{50\times50}$ show subsidence of the Conrad discontinuity and also according to the model of the upper crust (Figure 6.2(b));
-thinner lower crust as there is large regional low which according to Hall's (1974) model of the lower crust indicates thinning ;
-shallow Moho as deduced from Hall's model of the crust.
The above are characteristic parameters of the region south of the east-west imprint of the Uno Fault, referred to as magnetic boundary B_{EW} on *SQ18*.

The eastern boundary of the HML coincides with the position of the deep crustal structure the Kalinjala Mylonite Zone (*KMZ*). The western boundary of the HML (Gr_{HML}) which runs in a NE-SW direction coincides with surface mapped occurrences of the granitic intrusions (Hiltaba Suite). This western boundary also coincides with B_{NE} which is clearly visible on the '$\lambda > 46km$' and '$\lambda > 64km$'.

The $DMS_{25\times25}$ (Figure 6.12) shows an east-west magnetic trough which coincides with the position of the Polda Trough. The $DMS_{50\times50}$ (Figure 6.33) map represent the thickness of the upper crust and shows the deep magnetic horizon under the offshore part of the rift which is 35-40 km wide. The onshore part of the Polda rift is marked by an east-west lineament L_{PT} with deep magnetic sources on its southern side. This could be interpreted as a deep listric fault which dips towards the south.
The L_{PT} lineament truncates the deep crustal structure the Kalinjala Mylonite Zone (*KMZ*). On the '$\lambda > 64km$' map shown in Figure 6.17 the imprint of this structure is very clear. On both sides of the lineament L_{PT} magnetic anomalies show sharp cut. As discussed in Chapter 4 interpretation of the surface TMI field over the Polda Trough shows that the trough is not purely an extensional feature but involves also a strike slip component along the east-west direction with the southern side moved towards the west by approximately 35 km. This interpretation explains the observed sharp truncation of the anomalies visible on the residual field maps.

Chapter 7

Conclusions

7.1 Summary of the research

The prime aim of the research presented in this thesis was the determination of the structure and origin of the onshore Polda Trough and its relation to the continental structure, based on new aeromagnetic survey data.

In the course of the research and based on the literature review, it was decided to extend this project to study the deeper crust below the Polda rift. As there is no deep seismic sounding in the area the deeper crust was studied by application of energy spectra analysis of the available aeromagnetic data. The specific interest was focused on the analysis and the interpretation of the magnetic inhomogeneities within the deep crust in the tectonic provinces representing normal crust and rift zones.

As a result of the research, the margins of the onland rift are clearly defined, showing a much narrower trough than previously interpreted. The analysis and interpretation of geophysical data integrated with known geology suggest a post-Permian origin of the Polda rift. The interior structure of the studied eastern end of the rift shows the presence of relay ramps instead of previously interpreted cross-faults. The offshore part of the Polda rift which has not been covered by this research project may show a similar interior structure as detected onland; the reinterpretation of geophysical data should reveal the presence of relay ramps instead of cross-faults and basement swells as previously interpreted.

This thesis shows a new and successful way of obtaining information about the upper part of the crust which has great potential in the study of major regional structures. This new approach to deep crustal studies, which is based on the spectral analysis of the magnetic field, shows that the upper crustal layer is thicker under the Polda rift and indicates that the northern limit of the South Australian Rift System was along the Uno Fault which is located about 100 km north of the Polda rift.

The summary of the research discussed in the previous chapters, with more detailed conclusions, has been divided into two sections: results concerning the top 5 km of the upper crust in the Polda rift area and new information about the deep crust in South Australia with particular attention to the south-eastern Gawler Craton surrounding Polda rift,.

7.2 Sedimentary wedge and regional structures associated with the Polda rift.

The study of the top portion of the upper crust has been directed to that part of the Polda Trough which was covered by the 1987/88 aeromagnetic survey conducted over Eyre Peninsula by MESA and AGSO. The integration of results obtained from detailed geophysical studies together with geological interpretation led to conclusions as follows.

- The shape of the Polda rift is clearly defined by the aeromagnetic survey data as shown in Figure 4.10; the off-shore section of the rift is about 40 km wide; the on-shore section becomes a very narrow structure and is only 4-5 km wide; the eastern end of the rift is a monoclinal sag dipping towards the west. The east-west oriented rift bounding faults are sub-vertical (75°-80°), which is not a typical fault geometry for purely extensional rifts (Chapter 2).

- Evidence for strike slip movement can be seen in the central-eastern part of the rift where a magnetic anomaly observed on the southern margin of the rift moves approximately 35 km towards the east on the northern margin of the rift (Figure 4.10).

- Integration of geological data with results of detailed geophysical studies brought the following evidence concerning the origin of the Polda rift:
  - Sediments of the Coolardie Formation of Permian age have been preserved only within the narrow rift (Figure 4.26);
  - The thickness of the Permian revealed in drill holes within the Polda rift is little different from that found elsewhere in central-southern Australia. The fact that there is no evidence of the great thickness of this sequence means, that there was no extra deposition in a developing rift.
  - Sediments of Jurassic Polda Formation overlap onto the basement on the southern margin of the rift;
  - There is no indication for a pre-Jurassic origin of the Polda rift; Permian and older underlying rocks have been down faulted and preserved within the graben after the doming stage prior to the actual rifting phase;
  - The change in thickness of the Polda Formation observed within the Lock Coal Deposit across faults defined from the magnetic survey is evidence of syn-rift sedimentation of Jurassic age (Chapter 3, Chapter 4);
  - From the above evidence it is concluded that the Polda rift was initiated in post-Permian and pre-Jurassic time.

- Kimberlitic intrusions of Jurassic age (Chapter 3, Chapter 4) in the vicinity of the Polda rift (southern margin) indicate that the Polda structure or rift related structure extends into the lithosphere.

- The western, central and eastern parts of the rift have different geological character which has been established from the interpretation of the new magnetic data, reinterpretation of existing gravity profiles and confirmed by seismic results (Figure 4.29).
  - In Polda West, the 1987/88 aeromagnetic survey, which covers a 40 km off-shore section of the main rift, shows a thick sedimentary in-fill (up to 5 km) preserved within the 35-40 km wide fault-

bounded rift structure. The rift margins are defined by east-west trending steeply dipping (80°) normal faults arranged in an en echelon pattern;

- Polda Central extends from the shore line towards the centre of Eyre Peninsula as a narrow trough, only 4-5 km wide, with 1-2 km thick sedimentary in-fill. The rift boundary faults are steeply dipping east-west oriented normal step faults. On the northern margin of Polda Central basement rocks are covered by a very thin veneer of Tertiary and Quaternary sediments, whereas on the southern margin of the rift sediments of the Jurassic Polda Formation overlap the Precambrian basement.
- Polda East is the half-graben structure which has been down faulted east of the NW-SE running major fault F_{PT}^{NW}, and extends towards the eastern monocline margin of the rift. A set of east-west oriented normal step faults constitutes the northern margin, whereas the southern margin appears to be unfaulted as a continuation of the eastern structure. The southern part of this half-graben structure has been down faulted several hundred metres along the WNW-ESE oriented fault F_{PE}^{WNW}. In this part of the Polda rift, according to the interpretation of magnetic data, the maximum thickness of the sediments is about 2.4 km; there are several hundred metres of Neoproterozoic, as well as Permian and Jurassic rocks, and there is a substantial thickness of Eocene sediments which represent a secondary syn-rifting stage. As the Neoproterozoic rocks include two layers of volcanics, which are strongly magnetic and perhaps overprint the magnetic signature of the underlying basement, the magnetic data may not indicate the total thickness of the Precambrian sediments preserved within this Mesozoic rift.

- The thickness of the sediments in the western Polda rift ranges between 2 km and 5 km; in the central narrow part of the rift sediments were down faulted to a depth of 1 km, or even 2 km and at the eastern end of the rift sediments are 1.3-2.4 km thick.

- The structure within the Polda rift has been established from the interpretation of the new aeromagnetic data integrated with other geophysical evidence. In the western part of the Polda rift, where the rift structure is about 40 km wide, the contour map of the magnetic basement (Figure 5.15) constructed from results obtained from the energy spectral analysis of TMI and forward modelling of the east-west magnetic profiles, indicates the presence of two graben-like structures trending east-west in an en echelon pattern, separated by a narrow sub-parallel ridge. Such a configuration suggests that the northern graben continues towards the west, whereas the southern graben continues towards the east as a narrow rift. The dividing ridge represents the position of the relay ramp which is a characteristic feature of many rifts and is responsible for change of the polarity of the internal half-grabens. The northern graben is about 4.5 km deep, whereas the southern graben appears to be 4 km deep, and the dividing ridge shows 2.5 km depth.

- In the central part of the Polda rift where this structure becomes very narrow, the Lock Coal Deposit has been preserved within the rift on its northern side on the ramp between two east-west trending graben-like structures (Chapter 4). The northern graben becomes very shallow towards the west of the Lock Coal Deposit, whereas towards the east it continues as a deep trough. The southern graben appears to be 1-2 km deep in the vicinity of the Lock Coal Deposit.

- Analysis of the older tectonic maps of this region (i.e. Stagg et al., 1991) has shown a series of north-west striking cross-faults (accommodation zones) intersecting the Polda rift and controlling

the rift's interior structure. There is no evidence in the 1987/88 aeromagnetic survey data of such cross-faults within the area covered by this survey.

- The rift sediments produce negative gravity anomalies, but the interpretation of gravity field is complicated by density variations within the basement. The large negative gravity anomaly of -40 mgals detected by the regional gravity survey, near Elliston on the western coast of the Eyre Penninsula, occurs over an area where the sediments, according to the magnetic survey, are thin (700 m) so that the gravity anomaly is clearly in part due to the low density basement rocks and not due to the very thick sediments. As discussed in Chapter 4 the north-south gravity profile surveyed across the southern rift's margin indicates a strong gravity low within the rift zone, but as is shown in Figure 4.7 and Figure 4.31 this low also continues on the other (northern) side of the rift. Hence this negative gravity anomaly could not be on account of the trough's sedimentary fill only, but it obviously indicates the presence of a density contrast within the basement on the northern margin.

- The low gravity at the eastern end of the Polda Basin is due in part to the Tertiary basin (300 m thickness of Tertiary sediments with density contrast of 0.5 g/cm^3)

- The fault F_{PW}^{NB} bounding rift from the north (Figure 4.7) was recognised to be a pre-existing basement feature. This fault structure was dormant during the deposition of the Blue Range Beds in the Mesoproterozoic and was reactivated in the post-Mesoproterozoic.

- The Blue Range Beds of the Mesoproterozoic and the Kilroo Formation of the Neoproterozoic were considered by others to exist in the Itiledoo Basin. Based on the existing facts and interpretation of geophysics, it is difficult to conceive that the Blue Range Beds depositional setting was an early east-west graben. On the contrary, it could be thought that Blue Range Beds sediments were similar deposits to the Stuart Shelf structure setting or, alternatively that sediments were preserved in a shallow fold.

- The interpretation of the gravity field does not indicate the east-west fault boundaries of the Itiledoo Basin, which had, in the past, been claimed to exist (e.g. Flint, 1993).

- The geological evidence and information provided by geophysics in this study do not support the current model of the Blue Range Beds deposition within the east west trending, several hundred kilometres long, Itiledoo Basin (e.g. Rankin et al., 1993). There is no satisfactory evidence of the presence of Blue Range Beds sediments in the central part of the Polda rift.

- "Itiledoo Basin" West
  North of Elliston the maximum thickness of the Blue Range Beds detected from the interpretation of the seismic data is estimated to be about 600 m, and from the interpretation of the magnetic field approximately 700 m. There is no satisfactory evidence for the presence of Blue Range Beds within the narrow graben.
  In addition the Blue Range Beds sediments are preserved on the northern side of the northern boundary fault F_{PW}^{NM}, indicating that the Polda rift is not an essential part of the preservation of the Blue Range Beds.

- "Itiledoo Basin" East
  The contact between the Palaeoproterozoic basement rocks and unconformably overlying Mesoproterozoic sediments of the Blue Range Beds can be followed along the eastern end of the Polda rift. The Blue Range Beds exposure in a series of thin sheets about 4 km long appears through the Tertiary sedimentary cover. The Blue Range Beds sediments dip towards the west with much steeper angles than elsewhere (15° to 45°). From geological field observations it appears that these sequences are preserved in the fold structure and the thickness of the Blue Range Beds calculated subsequently is about 1500 m.

- "Itiledoo Basin" South-East
  The configuration of the magnetic field anomalies is consistent with the boundaries of the Blue Range Beds established on geological evidence. The basement rocks are magnetic and the Blue Range Beds sequences are non-magnetic; there is an evident north-south fault boundary on the western side of the outcrop of the Blue Range Beds. There is no evidence of the presence of shallow magnetic rocks within the Blue Range Beds depositional boundaries established from the magnetics.

- The generally accepted current model (e.g. Rankin et al., 1993) of the Itiledoo Basin implies that the Blue Range Beds sediments are preserved in the east-west elongated depositional basin. However, the 'Tectonic Sketch' of Kimba (Geological Map 1:250,000 Sheet) shows at the eastern end of the basin a north-south trough, and this is what is shown by the geophysical investigation presented in this thesis.

- According to other authors (e.g. Flint and Rankin, 1990; Flint, 1992) evidence for a Proterozoic origin of the Polda rift is the great thickness of halite beds and evaporate-bearing mudstone and sandstone found in the offshore section of the rift and assumed to be an equivalent of the Neoproterozoic Kilroo Formation. However, the Neoproterozoic Kilroo Formation intersected by drilling at the eastern end of the Polda rift cannot be definitely correlated with sediments encountered in oil-wells offshore at a distance of more than 170 km. The basis for such correlation is tenuous as the offshore sediments show strong oxidation, absence of fossil, and the only fact that can be established is that they are of prior-Permian age.

7.3 Crustal environment of the Polda rift, South Australia.

Knowledge of the deep crust in South Australia is limited; the information comes from studies based on travel times of minor earthquakes, seismic refraction profiles based on quarry blasts at Iron Baron and, recently shot deep seismic sounding profiles in the Officer Basin.

The energy spectral analysis method applied to aeromagnetic data sets allowed the study of crustal magnetic inhomogeneities and determination of magnetic interfaces within the crust to a depth of about 25 km. The results show a 5-25 km thick upper weakly magnetic crustal layer overlying a strongly magnetic lower crust.

The identification of the crustal layers detected by spectral analysis of TMI is still speculative. However, by a comparison with results of deep crustal studies in Canada, Ukraine and India some indirect evidence identifying its meaning exists.

- According to the study conducted by Hall (1974) over the Canadian Shield the thicker upper crustal layer is connected with regional broad lows, and the thinner upper crustal layer is associated with a high intensity of regional magnetic field (Chapter 6). In analogy to the magnetic model of the earth's crust under the Ukrainian Shield (Krutikhovskaya and Pashkevich, 1976) it can be concluded that the energy spectra analysis of TMI across South Australia indicates the presence of a similar weakly magnetic upper crustal layer overlying a strongly magnetic lower crust.

- In India the study of the Narmada-Son Lineament intersecting the Gondwana Graben, using both deep seismic sounding and energy spectra analysis of TMI, has established a similar relationship between an upper weakly magnetic crustal layer and the change of velocity from 6.1 km/sec to 6.9 km/sec (Rao et al., 1992).

- In South Australia the Iron Baron refraction seismic profile shows an upper crustal layer with a velocity of 5.93 km/sec and a lower layer with a velocity of 6.46 km/sec. To the west of the Torrens Hinge Zone the seismic boundary lies at a depth of about 10-12 km. To the east of the Torrens Hinge Zone below the Adelaide Geosyncline the boundary lies at a depth greater than 20 km. The study presented in this thesis shows that, the depth of the weakly magnetic layer on the western side of the Torrens Hinge Zone is 11-13 km and on the eastern side is 19-21 km.

Presented in Figures 6.30-6.31 are cross-plots of depths to the top of deep magnetic sources obtained from energy spectra analysis of TMI versus the intensity of the long wavelength magnetic anomaly field (low pass filter with λ>64 km; and upward continuation to a height of 10 km) show a linear trend with negative slope for the region of the south-western Gawler Craton and across the Adelaide Geosyncline. The statistical correlation between these two variables (statistical test shows that there is evidence of linear association at a 95% significance level) indicates a similar trend to that observed on the Canadian Shield for the thickness of the upper crustal layer established from deep seismic sounding. An analogy can also be drawn between results obtained from correlation of crustal thickness computed from spectral analysis of TMI with the intensity of the regional magnetic field across the south-western Gawler Craton and the Adelaide Geosyncline and results obtained from deep seismic sounding and analysis of long wavelength magnetic anomalies across the Canadian, Ukrainian and Baltic Shields and over the Gondwana crust in the Indian sub-plate. A low regional magnetic field over the Polda rift indicates a thicker upper crustal layer but thinner lower crust. The results of spectral analysis of TMI also indicate a thicker weakly magnetic upper crustal layer under the Polda rift than under the surrounding craton.

The spectral analysis of TMI and the long wave-length magnetic field show a north-south deep crustal structure (B_{NS}^{7km}) truncating the south-eastern Gawler Craton (Figure 6.25). The intersection of this boundary B_{NS}^{7km} with the Polda rift coincides with the change of geological character of the rift from a 35-40 km wide structure to the west of B_{NS}^{7km} to a very narrow (4-5 km wide) trough east of the observed boundary. The observed regular change of 'depth polarity' on the eastern and western sides of B_{NS}^{7km} indicates strike slip movement along B_{NS}^{7km}. The analysis of the TMI field over the

south-eastern Gawler Craton shows that an imprint of the Polda rift extends eastwards towards the Torrens Hinge Zone (Figure 6.36).

The deep magnetic sources map over the south-eastern Gawler Craton shows significant changes within the crust to the north and south of the east-west trending magnetic boundary B^{EW}_{50x50} (Figure 6.33) located about 50 km north of the Polda rift. The position of the observed boundary coincides with the surface location of the Uno Fault. The upper crustal layer in the southern part is much thicker than towards the north. It appears that the Uno Fault is a major crustal structure which extends to the deep interior of the lithosphere. The magnetic feature B^{EW}_{50x50} is sub-parallel to the Polda rift and may mark the northern boundary of the continental crust affected by tectonic processes connected with origin of the South Australian Rift System.

The interpretation of the whole of the South Australian crust based on energy spectral analysis of TMI will provide further useful information, both scientific and economic, and is continuing.

7.4 Concluding statement.

The research presented in this thesis clearly shows that properly interpreted geophysical data integrated with geology is essential for an understanding of the earth's structure. Many of the results obtained here will be beneficial for other researches when, as quoted from McLaren and Skinner (1987) in the beginning of this thesis '...it is already apparent that prospecting for deposits buried beneath thick blankets of surface rocks will become feasible. The search for buried mineral deposits will become intense over the next 50 years, and the places where searching is likely to be most rewarding will be in those countries that have made the long term investments needed to measure and map the earth's crust in the third dimension to depths of 15 or 20 km".

Appendix A

Theoretical aspects of the energy spectrum analysis method

A.1 Fundamentals of spectral analysis

An aperiodic function $f(x)$ of a space domain variable x can be synthesised by an infinite aggregate of sinusoids of all possible frequencies of differing amplitude and phase (Fourier, 1822). The Fourier transform of $f(x)$, assuming that $f(x)$ satisfies the Dirichlet's conditions, viz., $f(x)$ must be piecewise continuous and it must be integrable (Sneddon, 1951), provides information on the amplitude and phase relationships of these frequencies. The application of the Fourier transform to 2-D data allows a study of the spectral characteristics of functions of two space variables (x, y) such as a total magnetic field anomaly $\Delta t(x, y)$ described on the x, y – plane.

The Fourier transform of $f(x, y)$ is given by

$$\overline{F}(u, v) = \int_{-\infty}^{\infty}\int_{-\infty}^{\infty} f(x, y)e^{-i(ux+vy)}dxdy\,. \tag{1}$$

Based on the reciprocal relation of the Fourier transform,

$$f(x, y) = \frac{1}{4\pi^2}\int_{-\infty}^{\infty}\int_{-\infty}^{\infty}\overline{F}(u, v)e^{i(ux+vy)}dudv \tag{2}$$

where u and v are the angular frequencies in the x and y direction, respectively. Those variables are related to the spatial "frequencies" f_x and f_y as follows

$$u = 2\pi f_x \qquad \text{and} \qquad v = 2\pi f_y\,. \tag{3}$$

The energy density spectrum, which will be referred to as the energy spectrum, is derived from (1) and is given as

$$E(u, v) = \overline{F}(u, v) \circ \overline{F}^{*}(u, v)\,, \tag{4}$$

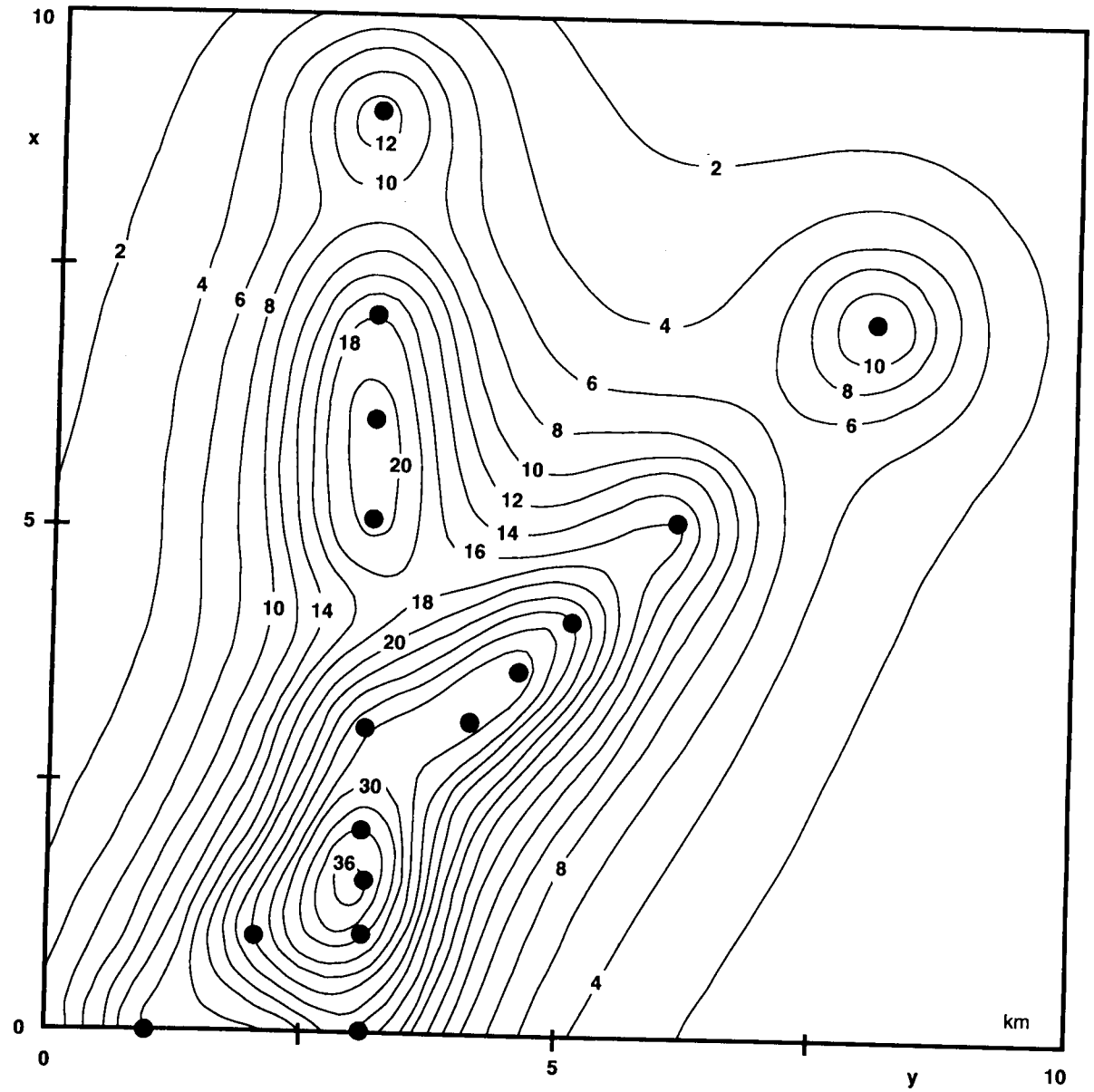

Figure A.1(a) Total magnetic intensity anomaly of 16 points poles at a depth of 1.6 km. After Spector (1968).

where $\overline{F}^{*}(u,v)$ is the complex conjugate of $\overline{F}(u,v)$. The function $\overline{F}(u,v)$ contains information on the amplitude and phase relationships of all the frequencies that make up the 2-D function $f(x,y)$. When this function is broken up into its real and imaginary parts, it is given by

$$\overline{F}(u,v) = R(u,v) - iQ(u,v) \tag{5}$$

and

$$\begin{matrix} R \\ Q \end{matrix}(u,v) = \int_{-\infty}^{\infty}\int_{-\infty}^{\infty} f(x,y) \begin{matrix} cos \\ sin \end{matrix}(ux+vy)dxdy\,. \tag{6}$$

The amplitude spectrum of $\overline{F}(u,v)$ is

$$A(u,v) = |\overline{F}(u,v)| = \sqrt{R^2+Q^2} \tag{7}$$

and its phase spectrum is

$$\Theta(u,v) = tan^{-1}\frac{Q}{R}\,. \tag{8}$$

Thus, the Fourier transform can be expressed as

$$\overline{F}(u,v) = A(u,v)e^{-i\theta(u,v)}$$

where R and $-Q$ are the real and imaginary components of $\overline{F}(u,v)$.

The energy spectrum is

$$E(u,v) = \left|\overline{F}(u,v)\right|^2 = R^2(u,v) + Q^2(u,v)\,. \tag{9}$$

According to the standard rule of harmonic analysis, the autocorrelation function is the Fourier transform of the energy spectrum. The autocorrelation function is defined in the (x,y) coordinate system and the result follows on taking the Fourier Transform:

$$C(\tau,\lambda) = \int_{-\infty}^{\infty}\int_{-\infty}^{\infty} f(x,y)\cdot f(x+\tau, y+\lambda)dxdy\,. \tag{10}$$

From the above equation it is evident that the autocorrelation function is related to the function $f(x,y)$ with the origin of coordinates displaced from $(0,0)$ to $(-\tau,-\lambda)$. The autocorrelation function indicates trends of the contours of function $f(x,y)$ in a particular direction. As is shown in Figures A.1(a)-(c) it will have a lobe in the same direction (Spector and Bhattacharyya, 1966; Spector, 1968).

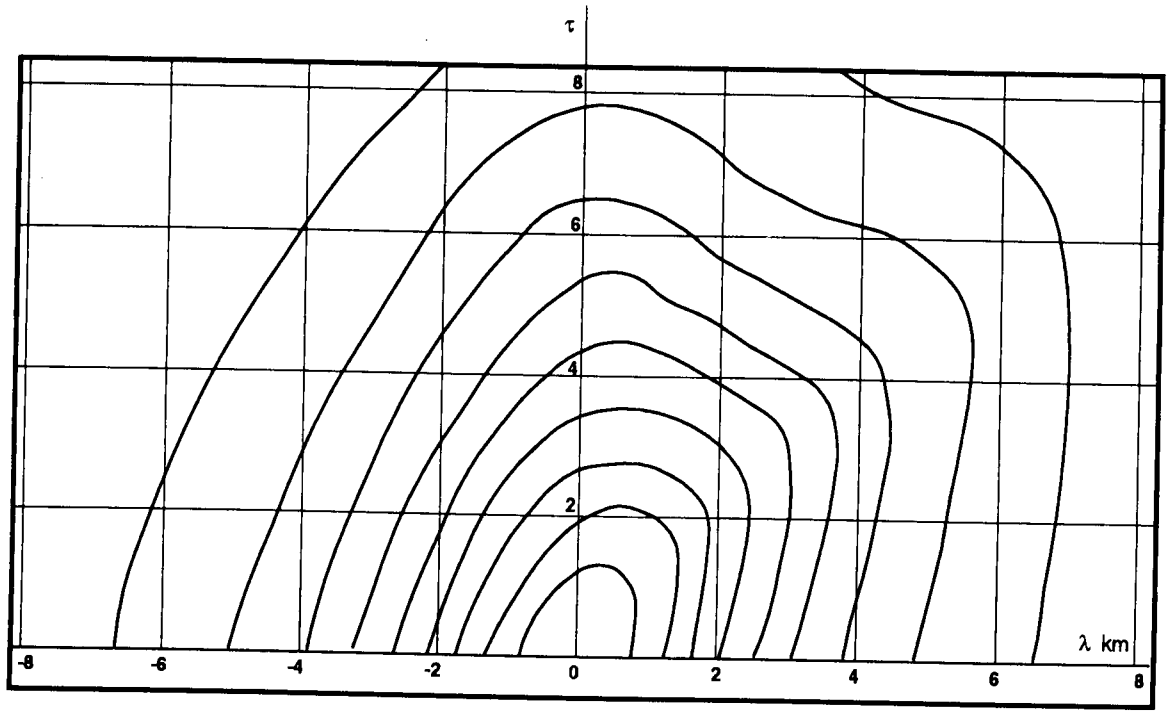

Figure A.1(b) Autocorrelation function (anomaly of 16 point poles at a depth of 16km). After Spector (1966).

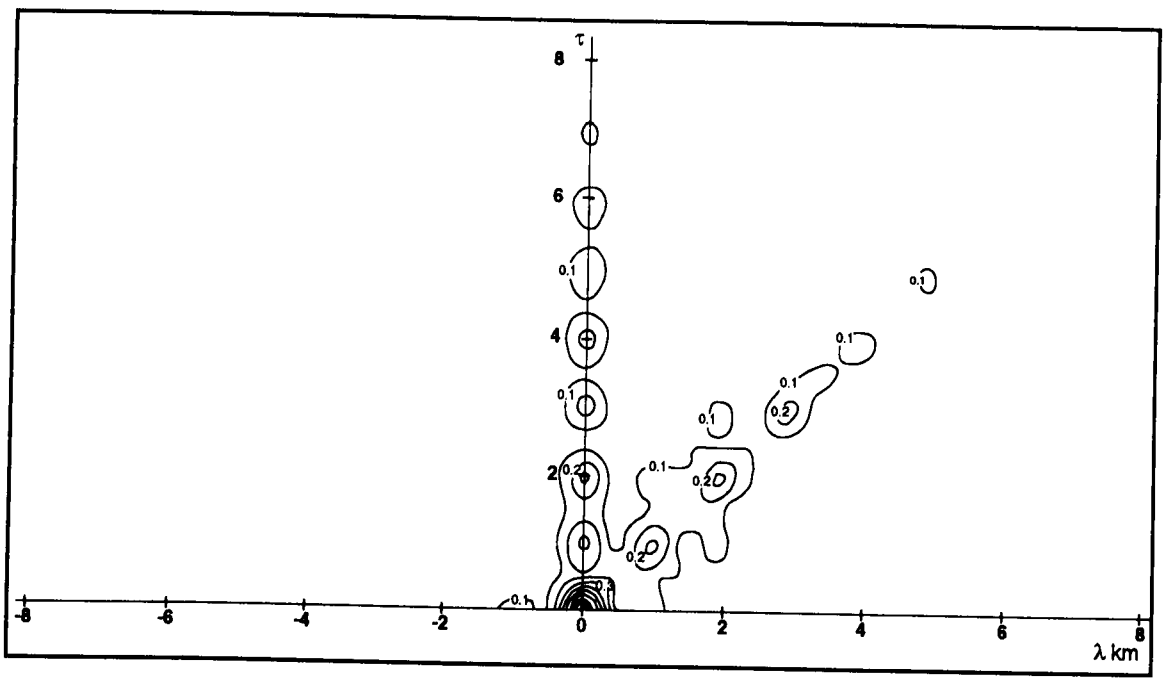

Figure A.1(c) Autocorrelation function, field downward continued to 1.44 km (anomaly of 16 point poles at a depth of 1.6 km) . After Spector (1968).

The autocorrelation function can also be expressed as

$$C(\tau,\lambda)=\frac{1}{4\pi^2}\int_{-\infty}^{\infty}\int_{-\infty}^{\infty}E(u,v)\cdot e^{i(u\tau+v\lambda)}dudv\,, \tag{11}$$

with the reciprocal relation

$$E(u,v)=\int_{-\infty}^{\infty}\int_{-\infty}^{\infty}C(\tau,\lambda)\cdot e^{-i(u\tau+v\lambda)}d\tau d\lambda\,. \tag{12}$$

The variables τ and λ are termed 'delays' or 'lags'.

The relationships in equations (4) and (11) imply that aperiodic functions with different phase spectra, but the same amplitude spectra, will have identical energy spectra and autocorrelation functions. Therefore, information contained in the phase spectrum is completely absent in both the energy spectrum and the autocorrelation function (Spector and Bhattacharyya, 1966; Spector, 1968).

A.2 The principles of spectral analysis of a simple magnetic model

The principles of energy spectral analysis allow application of this method to potential field theory, to study regional deep crustal structure from magnetic and gravity data. This method analyses characteristics of the potential field data in the frequency domain using Fast Fourier Transforms. There are some advantages of working in the frequency domain: the expressions of the potential field are relatively simple in comparison with the corresponding expressions in the space domain. They are given as a product of factors depending on the type of the observed field and the geometry and physical properties of the causative body (Shi, 1993).

The application of the Fourier transformation to the calculation of the vertical derivatives, and the upward and downward continuation of potential fields was well known and broadly published by many researchers in late fifties and early sixties (Tsuboi, 1959; Dean, 1958, Daneš,1962; Daneš, and Oncley, 1962; Bhattacharyya, 1965). Since the late fifties and sixties, the use of spectral techniques in the interpretation of potential field data has become widely accepted. Alldredge et al. published in 1963 the results of a frequency analysis of the total field values along a magnetic profile around the world. They plotted the sum of the squares of the amplitudes of a different frequency versus the wavelength of the harmonics, obtaining a bimodal distribution of the energy spectrum. Alldredge et al. interpreted the results as being due to crustal and core sources of the earth. McClure (1963) applied power spectra techniques to analyse long aeromagnetic profiles to study the Curie-point geotherm. Horton et al. (1964) applied power spectral and autocovariance techniques to aeromagnetic maps to analyse trend directions and other structural information.

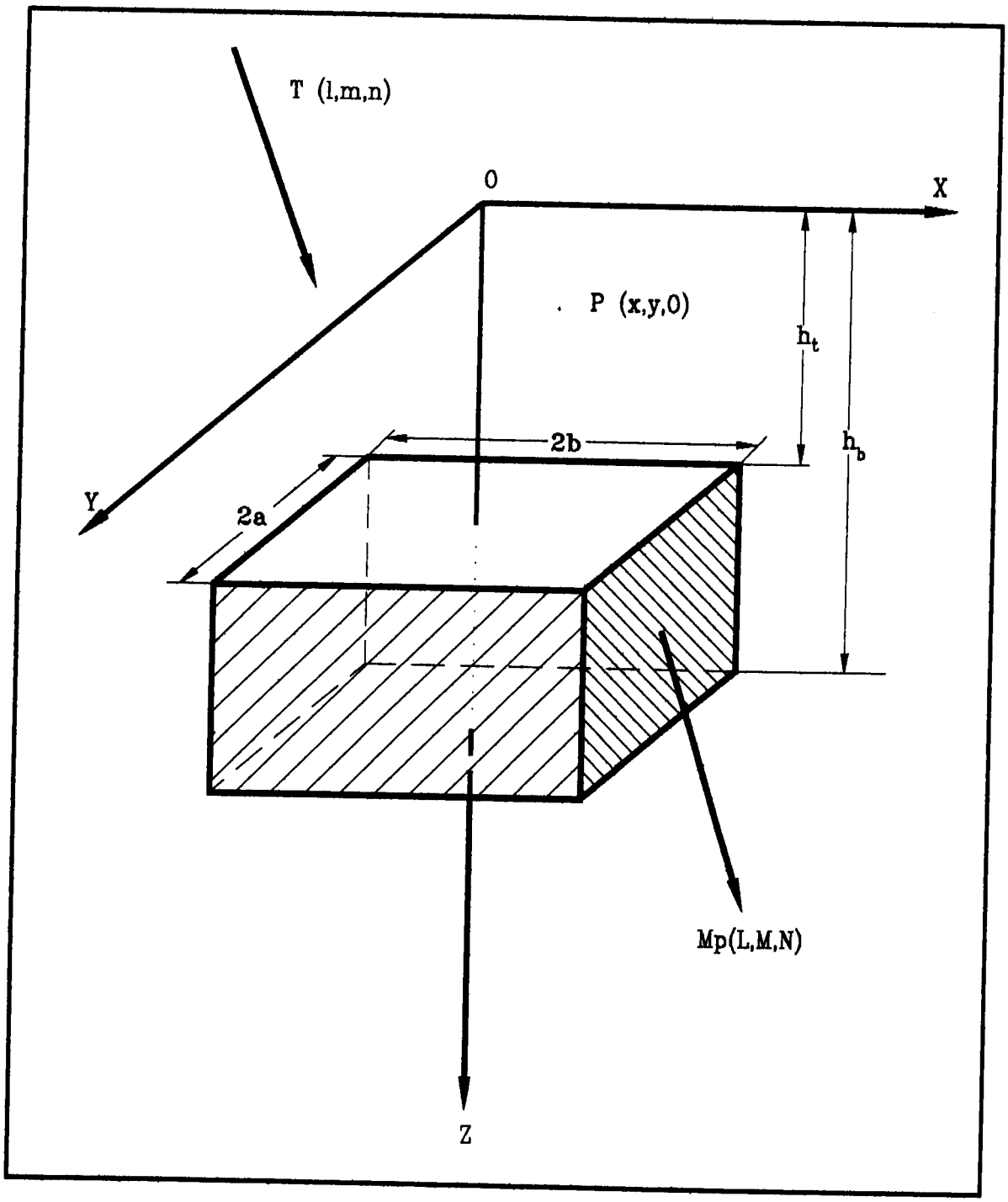

Figure A.2 The simple model of the vertical-sided, finite rectangular prism. After Bhattacharyya (1966).

Spectral analysis provides the possibility for having, not only an estimate of the depth to the top of the causative body, but also its horizontal dimensions. Studies of the spectral characteristics of the high-frequency anomalies derived from shallow sources and those which are mainly low-frequency contributors, derived from the deep-seated magnetic sources, provide a way of filtering out high-frequency components from the aeromagnetic map in order to obtain the broad crustal anomalies. One of the earliest works on the design of such filters was published by Goldstein and Ward (1964).

The very first publications by Odegard and Berg (1965) concerning spectral techniques as a tool for the interpretation of potential field data, describe the theoretical spectra produced by different model sources. The principles of the method are based on the fundamental work done by Bhattacharyya (1966a). This method was further developed and tested by Spector and Grant and published in 1970. Over the years many scientists contributed to the development of this method, analysing spectral effects of simple magnetic models: point pole, dipole, line of poles and dipoles, sphere, cylinder, dyke, rectangular and triangular prism, fault and step (Solovyev, 1962; Spector and Bhattacharyya, 1966; Bhattacharyya, 1965, 1966b; Spector, 1968; Bhattacharyya and Navolio, 1976; Bhattacharyya and Leu, 1977; Gudmundsson, 1966; Rao and Avasthi, 1973).

The principles of spectral analysis can be demonstrated with the use of Bhattacharyya's (1966a) description of the simple model of the vertical sided rectangular prism. If the total magnetic intensity field (TMI) due to a finitely extended prismatic body (see Figure A.2) be denoted by $T(x, y)$, the Fourier transform of it is as follow:

$$\overline{T}(u,v) = 2\pi I_p\left[\left[-lLu^2 - mMv^2 + nN(u^2+v^2) - \alpha_{12}uv - i\alpha_{13}u\sqrt{u^2+v^2} - i\alpha_{23}v\sqrt{u^2+v^2}\,\right]\right] \times \frac{4}{uv}\sin(ub)\sin(va)\frac{e^{-h_t(u^2+v^2)} - e^{-h_b(u^2+v^2)}}{u^2+v^2} \qquad (13)$$

where

T is the earth's magnetic field vector, which is defined by the direction cosines l, m, n;

I_p is the magnitude of the polarisation vector, which is characterised by L, M and N, the direction cosines;

$2a, 2b$ are the horizontal dimensions of the prismatic body along the x and y-axes, respectively;

h_t, h_b is the depth to the top and the bottom of the prism;

$\alpha_{12} = Lm + Ml$;

$\alpha_{13} = Ln + Nl$;

$\alpha_{23} = Mn + Nm$.

The equation (13) can be expressed as a product of simplified factors by introducing the following notation:

$$r = \sqrt{u^2 + v^2}$$

$$D(u,v) = \frac{(-lLu^2 - mMu^2 + nNr^2) - \alpha_{12}uv + i\alpha_{13}ur + i\alpha_{23}vr}{r^2}$$

$$B(u,v) = \frac{4}{uv} \sin ub \sin va$$

$$H(u,v) = e^{-h_t r} - e^{-h_b r} = e^{-h_t r}(1 - e^{-(h_b - h_t)r})$$

therefore,

$$\overline{T}(u,v) = 2\pi \cdot I_p \cdot D(u,v) \cdot B(u,v) \cdot H(u,v). \tag{14}$$

The Fourier transform of the total magnetic intensity field is now expressed as a simple product of the following factors:

$D(u,v)$ - dimensionless factor dependent on the geomagnetic latitude of the place (inclination of earth's magnetic field) and on the orientation of the polarisation vector, which after reduction to the pole becomes unity;

$B(u,v)$ - boundary effect or the horizontal dimension of the magnetic body factor;

$H(u,v)$ - function of the depth to the top of the causative body and the depth extent.

Transferring equation (13) into polar wave-number coordinates (r,θ) in the (u,v) frequency plane, the energy spectrum (which is the square of the Fourier amplitude spectrum) of the total magnetic intensity field over a single rectangular prism can be expressed (Spector and Grant, 1970) in the following form:

$$E(r,\theta) = |\overline{T}(u,v)|^2 = 4\pi^2 k^2 e^{-2hr}(1 - e^{-tr})^2 S^2(r,\theta)\Gamma_T^2(\theta)\Gamma_M^2(\theta) \tag{15}$$

where

$\theta = tan^{-1}\frac{u}{v}$ is the angle of the polarisation vector is relative to the direction of the earth's field;

$k = 4ab \cdot I_p$ is the magnetic moment/unit depth;

e^{-2hr} is the depth factor, in which h is the depth to the top of the body;

$1 - e^{-tr}$ is the thickness factor, $t = h_b - h_t$. For infinite depth extent this factor tends to unity.

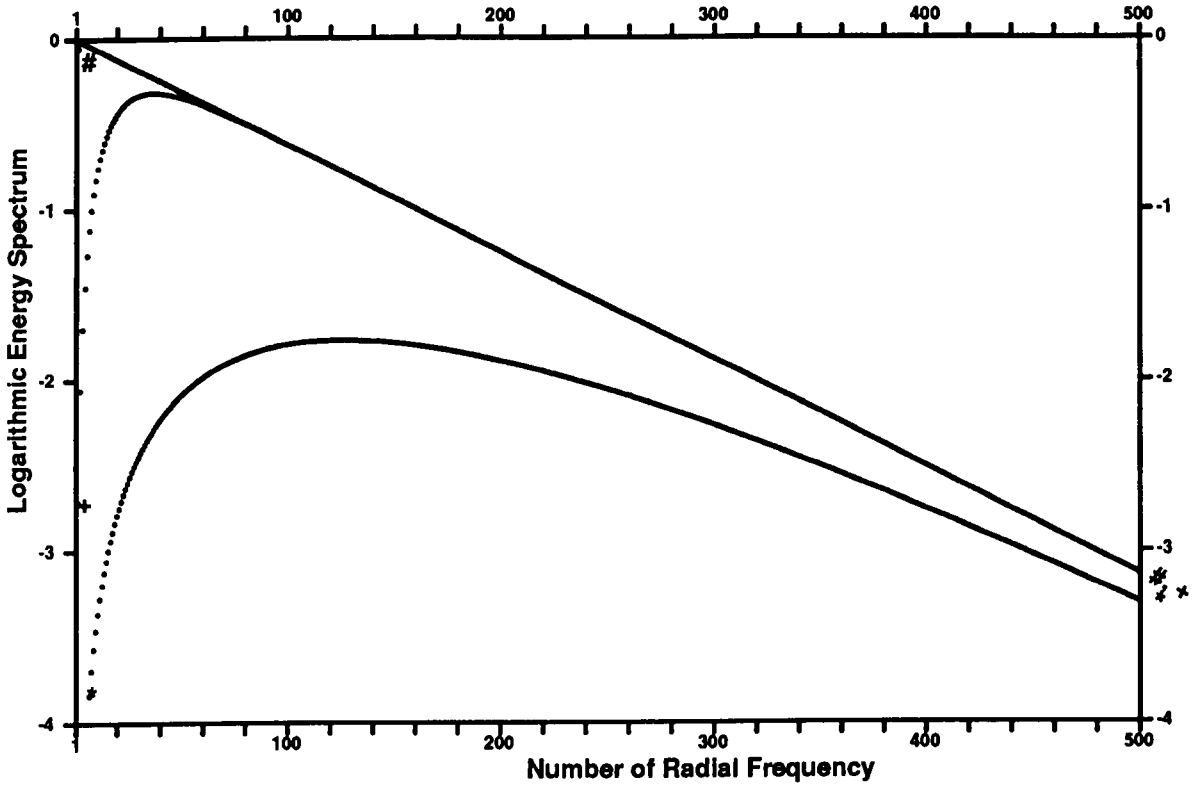

Figure A.3(a) Effect of finite thickness on the shape of the spectra. After Spector & Grant (1970)

Bottomless source

+ Limited depth extent source

* Thin plate source

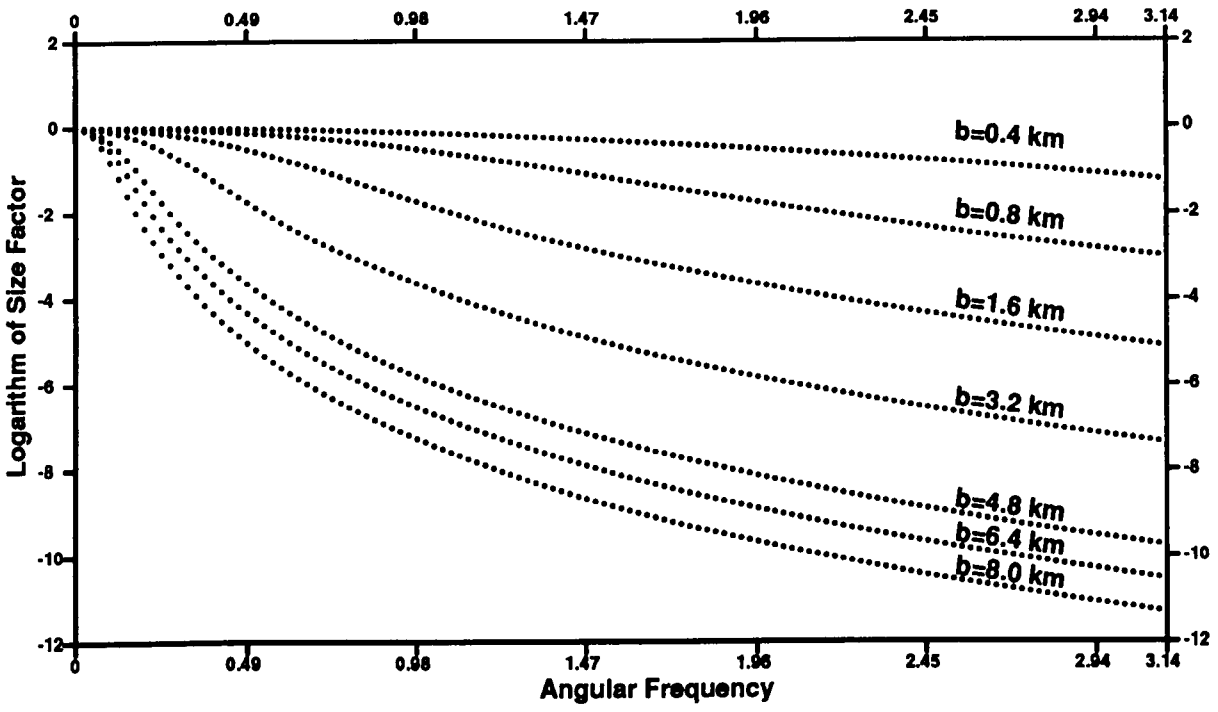

Figure A.3(b) Finite horizontal size effect. After Spector and Grant (1970).

b: the average of horizontal size

These last two factors (the depth and the thickness) are both related to the term $H(u,v)$ in equation (14).

$S(r,\theta)=\frac{sin(ar\cos\theta)}{ar\cos\theta}\cdot\frac{sin(br\sin\theta)}{br\sin\theta}$ is the horizontal size factor which

corresponds to the term $B(u,v)$ in equation (14);

$R_T(\theta)=n^2+(l\cos\theta+m\sin\theta)^2$ is the geomagnetic field factor;

$R_M(\theta)=N^2+(L\cos\theta+M\sin\theta)^2$, the factor of the polarisation vector.

The geomagnetic and polarisation factors correspond to the term $D(u,v)$ in equation (14).

The energy spectrum is further simplified when reduction to the magnetic pole (RTP) is applied. The energy spectrum of a magnetic body with infinite depth extent can be expressed by

$$E(r,\theta)=4\pi^2k^2e^{-2hr}S^2(r,\theta). \tag{16}$$

The characteristic of the spectrum for a single vertical prism is thus mainly dependent on two factors: depth e^{-2hr} and horizontal dimantion $S^2(r,\theta)$. The effect of these two factors on the energy spectrum will be discussed in Section A.3.

A.3 Properties of the energy spectra for the single prism model

(I) Depth and thickness factors

According to the expression for the energy spectrum in (15), the depth factor, for a body with infinite thickness, is represented by the function e^{-2hr}. Neglecting other influences, the logarithmic energy spectrum contains the simple linear term, $-2hr$. Therefore, the slope of the line, representing this simple function, indicates the depth to the top surface of the causative body.

Spector (1968) studied the shape of the spectrum and effect of the depth factor of a very thin ('laminar') and limited thickness ('finite') body. The depth factor has a non-linear logarithmic form (see Figure A.3(a))

$\log H(r)\approx -2hr+2\log(rt)$, for 'laminar' type

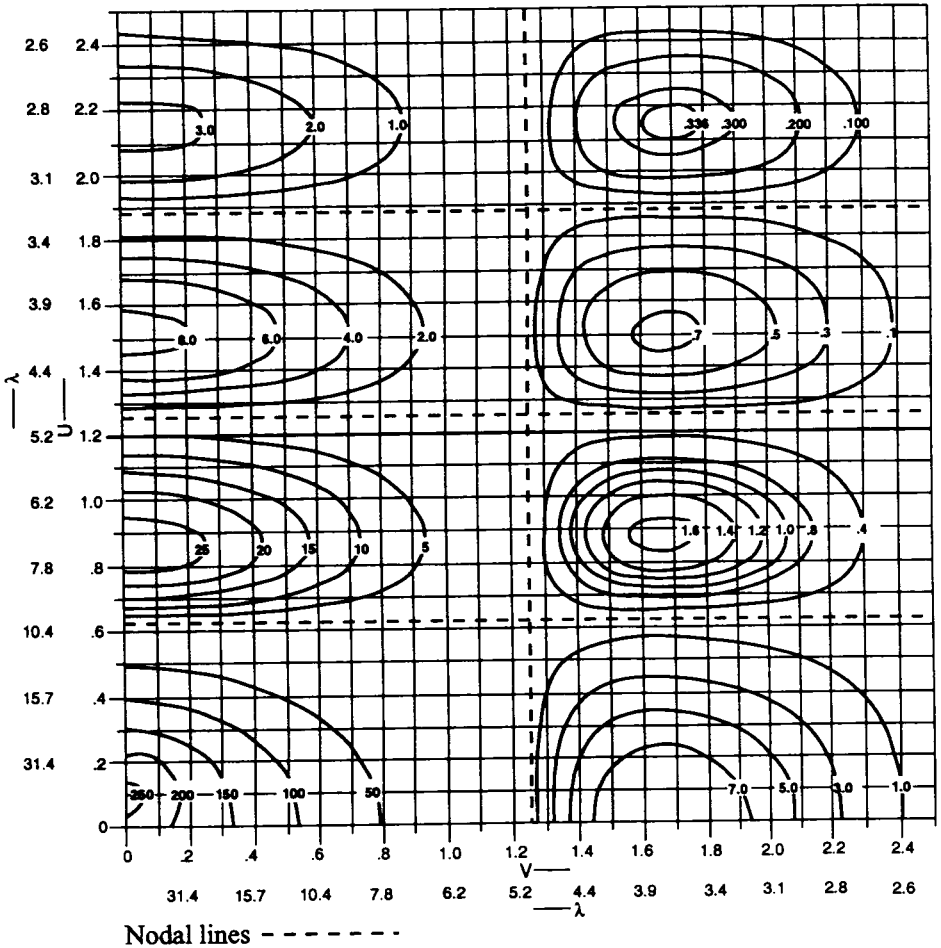

Figure A.4(a) Contour diagram of 2-D amplitude spectrum of the anomaly due to a prismatic body: 2a = 5, 2b = 10, h_t = 3.0, h_b = ∞. After Bhattacharyya (1966).

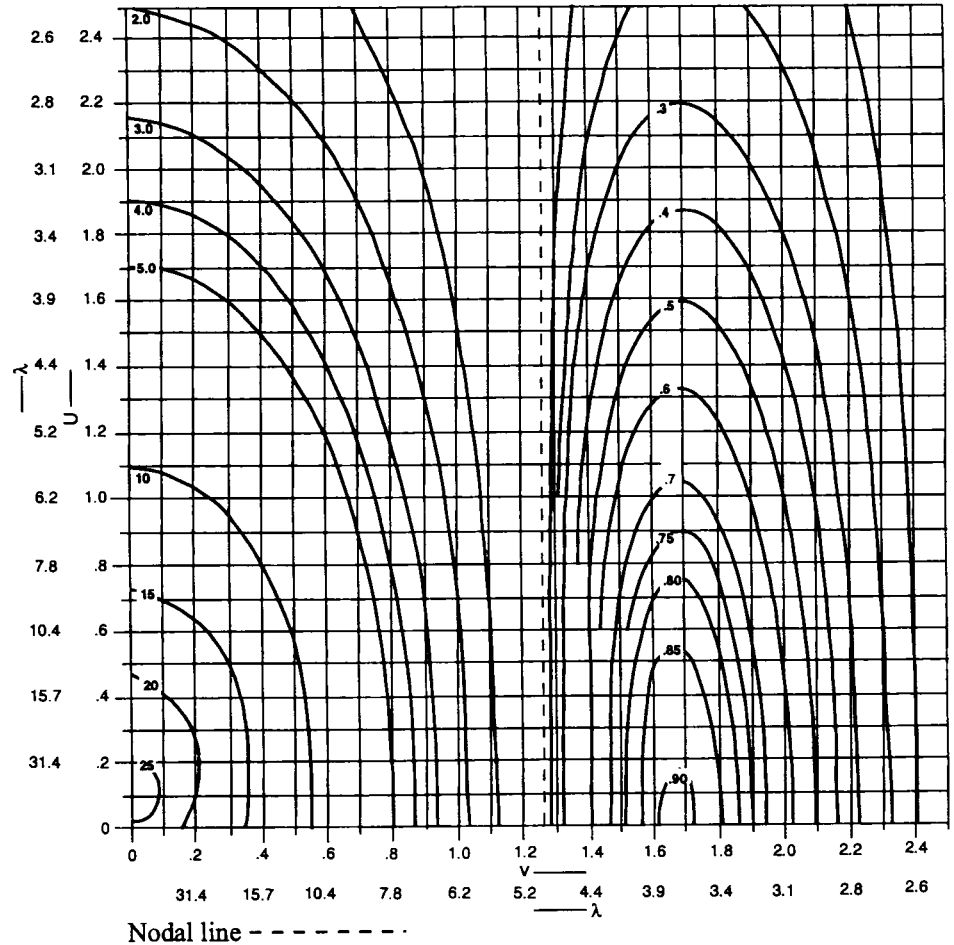

Figure A.4(b) Contour diagram of 2-D amplitude spectrum of anomaly due to a prismatic body: 2a = 5, 2b = 1, h_t = 3, h_b = ∞. After Bhattacharyya (1966).

and

$\log H(r) = -2hr + 2\log(1 - e^{-dr})$, for 'finite' type,

where t is a thickness of the laminar body and d is the finite depth extent.

The thickness factor $(1 - e^{-tr})$ has an influence on the shape of the energy spectrum graph. The spectrum for a bottomless body has a maximum at $r = 0$. A body with limited thickness will have a spectrum with a characteristic peak, resulting in the maximum of the energy spectrum moving towards the higher frequencies (Figure A.3(a)).

The empirical studies done by Vacquier et al. (1951) indicate that causative bodies which are found at great depth, i.e. $h > 1.5km$, can be treated as bottomless bodies. Therefore, the model of the infinite prism in the depth interpretation of aeromagnetic data described in the frequency domain is adequate.

(II) Horizontal dimension and orientation factors

The energy spectrum of bodies with finite horizontal dimensions is strongly dependent on the factor $S^2(r,\theta)$ or $B(u,v)$, which, as was already noted in equation (14), is given as

$$B(u,v) = \frac{4}{uv} sin(ub) sin(va) \tag{17}$$

This factor involves the horizontal dimensions and orientation of the body, i.e. its geometry (Bhattacharyya, 1966a, Spector, 1968). In the case of a bottomless prism oriented at an angle γ with a respect to the $x-$axis (Spector, 1968), the factor $S^2(r,\theta)$ in polar coordinates can be expressed as

$$S(r,\theta) = \frac{sin^2[arsin(\theta+\gamma)]}{[arsin(\theta+\gamma)]^2} \cdot \frac{sin^2[brcos(\theta+\gamma)]}{[brcos(\theta+\gamma)]^2}. \tag{18}$$

The effect of this factor on the energy spectrum plotted on the frequency plane (u,v) results in the presence of two equally spaced series of null lines, orthogonal to each other and oriented at the angle $\gamma + 90^\circ$ with respect to the $u-$axis. In Figures A.4(a)-(b) (Bhattacharyya, 1966a) are presented contour diagrams of the two-dimensional amplitude spectra for a prismatic body of infinite depth extent and of dimensions h_t=3, a=5 and b=10 in Figure A.4(a), and b=1 at part (b) of this figure. In this case magnetisation of the prism is assumed to be due to induction only and the axis points to the magnetic north. The dip of the magnetic field is $60^\circ N$. The distance between the consecutive null lines is a function of the horizontal dimensions of the body:

$$a = \frac{\pi}{v_2 - v_1} \quad \text{and} \quad b = \frac{\pi}{u_2 - u_1},$$

where $u_2 - u_1$ and $v_2 - v_1$ are the wavelengths of the periods on the u and v axes respectively.

Because of the presence in equations (17) and (18) of the sine function and of the reciprocal of the frequency $1/u$, $1/v$ and $1/r$, the energy spectrum, plotted along the radial frequency axis, has the characteristics of damped oscillation with maxima and minima, occurring at the frequencies given by $ub = tan(ub)$ (see Figure A.3(b)). The rapid decay in amplitude of the function from the first maximum at $u = 0$ to the first minimum, decreases towards the higher frequency, with a decrease in dimension b. Hence, with a decrease in the size of the horizontal dimension, the higher frequency component in this factor increases. The finite horizontal size factor is of great concern with regard to depth estimation, because of the influence of the rate of spectral decay with frequency.

Spector (1968) paid particular attention to the influence of the size factor $S(r,\theta)$ on the radial component of the logarithmic energy spectrum, which provides a depth estimate. Figure A.3(b) shows the effect of the finite size factor. The set of curves shows that an increase of the size of the horizontal dimension causes quicker decay of spectral energy in the lower frequency zone, resulting in increasing estimated depth values. The complexity of this factor causes difficulty in removing its effect on depth estimates.

A.4 Geomagnetic and magnetisation direction cosine factor

The orientation of the geomagnetic vector $\vec{T}_0$ and the orientation of the polarised magnetisation vector $\vec{M}$ are expressed by a factor, which is a product of two functions $R_T(\theta)$ and $R_M(\theta)$. The latter are functions of the wavenumber azimuth, $\theta = tan^{-1}(u/v)$, and are independent of the wavenumber magnitude $r = \sqrt{u^2 + v^2}$.

The direction cosine factor is not related to the depth or geometry of the model. Hence, neglecting all other influences, depth estimates are not affected by the orientation of $\vec{M}$ or $\vec{T}_0$ vectors.

The use of a single model for the analysis and interpretation of the potential field caused by complex geological structures cannot provide an accurate and reliable solution. Therefore, an application of multi-model energy spectra has to be considered.

A.5 Spectral analysis of an ensemble model

Aeromagnetic maps are composed of a very large number of different effects, which are due to bodies of a wide range of geometry, distribution and magnetic properties. These bodies represent a bulk variation in the distribution of ferromagnetic minerals within the host rock. Such a scenario can be represented by a large set of individual discrete magnetic bodies with suitable geometrical parameters and magnetisation.

Spector (1968) and Spector and Grant (1970) carried out theoretical and empirical research on the application of the energy spectra to the statistical model of an ensemble of bodies with varied depth, width, thickness and magnetisation and position parameters. They assumed that the observed total magnetic field anomalies were caused by several ensemble models. As long as the logic of statistics is applied, there is no need to use very complicated models to comprise the assemblage of models simulating a real geological situation. Accordingly, they adopted as a basic model the rectangular prism, originally described by Bhattacharyya (1966a), but it was Spector (1968) who first introduced the notion of an ensemble. In the collection of a large number of individual bodies, whose parameters cover a wide range of possible values, each individual model can be identified from the values assumed by the depth, size, magnetisation and position, referred to as coordinates in n-dimensional parameter space. Thus each body is associated with a point in space and the collection of such points is referred to as the ensemble.

Based on the fundamental concept of statistical mechanics, which postulates that the mathematical expectation of the value of the energy spectra function is equal to the ensemble average of the energy spectrum $< E >$, the effect of the energy spectrum from the statistical model can be expressed as an integration over the 7-dimensional parameter space

$$\langle E \rangle = \int \cdots \int E \cdot \Phi(a, b, t, h, I, D, M) dV ,$$

where

E is the energy spectrum expressed in equation (15);
Φ is the ensemble joint frequency distribution for the parameters a, b, t, h, I, D and M;
a, b, t, h are geometrical parameters of the bodies;
I is the inclination and D is the declination of the magnetic moment vector M.

On the assumption that each of the parameter space variables varies independently, the joint probability distribution function Φ is a product of individual prior frequency distribution functions;

$$\Phi(a, b, \ldots, M) = \Phi_1(a) \cdot \Phi_2(b) \cdot \Phi_3(t) \cdot \Phi_4(h) \cdot \Phi_5(I) \cdot \Phi_6(D) \cdot \Phi_7(M)$$

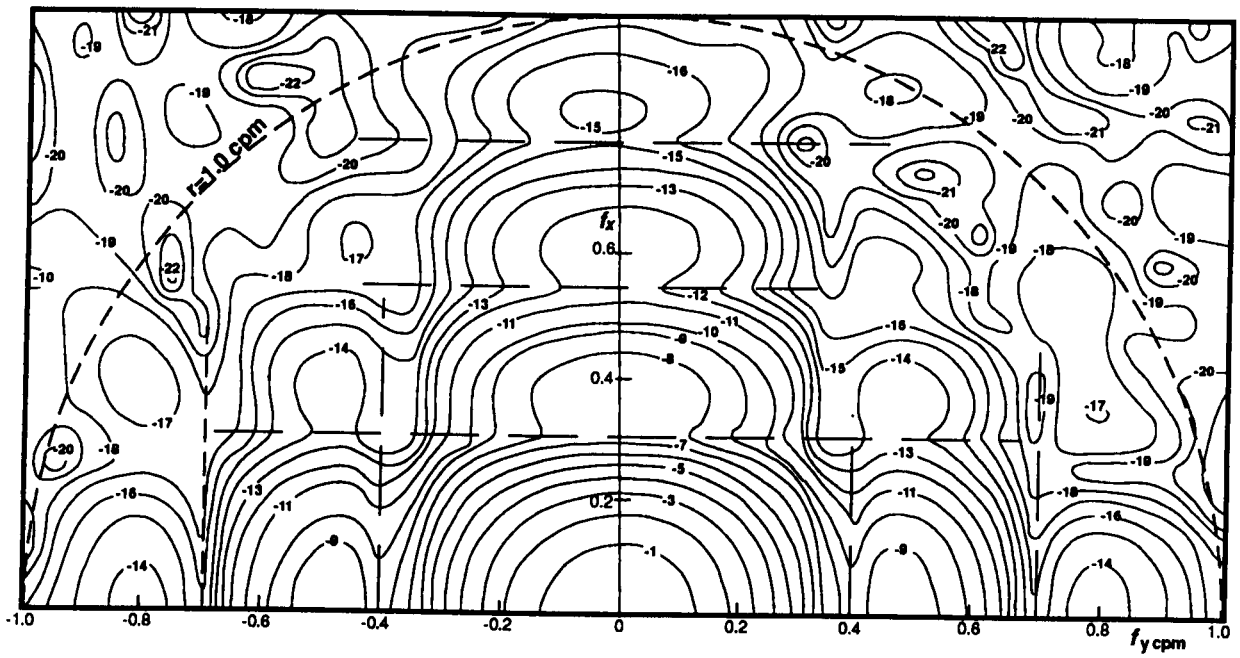

Figure A.5 Normalized logarithmic energy spectrum of map containing bottomless prism anomaly. After Spector (1968).

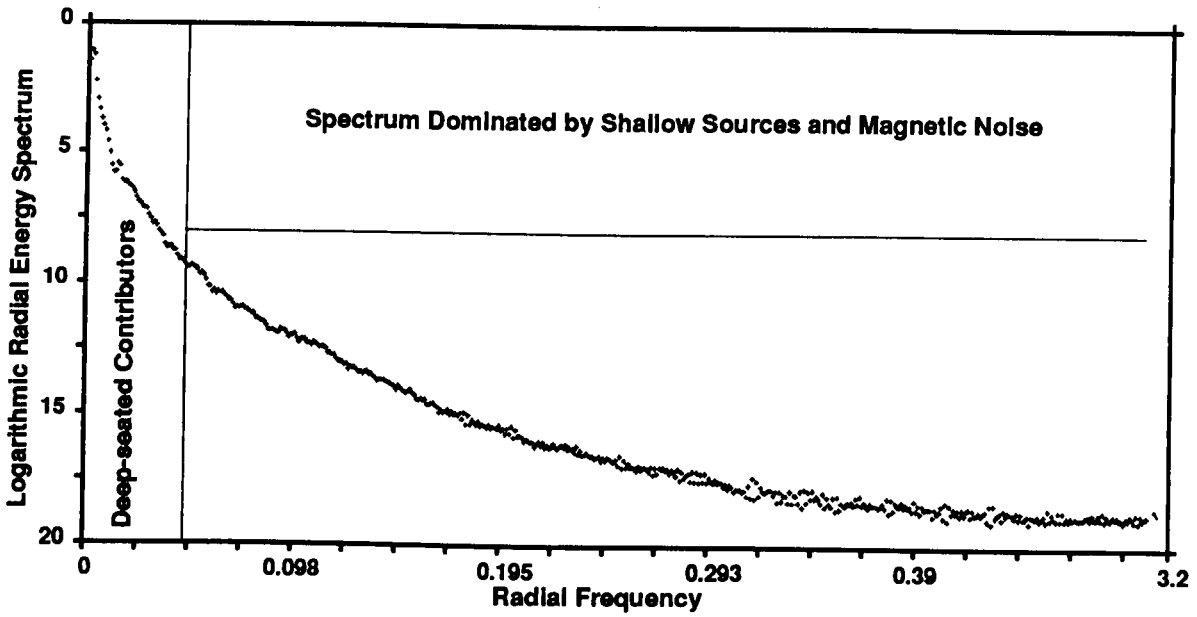

Figure A.6 Logarithmic radial energy spectrum of total magnetic intensity field.

Assuming also that each of the parameter's space variables has a uniform prior probability within a specified range (i.e. the width a is uniformly distributed in $(0,2\bar{a})$, b in $(0,2\bar{b})$, t in $(0,2\bar{t})$, h in $\bar{h}\pm\Delta h$, I in $\bar{I}\pm\Delta I$, and D in $\bar{D}\pm\Delta D$) an ensemble average of the energy spectrum $<E>$ is given as

$$\langle E\rangle = \frac{1}{V}\int\cdots\int E(r,\theta)\cdot da\cdot db\cdot dt\cdot dh\cdot dI\cdot dD\cdot dM, \tag{19}$$

where V is the 7-dimensional parallelepiped which is defined by the limits of the frequency distribution functions.

From the combination of equations (15) and (19) the expression for energy spectra can be written as

$$\langle E(r,\theta)\rangle = 4\pi^2\bar{k}^2\cdot\langle R_T(\theta)\rangle\cdot\langle R_M(\theta)\rangle\cdot\langle e^{-2hr}\rangle\langle(1-e^{-tr})^2\rangle\langle S^2(r,\theta)\rangle.$$

Under a further assumption that for a moderately large number of bodies the average values of magnetic inclination I and declination D will vary less than 20° of the geomagnetic field, and after reduction to the north magnetic pole, the new simplified form of the energy spectrum can be derived as

$$\langle E(r,\theta)\rangle = 4\pi^2\bar{k}^2\langle e^{-2hr}\rangle\langle(1-e^{-tr})^2\rangle\langle S^2(r,\theta)\rangle.$$

Such simplification is valid only if the anomaly patterns are depicted close to the specified characteristic for the particular magnetic latitude. The reduction of the energy spectrum to the north magnetic pole is no problem in the high latitudes ($R_T(\theta)$ is always known); however, care must be taken at low magnetic latitudes, close to the geomagnetic equator where $R_T(\theta)$ becomes exceedingly asymmetric.

A.6 Properties of the energy spectrum of the statistical model

The presentation of the energy spectrum in a map form (see Figure A.5) is less practical than a profile presentation. When the horizontal dimension $\bar{a}$ (or $\bar{b}$) is moderately large certain irregularities on the energy spectrum contours will occur due to the oscillatory nature of the function $<S^2(r,\theta)>$ which varies unstably with the angle θ. The radial component of the spectrum is averaged with respect to angle θ to reduce its effect.

The logarithm of the radial average of the energy spectra $E(r,\theta)$ is plotted versus radial frequencies r (Figure A.6). The radial energy spectrum is computed over the whole plane (u,v).

For the radius equal to the subsequent frequency intervals the energy spectra values are interpolated based on the values around the circle. Next, the energy spectra values are averaged along the circle for subsequent radius. Accordingly, the radial average energy spectrum can be expressed as follows:

$$\langle E(r)\rangle = 4\pi^2\bar{k}^2\langle e^{-2hr}\rangle\langle(1-e^{-tr})^2\rangle\langle S^2(r)\rangle, \tag{20}$$

where

$$\langle S^2(r)\rangle = \frac{1}{\pi}\int_0^{\pi}\langle S^2(r,\theta)\rangle d\theta\,. \tag{21}$$

Moreover, as an additional modification of the expression of the energy spectrum, the logarithm of the spectra is taken. The properties of the logarithmic form of the spectrum allows complete control of the influence of the ensemble parameters $\bar{k},\bar{h},\bar{t}$ and $\bar{a}$. As mentioned, for final analysis of the depth estimates, the logarithm of the radial average energy spectrum is plotted versus radial frequency (see Figure A.6).

(I) Effect of the ensemble average depth factor

The expression (20) of the radial spectrum includes the ensemble average depth $\bar{h}$ only in the factor $< e^{-2\bar{h}r} >$ which is equal to $\{e^{-2\bar{h}r}\cdot sin(h)\cdot(2r\Delta h)/4r\Delta h\}$, where Δh is the variation of the depths between models in each ensemble and is normally set at a value not greater than half of the ensemble average depth $|\Delta h| < 1/2\bar{h}$. When radial frequency values are less than the reciprocal of the ensemble average depth $r < 1/\bar{h}$, the value $< e^{-2\bar{h}r} >$ is equal to the term $e^{-2\bar{h}r}$ and the logarithm of this factor approximates to a straight line whose slope is $-2\bar{h}$. This slope is equal to the mean depth of the statistical model. The term $e^{-2\bar{h}r}$ is the dominating factor in the power spectrum.

(II) Effect of the mean depth extent factor

The mean depth extent of the magnetic sources $\bar{t}$ enters only into the factor

$$\langle(1-e^{-tr})^2\rangle = 1-(3-e^{-2\bar{t}r})(1-e^{-2\bar{t}r})/4\bar{t}r\,.$$

The depth extent factor is a complex function and plays an interesting role in shaping the power spectrum. The function, consisting of the depth factor and the depth extent factor, has a characteristic peak in the spectrum which moves towards the higher frequency with decreasing average thickness of the bodies (see Figure A.3(a)). In the case of a set of magnetic bodies with an unlimited depth extent (so that their bottom surfaces cannot be discerned through the window of analysis), the value of $\bar{t}$ becomes very large. The spectrum has its maximum at $r = 0$ and the peak does not appear on the graph at all (see Figure A.3(a)). Hence, from the characteristic shape of the

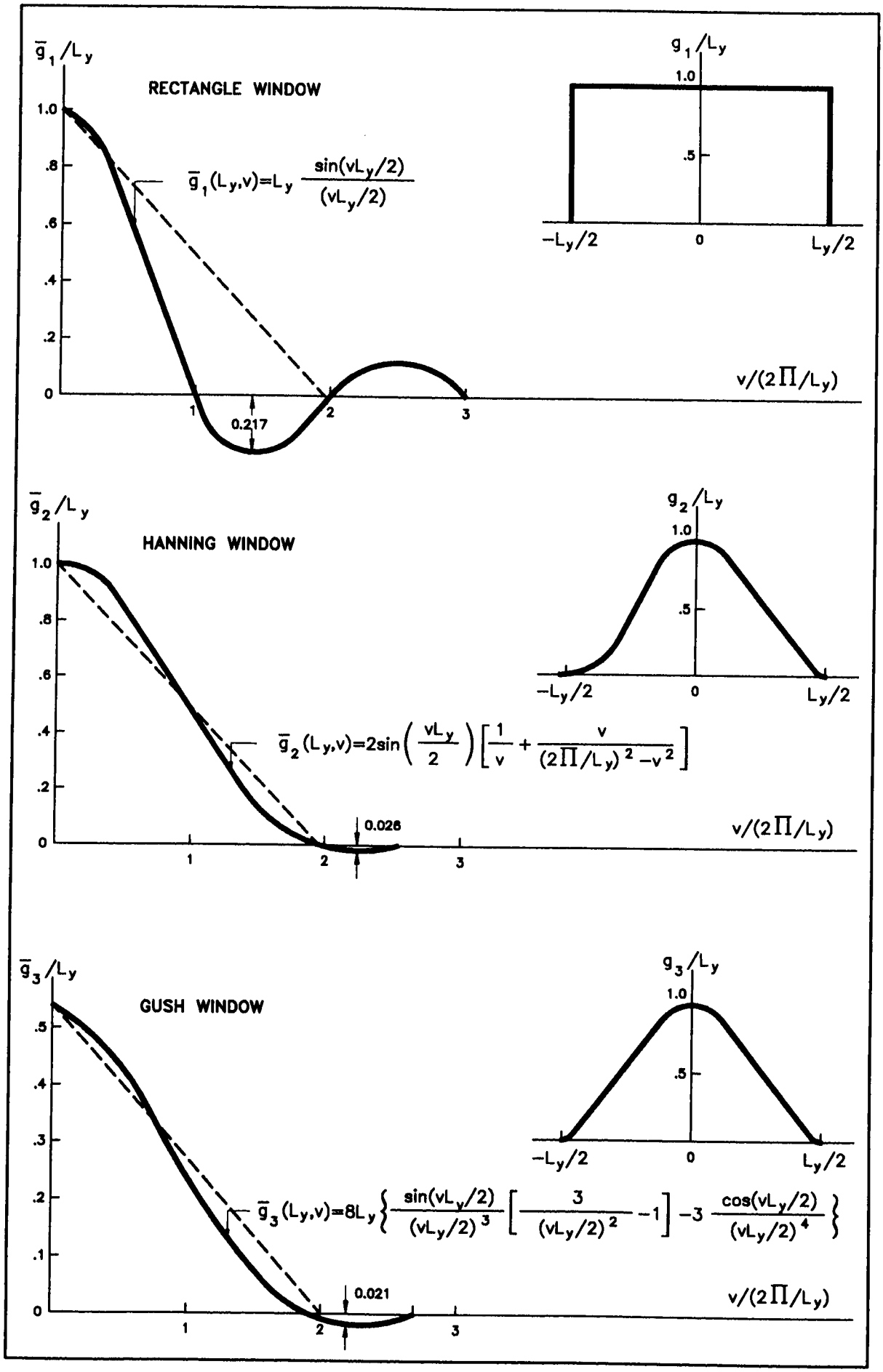

Figure A.7 Weighting functions and spectral windows.

spectrum and the position of the spectrum peak, the indication of limited/unlimited thickness of the ensemble of the bodies can be inferred, as Figure A.3(a) shows. Whether the assemblage of the models appears to have a limited depth extent, or not, will depend to a the great degree on the size of the analysed window.

(III) Effect of the finite map size (edge effect)

The definition of the energy spectrum assumes that the magnetic field function $F(x, y)$ is defined over the entire plane of observation. An aeromagnetic map can be considered as a 'window' through which only a part of the total magnetic intensity field is observed. Because analyses are carried out on a limited area, the knowledge of the magnetic field (or ' field function') is incomplete, and thus only an estimate of the true energy spectrum can be obtained. Spector (1968) proposed a synthetic solution to satisfy an assumption of complete definition by multiplying $F(x, y)$ with a weighting function, or 'space window' $G(x, y)$ vanishing outside the original 'window'. The original 'window' is the region of field definition: $-L_X/2 \le x \le L_X/2$ and $-L_Y/2 \le x \le L_Y/2$, where L_X, L_Y are the dimensions of the map and the origin of the coordinates system is set up at the centre of the map. The modified version of the total field intensity is defined as

$$F'(x, y) = F(x, y) \cdot G(x, y)$$

where its Fourier transform is

$$\overline{F}'(u, v) = \int_{-\infty}^{\infty} \int_{-\infty}^{\infty} [F(x, y) \cdot G(x, y)] \cdot e^{-i(ux+vy)} dxdy .$$

The Fourier transform of the product of two functions is the convolution of the transforms of the two functions:

$$\overline{F}'(u, v) = \frac{1}{4\pi^2} \overline{G} * \overline{T} .$$

Such an operation is a smoothing process on the transform $\overline{F}(u, v)$.

The simplest weighting function is the 'boxcar' function which has the value of unity over the original 'window' and is equal to zero elsewhere (see Figure A.7(a)). Its transform, or spectral window is

$$\overline{G}_1(u, v) = \overline{g}_1(L_X, u) \cdot \overline{g}_1(L_Y, v)$$

where

$$\overline{g}_1(L_Y, v) = L_Y \cdot \sin(vL_Y/2)/(vL_Y/2) .$$

The Fourier transform of the product of two functions is the convolution of the transforms of the two functions:

$$\overline{F}'(u,v) = \frac{1}{4\pi^2}\overline{G} * \overline{T}$$

Such an operation is a smoothing process on the transform $\overline{F}(u,v)$.

The simplest weighting function is the 'boxcar' function which has the value unity over the original 'window' and is equal to zero elsewhere (see Figure A.7(a)). Its transform, or spectral window is

$$\overline{G}_1(u,v) = \overline{g}_1(L_x,u)\cdot\overline{g}_1(L_y,v)$$

where

$$\overline{g}_1(L_y,v) = L_y\cdot\sin(vL_y/2)/(vL_y/2).$$

The function $\overline{g}_1(L_y,v)$ is illustrated in Figure A.7(a). At high frequencies, the sharp edges of the boxcar function would cause distortion if $\overline{G}_1(u,v)$ were convolved with $F(x,y)$. The boxcar function is thus undesirable. Spector also considered two other weighting functions: the 'Hanning window' and 'Gush window' (see Figure A.7(b)-(c)). The 2-dimensional extension of the Hanning window is a weighting function which decreases continuously to zero along the borders of the original window (Figure A.7(b)):

$$G_2(x,y) = \frac{1}{4}\left(1+\cos\left(\frac{2\pi x}{L_x}\right)\right)\cdot\left(1+\cos\left(\frac{2\pi y}{L_y}\right)\right), \quad \text{in } R$$

$$= 0 \qquad \text{elsewhere.}$$

R is the rectangular window on which the data has been collected.

The Fourier transform of this function is

$$\overline{G}_2(u,v) = \overline{g}_2(L_x,u)\cdot\overline{g}_2(L_y,v)$$

where

$$\overline{g}_2(L_y,v) = 2\sin\left(\frac{vL_y}{2}\right)\cdot\left[\frac{1}{v}+\frac{v}{\left(\frac{2\pi}{L_y}\right)^2 - v^2}\right]$$

The function $\bar{g}_2(L_y, v)$, as shown in Figure A.7(b), has a very small negative side-lobe compared to the function $\bar{g}_1$.

The third weighting function proposed by Spector (1968), the 'Gush window', decreases continuously to zero along the borders of the original window presenting the following form

$$G_3(x,y) = \left[1-(2y/L_y)^2\right]\cdot\left[1-(2x/L_x)^2\right], \qquad \text{in } R$$

$$= 0 \qquad \text{elsewhere.}$$

The Fourier transform is

$$\bar{G}_3(u,v) = \bar{g}_3(L_x,u)\cdot\bar{g}_3(L_y,v)$$

where

$$\bar{g}_3(L_y,v) = 8L_y\left\{\frac{\sin(vL_y/2)}{(vL_y/2)^3}\cdot\left[\frac{3}{(vL_y/2)^2}-1\right]-3\frac{\cos(vL_y/2)}{(vL_y/2)^4}\right\}.$$

The 'Gush window' as shown in Figure A.7(c) is similar in shape to the 'Hanning window'.

The problem of choosing the best designed weighting function was subjected to extensive research in the past (Blackman and Tukey, 1959; Hou et al., 1977).

Hou et al. (1977) designed a weighting function which has similar, but improved performance, compared to the 'Hanning window'. This window totally eliminates the negative side-lobes. The spectral window designed by Hou was applied to all computations of the energy spectra in this thesis.

A.7 Geomagnetic field factor - Reduction to the North Magnetic Pole

The energy spectrum of an aeromagnetic map is dependent on the orientation of the geomagnetic vector $\bar{T}_o$ i.e. the inclination I_E and declination D_E. The dependence of the energy spectrum on the orientation of the geomagnetic field vector is described by the following factor:

$$\Gamma_T(\theta) = sinI_E + icosI_E\cdot sin(D_E+\theta) = A + iB$$

where

$$A = \sin I_E \qquad \text{and} \qquad B = \cos I_E \cdot \sin(D_E + \theta)$$

and θ is the angular position on the frequency plane; $\theta = tan^{-1}\frac{u}{v}$.

In the energy spectrum this factor is expressed as

$$R_T(\theta) = 1 - \cos^2 I_E \cdot \cos^2(\theta + D_E) = A^2 + B^2 .$$

The factor $R_T(\theta)$ is a function of the argument θ, which distorts the energy spectrum from its otherwise symmetrical circular form having an extreme at

$$\theta_{max} = -D_E \pm \frac{\pi}{2} \qquad \text{and} \qquad \theta_{min} = -D_E ; -D_E + \pi .$$

In the high geomagnetic latitude (I_E) the distortion is significantly decreased. If an inclination I_E and a declination D_E are determined e.g. from the world magnetic charts, the effect of the orientation of the geomagnetic field vector $\vec{T}_o$ can be simply removed by dividing the energy spectrum by $R_T(\theta)$. Such an operation has the same effect as transformation of the TMI data to the North Magnetic Pole (RTP) i.e. vector $\vec{T}_o$ becomes perpendicular to the observation plane. The whole procedure simplifies the energy spectrum calculation and is necessary in the low and middle latitudes, where magnetic anomalies are asymmetric, as their maximum is usually not positioned above the centre of causative body.

The inverse transform of the complex spectrum expressed in its real and imaginary form

$$\overline{T}(u, v) = R - iP$$

will describe the pole-reduced spectrum in the following expression

$$\overline{T_1}(u, v) = \frac{AR + BP}{A^2 + B^2} - i\frac{AP - BR}{A^2 + B^2} .$$

A.8 Geomagnetic field factor - Remanent magnetisation

The magnetisation of the source consists of the vector sum of the induced magnetisation and the remanent magnetisation. If the demagnetisation effect is ignored, the induced magnetisation vector is equal to $k\vec{T}_o$, where k is the bulk magnetic susceptibility. The remanent or permanent magnetisation determines the angular displacement of the magnetisation vector from the direction of the geomagnetic vector $\vec{T}_o$. Fourier transformed aeromagnetic maps may indicate remanent magnetisation, if there is a consistent orientation of the remanent magnetisation vectors in the study area.

Under an assumption that causative bodies have uniform magnetisation $\vec{M}(I_X, D_X)$ the direction of the polarised magnetisation can be estimated from the energy spectrum, which will include the factor $\Gamma_T(\theta)\cdot\Gamma_M(\theta)$, where

$$\Gamma_M(\theta) = \sin I_x + i\cos I_x \cdot \sin(D_x + \theta) = \alpha + i\beta ,$$

and after reducing the energy spectrum to the magnetic pole the presence of the factor

$$R_M(\theta) = 1 - \cos^2 I_X \cdot \cos^2(\theta + D_X) = \alpha^2 + \beta^2$$

which has its extreme at

$$\theta_{max} = -D_X \pm \frac{\pi}{2} \qquad \text{and} \qquad \theta_{min} = -D_X; -D_X + \pi .$$

This function will have the minimum to maximum amplitude $\sin^2 I_X : 1$. From these characteristics both an inclination I_X and a declination D_X can be estimated.

To minimise or offset the influence of all other factors in the spectral expression, the energy spectrum could be averaged considering all computed values of the energy spectrum within the interval $r \pm \Delta r$ over the intervals $\Delta\theta$.

The procedure discussed above is based on the assumption that the effects of demagnetisation are not significant. In many cases, such as dykes, the direction of the induced magnetic moment is influenced by the geometry of the magnetic sources. Natural aeolotropy may occur if the width is significantly less than the strike-length of the body. The bulk susceptibility is smaller in the direction perpendicular to the plane of the body than in a direction parallel to it. This causes a deviation of the induced magnetic moment of the body from the direction of the geomagnetic

field, T_0, towards the plane of the body. The variation of the bulk susceptibility with the direction in the body is due to the demagnetisation effects (Grant & West, 1965) and may be considered as an additional component of the magnetisation which is added vectorially to the remanent magnetisation of the body and is reflected in the factor $R_M(\theta)$. Therefore, the true direction of the remanent magnetisation can be established only if the contribution of the demagnetisation effect is known.

A.9 Geomagnetic field factor - Double RTP

Aeromagnetic maps are sometimes very complex. If the distribution of the causative bodies has strong anisotropy in one or more directions, the energy spectrum will reflect the directions of such trends and, of course, will virtually preclude meaningful estimation of the direction of polarisation. Hence, the direction of a vector $\vec{M}$ can be usefully determined only in cases of simple-shaped single magnetic bodies with negligible natural aeolotropy.

Spector (1968) shows that the energy spectrum can also be applied in a different manner to detect the presence of sources with remanent magnetisation deflecting from the direction of the geomagnetic field $\vec{T}_o$. The inverse transform of the reduced to the pole energy spectrum will shape the magnetic anomalies to appear to be more symmetrical and positioned more directly above the causative bodies. If magnetic bodies are magnetised in a direction parallel with $\vec{T}_o$, and such transformation is repeated twice, the character of the magnetic anomalies will become more like gravity anomalies, either all positive or all negative and positioned directly over the sources. The bodies with magnetisation direction deviating from $\vec{T}_o$, i.e. having remanent magnetisation and/or strong natural aeolotropy will generate anomalies with both positive and negative components.

The operation of the double reduction to the North Magnetic Pole of the energy spectrum can be computed at all points on the frequency plane, assuming that the real and imaginary components of the complex spectrum and also the direction of the vector $\vec{T}_o$, i.e. its inclination I_E and declination D_E, are given.

Appendix B

Estimation of the average depth to the top of magnetic sources from the model data

The observed magnetic field is the sum of a regional field, residual field and a noise component. However, the distribution of magnetic sources is considered as a vertically superimposed multi-layer model with a random distribution of numerous sources around a discrete level. Therefore, the frequency components of magnetic anomalies being the effect of horizontally displaced causative sources occurring around a particular depth level, are all main contributors to the relevant section of the spectrum. The decay of the spectrum is approximated by linear segments whose slope is related to an average ensemble depth of a particular depth layer. Such an interpretation can only be applied to linear spectra, in which distinct linear segments correspond to separate depth ensembles, and which contain minimum effect from sources at different levels. As discussed in Section 5.13 energy spectral analysis method has its limitations, mainly due to:

- the effect of the horizontal dimensions of the causative bodies,
- the effect of the thickness factor.

The results of energy spectral analysis are also dependent on the distribution of the anomalies within the spectral window, and the dimensions of both the spectral window and the extension window (extrapolation array).

Energy spectra of several artificial models, composed of simple magnetic bodies and more complex multi-prism sets, were computed to test the accuracy of the depth estimates. The limitations of the method were also considered. The description of the analysed models and the computation results, are discussed below.

(I) Single prism model

The method was tested for a single vertical prism model with limited and unlimited depth extent, which was placed at various depth levels. Sample interval of the grid data generated for each model equals unity. The contour maps of the magnetic fields generated by each individual model and the relevant graphs of computed logarithmic radial energy spectrum are presented at Figures B.1-B.5. The estimated depth values and real depth to the top of computed model are listed in Table 5.2a.

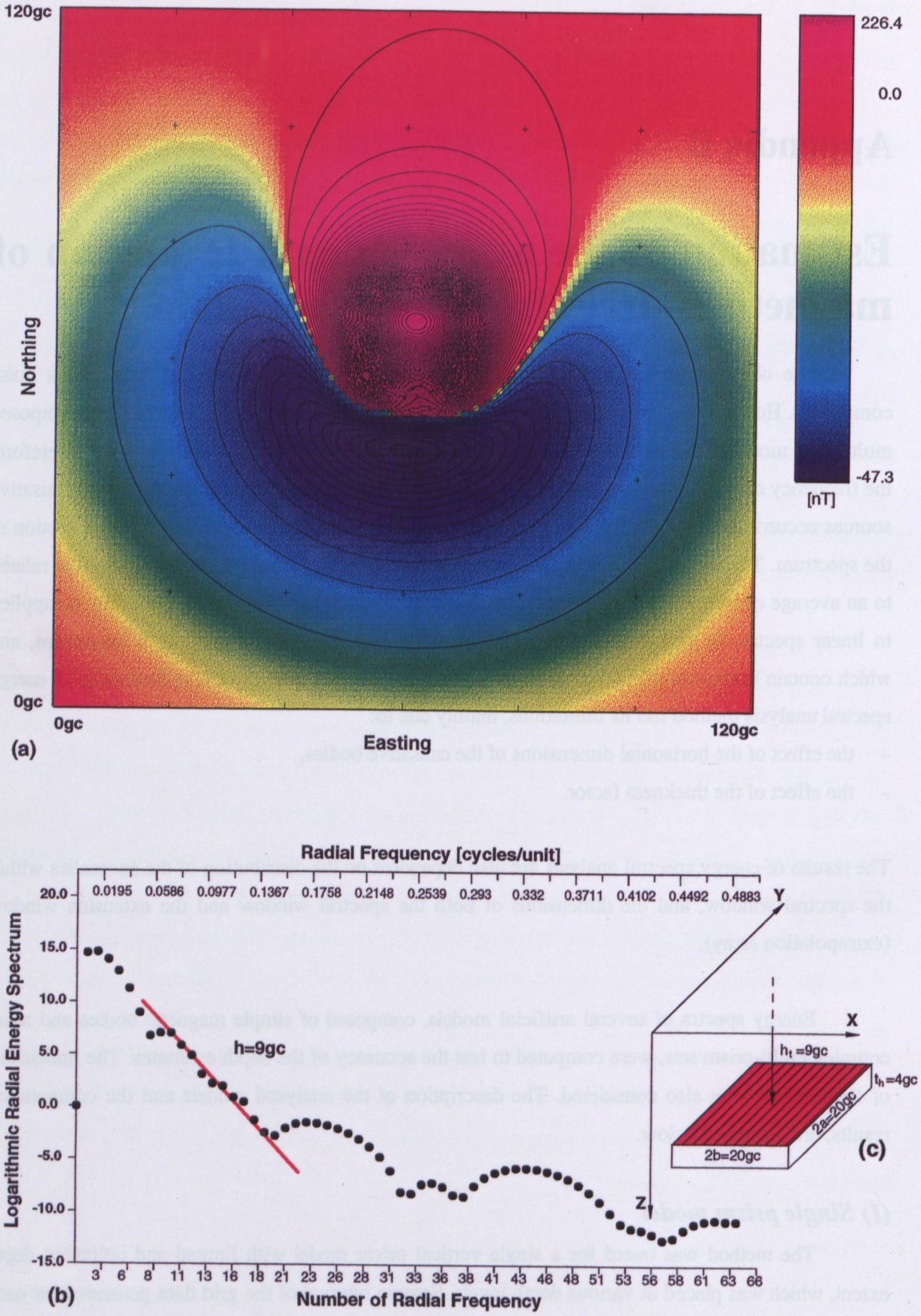

Figure B.1 Model data of shallow, thin, vertical-sided prism with large horizontal dimensions. The original map size 120x120gc, extension window 128x128gc, where gc=grid cell.
(a) Colour image with superimposed contours of the magnetic field.
(b) Logarithmic radial energy spectrum of the magnetic field.
(c) Parameters of the prism model.

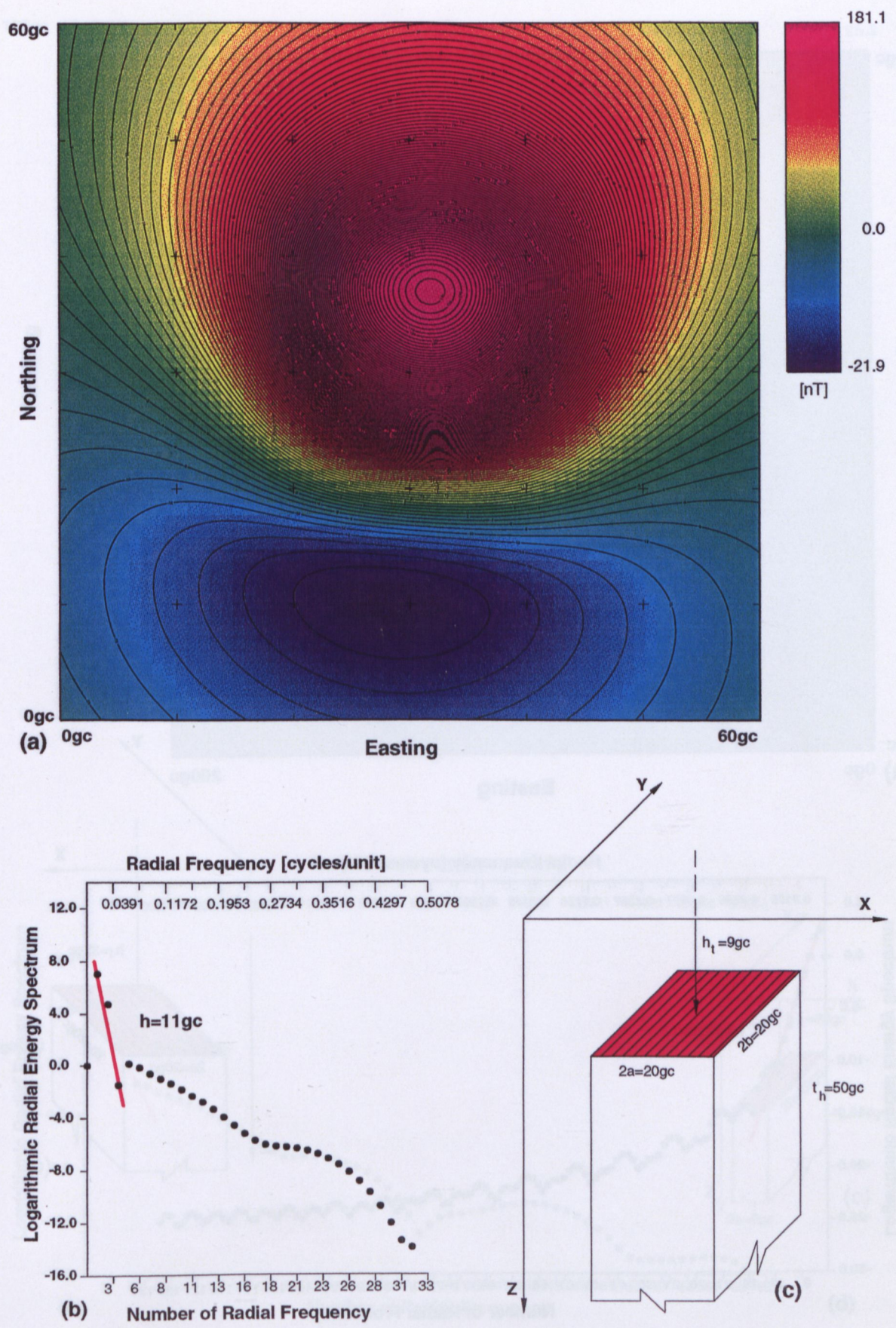

Figure B.2 Model data of shallow, large, vertical-sided prism with very large depth of extent. The original map size 60x60gc, extension window 64x64gc, where gc=grid cell.
(a) Colour image with superimposed contours of magnetic field.
(b) Logarithmic radial energy spectrum of the magnetic field.
(c) Parameters of the prism model.

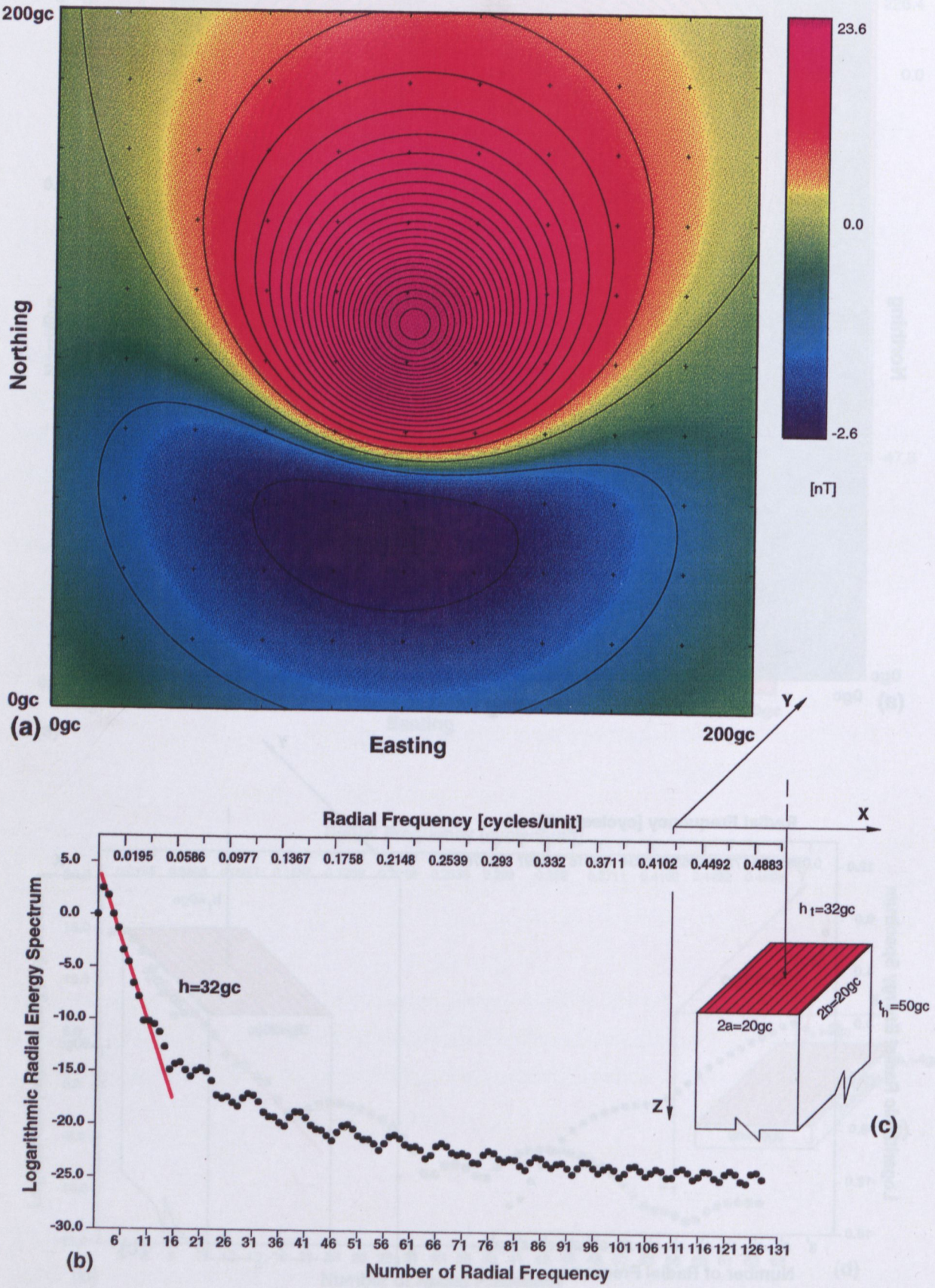

Figure B.3 Model data of deep, large, vertical-sided prism with very large depth of extent. The original map size 200x200gc, extension window 256x256gc, where gc=grid cell.
(a) Colour image with superimposed contours of the magnetic field.
(b) Logarithmic radial energy spectrum of the magnetic field.
(c) Parameters of the prism model.

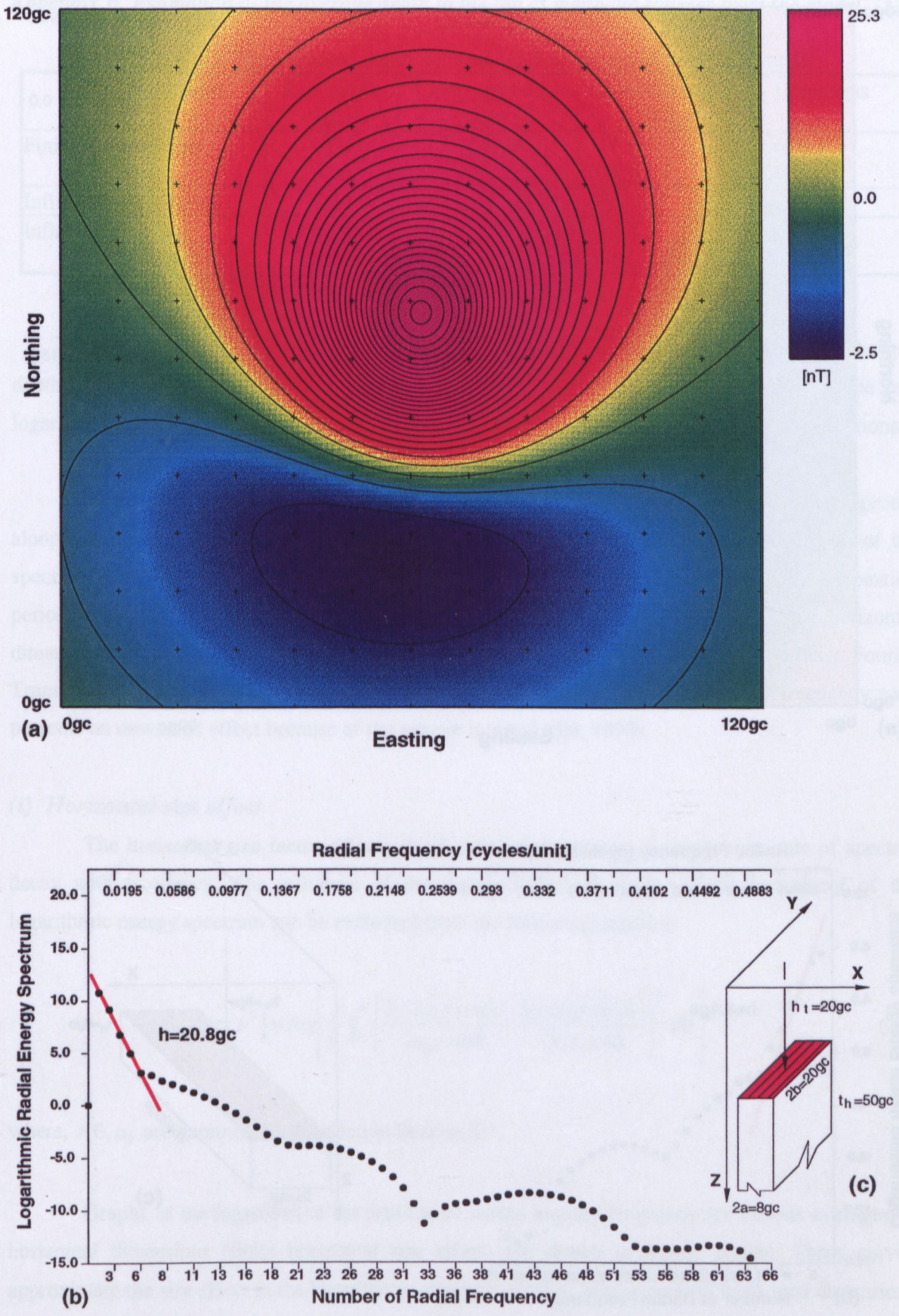

Figure B.4 Model data of deep, long and narrow, vertical-sided prism with large depth of extent. The original map size 120x120gc, extension window 128x128gc, where gc=grid cell.
(a) Colour image with superimposed contours of the magnetic field.
(b) Logarithmic radial energy spectrum of the magnetic field.
(c) Parameters of the prism model.

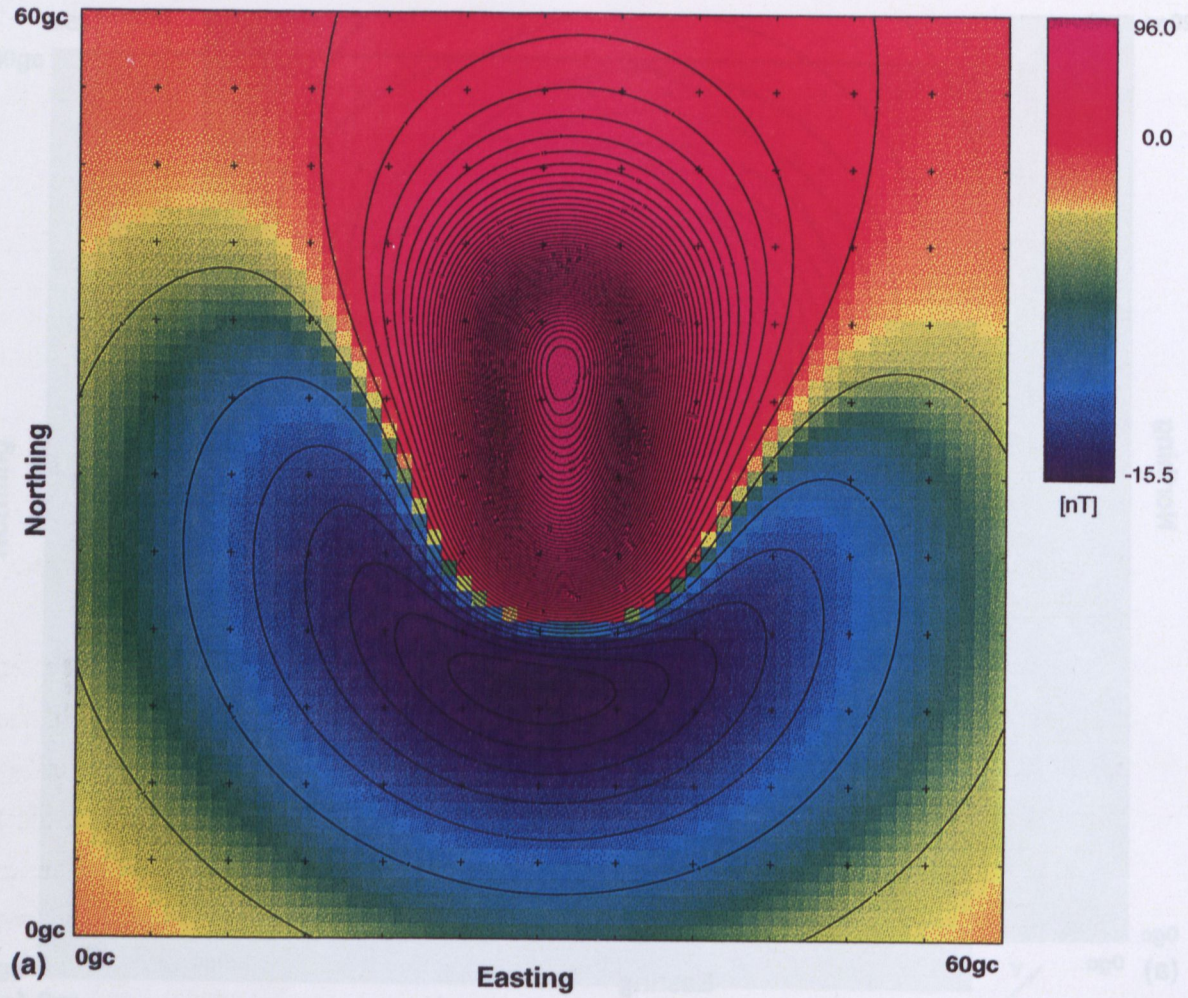

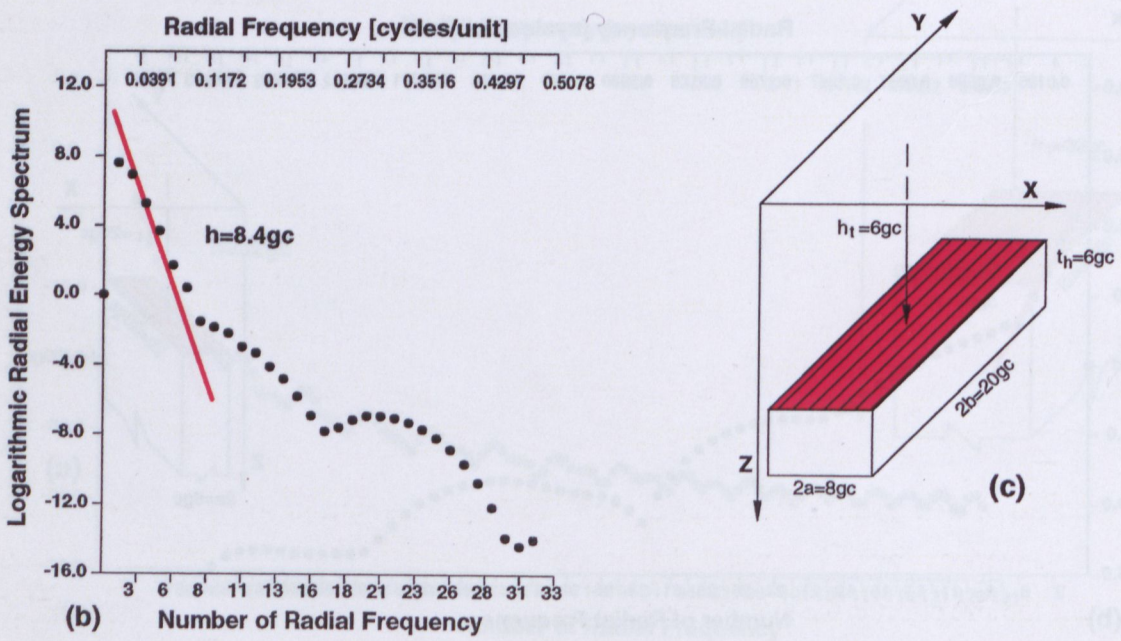

Figure B.5 Model data of shallow, long and narrow, vertical-sided prism with limited thickness. The original map size 60x60gc, extension window 64x64gc, where gc=grid cell.
(a) Colour image with superimposed contours of the magnetic field
(b) Logarithmic radial energy spectrum of the magnetic field.
(c) Parameters of the prism model.

Table B.1 The estimated depth and real depth to the top of computed model.

Model description	Real depth [gc]	Computed depth [gc]	Relative error [%]	Comments
Finite shallow prism	9.00	10.00	11.1	Figure B.1
	6.00	7.45	24.2	Figure B.5
Infinite shallow prism	9.00	11.50	16.7	Figure B.2
Infinite deep prism	32.00	33.08	3.4	Figure B.3
	20.00	20.80	4.0	Figure B.4

Depth unit [gc] = grid cell size

The results shown in Table B.1 indicate that the estimated depths are greater than the real depths. Errors in the results obtained are due to the effect of the horizontal size factor. The raw logarithmic radial energy spectrum needs to be corrected to obtain more accurate depth estimations.

The distribution of the energy spectrum of a single body has a characteristic period repeated along the whole frequency range, and is due to the horizontal size effect. The amplitude of the spectrum decays with the increase of frequency (Figure B.2(b) and Figure B.4(b)). Those repeating periods are not so distinct, when the extension array is considerably bigger than the horizontal dimensions of the analysed body. Due to the approximation of the spectrum by Fast Fourier Transformations, only the low frequency part of the spectrum is considered. The high frequency zone presents an unwanted effect because of the sample interval (Shi, 1993).

(i) Horizontal size effect

The horizontal size factor affects depth estimation because it changes the rate of spectral decay with frequency. The influence of the finite size effect on the radial component of the logarithmic energy spectrum can be evaluated from the following equation

$$log\left[< S(r) >^2\right] = log\left[\frac{1}{\pi}\int_0^{\pi}\left\{\frac{S_i(2a_0 r\sin\theta)}{2a_0 r\sin\theta}\cdot\frac{S_i(2a_0 r\cos\theta)}{2a_0 r\cos\theta}\right\}^2 d\theta\right] \qquad (22)$$

where, r, θ, a_0 are parameters described in Section 5.1.

Graphs of the logarithm of the size factor versus angular frequency for various averages of horizontal dimensions (finite horizontal size effect) are shown at Figure A.3(b). These curves approximate the size effect in the logarithmic energy spectrum. With increased horizontal dimensions of the analysed body, the estimated depth also increases, being the result of increased rate of decay of the curve representing the horizontal size effect.

The correction of the size effect is achieved by subtraction of the appropriate curve of the finite horizontal size effect (shown at Figure A.3(b)) from the radial component of the logarithmic

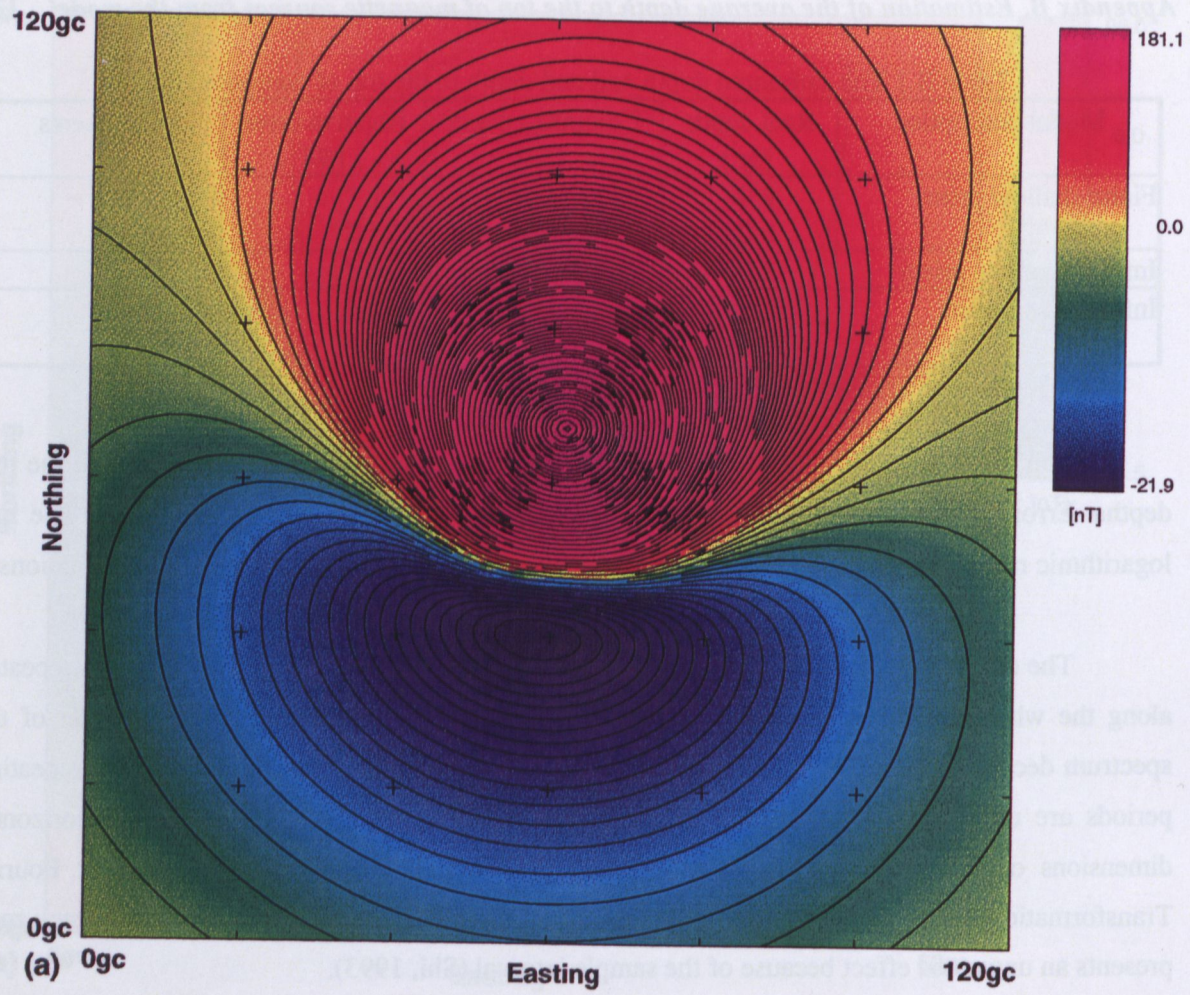

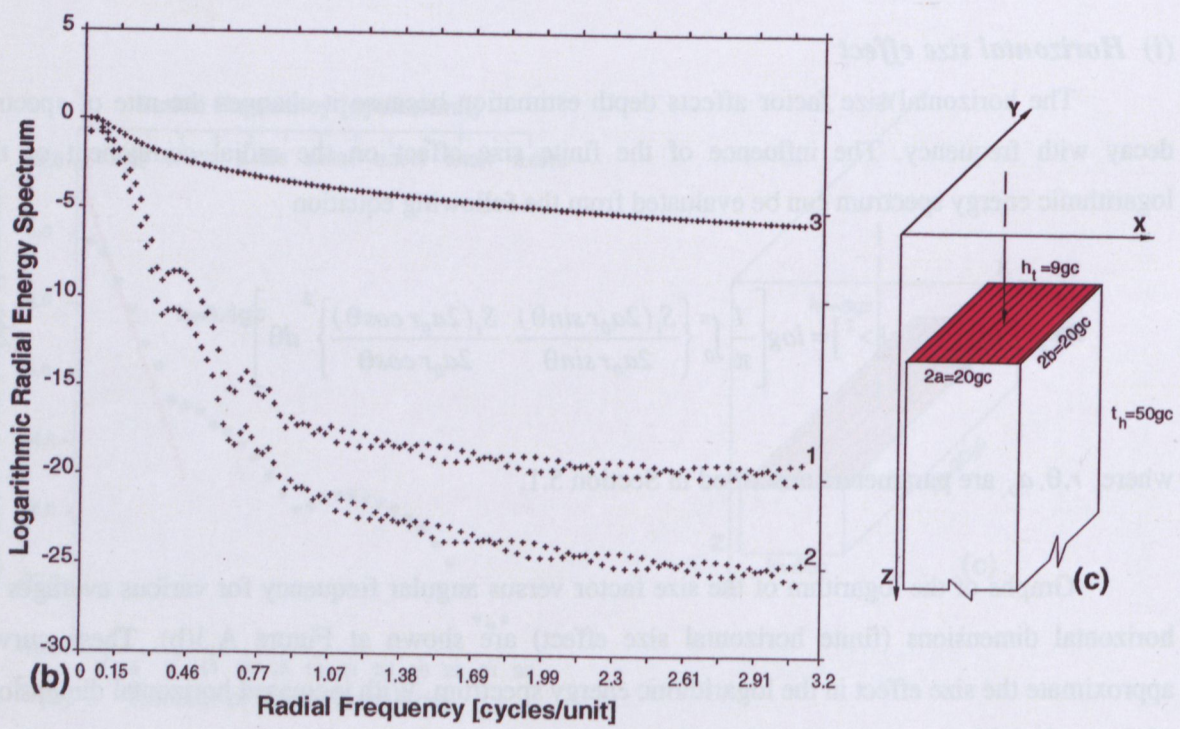

Figure B.6 Model data of shallow, large, vertical-sided prism with very large depth extent. The original window size 120x120gc, extension window 256x256gc, gc=grid cell.
(a) Colour image with superimposed contours of the magnetic field.
(b) Logarithmic radial energy spectra of the magnetic field prior '1' and after '2' size correction and 'horizontal size effect' curve '3'.
(c) Parameters of the prism model.

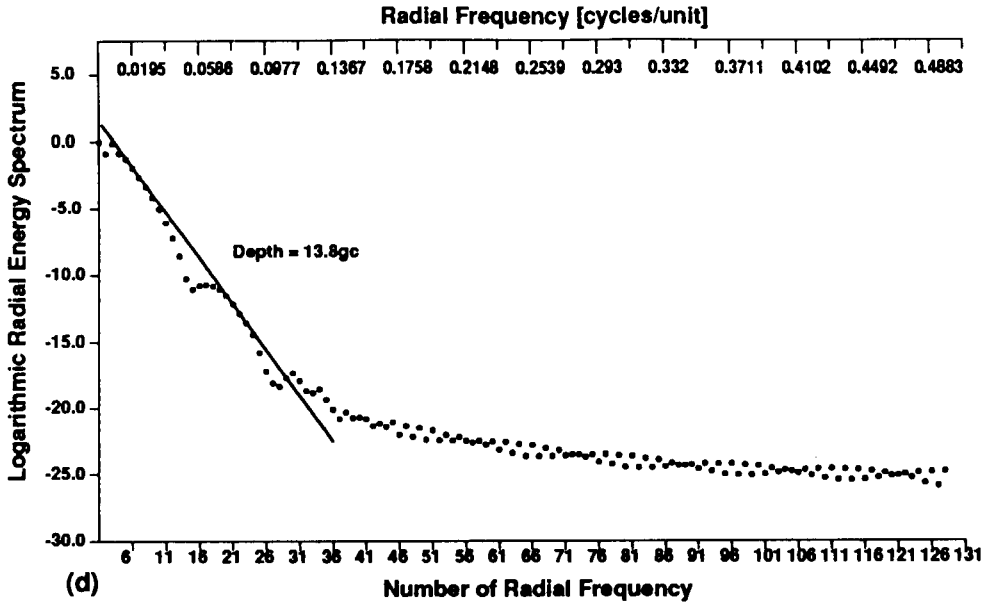

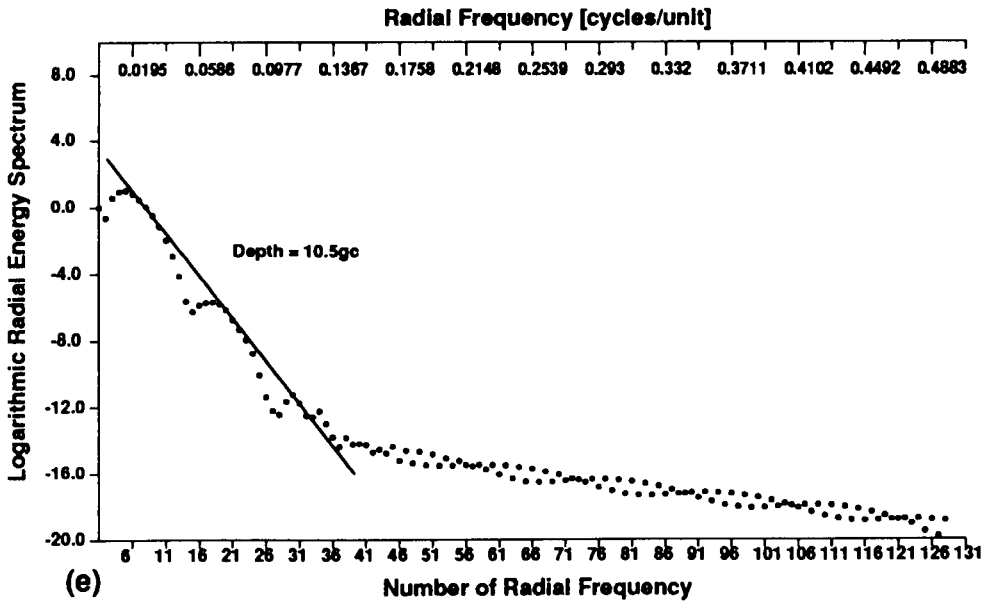

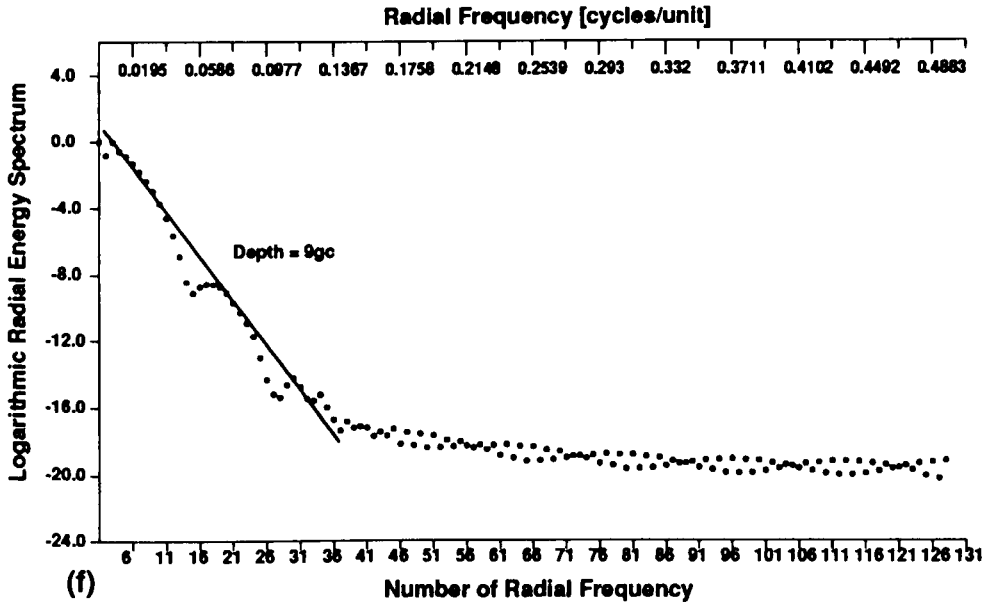

(d) Logarithmic radial energy spectrum of the magnetic field.
(e) Logarithmic radial energy spectrum of vertical gradient of the magnetic field.
(f) Logarithmic radial energy spectrum of vertical gradient of magnetic field with applied horizontal size correction.

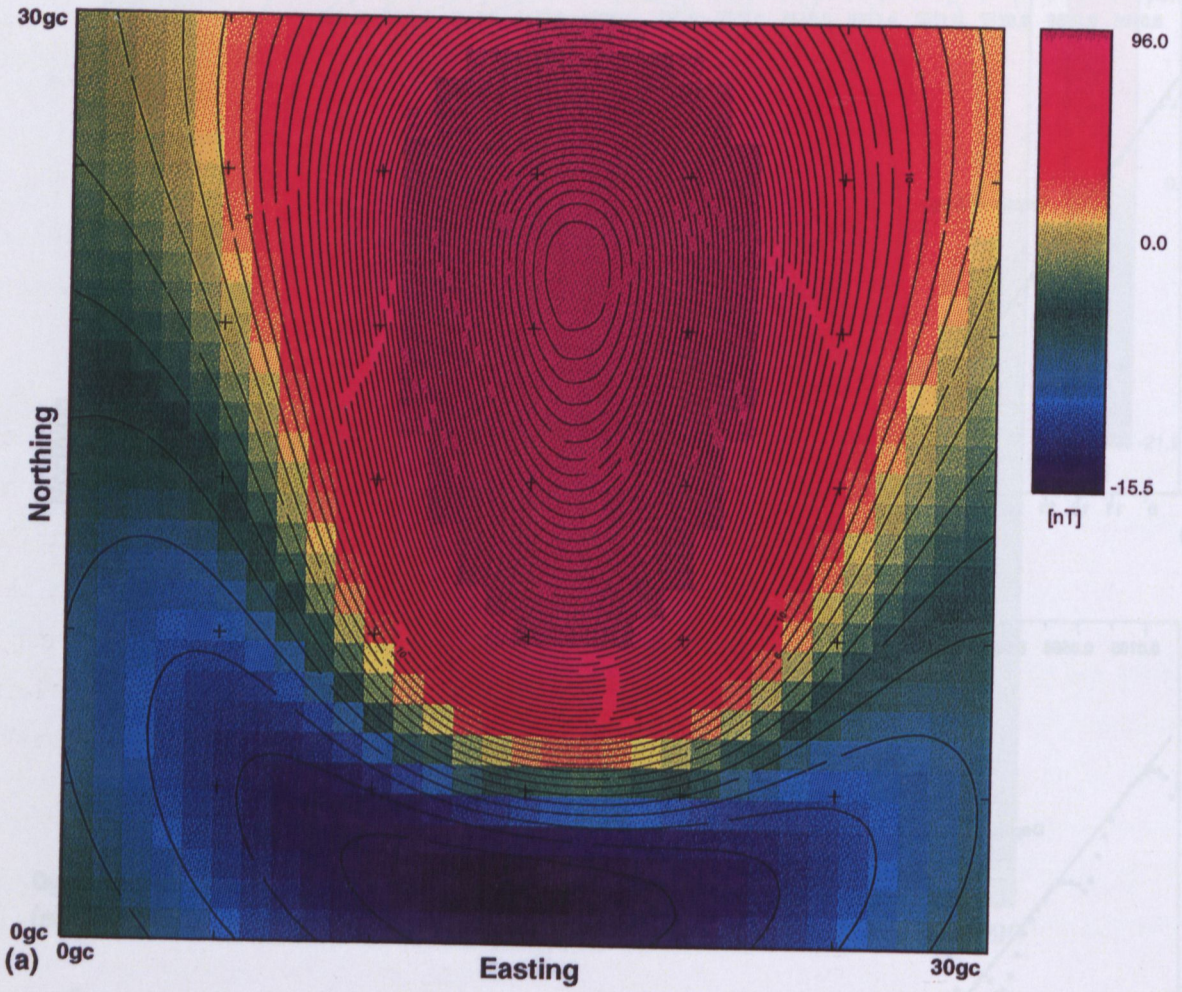

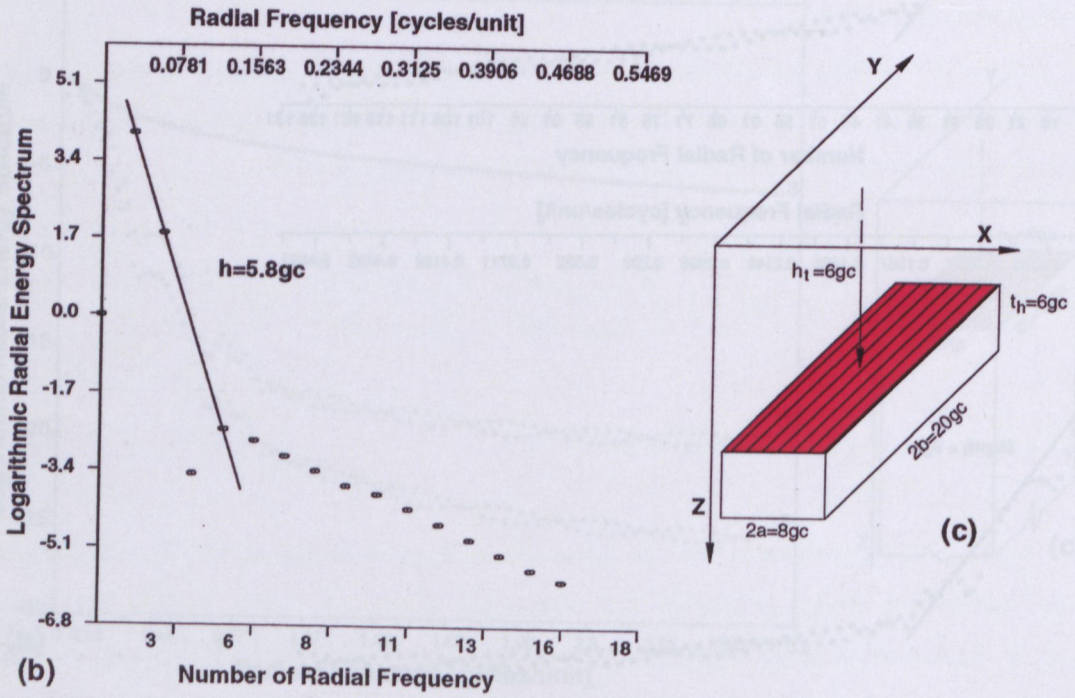

Figure B.7 Example of too small window size. Model data of shallow, thin, long and narrow, vertical-sided prism. The original map size 30x30gc, extension window 32x32gc.
(a) Colour image with superimposed contours of magnetic field.
(b) Logarithmic radial energy spectrum of the magnetic field.
(c) Parameters of the prism model.

energy spectrum. The size correction, called 'refining' (Spector, 1968), needs to be done prior to the depth analysis.

The effect of the horizontal size factor on the spectrum and consequently on the computed average depth of the causative bodies was tested for several models. Shallow magnetic sources with large horizontal extensions are of particular concern. The size correction is done using a computer program developed by Shi (1993).

Figure B.6 presents an example of the logarithmic radial energy spectrum, prior to and after a size correction, and a graph of the horizontal size effect computed for the shallow body which has large horizontal dimensions. To obtain a better correction, the spectrum was first computed over the vertical gradient of the magnetic field, and then followed by the spectrum 'refining' process. The application of the vertical gradient has some advantages; the regional field is reduced and the range of the magnetic anomalies is decreased. This approach to the energy spectrum computation has been proved and developed by Shi (1987, 1993). The real depth to the top of an analysed prism model equals 9gc. The estimated depth value obtained from the interpretation of

- the raw spectrum equals 11.5gc,
- the spectrum of the vertical gradient is approximately equal to 10.5 gc,
- the spectrum after the size correction also equals 9gc.

(ii) Extrapolation window

As discussed in Section 5.1.3, the size of the original window and the dimensions of the extension window (extrapolation array), need to be chosen properly. The depth estimation could be incorrect if the original window does not cover at least three quarters of an anomaly (Shi, 1993) and/or if the extension window is too small. Figures B.5 and B.7 demonstrate both an incorrect size and a proper size of the original window (map dimensions). The real depth to the top of the computed model is 20 grid units, where the depth values obtained from the energy spectrum are 16.8 grid units for too small an original window ($2^6 \times 2^6$), and 20.5 grid units for a larger original window size ($2^7 \times 2^7$). With index n equals 6 and 7 in the above, the data was extrapolated to an array $2^{n+1} \times 2^{n+1}$ in both cases.

(II) Ensemble of vertical prisms

Real geological situations can be simulated by superimposed multi-layers of magnetic sources. Such a multi-layer model is a statistical representation of an ensemble of several single vertical prisms randomly distributed within each layer. Table 5.2b includes geometrical parameters of the analysed model. A sample interval of the magnetic grid data created for each model is equal to unity.

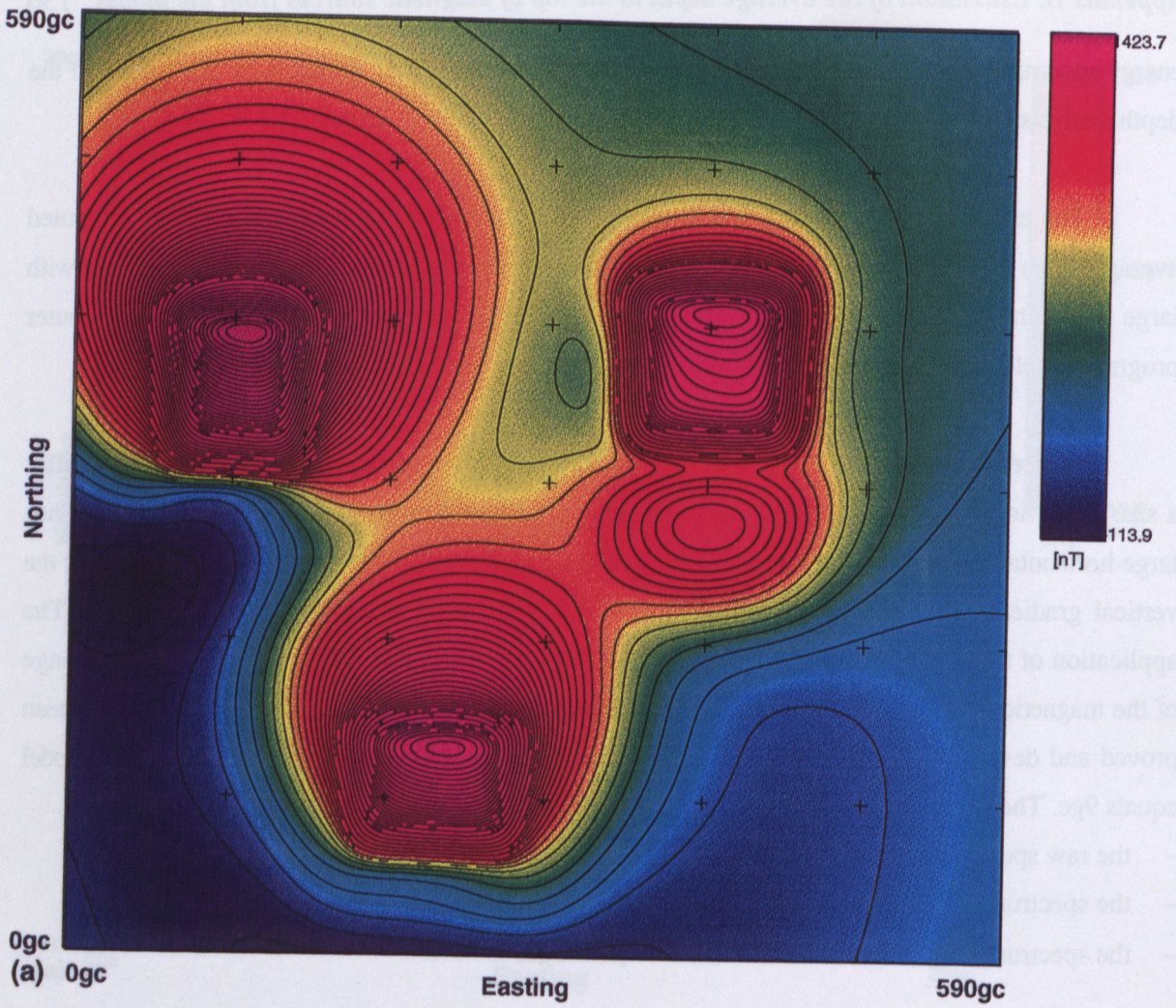

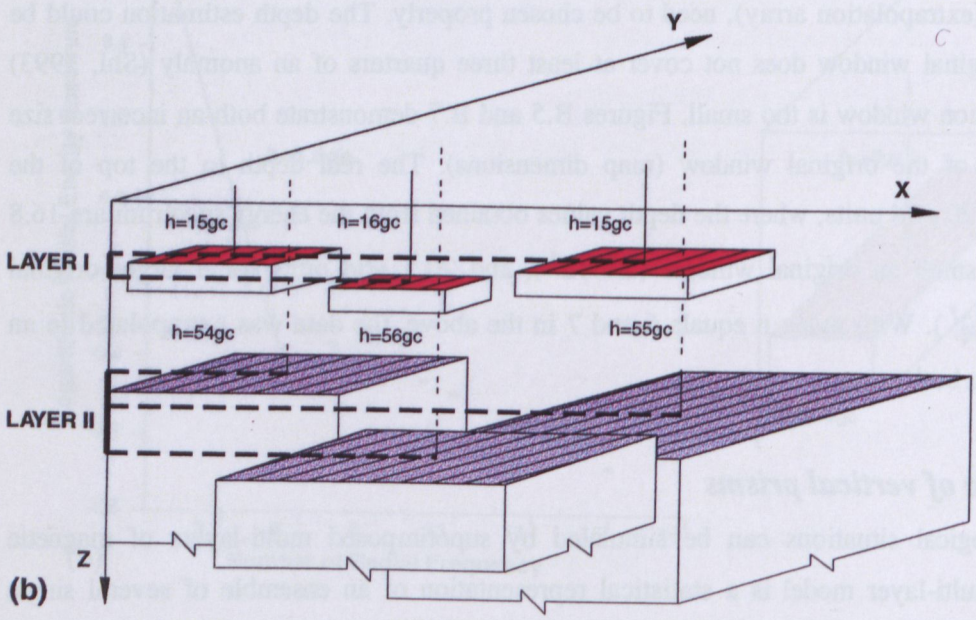

Figure B.8 **The multi-layer model data of an ensemble of six vertical-sided prisms.**
(a) Colour image with superimposed contours of the magnetic field.
(b) Parameters of the multi-prism model. Top-red surface of the shallow prisms represents statistical 'Layer I ' and top-blue surface of the deep prisms represents statistical 'Layer II'.

Table B.2 Geometrical parameters of the analysed model.

Body	*t[gc]*	*a[gc]*	*b[gc]*	h_t*[gc]*	*Statistical layer*	h_{ave}*[gc]*
P_1	25	80	100	15	I	16
P_2	35	100	100	15	I	16
P_3	35	100	80	16	I	16
P_4	250	150	150	54	II	55
P_5	330	100	100	55	II	55
P_6	300	150	180	56	II	55

t - thickness of the prism

a - width of the prism in the horizontal plane

b - length of the prism in the horizontal plane

h_t - depth to the top of the prism

h_{ave} -computed approximate average depth to the top of the ensemble of the prisms, laterally distributed within the particular layer.

The map of the magnetic field and the graph of the logarithmic radial spectrum of the ensemble model are presented at Figures B.8(a)-(d). As indicated, there are three distinct line segments representing adequate depth layers: 55gc, 16gc, and 1gc. The shallowest depth represents the sample interval; an average depth to the top of the middle layer equals approximately 16gc; the computed approximate average depth to the top of this ensemble equals 16gc. The deepest sources are clearly indicated on the spectrum by a distinct line segment, whose slope indicates an average depth 55gc. The results of the analyses show that the energy spectrum method successfully estimates the average depth to the top of each ensemble.

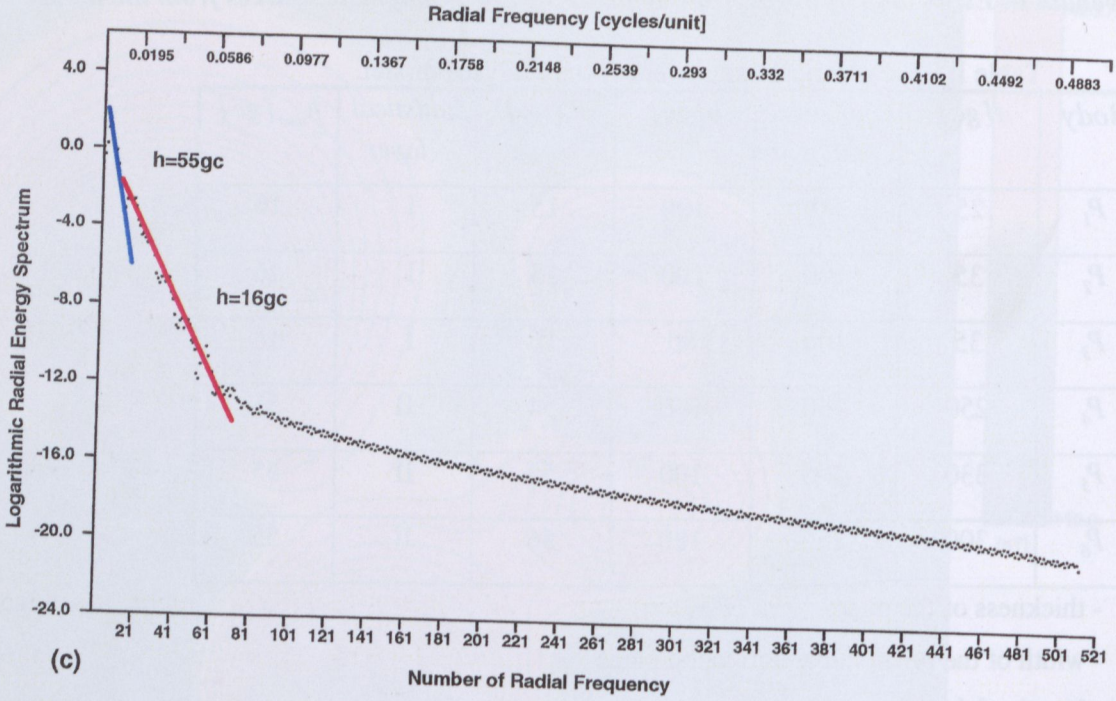

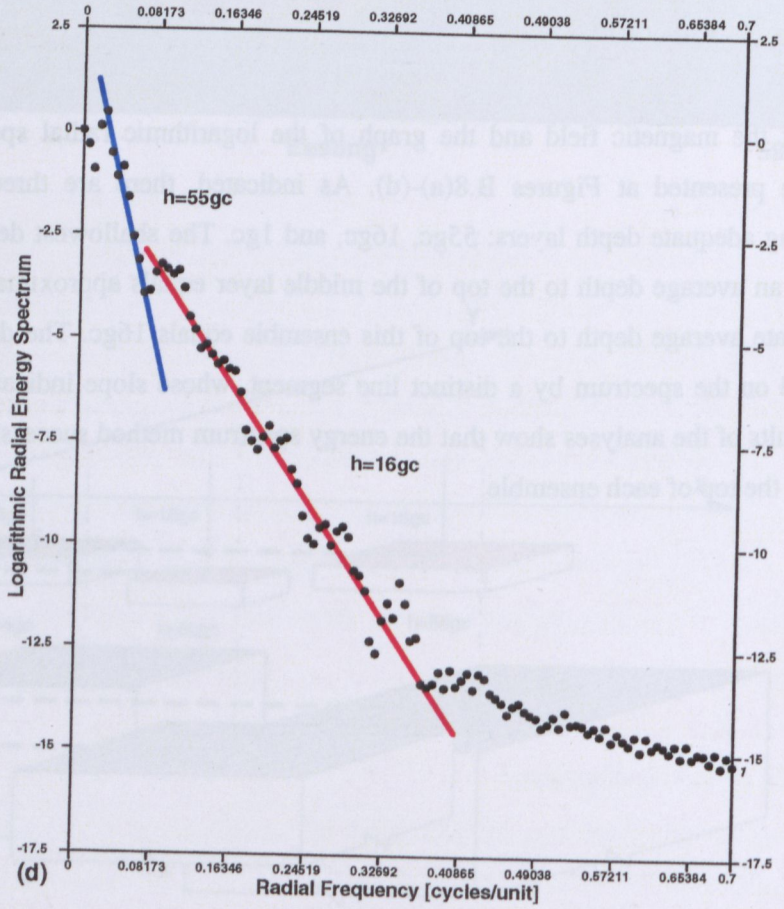

Figure B.8 (c) **Logarithmic radial energy spectrum of the TMI. Original window size 590x590gc with extension window 1024x1024gc, where gc=grid cell.**
(d) **Detail of the spectrum showing the low frequency part.**

References

Ajayi, C.O. and Ajakaiye, D.E., 1981, The origin and peculiarities of the Nigerian BenueTrough: another look from recent gravity data obtained from the middle Benue, *Tectonophysics*, 80: 285-303.

Allan, T.D., 1970, Magnetic and gravity fields over the Red Sea, *Philos. Trans. R. Soc.* London, Ser. A, 267: 153-180.

Alldredge, L.R., Van Voorhis, G.D. and Davis, T.M., 1963, Amagnetic profile around the world, *J. Geophys. Res.*, 68: 3679-3692.

Allen, P.A. and Allen, J.R., 1990, Basin Analysis. Principles and applications, *Blackwell Scientific Publications*.

Almond, D.C., 1986, Geological evolution of the Afro-Arabian dome, *Tectonophysics*, 131: 301-332.

Aplanov, S.V., 1987, Geodynamics of the early Mesozoic obsky Paleoocean, *Acad. Sci. USSR, P.P. Shirshov Inst. Oceanol.*, Moscow, 98 (in Russian).

Arkani-Hamed, J., 1988, Remnant magnetization of the oceanic upper mantle, *Geophys. Res. Lett.*, 15: 48-51.

Arkani-Hamed, J. and Strangway, D.W., 1985, Lateral variations of apparent magnetic susceptibility of lithosphere deduced from Magsat data, *J. Geophys. Res.*, 90: 2655-2664.

Artemjev, M.E. and Artyushkov, E.V., 1971, Structure and isostasy of Baikal Rift and the mechanism of rifting, *J. Geophys. Res.*, 76: 1197-1211.

Atchuta Rao, D., Ram Babu, H.V. and Sivakumar Sinha, G.D.J., 1992, Crustal structure associated with Gondwana graben across the Narmada-Son lineament in India: an inference from aeromagnetics, *Tectonophysics*, 212: 163-172.

Austin, P.M. and Williams, G.E., 1978, Tectonic development of late Proterozoic to Mesozoic Australia through plate motions possibly influenced by earth's rotation, *Journal of the Geological Society of Australia*, 25: 1-21.

Bailey, D.K., 1974, Continental rifting and alkaline magmatism, *In*: H. Sorenson (Ed.), *The alkaline rocks*, 148-159, John Wiley, New York.

Baker, B.H., Crossley, R. and Goles, G.G., 1978, Tectonic and magmatic evolution of the southern part of the Kenya rift valley, *In*: E.-R. Neumann and I.B. Ramberg (Eds), *Petrology and geochemistry of continental rifts*, Reidel, Dordrecht.

Baker, B.H. and Wohlenberg, J., 1971, Structure and evolution of the Kenya rift valley, *Nature*, 229: 538-542.

Baranov, V., 1957, A new method for interpretation of aeromagnetic maps: pseudo-gravimetric anomalies, *Geophysics*, 22: 359-383.

Barberi, F. and Varet, J., 1978, The Afar rift junction, *In*: E.-R. Neumann and I.B. Ramberg (Eds), *Petrology and geochemistry of continental rifts*, Reidel, Dordrecht, 55-69.

Barbier, F., Duvergé, J. and Le Pichon, X., 1986, Structure profonde de la marge Nord-Gascone. Implications sur le méchanisme de rifting et de formation de la marge continentale, *Bull. Cent. Rech. Explor.-Prod. Elf-Aquitaine*, 10(1): 105-121.

Bayer, H.-J., Hötzl, H., Jado, A. R., Röscher, B. and Voggenreiter, W., 1988, Sedimentary and structural evolution of the northwest Arabian Red Sea margin, *Tectonophysics*, 153: 137-152.

Beaumont, C., 1981, Foreland basins, *Geophysical Journal of the Royal Astronomical Society*, 65: 291-329.

Beaumont, C. and Sweeney, J. F., 1978, Graben generation of major sedimentary basins, *Tectonophysics*, 50: 19-23.

Behrendt, J. C. and Kiltgord, K. D., 1980, High sensitivity aeromagnetic survey of the U.S. Atlantic Continental Margin, *Geophysics*, 45: 1813-1846.

Behrendt, J. C., Le Masurier, W.E., Cooper, A.K., Tessensohn, F., Tréhu, A. and Damaske, D., 1991, Geophysical studies of the West Antarctic rift system, *Tectonics* 10/6: 1257-1273.

Ben-Avraham, Z. (Ed.), 1987, Symposium on 'Sedimentary basins within the Dead Sea and other rift zones', *Tectonophysics*, 141: 1-198.

Ben-Avraham, Z., 1992, Development of asymmetric basins along continental transform faults, *Tectonophysics*, 215: 209-220.

Bertram, Z., 1992, Development of asymmetric basins along continental transform faults, *Tectonophysics*, 215: 209-220.

Bhattacharji, S. and Koide, H., 1978, The origin and evolution of rifts and rift valley structures: a mechanistic interpretation. In: E.-R. Neumann and I.B. Ramberg (Eds), *Tectonics and geophysics of continental rifts*, Reidel, Dordrecht, 29-37.

Bhattacharyya, B.K., 1965, Two-dimentional harmonic analysis as a tool for magnetic interpretation, *Geophysics*, 30: 829-857.

Bhattacharyya, B.K., 1966a, A method for computing the total magnetization vector and dimensions of a rectangular block-shaped body from magnetic anomalies, *Geophysics*, 31: 74-96.

Bhattacharyya, B.K., 1966b, Continuous spectrum of the total magnetic field anomaly due to a rectangular prismatic body, *Geophysics*, 31: 96-121.

Bhattacharyya, B.K. and Leu, L.K., 1975a, Analysis of magnetic anomalies over Yellowstone National Park: mapping of Curie point isotherm surface for geothermal reconnaissance, *Journal Geophysical Research*, 80(30): 4461-4465.

Bhattacharyya, B.K. and Leu, L.K., 1975b, Spectral analysis of gravity and magnetic anomalies due to two-dimensional structures, *Geophysics*, 40: 993-1013.

Bhattacharyya, B.K. and Leu, L.K., 1977, Spectral analysis of gravity and magnetic anomalies due to rectangular prismatic bodies, *Geophysics*, 42: 41-50.

Bhattacharyya, B.K. and Navolio, M.E., 1976, A Fast Fourier Transform method for rapid computation of gravity and magnetic anomalies due to arbitrary bodies, *Geophys. Prosp.*, 24: 633-649.

Billings, M. P., 1942, *Structural Geology*, Prentice- Hall, Inc., New York.

Birch, F.S., 1982, Gravity models of the Albuquerque Basin, Rio Grande Rift, New Mexico, *Geophysics*, 47: 1185-1197.

Birdwell, R.J. and Potzick, C., 1981, Thermal regimes, mantle diapirs and crustal stresses of continental rifts, *Tectonophysics*, 73: 9-15.

Black, L.P., Ferguson, J. and Gray, P.T., 1993, A Jurassic U-Pb zircon age for a South Australian kimberlitic rock, *Quarterly Geological Notes, The Geological Survey of South Australia*, 125: 2-5.

Blackman, R.B. and Tukey, J.W., 1959, The measurement of power spectra, New York, Dover Publications, Inc.

Blakely, R.J., 1988, Curie temperature isotherm analysis and tectonic implications of aeromagnetic data from Nevada, *J. Geophys. Res.*, 93: 11817-11832.

Boeuf, M. G. and Doust, H., 1975, Structure and development of the southern margin of Australia, *APEA Journ.*, 15: 33-43.

Bolt, B.A., Doyle, H.A. and Sutton, D.J., 1958, Seismic observations from the 1956 atomic explosions in Australia, *Geophysical Journal of the Royal Astronomical Society*, 1: 135.

Bonatti, E. and Crane, K., 1984, Oceanic fracture zones, *Sci. Am.*, 250: 40-51.

Bosworth, W., 1985, Geometry of propagating continental rifts, *Nature*, 316: 625-627.

Bott, M.H.P. (Ed.), 1976, Sedimentary basins of continental margins and cratons, *Developments in Geotectonics 12*, Inter-Union Commission on Geodynamics: Scientific report No.27, Reprinted from *Tectonophysics* 36.

Bott, M.H.P., 1979, Subsidence mechanisms at passive continental margins, In: J.S. Watkins, ET AL. (Eds), Geological and geophysical investigations of continental margins, 3-10, *American Assoc. of Petroleum Geologists Memoir*, 29.

Bott, M.H.P., 1981, Crustal doming and the mechanism of continental rifting, In: J.H. Illies, Mechanism of graben formation, Reprinted from *Tectonophysics*, 73, Elsevier, Amsterdam.

Boyd, D.M., Shi, Z. and Kivior, I., 1993, Analysis of regional gravity and magnetic data as a guide for mineral exploration in the next century, SEG Conference, Moscow, Abstrct.

Bridwell, R.J., 1978, The Rio Grande Rift and a diapiric mechanism for continental rifting, In: E.-R. Neumann and I.B. Ramberg (Eds), *Tectonics and geophysics of continental rifts*, Reidel, Dordrecht, 73-80.

Bridwell, R.J. and Potzick, C., 1981, Thermal regimes, mantle diapirs and crustal stresses of continental rifts, In: J.H. Illies, Mechanism of graben formation, Reprinted from *Tectonophysics*, 73, Elsevier, Amsterdam.

Brown, L.D. et al., 1980, Deep structures of the Rio Grande Rift from seismic reflection profiling, *J. Geophys. Res.*, 85: 4773-4800.

Browne, S.E. and Fairhead, J.D., 1983, Gravity study of the Central African Rift System: a model of continental disruption, *Tectonophysics*, 94: 187-203.

Buck, W.R., 1986, Small-scale convection induced by passive rifting: the cause for uplift of rift shoulders, *Earth Planet. Sci. Lett.*, 77: 326-372.

Bullard, E.C., 1936, Gravity measurements in East Africa, *Philos. Trans. R. Soc*, London, A135: 265-281.

Burk, C.A. and Drake, C.L. (Eds), 1974, *The Geology of Continental Margins*, Springer-Verlag Berlin.

Burke, K., 1977, Aulacogens and continental break-up, *Ann. Rev. Earth Planet. Sci.*, 5: 371-396.

Burke, K., 1978, Evolution of continental rift systems in the light of plate tectonics, *In*: E.-R. Neumann and I.B. Ramberg (Eds), *Tectonics and geophysics of continental rifts*, Reidel, Dordrecht, 1-9.

Burke, K., Dessauvagie, T.F.J. and Whiteman, A.J., 1972, Geological history of the Benue valley and adjacent areas, *In*: T.F.J. Dessauvagie and A.J. Whiteman (Eds), *African Geology*, Ibadan University Press, 187-205.

Burke, K. and Dewey, J.F., 1970, Orogeny in Africa, *In*: T.F.J. Dessauvagie and A.J. Whiteman (Eds), *African Geology*, Ibadan University Press.

Burke, K. and Dewey, J.F., 1973, Plume generated triple junctions, key indicators in applying plate tectonics to old rocks, *Geological Journal*, 81: 406-433.

Burke, K. and Whiteman, A.J., 1973, Uplift, rifting and the break-up of Africa, *In*: D.H. Tarling and S.K. Runcorn (Eds), *Implications of continental drift to the Earth sciences*, Academic Press, New York, 735-755.

Byerly, P.E. and Stolt, R.H., 1977, An attempt to define the Curie point isotherm in northern and central Arizona, *Geophysics*, 42: 1394-1400.

Cain, J.C., Davis, W.M. and Regan, R.D., 1974, An *N=22* model of the geomagnetic field (abstract), *EOS,Trans. Am. Geophys. Union*, 56: 1108.

Cande, S.C. and Mutter, J.C., 1982, A revised identification of the oldest sea-floor spreading anomalies between Australia and Antarctica, *Earth Planet. Sci. Lett.*, 58: 151-160.

Capon, D., 1984, A geophysical study of the structure and geological history of the Polda Basin, S.A., University of Adelaide, Honours degree thesis (unpublished).

Carle, H.M. and Harrison, C.G.A., 1982, A problem in representing the core magnetic field of the earth using spherical harmonics, *Geophys. Res. Lett.*, 9: 265-268.

Carter, B.R., Barber, W. and Tait, E.A., 1963, The geology of parts of Adamawa, Bauchi and Bornu Provinces in northeastern Nigeria, *Bull. Geol. Surv. Nigeria*, 30:1-108.

Carter, B.R. and Scott, A.F., 1975, Gemini No.1 *well completion report*, Outback Oil Company N.L

Chang, H.K., Kowsmann, R.O., Figueiredo, A.M.F. and Bender, A.A., 1992, Tectonics and stratigraphy of the East Brazil Rift System: an overview, *In:* P.A. Ziegler (Ed.), *Geodynamics of rifting, Vol. II, Case history studies on rifts: North and South America and Africa, Tectonophysics*, 213: 97-138.

Chekunov, A.V., Gavrish, V.K., Kutas, R.I. and Ryabchun, L.I., 1992, Dnieper-Donetz palaeorift, *In:* P.A. Ziegler (Ed.), *Geodynamics of rifting, Vol. I, Case history studies on rifts: Europe and Asia, Tectonophysics*, 208: 257-272.

Christencen, N.I. and Fountain, D.M., 1975, Constitution of the lower continental crust based on experimental studies of seismic velocities in granulite, *Geol. Soc. Am. Bull.*, 86: 227-234.

Clark, I.F. and Cook, B.J. (Eds), 1983, *Perspectives of earth*, Australian Academy of Science, Canberra.

Clark, M.J. and Farmer, N., 1976, Biostratigraphic nomenclature for Late Palaeozoic rocks in Tasmania, *Royal Society of Tasmania, Papers and Proceedings*, 110: 91-109.

Clark, S.C., Frey, H. and Thomas, H.H., 1985, Satellite magnetic anomalies over subduction zones: The Aleutian Arc anomaly, *Geophys. Res. Lett.*, 12: 41-44.

Cleary, J., 1967, P-times of Australian stations from nuclear explosions, *Bulletin of the Seismological Society of America*, 57: 773-781.

Cleary, J., Simpson, D.W. and Muirhead, J.J., 1972, Variations in Australian upper mantle structure, from observations of the Cannikin explosion, *Nature*, 236: 111-112.

Cochran, J.R., 1983, A model for the development of the Red Sea, *AAPG Bull.*, 67: 41-69.

Cochran, J.R. and Martinez, F., 1988, Evidence from the northern Red Sea on the transition from continental to oceanic rifting, *Tectonophysics*, 153: 25-54.

Coleman, R.G. and McGuire, A.V., 1988, Magma systems related to the Red Sea opening, *Tectonophysics*, 150: 77-100.

Coles, R.L. and Currie, R.G., 1977, Magnetic anomalies and rock magnetizations in the southern Coast Mountains, British Columbia: possible relation to subduction, *Can. J. Earth Sci.*, 14: 1753-1770.

Collier, R., 1988, Sedimentary facies evolution in continental fault-bounded basins formed by crustal extension: the Corinth basin, Greece, Ph. D. Thesis, University of Leeds.

Collier, R., 1990, Eustatic and tectonic controls upon Quaternary coastal sedimentation in the Corinth basin, Greece, *Journal of the Geological Society,* London, 147: 301-314.

Collins, C.D.N., 1991, The nature of the crust-mantle boundary under Australia from seismic evidence, *In:* B.J., Drummond (Ed.), *The Australian lithosphere, Geological Society of Australia Special Publication,* 17: 67-80.

Connard, G., Couch, R. and Gemperle, M., 1983, Analysis of aeromagnetic measurements from the Cascade Range in central Oregon, *Geophysics,* 48: 376-390.

Conybeare, C.E.B., 1979, *Lithostratigraphic analysis of Sedimentary basins*, Academic Press, New York, London, Toronto, Sydney, San Francisco.

Cooper, B.J., 1980, Biostratigraphy of Permian samoles from SADME Lock no. 1, *South Australia, Department of Mines and Energy, Report Book,* 80-109.

Cooper, B.J. and Gatehouse, C.G., 1983, The Polda Trough: periodic sedimentation since the Proterozoic?, *Abstracts of the 6th Australian Geological Convention*, Geological Society of Australia, 117-118.

Cooper, B.J., Harris, W.K. and Myer, G.M., 1982, The Late Palaeozoic Coolardie Formation, Polda Basin, *Quarterly Geological Notes, The Geological Survey of South Australia,* 81: 9-13.

Coppin, R.J., 1967, Report on Colton reconnaissance refraction seismic survey, *SADME report* (unpublished), RB 65/71.

Cordell, L., 1979, Gravimetric expression of graben faulting in Santa Fe county and the Espanola basin, New Mexico, Guideb., 30th Field Conf., Santa Fe Couty, N. Mex. Geol. Soc., 59-64.

Cordell, L. and Grauch, V.J.S., 1985, Mapping basement magnetization zones from aeromagnetic data in the San Juan, New Mexico, *In:* W.J. Hinze (Ed.), *The utility of regional gravity and magnetic anomaly maps,* Society of Exploration Geophysicists.

Coutelle, A., Pautot, G. and Guennoc, P., 1991, The structural setting of the Red Sea axial valley and deeps: implications for crustal thinning processes. *In*: J. Makris, P.Mohr and R. Rihm (Eds), *Red Sea : British and early history of new oceanic basins, Tectonophysics*, 198: 395-409.

Cowan, D.R. and Cowan, S., 1993, Separation filtering applied to aeromagnetic data, *Exploration Geophysics,* 24: 429-436.

Coward, M.P., 1990, The Precambrian, Caledonian and Variscan framework to NW Europe, *In*: R.F.P. Hardman and J. Brooks (Eds), *Tectonic events responsible for Britain's oil and gas reserves,* The Geological Society of London.

CRA Exploration Pty Ltd, 1981, EL 670, Lock area, Progress reports, *South Australia. Department of Mines and Energy. Open File Envelope*, 4659 (unpublished).

CRA Exploration Pty Ltd, 1982a, EL 670, McLachlan; EL 687, Tuckey; EL 688, Sheringa. Progress reports on Polda Basin, South Australia, from 11/11/80 to 10/5/82, *South Australia. Department of Mines and Energy. Open File Envelope*, 3973 (unpublished).

CRA Exploration Pty Ltd, 1982b, Report on the surrender of Sheringa EL 688 and partial surrender of McLachlan EL 670 and Tuckey EL 687, Polda Basin, South Australia, 17th May 1982, *South Australia. Department of Mines and Energy. Open File Envelope*, 4659 (unpublished).

CRA Exploration Pty Ltd, 1983, EL 670, 1032, McLachlan. Progress and final reports from 10/8/82 to 7/3/83, *South Australia. Department of Mines and Energy. Open File Envelope*, 5078 (unpublished).

CRA Exploration Pty Ltd, 1985, EL 1216, Mount Wedge. Progress reports from 10/4/84 to 10/1/85, *South Australia. Department of Mines and Energy. Open File Envelope*, 5457 (unpublished).

CRA Exploration Pty Ltd and Shell Co. Australia Ltd, 1985a, EL 485, 876, 1182, Cleve Central. Progress and final reports from 6/6/79 to 12/10/85, *South Australia. Department of Mines and Energy. Open File Envelope*, 3541 (unpublished).

Crabb, T.N., Gerdes, R.A. and Nelson, R.G., 1985, A geophysical review of the Polda Basin, South Australia, *Bulletin of the Australian Society of Exploration Geophysics*, 16: 190-193.

Cratchley, C.R. and Jones, G.P., 1965, An interpretation of the geology and gravity anomalies of the Benue Valley, Nigeria, *Overseas Geol. Surveys Geophys.*, Paper No. 1, HMSO, London.

Dalmayrac, B. and Molnar, P., 1981, Parallel thrust and normal faulting in Peru and constraints on the state of stress, *Earth Planet. Sci. Lett.*, 55: 473-481.

Daneš, Z.F., 1962, Structure calculation from gravity data and density logs, *Soc. of Mining Engin. Transactions*, 223: 23-29.

Daneš, Z.F. and Oncley, L.A., 1962, An analysis of some second derivative methods, *Geophysics*, 27: 611-615.

Darracott, B.W., Fairhead, J.D., Girdler, R.W. and Hall, S.A., 1973, The East African Rift System, *In*: D.H. Tarling and S.K. Runcorn (Eds), *Implications of continental drift to the Earth sciences*, Academic Press, London and New York, Vol. 2, 757-766.

Dawson, J.B., 1977, Subcratonic crust and upper mantle models based on xenolith suites in kimberlite and nephelinitic diatremes, *J. Geol. Soc. London*, 134: 173-184.

Dawson, J.B., 1986, Geographic and time distribution of kimberlites and lamproites: relationships to tectonic processes, *In:* J. Ross (Ed.), *Kimberlites and related rocks, Vol.1, Their composition, occurrence, origin and emplacement,* GSA Special Publication No. 14, Blaclwell Scientific Publications, 323-342.

De Sitter, L.U., 1959, *Structural Geology*, McGraw-Hill Publishing Company Limited, New York, London, Toronto.

Dean, W.C., 1958, Frequency analysis for gravity and magnetic interpretation, *Geophysics*, 23: 97-127.

Denham, D., Simpson, D.W., Gregson, P.J. and Sutton, D.J., 1972, Travel times and amplitudes from explosions in northern Australia, *Geophysical Journal of the Royal Astronomical Society*, 28: 225-235.

Dewey, J.F., 1989, Extensional collapse of orogens, *Tectonophysics*, 7: 1123-1139.

Dietz, R.S. and Holden, J.C., 1970, Reconstruction of Pangea: breakup and dispersal of continents, Permian to present, *J. Geophys. Res.*, 75: 4939-4956.

Dixon, T.H., Stern, R.J. and Hussein, I.M., 1987, Control of Red Sea rift geometry by Precambrian structures, *Tectonics*, 6 (5): 551-571.

Dole, W.E. and Jordan, N.F., 1978, Slope mapping, *AAPG Bull.*, 62: 2427-2440.

Doyle, H.A. and Everingham, I.B., 1964, Seismic velocities and crustal structures in southern Australia, *Geophysical Journal of the Royal Astronomical Society*, 11: 141.

Drummond, B.J., 1988, A review of crust/upper mantle structure in the Precambrian areas of Australia and implications for Precambrian crustal evolution, *Precambrian Research*, 40/41: 101-106.

Drummond, B.J., Goncharov, A.G. and Collins, C.D.N., 1995, Upper crustal heterogeneities in Australian Precambrian provinces interpreted from deep seismic profiles and the Kola Superdeep Borehole, *AGSO Journal of Australian Geology and Geophysics*, 15: 519-527.

Drummond, B.J. and Collins, C.D.N., 1986, Seismic evidence for underplating of the lower continental crust of Australia, *Earth and Planetary Science Letters*, 79: 361-372.

Eggler, D.H. and McCallum, M.E., 1974, Xenoliths in diatremes of the western United States, *Yb. Carnegie Instn. Wash.*, 73: 294-300.

Egloff, F., Rihm, R., Makris, J., Izzeldin, Y.A., Bobsien, M., Meier, K., Junge, P., Noman, T. and Warsi, W., 1991, Contrasting structural styles of the eastern and western margins of the southern Red Sea: the 1988 SONNE experiment, *Tectonophysics*, 198: 329-353.

El-Isa, Z.H., Mechie, J. and Prodehl, 1986, A deep seismic sounding experiment in Jordan, *Dirasat*, 13: 271-281.

El-Isa, Z.H., Mechie, J. and Prodehl, 1987a Shear velocity structure of Jordan from explosion seismic data, *Geophys. J.R. Astron. Soc.*, 90: 265-281.

El-Isa, Z.H., Mechie, J., Prodehl, C., Makris, J. and Rihm, R., 1987b, A crustal structure study of Jordan derived from seismic data refraction data, *Tectonophysics*, 138: 235-253.

Elming, S.-A. and Törne, A., 1976, The blue road geotraverse: A magnetic ground survey and the interpretation of magnetic anomalies, *Geol. Foeren. Stockholm Forh.*, 98: 264-270.

England, P. and Houseman, G., 1984, On the geodynamic setting of kimberlite genesis, *Earth Pla. Sci. Lett.*, 67: 109-122.

Etheridge, M.A., Drummond, B.J. and Tucker, D.H., 1985, Evolution and internal structure of intracratonic sedimentary basins as seen by geophysics, *Bulletin of the Australian Society of Exploration Geophysics*, 16: 216-220.

Etheridge, M.A., Symonds, P.A. and Lister, G.S., 1990, Application of the detachment model to reconstruction of conjugate passive margins, *In:* A.J. Tankard and H.R. Balkwill (Eds), *Extensional tectonics and stratigraphy of the North Atlantic Margins, AAPG Mem.*, 46: 23-40.

Etheridge, M.A., Symonds, P.A., Powell, T.G. and Lister, G.S., 1988, Application of the detachment model for continental extension to hydrocarbon exploration in extensional basins, *APEA J.*, 28: 167-187.

Etheridge, M.A. and Vernon, R.H., 1983, Comment on "Seismic velocity and anisotrophy in mylonites and the reflectivity of deep crustal fault zones", *Geology*, 11: 487-489.

Evans, P.R., 1966, Mesozoic stratigraphic palynology in Australia, *Australasian Oil and Gas Journal*, 12: 58-63.

Fairhead, J.D., 1986, Geophysical controls on sedimentation within the African Rift System, In: L.E. Frostick et al. (Eds), Sedimentation in the African Rifts, *Geological Society Special Publication*, 25: 19-27.

Fairhead, J.D., 1988, Mesozoic plate tectonic reconstructions of the central South Atlantic Ocean: The role of the West and Central African rift system, *Tectonophysics*, 155: 181-191.

Fairhead, J.D. and Green, C.M., 1989, Controls on rifting in Africa and the regional tectonic model for the Nigeria and East Niger rift basins, In: B. Rosendahl (Ed.), Rifting in Africa, *J. Afr. Earth Sci. Spec. Publ.*, 8: 231-249.

Fairhead, J.D. and Okereke, C.S., 1988, Depths to major density contrasts beneath the West African Rift System in Nigeria and Cameroon based on spectral analysis of gravity data, *J. Afr. Earth Sci. Spec. Publ.*, 7: 769-777.

Falvey, D.A., 1974, The development of continental margins in plate tectonic theory, *Aust. Petrol. Explor. Assoc.*, 14: 94-106.

Falvey, D.A. and Middleton, M.F., 1981, Passive continental margins: evidence for a pre-breakup deep crustal metamorphic subsidence mechanism, *Oceanol. Acta, Colloque C3*: 103-114.

Falvey, D.A. and Mutter, J.C., 1981, Regional plate tectonics and evolution of Australia's passive continental margins, *BMR J. Geol. and Geophys.*, 6: 1-29.

Fanning, C.M., 1987, U-Pb geochronology of Broadview DDH1, Wangary Gneiss, Carpa Granite and Middle Cmp Granite, *AMDEL report*, G7155/88 (unpublished).

Fanning, C.M., Flint, R.B., Parker, A.J., Ludwig, K.R. and Blissett, A.H., 1988, Refined Proterozoic evolution of the Gawler Craton, South Australia, through U-Pb zircon geochronology, *Precambrian Research*, 40/41: 363-386.

Fanning, C.M., Ludwig, K.R., Forbes, B.G. and Preiss, W.V., 1986, Single and multiple grain U-Pb zircon analyses for the early Adelaidean Rook Tuff, Willouran Ranges, South Australia, *In:* 8th Australian Geological Convention, Adelaide, 1986, *Geological Society of Australia, Abstracts*, 15: 71-72.

Favre, P. and Stampfli, G.M., 1992, From rifting to passive margin: the examples of the Read Sea, Central Atlantic and Alpine Tethys, *Tectonophysics*, Elsevier Science Publishers B.V., Armsterdam, 215: 69-97.

Ferguson, J. and Sheraton, J.W., 1979, Petrogenesis of kimberlitic rocks and associated xenoliths of southeastern Australia, *In:* H.O. Meyer and F.R. Boyd (Eds), *Kimberlites, diatremes and diamonds: their geology, petrology and geochemistry, Proceedings 2nd International Kimberlite Conference, American Geophysical Union, Washington D.C.*, 1: 71-91.

Finlayson, D.M., 1982, Geophysical differences in the lithosphere between Phanerozoic and Precambrian Australia, *Tectonophysics*, 84: 287-312.

Finlayson, D.M., Collins, C.D.N., and Lock, J., 1984, P-wave velocity features of the lithosphere under the Eromanga Basin, Eastern Australia, including a prominent mid-crust discontinuity, *Tectonophysics*, 101: 267-291.

Finlayson, D.M., Cull, J.P. and Drummond, B.J., 1974, Upper mantle structure from the trans-Australia seismic survey (TASS) and other seismic refraction data, *J. Geol. Soc. Aust.*, 21: 447-458.

Finlayson, D.M., Prodehl, C. and Collins, C.D.N., 1979, Explosion seismic profiles, and implications for crustal evolution, in southeastern Australia, *BMR Journal of Australian Geology and Geophysics*, 4: 243-252.

Flint, R.B., 1989, Elliston map sheet, *South Australia, Geological Survey, Geological Atlas 1:250 000 Series*, sheet SI53-6.

Flint, R.B., 1992, Elliston, South Australia, *1:250 000 Geological Series - Explanatory. Notes, Department of Mines and Energy of South Australia*, Peacock Publications, Adelaide.

Flint, R.B., 1993, Itiledoo Basin: Blue Range Beds, *In:* J.F. Drexel, W.V. Preiss and A.J. Parker (Eds), *The geology of South Australia, Volume 1, The Precambrian, Mines and Energy of South Australia, Geological Survey of South Australia.*

Flint, R.B. and Parker, A.J., 1981, The Blue Range Beds, central Eyre Peninsula, *Quarterly Geological Notes, The Geological Survey of South Australia*, 80: 12-15.

Flint, R.B. and Parker, A.J. (Compilers), 1982, Tectonic map of South Australia, South Australia, *Geological Survey of South Australia, Maps of South Australia Series, 1: 2 000 000.*

Flint, R.B., Fanning, C.M. and Rankin, L.R., 1988a, Carappee Granite of central Eyre Peninsula, *Quarterly Geological Notes, The Geological Survey of South Australia*, 105: 2-6.

Flint, R.B., Fanning, C.M. and Rankin, L.R., 1988b, The Late Proterozoic Kilroo Formation of the Polda Basin, *Quarterly Geological Notes, The Geological Survey of South Australia*, 106: 16-23.

Flint, R.B. and Rankin, L.R., 1991, Kimba, South Australia, 1:250 000 Geological Series - *Explanatory Notes, Department of Mines and Energy of South Australia*, Peacock Publications, Adelaide.

Flöttmann, T., Kleinschmidt, G. and Funk, T., 1993, Thrust patterns of the Ross/Delamerian orogens in northern Victoria Land (Antarctica) and southeastern Australia and their implications for Gondwana reconstructions, *In:* R.H. Findlay, R. Unrug, M.R. Banks and J.J. Veevers (Eds), *Gondwana Eight, Assembly, Evolution and dispersal*, Balkema, Rotterdam, pp.131-139.

Flöttmann, T. and Oliver, R.L., 1994, Review of Precambrian-Palaeozoic relationships at the craton margins of southeastern Australia and adjacent Antarctica, *Precambrian Research*, 69: 293-306.

Foden, J., Song, S.H., Smith, P.B. and Van der Steldf, B., 1995, Geochemical evolution of lithospheric mantle beneath S.E. South Australia, in press.

Folkman, Y., 1981, Structural features in the Dead Sea - Jordan Rift zone, interpreted from a combined magnetic-gravity study, *Tectonophysics*, 80: 135-146.

Folkman, Y. and Bein, A, 1978, Geophysical evidence for a pre-Upper Jurassic fossil continental margin oriented east-west under central Israel, *Earth Planet. Sci. Lett.*, 39: 335-340.

Forman, D.J. and Shaw, R.D., 1973, Deformation of the crust and mantle in central Australia, *Bureau of Mineral Resources, Geology and Geophysics,Bulletin*, 144.

Fountain, D.M. and Salisbury, M.H., 1981, Exposed cross-sections through the continental crust: implications for crustal structure, petrology and evolution, *Earth Planet. Sci. Lett.*, 56: 263-277.

Fourier, J.B.J., 1822, *Théorie analytique de la chaleur.*

Fraser, A.R., and Tilbury, L.A., 1979, Structure and stratigraphy of the Ceduna Terrace region, Great Australian Bight, *APEA Journal*, 19: 53-65.

Freund, R., 1965, A model of structural development of Israel and adjacent areas since Upper Cretaceous times, *Geol. Mag.*, 102: 189-205.

Freund, R. and Garfunkel, Z. (Eds), 1981, The Dead Sea Rift, *Tectonophysics*, 80: 1-303.

Freund, R., Garfunkel, Z., Zak, I., Goldberg, M., Weissbrod, T. and Derin, B., 1970, The shear along the Dead Sea rift, In: N.L. Falcon, J.G. Gass, R.W. Girdler and A.S. Laughton (Eds), A discussion of the structure of the Red Sea and the nature of the Red Sea, Gulf off Aden and Ethiopia Rift Junction, *Philos. Trans. R. Soc. London, Ser. A*, 267: 107-130.

Frey, H., 1985, Magsat and POGO magnetic anomalies over the Lord Howe Rise: evidence against a simple continental crustal structure, *J. Geophys. Res.*, 90: 2631-2639.

Garfunkel, Z., 1981, Internal structure of the Dead Sea leaky transform (rift) in relation to plate kinematics, *Tectonophysics*, 80: 81-108.

Garfunkel, Z. and Bartov, Y., 1977, The tectonics of the Suez rift, *Geol. Surv. Isr. Bull.*, 71.

Garson, S.M. and Krs, M., 1976, Geophysical and geological evidence of the relationship of Red Sea transverse tectonics to ancient fractures, *Geol. Soc. Am. Bull.*, 87: 169-181.

Gasparini, P., Mantovani, M.S.M., Corrado, G. and Rapolla, A., 1979, Depth of Curie temperature in continental shields: A compositional boundary?, *Nature*, 278: 845-846.

Gatehouse, C.G., 1981a, Colton No. 1 - Well completion report, *South Australia, Department of Mines and Energy, Report Book*, 81/78.

Gatehouse, C.G., 1981b Tuckey No. 1 - Well completion report, *South Australia, Department of Mines and Energy, Report Book*, 81/19.

Gatehouse, C.G. and Cooper, B.J., 1982, The Late Jurassic Polda Formation, Eyre Peninsula, *South Australia, Geological Survey, Quarterly Geological Notes*, 81: 13-15.

Gaulier, J.M., Le Pichon, X., Lyberis, N., Avedik, F., Geli, L., Moretti, I., Deschamps, A. and Salah, H., 1988, Seismic study of the crust of the northern Red Sea and Gulf of Suez, *Tectonophysics*, 152: 55-88.

Gavrish, V.K., Zabello, G.D., Ryabchun, L.I., et al., 1989, *Geology and oil and gas occurrence of the Dnieper-Donetz Basin. Deep structure and geotectonic evolution*, Akad. Nauk Ukrainskoy CCR, Inst. Geol. Nauk, (in Russian).

Geil, K., 1991, The development of salt structures in Denmark and adjacent areas: the role of basin floor dip and differential pressure, *First Break*, 9: 467-483.

Gerdes, R.A., 1983, A geological appraisal of the basement configuration below the Polda Basin, Eyre Peninsula, *South Australia, Department of Mines and Energy report*, 83/61 (unpublished).

Gerdes, R.A., 1986, A geological appraisal of the graben beneath the Polda Basin, Eyre Peninsula, *South Australia, Quarterly Geological Notes, The Geological Survey of South Australia*, 99: 8-13.

Gersteling, R.W. and Maiden, K.J., 1975, Relinquishment report, El. 81, Lake MacFarlane area, South Australia, *South Australia, Department of Mines and Energy, Open file Envelope*, 2575 (unpublished).

Gibbs, A.D., 1984, Structural evolution of extensional basin margins, *J. Geol. Soc.* London, 141: 609-620.

Gibbs, A.D., 1987, Linked tectonics of the northern North Sea basin, *In*: C. Beaumont and A.J. Tankard (Eds), *Sedimentary basins and basin forming mechanisms*, Can. Soc. Pet. Geol. Mem., 12: 163-171.

Gibbs, A.D., 1989, Structural styles in basin formation, *In*: A.J. Tankard and H.R. Balkwill (Eds), *Extensional tectonics and stratigraphy of the north Atlantic margins,* Am. Assoc. Pet. Geol. Mem., 46: 81-93.

Ginzburg, A., Makris, J., Fuchs, K., Perathoner, B. and Prodehl, C., 1979a, Detailed structure of the crust and upper mantle along the Jordan-Dead Sea Rift and their transition toward the Mediterranean Sea, *J. Geophys. Res.*, 84: 5605-5612.

Ginzburg, A., Makris, J., Fuchs, K. and Prodehl, C., 1981, The structure of the crust and upper mantle in the Dead Sea Rift, *Tectonophysics,* 80: 109-119.

Ginzburg, A., Makris, J., Fuchs, K., Prodehl, C., Kaminski, W. and Amitai, U., 1979b, A seismic study of the crust and upper mantle of the Jordan-Dead Sea Rift and their transition toward the Mediterranean Sea, *J. Geophys. Res.*, 84: 1569-1582.

Girdler, R.W., 1978, Comparison of the East African Rift System and the Permian Oslo rift, *In*: I.B. Ramberg and E.-R. Neuman (Eds), *Tectonics and geophysics of continental rifts*, Reidel, Dordrecht, 329-345.

Girdler, R.W., 1990, The Dead Sea transform fault system, *Tectonophysics*, 180: 1-13.

Girdler, R.W., 1991a, The Afro-Arabian rift system - an overview, *Tectonophysics*, 197: 139-153.

Girdler, R.W., 1991b, The case for ocean crust beneath the Red Sea (Abstract), *Tectonophysics*, 198: 275-278.

Girdler, R.W., Fairhead,J.D., Searle, R.C. and Sowerbutts, W.T.C., 1969, The evolution of rifting in Africa, *Nature*, 224: 1178:1182.

Girdler, R.W. and Styles, P., 1974, Two stages seafloor spreading, *Nature*, 247: 7-11.

Girdler, R.W. and Underwood, M., 1985, The evolution of early oceanic lithosphere in the Southern Red Sea. *In*: G.F. Sharman and J. Francheteau (Eds), *Oceanic Lithosphere, Tectonophysics*, 116: 95-108.

Girod, M. (Ed.), 1978, *Les Roches Volcaniques*, Doin, Paris.

Goldberg, M. and Beyth, M., 1991, Tiran Island: an internal block at the junction of the Red Sea rift and Dead Sea transform, *Tectonophysics*, 198: 261-273.

Goldstein, N.E. and Ward, S.H., 1964, Numerical filtering of potential field signals, Abstracted in SEG Yearbook, 217-218.

Goleby, B.R., Shaw, R.D., Wright, C., Kennett, B.L.N. and Lambeck, K., 1989, Geophysical evidence for 'thick-skinned' deformation in central Australia, *Nature*, 337: 325-330.

Goleby, B.R., Kennett, B.L.N., Wright, C., Shaw, R.D. and Lambeck, K., 1990, Seismic profiling in the Proterozoic Arunta Block, central Australia: processing for testing models of tectonic evolution, *Tectonophysics*, 173: 257-268.

Goode, A.D., 1970, The petrology and structure of the Kala and Ewarara layered basic intrusions, Giles Complex, central Australia, University of Adelaide Ph.D. thesis (unpublished).

Grant, F.S. and West, G.F., 1965, Interpretation theory in applied geophysics, McGraw-Hill Book Co., Inc., New York.

Grant, N.K., 1971, South Atlantic, Benue Trough, and Gulf of Guinea Cretaceous triple junction, *Geol. Soc. Am. Bull.*, 82: 2295-2297.

Green, A.G., 1976, Interpretation of project Magnet aeromagnetic profiles across Africa, *Geophysical Journal*, 44: 203-228.

Greenhalgh, S.A., Singh, R. and Parham, R.T., 1986a, Earthquakes in South Australia, *Trans. R. Soc. Aust.*, 110(4): 145-154.

Greenhalgh, S.A., Tapley, D. and Singh, R., 1986b, Crustal structure of South Australia from earthquake and explosion data, *Geol. Soc. Aust., Abstracts*, 15: 87-88.

Greenhalgh, S.A., Tapley, D. and Singh, R., 1989, Crustal heterogeneity in South Australia, earthquake evidence, *Geophysical Journal.*, 96: 85-99.

Gregory, J.W., 1984, Contribution to the physical geography of British East Africa, *Geogr. J.*, 4: 290-315, 408-424, 505-514.

Griffiths, J.R., 1971, Continental margin tectonics and the evolution of southeastern Australia, *Australian Petroleum Exploration Journal*, 11: 75-79.

Guardado, J.R., Gamboa, L.A.P. and Lucchesi, C.F., 1990, Petroleum geology of the Campos Basin, Brazil, a model for producing Atlantic type basins, *In*: J.D. Edwards and P.A. Santogrossi (Eds), *Divergent/passive margin basins*, Am. Assoc. Pet. Geol. Mem., 48: 3-79.

Gudmundsson, G., 1967, Spectral analysis of magnetic surveys, *Geophysical Journal of Royal Astronomical Society*, 13: 325-337.

Guiraud, R., Issawi, B. and Bellion, Y., 1985, Les line'aments Guineo-Nubiens: un trait structural majeur a l'échelle de la Plaque Africaine, *C.R. Acad. Sc. Paris*, 300, II (1): 17-20.

Gunn, P.J., 1975, Mesozoic-Cainozoic tectonics and igneous activity - southeastern Australia, *J. Geol. Soc. Aust.*, 22: 215-222.

Gunn, P.J., 1984, Recognition of ancient rift systems: Examples from the Proterozoic of South Australia, *Exploration Geophysics*, 15: 85-97.

Haggerty, S.E., 1978, Mineralogical constraints on Curie isotherms in deep crustal magnetic anomalies, *Geophysical Research Letters*, 5: 105-108.

Haggerty, S.E. and Toft, P.B., 1985, Native iron in the continental lower crust: Petrological and geophysical implications, *Science*, 229: 647-649.

Hahn, A., Kind, E.G. and Mishra, D.C., 1976, Depth estimation of magnetic sources by means of Fourier amplitude spectra, *Geophysical Prospecting*, 24: 287-308.

Hale, L.D. and Thompson, G.A., 1982, The seismic reflection character of the continental crustal Mohorovicic discontinuity, *Journal of Geophysical Research*, 87: 4625-4635.

Hall, D.H., 1968, Regional magnetic anomalies, magnetic units, and crustal structure in the Kenora district of Ontario, *Can. J.Earth Sci.*, 5: 1277-1296.

Hall, D.H., 1974, Long-wavelength aeromagnetic anomalies and deep crustal magnetisation in Manitoba and Northwestern Ontario, Canada, *J. Geophys.*, 40: 403-430.

Hall, D.H., 1976, Crustal studies: their implications for the explorationist, *Bull. Aust. Soc. Explor. Geophys.*, 7: 53-59.

Hall, D.H., Coles, R.L. and Hall, J.M., 1979, The distribution of surface magnetization in the English River and Kenora subprovince of the Archean shield in Manitoba and Ontario, *Can. J.Earth Sci.*, 16: 1764-1777.

Hall, D.H. and Hajnal, Z., 1969, Crustal structure of northwestern Ontario. Refraction seismology, *Can. J.Earth Sci.*, 6: 81-99.

Hall, D.H., Noble, I.A. and Millar, T.W., 1985, Crustal structure of the Churchill-Superior boundary zone between 80° and 98°*W* longitude from Magsat anomaly maps and stacked passes, *Journal of Geophysical Research*, 90: 2621-2630.

Hall, S.A., Andreasen, G.E. and Girdler, R.W., 1977, Total intensity magnetic anomaly map of the Red Sea and adjacent coastal areas, a description and preliminary interpretation, In: Red Sea Research 1970-1975, *Saudi Arabian Dir. Gen. Min. Res., Bull.*, 22: F1-F15.

Halls, H.C., 1978, The late Precambrian central North American rift system. A survey of recent geological and geophysical investigations, *In*: I.B. Ramberg and E.-R. Neuman (Eds), *Tectonics and geophysics of continental rifts*, Reidel, Dordrecht, pp 111-123.

Hammons, R.H., 1966, Aeromagnetic survey offshore South Australia, OEL 33 and 58, *Bureau of Mineral Resources, Petroleum Search Subsidy Report*, 66/4620.

Hansen, R.O., Okubo, Y., Graf, R.J., Tsu, H. and Ogawa, K., 1983, Nationwide Curie point depth analysis of Japan, *SEG Expanded Abstract, EG&G Geometrics Technical Report* I, (unpublished).

Harding, A.W., Humphrey, T.J., Latham, A., Lunsford, M.K. and Strider, M.A., 1990, Controls on Eocene submarine fan deposition in the Witch Ground Graben, *In*: R.F.P. Hardman and J. Brooks (Eds), *Tectonic events responsible for Britain's oil and gas reserves*, The Geological Society of London.

Harris, W.K., 1964, Mesozoic Sediments of Polda Basin, Eyre Peninsula, *Quarterly Geological Notes, The Geological Survey of South Australia*, 12: 6-7

Harris, W.K. and Foster, C.B., 1974, Stratigraphy and palynology of the Polda Basin, Eyre Peninsula, *Mineral Resources Review, South Australia*, 136: 72-105.

Harrison, C.G.A., Carle, H.M. and Hayling, K.L., 1986, Interpretation of satellite elevation magnetic anomalies, *J. Geophys. Res.*, 91: 3633-3650.

Hatcher, R.D., Zeitz, I., Regan, R.D. and Abu-Ajamieh, M., 1981, Sinistral strike-slip motion on the Dead Sea Rift: confirmation from new magnetic data, *Geology*, 9: 458-462.

Hawkins, L.V., Hennion, J.F., Nafe, J.E. and Doyle, H.A., 1965, Marine seismic refraction studies on the continental margin to the south of Australia, *Deep Sea Res.*, 12: 479-495.

Hempton, M.R., 1987, Constraints on Arabian plate motion and extensional history of the Red Sea, *Tectonics*, 6: 687-707.

Herz, N., 1977, Timing of spreading in the South Atlantic: information from Brazilian alkalic rocks, *Bull. Geol. Soc. Am.*, 88: 101-112.

Herz, N., 1978, Basaltic and alkalic rocks of southern Brazil, *In*: E.-R. Neumann and I.B. Ramberg Eds.), *Petrology and geochemistry of continental rifts*, Reidel, Dordrecht, 154-162.

Hillis, R.R., 1991, Chalk porosity and Tertiary uplift, Western Approaches Trough, SW UK and NW French continental shelves, *Journal of Geological Society*, London 148: 669-679.

Hillis, R.R., 1992, A two-layer lithospheric compressional model for the Tertiary uplift of the southern United Kingdom, *Geophysical Research Letters*, 19(6): 573-576.

Horton, C.W., Hempkins, W.B. and Hoffman, A.A.J., 1964, A statistical analysis of some aeromagnetic maps from northwestern Canadian Shield, *Geophysics*, 29: 582-601.

Hospers, J., Rathore, J.S., Feng, J., Finstrøm, E.G. and Holthe, J., 1988, Salt tectonics in the Norwegian-Danish basin, *Tectonophysics*, 149: 35-60.

Hou, C., 1989, Method for calculating and compiling the map of Curie-point surface, *Computation Techniques for Geophysical and Geological Exploration*, 4: 306-311 (in Chinese).

Hou, C., Liu Xiofang, and others, 1977, Transformation of potential field by using 2D FFT, Beijng Computer Center, Ministry of Geology and Mineral Resources, Unpublished Report.

Hou, C. and Shi, Z., 1982, Interpretation system of potential field transform, *Computing Techniques for Geophysical and Geochemical Exploration*, *4*(13): 1-10, (in Chinese).

Hou, C. and Shi, Z., 1985, Experimental analysis for calculating depth of magnetic source via energy spectrum, *Dizhi Xinxi Jishu (Geological Information Technique)*, 1(1): 22-36, (in Chinese).

Howchin, W., 1918, The Geology of South Australia, *The Education Department, Adelaide*.

Illies, J.H., 1975, Recent and paleo-intraplate tectonics in stable Europe and the Rhinegraben rift system, *Tectonophysics*, 29: 251-264.

Illies, J.H., 1978, Two stages Rhinegraben rifting. *In*: E.-R. Neumann and I.B. Ramberg (Eds), *Tectonics and geophysics of continental rifts*, Reidel, Dordrecht, 63-71.

Illies, J.H. (Ed.), 1981, Mechanism of graben formation, Developments in Geotectonics 17, Selected papers of an ICG Symposium held during the 17th IUGG General Assembly, Canberra, Australia, December 5, 1979. Reprinted from *Tectonophysics*, 73, Inter-Union Commission on Geodynamics Scientific Report, 63, Elsevier Scientific Publishing Company, Amsterdam.

Jack, R.L., 1912,The geology of portion of the counties of LeHunte, Robinson and Dufferin, with special reference to underground water supplies, *South Australia, Geological Survey, Bulletin*, 1.

Jackson, J.A., 1987, Active normal faulting and continental extension, *In:* M.P. Coward, J.F. Dewey and P.L. Hancock (Eds), *Continental extensional tectonics*, Geological Society, London, Special Publication, 28: 3-17.

Jackson, J.A. and McKenzie, D., 1983, The geometrical evolution of normal fault systems, *Journal of Structural Geology*, 5: 471-482.

Jackson, J.A. and White, N.J., 1989, Normal faulting in the upper continental crust: observations from regions of active extension, *Journal of Structural Geology*, 11: 15-36.

Jarrige, J.-J., 1992, Variation in extensional fault geometry related to heterogeneities with basement and sedimentary sequences, *In:* P.A. Ziegler (Ed.), *Geodynamics of rifting, Vol. III, Thematic discussions, Tectonophysics*, 215: 161-166.

Jarrige, J.-J., Ott d'Estevou, P., Burollet, P.F., Montenat, C., Prat, P., Richer, J-P. and Thiriet, J-P., 1990, The multistage tectonic evolution of the Gulf of Suez and northern Red Sea continental rift from field observations, *Tectonophysics*, 9: 441-465.

Joffe, S. and Garfunkel, Z., 1987, Plate kinematics of the circum Red Sea - a re-evaluation, *Tectonophysics*, 141: 5-22.

Johnson, B.D., 1972, Crustal structure studies in Tasmania, *Ph.D. thesis, University of Tasmania*, Hobart.

Johnson, B.D., 1985, Viscous remanent magnetization model for the Broken Ridge satellite magnetic anomaly, *J. Geophys. Res.*, 90: 2640-2646.

Johnson, B.D. and Mayhew M.A., 1985, Interpretation of satellite magnetometer data, *4th ASEG Conference*, 1985.

Jordan, T.H. and Frazer, L.N., 1975, Crustal and upper mantle structure from S_P phases, *J. Geophys. Res.*, 80: 1504-1508.

Kabyshev, B.P., Shpak, P.F., Bilik, O.D. et al., 1989, *Geology and oil and gas occurrence of the Dnieper-Donetz Basin. Oil and gas occurrence*, Akad. Nauk Ukrainskoy CCR, Inst. Geol. Nauk, (in Russian).

Keen, C.E. (Ed.), 1979, *Crustal properties across passive margins*, Elsevier, Amsterdam.

Keen, C.E., Beaumont, C. and Boutilier, R., 1981, Preliminary results from a thermo-mechanical model for the evolution of Atlantic-type continental margins, *Oceanol. Acta, Colloque C3*: 123-128.

Keen, C.E., Beaumont, C. and Boutilier, R., 1982, A summary of thermo-mechanical model results for the evolution of continental margins based on three rifting processes, *In:* J.S. Watkins and C.L. Drake (Eds), *Studies in continental margin geology*, American Association of Petroleum Geologists, Memoir 34.

Keen, C.E. and De Voogd, B., 1988, The continent-ocean boundary at the rifted margin off Eastern Canada. New results from deep seismic reflectiion studies, *Tectonics*, 7(1): 107-124.

Khain, V.Ye., 1992, The role of rifting in the evolution of the earth's crust, *Tectonophysics*,215:1-7.

Khan, M.A. and Mansfield, J., 1971, Gravity measurements in the Gregory rift, *Nature*, Phys. Sci., 229: 72-75.

King, B.C., 1978, A comparison between the older (Karroo) rifts and the younger (Cainozoic) rifts of eastern Africa, *In*: E.-R. Neumann and I.B. Ramberg (Eds), *Tectonics and geophysics of continental rifts*, Reidel, Dordrecht, 347-350.

King, L.C., 1950, Outline and description of Gondwanaland, *Geol. Mag.*, 87: 353-359.

Kivior, I. and Boyd, D., 1995, Interpretation of high quality aeromagnetic data over the Polda Trough, *ASEG 11th Geophysical Conference and Exhibition, Petrh*, Abstract, *Australian Society of Exploration Geophysics, Preview*, 57: 129.

Kivior, I., Boyd, D., Shi, Z. and McClay, K.R., 1993, Crustal studies of South Australia based on energy spectral analysis of regional magnetic data, *Exploration Geophysics*, 24: 603-608.

Kovach, R.L. (Ed.), 1990, Conference on 'Geologic and tectonic processes of the Dead Sea rift zone' held at Standford University, Calif., Sept. 7-8, 1988, *Tectonophysics*, 180: 1-137.

Krutikhovskaya, Z.A., 1976, Problems of creating the earth's crust magnetic model for ancient shields (in Russian), *Geofiz. Sb.*, 73: 3-29.

Krutikhovskaya, Z.A. and Pashkevich, I.K., 1977, Magnetic model for the earth's crust under the Ukrainian shield, *Canadian Journal of Earth Sciences*, 14: 2718-2728.

Krutikhovskaya, Z.A. and Pashkevich, I.K., 1979, Long-wavelength magnetic anomalies as a source of information about deep crustal structure, *Journal of Geophysics*, 46: 301-317.

Kusznir, N.J. and Egan, S.S., 1989, Simple-shear and pure-shear models of extensional sedimentary basin formation: applications to the Jeanne d'Arc Basin, Grand Banks of Newfoundland, *In:* A.T. Tankard and H.R. Balkwill (Eds), Extensional tectonics and stratigraphy of the northern Atlantic margins, *Am. Assoc. Pet. Geol. Mem.*, 46: 305-322.

Kusznir, N.J., Karner, G.D. and Egan, S.S., 1987, Geometric, thermal and isostatic consequences of detachment in continental lithosphere and basin formation, *In:* C. Beaumont and A.T. Tankard (Eds), Sedimentary basins and basin-forming mechanisms, *Can. Soc. Pet. Geol. Mem.*, 12: 185-203.

Kusznir, N.J., Marsden, G. and Egan, S.S., 1991, A flexural-cantilever simple-shear/pure-shear model of continental lithosphere extension: applications to the Jeanne d'Arc Basin, Grand Banks and

Viking Graben, North Sea, *In:* A.M. Roberts, G. Yielding and B. Freeman (Eds), *The geometry of normal faults,* Geological Society, London, Special Publication, 56: 41-60.

Kwitko, G., 1982, Lock No. 1 well completion report, *South Australia, Department of Mines and Energy, Report Book,* 81/109.

LaBrecque, J.L., Cande, S.C. and Jarrard, R.D., 1985, Intermediate-wavelength magnetic anomaly field of the North Pacific and possible source distributions, *J. Geophys. Res.*, 90: 2549-2564.

Lambeck, K., 1984, Structure and evolution of the Amadeus, Officer and Ngalia Basins of central Australia, *Australian Journal of Earth Sciences*, 31: 25-48.

Lambeck, K., 1986, Crustal structure and evolution of the central Australian basins, *In*: J.G., Dawson, D.A., Carswell, J., Hall, K.H., Wedepohl (Eds), *The nature of the lower continental crust,* Geological Society, London, Special Publication, 24: 133-145.

Lambeck, K. and Burgess, G., 1992, Deep crustal structure of the Musgrave Block, central Australia: Results from teleseismic travel-time anomalies, *Australian Journal of Earth Sciences*, 39: 1-19.

Lambeck, K., Burgess, G. and Shaw, R.D., 1988, Teleseismic travel-time anomalies and deep crustal structure in central Australia, *Geophysical Journal*, 94: 105-124.

Lambeck, K. and Penny, C., 1984, Teleseismic travel-time anomalies and crustal structures in central Australia, *Phys. Earth Planet. Int.*, 34: 46-56.

Langel, R.A. and Estes, R.H., 1982, A geomagnetic field spectrum, *Geophysical Research. Letters*, 9: 250-253.

Latin, D.M., Dixon, J.E. and Fitton, J.G., 1990, Rift-related magmatism in the North Sea basin. *In*: D.J. Blundell and A.D. Gibbs (Eds), *Tectonic evolution of the North Sea rifts*, Claredon Press, Oxford, 101-144.

Le Bas, M.J., 1971, Peralkaline volcanism, crustal swelling and rifting, *Nature*, 230: 85-87.

Lees, G.M., 1952, Foreland folding, *Q. J., Geol. Soc.*, London, 108: 1-34.

Le Masurier, W.E. and Thomson, J.W. (Eds), 1990, Volcanoes of the Antarctic plate and Southern Ocean, *Antarctic Research Series*, 48, American Geophysical Union, Washington.

Leonov, G.P., 1980, *Historical geology. Principles and methods. Precambrian,* Moscow Univ. Publ. House, Moscow (in Russian).

Le Pichon, X. and Sibuet, J.C., 1981, Passive margins: a model of formation, *J. Geophys. Res.*, 86: 3708-3720.

Letouzey, J., Werner, P. and Marty, A., 1991, Fault reactivation and structural inversion. Backarc intraplate compressive deformations. Examples of the eastern Sunda shelf (Indonesia), *Tectonophysics*, 183: 341-362.

Lidiak, E.G., 1974, Magnetic characteristics of some Precambrian basement rocks, *J. Geophys.*, 40: 549-654.

Lister, G.S., Etheridge, M.A. and Symonds, P.A., 1986, Detachment faulting and the evolution of passive continental margins, *Geology*, 14: 245-250.

Lister, G.S., Etheridge, M.A. and Symonds, P.A., 1991, Detachment models for the formation of passive continental margins, *Tectonics*, 10: 1038-1064.

Logatchev, N.A., Rogozhina, V.A., Solonenko, V.P. and Zorin, Y.A., 1978, Deep structure and evolution of the Baikal rift zone. *In*: E.-R. Neumann and I.B. Ramberg (Eds), *Tectonics and geophysics of continental rifts*, Reidel, Dordrecht, 49-61.

Logatchev, N.A. and Zorin, Y.A., 1992, Baikal rift zone: structure and geodynamics. *In*: P.A. Ziegler (Ed.), *Geodynamics of rifting, I*, Case history studies on rifts: Europe and Asia, *Tectonophysics*, 208: 273-286.

Logatchev, N.A., Zorin, Y.A. and Rogozhina, V.P., 1983, Baikal rift: active or passive? - comparison of the Baikal and Kenya rift zones. *Tectonophysics*, 94: 223-240.

Lowes, F.J., 1966, Mean square values on sphere of spherical harmonic vector fields, *J. Geophys. Res.*, 71: 2179.

Ludwig, K.R., 1980, Calculation of uncertainties of U-Pb isotope data. *Earth and Planetary Science Letters*, 46: 212-220.

Makris, J., Allam, A., Mokhtar, T., Basahel, A., Deghani, G.A. and Bazari, M., 1983, Crustal structure at the northern western region of Saudi Arabian Peninsula and its transition to the Red Sea, *In*: Pan African Crustal Evolution in the Arabian-Nubian Shield, First Symp. I.G.C.P. 164, *Bull. Fac. Earth Sci., King Abdulaziz Univ.*, Jeddah, 6: 435-447.

Makris, J., Henke, H., Egloff, F. and Akamaluk, T., 1991a, The gravity field of the Red Sea and East Africa, *Tectonophysics*, 198: 369-381.

Makris, J. and Rihm, R., 1991, Shear-controlled evolution of the Red Sea : pull apart model. In J. Makris, P. Mohr and R. Rihm (Eds), Red Sea: British and Earth History of a New Oceanic Basins, *Tectonophysics*, 198: 441-446.

Makris, J., Tsironidis, J. and Richter, H., 1991b, Heat flow density distribution in the Red Sea, *Tectonophysics*, 198: 383-393.

Mathur, S.P., 1974, Crustal structure in southwest Australia from seismic and gravity data, *Tectonophysics*, 24: 151-82.

Mayhew, M.A., 1985, Curie isotherm surfaces inferred from high altitude magnetic anomaly data, *J. Geophys. Res.*, 90: 2647-2654.

Mayhew, M.A., Estes, R.H. and Myers, D.M., 1985a, Magnetization models for the source of the 'Kentucky anomaly' observed by Magsat, *Eart Planet. Sci. Lett.*, 74: 117-129.

Mayhew, M.A., Johnson, B.D. and Wasilewski, P.J., 1985b, A review of problems and progrss in studies of satellite magnetic anomalies, *J. Geophys. Res.*, 90: 2511-2522.

Mayhew, M.A., Thomas, H.H. and Wasilewski, P.J., 1982, Satellite and surface geophysical expression of anomalous crustal structure in Kentucky and Tennessee, *Earth Planet. Sci. Lett.*, 58: 395-405.

McClay, K.R., 1989, Physical models of structural styles during extension, In: A.J. Tankard and H.R. Balkwill (Eds), Extensional tectonics and stratigraphy of the North Atlantic Margins, *Am. Assoc. Pet. Mem.*, 46: 86-96.

McClay, K.R., 1990a, Extensional fault systems in sedimentary basins: a review of analogue model studies, *Marine and Petroleum Geology*, 7: 206-233.

McClay, K.R., 1990b, Deformation mechanics in analogue models of extensional fault systems, In: R.J. Knipe and E.H. Rutter (Eds), *Deformation Mechanics, Rheology and Tectonics*, Special Publication Geological Society of London, 54: 445-453.

McClay, K.R. and Ellis, P.G., 1987, Geometries of extensional fault systems developed in model experiments, *Geology*, 15: 341-344.

McClay, K.R. and Scott, A.D., 1991, Experimental models of hangingwall deformation in ramp-flat listric extensional faults systems, *Tectonophysics*, 188: 85-96.

McClay, K.R. and White, M., 1993, Analogue modelling of orthogonal and oblique rifting, *Marine and Petroleum Geology*.

McClure, D., 1963, Interpretation of long aeromagnetic profiles, The University of Alberta, Alberta, Master of Science thesis.

McClure, I., 1982a, Mercury 1 - well completion report, *South Australia, Department of Mines and Energy, Open file Envelope*, 4689 (unpublished).

McClure, I., 1982b, Columbia 1 - well completion report, *South Australia, Department of Mines and Energy, Open file Envelope*, 4737 (unpublished).

McConnell, R.B., 1980, A resurgent taphrogenic lineament of Precambrian origin in eastern Africa, *J. Geol. Soc.*, 137: 483-489.

McGetchin, T.R. and Siver, A.T., 1972, A crustal-upper mantle model for the Colorado Plateau based on observations of crystalline rock fragments in the Moses Rock Dike, *J. Geophys. Res.*, 77: 7022-7037.

McInerney, P.M., 1977, Seismic refraction investigations in the Polda Basin, *SADME unpublished report Bk.*, 77/74.

McInerney, P.M., 1978, Progress report: reappraisal of geophysical data, offshore Polda Basin, *Geological Survey of South Australia*, No. RB78/31.

McKenzie, D.P., 1978a, Active tectonics of the Alpine-Himalayan belt: The Aegean and surrounding regions, *Geophys. J. R. Astron. Soc.*, 55: 217-254.

McKenzie, D.P., 1978b, Some remarks on the development of sedimentary basins, *Earth Planet. Sci. Lett.*, 40: 25-32.

McKenzie, D.P. and Bickle, M.J., 1988, The volume and composition of melt generated by extension of the lithosphere, *Journal of Petrology*, 29: 625-679.

McLaren, D.J. and Skinner, B.J., 1987, Resources and world development, Wiley.

McLure, I., 1982, Columbia 1, offshore Polda Basin EPPSA 15 *well completion report, Australian Occidental Pty. Ltd.*

McPharlin, D., 1980, Preliminary report on gravity survey in the Polda Basin area, *Department of Mines and Energy, South Australia, Report Bk.* No. 80/82, D.M. No. 125/177.

Meissner, R., 1973, The 'moho' as a transition layer, *Geophys. Surveys*, 1: 195-216.

Meissner, R., 1986, The continental crust, a geophysical approach, *Int. Geophys. Ser.*, 34, Academic Press, London.

Milanovsky, E.E. and Malkov, B.A., 1980, Epochs of kimberlite volcanism and the global compressive and expansionary cycles of the earth. *Dokl. Akad. Nauk S.S.S.R., Earth Sci. Sect.*, 252: 62-65.

Milanovsky, E.E., 1978, Some problems of rifting development in the earth's history, *In*: E.-R. Neumann and I.B. Ramberg (Eds), *Tectonics and geophysics of continental rifts*, Reidel, Dordrecht, 385-399.

Milanovsky, E.E., 1981, Aulacogens of ancient platforms; problems of their origin and tectonic development, *Tectonophysics*, 73: 213-248.

Milanovsky, E.E., 1983a, Metaplatforms as regions of intermediate character between ancient platforms and folded belts, *Bull. Moscow Nat. Soc. Sect. Geol.*, 6: 48-68 (in Russian).

Milanovsky, E.E., 1983b, *Rifting in the earth's history. Rifting on the ancient platforms*, Nedra, Moscow (in Russian).

Milanovsky, E.E., 1983c, Major stages of rifting evolution in the earth's history, *Tectonophysics*, 94: 599-607.

Milanovsky, E.E., 1987, Rifting evolution in geological history, *Tectonophysics*, 143: 103-118.

Milanovsky, E.E., 1992, Aulacogens and aulacogeosynclines: Regularities in setting and evolution, *Tectonophysics*, 215: 55-68.

Milligan, P.R., (1989), Geomagnetic variations in South Australia: the Eyre Peninsula anomaly, unpublished Ph.D. Thesis, The Flinders University of South Australia.

Milligan, P.R. and White, A., 1988, Geological structure and geomagnetic variations in South Australia, Poster paper presented at the Australian Bicentenary Congress of Physicists, Eighth AIP Congress, University of NSW, Sydney.

Milligan, P.R., White, A. and Chamalaun, F., 1990, Extension of the Eyre Peninsula conductivity anomaly, *Exploration Geophysics.*

Milnes, A.R., Cooper, B.J. and Cooper, J.A., 1982, The Jurassic Wisanger Basalt of Kangaroo Island, South Australia, *Transactions of the Royal Society of South Australia,* 106: 1-13.

Milton, N.J., Bertram, G.T. and Vann, I.R., 1990, Early Palaeogene tectonics and sedimentation in the Central North Sea, *In*: R.F.P. Hardman and J. Brooks (Eds), *Tectonic events responsible for Britain's oil and gas reserves,* The Geological Society of London.

Mims, C.V.H., Powell,C. and Ellwood, B.B., 1990, Magnetic susceptibility of rocks in the Nutbush Creek ductile shear zone, Northern Carolina, *Tectonophysics*, 178: 207-223.

Mitchell, A.M. and Garson, M.S., 1976, Mineralisation at plate boundaries, *Minerals, Sci. and Engn.*, 8: 129-169.

Molnar, P. and Tapponnier, P., 1975, Cenozoic tectonics of Asia: effects of a continental collision, *Science*, 189: 419-426.

Morgan, P. and Barker, B.H. (Eds), 1983, Processes of continental rifting, Developments in Geotectonics 19, Selected papers from the Lunar and Planetary Institute Topical Conference on the Processes of Planetary Rifting, held in St. Helena, California, U.S.A., December 3-5, 1981. Reprinted from *Tectonophysics*, 94.

Mueller, S., 1978, Evolution of the earth's crust. *In*: E.-R. Neumann and I.B. Ramberg (Eds), *Tectonics and geophysics of continental rifts*, Reidel, Dordrecht, 11-28.

Mutton, A.J. and Shaw, R.D., 1979, Physical property measurements as an aid to magnetic interpretation in basement terrains, *Bull. Aust. Soc. Explor. Geophys.*, 10: 79-91.

Negi, J.G. and Arawal, P.K., 1986, Delineation of crustal layers by the spectral analysis of Bouguer gravity data: a case history for the Deccan Traps (India), *Tectonophysics*, 122: 135-147.

Negi, J.G., Arawal, P.K. and Rao, K.N.N., 1983, Three-dimensional model of the Koyna area of Maharashtra State (India) based on the spectral analysis of aeromagnetic data, *Geophysics*, 48: 964-974.

Nelson, R.G., 1972, A review of geophysical work in the Polda Basin - Eyre Peninsula, *Mineral Resources Review*, 136: 91-98.

Nelson, R.G., 1974, A re-evaluation of seismic velocities recorded in calcretes, Flinders Highway, Talia - Port Kenny - Streaky Bay section, *South Australia, Department of Mines, Report Book*, 74/175.

Nelson, R.G., Crabb, T.N. and Gerdes, R.A., 1986, A review of geophysical exploration in the Polda Basin, South Australia, *The APEA Journal*, 26: 319-333.

Neugebauer, H.J., 1983, Mechanical aspects of continental rifting, *Tectonophysics*, 94: 91-108.

Neumann, E.R. (Ed.), 1990, Rift zones in the continental crust of Europe - geophysical, geological and geochemical evidence: Oslo-Horn Graben, *Tectonophysics*, 178: 1-126.

Odegard, M.E. and Berg, J.W., 1965, Gravity interpretation using the Fourier integral, *Geophysics*, 30: 424-438.

Ofoegbu, C.O. and Mohan, N.L., 1990, Interpretation of aeromagnetic anomalies over part of southeastern Nigeria using three-dimensional Hilbert transformation, *Pure and Applied Geophysics*, 134: 13-29.

Okubo, Y., Graf, R.J., Hansen, R.O., Ogawa, K. and Tsu, H., 1985, Curie point depths of the Island of Kyushu and surrounding areas, Japan, *Geophysics*, 53: 481-494.

Olade, M.A., 1975, Evolution of Nigeria's Benue Trough: A tectonic model, *Geol. Mag.*, 112: 575-583.

Oliver, R.L., 1972, Some aspects of Antarctic-Australian geological relationships, *In:* R.J. Adie (Ed.), *Antarctic geology and geophysics*, Universitetsforlaget, Oslo, 859-864.

Oliver, R.L., Cooper, A.J. and Truelove, A.J., 1983, Petrology and zircon geochronology of Herring Island and Commonwealth Bay and evidence for Gondwana reconstructions, *In:* R.L. Oliver, P.R. James and J.B. Jago (Eds), *Antarctic Earth Science*, Cambridge University Press, 64-68.

O'Reilly, S.Y. and Griffin, W.L., 1985, A xenolith-derived geotherm for southeastern Australia and its geophysical implications, *Tectonophysics*, 111: 41-63.

Padovani, E.R. and Carter, J.L., 1977, Aspects of the deep crustal evolution beneath south central New Mexico, *In:* J.G. Heacock (Ed.), *The earth's crust*, AGU Mono, 20: 19-56.

Pal, P.C., Khurana, K.K. and Unnikrishnan, P., 1979, Two examples of spectral approach to source depth estimation in gravity and magnetics, *Pure and Applied Geophysics*, 117: 772-783.

Parker, A.J., 1978, Structural, stratigraphic and metamorphic geology of Lower Proterozoic rocks in the Cowell/Cleve district, eastern Eyre Peninsula, *University of Adelaide Ph.D. thesis*, (unpublished).

Parker, A.J., 1983, Whyalla map sheet, South Australia, *South Australia, Geological Survey, Geological Atlas 1:250 000 Series*, sheet SI53-8.

Parker, A.J., 1990, Gawler Craton and Stuart Shelf-regional geology and mineralisation, *In:* F.C. Hughes (Ed.), *Geology of the mineral deposits of Australia and Papua New Guinea*, Australian Institute of Mining and Metallurgy, Monograph Series, 14: 999-1008.

Parker, A.J., Fanning, C.M. and Flint, R.B., 1985, Geology, *In:* C.R. Twidale, M.J. Tyler and M. Davies (Eds), Natural history of Eyre Peninsula, *Royal Society of South Australia, Occasional Publications*, 4: 21-45.

Parker, A.J., Fanning, C.M., Flint, R.B., Martin, A.R. and Rankin, L.R., 1988, Archaean-Early Proterozoic granitoids, metasediments and mylonites of southern Eyre Peninsula, South

Australia, *Geological Society of Australia, Specialist Group in Tectonics and Structural Geology, Field Guide Series*, 2.

Parker, A.J. and Lemon, N.M., 1982, Reconstruction of the Early Proterozoic stratigraphy of the Gawler Craton, South Australia, *Journal of the Geological Society of Australia*, 29: 221-239 .

Parker, A.J. with contributions from **Preiss, W.V. and Rankin L.R.**, 1993, Geological framework, *In:* J.F. Drexel, W.V. Preiss and A.J. Parker (Eds), *The geology of South Australia, Volume 1, The Precambrian, Mines and Energy of South Australia, Geological Survey of South Australia.*

Parker, A.J., Rickwood, P.C., Baillie, P.W., McClenaghan, M.P., Boyd, D.M., Freeman, M.J., Pietsch, B.A., Murray, C.G. and Myers, J.S., 1987, Mafic dyke swarms of Australia, *In:* H.C. Halls and W.F. Fahrig (Eds), *Mafic dyke swarms, Geological Association of Canada, Special Papers*, 34: 401-417.

Parkin, L.W. with contributions by **Firman, J.B., Johns, R.K., Ludbrook, N.H., Thomson, B.P. and Wopfner, H.**, 1969, *Handbook of South Australian Geology*, Geological Survey of South Australia.

Patridge, A., 1976, Late Jurassic palynology of Gemini-1, Polda Trough offshore, South Australia, *ESSO Australia Ltd., Palaeontological Report*: 1976/6.

Perathoner, B., Fuchs, K., Prodehl, C. and Ginzburg, A., 1981, Seismic investigation of crust-mantle transition in continental rift systems - Jordan-Dead Sea Rift and Rhinegraben, *Tectonophysics*, 80: 121-133.

Planke, S., Skogseid, J. and Eldholm, O., 1991, Crustal structure off Norway, 62° to 70° north, *Tectonophysics*, 189: 91-107.

Plumb, K.A., Derrick, G.M., Needham, R.S. and Shaw, R.D., 1981, The Proterozoic of northern Australia. *In*: Hunter, D.R. (Ed.), *Precambrian of the Southern Hemisphere*, Elsevier, New York, 205-307.

Prodehl, C. and Mechie, J., 1991, Crustal thinning in relationship to the evolution of the Afro-Arabian rift system: a review of seismic-refraction data, *Tectonophysics*, 198: 11-327.

Preiss, W.V. (Compiler), 1987, The Adelaide Geosyncline-Late Proterozoic stratigraphy, sedimentation, palaeontology and tectonics, South Australia, *Geological Survey, Bulletin*, 53.

Quennell, A.M., 1958, The structural and geomorphic evolution of the Dead Sea Rift, *Q. J. Geol. Soc. London*, 114: 1-24.

Quennell, A.M., 1983, Evolution of the Dead Sea Rift - a review, *In*: A.M. Abed and H.M. Khaled (Eds), *Geology of Jordan*, 460-482.

Rabinowitz, P.D., 1974, The boundary between oceanic and continental crust in the western North Atlantic, *In*: C.A. Burk and C.L. Drake (Eds), *The geology of continental margins*, 67-84, Springer-Verlag, New York.

Ramberg, I.B., 1976, Gravity interpretation of the Oslo Graben and associated rocks, *Norges Geologishe Undersokelle Bull.*, 325.

Ramberg, I.B., Milanovsky, E.E. and Qvale, G. (Eds), 1984, Continental rifts - principal and regional characteristics, Tectonophysics, 143/1-3.

Ramberg, I.B. and Neumann, E.R. (Eds), 1978, *Petrology and geochemistry of continental rifts*, Reidel, Dordrecht.

Ramberg, I.B. and Spjeldanæs, N., 1978, *In*: E.-R. Neumann and I.B. Ramberg (Eds), *Tectonics and geophysics of continental rifts*, Reidel, Dordrecht, 167-194.

Rankin, L.R., 1993, Polda Basin, *In:* J.F. Drexel, W.V. Preiss and A.J. Parker (Eds), *The geology of South Australia, Volume 1, The Precambrian, Mines and Energy of South Australia, Geological Survey of South Australia.*

Rankin, L.R., Flint, R.B. and Fanning, C.M., 1988, The Bosanquet Formation of the Gawler Craton, *South Australia, Geological Survey, Quarterly Geological Notes*, 105: 12-18.

Rao, K.G.C. and Avasthi, D.N., 1973, Analysis of the Fourier spectrum of the gravity effect due to two-dimensional triangular prism, *Geophysical Prospecting*, 21: 526-542.

Rattigan, J.H., Gersteling, R.W. and Tonkin, D.G., 1977, Exploration geochemistry of the Stuart Shelf, South Australia, *Journal of Geochemical Exploration*, 8: 203-217.

Raymond, C.A. and LaBrecque, J.L., 1987, Magnetization of oceanic crust: thermoremanent magnetization or chemical remanent magnetization?, *J. Geophys. Res.*, 92: 8077-8088.

Reading, H.G., 1986, African tectonics and sedimentation, an introduction, *In*: L.E. Frostick et al. (Eds), *Sedimentation in the African Rifts*, Geological Society Special Publication, 25.

Regan, R.D. and Marsh, B.D., 1982, The Bangui magnetic anomaly: Its geological origin, *J. Geophys. Res.*, 87: 1107-1120.

Reynolds, D.J. and Rosendahl, B.R., 1984, Tectonic expression of rifting, *Trans. Am. Geophys. Union*, 65: 1116.

Richards, P.C., 1990, The early to mid-Jurassic evolution of the northern North Sea, *In*: R.F.P. Hardman and J. Brooks (Eds), *Tectonic events responsible for Britain's oil and gas reserves*, The Geological Society of London.

Richter, H., Makris, J. and Rihm, R., 1991, Geophysical observations offshore Saudi Arabia: seismic and magnetic measurements, *Tectonophysics*, 198: 297-310.

Riddihough, R.P., 1972, Regional magnetic anomalies and geology in Fennoscandia: a discussion, *Can. J. Earth Sci.*, 9: 219-232.

Rihm, R., Makris, J. and Möller, L., 1991, Seismic surveys in the northern Red Sea: asymmetric crustal structure, *Tectonophysics*, 198: 275-295.

Ringwood, A.E., 1975, *Composition and petrology of the earth's mantle*, McGraw Hill, New York, NY, 603.

Ro, H.E., Larsson, F.R., Kinck, I.J. and Husebye, E.S., 1990, The Oslo Rift - its evolution on the basis of geological and geophysical observations, *Tectonophysics*, 178: 11-28.

Roberts, S. and Jackson, J., 1991, Active normal faulting in central Greece: an overview, *In*: A.M Roberts, G. Yielding and B. Freeman (Eds), *The geometry of normal faults*, Reidel, Geological Society Special Publication N0 56, London, 125-142.

Roeser, H.A., 1975, A detailed magnetic survey of the southern Red Sea, *Geol. Jahrb.*, 13: 131-153.

Rosendahl, B.R., 1987, Architecture of continental rifts with special reference to East Africa, *Ann. Rev. Earth Planet. Sci.*, 15: 445-503.

Rosendahl, B.R., Kilembe, E. and Kaczmarick, K., 1992, Comparison of Tanganyika, Malawi, Rukwa and Turkana rift basins from analyses of seismic reflection data, *In:* P.A. Ziegler (Ed.), *Geodynamics of rifting, Vol. II, Case history studies on rifts: North and South America and Africa, Tectonophysics*, 213: 235-256.

Rotstein, Y., Bartov, Y. and Hofstetter, A., 1991, Active compressional tectonics in the Jericho area, Dead Sea Rift, *Tectonophysics*, 198: 239-259.

Rowan, I.S., 1968, Regional gravity survey of Kimba and Elliston 1:250000 map areas. *Mineral Resources Review*, South Australia, 128: 26-32.

Royden, L.H. and Horváth, F. (Eds), 1988, The Pannonian Basin, a study in basin evolution, *Am. Assoc. Pet. Geol. Mem.*, 45.

Ruder, M.E. and Alexander, S.S., 1986, Magsat equivalent source anomalies over the southeastern United States: implications for crustal magnetization, *Earth Planet. Sci. Lett.*, 78: 33-43.

Rudkewicz, M.Y., 1976, The history and dynamics of the development of the West Siberian platform, *Tectonophysics*, 36: 275-287.

Rutland, R.W.R., 1981, Structural framework of the Australian Precambrian. *In*: Hunter, D.R. (Ed.), *Precambrian of the Southern Hemisphere*, Elsevier, New York, 205-307.

Rutland, R.W.R., Parker, A.J., Pitt, W.V. and Murrell, B., 1981, The Precambrian of South Australia. *In*: Hunter, D.R. (Ed.), *Precambrian of the Southern Hemisphere*, Elsevier, New York, 205-307.

Salveson, J.O., 1978, Variations in the geology of rift basins - a tectonic model, Proc. 1978 Int. Symp. on the Rio Grande Rift, Santa Fé, N.M.

Schandelmeier, H. and Pudlo, D., 1990, The Central African Fault Zone (CAFZ) in Sudan: a possible continental transform fault, *Berliner Geowiss. Abh., Reihe A*, 120.1: 31-44

Schlinger, C.M., 1985, Magnetisation of lower crust and interpretation of regional magnetic anomalies; examples from Lofoten and Vesteralen, Norway, *J. Geophys. Res.*, 90: 11484-11504.

Schnetzler, C.C., 1985, An estimation of continental crust magnetization and susceptibility from Magsat data for the conterminous United States, *J. Geophys. Res.*, 90: 2617-2620.

Schuepbach, M.A. and Vail, P.R., 1980, Evolution of outer highs on divergent continental margins, *Continental Tectonics*, 50-62, National Academy of Science, Washington.

Sclater, J.G. and Christie, P.A.F., 1980, Continental stretching: an explanation of the post-mid-Cretaceous subsidence of the central North Sea basin, *J. Geophys. Res.*, 85: 3711-3739.

Segawa, J. and Oshima, S., 1975, Buried Mesozoic volcanic-plutonic fronts of the northwestern Pacific island arcs and their implications, *Nature*, 256: 15-19.

Sengör, A.M.C. and Burke, K., 1978, Relative timing of rifting and volcanism on earth and its tectonic implications, *Geophys. Res. Lett.*, 5: 419-421.

Shackleford, P.R.J., 1978, The determination of crustal structure in Adelaide Geosyncline using quarry blasts as seismic sources, *M.Sc. thesis, Department of Physics, University of Adelaide.*

Shackleford, P.R.J. and Sutton, D.J., 1979, Crustal structure in South Australia using quarry blasts, *In*: D. Denham (Ed.), *Crust and Upper Mantle of Southwest Australia, Austr. Bur. Miner. Resour., Rec.* 1979/2.

Shackleford, P.R.J. and Sutton, D.J., 1981, A first interpretation of crustal structure in the Adelaide Geosyncline in South Australia using quarry blasts, *J. Geol. Soc. Aust.*, 28: 491-500.

Shatsky, N.S., 1964, O progibakh donetskogo tipa (On the basins of the Donets type), Izbrannye Trudy, Vol. II, *Nauka*, Moscow, 544-553.

Sheridan, R.E., 1983, Phenomena of pulsation tectonics related to the breakup of the eastern North American continental margin, In: R.E. Sheridan, F.M. Gradstein et al. (Eds), *Init. Rep. DSDP*, 76: 897-909.

Shi, Z., 1993, Automatic interpretation of potential field data applied to the study of overburden thickness and deep crustal structure, South Australia, *Ph.D. thesis, Department of Geology and Geophysics, The University of Adelaide.*

Shive, P.N., Blakely, R.J., Frost, B.R. and Fountain, D.M., 1992, Magnetic properties of the lower continental crust, *In*: D.M. Fountain, R. Arculus and R.W. Kay (Eds), *Continental crust, Developments in Geotectonics*, 23, Elsevier, 145-177.

Shuey, R.T., Schellinger, D.K., Johnson, E.H. and Alley, L.B., 1973, Aeromagnetics and the transition between the Colorado Plateau and Basin and Range province, *Geology*, 1: 107-110.

Shuey, R.T., Schellinger, D.K., Tripp, A.C. and Alley, L.B., 1977, Curie depth determination from aeromagnetic spectra, *Geophysical Journal of Royal Astronomical Society*, 50: 75-101.

Simpson, D.W., 1973, P wave velocity structure of the upper mantle in the Australian region, Ph.D. thesis, Australian National University. Canbera.

Sleep, N.H., 1971, Thermal effects of the formation of Atlantic continental margins by continental break-up, *Geophysical Journal of Royal Astronomical Society*, 24: 325.

Smith, A.G. and Hallam, A., 1970, The fit of the southern continents, *Nature*, 225: 139-144.

Smith, R. and Kamerling, P., 1969, Geological framework of the Great Australian Bight, *APEA Journal*, 9: 60-66.

Sneddon, I.N., 1951, *Fourier transforms*, New York, McGraw-Hill Book Company, Inc.

Sollogub, V.B. and Chekunov, A.V., 1975, Deep structure and earth's crust evolution, *In*: *The earth's physics problems in the Ukraine*, Kiev, *Naukova Dumka*, 118-141.(in Russian)

Solovyev, O.A., 1962, Use of the frequency method for the determination of some parameters of magnetic bodies, Izv. Akad. Nauk, SSSR, *Sibirskoye Otedelniye Geologyai Geofizika*, 2: 122-125.

Spector, A., 1968, Spectral analysis of aeromagnetic data, *Ph.D. thesis, Department of Physics, University of Toronto*, Canada (unpublished).

Spector, A. and Bhattacharyya, B.K., 1966, Energy density spectrum and autocorrelation function of anomalies due to simple magnetic models, *Geophysical Prospecting*, 14: 242-272.

Spector, A. and Grant, F.S., 1970, Statistical models for interpreting aeromagnetic data, *Geophysics*, 35: 293-302.

Spector, A. and Grant, F.S., 1975, Comments on "Two-dimensional power spectral analysis of aeromagnetic field", *Geophysical Prospecting*, 23: 391.

Spector, A. and Grant, F.S., 1985, Comments and errata to Classic Papers, "Statistical models for interpreting aeromagnetic data", *Geophysical Prospecting*, 23: 391.

Spohn, T. and Schubert, G., 1982, Convective thinning of the lithosphere: a mechanism for the initiation of continental rifting, *J. Geophys. Res.*, 87: 4669-4681.

Sprigg, R.C., 1952, Sedimentation in the Adelaide Geosyncline and the formation of the continental terrace, *In:* M.F. Glaessner and R.C. Sprigg (Eds), *Sir Douglas Mawson Anniversary Volume*, University of Adelaide, 153-159.

Springbett, G.M., 1980, Polda Basin Coalfield - Lock Coal Deposit, South Australia: geological report, for Electricity Trust of South Australia, *South Australia, Department of Mines and Energy, Open file Envelope*, 3384 (unpublished).

Sproll, W.P. and Dietz, R.S., 1969, Morphological continental-drift fit of Australia and Antarctica, *Nature*, 222: 345-348.

Stagg, H.M.J. and Willcox, J.B., 1992, A case for Australia-Antarctica separation in the Neocomian (ca. 125 Ma), *Tectonophysics*, 210: 21-32.

Stagg, H.M.J., Willcox, J.B., Needham, D.J.L., O'Brien, G.W., Cockshell, C.D., Hill, A.J., Thomas, B. and Hough, L.P., 1991, Basins of the Great Australian Bight, Continental Margins Program, *Folio 5, BMR and SADME.*

Steel, R. and Ryseth, A., 1990, The Triassic-early Jurassic succession in the northern North Sea: megasequence stratigraphy and intra-Triassic tectonics, *In*: R.F.P. Hardman and J. Brooks (Eds), *Tectonic events responsible for Britain's oil and gas reserves*, The Geological Society of London.

Stein, R.S. and Barrientos, S.E., 1985, Planar high-angle faulting in the Basin and Range: Geodetic analysis of the 1983 Borah Peak, Idaho, Earthquake, *J. Geophys. Res.*, 90: 11355-11366.

Stewart, I.C.F., 1971, Seismic activity in 1969 associated with the eastern margin of the Adelaide Geosyncline, *Ibid.*, 18: 143-147.

Stewart, I.C.F., 1972, Seismic interpretation of crustal structures in the Flinders - Mt Lofty Ranges and gulf regions, South Australia, *Journal of the Geological Society of Australia*, 19: 351-362.

Stewart, I.C.F. and Mount, T.J., 1972, Earthquake mechanism in South Australia in relation to plate tectonics, *Journal of the Geological Society of Australia*, 19: 41-52.

Stewart, I.C.F., Slade, A. and Sutton, D.J., 1972, South Australia seismicity 1967-1971, *Journal of the Geological Society of Australia*, 19: 441-452.

Stewart, J.H., 1978, Rift systems in the western United States, *In*: E.-R. Neumann and I.B. Ramberg (Eds), *Tectonics and geophysics of continental rifts*, Reidel, Dordrecht, 89-119.

Stockdale Prospecting Ltd, 1992a, EL 1518, Mount Hope; Progress and final reports for the period 22/9/88 to 11/6/92, *South Australia. Department of Mines and Energy. Open File Envelope*, 8076 (unpublished).

Stockdale Prospecting Ltd, 1992b, EL 1517, Verran; Progress and final reports for the period 22/9/88 to 15/7/92, *South Australia. Department of Mines and Energy. Open File Envelope*, 8086 (unpublished).

Stockdale Prospecting Ltd, 1992c, EL 1527, Mount Wedge; Progress and final reports for the period 12/10/88 to 11/6/92, *South Australia. Department of Mines and Energy. Open File Envelope*, 8087 (unpublished).

Stockdale Prospecting Ltd, 1992d, EL 1694, Venus Bay; Progress and final reports for the period 9/1/91 to 15/7/92, *South Australia. Department of Mines and Energy. Open File Envelope*, 8422 (unpublished).

Stracke, K.J., Ferguson, J. and Black, L.P., 1979, Structural setting of kimberlites in southeastern Australia, *In:* H.O. Meyer and F.R. Boyd (Eds), *Kimberlites, diatremes and diamonds: their geology, petrology and geochemistry, Proceedings 2nd International Kimberlite Conference, American Geophysical Union, Washington D.C.*, 1: 71-91.

Stuart, G.W., Fairhead, J.D., Dorbath, L. and Dorbath, C., 1985, A seismic refraction study of the central structure associated with the Adamawa plateau and Garoua Rift, Cameroon, West Africa, *Geoph. J. R. Astron. Soc.*, 81: 1-12.

Suess, E., 1885, *Das Antlitz der Erde*, Vol. 1, Tempsky, Prag.

Sultan, M., Arvidson, R.E. and Duncan, I.J., 1988, Extension of the Najd Shear System from Saudi Arabia to the central Eastern Desert of Egypt based on integrated field and Landsat observations, *Tectonics*, 7 (6): 1291-1306.

Talwani, M., Mutter, J., Houtz, R. and König, M., 1978, The margin south of Australia - a continental margin palaeorift, *In*: E.-R. Neumann and I.B. Ramberg (Eds), *Tectonics and geophysics of continental rifts*, Reidel, Dordrecht, 203-219.

Tarlowski, C., Simonis, F., Whitaker, A. and Milligan, P., 1991, The magnetic anomaly map of Australia, *Exploration Geophysics*, 23(1/2): 339-342.

Taylor, D., 1975, Micropaleontological study of Outback Oil Gemini-1 well.

Taylor, P.T., 1983, Magnetic data over the Arctic from aircraft and satellites, *Cold Regions. Sci. Technol.*, 7: 35-40.

Teisserenc, P. and Villemin, L., 1990, Sedimentary basin of Gabon-geology and oil systems, *In:* J.D. Edwards and P.A. Santogrossi (Eds), *Divergent/passive margin basins*, Am. Assoc. Pet. Geol. Mem., 48: 117-199.

Ten-Brink, U.S. and Ben-Avraham, Z., 1989, The anatomy of a pull apart basin: seismic reflection observations of the Dead Sea Basin, *Tectonics*, 8 (2): 333-350.

Thomas, L., 1969, Rayleigh wave dispersion in Australia, *Bull. Seism. Soc. Am.*, 59: 167.

Thompson, R.N. and Gibson, S.A., 1994, Magmatic expression of lithospheric thinning across continental rifts, *Tectonophysics*, 233: 41-68.

Thomson, B.P., 1969a, Precambrian crystalline basement, *In:*L.W. Parkin (Ed.), *Handbook of South Australian geology*, Geological Survey of South Australia, pp.21-48.

Thomson, B.P., 1969b, Precambrian basement cover: the Adelaide System, *In:*L.W. Parkin (Ed.), *Handbook of South Australian geology*, Geological Survey of South Australia, pp.49-83.

Thomson, B.P., 1970, A review of the Precambrian and Lower Palaeozoic tectonics of South Australia, *Transactions of the Royal Society of South Australia*, 94: 193-221.

Thomson, B.P. (Compiler), 1980, Geological map of South Australia, *South Australia, Geological Survey of South Australia, Maps of South Australia Series, 1: 2 000 000.*

Thomson, B.P., Daily, B., Coats, R.P. and Forbes, B.G., 1976, Late Precambrian and Cambrian geology of the Adelaide 'geosyncline' and Stuart Shelf, South Australia, *25th International Geological Congress, Sydney, Excursion Guide*, 33A.

Toft, B. and Haggerty, S.E., 1988, Limiting depth of magnetisation in cratonic lithosphere, *Geophysical Research Letters*, 15(5): 530-533.

Tron, V. and Brun, J-P., 1991, Experiments on oblique rifting in brittle-ductile systems, *Tectonophysics*, 188: 71-74.

Truswell, E.M., 1978, Palynology of the Permo-Carboniferous in Tasmania, *Tasmania, Geological Survey, Bulletin*, 6.

Tsuboi, C., 1959, Application of double Fourier series to computing gravity anomalies and other gravimetrical quantities at higher elevations from surface gravity anomalies, *Report no. 2*, The Ohio State University, Institute of Geodesy, Photogrammetry, and Cartography.

Uyeda, S., 1981, Subduction zones and back-arc basins - a review, *Geol. Rundsch.*, 70(2): 552-569.

Uyeda, S., 1982, Subduction zones: an introduction to comparative subductology, *Tectonophysics*, 81: 133-159.

Uyeda, S. and Kanamori, H., 1979, Back-arc opening and mode of subduction, *J. Geophys. Res.*, 84: 1049-1062.

Uyeda, S. and Miyashiro, A., 1974, Plate tectonics and the Japanese Islands: a synthesis, *Geol. Soc. Am. Bull.*, 85: 1159-1170.

Vacquier, V., Steenland, N.C., Henderson, R.G. and Zietz, I., 1951, Interpretation of aeromagnetic maps, *Geol. Soc. Amer.*, Mem., 47: 151.

Veevers, J.J., 1974, Western continental margin of Australia, *In*: C.A. Burk and C.L. Drake (Eds), *The geology of continental margins*, 605-616, Springer-Verlag, New York.

Veevers, J.J. (Ed.), 1984, *Phanerozoic earth history of Australia*, Clarendon Press, Oxford.

Veevers, J.J., 1990, Antarctica-Australia fit resolved by satellite mapping of oceanic fractures zones, *Australian Journal of Earth Sciences*.

Veevers, J.J. and Eittreim, S.L., 1988, Reconstruction of Antarctica and Australia at breakup (95 ± 5 Ma) and before rifting (160 Ma), *Australian Journal of Earth Sciences*, 35: 355-362.

Veevers, J.J., Stagg, H.M.J., Wilcox, J.B. and Davies, H.L., 1990, Pattern of slow spreading (<4mm/year) from breakup (96 Ma) to A20 (44.5 Ma) off the southern margin of Australia, *BMR Journal of Australian Geology and Geophysics*, 11: 499-507.

Venturelli, G., Thorpe, R.S., Dal Piaz, G.V., Del Moro, A. and Potts, P.J., 1984,Petrogenesis of the calc-alkaline, shoshonitic and associated ultrapotassic Oligocene volcanic rocks from the Northwestern Alps, Italy, *Contrib. Mineral. Petrol.*, 86: 209-220.

Verall, P., 1989, Speculations on the Mesozoic-Cenozoic tectonic history of the western United States. *In:* A.J. Tankard and H.R. Balkwill (Eds), *Extensional tectonics and stratigraphy of the North Atlantic Margins, Am. Assoc. Pet. Geol. Mem.*, 46: 615-631.

Vierbuchen, R.C., George, R.P. and Vali, P.R., 1982, A thermal-mechanical model of rifting with implications for outer highs on passive continental margins, *In*: J.S. Watkins and C.L. Drake (Eds), *Studies in continental margin geology, Am. Assoc. Pet. Geol. Mem.*, 34: 765-778.

Vine, F.J. and Hess, H.H., 1970, Sea floor spreading, *In*: *The Sea, Int.*, 4: 587-622, Interscience, New York.

Vogel, A. and Lund, C.E., 1970, Combined interpretation of the Trans-Scandinavian seismic profile, section 2-3. *University of Uppsala, Report No. 4*, Uppsala, Sweden.

Voggenreiter, W. Höltz, H. and Mechie, J., 1988, Low-angle detachment origin for the Red Sea rift system, *Tectonophysics*, 150: 51-75.

Vogt, P.R., Cherkis, N.Z. and Morgan, G.A., 1983, Project Investigator-1: Evolution of the Australia-Antarctic discordance deduced from a detailed aeromagnetic study, *In:* R.L. Oliver, P.R. James and J.B. Jago (Eds), *Antarctic Earth Science*, Australian Academy of Science, Canbera, 608-613.

Von der Borch, C.C., 1980, Evolution of the Late Proterozoic to Early Paleozoic Adelaide Foldbelt, Australia: comparison with post-Permian rifts and passive margins, *Tectonophysics*, 70: 115-134.

Von der Borch, C.C., Conolly, J.R. and Dietz, R.S., 1970, Sedimentation and structure of the continental margin in the vicinity of the Otway Basin, southern Australia, *Marine Geology*, 8: 59-83.

Wang Hongzhen and Qiao Xiefu, 1984, Proterozoic stratigraphy and tectonic framework of China, *Geol. Mag.*, 121(6): 599-614.

Wasilewski, P. and Mayhew, M.A., 1982, Crustal xenolith magnetic properties and long wavelength anomaly source requirements, *Geophysical Research Letters*, 9 (4): 329-332.

Wasilewski, P., Thomas, H.H. and Mayhew, M.A., 1979, The Moho as a magnetic boundary, *Geophysical Research Letters*, 6 (7): 541-544.

Watkins, J.S., Montadert, L. and Dickerson, P.W. (Eds), 1979, Geological and geophysical investigations of continental margins, *The American Association of Petroleum Geologists, Memoir 29.*

Watkins, J.S., Zhiqiang, F. and McMillen, K.J. (Eds), 1992, Geology and geophysics of continental margins, *The American Association of Petroleum Geologists, Memoir 53.*

Webb, A.W., 1979, Geochronology of the eastern basement rocks, Progress report 22, *South Australia, Department of Mines and Energy, Open file Envelope*, 2136: 337-341 (unpublished).

Webb, A.W., Thomson, B.P., Blissett, A.H., Dally, S.J., Flint, R.B. and Parker, A.J., 1982, Geochronology of the Gawler Craton, South Australia, *South Australia, Department of Mines and Energy, Report Book*, 82/86.

Webb, A.W., Thomson, B.P., Blissett, A.H., Dally, S.J., Flint, R.B. and Parker, A.J., 1986, Geochronology of the Gawler Craton, South Australia, *Australian Journal of Earth Sciences*, 33: 119-143.

Weissel, J.K. and Hayes, D.E., 1971, Asymmetric spreading south of Australia, *Nature*, 231: 517-521.

Weissel, J.K. and Hayes, D.E., 1972, Magnetic anomalies in the southeastern Indian Ocean, *In:* D.E. Hayes (Ed.), *Antarctic Oceanology II: The Australian-New Zeland Sector, Antarctic Res. Ser.*, 19: 165-196.

Weissel, J.K. and Hayes, D.E., 1974, The Australian-Antarctic discordance: new results and implications, *Journal of Geophysical Research*, 84: 4572-4582.

Weissel, J.K., Hayes, D.E. and Herron, E.M., 1977, Plate tectonics synthesis: The displacements between Australia, New Zealand, and Antarctica since the Late Cretaceous, *Marine Geology.*, 25: 231-277.

Wells, A.T., Forman, D.J., Randford, L.C. and Cook, P.J., 1970, Geology of the Amadeus Basin, central Australia, Bull. Bur. Miner. Resour., *Geol. Geophys. Aust.*, 100.

Wernicke, B., 1981, Low-angle normal faults in the Basin and Range province: Nappe tectonics in an extending orogen, *Nature.*, 291: 645-648.

Wernicke, B., 1985, Uniform-sense normal simple shear of the continental lithosphere, *Canadian Journal of Earth Sciences.*, 22: 108-125.

White, A. and Milligan, P.R., 1984, A crustal conductor on Eyre Peninsula, South Australia, *Nature*, 310: 219-221.

White, A. and Milligan, P.R., 1986, Geomagnetic variation anomaly on Eyre Peninsula, South Australia, *Exploration Geophysics*, 17: 32-34.

White, A. and Polatayko, O.W., 1985, Electrical conductivity anomalies and their relationship with the tectonics of South Australia, *Geophysical Journal of the Royal Astronomical Society*, 80: 757-771.

White, R.E., 1969, Seismic phases recorded in South Australia and their relation to crust structure, *Geophysical Journal of the Royal Astronomical Society*, 17: 249-261.

White, R.S. and McKenzie, D.P., 1988, Formation of the "steer's head" geometry of sedimentary basins by differential stretching of the crust and mantle, *Geology*, 16: 250-253.

White, R.S. and McKenzie, D.P., 1989a, Volcanism at rifts, *Scientific American*, 7: 44-55.

White, R.S. and McKenzie, D.P., 1989b, Magmatism at rift zones: the generation of volcanic continental margins and flood basalts, *Journal of Geophysical Research*, 94: 7685-7729.

White, R.S., Spence, G.D., Fowler, S.R., McKenzie, D.P., Westbrook, G.K. and Bowen, A.N., 1987, Magmatism at rifted continental margins, *Nature*, 330: 439-444.

Whiteman, A., Naylor, D., Pegrum, R. and Rees, G., 1975, North Sea troughs plate tectonics, *Tectonophysics*, 26: 39-54.

Willcox, J.B., 1978, The Great Australian Bight - a regional interpretation of gravity, magnetic, and seismic data from the Continental Margin Survey, Bur. Miner. Resour. Austr., Rep. 201.

Willcox, J.B. and Stagg, H.M.J., 1990, Australia's southern margin: a product of oblique extension, *Tectonophysics*, 173: 269-281.

Williams, L.A.J., 1978, The volcanological development of the Kenya rift, *In*: E.-R. Neumann and I.B. Ramberg (Eds), *Petrology and geochemistry of continental rifts*, Reidel,Dordrecht, 101-121.

Willock, C., 1974, *Africa's rift valley*, The World's Wild Places/Time-Life Books, Amsterdam.

Wilson, M. and Guiraud, R., 1992, Magmatism and rifting in Western and Central Africa, from Late Jurassic to Recent times, *Tectonophysics*, 213: 203-225.

Withjack, M.O., Olson, J. and Peterson, E., 1990, Experimental models of extensional forced folds, Am. Assoc. Pet. Geol. Bull., 74: 1038-1054.

Wopfner, H., 1969, Depositional history and tectonics of South Australian sedimentary basins, *Mineral Resources Review, South Australia*, 133: 32-50.

Wright, J.B., 1968, South Atlantic continental drift and the Benue Trough, *Tectonophysics*, 6: 301-309.

Wright, J.B., 1970, The Benue Valley - a rip in the African continent, *The Nigerian Field*, 35: 78-85.

Wyllie, P.J., 1986, Genesis of kimberlites and some low-SiO_2, *In:* J. Ross (Ed.), *Kimberlites and related rocks, Vol.1, Their composition, occurence, origin and emplacement*, GSA Special Publication No. 14, Blacklwell Scientific Publications, 601-615.

Wyatt, B.A., Shee, S.R., Griffin, W.L., Zweistra, P. and Robinson, H.R., 1991, The petrology of the Cleve kimberlite, Eyre Peninsula, South Australia, *Proceedings of the 5th Kimberlite Conference, Brasilia, CPRM Special Publication*, 2(91): 463-465.

Ziegler, P.A., 1988, Evolution of the Arctic-North Atlantic and the Western Tethys, *Americ. Assoc. Pet. Geol. Mem.*, 43.

Ziegler, P.A., 1989, Evolution of the Laurussia, a study in late Palaeozoic plate tectonics, Kluwer, Dordrecht, 102.

Ziegler, P.A., 1990, *Geological Atlas of Western and Central Europe*, Shell Int. Pet. Mij. and Geol. Soc. London

Ziegler, P.A., 1992a, Plate tectonics, plate moving mechanisms and rifting, *In*: P.A. Ziegler (Ed.), *Geodynamics of rifting*, Vol. 3, Thematic discussions, *Tectonophysics*, 215: 9-34.

Ziegler, P.A., 1992b, Geodynamics of rifting and implications for hydrocarbon habitat, *In*: P.A. Ziegler (Ed.), *Geodynamics of rifting*, Vol. 3, Thematic discussions, *Tectonophysics*, 215: 221-253.